FLEXURAL - TORSIONAL ELASTO - PLASTIC BUCKLING

IN FLAT STIFFENED PLATING

by

Petros Andreas Caridis B.Sc. (Eng.) M.Sc. Dipl. Ocean Eng.

A Thesis Submitted for the Degree of

Doctor of Philosophy

in the Faculty of Engineering, University of Glasgow

August 1987

To Carmen and Anna - Maria

CONTENTS

ACKNOWLEDGEMENTS

The work presented in this thesis was carried out in the Department of Naval Architecture and Ocean Engineering, Glasgow University, during the period 1982-7. It has formed part of the Science and Engineering Research Council/Department of Energy Cohesive Buckling Programme and has been funded by these organisations. The experimental work reported was supported by the Ministry of Defence (ARE Dunfermline) and additional funding was obtained from A/S Veritec, Oslo, to carry out the parametric studies presented in Chapter 5. All the above organisations are thanked for the financial assistance given.

The theoretical work presented herein was conducted under the general supervision of Dr. P.A. Frieze.His assistance, encouragement and detailed advice throughout are gratefully acknowledged. Within the Department I wish to thank Professor D. Faulkner whose teaching at earlier times inspired the author to pursue research work in this field. Without his efforts to secure funding throughout the period of research this work would not have been brought to a successful completion. At this point I wish to also acknowledge the efforts made by Dr. P. Mayo, formerly Administrative Assistant within the Department, in the general administration of the correspondence relating to this project and in particular for the personal interest that he has shown.

The experimental work was carried out in collaboration with Mr. G. Sands, who supervised the preparation of the models, the test procedure and prepared the results which are given in a separate report. The technical expertise and patience of Mr. J. Fulton in preparing the models for testing is also acknowledged.

Discussions carried out with Dr. E. Samuelides in relation to the dynamic aspects of the work assisted in the development of the theoretical formulation presented in Chapter 6.

A number of figures have been prepared by Mrs. R. Young, within the Faculty of Engineering, and her assistance is also acknowledged.

I finally wish to express my heartfelt gratitude towards my wife for the continuous support and encouragement I received from her throughout.

INTRODUCTION

The importance of thin-walled structures in weight-critical design is evident from the wide application that these have found in the naval, aeronautical and more recently the offshore industry.

In the marine field, flat stiffened panels have formed the basic component of ship construction since the early years of this century and as such they have been subjected to the types of loading that a ship generally undergoes during its lifetime. The most critical condition which a vessel normally experiences is compression of the strength deck when in a sagging condition. Compressive loading in stiffened plates generally leads to some form of buckling collapse which may involve the shell plating, the stiffening elements, or both and consequently a thorough understanding of the various modes of buckling failure is essential, particularly as during the past decade thin-walled structures have found new fields of application in weight-critical design in the offshore industry.

Buckling in stiffened panels has been the subject of extensive research over several decades and foremost attention has been given to the analysis of plate behaviour. The analysis of individual structural components has been supplemented with that of the study of units consisting of plating combined with longitudinal and/or transverse stiffening elements and to this end many techniques have been developed.

Initial imperfections which arise during production, fabrication and the later life of the structure can lead to not insignificant reductions in strength and for this reason their presence has been studied in detail and is allowed for in most rigorous formulations. One other cause of deviations from perfect plate behaviour is the presence of residual stresses which arise during production and fabrication. These are also associated with the out-of-plane distortions which are caused by welding. Both factors have been studied extensively and reasonably good understanding of their effects has been gained.

One of the aspects of stiffened plate behaviour under compressive loading which has not however been given sufficient attention is flexural-torsional buckling; this involves

the combined action of the plate and the longitudinal stiffening elements.

The analysis of the flexural-torsional buckling behaviour of stiffened plates presents many problems because it is a complex mode of failure, characterised by a twisting of the stiffener about its line of attachment to the plating. The deformation also involves transverse and longitudinal flexure and is particularly likely to occur in short, flexurally stiff girders and in stiffeners with low lateral-torsional rigidity such as flatbars and bulb sections.

In conventional design procedures stiffener flexural-torsional (tripping) behaviour is treated as a secondary mode of failure and is prevented from occurring by limiting the proportions of stiffeners, to ensure that material failure becomes critical. Experimental research [1] has shown that when tripping failure occurs, the buckling mode is a 'brittle' one, demonstrating little ductility after its onset.

In the past, a wide variety of techniques have been used to tackle aspects of this problem and to date the energy method has been used most effectively in providing guidance in design. Closed form solutions to the equations which describe the behaviour of the shell plating and the stiffener cannot be obtained and when interactive behaviour arises, this complicates the analysis further since interactions with adjoining structural elements have to be considered when specifying boundary conditions. Irrespective of the problems peculiar to this mode of failure, the implementation of realistic boundary conditions is still difficult, despite the progress achieved by the use of numerical methods. The task becomes one of solving more than one set of coupled partial differential equations and this presents formidable problems when attempting to obtain analytical solutions. Each type of stiffener cross-section (flatbar, teebar, anglebar, bulb section) has its own flexural-torsional characteristics and has to be considered separately.

It is common practice in the offshore and shipbuilding industry to fit tripping brackets or other means of lateral support at regular spacings along the length of stiffeners. This has been criticised [2] on several counts and in particular because:

- if lateral movement were to take place, it is doubtful whether the brackets would

provide sufficient support against tripping.

- the determination of optimum spacings between lateral supports is at present conducted in a simplified manner which ignores the detrimental effect of the adjoining plating. In general, this would have buckled before tripping stress levels were reached.

- the cost of production, installation and maintenance of tripping brackets may well exceed that of stiffeners whose scantlings have been determined in a rational manner.

Central to the aim of this thesis is the development of a method which can address itself succesfully to the problems which are confronted when analysing stiffened plating. The importance of this category of structural component cannot be overestimated as it forms the building block upon which so much engineering construction is based. It is hoped that the method will be shown to be capable of overcoming the problems mentioned above and that it may prove to be a useful tool in gaining a better understanding of the behaviour of flat stiffened plates and in particular of their flexural-torsional behaviour.

The thesis is subdivided into seven chapters. In the first of these current and past work is reviewed. Stiffener tripping is considered and stiffened plates in general are discussed as the various modes of failure are interrelated. The literature on the flexural-torsional behaviour of stiffeners is not as extensive as one might expect and this reflects in part the prevalent feeling that it is a secondary mode of failure and does not therefore merit as much attention.

The equations used to describe the behaviour of the plate and stiffener are given in the second chapter. The von Karman equations (allowing for initial imperfections) are used for both the plate and the stiffener and incremental kinematic relationships are implemented to relate strains to in-plane and out-of-plane deflections. Intermediate levels of deformations are assumed and therefore large-deflection small-strain behaviour is appropriate. The conditions along the boundaries are considered next and the approach used to allow for material nonlinearity is described. The material behaviour is modelled using the von Mises yield criterion on a multilayer basis, in

conjunction with the Prandtl-Reuss flow rule. Elasto-plastic tangential multilayer rigidities are obtained and used to relate multilayer strains to corresponding stresses. In the final section of this Chapter, the equations which describe column type behaviour of the whole cross-section are given.

Chapter 3 is concerned with the application of the numerical method. A brief discussion on finite difference methods is followed by a description of iterative methods and in particular gradient methods one of which is Dynamic Relaxation (DR), the method used in this work. The numerical modelling of the boundary conditions is described in some detail and validation exercises are carried out to check the overall accuracy of the procedure.

Results from correlation studies with a series of tests carried out at Glasgow University are presented in Chapter 4. Detailed results from the tests are found elsewhere, and in this chapter a brief description of the experimental programme is followed by results obtained from the numerical analysis. These are compared with the test data. In all, seven model tests were considered all of which involved flatbar stiffeners. Of these, four were subjected to axial compression, two were loaded under lateral pressure and one was subjected to combined loading.

Studies concerning the effect of various geometrical and material parameters on the local torsional failure of flatbar stiffeners are carried out in Chapter 5.

An extension of the method to study the dynamic behaviour of unstiffened and stiffened plating is described in Chapter 6. Suitable modifications were made to the DR algorithm in order to convert the method to a real-time procedure. It was found necessary to include the effect of strain rate which can affect the overall behaviour significantly. The modified procedure was used to determine the final deflection and other aspects of the transient response of a series of impacted flat plates. These plates were tested at Glasgow University as part of a study on ship collisions.

The thesis ends with a summary of the major achievements of the work, and indicates where further effort is required.

CHAPTER ONE

LITERATURE REVIEW

A significant research effort has been carried out into the behaviour of flat stiffened plating. In this Chapter the variety of approaches that have been implemented will be indicated and in addition, certain of the more important aspects of stiffened plate response with particular regard to the lateral torsional instability of stiffeners will be considered.

1.1 Brief Historical Background

The foundations of structural mechanics were laid during the eighteenth century by Hooke [3], Daniel [4] and Jacob Bernoulli [5] and Euler [6] who studied the strength and deflection properties of elastic beams. These initial studies led to the consideration of the more complex problem of plate stability which was tackled during the nineteenth century by French mathematicians and scientists, following the work of Coulomb. In 1821, Navier published a paper containing the fundamental equations of the mathematical theory of elasticity [7]. Flexural and membrane effects were allowed for in 1877 by Kirchhoff [8], and by the end of the nineteenth century the governing equation for thin isotropic plates was in the form commonly encountered today. Further developments by Foppl [9], von Karman [10] and Marguerre [11] during the first part of the twentieth century led to the formulation that enables the postbuckling response of imperfect flat plates to be studied.

Solutions to this equation for particular boundary conditions were initially given by Bryan [12] in 1891, Timoshenko [13] in 1907 and Hencky [14] in 1921. Hencky was one of

the first to apply a finite difference method to plate buckling problems. Other boundary conditions and cases of loading were considered later by Way [15], Levy [16], Coan [17], Yamaki [18] and Walker [19] amongst others.

Contemporary solution techniques may be broadly classified into two groups. Firstly classical methods, originally developed during the nineteenth century and based on either:

i) energy principles,
ii) direct integration of the governing differential equation,
iii) variational principles (Rayleigh-Ritz, Galerkin).

Secondly numerical techniques which employ any one of a large variety of methods. Finite difference and finite element methods have nowadays become established tools of the structural analyst and design formulations are increasingly based on results derived from these.

The problem of material nonlinearity was first treated mathematically by Levy and Saint Venant during the mid-nineteenth century. The concept of yield criterion was introduced by Tresca in 1864 and following a period of experimental research various other criteria were proposed by other researchers. The most successful one, based on mathematical considerations, was that due to von Mises in 1913 [20] and this is now extensively used. Approximate criteria such as those due to Ilyushin [21], Ivanov [22] and later Ilyushin's criterion as modified by Crisfield [23] have also been used in order to reduce the cost of computational procedures.

Probably the most accurate formulation for the post-yield response of materials which is in use today is that proposed by Reuss in 1930 [24], following the work of Prandtl during the 1920s.

1.2 Recent Developments in Stiffened Plate Research

The difficulties that arise in the analysis of stiffened plating stem from a variety of sources. In this section, some of the most important of these are discussed against the

background of work carried out in recent years.

As mentioned in the previous section, the equations representing the large deflection behaviour of unstiffened plates with initial imperfections have been derived and solved for a number of different types of boundary conditions, using analytical and numerical methods. For the analysis of stiffened plates, amongst the most commonly used techniques are the following:

- Orthotropic plate theory [25]
- Plate-beam analysis [26]
- Beam-column (effective-width type approach) [27]
- Effective-stress approach [28]
- Finite element methods [29,30]
- Finite difference methods [31]

In all of the above, particular simplifying assumptions have been made or are implicit in the equations used.

Orthotropic plate theory has been used to analyse plating bearing a number of stiffeners in one or two orthogonal directions. For a small number of stiffeners however, the method proves less accurate and since the stiffness properties of the stiffeners are 'merged' with those of the plating, no detailed design data for them can be obtained.

Plate-beam analysis combines the large deflection equations representing plate behaviour with beam equations to represent the action of stiffeners. The method was first proposed by von Karman [10] and has been used by Shade [32], Reissner [33] and Odqvist [34] amongst others to analyse stiffened plates in conjunction with the effective breadth concept. It has recently been used by Smith [26] in the folded plate analysis of ship structures and elastic torsional buckling stresses have been obtained. In beam theory, shear stress terms are not included and thus a rigorous treatment of stiffener behaviour cannot be carried out.

In the beam-column (strut) approach, a plate bearing a number of stiffeners is divided into strips consisting of one stiffener and associated width of plating which are

analysed in isolation in order to determine the bending, buckling and flexural response of the cross-section. Recent research into steel box-girder bridge design has led to the implementation of the Perry-Robertson formula [27,35], based on this approach, which provides a simple yet reasonably rigorous design method.

Dwight and Little [36] however have criticised effective-width methods in general as being based upon the assumption that local buckling always occurs, whereas it is well-known that for high slenderness ratios local buckling may not occur until after the process of overall collapse is well developed. They have used instead an effective-stress approach, using the actual load-end shortening curves of plate elements.

Using finite element methods, Harris and Pifko [37] developed an elasto-plastic analysis procedure for stiffened plates. This was based on compatible plate bending and beam-column elements. Anisotropy and work-hardening were also allowed for. In their analysis however, the beam-column element used did not have torsional-flexural characteristics and was not used to study the torsional buckling behaviour of the stiffeners. Finite elements methods have also been used in combination with analytical techniques. Crisfield [30] developed a combined f.e.m./Rayleigh-Ritz elasto-plastic formulation in which the torsional response of the stiffener was not allowed for. Komatsu, Nara and Kitada [38] used a combined f.e.m./modal analysis method to study orthogonally stiffened plates in the elasto-plastic range and compared their results with a series of tests. The constraint method of analysis, applied to finite elements and introduced by Szabo et al. [39] was applied to the study of stiffened plates by Rossow and Ibrahimkhail [40]. In this study, plate-stiffener behaviour was modelled as a plate-beam.

From the mathematical point of view, the exact analysis of thin stiffened plates consists of solving two or more simultaneous sets of coupled partial differential equations for specified boundary conditions. Each set consists of two second order linear equations and one fourth order linear equation. The boundary conditions along the plate and stiffener edges may vary but are fixed along the unloaded, longitudinal edges of the stiffener. Exact analytical solutions for this type of problem have not been carried out and are not likely to be explored in the future because the advent of numerical techniques means that solutions can be obtained much more readily.

The effects of initial imperfections and residual welding stresses have been studied extensively for flat plates. For unstiffened compressed plates, increasing the magnitude of initial imperfections causes a reduction in ultimate strength, whereas residual welding stresses cause serious reductions only near yield strain levels [41].

Much less work is available on stiffened plates. A parametric study using a beam-column approach by Moolani and Dowling [42] showed that for stiffened plates with a slenderness ratio of around unity, increasing the initial imperfections causes significant reductions in column strength, particularly for low values of the ratio of stiffener/plate area. Murray [43] used the Perry-Robertson formula to predict collapse of axially compressed stiffened plates and considered the effects of eccentricity of the applied loading. A design method is outlined in his paper and the initiation of yielding is proposed in order to estimate the maximum strength of the cross-section.

Classical finite difference methods have a long history of application in plate analysis and during the past decade several f.d. based methods have been used. Djahani [44] carried out an analysis of stiffened plates under lateral pressure and edge compression using a modified Newton-Raphson method in conjunction with Aitken's δ^2-method. This formulation used thin plate and beam theory. Webb and Dowling [45] later used dynamic relaxation in an elasto-plastic analysis of stiffened plates based on Djahani's approach to the interaction of forces and at the plate-stiffener intersection. In this study the torsional behaviour of the stiffener was approximated and a variety of stiffener cross-sections were modelled.

1.3 Mode and Component Interactions in Stiffened Plates

Apart from questions concerning the equations used to describe stiffened plate response, several other factors of importance have in recent years been receiving the attention of researchers. Geometrical nonlinearity involves the process of interaction of the different buckling modes of each member (local, overall) and also the interaction of the components of the stiffened plate (stiffener and shell plating). The physical complexity is reflected by the highly nonlinear equations that describe this type of behaviour. On the other hand, a formulation that enables stiffener bending, twisting and

flexure to be studied necessitates the use of the Marguerre equations.

The first explicit study of mode interaction was that by van der Neut [46]. A simplified model based on overall buckling was proposed in order to study local and overall column buckling in the elastic range, including the effect of initial imperfections. An alternative approach by Koiter and Pignataro [47] using energy functionals has also been presented and experimental work in Britain by Thomson, Tulk and Walker [48] has been carried out on stiffened plates. In (49), Tulk and Walker reported that for a particular geometry, although each panel component would individually exhibit stable postbuckling response, they would interact to give unstable behaviour. Fok, Rhodes and Walker [50] presented a simplified theoretical model of the local elastic buckling of stiffeners and compared results with small-scale tests. This analysis was extended in (51) to allow for initial imperfections. The coupling of local and overall modes was modelled using linear and rotational springs by Croll [52], for box columns and stiffened plates. The effect of initial imperfections has been studied by Tvergaard [53] who showed that imperfections move the 'optimum' away from coincident buckling mode design. More recently, Svensson and Croll [54] gave solutions to the equations governing mode interaction for small imperfections in the van der Neut model.

In (55), Maquoi and Massonet reviewed the work carried out until that time on the mode interaction problem. They concluded that, regarding box columns, from a theoretical standpoint the formulation by Graves-Smith [56], which allowed for the plastic reserve of strength, was the most accurate one although in practice the optimum could still be determined by coincident buckling design since for box columns little variation is noted near the optimum.

The 'exact' boundary conditions at the intersection of two flat plates were first modelled numerically by Frieze and Dowling [57] and Frieze [58] for the case of axially loaded box columns in the elastic and elasto-plastic range.

1.4 Classical Methods for the Lateral Torsional Instability Analysis of Stiffeners

The problem of lateral torsional instability in beams and stiffened plates was recognised during the previous century and following the work of Saint-Venant on torsion,

Prandtl, Mitchell and Timoshenko studied the lateral torsional behaviour of beams. Their work concentrated on developing a method to determine the moment of inertia of the cross-section in order to prevent elastic torsional buckling. Timoshenko [59] and Barbre [60] later extended this work to stiffened plates. Before the Second World War, extensive work was carried out in the U.S. by N.A.C.A. in order to provide structural design data for aircraft. This concentrated mainly on stiffened and unstiffened plates under various boundary conditions. Within this context, Seide [61] evaluated expressions for effective moments of inertia of panels with Z-section stiffeners which are used in aircraft structures.

Torsional buckling of open thin-walled sections was first considered by Wagner [62] based on the assumption that the centre of rotation of the cross-section during buckling coincides with the shear centre. Since this was shown not to be correct [63] the results of Wagner's analysis are not exact.

In 1936 Bleich and Bleich [63] treated the problem in a generalised manner by allowing for the effects of bending, twisting and buckling. The fundamental differential equations of the problem were derived from the theorem of stationary potential energy and it was established that, in the general case, if the displacements of the shear centre are used as co-ordinates instead of the displacements of the centroid, the usual differential equations retain their validity [64]. In this treatment however a term in the expression for the potential energy was omitted; this was later included in a more refined treatment by Kappus [65].

Theoretical results obtained by the above authors [62,63] were compared by Kappus [65] and are reproduced here in Fig. 1.1. In this diagram the effect of aspect ratio on the elastic torsional buckling stress of a channel section with elements of equal breadth, i.e. a=b, are indicated. It is seen that the differences that arise tend to become smaller with increasing column length as the torsional buckling stress approaches the Euler stress.

Other authors working during the same period on the torsional buckling problem of columns were Lundquist and Fligg [66], Timoshenko [67], and Goodier [68].

In all the above mentioned work, it was assumed that plane cross-sections may warp

but that the geometric shape did not change; the theories considered overall (primary) column failure as opposed to local failure characterised by distortion of the cross-section. It was only in later work that account was taken of overall and local failure modes and their interaction, as described in the preceding section.

The theorem of stationary potential energy which was used by Kappus [65] and Bleich and Bleich [63] states that "the amount of total potential energy $U = V + U_w$ does not change when the structure passes from its configuration of equilibrium to an infinitesimally near adjacent configuration". Thus,

$$U = V + U_w = \text{stationary} \tag{1.1}$$

where U = total potential energy of the system
V = internal strain energy
U_w = potential energy of the external loads

According to the calculus of variations, for an integral of the form:

$$I = \int F(x,y,y',y'')\, dx \tag{1.2}$$

the function y=y(x) which makes the expression I stationary is given by:

$$F(y) - \frac{d}{dx} F(y') + \frac{d^2}{dx^2} F(y'') = 0 \tag{1.3}$$

This is the Eulerian differential equation of I which may be used to obtain a solution to the stationarity problem that has been posed.

Bleich [64] treated the stiffener using beam theory and applied the stationary potential energy theorem in order to derive critical elastic buckling stresses under the following assumptions:

i) Distortions of the cross-section are ignored

ii) The angle of twisting is small

iii) The energy of external shearing stresses is small.

The internal energy V consists of strain energy due to the longitudinal stress V_1 and shearing stresses V_2. Therefore,

$$V_1 = \frac{1}{2}\int_0^1 \left[E\tau \left(a^2 I_y + \Gamma \right) \beta''^2 \right] dz \qquad (1.4a)$$

$$V_2 = \frac{1}{2}\int_0^1 \left[G\tau K \beta'^2 \right] dz \qquad (1.4b)$$

and $$V = V_1 + V_2 \qquad (1.5)$$

The potential energy of the external loads, U_w, is given by:

$$U_w = -\frac{1}{2}\int_0^1 \sigma \left[Aa^2 + 2Aay_0 + I_p \right] \beta'^2 \, dz \qquad (1.6)$$

where

ß = angle of twist

E = Young's Modulus

τ = E_t / E (E_t = tangent modulus)

a = distance from shear centre to axis of enforced rotation

I_y = principal moment of inertia about y-axis

G = shear modulus

Γ = longitudinal warping constant

K = torsional constant

σ = compressive stress on end surfaces

A = area of cross-section

y_o = distance from centroid to neutral axis

I_p = polar moment of inertia with respect to shear centre

dz = incremental distance along length of column

I_{pc} = polar moment of inertia with respect to axis of enforced rotation.

and consequently the total potential energy of the system, U, is:

$$U = \frac{1}{2}\int_0^l \left[E\tau\,(a^2 I_y + \Gamma)\,\beta''^2 + G\tau K\beta'^2 - \sigma\,(Aa^2 + 2Aay_0 + I_p)\,\beta'^2 \right] dz \qquad (1.7)$$

Since $I_p = I_x + I_y + Ay_0^2$, I_x, I_y being the principal moments of inertia of the cross-section, the following form is obtained:

$$U = \frac{1}{2}\int_0^l \left[E\tau\,(a^2 I_y + \Gamma)\,\beta''^2 + (G\tau K - \sigma I_{pc})\beta'^2 \right] dz \qquad (1.8)$$

The corresponding Eulerian equation is:

$$E\tau\,(a^2 I_y + \Gamma)\,\beta^{IV} + (\sigma I_{pc} - G\tau K)\,\beta'' = 0 \qquad (1.9)$$

Letting $\beta = C \sin(n\pi z/l)$

where C is the magnitude of the rotation

n is an integer (1,2,....)

z is the length along the column

l is the length of the column

the equation can be integrated for simply supported boundary conditions to give:

$$\sigma_{cr} = \frac{\pi^2 E\tau}{l^2}\left[\frac{a^2 I_y + \Gamma}{I_{pc}} + \frac{Gl^2 K}{\pi^2 E I_{pc}}\right] \qquad (1.10)$$

where σ_{cr} is the critical torsional buckling stress corresponding to the fundamental buckling mode (n=1). The preceding approach forms the basis of the energy method which has been used by several authors and implemented in classification society rules [69,70]. Windenburg [71] considered the proportions of tee-bar stiffeners to ensure against:

i) Web local buckling
ii) Twisting instability
iii) Flange local buckling

The differential equation of the deflection surface of the web was integrated for simply supported boundary conditions and elastic restraint at the intersection with the flange. In this treatment, in-plane deflections were ignored and a reduced modulus was used for the plastic range. Later work has shown that this treatment is optimistic due to interaction effects. More complex cases of loading have been handled using interaction curves [72,73]. Argyris and Dunne [74] have given detailed analyses for various failure modes (flexural, flexural-torsional) for panels with several stiffeners. Critical elastic stresses were obtained for aircraft-type structures.

Faulkner [72,75,76] has proposed several equations for the determination of elastic tripping stresses, based on the energy method. The problem of interaction with the plate and the complexities arising from this are acknowledged. A simplified treatment is carried out in which it is assumed that the lowest tripping stress occurs when the plate elements and the stiffener buckle with the same half wave lengths, leading to the following equation:

$$\sigma_{cr} = \frac{G\{J+(E/G)(m\pi/a)^2(I_z\bar{z}^2+\Gamma)\}/I_0 + C_0 a^2/m^2\pi^2 I_0}{1+C_0 a^2/m^2\pi^2\sigma_p I_0} \qquad (1.11)$$

where

J = Saint Venant torsion constant for stiffener

m = number of half-waves along length

a = length of plate

I_z = second moment of area about web cross-section (= $dt^3/3$)

$\bar{z}$ = height of centroid

Γ = longitudinal warping constant (= $I_z d^2/4$)

I_o = polar moment of inertia about the toe (= $td^3/12 + I_z$)

C_o = rotational spring constant (= $Et^3/3b$)

σ_p = plate elastic buckling stress (= $0.903E(t/d)^2\{a/m+m/a\}^2$)

In this equation the stiffener is assumed to have a constant rotational restraint C_o along the edge in contact with the plate, the second term in the denominator representing the destabilising effect of the plate. In theory, if the rotational restraint becomes negative due to plate buckling effects the tripping stress is reduced. Inelastic effects are allowed for by the use of the structural tangent modulus E_t.

In an extensive study on the subject, Adamchak [73] employed the energy method and presented a series of design-orientated equations for axial, lateral and combined loading. Flatbar and tee-bar stiffeners were considered and plasticity effects were allowed for, again using the structural tangent modulus. It was noted that since plate effectiveness was dependent upon initial imperfections, critical torsional buckling stresses could be significantly reduced in their presence. Adamchak also found that the assumption that the web of a stiffener remained locally undeformed in its own plane led to higher buckling stresses than those obtained from a finite element analysis. A simplified treatment to allow for this in the case of symmetrical stiffeners was included and resulted in a quadratic equation for the buckling stress. Examples of these and other design equations are included in Appendix A.

In a paper by Bijlaard [77], longitudinally and transversely stiffened plates were studied and elastic solutions obtained by direct integration of beam equations which were used to represent stiffener action

1.5 Numerical Methods

Of the general purpose finite-element packages available none has to date been used to investigate the tripping problem. Det norske Veritas [78,79], have compared the results from two such packages (STAGSC, NV390) with test data on flatbar stiffeners used in flat panels. Good agreement was found when the stiffener was assumed clamped to the plate. When however a simple support was used, large discrepancies between the two predictions were observed.

As mentioned in Section 1.2, plate-beam analysis [26] has also been used to obtain elastic torsional buckling stresses. The method has not however been extended to the plastic range. Skaloud and Kristek [80] have analysed stiffened plating and have considered a variety of stiffener cross-sections. Folded-plate theory was applied in the elastic range in order to obtain optimum stiffener spacings and dimensions. It was found that the results did not differ appreciably from classical theory.

In (81) Guedes Soares and Soreide discuss the results of recent work on both stiffened and unstiffened plates using numerical and analytical techniques. The more important factors which affect behaviour are considered and results are given for flat plates under axial compression. Design methods for stiffened plates based on the effective width approach and the Perry-Robertson equation are also compared.

The elastic postbuckling range for stiffeners failing by torsional instability was examined theoretically by Ellinas and Croll [82]. The large deflection equations and boundary conditions were linearised by employing a perturbation scheme. Finite differences were subsequently employed and the resulting linear simultaneous algebraic equations solved. Good agreement with test results was noted, although it is felt that the method was cumbersome and any attempt at extending this type of analysis to the elasto-plastic range could meet with mathematical as well as conceptual difficulties.

A theoretical model for simply supported stiffeners based on Wagner's original equation was developed by Rogers and Dwight [83]. Plasticity effects were included and results compared with test data (described in Section 1.6). The stress-strain curves

obtained were similar to equivalent ones for plates; at high depth/thickness ratios a clearly defined post-buckled range was found. The effects of residual stresses and initial imperfections were also studied. It was found that imperfections did not affect the response appreciably although residual stresses caused a deterioration in strength in lightly welded plating which however was not amplified significantly by heavy welding. This is consistent with the behaviour of simply supported plates as found by Dowling and Frieze [84]. A strength formula, based on the Perry-Robertson equation was proposed for long simply supported stiffeners.

In another study carried out at ARE (Dunfermline) [85], the behaviour of bulb and tee-bar sections were compared using a folded plate analysis procedure. The study was limited to the elastic range and it was found that bulb sections were less efficient, partly because they are more susceptible to lateral-torsional instability.

The large-deflection plate equations were solved for flatbar stiffeners using simplified boundary conditions by Bradfield [86]. A constant rotational restraint along the intersection with the base plate was assumed and a finite difference formulation implemented to solve the equations. Plasticity was modelled using the Ilyushin yield criterion, as modified by Crisfield. A study of the effect of rotational restraint showed that strength is relatively insensitive to it, as demonstrated in the accompanying diagram.

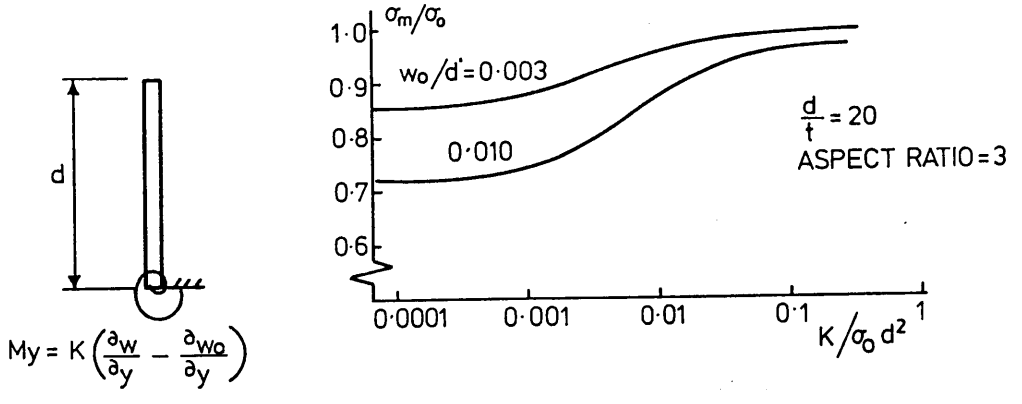

The effect of initial distortions here seems greater than that found by Rogers and Dwight [83].

1.6 Experimental Research

Bleich [64] discusses the earliest results from tests carried out in this field. Experimental work on torsional buckling was first conducted on aluminium panels used in aircraft structures by Wagner and Pretschner [87]. In the 1930s and 1940s further work was carried out on panels with Z-section and bulb stiffeners [88]. Later tests were conducted using magnesium and steel alloys, also for aircraft-type structures.

More recently, tests have been performed for ship-type structures at Cambridge University [89] and Det norske Veritas [79]. An extensive series of tests relating to the civil engineering field (box girder bridges) was carried out at Manchester University by Horne and Narayanan [90,91].

The work at Cambridge consisted of a series of axial compression tests on flatbars and bulb flats. Fifty-eight flatbars were treated with their longitudinal centrelines supported, thus providing two simply-supported webs with their common attached edge constrained to stay straight by symmetry. The tests covered nine slendernesses in the range $28 > d/t > 9$. Twelve models consisting of sections 150mm wide x 7mm thickness x 28mm bulb overall thickness arranged as cruciforms, were also tested. The purpose of these tests was to provide a means of comparison for a theoretical approach that was developed in parallel. The effects of residual welding stresses and imperfections were included.

At Manchester University [91] the tests were carried out on axially compressed stiffened steel plating and both plate and stiffener induced failure was examined. It was found that in general, rapid unloading was experienced following stiffener induced collapse. Comparisons with the Merrison box girder bridge design rules indicated that the rules were in general conservative except for simply supported bulb flats, and to a lesser degree for wider flange angles, where they appeared to be optimistic.

1.7 Design Rules - Implementation and Present Practice

The traditional, empirical approach to the drafting of codes relies on the reappraisal of

past recommendations in the light of new experience. The fundamental drawback to this approach however, lies in the inability to obtain a real understanding of the basic mechanics of the structure in question. Consequently, by not being able to accurately interpret and generalise the data that has been obtained, rules which usually tend to be conservative are adhered to.

Few practical structural mechanics problems can be solved in a quick and easy manner, so when a situation involving a complicated structural arrangement coupled with a non-idealised distribution of loading arises, simplifying assumptions are necessarily made in order to provide guidance to the designer.

Progress in the past few decades is beginning to be reflected in design rules and the attitudes of one particular group of engineers involved in drafting plate buckling rules some years ago were expressed as follows:

> "It is recognised that progress has been achieved in solving von Karman's nonlinear differential equations for initially perfectly flat plates, in solving Marguerre's nonlinear differential equations which have small initial geometrical imperfections and in applying finite element methods to geometrical and material non-linearities in plate problems"[92].

It should be added, however, that not all bodies responsible for the drafting of rules follow an approach such as the above.

From Appendix A it is apparent that a variety of different approaches have been adopted in some of the recently drafted design codes on the question of stiffener design. In merchant vessels it is common practice to use flatbar and bulb section stiffeners whereas in warships tee-bar stiffeners are extensively used.

Det norske Veritas provide a simple criterion for the design of flatbars; rearranging the formula contained in the Appendix leads to $\beta < 0.4$ where $\beta = (b/t)\ (\sigma_0/E)^{1/2}$. Webs designed in accordance with this formula lie in the region where for simply supported plates $\sigma_m = \sigma_0$ [93] (where σ_m is the ultimate strength). In other words, torsional buckling is designed out of stiffeners and yielding becomes the failure criterion.

Although the British steel bridge design code (BS 5400) has a different format [94], results are close to those obtained using the DnV formula. The same is true of the Lloyds' Register of Shipping Rules which also exclude tripping as a form of failure by limiting the proportions of flatbar stiffeners [69]. Strength of primary stiffening elements is checked throughout by use of the section modulus of the cross-section.

For plating bearing tee-bar stiffeners the Royal Navy uses a weighted average of the stiffener torsional buckling stress and the plate buckling stress. Following comparisons of theoretical predictions with experimental results obtained from full-scale tests [1], it was decided to specify that torsional buckling stresses at the preliminary design stage should not be less than the panel average compressive failure stress, this being calculated using an iterative method developed by Faulkner et al. [75]. Final design would involve a finite-element program developed at ARE (Dunfermline) [85].

Drymakis [95] compared the results obtained from several elastic torsional buckling design formulae for tee-bar stiffeners including some of those mentioned above. He found that Bleich's formula predicted generally higher stresses than any of the other methods. Overall, an appreciable amount of scatter was noted when buckling stresses were plotted against several geometrical parameters.

One of the underlying assumptions that has been made in deriving explicit expressions for stiffener torsional buckling stresses is that the stiffener is attached to the plating in a simply supported manner. The thinking behind this goes back to the earliest work on the subject, namely Windenburg, Bleich, et al. At first glance this may appear to be a conservative criterion, especially when the stiffener is considered in isolation. However, since plate flexural buckling stresses are generally lower than stiffener torsional buckling stresses, when the plate approaches its limit it will act in a destabilising manner on the stiffener (provided interframe buckling does not occur), so that the torsional buckling stress will be reduced. In actual practice interaction effects will come into play, particularly those relating to stiffener interframe buckling, considerably complicating the response. Classical methods cannot at this stage provide an exact solution and few design equations make any attempt at allowing for this, although in certain treatments the effect of the rotational restraint arising from the plate

is allowed for [72,73]. In a folded plate analysis [85], Smith also allowed for the destabilising effect of plating and found that for relatively slender stiffeners, the simply supported condition was more accurate. He concluded however that since the plating exerts a substantial restraining effect on the torsional buckling of tee-bars, neither the simply supported nor the clamped condition provide satisfactory results. In other words, the 'true' condition will depend on the slenderness of the stiffener relative to that of the plate.

1.8 Concluding Remarks

It is thus seen that the study of the torsional response of stiffeners attached to flat plating has over a period of fifty years attracted the application of a variety of approaches, of which probably the most important has been the energy method which has been based on small-deflection theory. The tangent modulus concept has been used to allow for plasticity while various simplifying assumptions concerning buckling modes and interaction effects have been made. The complexity of the problem necessitates the use of a method capable of successfully allowing for the more important effects that govern stiffener torsional behaviour, namely large deflections, plasticity and mode and component interactions. Numerical techniques have proven to be powerful tools in the nonlinear analysis of structures, the most successful of which have been the finite element method (FEM) and the finite difference method (FD). In this thesis, a large-deflection FD elasto-plastic formulation has been used and 'exact' boundary conditions at the plate/stiffener intersection have been modelled. Local and overall failure modes are modelled and thus full interaction effects may been studied.

CHAPTER TWO

ELASTO - PLASTIC ANALYSIS OF FLAT STIFFENED PLATING

The equations used to describe the behaviour of flat stiffened plating are presented in this Chapter. The modelling of the behaviour of the material is described in detail and the yield criterion is derived from conditions of plane stress, following Hill [96]. The Prandtl-Reuss flow rule is also described and used to obtain the elements of the matrix of multilayer rigidities, in a manner similiar to Harding [97]. Finally the boundary conditions acting along the panel edges and the plate-stiffener intersection are described for the general case in which the panel forms part of an orthogonally stiffened grillage.

2.1 Equilibrium Equations for Thin Flat Plates

As mentioned earlier a large variety of formulations have been developed in order to represent both unstiffened and stiffened plate behaviour. The von Karman equations are obtained when the analysis of unstiffened thin flat plates is based on coupled direct force and moment terms. A variety of approaches may be used to derive these and are available in the literature [98]. Analytical and numerical solutions in conjunction with corresponding kinematic relationships and constitutive relations have been obtained for several types of boundary conditions. The equations which were originally derived by von Kármán, and later modified by Marguerre to allow for initial geometrical imperfections, are as follows:

$$\frac{\partial^2 M_x}{\partial x^2} + 2\frac{\partial^2 M_{xy}}{\partial x \partial y} + \frac{\partial^2 M_y}{\partial y^2} + N_x\left(\frac{\partial^2 w}{\partial x^2} + \frac{\partial^2 w_o}{\partial x^2}\right) + 2N_{xy}\left(\frac{\partial^2 w}{\partial x \partial y} + \frac{\partial^2 w_o}{\partial x \partial y}\right) +$$

$$N_y\left(\frac{\partial^2 w}{\partial y^2} + \frac{\partial^2 w_o}{\partial y^2}\right) + q = 0 \qquad (2.1a)$$

$$\frac{\partial N_x}{\partial x} + \frac{\partial N_{xy}}{\partial y} = 0 \qquad (2.1b)$$

$$\frac{\partial N_y}{\partial y} + \frac{\partial N_{xy}}{\partial x} = 0 \qquad (2.1c)$$

where

x,y	are the cartesian coordinates defining the plane of the plate
w	is the deflection in the direction normal to the plate
N_x,N_y	are the in-plane forces per unit width of plate (stress resultants) acting in the x and y directions.
N_{xy}	is the inplane shear force/unit width of plate acting tangentially along the faces of the element.
M_x,M_y	are the bending moments/unit width of plate acting in the (x-w) and (y-w) planes respectively.
M_{xy}	is the twisting moment/unit width of plate acting in the plane of the faces of the element (using reversed signs).
w_o	is the initial deformation of the plate in the w-direction, and
q	is the (external) pressure acting on the plate in the 'w' direction as shown in Fig. 2.1.

It is seen that these form a set of linear partial differential equations which are coupled since, in the first of these, in-plane direct and shear stress resultants are included. These terms are required when studying postbuckling behaviour and when omitted lead to linear plate theory. In a more rigorous treatment, the effect of plate thickness also needs

to be considered. This complicates the analysis considerably and the additional terms are of practical importance only near the edges and around holes which are not large in comparison with the thickness of the plating [99]. Thus in thin plate theory transverse forces are neglected and the usual assumption of isotropy is no longer valid.

The Marguerre equations are used to describe local buckling in thin flat plates. As such they are the appropriate equations to use in order to describe the local torsional behaviour of flatbar stiffeners when solved in conjunction with the corresponding boundary conditions. In this analysis they have been used to model the response of both the base plate and the stiffener. In existing analyses of stiffened plating, the beam-column equations have been used to model stiffener behaviour but these however cannot allow for the torsional mode of failure which depends on the local bending and twisting of the stiffener about its line of attachment to the plating. The third failure mode, column buckling, is described by the beam-column equations and therefore in a full analysis the interaction between local and overall failure modes needs to be considered.

2.2 Kinematic Relationships

The strain-displacement relations used are based on classical plate theory and again, terms of second order are ignored. Donnell [100] has derived exact expressions based on the Kirchhoff assumption but justifies the omission of higher order terms on the basis that strains and slopes are small compared with unity. The present analysis deals with intermediate levels of deformations and thus the use of the approximate expressions is justified. Since an incremental formulation is required in the flow theory of plasticity used to model material behaviour, the kinematic relationships are cast in the following form:

$$\Delta\varepsilon_x = \left(\frac{\partial u}{\partial x} - \frac{\partial u_p}{\partial x}\right) + \frac{1}{2}\left(\frac{\partial w}{\partial x} - \frac{\partial w_p}{\partial x}\right)\left(\frac{\partial w}{\partial x} + \frac{\partial w_p}{\partial x} + 2\frac{\partial w_o}{\partial x}\right) \tag{2.2a}$$

$$\Delta\varepsilon_y = \left(\frac{\partial v}{\partial y} - \frac{\partial v_p}{\partial y}\right) + \frac{1}{2}\left(\frac{\partial w}{\partial y} - \frac{\partial w_p}{\partial y}\right)\left(\frac{\partial w}{\partial y} + \frac{\partial w_p}{\partial y} + 2\frac{\partial w_o}{\partial y}\right) \tag{2.2b}$$

$$\Delta\gamma_{xy} = \left(\frac{\partial u}{\partial y} - \frac{\partial u_p}{\partial y}\right) + \left(\frac{\partial v}{\partial x} - \frac{\partial v_p}{\partial x}\right) + \frac{\partial w}{\partial x}\frac{\partial w_p}{\partial y} - \frac{\partial w}{\partial x}\frac{\partial w_p}{\partial y} +$$

$$\left(\frac{\partial w}{\partial x} - \frac{\partial w_p}{\partial x}\right)\frac{\partial w_o}{\partial y} + \left(\frac{\partial w}{\partial y} - \frac{\partial w_p}{\partial y}\right)\frac{\partial w_o}{\partial x} \qquad (2.2c)$$

$$\Delta\phi_x = -\left(\frac{\partial^2 w}{\partial x^2} - \frac{\partial^2 w_p}{\partial x^2}\right) \qquad (2.3a)$$

$$\Delta\phi_y = -\left(\frac{\partial^2 w}{\partial y^2} - \frac{\partial^2 w_p}{\partial y^2}\right) \qquad (2.3b)$$

$$\Delta\phi_{xy} = -\left(\frac{\partial^2 w}{\partial x \partial y} - \frac{\partial^2 w_p}{\partial x \partial y}\right) \qquad (2.3c)$$

where

$\Delta\varepsilon_x$, $\Delta\varepsilon_y$	are incremental strains in the x,y directions
$\Delta\gamma_{xy}$	is the incremental shear strain
$\Delta\phi_x$, $\Delta\phi_y$	are incremental curvatures in the x,y directions
$\Delta\phi_{xy}$	is the incremental twisting curvature
$\frac{\partial u}{\partial x}, \frac{\partial u}{\partial y}, \frac{\partial v}{\partial x}, \frac{\partial v}{\partial y}$	are strains arising from in-plane deflections
$\frac{\partial^2 w}{\partial x^2}, \frac{\partial^2 w}{\partial y^2}$	are curvatures in the plating in the x,y directions

$\frac{\partial^2 w}{\partial x \partial y}$ is the twisting curvature in the plating

The subscipt p indicates values of the displacements at the end of the previous increment. The above expressions (2.2) give the membrane strains acting at the neutral axis of the plate. In order to obtain strains at other positions through the thickness of the plate, use is made of the Kirchhoff assumption. Thus

$$\varepsilon_{,z} = \varepsilon + z\,\phi \tag{2.4}$$

where $\varepsilon_{,z}$ is the strain at a distance z from the neutral axis. This linear relationship simplifies the analysis since forces and moments acting on the plate can be found directly from the deflection of the middle surface of the plate, because in classical plate theory this is assumed to be a function of the coordinates x,y only. In explicit form the strains become:

$$\Delta\varepsilon_{x,z} = \Delta\varepsilon_x + z\ \Delta\phi_x \tag{2.5a}$$

$$\Delta\varepsilon_{y,z} = \Delta\varepsilon_y + z\ \Delta\phi_y \tag{2.5b}$$

$$\Delta\gamma_{xy,z} = \Delta\gamma_{xy} + 2z\,\Delta\phi_{xy} \tag{2.5c}$$

The multilayer strains are required to model the material behaviour in conjunction with the yield criterion, attributed to von Mises et al., as described in the next section.

2.3. Material Behaviour - The Ideal Plastic Body

During the past decade, the von Mises yield criterion has increasingly been combined with the Prandtl-Reuss flow rule to model the material behaviour of steel structures. Computer storage capacity and processor speed limitations have forced researchers in certain cases to use approximate theories to overcome these problems. It may be expected however that in future, developments in computer hardware will lift these restrictions and make the application of rigorous theory more widely possible.

It is recognised that at any point in a structure, the growth of plasticity proceeds gradually through the thickness of the plate, making use of a multilayer approach desirable. In this treatment, the material is considered to possess the properties of an ideal plastic body [96] for which the following assumptions are made:

i) The effects of time and temperature are neglected. Thus creep and thermal phenomena are ignored although in a dynamic analysis the strain rate effect may be included.

ii) The material is treated as being uniform on the microscopic scale , i.e. the Bauschinger effect and hysteresis are not allowed for. The material is further assumed to be isotropic although the treatment may be readily generalised to allow for the effects of anisotropy. It is not intended to be used to study the effects of plastic anisotropy.

iii) Size effects are neglected. These may be due to grain size, inclusions, or the irregular propagation of slip fields.

2.4 Yield Criterion

The von Mises yield criterion was proposed in 1913 [20] following a period of experimental research during which numerous other criteria were put forward. In general, a law defining the limit of elasticity under any possible combination of stresses is required; this is called a criterion of yielding. Since, for an isotropic material, plastic yielding depends only on the magnitudes of the principal applied stresses, and not on their directions, any yield criterion may be expressed as

$$f(J_1,J_2,J_3) = 0 \qquad (2.6)$$

where J_1,J_2 and J_3 are the first three invariants of the stress tensor σ_{ij}. They are defined by:

$$J_1 = \sigma_1 + \sigma_2 + \sigma_3 \qquad (2.7a)$$

$$J_2 = -(\sigma_1\sigma_2 + \sigma_2\sigma_3 + \sigma_3\sigma_1) \qquad (2.7b)$$

$$J_3 = \sigma_1 \sigma_2 \sigma_3 \tag{2.7c}$$

where σ_1, σ_2 and σ_3 are the three principal stresses. Experimental data show that yielding is, to a first approximation, unaffected by hydrostatic pressure, either applied alone or superimposed on any other state of stress. For the ideal plastic body therefore, yielding depends only on the deviatoric or reduced stress tensor. Thus,

$$\sigma_{ij}' = \sigma_{ij} - \sigma \delta_{ij} \tag{2.8}$$

where $\sigma = \sigma_{ij} / 3$ is the hydrostatic component of stress and δ_{ij} is the Kronecker delta. The principal components are not independent since $\sigma_1' + \sigma_2' + \sigma_3'$ is identical to zero. The yield criterion reduces to the form:

$$f (J_2', J_3') = 0 \tag{2.9}$$

where

$$J_2' = - (\sigma_1' \sigma_2' + \sigma_2' \sigma_3' + \sigma_3' \sigma_1') = \frac{1}{2} (\sigma_1'^2 + \sigma_2'^2 + \sigma_3'^2) = \frac{1}{2} \sigma_{ij}' \sigma_{ij}' \tag{2.10a}$$

$$J_3' = \sigma_1' \sigma_2' \sigma_3' = \frac{1}{3} (\sigma_1'^3 + \sigma_2'^3 + \sigma_3'^3) = \frac{1}{3} \sigma_{ij}' \sigma_{jk}' \sigma_{ki}' \tag{2.10b}$$

Most of the yield criteria that were suggested during the latter part of the nineteenth century conflict with experimental data in that they predict that hydrostatic stress always influences yielding. Von Mises proposed that yielding occurred when J_2' reached a critical value, in other words that it was independent of J_3'. His criterion can be written in the following alternative forms:

$$2 J_2' = \sigma_{ij}' \sigma_{ij}' = \sigma_1'^2 + \sigma_2'^2 + \sigma_3'^2 = 2K^2 \tag{2.11a}$$

$$J_2' = \frac{1}{6} \left[(\sigma_1 - \sigma_2)^2 + (\sigma_2 - \sigma_3)^2 + (\sigma_3 - \sigma_1)^2 \right] = K^2 \tag{2.11b}$$

$$(\sigma_x - \sigma_y)^2 + (\sigma_y - \sigma_z)^2 + (\sigma_z - \sigma_x)^2 + 6(\tau_{yz}^2 + \tau_{zx}^2 + \tau_{xy}^2) = 6K^2 \qquad (2.11c)$$

where K depends of the amount of pre-strain. Hencky suggested that the physical implication of the above criterion was that yield begins when the recoverable elastic energy of distortion reaches a critical value. A complementary interpretation, due to Nadai, is that yielding begins when the shear stress acting over the octahedral planes reaches a certain value. This may be shown to be mathematically equivalent to the above interpretations, since:

$$\tau_{ns} = \sigma_{ij}\, l_{in}\, l_{js} \qquad (2.12)$$

where τ_{ns} is the shear stress acting over the octahedral plane, lying at equal angles to the three principal axes and l_{in}, l_{js} are direction cosines. Expressing equation 2.12 in vector form,

$$\tau_{ns}^2 = (\sigma_1 - \sigma_2)^2 l^2 m^2 + (\sigma_2 - \sigma_3)^2 m^2 n^2 + (\sigma_3 - \sigma_1)^2 n^2 l^2 \qquad (2.13)$$

where l, m and n are direction cosines. Since l=m=n for an octahedral plane and $l^2 + m^2 + n^2 = 1$, then $l^2 = 1/3$. Hence,

$$\tau_{ns}^2 = 2/9\,[(\sigma_1 - \sigma_2)^2 + (\sigma_2 - \sigma_3)^2 + (\sigma_3 - \sigma_1)^2]$$

and substituting in equation 2.11b the following form is obtained:

$$6J_2' = [(\sigma_1 - \sigma_2)^2 + (\sigma_2 - \sigma_3)^2 + (\sigma_3 - \sigma_1)^2] = 9/2\ \tau_{ns}^2$$

Therefore $$\tau_{ns}^2 = 2/3\ J_2' \qquad (2.14a)$$

and thus $$K^2 = 3\,\tau_{ns}^2 / 2 \qquad (2.14b)$$

In this analysis the transverse stresses are assumed to be zero ($\sigma_z = 0$). The yield criterion therefore becomes:

$$\sigma_x^2 + \sigma_y^2 - \sigma_x\sigma_y + 3\,\tau_{xy}^2 \leq 3\,K^2 \leq \sigma_y^2 \qquad (2.15)$$

The representation of this equation in two dimensions is shown in Fig. 2.2a and it is seen that it is an ellipse. Permissible stress and strain paths are indicated in Fig. 2.2b.

2.5 The Flow Rule

The flow theory of plasticity is based on the fact that unique relations do not exist in general between stress and strain components in the plastic region; the strain depends not only on the final state of stress, but also on the loading history. Stress-strain relations which are valid in the theory of elasticity have to be replaced by relations between increments of stress and strain [101].

Within the framework of behaviour of the ideal plastic body and having accepted the validity of the yield criterion it is possible to obtain a flow rule describing the plastic behaviour of the material [101]. For a non-workhardening material,

$$\Delta\,\sigma_{ij,z}\;\Delta\,\varepsilon_{ij,z}^{(p)} = 0 \qquad (2.16)$$

when plastic deformations occur. In the above equation,

- $\Delta\,\sigma_{ij,z}$ are the increments in elasto-plastic stress at any distance z from the neutral axis
- $\Delta\,\varepsilon_{ij,z}^{(p)}$ are the increments in plastic strain at any distance z.

The von Mises yield function f is a function of the total stresses $\sigma_{ij,z}$ and not of the strains $\varepsilon_{ij,z}$ such that $f(\sigma_{ij,z}) \leq 0$ prevails. Any change in stress during plastic flow must therefore satisfy the relation:

$$df = \left[\frac{\partial f}{\partial \sigma_{ij}}\right]^{T}_{,z} \Delta \sigma_{ij,z} = 0 \qquad (2.17)$$

where T denotes transpose. From equations 2.16 and 2.17 it is evident that

$$\Delta \varepsilon^{(p)}_{ij,z} = \lambda \left[\frac{\partial f}{\partial \sigma_{ij}}\right]_{,z} \qquad (2.18)$$

where λ is a constant of proportionality termed the plastic strain rate multiplier. The above expression gives the rule of plastic flow, generally known as the Prandtl-Reuss flow rule.

If $\lambda > 0$ loading on the yield surface is occurring
$\lambda = 0$ pure plastic flow is occurring
$\lambda < 0$ unloading from the yield surface takes place.

2.6 Elasto-Plastic Tangential Multilayer Rigidities

Hooke's law may be applied to the difference between the total and plastic strain increments in order to obtain a stress-strain relation valid in the elastic range:

$$\Delta \sigma_{ij,z} = E_{ij} \left(\Delta \varepsilon_{ij,z} - \Delta \varepsilon^{(p)}_{ij,z} \right) \qquad (2.19)$$

where E_{ij} is the matrix of elastic rigidities which for an isotropic elastic material is given by:

$$E_{ij} = \frac{E}{1-\nu^2}\begin{bmatrix} 1 & \nu & 0 \\ \nu & 1 & 0 \\ 0 & 0 & \frac{1-\nu}{2} \end{bmatrix} \qquad (2.20)$$

By substituting from equation 2.18,

$$\Delta \sigma_{ij,z} = E_{ij} \left(\Delta \varepsilon_{ij,z} - \lambda \left[\frac{\partial f}{\partial \sigma_{ij}} \right]_{,z} \right) \qquad (2.21)$$

The plastic strain rate multiplier λ is obtained by substituting equation 2.21 in equation 2.17 to give:

$$\left[\frac{\partial f}{\partial \sigma_{ij}} \right]^{T}_{,z} E_{ij} \left(\Delta \varepsilon_{ij,z} - \lambda \left[\frac{\partial f}{\partial \sigma_{ij}} \right]_{,z} \right) = 0$$

giving

$$\lambda = \frac{1}{r} \left[\frac{\partial f}{\partial \sigma_{ij}} \right]^{T}_{,z} E_{ij} \quad \Delta \varepsilon_{ij,z} \qquad (2.22)$$

where

$$r = \left[\frac{\partial f}{\partial \sigma_{ij}} \right]^{T}_{,z} E_{ij} \left[\frac{\partial f}{\partial \sigma_{ij}} \right]_{,z}$$

Substituting back in equation 2.21

$$\Delta \sigma_{ij,z} = E^{*}_{ij} \quad \Delta \varepsilon_{ij,z} \qquad (2.23)$$

so $$E^{*}_{ij,z} = E_{ij}\left(I - \frac{1}{r}\ \sigma\ E_{ij}\right)_{,z} \qquad (2.24)$$

at any layer z. In the above equation, $\sigma = \left[\frac{\partial f}{\partial \sigma_{ij}}\right]_{,z}\left[\frac{\partial f}{\partial \sigma_{ij}}\right]^{T}_{,z}$

Explicit expressions for the elements of the tangential modular matrix of multilayer rigidities will now be obtained. Using equation 2.15, the elements of the vector

$\left[\frac{\partial f}{\partial \sigma_{ij}}\right]^{T}_{,z}$ are:

$$\left[\frac{\partial f}{\partial \sigma_{ij}}\right]^{T}_{,z} = \begin{bmatrix} \frac{\partial f}{\partial \sigma_x} \\ \frac{\partial f}{\partial \sigma_y} \\ \frac{\partial f}{\partial \tau_{xy}} \end{bmatrix}^{T}_{,z} = \frac{1}{\sigma_0^2}\begin{bmatrix} 2\sigma_x - \sigma_y & 2\sigma_y - \sigma_x & 6\tau_{xy} \end{bmatrix} \qquad (2.25)$$

Combining with equation 2.20 expressions for **r** and σ are obtained:

$$r = \frac{E}{1-\nu^2}\left[\frac{\partial f}{\partial \sigma_x}\left(\frac{\partial f}{\partial \sigma_x} + \nu\frac{\partial f}{\partial \sigma_y}\right) + \frac{\partial f}{\partial \sigma_y}\left(\nu\frac{\partial f}{\partial \sigma_x} + \frac{\partial f}{\partial \sigma_y}\right) + \frac{1-\nu}{2}\left(\frac{\partial f}{\partial \tau_{xy}}\right)^2\right] \qquad (2.26)$$

$$\sigma = \begin{bmatrix} (\frac{\partial f}{\partial \sigma_x})^2 & \frac{\partial f}{\partial \sigma_x}\frac{\partial f}{\partial \sigma_y} & \frac{\partial f}{\partial \sigma_x}\frac{\partial f}{\partial \tau_{xy}} \\ \frac{\partial f}{\partial \sigma_x}\frac{\partial f}{\partial \sigma_y} & (\frac{\partial f}{\partial \sigma_y})^2 & \frac{\partial f}{\partial \sigma_y}\frac{\partial f}{\partial \tau_{xy}} \\ \frac{\partial f}{\partial \sigma_x}\frac{\partial f}{\partial \tau_{xy}} & \frac{\partial f}{\partial \sigma_y}\frac{\partial f}{\partial \tau_{xy}} & (\frac{\partial f}{\partial \tau_{xy}})^2 \end{bmatrix}_{,z} \qquad (2.27)$$

σ is seen to be symmetrical.

Substituting from equations 2.26 and 2.27 into 2.24 the elements of the tangential multilayer elasto-plastic modular matrix are obtained.

$$\mathbf{E}^*_{ij,z} = \begin{bmatrix} E_{11} & E_{12} & E_{13} \\ E_{21} & E_{22} & E_{23} \\ E_{31} & E_{32} & E_{33} \end{bmatrix}_{,z} = \mathbf{E}_{ij} \begin{bmatrix} 1-E_{11}' & -E_{12}' & -E_{13}' \\ -E_{21}' & 1-E_{22}' & -E_{23}' \\ -E_{31}' & -E_{32}' & 1-E_{33}' \end{bmatrix}_{,z} \qquad (2.28)$$

Where E_{11}', E_{12}', ... E_{33}' are the elements of the 'plastic reduction' matrix resulting from the evaluation of $(1/\mathbf{r})\sigma\cdot$ These become zero when unloading takes place.

Substituting equation 2.20 in the above, the matrix of multilayer elasto-plastic rigidities is obtained:

$$E^{*}_{ij,z} = \frac{E}{1-\nu^2}\begin{bmatrix} 1-E_{11}'-\nu E_{21}' & -E_{12}'+\nu(1-E_{22}') & -E_{13}'-\nu E_{23}' \\ -E_{21}'+\nu(1-E_{11}') & -E_{22}'-1-\nu E_{12}' & -E_{23}'-\nu E_{13}' \\ -(\frac{1-\nu}{2})E_{31}' & -(\frac{1-\nu}{2})E_{32}' & \frac{1-\nu}{2}(1-E_{33}') \end{bmatrix}_{,z} \qquad (2.29)$$

for an isotropic elastic rigid-plastic material obeying the von Mises yield criterion. The plastic strain rate multiplier is found using equations 2.24, 2.25 and 2.26.

$$\lambda = \left[\frac{\frac{\partial f}{\partial \sigma_x}(\Delta\varepsilon_x + \nu\Delta\varepsilon_y) + \frac{\partial f}{\partial \sigma_y}(\Delta\varepsilon_y + \nu\Delta\varepsilon_x) + \frac{1-\nu}{2}\frac{\partial f}{\partial \tau_{xy}}\Delta\gamma_{xy}}{\frac{\partial f}{\partial \sigma_x}(\frac{\partial f}{\partial \sigma_x} + \nu\frac{\partial f}{\partial \sigma_y}) + \frac{\partial f}{\partial \sigma_y}(\frac{\partial f}{\partial \sigma_y} + \nu\frac{\partial f}{\partial \sigma_x}) + \frac{1-\nu}{2}(\frac{\partial f}{\partial \tau_{xy}})^2} \right]_{,z} \qquad (2.30)$$

λ is seen to have units of $\left[\frac{\partial f}{\partial \sigma_{ij}}\right]^{-1}_{,z}$.

The multilayer elasto-plastic stress-strain relations (equation 2.21) are:

$$\begin{bmatrix} \Delta\sigma_x \\ \Delta\sigma_y \\ \Delta\tau_{xy} \end{bmatrix}_{,z} = \begin{bmatrix} E_{11} & E_{12} & E_{13} \\ E_{21} & E_{22} & E_{23} \\ E_{31} & E_{32} & E_{33} \end{bmatrix}_{,z} \begin{bmatrix} \Delta\varepsilon_x \\ \Delta\varepsilon_y \\ \Delta\gamma_{xy} \end{bmatrix}_{,z} \qquad (2.31)$$

at any layer z. The total stress acting at any point in the plate during a particular load increment is thus given by:

$$\sigma_{ij,z} = (\sigma_{ij,z})_p + \Delta\sigma_{ij,z}$$
$$= (\sigma_{ij,z})_p + E^*_{ij,z}\,\Delta\varepsilon_{ij,z} \qquad (2.32)$$

where p denotes the value obtained during the previous increment. Numerical integration is used to obtain stress resultants at any node. Typically,

$$N_{x,y} = \int_{-t/2}^{+t/2} \sigma_{x,y}\, dz \qquad (2.33a)$$

$$M_{x,y} = \int_{-t/2}^{+t/2} \sigma_{x,y}\, z\, dz \qquad (2.33b)$$

2.7 Boundary Conditions along Stiffened Plate Edges

As mention in section 2.1 the von Karman equations have been adopted to represent the behaviour of the base plate and the stiffener. Thus, boundary conditions corresponding to the solutions of equations 2.1a, 2.1b, 2.1c have to be specified.

Equation 2.1a can be shown to be of fourth order in w, the out-of-plane deflection, for which two boundary conditions are required along each edge. Equations 2.1b, 2.1c which yield solutions describing the in-plane behaviour require another two conditions. The actual choice of conditions adopted along each edge corresponds to the behaviour of that edge, which will thus be described in an exact manner, within the limitations of thin plate theory. In total, four conditions are required and in this section each edge of the stiffened plate will be considered in turn. The following sketch shows the four degrees of freedom for which boundary conditions are specified along each edge.

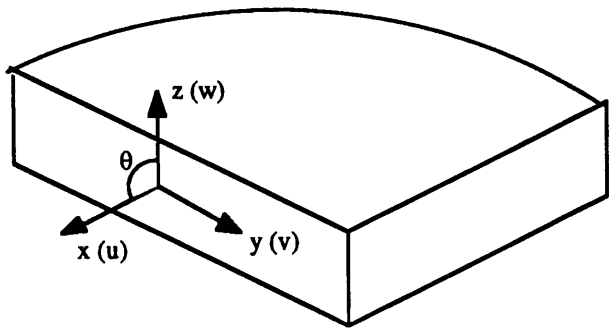

In practice, stiffened panels do not exist in isolation. They form part of a continuous system of shell plating, which in most cases is stiffened in orthogonal directions. Stiffening in the direction of the principal applied external loading normally predominates. In the case of a hull girder the bending moments due to static and dynamic loads usually dominate, so ship structures are usually stiffened longitudinally.

The stiffened panel which is treated here in isolation experiences in real conditions different restraints along each edge. For example, the longitudinal edge of a panel adjacent to a deck side will be subject to substantially different transverse in-plane conditions compared with the other three edges. In the present analysis, the same conditions are assumed to hold along opposite edges of a panel which is considered to form part of uniformly compressed grillage. Such a grillage is composed of deep transverses and longitudinal stiffeners of various cross-sections. The longitudinal stiffeners are attached to the plating and to deep transverses at the intersections indicated in Fig. 2.3; both the plating and the stiffeners are generally continuous through the transverse girders.

It is reasonable to assume that out-of-plane deflections of the plating along the lines of attachment to the deep transverse are zero ($w = 0$), since the relative deflections of the transverses will be significantly smaller than those of the plating. The magnitude however of the rotational restraint along these edges is unknown and therefore a lower bound condition is chosen. The edges are thus treated as being simply-supported, i.e. $M_x = 0$.

External loading is applied in such a way that the edges are uniformly compressed. This condition holds true for panels which are located near the centreline of the grillage. The alternative to applying a uniform edge displacement would be to apply an appropriate stress distribution along the boundary. In the linear elastic range, good estimates of the magnitude and distribution of this could be obtained. Following buckling, however, and when interaction effects come into play, it would become more difficult to achieve.

The boundary conditions just described are also valid for the loaded edges of the stiffener. The last condition along the loaded edges which requires consideration is that of transverse in-plane behaviour. This is governed by the shear restraint provided by the deep transverses to both elements of the stiffened plate. From considerations of continuity, symmetry can be applied and thus, for the plate,

$$\frac{\partial N_{xy}}{\partial x} = 0 \tag{2.34a}$$

Similarly, for the stiffener,

$$\frac{\partial N_{xyw}}{\partial x} = 0 \tag{2.34b}$$

The transverse movement of the stiffener at its junction with the transverse girder and the shell plating must also be consistent with the out-of-plane deflection of the plating at that position, which is here assumed to be zero (w = 0). Therefore at that point,

$$v_w = 0 \tag{2.35}$$

The unloaded, longitudinal edges of the plating are considered as lying halfway between adjacent stiffeners. Assuming that the shell plating exhibits identical behaviour for each panel, symmetry can be used to determine out-of-plane deflections, rotations and shear restraints along these edges. Therefore,

$$\frac{\partial w}{\partial y} = 0 \qquad \frac{\partial M_y}{\partial y} = 0 \qquad N_{xy} = 0 \tag{2.36}$$

The in-plane behaviour perpendicular to the edge is treated as being 'constrained'. For this type of boundary, the edge is allowed to move transversely in a straight line in such a way that the total transverse force acting along the edge is zero,

$$v = \text{constant such that } \int_0^1 N_y \, dx = 0 \qquad (2.37)$$

Apart from the plate-stiffener intersection which is to be described in the next section, the remaining boundary which requires to be considered is the unattached edge of the stiffener. For a flatbar this consists of one free edge while for a tee-bar it consists of two free edges. In both cases the following conditions hold :

$$M_y = 0 \qquad N_{xy} = 0 \qquad N_y = 0 \qquad (2.38a)$$

$$Q_y = \frac{\partial M_y}{\partial y} + \frac{\partial M_{xy}}{\partial x} \qquad M_{xy} = 0 \qquad (2.38b)$$

Q_y being the shear force acting along the boundary edge.

This provides five conditions whereas only four are admissible in thin plate theory. Reduction to four is achieved by combining the two conditions represented by 2.38b. This is accomplished by replacing the in-plane forces represented by M_{xy} by an equivalent system of forces which act as shown in the diagram overleaf.

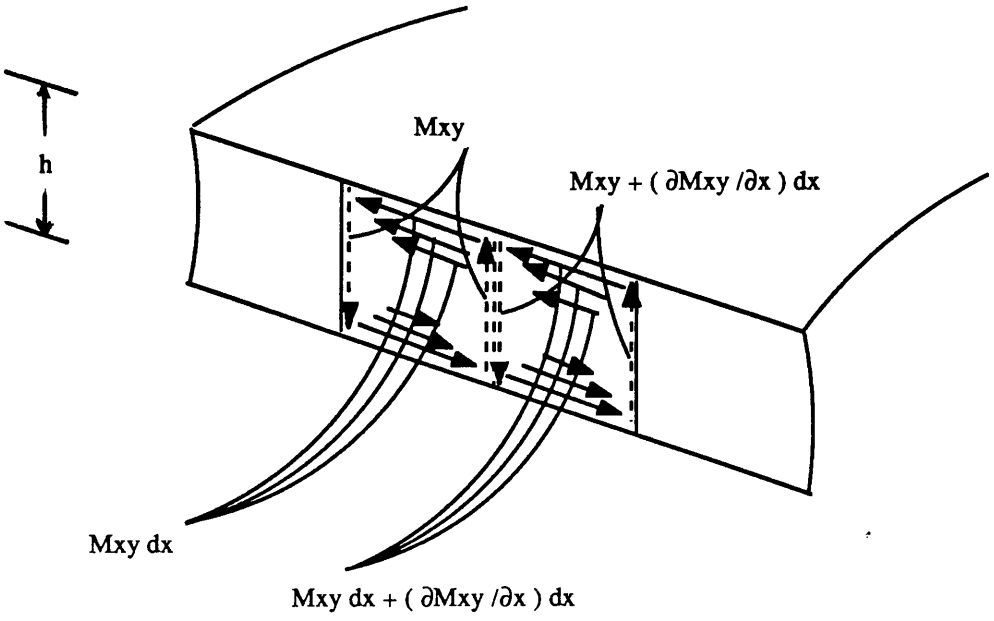

This is based on the assumption that the behaviour of the stiffener will not be changed if the forces which give rise to the twisting couple $M_{xy}dx$ which acts on an element dx, are replaced by two forces perpendicular to the edge, of magnitude M_{xy} and distance dx apart[100]. This substitute force is equivalent to a shear force given by:

$$Q_y' = \frac{\partial M_{xy}}{\partial x} \tag{2.39}$$

so that the joint requirement regarding twisting moments and shearing forces Q_y becomes:

$$Q_y + Q_y' = V_y = 0 \tag{2.40a}$$

$$\therefore \quad V_y = \frac{\partial M_y}{\partial y} + 2\frac{\partial M_{xy}}{\partial x} = 0 \tag{2.40b}$$

As in section 2.1, reversed signs have been used for the twisting moments. The term V_y is known as the Kirchhoff force which acts perpendicularly to the edge; it is zero

when the edge is free.

2.8 Boundary Conditions along the Plate-Stiffener Intersection

It was seen previously that out-of-plane displacements along the panel edges were set equal to zero ($w = 0$). This was based on the assumption that the effects of interaction of the panel edges with adjacent structural elements can be ignored; it was necessary to make this assumption so as to be able to model one section of an orthogonally stiffened grillage. When modelling the intersection of the base plate with the stiffener, in order that the intersection may be represented correctly, the effects of edge deformations and forces have to be allowed for. The boundary conditions along a plate edge can be expressed in terms of either displacements or forces. Therefore, along the intersection, eight conditions in total have to be specified.

Structural continuity dictates that the out-of-plane deflections of the base plate and stiffener are set equal to the corresponding in-plane deflections of the other element. Thus, for the co-ordinate system used in Fig. 2.4a.

$$w_p = - v_w \tag{2.41a}$$

$$w_w = + v_p \tag{2.41b}$$

Compatibility of deflections in the longitudinal direction gives:

$$u_p = u_w \tag{2.42}$$

In this treatment it is assumed that the plate and stiffener remain at right angles during deformations. This is valid insofar as the weld along the junction does not permit any rotation, which seem reasonable considering the relative stiffness of double fillet welds. For intermittent welds this will not necessarily be true. Along the intersection therefore,

$$\frac{\partial w_w}{\partial y} = \frac{\partial w_p}{\partial y} \tag{2.43}$$

The out-of-plane displacements of the plate and stiffener along the intersection give rise to interaction forces acting in the plane of the other component. In the previous section it was seen that for a free edge,

$$V_y = \frac{\partial M_y}{\partial y} + 2\frac{\partial M_{xy}}{\partial x} = 0 \qquad (2.44)$$

where V_y is the Kirchhoff shear force acting in a direction perpendicular to the plate edge. When the components of the stiffened plate interact, $V_y \neq 0$ and now represents the interaction force along the junction. Since the edges remain at right angles along the intersection, the interaction force is identically equal to the in-plane force acting along the corresponding edge. Therefore,

$$N_{yp} = \frac{\partial M_{yw}}{\partial y} + 2\frac{\partial M_{xyw}}{\partial x} \qquad (2.45a)$$

$$N_{yw} = \frac{\partial M_{yp}}{\partial y} + 2\frac{\partial M_{xyw}}{\partial x} \qquad (2.45b)$$

where N_{yw}, N_{yp} are forces acting in the planes of the web and stiffener respectively, as shown in the following diagrams.

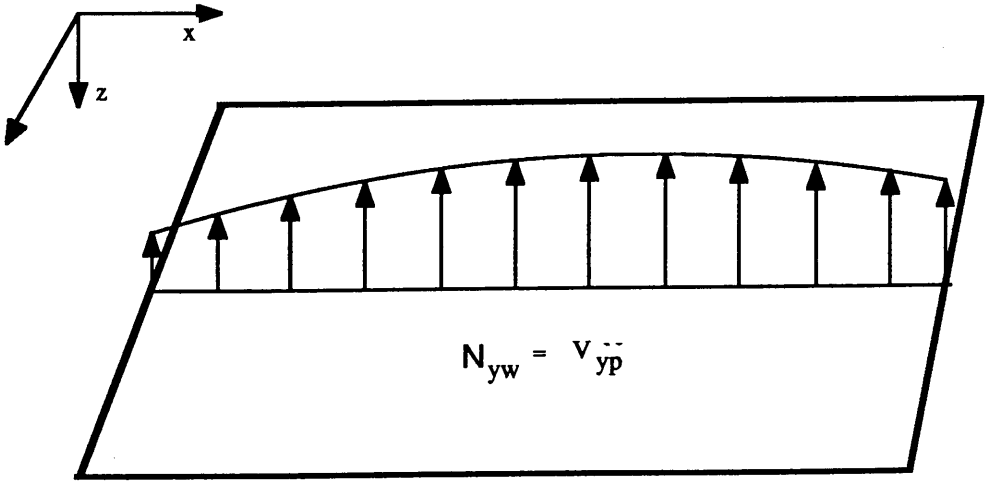

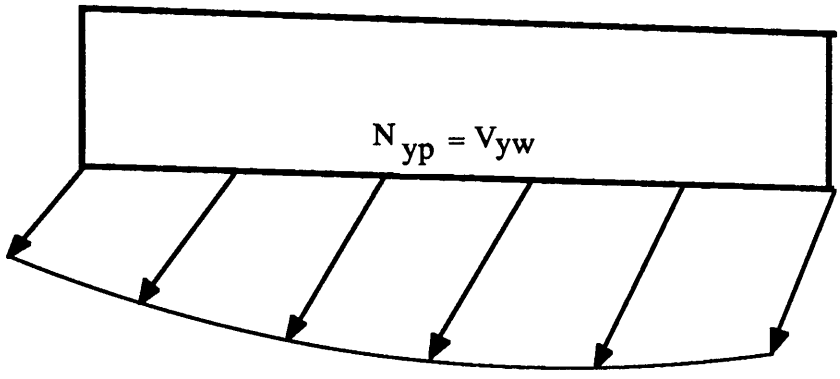

Shear flow requirements imply equilibrium of shear forces across the plate-stiffener intersection as shown below:

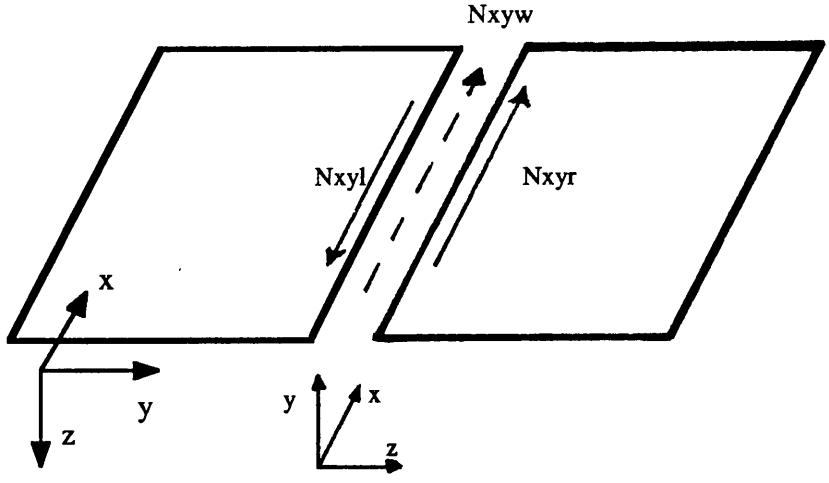

For the coordinate system chosen, the following relationship holds:

$$N_{xyw} = N_{xyr} - N_{xyl} \tag{2.46}$$

Finally, in order to introduce flexural continuity, equilibrium of the transverse bending

moments has to be satisfied. A discontinuity in the base plate moments M_y arises, as shown below:

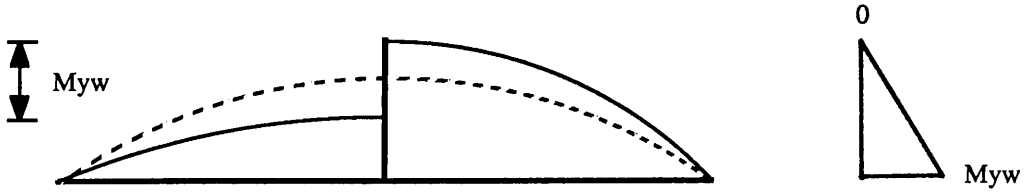

The presence of the stiffener gives rise to a line of moments M_{yw} which act along the intersection with the base plate. These are introduced using the following relations :

$$M_{yl} = M_y - \frac{M_{yw}}{2} \qquad (2.47a)$$

$$M_{yr} = M_y + \frac{M_{yw}}{2} \qquad (2.47b)$$

In this way, the discontinuity can be modelled in an exact manner. More details concerning this and the preceding equations shall be given in the next Chapter in which the application of finite differences and interlacing meshes shall be described.

Finite differences have already been used in conjunction with dynamic relaxation to model the nonlinear interaction of plate elements. Stiffened plates and box-columns have been studied and the present work is an extension of these applications.

Using plate and beam theory, Basu, Djahani and Dowling [102] developed a large deflection elastic analysis for thin plates bearing flatbar stiffeners. The interaction was modelled by deriving line forces representing stiffener action and including them in the equation of equilibrium of the plate. Finite differences and a modified Newton-Raphson method were used to solve the matrix equation. Aitken's δ^2-extrapolation method was also incorporated to accelerate convergence. The line force terms used to represent stiffener action consisted of components acting in the longitudinal and tranverse

directions and a couple simulating the torsional moment. These components were obtained from beam theory and thus local buckling effects were not allowed for.

Djahani [44] later extended this analysis to the elasto-plastic range in a study of stiffened plating. The same interaction formulation was used by Webb and Dowling [45] who used dynamic relaxation to solve the equations of equilibrium for the stiffened plate. The analysis was valid in the elasto-plastic range and tee-bar and angle-bar sections were also considered.

Lamas [103] analysed shear lag effects arising from point loads on box girders. He also considered the effects of discrete longitudinal stiffeners in the compression flange. In describing plate-stiffener interaction, the approach proposed by Basu, Djahani and Dowling [102] was used, with some simplifications. Lamas drew attention to the fact that due to the way in which the plate-stiffener boundary was modelled, the line forces were treated as though they were distributed over a finite width equal to the mesh spacing. The discontinuities actually present at the intersection were consequently not modelled in an exact manner.

Work on box-columns has progressed along different lines, however, and it is with an approach adopted in this field that the procedure used here most closely relates. Frieze and Dowling [57] and Frieze [58] analysed the behaviour of short rectangular box-columns in the elastic and elasto-plastic range respectively. The Marguerre equations were used to represent the action of the web and flange elements of the column and interaction equations analogous to 2.41-2.47 were used.

2.9 Local - Overall Buckling Mode Interaction

The importance of interaction between local and overall buckling modes in stiffened plates has already been highlighted in Chapter 1 in which current and past work in this field was discussed (Section 1.3). It was mentioned that mode interaction can lead to lower buckling loads than if only one failure mode prevailed; consequently it is necessary to examine to what extent this affects the behaviour of stiffened plates and also to evaluate over what range of geometries it is important. For long panels, column effects become significant and have to be included in the analysis.

The equilibrium equations which describe local behaviour in thin plates cannot be used to allow for column action and it becomes necessary to introduce an additional beam-column equation to accomplish this. To model the interaction of modes in an 'exact' manner, the equations describing local and overall behaviour have to be solved simultaneously.

The equations which describe beam-column behaviour of a cross-section can be derived by considering equilibrium perpendicularly to the axis of the cross-section and rotationally about one end of it, as shown below:

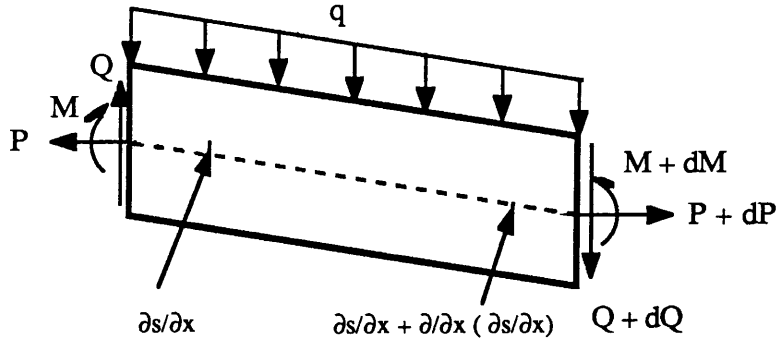

The resulting equations are:

$$\frac{d^2M}{dx^2} + P\left(\frac{d^2s}{dx^2} + \frac{d^2s_0}{dx^2}\right) + q = 0 \qquad (2.48a)$$

$$\frac{dP}{dx} = 0 \qquad (2.48b)$$

where M = moment about the neutral axis of the cross-section

P = axial force

s = deflection perpendicular to axis of beam-column

s_0 = initial lateral deflection of beam-column

The constitutive relations from which the values of P and M can be found are:

$$P = \int N_x \, dy \tag{2.49a}$$

$$M = \int N_x \, y \, dy \tag{2.49b}$$

where N_x are stress resultants acting in the longitudinal direction; these are found from the constitutive equations for local behaviour. For column action, the appropriate incremental kinematic relationships are:

$$\Delta\varepsilon_x^s = \left(\frac{\partial u}{\partial x} - \frac{\partial u}{\partial x}p\right) + \frac{1}{2}\left(\frac{\partial s}{\partial x} - \frac{\partial s}{\partial x}p\right)\left(\frac{\partial s}{\partial x} + \frac{\partial s_o}{\partial x} + 2\frac{\partial s}{\partial x}\frac{\partial s_o}{\partial x}\right) \tag{2.50a}$$

$$\Delta\phi_x^s = -\left(\frac{\partial^2 s}{\partial x^2} - \frac{\partial^2 s}{\partial x^2}p\right) \tag{2.50b}$$

where $\Delta\varepsilon_x^s$ = incremental strain along axis of column

$\Delta\phi_x^s$ = incremental curvature of column arising from lateral deflections s.

The above relations apply to a general cross-section. In the case of a flatbar stiffened plate, the axial force and moment are found from:

$$P = \int_0^d N_{xw} \, dy + \int_0^{b_p} N_{xp} \, dy \tag{2.51a}$$

$$M = \int_0^d N_{xw} \, y \, dy + P_{pl} \, z_{pl} \tag{2.51b}$$

where N_{xp}, N_{xw} are the plate and stiffener local stress resultants and P_{pl} is the total

axial force on the base plate. Having established the relations which describe beam-column action it is necessary to consider how the interaction with local behaviour is to be achieved.

To model the interaction between the two types of behaviour it is necessary to use a global formulation in which the terms describing the individual modes are included. This formulation is obtained by combining the kinematic relationships for the strains in the longitudinal direction, in which coupling occurs. The total, global axial strain along the neutral axis is therefore given by:

$$\varepsilon_x^G = \frac{\partial u}{\partial x} + \frac{1}{2}\left(\frac{\partial w}{\partial x}\right)^2 + \frac{\partial w}{\partial x}\frac{\partial w_o}{\partial x} + \frac{1}{2}\left(\frac{\partial s}{\partial x}\right)^2 + \frac{\partial s}{\partial x}\frac{\partial s_o}{\partial x} \qquad (2.52)$$

where the first term is the strain arising from pure compression, the following two terms arise from local out-of-plane behaviour and the last two arise from column action. The global strain increases by $-z(\partial^2 s/\partial x^2)$ at a distance z from the neutral axis of the cross-section. It is not necessary to consider strains in the other directions because beam-column action does not affect these. Additionally, equilibrium in the longitudinal direction is achieved using the equation describing local behaviour (2.1b) and thus equation 2.48b is not included in the analysis.

The stress resultants used in the local formulation now become global stress resultants [104]. The total axial force P and the moment M are found by integrating along the breadth of the cross-section, at each node. This integration is performed numerically using an approximate method (e.g. Simpson's First Rule).

CHAPTER THREE

SOLUTION OF GOVERNING EQUATIONS

USING DYNAMIC RELAXATION

As mentioned in Chapter 1, from the mathematical point of view, the task that has been posed involves the solution of two or more simultaneous sets of partial differential equations, each of which describes the behaviour of a panel component (plate, web, flange). Each set consists of two second order linear equations and one fourth order linear equation in three variables (u,v,w). This becomes apparent when compatibility relations valid in the elastic range are substituted in equations 2.1 . Coupling of the sets of pde's occurs along common boundaries where the solutions obtained have to be compatible. A set of 'dependent' boundary conditions therefore exists along the intersection of the panel components, for each of which compatibility of displacement and forces is required.

Systems of pde's have been solved using any one of a large number of numerical techniques developed during the past fifty years. Satisfactory results, however, depend partly on the choice of method employed. Experience has shown that good results are obtained by 'natural' methods, i.e. those in which a direct mathematical analogy to the physical situation exists [105]. It will become apparent in this Chapter that Dynamic Relaxation is in this sense very much a 'natural' method; the method was originally conceived to represent the undamped harmonic motion of tidal waves. Its application to structural mechanics static problems was made possible by adding a damping term which ensures that a steady state solution is obtained. This solution is the same as that of the statical problem that has been set although a formal proof of this has not yet been given.

3.1 Finite Difference Methods and Dynamic Relaxation

One of the earliest applications of finite differences was carried out by Richardson [106] who obtained approximate solutions to differential equations describing stresses in a dam. In 1921, Hencky [14] employed finite differences to solve the large deflection equations of flat plates into which a stress function had been introduced (Föppl). The importance of numerical methods was recognised, but only after the Second World War with the advent of high-speed computing could they realise their true potential.

The power of finite differences lies in their ability to provide solutions to differential equations for which analytical solutions cannot be obtained. This, however, is achieved at the expense of accuracy because the continuum is replaced by a grid at the nodes of which the equation is solved. The approximate solution approaches the exact solution when the number of grid points is increased. In classical finite difference methods, the solution of a set of simultaneous equations is thus required, each of which describes the behaviour at one grid point . It becomes evident that for a large number of points the amount of computation becomes excessive for hand-calculation and at this stage computing facilities become indispensable. The problem often becomes one of matrix inversion and to this end many algorithms have been developed to generate solutions.

In 1960, Otter and Day gave analytical and computer solutions to the equations describing tidal flow [107]. Physical considerations led to the implementation of a procedure which forms the basis of Dynamic Relaxation. Day later applied this to the analysis of concrete pressure vessels [108] and the small deflection behaviour of plates [109].

Although the DR algorithm is applied with a finite difference representation, it differs from classical finite difference methods in a fundamental way. It is not necessary to carry out a matrix assembly and subsequent inversion because DR uses an iterative procedure which follows a process of substitution. The available computer storage is thus utilised more efficiently and the solution can be obtained more quickly. When using DR, considerations involving matrix bandwidth do not arise, as in finite element methods. Nonetheless, DR has been combined with a finite element representation [110].

It was concluded, however, that the finite difference representation is more suitable because in this case the algorithm converges more rapidly.

During the past 20 years DR has been used to solve progressively more complex problems. Geometrical [111,112,113,114] and material [97,115,116] nonlinearities have been successfully incorporated and a variety of structural configurations have been analysed [115,116,117]. In nearly all these cases, static solutions have been obtained. At the same time, significant advances have been made in making DR more efficient from the point of view of 'numerical performance', i.e. stability and convergence [118,119,120,121,122,123].

3.2 Theoretical Basis of DR - Gradient Methods

In Dynamic Relaxation, the equations of equilibrium of flat plates are treated as damped equations of motion, i.e.

$$\rho \ddot{X} + C\dot{X} = P \tag{3.1}$$

where ρ, C, P are mass densities, damping and forcing functions respectively. When solving the thin plate equations, P is in each case set equal to the l.h.s. of equations 2.1. Therefore,

$$\rho_w \frac{\partial \dot{w}}{\partial t} + C_w \dot{w} = P_w \quad (= \text{out-of-balance force, equation 2.1a}) \tag{3.2a}$$

$$\rho_u \frac{\partial \dot{u}}{\partial t} + C_u \dot{u} = P_u \quad (= \text{out-of-balance force, equation 2.1b}) \tag{3.2b}$$

$$\rho_v \frac{\partial \dot{v}}{\partial t} + C_v \dot{v} = P_v \quad (= \text{out-of-balance force, equation 2.1c}) \tag{3.2c}$$

where ρ_w, ρ_u, ρ_v are mass densities

C_w, C_u, C_v are viscous damping coefficients

$\dot{w}$, $\dot{u}$, $\dot{v}$ are velocities in the three orthogonal directions

t is time.

Taking central finite differences in time, equation 3.2a becomes:

$$\rho_w \frac{\dot{w}_{t+\Delta t/2} - \dot{w}_{t-\Delta t/2}}{\Delta t} + C_w \frac{\dot{w}_{t+\Delta t/2} + \dot{w}_{t-\Delta t/2}}{2} = P_w(t) \qquad (3.3)$$

Introducing a non-dimensionalised viscous damping coefficient

$$k_w = \frac{C_w \Delta t}{\rho_w} \qquad (3.4)$$

After rearranging, equation 3.3 becomes:

$$\dot{w}_{t+\Delta t/2} = \frac{1-k_w/2}{1+k_w/2} \dot{w}_{t-\Delta t/2} + \frac{\Delta t}{\rho_w (1+k_w/2)} P_{w(t)} \qquad (3.5)$$

The velocity is then integrated to give the displacement at time t+Δt:

$$w_{t+\Delta t} = w_t + \Delta t \, \dot{w}_{t+\Delta t/2} \qquad (3.6)$$

In the next cycle of calculations, $w_{t+\Delta t}$ becomes w_t and corresponding forces and moments may be obtained. It is apparent from equation 3.6 that the DR algorithm is an explicit three-term recursion formula since three time levels are involved (t, t+Δt, t+Δt/2). Explicit operators are conditionally stable and thus suitable time step and density parameters have to be chosen.

It was mentioned earlier that solutions using classical finite difference methods involve

the inversion of the (stiffness) matrix relating deflections to forces and moments. The problem can be seen to be of the type:

$$\mathbf{A}\,\mathbf{x} + \mathbf{b} = \mathbf{0} \tag{3.7}$$

where **A** is symmetric with positive definite coefficients

b is the vector of constant terms

x is the vector of unknowns.

The linear system 3.7 may be interpreted as a minimising problem, because the quadratic form

$$Q = \frac{1}{2}(\mathbf{x}, \mathbf{Ax}) + (\mathbf{b}, \mathbf{x}) \tag{3.8}$$

has its only minimum at the point $-\mathbf{A}^{-1}\,\mathbf{b}$ [120]. This can be presented graphically if it is assumed that the generally multi-dimensional vector **x** is reduced to one dimension. Thus the following representation is obtained.

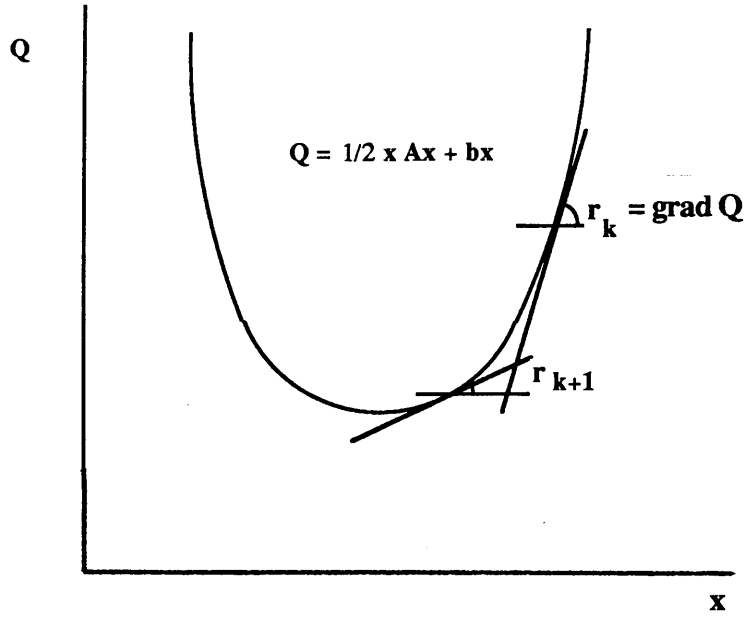

The minimum value of **Q** occurs when **dQ = 0**, i.e.

$$\mathbf{x} = \mathbf{A}^{-1}\mathbf{b} \tag{3.9}$$

Iteration methods generally start with an arbitrary initial vector $\mathbf{x_0}$ and generate from it a sequence of approximants $\mathbf{x_1}, \mathbf{x_2}, \mathbf{x_3}, \ldots$ which under certain conditions, converge to the solution $\mathbf{A^{-1}b}$. The way in which $\mathbf{x_{k+1}}$ is computed from its predecessors is characteristic of the method. The results of substituting an approximant $\mathbf{x_k}$ into the original equation is called the residual vector $\mathbf{r_k}$ of $\mathbf{x_k}$.

$$\mathbf{r_k} = \mathbf{A}\,\mathbf{x_k} + \mathbf{b} \tag{3.10}$$

Thus,
$$\mathbf{A^{-1}}\,\mathbf{r_k} = \mathbf{x_k} + \mathbf{A^{-1}}\,\mathbf{b} \tag{3.11}$$

It follows that $\lim_{k\to\infty} \mathbf{r_k} = 0$ is a necessary and sufficient condition for the convergence of an iteration method. From the preceding diagram it is seen that the magnitude of the residual vector is equal to the gradient of the tangent to **Q**, namely

$$\mathbf{r_k} = \mathbf{A}\,\mathbf{x_k} + \mathbf{b} = \text{grad } \mathbf{Q} \tag{3.12}$$

If an iteration method computes the next approximant $\mathbf{x_{k+1}}$ in such a way that $\Delta\mathbf{x_k}$ (= $\mathbf{x_{k+1}} - \mathbf{x_k}$) is a linear combination of the gradient vectors of **Q** taken at the preceding points, $\mathbf{x_0}, \mathbf{x_1}, \mathbf{x_2}, \ldots, \mathbf{x_k}$, then the method is called a gradient method.

Stiefel [120] has shown that for optimum convergence, the recursion formula:

$$\mathbf{x_{k+1}} = \mathbf{x_k} + \Delta\mathbf{x_k} \tag{3.13}$$

is of the form $\mathbf{x_{k+1}} = \mathbf{x_k} + \dfrac{1}{q_k}\,(\mathbf{r_k} + e_{k-1}\,\Delta\mathbf{x_{k-1}})$ $\qquad k = 1,2,\ldots$

$$e_{k-1} = 0 \qquad k = 0 \qquad (3.14)$$

where q_k, e_k are relaxation coefficients.

Various types of recursion formulae have been proposed, the earliest being that of Richardson. Frankel proposed the following method:

$$q_0 = \frac{a+b}{2} \qquad e_{-1} = 0 \qquad k = 0$$

$$q_k = \left(\frac{\sqrt{a} + \sqrt{b}}{2}\right)^2 \qquad e_{k-1} = \left(\frac{\sqrt{a} - \sqrt{b}}{2}\right)^2 \quad k > 0 \qquad (3.15)$$

where a, b are the minimum and maximum eigenvalues of the stiffness matrix. This method was termed the "second order Richardson process". Rearranging equations 3.13 and 3.14 as:

$$\Delta x_k = x_{k+1} - x_k = \frac{1}{q_k} (r_k + e_{k-1} \Delta x_{k-1}) \qquad (3.16)$$

and substituting from equation 3.15, the following form is obtained:

$$\Delta x_k = \left(\frac{2}{\sqrt{a} + \sqrt{b}}\right)^2 \left[r_k + \left(\frac{\sqrt{a} - \sqrt{b}}{2}\right)^2 \Delta x_{k-1} \right] =$$

$$= \left(\frac{\sqrt{a} - \sqrt{b}}{\sqrt{a} + \sqrt{b}}\right)^2 \Delta x_{k-1} + \frac{4}{\left(\sqrt{a} + \sqrt{b}\right)^2} r_k \qquad (3.17)$$

Since for the DR algorithm

$$\Delta w_{t+\Delta t/2} = w_{t+\Delta t} - w_t =$$

$$= \frac{1-k_w/2}{1+k_w/2} w_{t-\Delta t/2} + \frac{\Delta t^2}{\rho_w (1+k_w/2)} P_{w(t)} \qquad (3.18)$$

it becomes apparent that the DR algorithm is identical to Frankel's method. Comparing coefficients,

$$\frac{1-k_w/2}{1+k_w/2} = \left(\frac{\sqrt{a}-\sqrt{b}}{\sqrt{a}+\sqrt{b}}\right)^2 \qquad (3.19a)$$

$$\frac{\Delta t^2}{\rho_w (1+k_w/2)} = \frac{4}{(\sqrt{a}+\sqrt{b})^2} \qquad (3.19b)$$

the following condition for numerical stability is obtained:

$$\frac{\Delta t^2}{\rho_w} = \frac{4}{a+b} \qquad (3.20)$$

Consequently it becomes necessary to find a, b which are the minimum and maximum eigenvalues of the stiffness matrix. The maximum eigenvalue, b, is found using Gershgorin's theorem which states that

$$|b| \le b_G = \max_i \sum_{j=1}^{N} |S_{ij}| \qquad (3.21)$$

where b_G is the Gershgorin bound and S_{ij} are the coefficients of individual rows. In order to obtain S_{ij} numerical differentation is used, an example of which is given in Appendix B. Although it is not easy to find the minimum eigenvalue a, in most cases

$$a \ll b \tag{3.22}$$

and thus

$$\frac{\Delta t^2}{\rho} = \frac{4}{b_G} \tag{3.23}$$

ensures stability of the procedure. Cassell quotes values of a and b for a square plate for which $a/b < 0.0006$ for 70 degrees of freedom [116]. One case in which the present author found that the above condition did not give a stable iteration was in the elastic solution of an axially compressed column. For this case, stability was obtained by multiplying b_G by 1.25.

In order to minimise computational costs, various researchers studied the problem of convergence when analysing statics problems [119,120,122,123]. If the real density of the material, ρ, is used in equation 3.2, the structure vibrates in its fundamental mode, which corresponds to the natural period. In order to obtain a fully damped solution , it is necessary to perform at least 3T/2 iterations, where T is the natural period [112].

Since in static analyses the true transient response is of no interest, suitable values of Δt and ρ can be chosen in order to accelerate the rate of convergence. In recent work, most researchers have arbitrarily given Δt the value of 1 and have used equation 3.23 to determine ρ. Thus,

$$\rho = \frac{1}{4} b_G \tag{3.24}$$

Having established conditions for numerical stability , the sequence of calculations within each iterative cycle has to be considered. The output from the DR algorithm consists of deflections at the nodes of the plate and stiffener grids; these are used as input for the subsequent cycle. Calculations typically proceed as outlined below:

a. Kinematic relationships are used to obtain incremental strains.

b. Total stresses are found using equation 2.31.

c. Nodal stress resultants (force/unit width, moment/unit width) are found by integrating numerically the total stresses.

d. Boundary conditions for stress resultants are applied.

e. Fictitious densities (ρ_u, ρ_v, etc.) are found.

f. Equations of equilibrium are applied and out-of-balance forces (P_u, P_v, etc.) are found.

g. Nodal velocities are determined using equation 3.5.

h. The velocities are integrated using equation 3.6 to give displacements.

i. Displacement boundary conditions are set.

Calculations are performed at each stage for both plate and stiffener nodes so that the equations of equilibrium for each panel component are relaxed simultaneously. Thus, when convergence is achieved, the boundary conditions along the common edges are satisfied. Convergence is checked by monitoring

- deflections at critical locations
- velocities
- the total kinetic energy content of the structure, given by:

$$K.E. = \frac{1}{2} \text{ x (mass) x } \sum_{i,j=1}^{imax,jmax} (\dot{u}^2 + \dot{v}^2 + \dot{w}^2)$$

During the first few cycles of an increment the velocities generally increase. They then gradually decrease and the deflections reach steady values about which small oscillations take place; that is, the velocities still fluctuate but with much smaller values. At this point, the kinetic energy reaches a minimum.

3.3 Choice of Finite Difference Grid - Interlacing Meshes

When an equation involving two or more dependent variables is discretised using a finite difference grid, in certain cases it becomes advantageous to use interlacing meshes. Each variable is evaluated at the nodes of one or other of the meshes. It is possible to use two or more interlacing grids.

Gilles [124] has shown that the use of interlacing meshes enables one to deal with differential equations of lower order than if one variable is first eliminated between the governing equations. This is the case when a stress function is introduced into the von Karman equations. A second advantage is that the 'coupling' effects between dependent variables (u, v, w) can be more accurately represented. This becomes evident when comparing the finite differences expressions for various terms in the equations.

Consider, for example, equation 2.16 which describes longitudinal equilibrium in the plate. If expressions for large deflection elastic strains (ignoring initial imperfections) are substituted, the equation takes the form

$$C_x\left[\frac{\partial^2 u}{\partial x^2}+\frac{\partial w}{\partial x}\frac{\partial^2 w}{\partial x^2}\right]+C_{xy}\left[\frac{\partial^2 u}{\partial y^2}+\frac{\partial^2 v}{\partial x\partial y}+\frac{\partial^2 w}{\partial x\partial y}\left(\frac{\partial w}{\partial x}+\frac{\partial w}{\partial y}\right)\right]=0 \quad (3.25)$$

The corresponding finite difference expressions for $\frac{\partial u}{\partial x}$, $\frac{\partial^2 u}{\partial x^2}$, $\frac{\partial^2 v}{\partial x\partial y}$ obtained when using a non-interlacing square grid as shown below are:

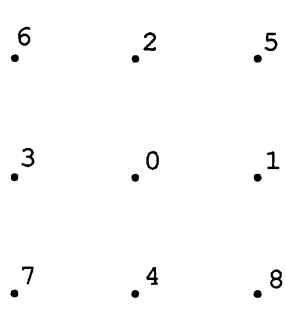

$$\frac{\partial u}{\partial x}\cong\frac{u_1-u_0}{a}$$

$$\frac{\partial^2 u}{\partial x^2}\cong\frac{1}{a}\left(\frac{u_1-u_0}{a}-\frac{u_0-u_3}{a}\right) \quad (3.26)$$

$$\frac{\partial^2 v}{\partial x\partial y}\cong\frac{1}{2a}\left(\frac{u_5-u_8}{2a}-\frac{u_6-u_7}{2a}\right)$$

where the orders of the errors involved are proportional to the squares of the denominators (size of mesh). It is thus evident that the use of the above approximation for the third term introduces larger errors in the equation than the other terms since the effective length is doubled.

The use of a second interlacing mesh, at the nodes of which v is found, reduces the error since the effective mesh length becomes 'a' when evaluating the finite difference expression for $\partial^2 v/\partial x \partial y$.

Gilles also noted that a disadvantage associated with using more than one mesh is that the independent variables are not found at the same points. In the past this has not proven to be a serious drawback although when considering the finite difference representation of the junction of two plate elements (e.g. plate-stiffener junction), this has to be borne in mind when deciding how the intersection is to be represented (Section 3.7).

Following past practice [97,115] the von Karman equations were solved on interlacing grids as shown in the diagram

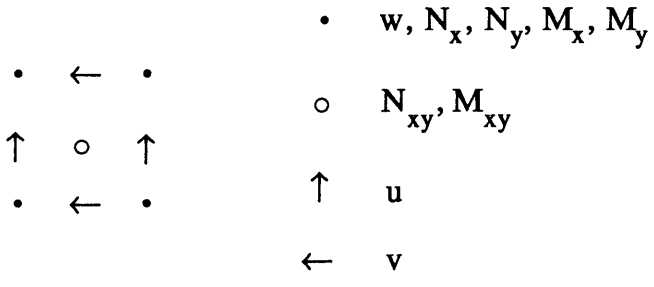

where the • nodes are used to define the edges of the plate.

The calculation of the yield function, however, involves stresses (σ_x, σ_y, τ_{xy}) at both • and o nodes ('w' nodes and 'shear' nodes). The arrangement described above generates values of σ_x, σ_y at • nodes and τ_{xy} at o nodes. The remaining values which are required can be obtained either by averaging existing stresses or by calculating first the required strains (ε_x, ε_y, γ_{xy}) and then using corresponding elasto-plastic relations. In order to reduce storage requirements, Frieze [115] chose the first alternative. In the present work, however, the second alternative was followed since computer facilities which are now available do not pose such restrictions.

3.4 Finite Difference Form of Equations

Before embarking on the derivation of finite difference expressions using the mesh scheme described previously, it is necessary to consider the calculations carried out within each relaxation cycle. These involve discretisation in space and time as specified by the DR algorithm. The discretisation in time uses a central difference scheme, while in this section expressions for the spatial discretisation will be given.

The kinematic relationships (equations 2.2 and 2.3) are linear combinations of strains due to in-plane and out-of-plane deflections. In order to derive finite difference expressions for these, the Taylor series can be used and simple central difference forms obtained. Direct strains $\Delta\varepsilon_x$, $\Delta\varepsilon_y$ are required at the w-nodes and shear strains $\Delta\gamma_{xy}$ are required at the shear nodes. The resulting expressions for the discretised component strains are given in Table 3.1 together with their associated orders of error. It is seen that the maximum error is of the order of $\Delta x\Delta y$, and that this is directly dependent on the type and size of mesh used. If non-interlacing meshes were used the error would have been of the order of $(\Delta x\Delta y)^2$.

Table 3.1 Finite Difference Expressions for Strains and Curvatures

Strain	Discretised Form	Approximation	Order of Error
$\partial u/\partial x$	$\Delta u/\Delta x$	$(u_{i,j}- u_{i-1,j})/\Delta x$	Δx
$\partial v/\partial y$	$\Delta v/\Delta y$	$(v_{i,j} - v_{i,j-1})/\Delta y$	Δy
$\partial w/\partial x$	$\Delta w/\Delta x$	$(w_{i+1,j} - w_{i-1,j})/2\Delta x$	Δx^2
$\partial w/\partial y$	$\Delta w/\Delta y$	$(w_{i,j+1} - w_{i,j-1})/2\Delta y$	Δy^2
$\partial^2 w/\partial x^2$	$\Delta^2 w/\Delta x^2$	$(w_{i+1,j} - 2w_{i,j} +w_{i-1,j})/\Delta x^2$	Δx^2
$\partial^2 w/\partial y^2$	$\Delta^2 w/\Delta y^2$	$(w_{i,j+1} - 2w_{i,j} +w_{i,j-1})/\Delta y^2$	Δy^2
$\partial u/\partial y$	$\Delta u/\Delta y$	$(u_{i,j+1}- u_{i,j})/\Delta y$	Δy
$\partial v/\partial x$	$\Delta v/\Delta x$	$(v_{i+1,j} - v_{i,j})/\Delta x$	Δx
$\partial w/\partial x$	$\Delta w/\Delta x$	$(w_{i+1,j} - w_{i,j} + w_{i+1,j+1} -w_{i,j+1})/2\Delta x$	Δx^2
$\partial w/\partial y$	$\Delta w/\Delta y$	$(w_{i+1,j+1} - w_{i+1,j} + w_{i,j+1} -w_{i,j})/2\Delta y$	Δy^2
$\partial^2 w/\partial x\partial y$	$\Delta^2 w/\Delta x\Delta y$	$(w_{i+1,j+1} - w_{i+1,j} -w_{i,j+1} + w_{i,j})/\Delta x^2\Delta y$	$\Delta x\Delta y$

In the above table expressions are given for $\partial w/\partial x$ and $\partial w/\partial y$ at both 'w' and shear nodes. The strains which result are substituted in equations 2.3 to obtain corresponding

incremental multilayer strains. Previous researchers,[97,104] have found that the improvement achieved by increasing the number of levels beyond five is outweighed by the accompanying increase in computational cost. For this reason the number of levels in the present work was limited to five.

The multilayer strains are then used to obtain total multilayer stresses which are subsequently integrated numerically using Simpson's First Rule. The stress resultants which are obtained are substituted in the equations of equilibrium which are cast in finite difference form.

3.5 Discretisation of Boundary Conditions

The application of non-interlacing and interlacing meshes in modelling plate boundaries using DR has been described in several papers. Rushton used non-interlacing meshes and considered several types of edges (simply supported, rotationally clamped, free) in the elastic range [110, 112,113,114]. Frieze has given a generalised formulation valid in the elasto-plastic range [115]. This description, however, was intended only for a single-layer representation, using the Ilyushin criterion. Harding utilised a multilayer approach but used integrated rigidities [97]. In his method the description of the edges was similar to that of Frieze. In this thesis, multilayer rigidities have been used and consequently it is necessary to reconsider the representation of the edges.

Of importance in buckling problems is the out-of-plane behaviour and in this section a generalised description suitable for rigorous multilayer solutions will be given. It will seen that this reduces to fairly simple forms in the usual cases of simply supported, rotationally clamped and free edges.

The slope of the edge x = 0 of a flat plate is in general governed by:

$$M_x = - k_r \frac{\partial w}{\partial x} \qquad (3.27)$$

where k_r is a rotational spring stiffness ($\infty \geq k_r \geq 0$). At any level of loading, the current value of the stress resultant is given by:

$$M_x = \int_{-t/2}^{+t/2} \sigma_{x,z}\, z\, dz \tag{3.28}$$

where $\sigma_{x,z}$ are the total stresses acting at a distance z from the mid-thickness layer of the plate. The stresses $\sigma_{x,z}$ are found from equation 2.31 and thus

$$M_x = \int_{-t/2}^{+t/2} (\sigma^p_{x,z} + \Delta\sigma_{x,z})\, z\, dz \tag{3.29}$$

where p denotes the value at the end of the previous increment. Elasto-plastic relations are used to obtain incremental stresses from incremental strains and at any distance z from the neutral axis:

$$\Delta\sigma_{x,z} = E_{11,z}\, \Delta\varepsilon_{x,z} + E_{12,z}\, \Delta\varepsilon_{y,z} + E_{13,z}\, \Delta\gamma_{xy,z} \tag{3.30}$$

Using equations 2.4 and 2.3a $\Delta\varepsilon_{x,z}$ is obtained in the following form:

$$\Delta\varepsilon_{x,z} = \Delta\varepsilon_{x,z=3} - z \left(\frac{\partial^2 w}{\partial x^2} - \frac{\partial^2 w}{\partial x^2}p \right) \tag{3.31}$$

Thus at layer z=1 (along the surface),

$$\Delta\sigma_{x_{z=1}} = E_{11_{z=1}} \left[\Delta\varepsilon_{x_{z=3}} - \frac{T}{2} \left(\frac{\partial^2 w}{\partial x^2} - \frac{\partial^2 w}{\partial x^2}p \right) \right] + E_{12_{z=1}}\, \Delta\varepsilon_{y_{z=1}} + E_{13_{z=1}}\, \Delta\gamma_{xy_{z=1}} \tag{3.32}$$

Similar expressions can be obtained for z = 2, 4, 5 and these are substituted in equation 3.29 to give:

$$M_x = \frac{T^2}{12}\left[\frac{1}{2}(\sigma_{x_{z=1}} - \sigma_{x_{z=5}}) + \sigma_{x_{z=2}} - \sigma_{x_{z=4}} \right] =$$

$$= M_x^p + \frac{T^2}{12}\left[\frac{1}{2}(\Delta\sigma_{x_{z=1}} - \Delta\sigma_{x_{z=5}}) + \Delta\sigma_{x_{z=2}} - \Delta\sigma_{x_{z=4}} \right] =$$

$$= M_x^p + \frac{T^2}{12}\left[\frac{1}{2}\{ E_{11_{z=1}} (\Delta\varepsilon_{x_{z=3}} + \frac{T}{2}(\frac{\partial^2 w}{\partial x^2} - \frac{\partial^2 w}{\partial x^2}p)) + E_{12_{z=1}} \Delta\varepsilon_{y_{z=1}} + \right.$$

$$E_{13_{z=1}} \Delta\gamma_{xy_{z=1}} - E_{11_{z=5}} (\Delta\varepsilon_{x_{z=3}} - \frac{T}{2}(\frac{\partial^2 w}{\partial x^2} - \frac{\partial^2 w}{\partial x^2}p)) - E_{12_{z=5}} \Delta\varepsilon_{y_{z=5}} - E_{13_{z=5}} \Delta\gamma_{xy_{z=5}} \} +$$

$$E_{11_{z=2}} (\Delta\varepsilon_{x_{z=3}} + \frac{T}{4}(\frac{\partial^2 w}{\partial x^2} - \frac{\partial^2 w}{\partial x^2}p)) + E_{12_{z=2}} \Delta\varepsilon_{y_{z=2}} + E_{13_{z=2}} \Delta\gamma_{xy_{z=2}} -$$

$$\left. E_{11_{z=4}} (\Delta\varepsilon_{x_{z=3}} - \frac{T}{4}(\frac{\partial^2 w}{\partial x^2} - \frac{\partial^2 w}{\partial x^2}p)) - E_{12_{z=4}} \Delta\varepsilon_{y_{z=4}} - E_{13_{z=4}} \Delta\gamma_{xy_{z=4}} \right]$$

(3.33)

where $$M_x^p = \frac{T^2}{12}\left[\frac{1}{2}(\sigma_{x_{z=1}}^p - \sigma_{x_{z=5}}^p) + \sigma_{x_{z=2}}^p - \sigma_{x_{z=4}}^p \right]$$

The coefficients of $\frac{\partial^2 w}{\partial x^2}, \frac{\partial^2 w}{\partial x^2}p$ are equal to the integrated elasto-plastic rigidity, D*, given by

$$D^* = \int_{-t/2}^{+t/2} E_{11,z}\, z^2\, dz \qquad (3.34)$$

After substituting equation 3.34 into equation 3.33, rearranging and letting the

remainder of the r.h.s. of equation 3.33 equal to α, equation 3.27 becomes:

$$- k_r \frac{\partial w}{\partial x} = \alpha - D^* \frac{\partial^2 w}{\partial x^2} \tag{3.35}$$

Using finite difference expressions for $\frac{\partial w}{\partial x}, \frac{\partial^2 w}{\partial x^2}$, equation 3.35 becomes :

$$- k_r \frac{w_{int} - w_{ext}}{2\Delta x} = \alpha - D^* \frac{w_{int} - 2w_b + w_{ext}}{\Delta x^2} \tag{3.36}$$

Collecting terms and dividing by ($k_r\Delta x/2 + D^*$) an explicit form is obtained for w_{ext}:

$$w_{ext} = \left[\frac{\frac{k_r \Delta x}{2} - D^*}{\frac{k_r \Delta x}{2} + D^*} \right] w_{int} + \left[\frac{2D^*}{\frac{k_r \Delta x}{2} + D^*} \right] w_b + \left[\frac{\Delta x^2 \alpha}{\frac{k_r \Delta x}{2} + D^*} \right] \tag{3.37}$$

This expression gives in generalised form the fictitious out-of-plane deflections along the edge x = 0 in the elasto-plastic range. It is based on the use of multilayer rigidities and strains and is an approximate result because second order terms involving shear strains and curvatures have not been included and the incremental strains which are used are obtained in the previous cycle. The effect of this is to reduce the rate of convergence although accounting for it more rigorously would considerably complicate the analysis. The cases which are of practical interest are the simply supported, clamped and free edges. In the elastic range, equation 3.37 reduces to:

$$w_{ext} = \left[\frac{\frac{k_r \Delta x}{2} - D^*}{\frac{k_r \Delta x}{2} + D^*} \right] w_{int} + \left[\frac{2D^*}{\frac{k_r \Delta x}{2} + D^*} \right] w_b \qquad (3.38)$$

For simply supported edges, $w_b = 0$, $k_r = 0$. Hence

$$w_{ext} = - w_{int} \qquad (3.39)$$

Along clamped edges, $w_b = 0$, $k_r = \infty$. Hence

$$w_{ext} = w_{int} \qquad (3.40)$$

In the elasto-plastic range, out-of-plane deflections along simply supported edges are given by:

$$w_{ext} = - w_{int} + \frac{\Delta x^2}{D^*} \alpha \qquad (3.41)$$

Along clamped edges deflections are given by equation 3.40. Out-of-plane deflections along free edges are found from:

$$w_{ext} = 2w_b - w_{int} + \frac{\Delta x^2}{D^*} \alpha \qquad (3.42)$$

Different values of spring stiffness k_r, may be used to represent conditions of intermediate rotational restraint.

Conditions of in-plane restraint act parallel and perpendicular to each plate edge. Displacements parallel to the plate edges shall be considered first. For the unloaded longitudinal edges of an axially compressed panel forming part of an orthogonal grillage, the displacements u are determined from the equation of equilibrium (equation 2.1b). The condition $\partial N_{xy} / \partial y = 0$ is satisfied by setting $N_{xyext} = N_{xyint}$. Similarly

the displacements along the transverse edges are found using equation 2.1c and $\partial N_{xy} / \partial x = 0$, giving $N_{xyext} = N_{xyint}$.

For panels which are loaded under lateral pressure with edges that are fully built-in, the displacements along the edges are zero, i.e. $v = 0$ ($u = 0$). For the elastic range this condition is sufficient to fully define the problem. In the plastic range, however, the tangential shear condition has to be determined along the edge in order to evaluate the yield function. This is accomplished by rearranging the equation of equilibrium along the edge. Thus, along the edge $y = 0$,

$$\frac{\partial N_{xy}}{\partial x} + \frac{\partial N_y}{\partial y} = 0 \tag{3.43}$$

$$N_{xy_{ext}} = N_{xy_{int}} + \Delta x \frac{\partial N_y}{\partial y} \tag{3.44}$$

The shear stress resultant can then be found by averaging internal and external values:

$$N_{xy_b} = \frac{1}{4} \sum_{i,j=1}^{2} N_{xy_{i,j}} \tag{3.45}$$

The displacements perpendicular to each plate edge depend either on the condition of loading or on the restraint across that edge. For a uniformly compressed edge, the displacement along the boundary is constant:

$$u_b = \frac{(u_{int} + u_{ext})}{2} \tag{3.46}$$

Therefore $$u_{ext} = 2u_b - u_{int} \tag{3.47}$$

For a fully built-in edge loaded under lateral pressure, this becomes:

$$u_{ext} = - u_{int} \tag{3.48}$$

On the other hand, the longitudinal unloaded edges can be either:

- restrained ($v = 0$)
- constrained (v = constant such that $\int N_y dx = 0$)
- unrestrained ($N_y = 0$)

The first of these conditions is achieved by setting

$$v_b = \frac{(v_{int} + v_{ext})}{2} = 0 \tag{3.49}$$

$$\therefore \; v_{ext} = - v_{int} \tag{3.50}$$

The constrained edge is described by equation 2.37. Frieze [41] satisfied this condition by treating the expression containing the integral sign as an equation of equilibrium which was then relaxed using the DR format. Thus,

$$\dot{v}_b^{t+\Delta t/2} = \frac{1-k_{v_b}/2}{1+k_{v_b}/2} \dot{v}_b^{t-\Delta t/2} + \frac{\Delta t}{\rho_{v_b}(1+k_{v_b}/2)} \left[\int_0^1 N_y \, dx \right] \tag{3.51a}$$

$$v_b^{t+\Delta t} = v_b^t + \Delta t \, \dot{v}_b^{t+\Delta t} \tag{3.51b}$$

$$\therefore \; v_{ext} = 2 v_b - v_{int} \tag{3.52}$$

The total force acting on the edge was found by numerical integration using the trapezoidal rule.

For unrestrained edges, the constitutive equation relating N_y to the in-plane strain $\Delta\varepsilon_y$ was used and an explicit expression for v_{ext} obtained.

$$N_y = \int_{-t/2}^{+t/2} \sigma_y \, dz = 0 \tag{3.53}$$

Using equation 2.32a,

$$N_y = \int_{-t/2}^{+t/2} (\sigma_y^p + \Delta\sigma_y) \, dz = \int_{-t/2}^{+t/2} \sigma_y^p \, dz + \int_{-t/2}^{+t/2} \sigma_y^p \, dz$$

Therefore,
$$N_y^p + \int_{-t/2}^{+t/2} \Delta\sigma_y \, dz = 0 \tag{3.54}$$

and since $N_y = N_y^p = 0$,
$$\int_{-t/2}^{+t/2} \Delta\sigma_y \, dz = 0 \tag{3.55}$$

Applying Simpson's Rule for five ordinates,

$$\Delta\sigma_{y_{z=1}} + \Delta\sigma_{y_{z=5}} + 2\Delta\sigma_{y_{z=3}} + 4(\Delta\sigma_{y_{z=2}} + \Delta\sigma_{y_{z=4}}) = 0 \tag{3.56}$$

The incremental stress at the mid-thickness position is given by

$$\Delta\sigma_{y_{z=3}} = E_{21_{z=3}} \Delta\varepsilon_{x_{z=3}} + E_{22_{z=3}} \Delta\varepsilon_{y_{z=3}} + E_{23_{z=3}} \Delta\gamma_{xy_{z=3}} \tag{3.57}$$

where the incremental strains are given by equation 2.2. Substituting for $\Delta\varepsilon_{y_{z=3}}$,

$$\Delta\sigma_{y_{z=3}} = E_{21_{z=3}} \Delta\varepsilon_{x_{z=3}} + E_{22_{z=3}} \left[\left(\frac{\partial v}{\partial y} - \frac{\partial v}{\partial y}p\right) + \frac{1}{2}\left(\frac{\partial w}{\partial y} - \frac{\partial w}{\partial y}p\right)\left(\frac{\partial w}{\partial y} + \frac{\partial w}{\partial y}p + 2\frac{\partial w_0}{\partial y}\right) \right] +$$

$$+ E_{23_{z=3}} \Delta\gamma_{xy_{z=3}} \tag{3.58}$$

and since $$\frac{\partial v}{\partial y} = \frac{v_{int} - v_{ext}}{\Delta y} \tag{3.59}$$

v_{ext} can be found by rearranging equations 3.57, 3.58 and 3.59. For the edge y = 0,

$$v_{ext} = v_{int} - \Delta y \left[\{\Delta\sigma_{y_{z=3}} - E_{21_{z=3}} \Delta\varepsilon_{x_{z=3}} - E_{23_{z=3}} \Delta\gamma_{xy_{z=3}}\}/E_{22_{z=3}} + \frac{\partial v}{\partial y} p \frac{1}{2}\left(\frac{\partial w}{\partial y} - \frac{\partial w}{\partial y} p\right)\right.$$

$$\left.\left(\frac{\partial w}{\partial y} + \frac{\partial w}{\partial y} p + 2\frac{\partial w_0}{\partial y}\right)\right] \tag{3.60}$$

Having described how fictitious deflections are obtained along the edge of the panel, it is necessary to consider how the forces act in the three types of conditions considered.

For simply supported edges, the appropriate condition is, for edges parallel to the y-axis, $M_x = 0$. The other conditions which are usually associated with the simply supported edge are $w = 0$, $N_{xy} = 0$, and any one of the conditions perpendicular to the edge. The free edge is satisfied by setting, for edges parallel to the x-axis,

$$M_y = 0 \qquad N_y = 0 \qquad N_{xy} = 0 \tag{3.61}$$

and $$\frac{\partial M_y}{\partial y} + 2\frac{\partial M_{xy}}{\partial x} = 0 \tag{3.62}$$

The last condition is rearranged and applied as follows:

$$M_{y_{ext}} = M_{y_{int}} + 2\Delta y \frac{\partial M_{xy}}{\partial x} \tag{3.63}$$

The value of $\partial M_{xy}/\partial x$ is required along the edge and therefore M_{xyext}. This is obtained by extrapolating internal values at the shear nodes since interlacing meshes are used.

3.6 Isolated Flatbar Stiffeners

In marine structures, stiffeners are usually attached to the shell plating by some type of welding process. In order to model the rotational restraint provided to the stiffener by the shell plating and vice versa, various simplifying assumptions have been made (See Chapter 1).

Before considering the problem of interactive buckling, a limited study of the behaviour of isolated stiffeners was conducted and is reported in this section. For the study, two computer programs were prepared. The first, STATEL, performs a static elastic analysis of a flat plate loaded under edge displacement and/or lateral pressure. The second, STAPL, is an extension of the first and allows for the effects of material non-linearity. Both programs use a large deflection formulation of the von Karman equations and plasticity is treated according to the von Mises yield criterion, as described in Chapter 2. The equations of equilibrium are solved using Dynamic Relaxation on an interlacing finite difference grid. The boundary conditions that were considered are given in the table below.

Table 3.2 Isolated Plate - Boundary Conditions

Loaded edges Simply supported	Loaded edges Clamped
S-S-S-S	C-C-C-C
S-S-S-F	C-C-C-F
S-C-S-F	C-S-C-F

where S is simply supported, C is clamped, and F is a free edge.

The solution obtained for an imperfect, square plate of moderate slenderness and

simply supported on all sides is compared in Fig. 3.1 with that derived analytically by Yamaki [18]. An 8 x 8 mesh was used and it is seen that good correlation was obtained with respect to both the buckling load and the postbuckling response.

The simply supported plate is compared with a plate having one unloaded edge free and the other unloaded edge simply supported or clamped in Fig. 3.2. The buckling loads were checked against Timoshenko's solutions [99] and good agreement was obtained. From Fig. 3.2 it is seen that, as expected, the effect of the free edge is to reduce the buckling load. The stiffness of the plate is not however noticeably affected in the postbuckling range for this particular geometry (square plate), and the plate continues to carry further load. It is of interest to note that the rotational restraint has comparatively little effect on the buckling load and also that only in the postbuckling range do the out-of-plane deflections begin to differ appreciably. Similar conclusions can be drawn in relation to clamped plates, as depicted in Fig. 3.3. Comparing the results presented in Figs 3.2 and 3.3 shows however that the rotational restraint along the loaded edges affects the buckling stress level considerably.

The effect of slenderness ratio on the behaviour of simply supported square plates with one unloaded edge free is shown in Fig. 3.4. It is noted that even though for the more slender plates the buckling loads are considerably reduced, in the postbuckling range all plates exhibit a substantial reserve of strength.

One parameter however which does affect the postbuckling behaviour of the plates is the aspect ratio. In Fig. 3.5, a series of plates with b/t = 60 and $w_0/t = 0.10$ are examined and it is seen that, as a/b is increased, the buckling load decreases and becomes more clearly defined. For these plates, the initial imperfection profiles chosen were:

Table 3.3 Isolated Plate Imperfection Profiles

Aspect Ratio	Imperfection Profile
0.875	single half-sine
1.0	single half-sine

Table 3.3 (cont'd)

1.5	single half-sine
2.0	double half-sine
3.0	triple half-sine

The deflections which are plotted were in all cases measured midway along the free edge of the plate.

Elasto-plastic solutions using the second program, STAPL, are presented in Figs 3.6a and 3.6b. The plate analysed was identical to that for which solutions have been obtained by Harding [97] and Frieze [115]. The properties of this plate are as follows:

Table 3.4 Isolated Plate particulars for Elastoplastic Analysis

Aspect ratio	a/b	0.875
Slenderness ratio	b/t	55
Max initial imperfection	w_o	b/1000
Young's Modulus	E	207
Poisson's ratio	ν	0.3
Yield stress	σ_o	250

The stress-strain curve for the simply supported case (S-S-S-S) was indistinguishable from that of Harding, who also solved the von Karman equations using dynamic relaxation. In his case the von Mises yield criteria and the Prandtl-Reuss flow rule were employed but he did not correct for penetrations of the yield surface. Presumably small enough load increments were chosen to ensure that (i) the numerical stability was not jeopardised and (ii) the spread of plasticity was correctly monitored.

The peakiness of the simply supported plate response does not arise in the other two cases for which the ultimate strengths (σ/σ_o) are 0.60 and 0.52 for the free-clamped and the free-simply supported plate respectively. In these two cases elastic buckling occurred at average stress ratios of 0.38 and 0.30, i.e. at much lower levels than the corresponding peak loads, in contrast with the S-S-S-S case in which elastic buckling

and yielding coincided.

Stress-strain curves for plates having the same geometrical and material properties but with clamped edges are presented in Fig. 3.6. For these cases, both the loaded edges and the unloaded supported edges are also restrained in the transverse direction. The plate with all edges clamped reaches the squash load (σ/σ_o = 1.0) and plastic buckling ensues. The load then gradually drops off but the plate is seen to be capable of carrying a substantial load well into the postfailure region. The slight increase in strains preceding the squash load is due to first yield. The plates with one edge free also fail by plastic buckling, very soon after first yield is reached. In none of these cases does elastic buckling occur.

Comparing Figs 3.6a and 3.6b it is observed that in the linear elastic range the stiffness of the plate depends on the boundary condition along the loaded edges. Furthermore, the rotational restraint along the unloaded supported edges is of secondary importance for square plates and only really affects the response in the postfailure regime.

3.7 Discretisation of Plate-Stiffener Intersection

The equations describing conditions of equilibrium along the junction have been presented in Section 2.8. To implement the finite difference scheme in the most efficient manner possible, it is necessary to consider the various options that are available when representing the intersection.

For non-interlacing meshes, the obvious arrangement is to have plate and stiffener nodes coinciding along the boundary. This ensures that compability of deflections and stress resultants (forces, moments) is achieved with the minimum amount of error. For interlacing meshes on the other hand, the following additional factors have to be considered:

- the representation of the discontinuities in the distribution of the stress resultants (M_y,N_{xy})
- the ease with which the finite difference expressions can be incorporated in the numerical procedure

- the minimisation of errors resulting from the use of finite difference approximants
- the minimisation of computation time.

It is possible to have either 'w' or 'shear' nodes along the intersection, giving rise to two finite difference schemes. Both options were considered and it was decided to position 'w' nodes from each grid along the intersection. The use of intersecting shear nodes gives rise to larger discretisation errors in the equations of longitudinal equilibrium (2.42 and 2.46). In addition, the representation of the discontinuities in M_y, N_{xy} is more complicated.

To improve the accuracy a stage further, 'auxiliary' nodes located in the plate on either side of the stiffener were introduced. These were used to improve the representation of equations 2.45a, 2.45b and 2.47 describing the distributions of in-plane forces and the torsional moment. The resulting arrangement is shown in Fig. 3.7.

In the remaining part of this section, each condition shall be examined in turn and the corresponding finite difference representation described. The principle upon which the equations were introduced into the numerical procedure is that, if a displacement condition is adopted for one panel component, then force equilibrium is used for the corresponding condition on the adjoining panel component [57,58].

3.7.1 Longitudinal Equilibrium

The equations of equilibrium in the longitudinal direction are:

$$\frac{\partial N_{x_p}}{\partial x} + \frac{\partial N_{xy_p}}{\partial y} = 0 \qquad (3.64a)$$

$$\frac{\partial N_{x_w}}{\partial x} + \frac{\partial N_{xy_w}}{\partial y} = 0 \qquad (3.64b)$$

for the plate and web, respectively. These are solved in discretised form at the 'u' nodes of each grid (u_p, u_w). Along the intersection, u_p and u_w coincide and the total

force acting at either 'u' node consequently consists of contributions from both panel components. Equilibrium is achieved by summing the longitudinal forces acting at the 'u' nodes, solving the equation of equilibrium for u_w and then setting the displacements in the plate equal to those in the web ($u_p = u_w$).

The stress resultants N_x acting on each panel component are shown in separated form in Fig. 3.8. It is seen that the longitudinal force arising along the intersection due to stiffener action is $N_{xw}\Delta y_w/2$. The corresponding force in the base plate is $N_{xp}\Delta y_p$ and therefore the total longitudinal force at any point along the intersection arising from direct stresses is:

$$N_x (\Delta y_p + \Delta y_w/2) = N_{x_p}\Delta y_p + N_{x_w}\Delta y_w/2 \qquad (3.65)$$

where N_x is the mean longitudinal stress resultant at any position along the intersection.

$$\therefore\ N_x = N_{x_p} \left(\frac{\Delta y_p}{\Delta y_p + \Delta y_w/2}\right) + N_{x_w} \left(\frac{\Delta y_w/2}{\Delta y_p + \Delta y_w/2}\right)$$

$$\therefore\ \frac{\partial N_x}{\partial x} = \frac{\partial N_{x_p}}{\partial x} \left(\frac{\Delta y_p}{\Delta y_p + \Delta y_w/2}\right) + \frac{\partial N_{x_w}}{\partial x} \left(\frac{\Delta y_w/2}{\Delta y_p + \Delta y_w/2}\right) \qquad (3.66)$$

The shear forces acting along the intersection due to plate and stiffener action are $N_{xyp}\Delta x$ and $N_{xyw}\Delta x$ respectively ($N_{xyp} = (N_{xypl} + N_{xypr})/2$). Summing as previously and differentiating with respect to y,

$$\frac{\partial N_{xy}}{\partial y} = \frac{\partial N_{xy_p}}{\partial y} \left(\frac{\Delta y_p}{\Delta y_p + \Delta y_w/2}\right) + \frac{\partial N_{xy_w}}{\partial y} \left(\frac{\Delta y_w/2}{\Delta y_p + \Delta y_w/2}\right) \qquad (3.67)$$

The equation of equilibrium along the intersection therefore becomes:

$$\left(\frac{\partial N_{x_p}}{\partial x} + \frac{\partial N_{xy_p}}{\partial y}\right)\left(\frac{\Delta y_p}{\Delta y_p + \Delta y_w/2}\right) + \left(\frac{\partial N_{x_w}}{\partial x} + \frac{\partial N_{xy_w}}{\partial x}\right)\left(\frac{\Delta y_w/2}{\Delta y_p + \Delta y_w/2}\right) = 0 \quad (3.68)$$

It is seen that if either panel component is considered alone, the equation reduces to the usual form. In order to satisfy shear flow requirements along the boundary the external fictitious shear stress resultant is required (N_{xywext}). This is obtained by substituting:

$$N_{xy_wb} = \frac{1}{2}\left(N_{xy_{wint}} + N_{xy_{wext}}\right)$$

in equation 2.46, where N_{xywb} is the shear stress resultant along the boundary giving:

$$N_{xy_{wext}} = 2\left(N_{xy_{pl}} - N_{xy_{pr}}\right) - N_{xy_{wint}} \quad (3.69)$$

A better approximation for (N_{xypl} - N_{xypr}) along the intersection is obtained by linear extrapolation of the shear stress resultants on either side of the stiffener as shown in the following diagram.

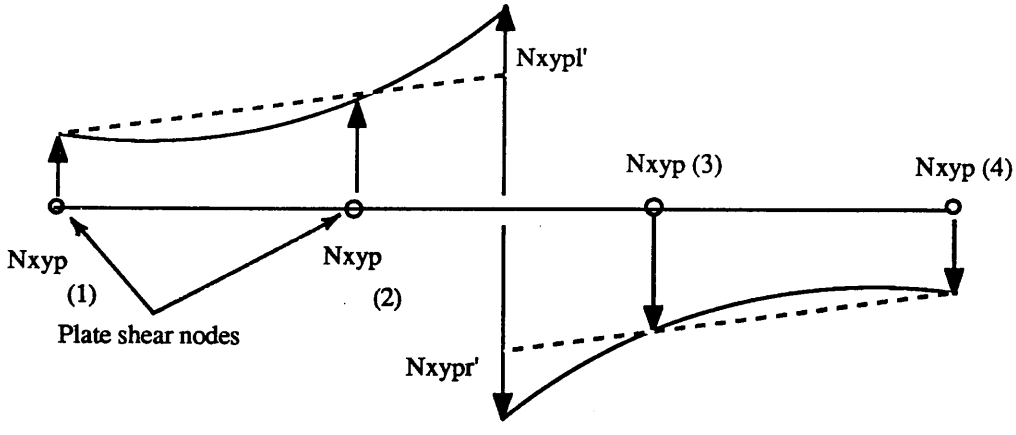

$$N_{xy_{pl}}' = (3N_{xy_{pl2}} - N_{xy_{pl}})/2$$

$$N_{xy_{pr}}' = (3N_{xy_{p3}} - N_{xy_{p4}})/2$$

$$\therefore N_{xy_{wext}} = 3(N_{xy_{pl}}' - N_{xy_{pr}}') + N_{xy_{pl2}} - N_{xy_{pr2}} - N_{xy_{winy}} \quad (3.70)$$

The equation obtained above is used to satisfy shear flow requirements along the plate-stiffener interface.

3.7.2 Equilibrium Normal to the Stiffener

Equilibrium in the direction normal to the stiffener is governed by a) the action of a Kirchoff force, Q_w, on the plate arising from out-of-plane movement of the stiffener along the intersection and b) by compatibility of deflections in this direction (equations 2.41b and 2.45a). The Kirchoff force acts in the plane of the plate and represents a body force (Figs 3.9a, 3.9b). This gives rise to a discontinuity in the distribution of in-plane forces, N_{yp}. The terms required for the calculation of Q_w are indicated in Fig. 3.9c. The twisting moments M_{xyw} which are determined at the shear nodes are in this case required at the 'w' nodes and are obtained from the expression :

$$M_{xy_w} = \int_{-t/2}^{+t/2} \tau_{xy_w} \, z \, dz \quad (3.71)$$

where τ_{xyw} are multilayer shear stresses along the edge of the stiffener. To represent the discontinuity in the distribution of plate transverse forces N_{yp} due to the body forces Q_w, auxiliary nodes on either side of the stiffener were introduced. In this manner, the 'smearing' effect which arises when nodes at a distance Δy_p are used is avoided. The Kirchhoff force Q_w acts on the left-hand and right-hand side sections of the plate and is introduced using the following equations:

$$N_{ypl} = N_y - \frac{Q_w}{2} \tag{3.72a}$$

$$N_{ypr} = N_y + \frac{Q_w}{2} \tag{3.72b}$$

allowing for the directions of the co-ordinate axes. The conditions of equilibrium normal to the stiffener are implemented in the numerical procedure in the following order:

1. Force and moment stress resultants along the stiffener edge are found using numerical integration.
2. Kirchhoff force terms are found from equation 2.45a.
3. In-plane forces acting on the plate on either side of the stiffener are found using equation 2.45b.
4. Transverse in-plane displacements in the plate, v_p, are found from the equation of equilibrium (2.1c).
5. Stiffener out-of-plane deflections, w_w, are found at the intersection using the displacement compatibility equation.

3.7.3 Equilibrium in the Plane of the Stiffener

Equilibrium in the plane of the stiffener is similarly governed by the action of the Kirchhoff force Q_p due to the out-of-plane deflections of the plate and by compatibility of deflections (w_p, v_w). The sign convention for the coordinate axes used is indicated in the following diagram.

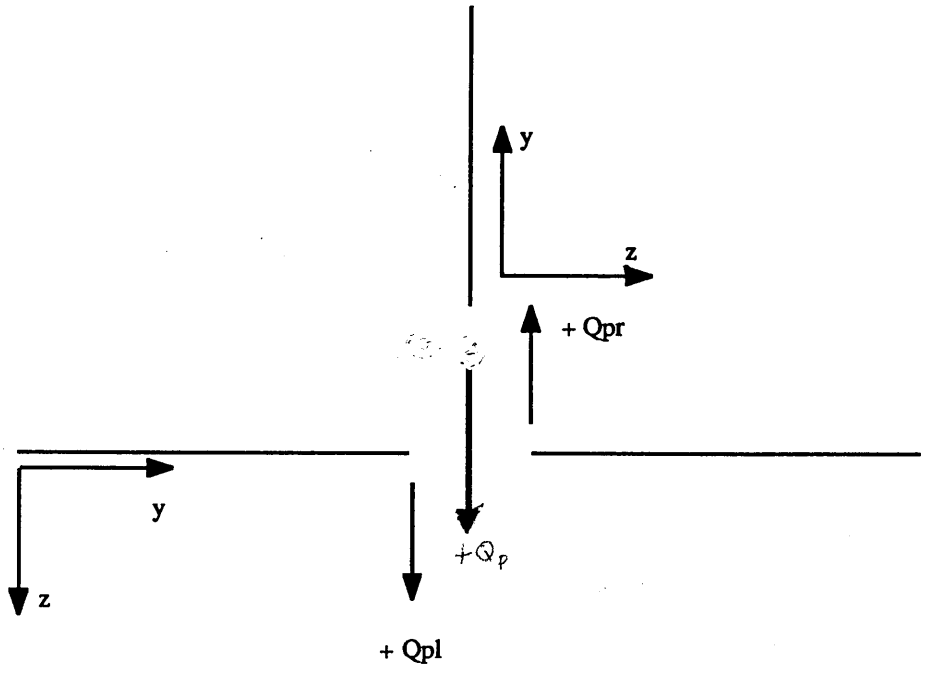

From the diagram, $Q_p = Q_{pr} - Q_{pl}$

where,
$$Q_{pr} = \frac{\partial M_{ypr}}{\partial y} + 2\frac{\partial M_{xypr}}{\partial x} \tag{3.73a}$$

$$Q_{pl} = \frac{\partial M_{ypl}}{\partial y} + 2\frac{\partial M_{xypl}}{\partial x} \tag{3.73b}$$

The force acting perpendicularly to the attached edge of the stiffener, N_{yw}, is equal to Q_p, the Kirchhoff force. Thus,

$$N_{yw} = \frac{\partial M_{ypr}}{\partial y} + 2\frac{\partial M_{xypr}}{\partial x} - \frac{\partial M_{ypl}}{\partial y} - 2\frac{\partial M_{xypl}}{\partial x} \tag{3.74}$$

along the intersection. For compatibility of deflections,

$$w = -\frac{(v_{wint} + v_{wext})}{2} \tag{3.75}$$

where v_{wext} is determined by rearranging the force-strain equation perpendicular to the attached edge. In this manner, compatibility of forces and deflections is achieved. The sequence of calculations in the numerical procedure is as follows:

1. Force and moment stress resultants in the base plate are determined.
2. Kirchhoff forces Q_p acting along the plate-stiffener intersection are then obtained.
3. The stiffener in-plane vertical force, N_{yw}, along the intersection is set equal to the Kirchhoff force.
4. The fictitious value for the stiffener vertical deflection, v_{wext}, is obtained as described above.
5. Compatibility of deflections is achieved by employing equation 3.75.

3.7.4 Rotational Equilibrium

The conditions governing rotational equilibrium involve the transversely acting bending moments M_y, and the rotations $\partial w/\partial y$ at the intersection. The rotational action of the stiffener produces a discontinuity in the distribution of the bending moments in the plate, as shown schematically in Chapter 2 (Section 2.8). To reproduce this using the finite difference scheme use is made of the auxiliary nodes located on either side of the stiffener. Since the geometry of the plate does not change on either side of the stiffener, it may be assumed that the bending moments M_{yw} are distributed equally between the two plate sections.

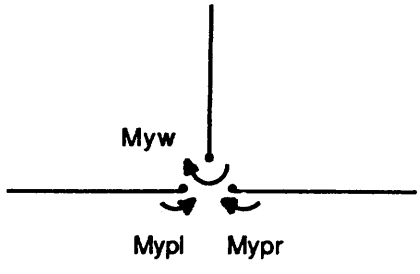

Thus, from the diagram,

$$M_{ypl} = M_{yp} - \frac{M_{yw}}{2} \tag{3.76a}$$

$$M_{ypr} = M_{yp} + \frac{M_{yw}}{2} \tag{3.76b}$$

where M_{ypl}, M_{ypr} act on the left-hand and right-hand sides of the base plate respectively. Geometrical compatibility is represented by equation 2.43. Casting in finite difference terms and rearranging, this becomes:

$$w_{w_{ext}} = w_{w_{int}} - 2\,\Delta y_w \frac{\partial w_p}{\partial y} \tag{3.77}$$

The use of this equation ensures that the plate and stiffener always deform at right angles.

To ensure numerical stability of the equations derived in this section, the Gershgorin bounds of the additional terms were included in the expressions for the fictitious densities along the intersection.

3.8 Elastic Response of Flat Stiffened Plating

Results obtained using the equations derived previously will now be described and compared with beam and plate theory. Before considering the combined interactions which arise when lateral torsional buckling occurs, each condition will be examined separately.

Lateral pressure loading on the base plate of a stiffener- plate combination gives rise to interaction forces in the plane of the stiffener, as described in Section 2.7. In order to check equilibrium in the longitudinal and transverse directions, a stiffened plate whose

particulars are given in Fig. 3.10 was analysed. Lateral pressure loading was applied to the plate whose longitudinal edges were free to move out-of-plane, the whole cross-section being supported at each end in such a way that the displacement of the intersection in the plane of the stiffener was zero, although different conditions could be applied to the transverse edges of the stiffener.

In-plane movement of the supported edges was allowed and the axial force at each node along the edges was set equal to zero ($N_x = 0$, $N_{xw} = 0$). The transverse displacement of the stiffener at the supported edges was treated in the following ways:

i) $N_{xy_w} = 0$ (unrestrained)

ii) $\dfrac{\partial N_{xy_w}}{\partial x} = 0$ (partially restrained)

iii) $v_w = 0$ (fully restrained)

Case (i) represents an isolated cross-section receiving no support from the adjoining structure at the propped edges other than at the plate-stiffener intersection. In case (ii), a symmetrical shear stress distribution is assumed along the transverse esges and case (iii) corresponds to a fully restrained edge (upper bound).

The results showed minimal differences for cases (ii) and (iii) since for case (ii) the transverse displacements v_w along the stiffener edge were several orders of magnitude smaller than at any other location. The curves produced in Figs 3.11a and 3.11b correspond to case (ii).

The longitudinal stresses in the plate and stiffener are compared with beam theory in Figs 3.11b, and 3.11c. Figure 3.11a shows the Kirchoff force acting along the stiffener in the range $L/2 > x > 0$. It is seen that for the range $x > L/4$ end-effects are negligible and the magnitude of the interactive force agrees well with the analytical result ($Q_p = 6480$ N/m). In Fig. 3.11b the longitudinal force along the stiffener tip is plotted for the range $L/2 > x > 0$ and compared with linear beam theory ($N_x = \sigma_x t = Myt/I$). The distribution across the depth of the stiffener at $x = L/2$ is plotted in Fig. 3.11c, and again good agreement is observed. The distribution of shear flow in the

cross-section at x = L/4 is compared with beam theory in Fig. 3.12. In deriving the exact shear flow distribution, sections at x = 7L/32 and 9L/32 were considered and numerical integration performed. The distribution of longitudinal stress resultants (N_x) in the plate at x = L/2 is plotted in Fig. 3.13. From this, the effective breadth of the section was calculated and compared with that given in Table EB1 [126]. The data contained in this table were produced in a study of shear lag using a finite element program.

Rotational and transverse equilibrium along the intersection in the base plate were examined using an alternative arrangement. In order to apply a known load to the plate along the intersection in the transverse direction, the stiffener was treated as a cantilever subjected to a uniformly distributed load, as shown in Fig. 3.14. In this manner, the bending moment and reaction force along the attached edge can be readily compared with beam theory.

The combined effects of the interactions when lateral torsional buckling of the stiffener occurs are illustrated in Figs 3.16a and 3.16b. A rectangular cross-section whose particulars are given in Table 3.5 was loaded in axial compression. The stiffener was analysed

i) isolated
ii) attached to a flat plate

When considering (ii), the stiffened plate was modelled as being either simply supported or rotationally clamped. The unloaded edges of the base plate were treated as being either constrained (v = const, $\partial M_y/\partial y = 0$) or rotationally clamped and supported against out-of-plane displacement ($N_y = 0$, $w = 0$). For the stiffened plate when clamped, the longitudinal unloaded edges of the base plate were restrained from deflecting in the out-of-plane direction (w = 0).

Table 3.5 Stiffener and Base Plate Particulars

Length/depth	a/d	7.8125
Depth/thickness	d/t_w	40

Table 3.5 (cont'd)

Initial imperfection	w_{ow}/t_w	1/20
Buckling stress	σ_{cr} (N/mm^2)	155
Buckling strain	ε_{cr} ($\mu\varepsilon$)	749
Aspect Ratio (plate)	a/b	1.67
Slenderness	b/t_p	72

The buckling stress given above was obtained using the standard equation developed using plate theory [99] in which the constant k had the value 1.328. This corresponds to the solution of a long plate with S-C-S-F edges. The following observations may be made in relation to Fig. 3.16:

i) For the aspect ratio considered, (a/d = 7.8125) the effect of rotational restraint along the loaded edge for the isolated stiffener (C-C-C-F versus S-C-S-F) is of secondary importance. This may be contrasted with the previous case described in Section 3.6 in which a square plate was considered.

ii) The pre-buckling behaviour follows the same path in all cases, although the S-I-S-F (I designates intersecting edge) plate exhibits a slightly lower stiffness, which is to be expected since in this case the base plate is simply supported along the loaded edges and partially restrained against out-of-plane movement along the longitudinal edges ($\partial w/\partial y = 0$).

iii) Buckling occurs at approximately the same stress levels in all cases. The calculated values were determined from Fig. 3.16 and are compared with plate theory in Table 3.6.

iv) Following buckling, substantially different paths are followed by the isolated and attached stiffeners. In the former case, torsional buckling leads to collapse of the cross-section whereas the attached stiffener continues to carry further load.

Figure 3.16 shows the corresponding average stress-deflection behaviour. In all cases,

buckling is characterised by a sudden, sharp increase in lateral deflection. This may be contrasted with plates which do not have a free edge and which buckle more gradually, notwithstanding the effect of initial imperfections.

Table 3.6 Buckling Stresses and Strains

		Stress (N/mm^2)	Strain ($\mu\varepsilon$)
Plate theory	S-C-S-F	155.0	749.0
Isolated	S-C-S-F	155.2	750.2
Isolated	C-C-C-F	158.2	813.4
Attached	S-I-S-F	127.1	660.1
Attached	C-I-C-F	154.3	746.0

It is seen from Table 3.6 that the numerical procedure predicts elastic buckling of the stiffener quite accurately. It is also apparent from (iv) that it is necessary to study the effect of interaction in more detail, since stiffener design based on isolated plate equations does not allow for the presence of the shell plating. In the next section the elasto-plastic behaviour of stiffened plating is briefly considered and some of the problems that arise when using dynamic relaxation are discussed.

3.9 Elasto-plastic Response of Flat Stiffened Plating

The behaviour of thin-walled structures under axial compression is affected by plasticity to such an extent that the load at which the plastic regime is entered is usually identified with the collapse of the section. Flat structures generally exhibit little post-yield strength since yielding spreads rapidly reducing the effective area of the section. The load carried is then shed to adjoining members with the possibility of buckling being precipitated and/or leading to overall failure.

Consequently, when performing an ultimate strength analysis it is necessary to allow for material non-linearity. In the case of stiffened plating, the overall behaviour can be classified according to the relative load-carrying capacity of the stiffener to that of the plate, i.e:

i) stiffeners which are torsionally weak

ii) stiffeners which are torsionally strong

iii) stiffeners whose load-carrying capacity is similar to that of the plating

In the first category, stiffener lateral torsional buckling occurs first, usually followed by yielding which leads to local collapse. The load is at each stage shed to the plate which may continue in a stable condition although generally this is unlikely particularly after yielding of the stiffener.

Torsionally strong stiffeners continue carrying load after local failure of the shell plating. Design codes generally ensure that the stiffener torsional failure load is greater than the shell plate buckling load.

The third category comprises stiffeners whose cross-sectional area is similar to that of the associated plate. Under these conditions, the failure of either section may lead to overall collapse of the plate stiffener combination, since the load shed by a weaker member will be sufficient to cause failure in the stronger member.

Beam-column behaviour has not been mentioned since it is generally associated with overall collapse of the cross-section and concerns panels of higher aspect ratios.

In the next two Chapters, the behaviour of stiffened plates with flatbar stiffeners will be considered. Chapter 4 is concerned with correlation studies of a series of small scale tests carried out at Glasgow University.In Chapter 5 the results from a series of parametric studies will be presented, the emphasis being on short panels with flatbar stiffeners. The use of dynamic relaxation to solve the equations of equilibrium proved not to be without its problems; when analysing a panel described by category (iii) numerical instability arose when plates of high aspect ratios buckled elasto-plastically, to be followed immediately by stiffener collapse. It was not found possible to obtain an accurate picture of the buckling phenomenon using the numerical procedure in its conventional form and it became necessary to develop a method capable of treating buckling as a dynamic phenomenon. The theoretical basis for a real-time simulation capable of describing the dynamic aspects of interactive elasto-plastic buckling is given in Chapter 6.

CHAPTER FOUR

EXPERIMENTAL PROGRAMME AND CORRELATION STUDIES WITH NUMERICAL ANALYSIS

A series of tests on flatbar stiffened plating was carried out in order to provide a basis for comparison with the numerical procedure. The tests were conducted in the Civil Engineering Structures Laboratories at Glasgow University. In previous experimental work, the local buckling of flat stiffeners in steel plating has not been considered in the elasto-plastic range, although test results are available for materials of high elastic strain capacity (Araldite epoxy resin) in which interactive effects were studied [49].

4.1 Experimental Programme

4.1.1 Description of Models and Test Rig

In order to evaluate the capability of the numerical procedure to predict local torsional buckling of a stiffener, it was decided to use a plate bearing a torsionally weak stiffener. This would ensure that failure of the stiffener preceded failure in the base plate; in addition, interaction effects would not significantly influence the overall behaviour of the panel. The geometry that resulted was not representative of stiffened plating used in practice but this does not detract from the general applicability of the procedure since other geometries can be analysed equally well. Other factors which were taken into account in designing the models were:

- axial compression, lateral pressure and combined loading could be applied

- the overall length should be such that the models could be fitted into an existing pressure chamber
- the test specimens should be readily amenable to numerical analysis.

The above considerations led to the configuration shown schematically in Fig. 4.1. The test specimen consisted of a base plate of dimensions 250 x 150 x 3 mm and a stiffener of dimensions 250 x 32 x 0.8 mm welded to the base plate along its centreline. The stiffened plate was welded to a rectangular box section and formed one side of it. The elastic buckling stresses for the stiffener and base plate were checked to confirm that stiffener buckling would precede that of the base plate. The dimensions and material properties of the box were chosen so that it would not fail in the range of applied loading.

Two box sections were constructed and each whole model was stress-relieved prior to testing. Tensile test specimens were also stress-relieved under the same conditions. In addition to the stiffener dimensions specified above, a narrower stiffener of height 25 mm was used. Details concerning test specimen dimensions are given in the following table.

Table 4.1 List of Model Tests

Model No.	Applied Loading	Stiffener Height (mm)
1	Axial	32
2	Axial	32
3	Combined	32
4	Pressure	32
5	Axial	25
6	Pressure	25
7	Combined	25
8	Axial	25

4.1.2 Preliminary Measurements and Test Procedure

Prior to testing, detailed measurements regarding the following were carried out:

- overall model dimensions
- plate and stiffener thicknesses
- plate and stiffener initial imperfections
- tensile tests of coupons extracted from plating used in each model component.

Model overall dimensions, thicknesses and yield stresses are summarised in Table 4.2 overleaf.

It is observed that stiffener yield stresses are higher than corresponding base plate yield stresses. The original specifications sought the opposite but it is felt that overall behaviour of the stiffened plate would not be substantially affected since the stiffener was designed to fail by lateral buckling before the base plate reached its elastic limit.

Initial distortions were measured in both the stiffener and the base plate. Similar trends were observed in all models, although the profile of the stiffener free edge differed in each case. The profile of the base plate in the longitudinal and transverse directions appeared to have been affected by the welding along the transverse edges and the plate-stiffener junction respectively. As a result, the ends of the base plate were pulled upwards towards the stiffener. In the transverse direction, a 'hogs-back' type effect was observed [127].

The stiffener initial distortions were small and evidently not seriously affected by the welding. A certain amount of twist was noted and several half-sine waves were detected along the free edge. Maximum distortions for all models lay in the range:

$$0.11 \text{ mm} > w_{ow} > -0.50 \text{ mm}$$
$$0.50 \text{ mm} > w_{op} > +0.35 \text{ mm}$$

Following the above measurements, electrical strain gauges were attached to the

Table 4.2 Test Specimen Dimensions and Yield Stresses

Model No.	Length	Breadth	Stiffener Height	Thicknesses		Yield Stresses	
				Plate	Stiffener	Plate	Stiffener
	(mm)	(mm)	(mm)	(mm)	(mm)	(N/mm^2)	(N/mm^2)
1	249.33	149.47	32.1	3.496	0.833	227	311
2	248.20	149.47	32.1	3.382	0.834	227	311
3	248.60	148.77	32.0	3.349	0.835	236	272
4	248.69	148.80	31.9	3.350	0.850	236	272
5	248.34	148.49	25.0	3.338	0.854	228	289
6	248.48	148.50	25.0	3.364	0.845	239	327
7	247.64	148.41	25.1	3.394	0.819	231	307
8	247.63	148.44	25.1	3.333	0.817	231	307

stiffener and base plate. The model was then positioned on a steel block to which linearly variable displacement transducers (LVDTs) used to measure deflections, were attached. The layout is shown in Figs 4.2a and 4.2b and the locations of strain gauges and transducers are indicated in Figs 4.4 and 4.5. The steel block with the model in position was then placed between the upper and lower plattens of the compression machine (axial load tests) or inside the cylindrical pressure chamber (Fig. 4.6). The 1000-ton Losenhausen compression machine used, with the model in position, is shown in Fig. 4.4. During the tests, results from the strain gauges and transducers were processed by an MBM 5000 data logger interfaced to a PDP-8 mini-computer.

The preliminary measurements described above were used as input data for the numerical procedure in the correlation studies. The incorporation of yield stress and overall dimensions presented no difficulty. However, the use of the initial imperfection measurements required a preliminary procedure to be carried out, which was necessary because the measurement points and grid co-ordinates did not coincide. The procedure followed for the development of component 'surfaces' is indicated in Fig. 4.7. Standard routines in which Chebychev polynomials are implemented were used to give values for the initial imperfections at the required positions. A series of trial runs was performed to choose the polynomial degrees which gave the best fit and for the base plate values of 8 and 6 in the longitudinal and transverse directions respectively were used; for the stiffener, values of 8 and 3 gave satisfactory results.

4.1.3 Representation of Boundary Conditions

In this section, the numerical representation of the plate and stiffener edges under test conditions will be described. Idealised conditions are summarised in Fig. 4.8 and the actual model is shown in Fig. 4.2.

As is apparent from Fig. 4.8, the stiffened plate was welded continuously to the box section along the longitudinal and transverse edges. Appropriate conditions are

therefore those of a rotationally clamped, isolated panel, since any rotation along the edges would necessarily involve concurrent rotation of the box section. The dimensions of the box were such that for the applied range of loading rotations along the edges could effectively be ignored. For the plate and stiffener in the longitudinal direction, therefore

$$\frac{\partial w}{\partial x} = 0 \qquad \frac{\partial w_w}{\partial x} = 0 \tag{4.1}$$

and for the plate in the transverse direction,

$$\frac{\partial w}{\partial y} = 0 \tag{4.2}$$

The base plate and stiffener were further assumed not to deflect in the out-of-plane direction along the welded edges. During the actual tests (axial compression in particular), the box section components moved perpendicularly to the direction of loading. It was considered reasonable to assume that any translation of the edges was such that deflections in one part of the stiffened plate relative to those in another would be small and not cause any premature failure or other unintended effects (i.e. rigid body translation does not give rise to any internal strains). Thus,

$$w = 0 \qquad w_w = 0 \tag{4.3}$$

along all edges (except for the free edge and the plate-stiffener junction).The transverse edges were further assumed to be partially restrained by a symmetrical shear stress distribution described by:

$$\frac{\partial N_{xy}}{\partial x} = 0 \qquad \frac{\partial N_{xy_w}}{\partial x} = 0 \tag{4.4}$$

Along the longitudinal edges of the base plate, translations also depend on the shear restraint provided by the box section. Since (for axial compression) the whole cross-section was uniformly loaded, the effects of shear along the edge would be small and thus the equation

$$N_{xy} = 0 \tag{4.5}$$

was used to approximate the shear condition along the longitudinal edges. Finally, the transverse in-plane condition along the same edges has to be considered. The in-plane forces, N_y, give rise to out-of-plane deflections in the box. Since however the bending restraint in the box is relatively small, it can be assumed that the edges are free to move and therefore

$$N_y = 0 \tag{4.6}$$

The transverse deflections are thus governed by the external loading and Poisson's effect. For specimens loaded in axial compression the external loading was applied as a uniform displacement of the transverse edge, as described in Chapter 3. For Model Nos. 4 and 6 to which only lateral pressure was applied, the transverse edges were assumed to be fully built-in.

4.1.4 Convergence Studies

A study involving a stiffened plate of similar geometric and material properties to the models was performed to determine the effect of mesh size on convergence. The elastic buckling load for the stiffener was chosen as a criterion for this study and four different mesh sizes were considered, as shown in the following table.

Table 4.3 Convergence Studies

Mesh No.	Plate Mesh	Stiffener Mesh	$\frac{\Delta x}{\Delta y}$	$\frac{\Delta x}{\Delta y_w}$	No. of Nodes
1	14 x 8	14 x 4	0.952	2.230	210
2	16 x 10	16 x 4	1.042	1.953	272
3	18 x 10	18 x 6	0.926	2.604	342
4	20 x 12	20 x 6	1.000	2.344	420

The results from this study are summarised in Figs 4.9a and 4.9b which correspond to cases of axial compression and lateral pressure. The stiffener buckling loads corresponding to Mesh no. 4 have been used as datum points. It is seen that for an increase in 76 nodes (Mesh 3 to Mesh 4) that the corresponding changes in the buckling loads are approximately 1%. Discretisations corresponding to Mesh no.4 were thus used in all correlation studies.

4.2 Correlation Studies of Axial Compression Tests

Model Nos. 1, 2, 5 and 8 were loaded under axial compression, consisting of a uniformly applied displacement of the transverse edges. Test results were presented in the form of load-strain and load-end compression diagrams and these were used to determine critical buckling and plastic collapse loads an d strains [127]. The features of the load-strain response for the stiffener tip are shown in Fig. 4.1c from which critical loads and strains may be obtained.

Upon application of the load, the strains along the stiffener tip increase in compression, the divergence betwen them depending on the initial imperfections. When buckling occurs, the strains diverge noticeably and continue doing so until plastic collapse occurs. At plastic collapse, the local behaviour of the stiffener changes as load begins to be shed to the base plate and/or the box, and a change in gradient occurs in the load-

strain diagram. The post-failure path depends on the shape adopted by the stiffener and the magnitude of the load carried locally.

To be able to compare the analytically and experimentally determined loads directly, it was necessary to calculate theoretically the load carried by the model cross-section for each load increment. Since only the plate and stiffener were analysed numerically, an approximate method had to be employed to estimate the load carried by the box section. The dimensions and yield stress of the box were chosen so that failure would not arise before failure of the stiffened plate. Therefore the box could be treated as behaving in the linear elastic range (yield stress = 430 N/mm^2, thickness = 10 mm). The load was thus estimated from:

$$P_{box} = E\,A\,\varepsilon_{app} \tag{4.7}$$

and the total load carried by the model was obtained from:

$$P_{mod} = P_{box} + P_{pl} + P_{stif} \tag{4.8}$$

This is an approximate method and it is possible a more refined technique would lead to better correlation of the critical loads. The analytical results for each study are presented in diagrams of:

- load-end shortening curves for the stiffener, base plate, stiffened plate and model cross-section.
- load-strain curves for local longitudinal strains along the stiffener tip
- load-deflection diagrams for stiffener and base plate out-of-plane deflections

The positions at which local strains and deflections were measured were those at which strain gauges and transducers were placed during the tests.

4.2.1 Model No. 1

4.2.1.1 Stiffener Response ($d/t_w = 38.5$)

The theoretical and experimental results obtained relate to overall and local stiffener behaviour. The theoretical response seen in Fig. 4.11 demonstrates three phases of behaviour:

- elastic pre-bifurcation	(0 - 3991 N)
- postbuckling	(3991 - 5547 N)
- unloading	(5547 - 5511 N)

The geometrical initial imperfections consisted of a three half-sine wave along the stiffener tip, with a tilt whose magnitude increased slightly towards the free edge. Stiffener misalignment in the longitudinal direction along the line of attachment to the base plate was 0.05 mm (small).

During the initial stages of loading, the out-of-plane deflections increased in the same direction as the initial imperfections. The stiffener tip adopted a three half-sine waveform which it maintained until the postbuckling range was reached. Elastic buckling commenced at a load of 3991 N and an end shortening of 0.193 mm (Fig. 4.11). At this load, the average buckling stress and strain along the loaded edge were 149.3 N/mm^2 and 775 $\mu\varepsilon$ respectively. The Timoshenko buckling load for a S-C-S-F plate is 167.2 N/mm^2 and the corresponding strain is 808 $\mu\varepsilon$. The model load at 3991 N was predicted to be 569.7 kN.

Following buckling, the analysis indicated that the stiffener tip maintained the three half-sine waveform which persisted throughout the rest of the load history. Plastic collapse was predicted to occur at a load of 5547 N and an end shortening of 0.421 mm. At this load the total load on the model was predicted to be 1172 kN and the

corresponding strain 1688 με. Plasticity was first detected in the stiffener after elastic buckling and developed in way of the buckle at the mid-length position. Following plastic collapse a slight drop in the load carried by the stiffener was observed and plasticity redistributed about the quarter points. Theoretical and experimental local buckling loads are compared in the following table.

Table 4.4 Model No. 1 - Comparison of Critical Strains and Loads

Strain Gauge Pair	1/2	3/4	5/6	7/8	11/12	13/14	15/16
Critical Strain	725	804	800	744	800	760	750
(με)	850	825	650	660	675	760	900
Critical Buckling	580	550	525	475	550	550	550
Load (kN)	450	525	350	340	320	325	350
Plastic Collapse	925	925	760	775	890	900	800
Load (kN)	-	-	-	-	-	-	-

In the table the lower values are the test results given in (127) while the upper values are the theoretical results derived using Figs 4.12a and 4.12b. Detailed information concerning local plastic collapse loads was not given for the test data. As is evident from the table, the predicted buckling strains are fairly constant at approximately 769 με. The test results however indicate that some bending arose which precipitated earlier buckling at 660 με at the midlength position. For gauge nos 3/4 and 13/14, the critical strains agree quite well but the differences increase towards the midlength position. The mean value of the test buckling strains along the stiffener tip was 760 με, and the corresponding buckling load was 320 kN. The test plastic collapse load was found to

be 935 kN although collapse commenced at 890 kN [127]. At 935 kN the average test strain was 1203 με.

There are several reasons as to why discrepancies exist between the predicted and observed results. Bending of the stiffener in its own plane occurred because of eccentricity of the applied loading and rotation of the loaded edges. It was not possible to know the distribution of strains across the loaded edges and in addition the load carried by the model cross-section was estimated in only an approximate manner. The fact that bending occurred is supported by the lower than expected midlength buckling strain and load.

The predicted buckling loads given in Table 4.4 were checked against load-deflection curves (Fig. 4.13) for the stiffener. This figure shows that buckling developed gradually as a result of initial imperfections and that in the post-failure regime a large buckle developed in way of gauge nos 5 and 6.

4.2.1.2 Base Plate Response

Since the base plate was designed so as not to buckle in the elastic range, failure was governed by material response. The material was modelled as elastic-rigid plastic and as a result the load carried increased until the squash load was reached. The onset of yielding was predicted at a load of 110.9 kN and an average strain of 981 με (yield strain =1097 με). Plasticity developed as a full-depth phenomenon from the central region and covered approximately three quarters of the plate area, the loaded edges remaining elastic.

The squash load was predicted to be 118.5 kN and from that point onwards the load remained constant (Fig. 4.14). A limited amount of out-of-plane deflections but no buckling were predicted by the numerical procedure.

4.2.1.3 Stiffened Plate Response

Because of the relatively slender stiffener compared with the plate ($A_w/A_p = 0.057$) the applied load was carried substantially by the plate, overall failure depending on plate failure.

The load-end shortening curve (Fig. 4.15) demonstrates this, when compared with Fig. 4.14. The relatively small contribution of the stiffener to the strength of the cross-section is evident by the small drop in the drop in load which occurred when the stiffener buckled. With increasing end shortening, the load carried remained constant at 123.7 kN, any further applied load being carried by the box section (theoretical squash load = 126.9 kN).

The effects of stiffener-plate interaction were secondary and did not affect the overall behaviour. This was in agreement with the general response noted during the test.

4.2.1.4 Overall Model Response

The behaviour of the model cross-section is shown in Fig. 4.16. It is seen that the load increases linearly until stiffened plate failure, at which point a slight reduction in gradient is noted. Stiffener buckling at 570 kN could not be detected in the model response curve. At 820 kN, however, a noticeable change in gradient is observed. The corresponding load on the stiffened plate was 123 kN and at that point the base plate resulted in load being shed to the stiffener which had already buckled and the box section, which continued carrying additional load. The load that was shed to the stiffener led shortly after to its plastic collapse. Thus the discontinuity in the load-end shortening curve for the model section arises from yielding in the base plate which also precipitated plastic collapse in the stiffener.

4.2.2 Model No.2

4.2.2.1 Stiffener Response ($d/t_w = 38.5$)

The initial distortions of the stiffener for this model were characterised by a large very localised deflection at a distance of 14 mm from the lower loaded edge. This was produced accidentally prior to testing and had a magnitude of approximately 0.50 mm (0.6 x thickness). The correlation of this test was thus made more difficult because of the presence of

- an exceptionally large very localised initial distortion
- an associated residual stress distribution

The distribution of residual stresses in way of the damage could not be quantified and therefore was not modelled whereas the initial distortions were reproduced quite satisfactorily using the Chebychev polynomial method.

The theoretical load-end shortening response of the stiffener is shown in Fig. 4.17. The behaviour is linear up to a load of 2751 N (end shortening = 0.13 mm). Elastic buckling commenced at 2751 N and the average stress and strain across the loaded edge were 102.7 N/mm^2 and 549 $\mu\varepsilon$. Load continues to be carried up to 5151 N, corresponding to an end shortening of 0.499 mm. At this point plastic collapse occurs, the average stress and strain being 192.4 N/mm^2 and 1013 $\mu\varepsilon$ respectively.

Compared with Model No. 1 it is noted that in this case the initial buckling strain is much lower and this can be attributed to the differences in initial distortions. For this model, surface plasticity was induced following buckling. The stiffener plastic collapse load of 5151 N was slightly lower than in the previous test but in the post-failure regime the load-end compression curve had a similar shape.

During the test, buckling developed from 191 kN (load on model) and became fully

developed in way of gauge nos 11/12. After critical buckling two buckles grew at distances of 95 mm and 155 mm from the top of the stiffener (gauge pairs 5/6, 11/12 respectively). The predicted profile consisted of a three half-sine waveform which is apparent from Fig. 4.19.

The local longitudinal strains determined analytically are shown in Figs 4.18a and 4.18b and are compared with test results in the following table.

Table 4.5 Model No. 2 Comparison of Critical Strains and Loads

Strain Gauge Pair	1/2	3/4	5/6	7/8	11/12	13/14	15/16
Critical Strain	700	707	725	611	723	589	615
($\mu\varepsilon$)	1020	800	750	700	625	650	785
Critical Load	543	525	562	457	600	437	500
(kN)	600	375	380	350	300	345	375
Plastic Collapse	950	1025	843	955	937	1010	1000
Load (kN)	950	950	950	975	950	950	950

From the above table it is apparent that the critical buckling strains agree quite well. Buckling of the stiffener is predicted in way of gauge nos. 13/14, which are the closest to the localised initial distortion. The critical loads appear to be overestimated by the theoretical approach as for the previous model.

The possibility of nonlinear behaviour of the box section did not arise because after each test the model retained it's original overall dimensions. Therefore the approximate method described earlier in this Chapter can be expected to give satisfactory results. On the other hand there is good agreement in the plastic collapse loads, the maximum difference being 8%, in way of gauge nos. 7/8.

The numerical procedure predicted the onset of plasticity in the stiffener along the tip and the intersection with the base plate at a strain of 1007 με, i.e. after elastic buckling. The number of yielded zones increased until the plastic collapse load was reached, following which gradual unloading occurred. During unloading, the spread of plasticity decreased very slowly.

4.2.2.2 Base Plate Response

The general remarks made concerning Model No.1 apply also to Model No.2. The plate deflected away from the stiffener, in sympathy with the initial imperfections and no local buckling was observed (Fig. 4.20).

The onset of plasticity occurred at an average strain of 1007 με (yield strain = 1097 με) and a load of 105.5 kN. The plate failed at 114.6 kN, i.e. just before the theoretical squash load of 114.75 kN was reached. Following failure, the load carried by the plate remained constant and the yielded zones spread throughout the volume of the plate which thus behaved as a plastic membrane.

4.2.2.3 Stiffened Plate Response

Comparison of Figs 4.15 and 4.21 shows that the response of the stiffened plate in Model No. 2 was similar to that of Model No. 1. This was to be expected considering the generally similar geometric and material properties of both models. The load increased until yielding of the base plate caused failure of the whole cross-section at 119.64 kN (theoretical squash load = 122.93 kN). Following failure the load carried remained constant without producing overall collapse of the cross-section.

4.2.2.4 Overall Model Response

The response of the model cross-section is shown in Fig. 4.22. It is seen that this is

similar to Model No.1 and the slight reduction in slope precedes stiffened plate failure. This is because failure was identified with the condition of maximum load rather than the point of change of gradient of the curves in Figs 4.20, 4.21. The theoretical squash load for the model was calculated to be 1413 kN and the corresponding strain was 2069 $\mu\varepsilon$ (end shortening = 0.517 mm).

4.2.3 Model No. 5

4.2.3.1 Stiffener Response ($d/t_w = 29.3$)

The stiffener for this model was stockier than in the previous cases. It was therefore expected that the buckling load would be higher since linear theory states that it is inversely proportional to the square root of the slenderness ratio (d/t_w). This was indeed confirmed by both the theoretical and the experimental results.

For this case, the geometrical initial imperfections consisted of a tilt of increasing magnitude towards the free edge and a two half-sine waveform of amplitude 0.15 mm along the stiffener tip. Misalignment along the longitudinal direction was 0.1 mm along the intersection with the base plate.

The theoretical average load-end shortening response is shown in Fig. 4.23 and can be subdivided into three sections:

- elastic pre-bifurcation	(0 - 4504 N)
- postbuckling	(4504 - 5037 N)
- post-collapse	(5037 - 4934 N)

During the initial stages of loading, the lateral deflections followed the shape of the initial imperfections. At higher loads the stiffener profile changed to a six half-sine waveform which became fully apparent at 3500 N and remained stable until the

postbuckling range was reached.

The change in gradient associated with elastic buckling occurred at 4504 N (end shortening = 0.285 mm). The average stress and strain across the loaded edges at this load were 211 N/mm^2 and 1145 με. The corresponding load on the model was 828 kN.

The test results showed that it was difficult to detect buckling from the strain distributions along the stiffener tip because no great changes were noted before 828 kN. It appeared that a series of local buckles were produced along the length of the stiffener and that these became fully formed at 446 kN [127]. This seems to agree with the change in profile predicted by the analysis at a model load of 641 kN (stiffener load = 3500 N).

The analysis indicated that yielding arose in the stiffener at 4760 N. The postbuckling range is seen to be reduced in comparison with that of the slenderer stiffeners (Figs 4.11 and 4.17). Load continued to be carried up to 5037 N, at which point the total load carried by the model was predicted to be 952.4 kN. Plastic collapse from test data was found to be in the range 950-1000 kN.

The variations in longitudinal strain with model load are indicated in Figs 4.24a and 4.24b. It is apparent that elastic buckling cannot be clearly detected in way of these gauges. A detailed examination of additional results revealed that a local plastic buckle appeared 40 mm from the clamped loaded edge and could be detected at 815 kN.

Following buckling the strains along the stiffener tip continued to increase without noticeable divergence until the yield strain (1396 με) was reached. For gauge nos 3/4, this occurred at 937 kN and at this point the strains diverged noticeably. This is also apparent in Fig. 4.25 which demonstrates that following failure a plastic buckle developed in way of transducer nos 5,6. At plastic collapse, strain reversal took place at the outer surface still in the elastic range whilst the strain along the inner surface

continued to increase. Similar behaviour was exhibited by some other gauges (Figs 4.24a, 4.24b). Plasticity developed in way of the local buckle near the clamped edge and along the stiffener tip.

4.2.3.2 Base Plate Response

In a similar manner to Model Nos. 1 and 2 the program predicted that the base plate would deflect away from the stiffener during the initial stages of loading. Yielding commenced at a load of 106.3kN at an average applied strain of 1013 με (yield strain = 1101 με) i.e. before buckling occurred in the stiffener. The volume of yielded zones increased until nearly the whole plate became plastic. Following stiffener buckling at a load of 112.75 kN, a buckle developed in the plate near midlength. At this load level the plate was behaving as a plastic membrane. Failure occurred at a load of 112.89 kN, i.e. just below the theoretical squash load of 113.01 kN. The plate subsequently carried load at the same level (Fig. 4.26).

During the test, plastic buckling was detected in the plate at a model load of 1230 kN. This is a much higher load than predicted by the analysis and it is possible that buckling had arisen earlier but was not detected.

4.2.3.3 Stiffened Plate Response

The theoretical load-end shortening curve for the stiffened plate is given in Fig. 4.27. For Model No. 5, as in the previous cases, a substantial part of the load was carried by the plate and this increased until it developed as a plastic membrane. At 1013 με the plate started yielding. This was followed by stiffener buckling at 1145 με. The local buckle in the plate developed at this point and at 1233 με the stiffener commenced yielding. It appears therefore that the load shed by the base plate precipitated failure of the stiffener. Following failure of the cross-section, the load continued to be carried at the same level since column failure did not arise.

4.2.3.4 Overall Model Response

Figure 4.28 shows that the load carried by the model cross-section as predicted theoretically increased linearly up to 828 kN. A slight change in gradient is noted at that point, following which the response continues as a straight line. At that point local buckling in the stiffened plate occurred (end shortening = 0.285 mm). At higher loads the end shortening curve increased linearly and reductions associated with yielding and failure of the stiffened plate could not be detected.

4.2.4 Model No. 8

As a result of the Model No. 7 test, local buckling was produced in the stiffener. Following renumbering, this local buckling became an (enlarged) initial distortion for Model No.8. The strains arising from the buckling were measured along the stiffener tip and are illustrated in Fig. 4.29 from which it is evident that the strains are elastic throughout. In correlating this test, the initial imperfection measurements taken after the test on Model No. 7 were used as initial distortions. These are indicated in Figs 33 [127] and 35 [127]. It is seen that the effect of the combined loading test did not produce any significant changes in the base plate profile. Comparison of Figs 32 [127] and 35 [127] shows however that two local buckles were produced in the stiffener by the combined loading test at 50 mm and 130 mm from the top loaded edge. The general profile of the stiffener was not otherwise significantly affected.

The effect of the residual strains in the stiffener and base plate arising from the buckling was not allowed for in correlating Model No. 8, because their magnitudes and distributions were not known. In principle, it would have been possible to generate the strain distributions produced by the Model No. 7 test, but certain strain gauges used to determine axiality did not operate correctly. It was therefore not possible to determine with sufficient accuracy the distribution of longitudinal strains so no simulation was attempted.

The differences in initial conditions produced departures between the theoretical and experimental results and these are considered in further detail in the next section.

4.2.4.1 Stiffener Response ($d/t_w = 30.7$)

From Fig. 4.30 it is seen that the predicted response consists of:

- elastic pre-bifurcation	(0 - 4609 N)
- post-buckling	(4609 - 4936 N)
- unloading	(4936 - 4855 N)

The geometry of the stiffener cross-section for this model was similar to that of Model No. 5 ($d/t_w = 29.3$) which was also tested under axial compression. Comparison of Fig. 4.30 with Fig. 4.23 shows that the overall response of both models is similar.

The initial imperfection profile of the stiffener shows that apart from the two localised buckles there also existed a slight tilt whose magnitude increased towards the stiffener tip. The longitudinal profile along the tip consisted of a five half-sine waveform.

During the initial stages of loading the stiffener deflections followed this profile until elastic buckling occurred at 4609 N, a slightly higher load than for Model No. 5 (4504 N). A direct comparison between the load-axial strain curves obtained experimentally and numerically (Figs 4.31a and 4.31b) cannot be made since residual strains were not allowed for in the latter case. Comparing Fig. 4.24a, 4,24b with Figs 4.31a, 4.31b for Model No. 5 shows that the effect of the larger initial imperfections is to produce a greater divergence before buckling. At buckling, no further divergence is noted and the critical buckling load which was determined from Fig. 4.30 (3951 N) corresponds to a total model load of 791 kN. The five half-sine wave profile of the stiffener did not change at this point. The test results however indicate the presence of a localised buckle near the clamped loaded edge (gauges 13/14) at a load of 345 kN. This was not predicted theoretically, possibly because of the differences in initial strain distributions.

Following elastic buckling, the stiffener continued to carry load up to 4936 N, corresponding to a plastic collapse load of 1047 kN (Fig. 4.30). At peak load, the total axial load on the model was estimated from Figs 4.31a and 4.31b to be 929 kN. During this part of the response stiffener deflections continued to increase. From Fig. 4.32 it is seen that no local buckling was predicted in the stiffener at mid-length before the peak load was reached. As in the case of Model No. 5, the reserve of post-buckling strength was lower than that observed in Models Nos 1 and 2.

Following peak load, the load carried by the stiffener decreased gradually for larger values of end-compression. The load end-compression curve (Fig. 4.30) was noted to be similar to that of Model No. 5 (same slenderness ratio). Stiffener deflections at mid-length decreased at higher applied strains and a local plastic buckle developed at a distance of 75 mm from the clamped loaded edge. It's appearance was already evident when the peak load was reached.

Plasticity was entered following stiffener buckling at 4609 N and was first apparent along the free edge, at midlength. In the post-buckling range plasticity developed further along the intersection with the base plate and as deflections increased further it became concentrated about the quarter points. The local buckle which had already developed became plastic as higher loads were applied. During the unloading part of the response, plasticity was evident in way of the local buckle and along the intersection with the base plate, the remaining volume of the stiffener behaving elastically. Overall failure was thus characterised by the appearance of a local plastic buckle; as in the case of Model No. 5, the loaded edges remained elastic throughout the loading history.

4.2.4.2 Base Plate Response

The theoretical response of the base plate was similar to that of the previously described cases (Model Nos 1, 2 and 5). The plate deflected away from the stiffener in sympathy with the initial imperfections. At midlength, a shallow sinusoidal shape was produced

whereas near the loaded edges twin peaks arose. The load carried by the plate increased until yielding occurred and then remained constant (elastic rigid-plastic material) as shown in Fig. 4.33. Following stiffener buckling, a local plastic buckle appeared in the plate. With increasing load, deflections near the stiffener buckle increased away from the stiffener as the plate deformations continued to grow. During the test, the base plate buckled plastically in two locations, both in way of the two stiffener buckles which had been produced during the testing of Model No. 7. As in the case of the other axial compression tests, plasticity arose in the central region of the plate. For Model No. 8 the onset of plasticity occurred before stiffener buckling. The loaded edges of the plate became plastic and for larger values of end compression the whole area of the plate became plastic apart from the clamped loaded edges (Fig. 4.34).

4.2.4.3 Stiffened Plate Response

The theoretical response of the stiffened plate is shown in Fig. 4.35. It is seen that since a small proportion of the load was carried by the stiffener ($A_w/A_p = 0.038$), failure was dependent on plate collapse. The stiffened plate carried load until the base plate yielded; following this, the load remained constant. Overall collapse did not occur for the range of applied loading, in agreement with test results. It is seen that stiffener failure gave rise to a localised plastic buckle in the plate which was not however extensive enough to produce overall collapse. With increased loading it is expected that plastic hinges would have developed along the loaded edges leading to overall collapse of the cross-section.

4.2.4.4 Overall Model Response

The load-carrying capability of the model as predicted theoretically is shown in Fig. 4.36. A substantial part of the load was carried by the box and the failure of the base plate at 952 kN produced only a small change in the load end-compression curve.

When failure of the stiffener occurred the model load was 929 kN. The experimental

result was 950 kN. It is thus seen that reasonably close correlastion was achieved using the simple linear relationship described in Section 4.2.

4.3 Correlation Studies of Lateral Pressure Tests

The two models tested under lateral pressure (Nos. 4 and 6) were placed inside a cylindrical pressure chamber filled with water. The test set-up is shown in Fig. 4.6. It is seen that the pressure chamber was positioned on an I-section column supported by the lower platen of the axial compression machine. Following the fitting of the model inside the chamber, the upper piston was moved into position. Access holes for strain gauge and transducer wires, air bleed and water fill are shown in the diagram.

Water was fed to the chamber using a hand-operated pump and at the same time air was bled using a valve located on the upper piston. At zero pressure, a small gap was maintained between the disc and the upper surface of the model. The axial compression machine was operated in displacement control during the test and thus a constant displacement could be maintained between the upper and lower platens. During the test, measurements were taken at pressure intervals of 50 kN/m^2. A small pressure load was exerted on the upper surface of the model since the applied loading was hydrostatic. During the initial stages of loading and prior to buckling the stiffener and plate can be considered as a beam clamped at both ends. Under these conditions, the longitudinal strain in the stiffener tip varies from compressive at midspan to tensile at the ends. At buckling, the parabolic shape of the strain distribution changes because redistribution occurs. The strain measurements obtained during the test were thus used to determine the lateral buckling pressure for the stiffener. The same approach was used to interpret the results from the numerical analysis and comparisons between the predicted and experimental local distributions for the two models are given in Tables 4.6 and 4.7. The results obtained from the numerical analysis procedure are presented in the form of :

- Pressure - longitudinal stiffener tip strain diagrams
- Pressure - lateral deflection diagrams (stiffener, base plate)
- Growth of plasticity with pressure (stiffener, base plate)

4.3.1 Model No. 4

4.3.1.1 Stiffener Response ($d/t_w = 37.5$)

A brief description of the behaviour of a stiffener whose associated plating is loaded under lateral pressure is given in [127], Section 5.3. For pre-bifurcation loads, the longitudinal strains along the stiffener tip vary from compressive at midspan to tensile at the ends. Figure 4.37 shows the distribution obtained numerically at various stages of loading. The variation of longitudinal strain along the stiffener tip and lateral deflections in way of the transducers is given in Figs 4.38 and 4.39 respectively. Compressive strains of increasing magnitude develop during the pre-buckling range and minimal divergence is observed. This indicates that tensile strains acting at the clamped ends reduced the effect of initial imperfections. Figure 4.39 confirms that negligible lateral movement of the stiffener is predicted in the pre-buckling range. The observed deflections were however much larger and this may be due to differences in initial imperfections, although symmetry would suggest any lateral deflections should be minimal.

During the test, buckling occurred at midspan at a pressure of 440 kN/m^2 and a local strain of 950 $\mu\varepsilon$. Corresponding theoretical results are 515 kN/m^2 and 1045 $\mu\varepsilon$ respectively. A full comparison for the remaining strain gauges is given in the following table.

Table 4.6 Model No.4 Comparison of Buckling Strains and Pressures

Strain Gauge Pair	1/2	3/4	5/6	7/8	11/12	13/14	15/16
Critical strains	+334	477	909	1045	909	477	+363
($\mu\varepsilon$)	*	360	875	950	950	38	*
Critical Buckling	552	549	530	515	521	549	602
Pressure (kN/mm^2)	*	440	465	440	440	440	*
Plastic Collapse	890	890	890	*	894	894	890
Pressure (kN/mm^2)	710	710	*	610	710	*	780

Unless indicated otherwise, strains are compressive.

During the test, two alternating local buckles were produced at midspan, of total length approximately 80 mm. The predicted profile consisted of a two half-sine waveform with nodes at approximately 100 mm from each other. This difference in buckled shapes may have contributed to the differences between the observed and predicted values of the local strains. The predicted buckling and plastic collapse pressures are consistently larger than the test values.

The onset of plasticity in the stiffener was predicted to occur at the ends adjacent to the free edge. At these positions high tensile local strains developed in the longitudinal direction. Yield grew to a full through-thickness phenomenon at 250 kN/m^2 but did not spread to other parts of the stiffener. At 475 kN/m^2, full-depth yielding had spread along the clamped ends. Following buckling, plasticity developed across the stiffener breadth at midspan, covering a triangular region with one apex at the intersection with the base plate (Fig. 4.40).

The effect of pressure on the longitudinal strains in the plastic range is shown in Fig.

4.37. With increasing load the magnitudes of the local strains increased but the regions of compressive/tensile strains remained essentially unaltered. Following buckling, tensile strains developed on either side of the buckle at midlength (Figs 4.37b and 4.37c).

4.3.1.2 Base Plate Response

Since the expected failure mode was torsional buckling of the stiffener, it was anticipated that following its suffering elastic lateral buckling, an additional load would be carried by the base plate. That is, following stiffener buckling, overall response would be governed by plate response and the contribution of the stiffener would be small. The plate dimensions were chosen such that it's failure would precede any failure in the supporting box and in addition, it was expected that any longitudinal in-plane movement in the stiffened plate boundaries would be small. On this basis, the plate end boundaries were modelled as being rotationally clamped and restrained. During the test, a small amount of in-plane movement in the longitudinal direction was observed (0.07 mm) but following removal of the load, the ends of the stiffened plate returned to their original positions.

The failure mechanism of a thin long plate clamped at the edges and fully built-in has been established and described in detail in earlier work [128,129,130]. The importance of membrane stresses in carrying additional loads has been demonstrated theoretically and experimentally and it has been shown that collapse is resisted at pressures considerably in excess of those at which first yield occurs. Initial yield commences at the plate edges midway along the length. With further load, plasticity spreads towards the corners and a centre plastic hinge then forms. The centre hinge subsequently expands towards the edges of the plate until finally a pure plastic membrane is formed. Even at this stage, however, additional load may be carried due to the action of the membrane stresses.

The predicted change in gradient in the pressure-lateral deflection curve (Fig. 4.41) associated with the formation of edge plastic hinges occurs at approximately 600

kN/m^2. The corresponding test value was 620 kN/m^2. Following this, it is seen that the load continues to be carried until 1000 kN/m^2 but with increasing lateral deflections. Figure 4.42 shows the spread of plasticity in the base plate at various stages of loading, following first yield. At 850 kN/m^2, (Fig. 4.42b) the centre hinges have grown along each edge. The effect of further loading is seen in Fig. 4.42c in which approximately half the plate area is elasto-plastic with plasticity spreading towards the ends. It is seen that the growth of plasticity is inhibited along the intersection with the stiffener, since a certain proportion of the total load is borne by it.

Figure 4.38b shows the variation in longitudinal strains at gauge nos 17 and 19 which were located at midspan in the plate at positions equidistant from the stiffener. A change in gradient is noted at 600 kN/m^2 and the axial strains start decreasing until compressive strains arise. An examination of the complete strain field confirmed that tensile longitudinal strains acted at other parts of the plate. Along the longitudinal edges, however, and in way of gauge nos 17 and 19 a local compressive strain field developed. This is attributed to the action of shear forces along these edges which restrained the movement of the plate.

4.3.2 Model No. 6

4.3.2.1 Stiffener Response ($d/t_w = 29.6$)

Model No. 6 was also tested under lateral pressure and differed from Model No. 4 in that a stockier stiffener was used. Although the external loading was only lateral pressure, a small amount of axial compression also acted on the model. For this model, this caused difficulties in correlating the distributions of longitudinal strains along the stiffener tip in the elastic range which was further complicated by the fact that since the box was not completely rigid, a limited amount of rotation of the stiffener ends took place.

Figures 4.43a and 4.43b which show the variation of longitudinal strain with lateral

pressure are used to obtain critical local buckling pressures. The results are summarised in the following table.

Table 4.7 Model No.6 Comparison of Buckling Strains and Pressures

Strain Gauge Pair	1/2	3/4	5/6	7/8	11/12	13/14	15/16
Critical strains ($\mu\varepsilon$)	+409 *	723 *	1363 590	1568 1070	1318 1100	704 1100	+409 *
Critical buckling pressure (kN/mm^2)	600 *	600 *	600 675	570 675	600 675	600 650	600 *

The diagrams show that little divergence occurred prior to buckling since the magnitudes of the initial distortions were small. At midspan, elastic buckling was predicted to occur at a pressure of 570 kN/m^2 and a strain of 1568 $\mu\varepsilon$. The corresponding test results are 675 kN/m^2 and 1070 $\mu\varepsilon$.

The critical buckling pressures and strains were obtained from the test results using the lateral pressure-longitudinal strain diagrams and also by observing the change in shape of the strain distribution along the stiffener tip. Using this last criterion, the buckling pressure was estimated to be 682 kN/m^2. Both results appear to agree reasonably well with the average predicted buckling pressure of 595 kN/m^2, although the predicted local critical strains are greater. From Fig. 4.44 lateral buckling appears to have occurred at 570 kN/m^2. The spread of plasticity in the stiffener is indicated in Fig. 4.45.

No further load increments were applied beyond 1000 kN/m^2 because divergence of the numerical procedure occurred; the plastic collapse level for the stiffener was thus not

reached (test result = 1550 kN/m^2).

4.3.2.2 Base Plate Response

It was expected that the plate behaviour for this test would be broadly similar to that of Model No. 4. The increase in lateral deflection is plotted against pressure in Fig. 4.46. It is seen that at midlength (transducer no.8) a change in gradient occurred at approximately 600 kN/m^2. At this pressure the stiffener buckled and load was shed to the base plate. The edges of the base plate became elasto-plastic and at 850 kN/m^2 the central portion of the plate also became elasto-plastic. Further loads were accompanied by additional increases in lateral deflections and large deflection effects meant that the lateral pressure load was carried by membrane strains in the plate.

A comparison of predicted and measured deflections showed however that the measured values were substantially smaller than the predicted ones. This may have occurred because of differences between the actual and theoretical load distributions at the ends which caused plasticity to spread in the theoretical model at lower pressure levels, leading to earlier failure.

4.4 Correlation Study of Combined Loading Test

Two models were originally scheduled for combined loading tests. Due to problems that arose during the testing of Model No. 7 however, this was not carried out to completion and the same stiffened plate was re-tested under axial compression alone, as Model No. 8. Thus in this section only one combined loading test, Model No.3, is reported. The layout of the test rig used is shown in Fig. 4.6.

For Model No.3 the stiffener depth/thickness ratio was 38.3. The effects of initial imperfections and yielding were included in the numerical procedure in the same manner as for the previous analyses. Boundary conditions are as shown in Fig. 4.8 and are described in detail in Section 4.1.3. Results from previous tests were used to

determine a linear relationship between the lateral pressure and applied edge compression (Fig. 4.9) which was implemented during the test. The same relationship was used in the theoretical analysis.

4.4.1 Model No. 3

4.4.1.1 Stiffener Response

In this test the loading on the stiffener consisted of the following:

- a component of the total axial compression applied to the model by the upper and lower platens.

- an interactive force along the line of attachment to the base plate due to the out-of-plane behaviour of the plate, resulting from the lateral pressure and amplified by the axial load.

From Fig. 4.6 it is seen that the model was totally immersed in water inside the pressure chamber. In calculating the axial load on the model during the test, account was taken of the effect of hydrostatic loading on the model (reference (127), Appendix 2). During preliminary runs it was found that the longitudinal strains along the stiffener tip did not agree well with those measured during the test. This was attributed to, firstly, the fact that the applied compressive load was not distributed uniformly along the transverse edges of the stiffener and secondly, that the box section to which the stiffened plate was welded to was not infinitely rigid.

Both factors contributed to a limited amount of rotation of the ends of the stiffener. In order to overcome the discrepancies that were observed, a modified, linearly varying distribution of displacements was applied and adjusted so that reasonable agreement between the theoretical and experimental strain distributions was obtained in the pre-

buckling range. The same linear distribution was then applied throughout the complete load cycle. The resulting strain distributions at other loads are also indicated in the same diagram.

Theoretical results for the growth of longitudinal strain along the stiffener tip are given in Fig. 4.47. The locations of the gauges are as for the other tests (Fig. 4.4). The results obtained for local buckling are summarised in the following table and are compared with test results.

Table 4.8 Model No.3 Comparison of Buckling Strains and Loads

Strain Gauge Pair	3/4	5/6	7/8	11/12	13/14
Critical Strains	580	*	627	651	604
($\mu\varepsilon$)	510	500	*	425	475
Critical Buckling	191	*	191	191	191
Load (kN)	150	150	*	150	150
Critical Buckling	78	78	78	78	78
Pressure (kN/m^2)	61	51	*	61	61
Plastic Collapse	320	*	344	332	344
Load (kN)	325	325	(325)	325	325
Plastic Collapse	130	*	140	135	140
Pressure (kN/m^2)	131	131	(131)	131	131

The theoretical critical stiffener strains are seen to be larger than those obtained experimentally. It was also noted that the theoretical profile of the strains changed when plastic collapse occurred and gave rise to two dips near midlength which did not appear

in the corresponding test distribution. It is possible that such reductions did arise but were not detected because the strain gauges were not positioned at appropriate locations.

The theoretical critical buckling strain along the stiffener tip at midspan is seen from the table to be 627 με; the relevant pressure is 78 kN/m^2. Corresponding test results for the midspan position were not available because of damage to the strain gauges. A re-examination of Fig. 4.47 shows however that divergence arose in the strains at much lower load levels, making it difficult to pinpoint accurately the critical buckling load. This is also evident in Fig. 4.48 in which lateral deflections of the stiffener tip are plotted against lateral pressure.

Another factor contributing to this discrepancy is the changing rotational rigidity of the loaded edges of the stiffener. It is not possible to accurately model the behaviour of the loaded edges since the conditions there change with increasing load.

The critical buckling load may alternatively be obtained from the load-end shortening response of the stiffener (Fig. 4.49). A change in gradient is noted at approximately 2000 N corresponding to a model load of 198 kN and a lateral pressure of 80 kN/m^2. The applied compressive strain at this load was 250 με and 550 με at the lower and upper edges of the stiffener respectively (mean = 400 με). Differences in this case are 33% and 25% for the stiffener tip strains and buckling loads respectively and are larger than those estimated previously.

During the test the stiffener buckled into three half-sine waves along its tip. The same profile was generated by the numerical analysis. A comparison of the deflections showed that in the pre-buckling range, the observed deflections were much larger than the predicted ones. Following buckling, however, and in the plastic region, the deflections agreed fairly well. At the peak load of 577 kN and 231 kN/m^2 pressure, the deflection of the stiffener tip at midlength was 3.45 mm (test) and 3.90 mm (theoretical) (Figs 68 [127] and 4.48). The average theoretical and observed plastic collapse loads

(Table 4.8) are 141 kN/m^2 and 131 kN/m^2 respectively and these differ by approximately 7%.

Alternatively Fig. 4.49 may be used and from this the theoretical plastic collapse load is found to be 2904 N at an end-compression of 0.137 mm. This corresponds to a total load on the model of 581 kN (233 kN/m^2) and is seen to be higher than the previously determined result.

The longitudinal midlayer strains remained compressive during the whole load cycle because the applied axial load dominated the response. Plasticity spread following elastic buckling from the tip at midlength in the region of the buckle: it was first observed at an axial load of 267 kN (pressure = 107 kN/m^2). At peak load, the central region of the stiffener was elasto-plastic, the loaded edges remaining elastic. During unloading, the profile changed to a single half-sine wave which remained when all loading was removed. Plasticity was confined to a narrow band at midlength the remaining part of the stiffener behaving elastically (Fig. 4.50).

4.4.1.2 Base Plate Response

The combination of axial compression and lateral pressure that was applied to the model ensured that the plate deflected away from the stiffener, in sympathy with the initial imperfections. The plate profile consisted of a single half-sine wave form in both the longitudinal and transverse directions. At the lower levels of loading, the shape of the transverse profile was not noticeably affected by the presence of the stiffener. At loads exceeding 250 kN and up to stiffener collapse however, a flattening was noted in the vicinity of the stiffener. The variation of lateral deflection with pressure is shown in Fig. 4.51. It is seen that the response is linear until stiffener failure, at which point a change in gradient occurs. The longitudinal strains remained compressive throughout the load cycle, the response being dominated by the axial compression. Plate buckling did not occur and the same profile was maintained throughout.

Plasticity was initiated along the loaded edges near the junction with the stiffener at a load of 396 kN (the stiffener started buckling at 200 kN and 80 kN/m^2 pressure). A limited number of nodes along the unloaded edges at mid-length also became elasto-plastic. During unloading, all plate nodes behaved elastically. The residual deflection in the base plate (Fig. 4.51) arises because of plastic straining during the loading path.

The load end-shortening response of the plate is shown in Fig. 4.52. It is seen that the behaviour is linear up to approximately 58 kN at which point stiffener collapse occurred. The relatively small effect of the induced plasticity is evident from the almost complete recovery of the end shortening curve.

4.4.1.3 Stiffened Plate Response

The response of the stiffened plate was similar to that of the axially loaded test specimens described previously. The effect of lateral pressure was seen to be of secondary importance. The major part of the applied compressive load was borne by the base plate which did not fail.

The load end-shortening response for the stiffened plate (Fig. 4.53) is similar to that obtained for the base plate, the differences being attributed to the presence of the stiffener which carried a small proportion of the load. Interaction effects for this model were evident only in the transverse profile of the base plate but did not affect the overall response of the stiffened plate.

4.4.2 Model No. 7

Model No. 7 was originally scheduled to be tested under combined loading involving axial compression and lateral pressure. It was not possible however to carry out the test as originally planned because of problems that became apparent at the initial stages of loading. Failure of some strain gauges resulted in lack of axiality in the model and with increased loading the top end of the model became indented by the hardened steel ball

transmitting the load. The test was stopped and it was found that local buckling had occurred in the stiffener. The resulting distribution of measured strains along the stiffener tip is given in Fig. 4.29. It was decided to repeat the test and apply axial compression alone because of the general difficulty in aligning the model axially within the pressure chamber. Initial imperfections were measured and the test carried out as Model No. 8, described in Section 4.2.4.

4.5 Concluding Remarks and Comparisons with Other Formulations

The response of seven flat stiffened plates has been compared in detail with results obtained from a large-deflection elasto-plastic analysis procedure. Several aspects of the behaviour of the stiffener and the base plate have been examined and critical buckling strains and loads and plastic collapse loads have been compared with test measurements. The results from the correlation studies are summarised in Table 4.9 overleaf. Theoretical buckling and plastic collapse loads and strains have been obtained using:

load end compression diagrams	(overall behaviour)
strain distributions along the stiffener tip	(local behaviour)

Theoretical and observed buckling modes have also been compared and the growth of plasticity has been described. Of the seven cases studied, four involved axial compression, two involved lateral pressure and one involved combined loading.

For the cases involving axial compression the predicted stiffener local buckling loads were much larger than the test values. Much better agreement was obtained in the estimation of the plastic collapse loads. A simple check was carried out on the test results and it was found that the measured externally applied end-compressive loads and the local strains at buckling levels did not satisfy the simple linear stress-strain relationship as expected; as described earlier in this Chapter this was used to estimate the total load on the model in the theoretical approach. At plastic collapse better

Table 4.9 Correlation Studies - Summary of Results

Model No	1	2	5	8	4	6	3
Loading	Axial	Axial	Axial	Axial	Lat. Pressure		Combined
Critical Buckling	775 (1)	549	1145	1140	1045	1568	627
Strain (με)	660	700	1200	1000	950	1070	472
Critical Buckling	475	457	815	863	-	-	191
Load (kN)	340	350	480	345	-	-	156
Critical Buckling	-	-	-	-	515	570	78
Pressure (kN/m^2)	-	-	-	-	440	675	63
Plastic Collapse	775	900	952	914	-	-	344
Load (kN)	935	975	975	950	-	-	325
Plastic Collapse	-	-	-	-	890	- (2)	140
Pressure (kN/m^2)	-	-	-	-	706	1550	131
Buckling Modes	3	3	2/6	5	4	4	3
	3/4	5	2/6	4	4	5	3
Base Plate	No	No	Yes	Yes	No	No	No
Failure	No	No	Yes	Yes	No	Yes	No
Overall Collapse	No	No	No	Yes	No	No	No
of Stiffened Plate	No	No	No	Yes	No	No	No

(1) (theory/test results)

(2) plastic collapse pressure not reached

agreement was obtained and this indicates that the fault may lie with the instrumentation used. For this reason the measured critical local strains and the average applied edge compressive strains were treated as a more reliable basis for purposes of comparison with the predicted values.

In the case involving combined loading (Model No. 3) it was found necessary to allow for stiffener end-rotation and this gave results which correlated better with the test values. However other problems which have already been discussed did not allow the buckling loads and strains to be predicted with the accuracy that was hoped for. Nonetheless the plastic collapse loads were predicted to a satisfactory degree of accuracy.

In the remaining part of this section a comparison of the critical buckling strains measured during the axial compression tests with several analytical formulations will be carried out. The results of this comparison are contained in Table 4.10. The analytical approaches which were checked are included in Appendix A and have been proposed or are currently in use in design codes to predict tripping. In all cases the loaded edges of the stiffener are assumed simply supported and various assumptions are made for the rotational restraint along the intersection with the base plate.

The data given in Table 4.10 represents elasto-plastic stiffener average buckling strains. From the table it is apparent that the results fall into two distinct categories: those in which some form of rotational restraint is assumed and those in which the stiffener is treated as being simply supported. In the former case the prediction of tripping stresses is significantly more accurate, for both slendernesses (30, 40).

In cases (4), (8) and (9) elasto-plastic collapse is allowed for by use of the Ostenfeld-Bleich parabola and the structural proportional limit p_r, set equal to 0.5.

Table 4.10 Comparison of Critical Buckling Strains for Several Design Formulae with Test Results and Numerical Analysis

Case			d/t = 40	d/t = 30
1	Test Results		**680** (1)	**1100** (1)
2	Numerical Analysis		662 (1)	1151 (1)
3	R.N. code [141]		253	440
4	Faulkner [72]		1000 (913)(2)	1297
5	Timoshenko [144]	(S-S-S-F)	267	470
6	Timoshenko [144]	(S-C-S-F)	750	1338
7	Rogers and Dwight [83]		322	466
8	Adamchak [72]	($C_0 = 0$)	269	439
9	Adamchak [72]	($C_0 > 0$)	956	1145

(1) This represent the average value for the two tests for this stiffener slenderness. Average dimensions and yield stresses were used to determine tripping stresses using the design formulae.

(2) The value in brackets is for a simply supported base plate.

The Royal Navy code assumes that the stiffener is simply supported along the intersection wih the base plate and consequently the mode shape consists of a single half-sine wave. This leads to an unnecessarily conservative result which ignores the support provided by the plating.

Faulkner's equation predicts elasto-plastic tripping at 207 N/mm^2 (1000 $\mu\varepsilon$) and an allowance is made for the rotational restraint (constant value, given by $C_o = Et^3/3b$). Collapse depends upon plate behaviour and thus the plate boundary conditions affect the response of the stiffener indirectly. Both clamped and simply supported edges were checked and it was found that for the simply supported case the stiffener buckling load was about 10% lower (Table 4.10).

The equation used by Rogers and Dwight contains a term which allows for pure torsion and an additional term which includes the longitudinal slenderness (a/d) of the stiffener. Simply supported edges all round are assumed and thus the result is similar to that obtained using the R.N. code equation.

Timoshenko's two equations give fairly good estimates of the buckling stress although no allowance is made for the presence of the shell plating. For the simply supported case (S-S-S-F) there is no significant reduction in buckling stress (value of the constant k) for long stiffeners (aspect ratios greater than 3). For the case in which the attached edge is assumed clamped (S-C-S-F) a minimum value is reached for an aspect ratio of 1.6.

Adamchak's equations allow for plate behaviour and several approaches are suggested with regard to estimating the rotational restraint. In the tabulated results a 'minimum' restraint has been assumed. Nevertheless, Table 4.10 shows that the value of C_o is overestimated by both this approach and that proposed by Faulkner and consequently the predicted buckling modes do not agree with the ones observed. During the tests, up to 6 half-sine waves were noted along the stiffener tip for the four cases in question,

whereas the analytical predictions gave values of 10 and 11. It is therefore necessary to treat these formulations with caution since the tripping stresses which are predicted may be higher than those which can actually occur. The comparison indicates that a 'minimum' restraint approach is required in order to obtain realistic values for tripping stresses and also to predict buckling mode shapes with some degree of accuracy. An allowance for plate flexure may give more accurate results for the rotational restraint; this can be included in formulations suitable for use at the preliminary design stage.

CHAPTER FIVE

PARAMETRIC STUDIES ON THE LOCAL BEHAVIOUR OF FLAT STIFFENED PLATING

In this Chapter, results from a series of studies on stiffened plates under axial compression are presented. The aspect ratios considered were with one exception (a/b = 4) limited to a/b<2 (short panels) and the stiffener was proportioned so that lateral torsional elasto-plastic buckling occurred. The panel analysed was treated as forming part of a continuous section of plating bearing several stiffeners of identical profiles and dimensions (orthogonally stiffened grillage). Out-of-plane support was assumed to be provided by deep transverses along the loaded edges, as indicated in Fig. 2.8. A fuller description of the boundary conditions used is given in Section 2.7. A 'standard' panel whose dimensions and material properties were varied was chosen, bearing in mind the range of interest in practical cases.

Table 5.1 Properties of Standard Panel

Aspect Ratio	a/b	1
Slenderness	b/t_p	60

Table 5.1 (cont'd)

Stiffener Slenderness	d/t_w		10
Young's Modulus	E	kN/mm^2	207.0
Poisson's Ratio	ν		0.3
Plate yield stress	σ_{op}	N/mm^2	245.0
Stiffener yield stress	σ_{ow}	N/mm^2	245.0

The non-dimensional slenderness ratios for the plate and stiffener (β_p, β_w) based on the above data are 2.064 and 0.344 respectively. The effect of residual stresses was not studied, the purpose being to study stress-free plates initially. As indicated in Fig. 2.8, axial compression is applied as a uniform displacement along the loaded edges; compression is applied until the average strain reaches three times the yield strain.

5.1 Base Plate and Stiffener Aspect Ratio

Elastic theory states that unstiffened rectangular plates buckle such that each buckle has an aspect ratio of approximately unity. When elasto-plastic buckling is considered, it has been shown analytically by Ueda and Tall that for simply supported plates the lowest ultimate load is carried when the aspect ratio lies in the range $0.8 > a/b > 0.7$ [131]. Moxham [132] observed in large scale tests that as the deformation proceeded, there was an initial buckling phase with several half-waves and afterwards only one plastic buckled zone was developed, with an aspect ratio of 0.875. Longer plates in general are stiffer and stronger but show a steeper post-collapse unloading. Frieze [41] found that the effect of aspect ratio was dependent on the magnitude of initial distortions and the boundary conditions. He concluded that the results for a square plate would generally give conservative estimates of the strength and stiffness of long plates.

Concerning the stiffener, there appears to be a lack of understanding with regard to the

effect of length on its lateral-torsional behaviour. It can be shown that the lowest tripping stress occurs in one half wavelength and depends upon the length, as in the case of columns. This provides a basis for choosing the spacing of intermediate lateral supports [2] and has been used in design codes.

If however the effect of the plating is included in the analysis by assuming a rotational restraint along the stiffener toe, the minimum tripping stress does not any more depend upon the length [2]. On this basis the usefulness of tripping brackets is brought into question and it is therefore important to investigate further the effect of length on stiffener behaviour.

Of the methods used in recent years to analyse stiffened plates, numerical analysis routines and the Perry-Robertson effective width approach have been amongst the most successful. Carlsen [133] used the program STAGS which employs the finite difference method. In this, the stiffener is assumed to fail by an overall collapse mechanism and torsional failure is not considered. For stocky panels, the program predicted failure in the stiffener due to plastic squashing of the section and for high aspect ratios failure with rapid unloading occurred shortly after yielding along the free edge.

In this study the value of a/b was varied by changing the length of the cross-section in conjunction with the plate imperfections. This was done so as to maintain throughout the same level of curvature in the plate. When considering plate aspect ratio a slender stiffener ($d/t_w = 40$) was used and its out-of-plane imperfections were set equal to zero. The purpose of this was to permit plate behaviour to be studied before introducing a combined flexural- twisting mode of failure in the stiffener which would interact with that of the plate. The ratio of stiffener/plate cross-sectional area was kept constant at 0.16.

When considering the effect of aspect ratio on the stiffener, the values of initial distortions used were based on the average values specified in the 1982 edition of the 1977 DnV Offshore Rules [70]. The base plate initial distortions are given as a function

of breadth, the maximum acceptable being b/100. For flatbar stiffeners the initial distortions are specified as a function of length, the maximum acceptable being 0.0015a. In this study the values used were b/200 and 0.00075a respectively. For both the base plate and the stiffener a sinusoidal profile was used.

The results obtained in each case are presented in terms of average stress-strain curves and peak load-aspect ratio curves. Average stress-strain curves for the base plate are given in Fig 5.1a. These cover the range $0.40 \leq a/b \leq 2.0$, which includes the minimum strength curve. Peak loads are plotted against aspect ratio in Fig. 5.1c and extend up to a/b = 2.0. The curves included in Fig. 5.1a are seen to be of generally similar shape and a reduction in stiffness due to yielding is noted above $0.60\varepsilon_0$. No sharp reduction is noted at the peak load and this is characteristic of the range of aspect ratios considered. In the post-peak range the drop in load carried is not large and is uniform throughout the loading range considered. Figure 5.1c shows that at aspect ratios greater than 1.5 the peak load approaches the squash load although it is expected that imperfection profiles with more than one half wavelength would reduce it. The reduction in the peak load of the stiffener shown in Fig. 5.1c is due to longitudinal flexural effects. Elasto-plastic collapse occurred at midlength along the free edge and plasticity gradually spread in the transverse direction, towards the intersection with the base plate. The curve given for the stiffened plate is similar to that of the base plate because the stiffener was slender ($d/t_w = 40$) and carried a small proportion of the total load (15%).

Corresponding strength curves for the stiffener are shown in Figs 5.2a and 5.2b. It is seen that for the slender stiffener ($d/t_w = 40$) the peak load decreases as the length is increased and the transition to the post-failure regime becomes more marked with increasing panel length. Stiffener stress-strain curves for plates with aspect ratios of 1.0 and 2.0 and 4.0 are shown in Fig. 5.2b. It is seen that there is no substantial decrease in the peak load between the three curves. The drop following peak load becomes much sharper with increasing aspect ratio and for an aspect ratio of 4.0 the pre-peak stiffness is higher as is the peak load. Similar results were obtained for an aspect ratio of 3.0

(not included in the diagram).

These two diagrams show that stiffeners which do not fail by tripping but in a longitudinal flexural mode can carry up to 90% of the squash load even for high slenderness ratios (d/t_w = 40). However if a lateral-torsional mode is introduced, the maximum load decreases considerably even for relatively stocky stiffeners; Fig. 5.1 shows that for a stiffener of slenderness of 10 the peak load is reduced to approximately 50% of the squash load. Longer plates have not been studied because

- overall behaviour is then also affected by column effects and
- it is necessary to investigate further the effect of initial imperfections on the response of plates in order to employ the appropriate profiles in the study of the stiffened plate.

The effects of initial imperfections will be considered in more detail in the next section.

It has been seen that aspect ratios at which minimum strength curves are obtained for the base plate and stiffener do not coincide and therefore if a design procedure is to be based on this type of approach, it is necessary to consider the behaviour of the plate and stiffener separately. On the other hand, if the minimum strength curve of the overall cross-section is used this will lead to the choice of a unique aspect ratio for a particular geometry. The main purpose of the studies which follow is to obtain comparative results and for this reason the aspect ratio was kept constant and equal to the minimum for that of a base plate of slenderness b/t_p= 60. For stockier cross-sections the critical value of a/b would be expected to decrease and for more slender stiffeners to increase. For a stiffener/plate area ratio of 0.66 the minimum strength was predicted to occur for at a value of a/b = 0.50.

5.2 Initial Imperfections

The initial imperfections considered were limited to sinusoidal out-of-plane distortions.

Base plate and stiffener imperfections were examined separately and for the base plate the range considered was $0.025 \leq w_{op}/t_p \leq 0.25$, with zero stiffener imperfections. For the stiffener the range considered was $0.0 \leq w_{ow}/t_w \leq 0.0015a$ with an imperfection in the base plate of b/200. These represent the range of values to be found in practical panels used in the construction of offshore structures, as envisaged by the DnV Rules 70.

The response of the base plate is, as expected, influenced by imperfections to a much greater extent than that of the stiffener (compare Figs 5.3a and 5.3b). A reduction in pre-peak stiffness was observed and this was accompanied by a corresponding reduction in peak load. For an imperfection of $0.025t_p$ the peak load was found to be $0.97\ \sigma_{op}$ and for an imperfection of 0.25t this dropped to $0.75\ \sigma_{op}$, a reduction of 22%. In the post-collapse range, the load carried gradually reduced for the smaller imperfections. For the larger imperfections, the strength curves flattened out and the load carried for an imperfection of $0.15t_p$ (average value) was $0.68\ \sigma_{op}$ at three times the yield strain.

For the smaller imperfections, yielding commenced at $0.92\varepsilon_o$ and developed over approximately three quarters of the total area of the base plate. In the post-peak range, some unloading was observed. For larger imperfections plate (surface) yielding commenced at significantly lower compressive strains ($0.60\varepsilon_o$ for an imperfection of $0.25t_p$) indicating the influence of initial imperfections on material behaviour.

The effects of imperfections in the base plate on the stiffener, base plate and stiffened plate are shown in Figs 5.3a-c. Figure 5.3b shows that, for slender stiffeners, with increasing end-compression the effect of the imperfections increases. A reduction in stiffness is observed before the peak load is reached. This drops from $0.98\ \sigma_{ow}$ ($w_{op} = 0.025t_p$) to $0.90\ \sigma_{ow}$ for an imperfection of $0.25t_p$ (a drop of 9%). In the post-failure range, the effect of plate imperfections on the stiffener is seen to be much less signficant and the strength curves converge to a value of $0.78\ \sigma_{ow}$. For stockier stiffeners ($d/t_w = 10$), the influence of plate imperfections was found to be much

smaller.

For the larger plate imperfections, the onset of yield in the stiffener occurred much earlier, although the change was not found to be significant (from one yield strain at $w_{op} = 0.025t_p$ to $0.95\varepsilon_0$ at $0.25t_p$), the uniaxial yield strain being 1184με. For very small plate imperfections the stiffener was capable of attaining full yield.

The strength curves of the stiffened plate (Fig. 5.3c) generally follow those of the base plate (Fig. 5.3a) and the above-mentioned comments apply in this case also. For larger values of A_w/A_p it would be expected that stiffener behaviour would affect overall behaviour to a much greater extent, particularly for the larger initial imperfections.

The effect of imperfections on slender stiffeners ($d/t_w = 40$) is indicated in Fig. 5.4. The range of imperfections studied was $0.025 \leq w_{ow}/t_w \leq 0.25$. There is a reduction in pre-peak stiffness with increasing imperfections caused by earlier yielding and this is followed by a corresponding reduction in peak load. After failure the load-carrying capacity reduces uniformly for all the curves in question. The effect of stiffener imperfections on plate behaviour is small, as shown in the adjacent diagram but for higher values of A_w/A_p it would be expected to be more pronounced.

A study of the behaviour of stocky stiffeners ($d/t_w = 10$) was also carried out over the same range of imperfections. No noticeable reduction in load-carrying capacity was observed in these and for slendernesses in the range $40 \geq d/t_w \geq 10$ the effect could be quantified by some form of interpolation.

Strength curves for stiffened plates designed to BS5400 and DnV Rules are shown in Figs 5.5a-b. The stiffened plate with zero imperfections is included for purposes of comparison. The DnV rules permit larger imperfections than the BS5400 rules and as a result:

i) the load-carrying capacity of the whole cross-section is reduced

ii) the stiffness of both the plate and the stiffener are also reduced.

The differences in ultimate strength noted from the diagrams are 30% and 20% for the base plate and the stiffener respectively. The values of imperfections used have been tabulated in the diagrams in non-dimensionalised form so that they can be compared directly.

5.3 Base Plate Slenderness

The value of b/t_p is the one of the most important geometrical parameters in stiffened plate design because it has direct influence on the overall load-carrying capacity of the cross-section and also its mode of failure. The range of values considered here covers those commonly encountered in marine structures ($30 \leq b/t_p \leq 85$). Four values have been used, namely 30, 40,60 and 85. The first two of these correspond to 'stocky' plates, the latter two to 'slender' plates. The aspect ratio of the cross-section was maintained constant at 0.60, as discussed earlier. Three values of the ratio of stiffener/plate area were considered, namely 0.11, 0.20 and 0.30 and results for these are given in Figs 5.6-5.17.

The results for each case are presented as average stress-strain curves for the:

a) flatbar stiffener

b) base plate

c) stiffened plate

The effect of base plate slenderness is indicated for each stiffener slenderness and stiffener/plate area ratio and strength curves for four values of b/t_p are plotted in each diagram. The peak loads obtained from these curves have been tabulated and are included in Tables 5.2a-c. Each of these tables corresponds to one value of stiffener to

Table 5.2a Effect of Base Plate and Stiffener Slenderness for Short Stiffened Plates

$a/b = 0.60$ $\sigma_{op} = 245\ N/mm^2$ $\sigma_{ow} = 245\ N/mm^2$

$A_w/A_p = 0.1,1$ $w_{op} = b_p/200$ $w_{ow} = 0.00075a$

d/t_w	b/t_p	β_p	β_w	σ_p/σ_{op}	σ_w/σ_{ow}	σ/σ_o
8	30	1.03	0.275	1.0	0.98	1.0
8	40	1.376	0.275	0.91	0.77	0.89
8	60	2.064	0.275	0.73	0.71	0.73
8	85	2.924	0.275	0.48	0.65	0.48
10	30	1.03	0.344	1.0	0.97	1.0
10	40	1.376	0.344	0.91	0.79	0.89
10	60	2.064	0.344	0.73	0.70	0.73
10	85	2.924	0.344	0.49	0.62	0.49
16	30	1.03	0.55	1.0	0.94	0.98
16	40	1.376	0.55	0.91	0.82	0.90
16	60	2.064	0.55	0.73	0.79	0.73
16	85	2.924	0.55	0.48	0.72	0.50
20	30	1.03	0.688	1.0	0.93	0.99
20	40	1.376	0.688	0.91	0.83	0.90
20	60	2.064	0.688	0.73	0.79	0.73
20	85	2.924	0.688	0.48	0.74	0.50

Table 5.2b Effect of Base Plate and Stiffener Slenderness for Short Stiffened Plates

$a/b = 0.60$ $\sigma_{op} = 245\ N/mm^2$ $\sigma_{ow} = 245\ N/mm^2$

$A_w/A_p = 0.20$ $w_{op} = b/200$ $w_{ow} = 0.00075a$

d/t_w	b/t_p	β_p	β_w	σ_p/σ_{op}	σ_w/σ_{ow}	σ/σ_o
10	30	1.03	0.344	1.0	1.0	1.0
10	40	1.376	0.344	0.93	1.0	0.94
10	60	2.064	0.344	0.68	1.0	0.72
10	85	2.928	0.344	0.49	1.0	0.56
20	30	1.03	0.688	1.0	1.0	1.0
20	40	1.376	0.688	0.95	1.0	0.96
20	60	2.064	0.688	0.74	1.0	0.76
20	85	2.928	0.688	0.56	0.94	0.62
30	30	1.03	1.03	1.0	0.99	1.0
30	40	1.376	1.03	0.96	0.99	0.96
30	60	2.064	1.03	0.76	0.90	0.78
30	85	2.928	1.03	0.58	0.83	0.63
40	30	1.03	1.376	1.0	0.83	1.0
40	40	1.376	1.376	0.95	0.85	0.89
40	60	2.064	1.376	0.76	0.73	0.76

Table 5.2c Effect of Base Plate and Stiffener Slenderness for Short Stiffened Plates

$a/b = 0.60$ $\sigma_{op} = 245$ N/mm^2 $\sigma_{ow} = 245$ N/mm^2

$A_w/A_p = 0.30$ $w_{op} = b/200$ $w_{ow} = 0.00075a$

d/t_w	b/t_p	β_p	β_w	σ_p/σ_{op}	σ_w/σ_{ow}	σ/σ_o
10	30	1.03	0.344	0.99	1.0	1.0
10	40	1.376	0.344	0.89	1.0	0.91
10	60	2.064	0.344	-	(1.0)	-
10	85	2.928	0.344	-	(1.0)	-
20	30	1.03	0.688	1.0	1.0	1.0
20	40	1.376	0.688	-	(1.0)	-
20	60	2.064	0.688	0.72	1.0	0.77
20	85	2.928	0.688	0.54	>0.95	0.62
30	30	1.03	1.03	1.0	1.0	1.0
30	40	1.376	1.03	0.96	0.98	0.96
30	60	2.064	1.03	0.75	0.86	0.78
30	85	2.928	1.03	0.58	0.80	0.63
40	30	1.03	1.376	0.98	0.95	0.98
40	40	1.376	1.376	0.95	0.88	0.92
40	60	2.064	1.376	0.75	0.73	0.74

plate area ratio. In general, with increasing plate slenderness the stiffness of the stiffener reduces and is accompanied by a corresponding reduction in peak load. Stiffeners attached to stocky plates (b/t_p = 30, 40) reach the squash load whereas for the slenderer plates there is a reduction in load-carrying capacity. For the stiffeners failure is accompanied by a sharp transition to the post-failure region and a subsequent loss in strength which is only secondarily affected by the slenderness of the base plate.

Similar comments apply also to the response of the base plate; in this case failure is characterised by a more gradual transition and the loss in strength that follows is also gradual, this being generally attributable to the boundary conditions used (simply supported edges). The slenderness was found to affect the peak load and pre-peak stiffness significantly and for the more slender plates departure from linear elastic behaviour occurs well before yielding.

The results obtained from these diagrams have been summarised as maximum strength - slenderness curves (Figs 5.21 - 5.22). The effect of base plate slenderness on stiffener strength is evident in these diagrams and it seen that stiffeners attached to stocky plates (b/t_p = 30, 40) can reach the squash load for values of d/t_w of up to 30. Stiffeners attached to slender plating (b/t_p = 60, 85) reach the squash load for lower values of slenderness (d/t_w = 15-20), depending on the value of b/t_p. The response is similar for both cases of A_w/A_p considered (0.20, 0.30).

5.4 Stiffener Slenderness

Existing design codes ensure that torsional failure does not arise in stiffeners by setting upper limits to the value of d/t_w. In this manner, failure by yielding is precipitated and this is identified with overall failure of the cross-section. The present study has confirmed previous results that initial yielding is closely followed by failure of the cross-section. It has also been found that in 'short' panels material failure is dominant over the practical range of stiffener slendernesses and that torsional behaviour reduces the strength by only a small amount. Lateral-torsional behaviour becomes more

important in cases where interframe buckling occurs and thus rotation of the stiffener loaded edge arises. It is also important for longer panels in which coupling with column failure occurs. In order to investigate this, a separate study is required in which column behaviour is included.

The effects of stiffener slenderness are apparent from Figs 5.21a and 5.22a in which β_w is plotted against stiffener peak load. For column-type behaviour the slenderness is usually defined in terms of the length and the radius of gyration; in this case it is more appropriate to use the equivalent 'plate' slenderness since local behaviour is studied. These diagrams show that for stiffeners attached to stocky plating the peak load is reached, provided $d/t_w < 30$. For stiffeners attached to plating with $b/t_p = 60$ the limit is $d/t_w = 20$ and for $b/t_p = 85$ stiffeners with a slenderness greater than 10 experience reductions in peak load.

The effect of stiffener slenderness on base plate response is indicated in Figs 5.21b and 5.22b. For a value of A_w/A_p of 0.20 it is seen that the more slender stiffeners provide greater support to the base plate. For $A_w/A_p = 0.30$ the stockiest stiffeners provide the greatest support although the effect is in general less clear. In order to clarify this it is necessary to generate results for higher values of A_w/A_p .

5.5 Stiffener/Plate Area Ratio

In practical cases the value of A_w/A_p can range up to 1.0, depending on the type of stiffener and the panel in question. In this study, stiffened plates were considered over the range 0.10 to 0.30. The effect of varying A_w/A_p is evident from Tables 5.2b-c and Figs 5.21a, 5.22a. It is observed that increasing the size of the stiffener produces:

- reductions in plate strength
- increases in stiffener strength

This occurs because the distribution of the load carried by the cross-section changes.

The overall load carried is not significantly affected and the slender stiffeners (d/t_w = 30, 40) attached to stocky plating experience the largest increases in peak load.

The results from a second study for higher area ratios are plotted in Figs 5.18a-c and the peak loads are included in Table 5.3 below. These show that when A_w/A_p is increased the strength of the cross-section increases; in this case the stiffener reaches the squash load when the area ratio exceeds the value of 0.40.

Table 5.3 Effect of Stiffener/Plate Area Ratio for Short Stiffened Plates

$a/b = 0.60$ $\quad \sigma_{op} = 245$ N/mm^2 $\quad \sigma_{ow} = 245$ N/mm^2

$w_{op} = b/200$ $\quad w_{ow} = 0.00075a$

b/t_p	d/t_w	A_w/A_p	σ_p/σ_{op}	σ_w/σ_{ow}	σ/σ_o
60	20	0.11	0.73	0.79	0.73
60	20	0.20	0.73	0.90	0.76
60	20	0.40	0.73	0.97	0.80
60	20	0.60	0.74	1.0	0.84

5.6 Effect of Yield Stress

This study was undertaken to examine to what extent changes in yield stress affect the maximum strength of the cross-section and the distribution of load between the base plate and the stiffener. In all the cases analysed failure occurred by yielding. The values of yield stress considered were in the range 200 N/mm^2 $\leq \sigma_o \leq$ 355 N/mm^2 and results are plotted in Figs 5.19a-b.

Table 5.4 Effect of Yield Stress for Short Stiffened Plates

$a/b = 0.60$	$b/t_p = 60$	$w_{op} = b/200$
$A_w/Ap = 0.11$	$d/t_w = 10$	$w_{ow} = 0.00075a$

σ_{op}	σ_{ow}	σ_p/σ_{op}	σ_w/σ_{ow}	σ/σ_o
200	200	0.78	0.93	0.80
245	355	0.74	0.86	0.77
355	245	0.66	0.91	0.68
300	300	0.76	0.95	0.79
355	355	0.66	0.88	0.78

It appears that for the base plate, increases in yield stress produce relative reductions in the ultimate strength. For the stiffener the maximum decrease in peak strength is relatively smaller and it can be expected that it would depend on the slenderness. All strength curves exhibit the same characteristic transition to the postfailure regime for the stiffener and base plate and the behaviour of the cross-section as a whole is dominated by plate behaviour ($A_w/A_p = 0.11$). For constant plate yield stress decreases in σ_{ow} produce increases in σ_w/σ_{ow} (cases 3,5). The same is observed in the case of the base plate for constant stiffener yield stress.

5.7 Effect of Clamped Edges

In this section the response of simply supported plates forming part of a grillage is compared with that of isolated clamped plates. The boundary conditions which were used are shown in Figs 2.8 and 4.8 respectively and the geometries are included in the following table, in which maximum strengths are compared. The study concentrated on the effect of the rotational restraint for different plate and stiffener slendernesses.

Table 5.5 Comparison of Simply Supported and Clamped Stiffened Plates

$a/b = 0.60$ $\quad w_{op} = b/200$ $\quad w_{ow} = 0.0$

$\sigma_{op} = 245\ N/mm^2$ $\quad \sigma_{ow} = 245\ N/mm^2$

		Simply Supported			Clamped		
d/t_w	b/t_p	σ_w/σ_{ow}	σ_p/σ_{op}	σ/σ_o	σ_w/σ_{ow}	σ_p/σ_{op}	σ/σ_o
10	30	0.97	1.0	1.0	0.98	1.0	1.0
10	40	0.79	0.91	0.89	0.93	1.0	1.0
10	60	0.70	0.73	0.72	0.96	1.0	1.0
10	85	0.62	0.49	0.49	0.70	0.83	0.81
8	60	1.0	0.81	0.90	1.0	1.0	1.0
16	60	0.98	0.81	0.86	0.99	1.0	1.0
20	60	0.98	0.81	0.85	0.99	1.0	1.0
40 [1]	60	0.72	0.72	0.72	0.82	0.98	0.95

[1] in this case $w_{ow} = 0.00075a$

Fig. 5.20a shows that for a range of plate slendernesses the implementation of the clamped condition leads to increased stiffness in the pre-peak range for the stiffeners as well as to higher peak loads. The strength of stiffeners attached to plates with $b/t_p = 40$ approach the squash load, the largest increase being observed for $b/t_p = 60$ (26%). For the base plate the effect of clamping produces increases in maximum strength, especially for the higher slenderness ratios. For $b/t_p = 85$ the increase was found in strength was found to be $0.34\sigma_{ow}$ (70%).

The effect of clamping for different stiffener slendernesses is not as important for stiffener behaviour although an increase in strength was noted for $d/t_w = 40$ from 0.72 to $0.82\sigma_{ow}$ (Table 5.5).

It is thus concluded that for the practical range of slenderness ratios, the effect of clamping produces more significant changes in plate behaviour than in stiffener behaviour.

CHAPTER SIX

DYNAMIC RESPONSE OF UNSTIFFENED AND STIFFENED FLAT PLATING

At the end of Chapter 3 it was stated that when analysing a stiffener whose load-carrying capacity was of the same order as that of the plate, numerical instability can arise if Dynamic Relaxation is used in its conventional, static form. This occurs because rapid collapse may follow buckling in either the plate or the stiffener, the proportion of load being shed to the adjoining member precipitating buckling in this as well. As a result, the load-deflection path cannot be traced since rapid out-of-plane motion causes the procedure to diverge. It would thus seem evident that it is necessary to treat this type of interactive buckling as a dynamic phenomenon.

The implementation of Dynamic Relaxation to achieve this will be described in this Chapter and results will be given for a dynamic analysis of a flat plate subjected to a lateral impact load. The results will be compared with test data and a similar analysis using a finite strip method [135].

6.1 Use of Dynamic Relaxation as a Real-Time Procedure

In conventional static solutions, when DR is used to analyse a structure a load increment is imposed upon it and a number of iterations are performed until

equilibrium is reached, i.e. the out-of-balance forces resulting from the imposed load converge to zero. In these analyses, stability is governed by time increment and mass density terms (Δt, ρ_u, ρ_v, ρ_w) and convergence by damping constants. For example, the out-of-balance force in the 'w' direction is given by:

$$P_w = \rho_w \frac{\partial \dot{w}}{\partial t} + C_w \dot{w} \qquad (6.1)$$

where P_w is identically equal to the left-hand side of equation 2.1a and ρ_w, C_w are mass density and damping terms. Because DR has not been concerned with the dynamic behaviour as such, fictitious mass densities and unit time steps have been introduced purely to achieve the most rapid convergence to the static solution.

In structural mechanics the majority of problems fall into one of three physical categories: equilibrium problems, eigenvalue problems and propagation problems [105].

Equilibrium problems are those of steady state in which the equilibrium configuration within the domain is to be determined by solving a particular differential equation subject to certain boundary conditions. If the domain of integration is closed and bounded, the problem is called a boundary value problem. It is apparent that the determination of equilibrium stresses in an elastic plate falls into this category.

When critical values of certain parameters are to be determined in addition to the corresponding steady state configuration the problem becomes an eigenvalue one, and for flat plate equations eigenvalues correspond to buckling stresses.

The third category is that of propagation problems in which an unsteady or transient response is analysed, given certain initial conditions (values). The solution of the equations describing the dynamic behaviour of flat plates subjected to in-plane and/or lateral loads belongs to this category and is achieved by satisfying the geometrical boundary conditions and initial values.

It is thus apparent that the implementation of a combined static/dynamic analysis involves the solution of two essentially different types of problem. Nonetheless, the means by which numerical stability is achieved in the DR static solution can also be used in the dynamic case, provided the true material density and an appropriate time step are used.

The time step used in other techniques is determined in various ways [112,117]. For methods which are unconditionally stable (implicit operators), no restrictions exist but for explicit operators a maximum value is required otherwise convergence is not achieved. In the past this upper limit has been determined by several authors by considering the propagation velocity C of a plane stress wave within the plate. Since $C = \Delta x/\Delta t$, the time increment can be found from $\Delta t = \Delta x/C$ where Δx is the mesh size. When DR is used to carry out a static analysis, stability is ensured by determining the Gershgorin bounds of the equations of equilibrium at each node. This analysis can also be used in a dynamic analysis since:

$$\rho = \frac{\Delta t^2 b_G}{4} \tag{6.2}$$

Rearranging,

$$\Delta t = \sqrt{\frac{4\rho}{b_G}} \tag{6.3}$$

where b_G is the maximum value of the Gershgorin bound calculated in the u, v and w directions. For mild steel, the speed of propagation of a stress wave $C = 5.4 \times 10^{-4}$ secs. The Gershgorin bound of the linear terms of the equilibrium equation of a flat plate using equation 6.3 gives $\Delta t = 0.1309 \times 10^{-4}$ secs. Thus,

$$\Delta t < \frac{\Delta x}{C} \tag{6.4}$$

and when nonlinear terms are included, the time increment decreases further. From physical considerations, therefore, the time taken for the stress wave to travel between two adjacent nodes represents an upper bound to the time step which is used in a numerical procedure involving an explicit operator. A dynamic analysis using Real-Time DR can therefore be used to describe only a short period in the overall time history of the structure. This does not pose any serious restrictions when analysing the true dynamic behaviour, since the period of a plate transient response is short (a few milliseconds). If however it as attempted to trace out a full load deflection static response using the dynamic procedure, the number of iterations required increases to such an extent that it becomes impracticable to perform such a calculation. The dynamic analysis is therefore limited to the study of the range of loading in which interactive buckling takes place, the rest of the response being treated in the conventional manner.

6.2 Governing Equations

The dynamic behaviour is described by the modified von Karman equations assuming rotary inertia can be neglected. Therefore,

$$\rho_w \frac{\partial \dot{w}}{\partial t} + C_w \dot{w} = P_w \tag{6.5a}$$

$$\rho_u \frac{\partial \dot{u}}{\partial t} + C_u \dot{u} = P_u \tag{6.5b}$$

$$\rho_v \frac{\partial \dot{v}}{\partial t} + C_v \dot{v} = P_v \tag{6.5c}$$

Since real densities are used throughout, $\rho_w = \rho_u = \rho_v = \rho$. Constant acceleration is assumed during a time interval Δt, and thus velocities at $t = t + \Delta t/2$ are obtained in terms of the previous velocities.

$$\dot{w}_{t+\Delta t/2} = \dot{w}_{t-\Delta t/2} + \frac{\Delta t}{\rho} P_w \tag{6.6a}$$

$$\dot{u}_{t+\Delta t/2} = \dot{u}_{t-\Delta t/2} + \frac{\Delta t}{\rho} P_u \tag{6.6b}$$

$$\dot{v}_{t+\Delta t/2} = \dot{v}_{t-\Delta t/2} + \frac{\Delta t}{\rho} P_v \tag{6.6c}$$

Using central differences in time, the velocities are then integrated to obtain displacements at $t = t + \Delta t$ as for the static solution.

6.3 Material Nonlinearity - Effect of Strain Rate

Geometrical nonlinearity is governed by the same equations as used in the static case. Dynamic effects do however affect material behaviour since the yield stress is dependent upon the strain rate [136,137,138,139]. For a stress increment to remain on the yield surface, the total differential of the yield function f is equal to zero, i.e.:

$$\frac{\partial f}{\partial \sigma_Y} \Delta\sigma_Y + \left[\frac{\partial f}{\partial \sigma}\right]^T \Delta\sigma = 0 \tag{6.8}$$

For the von Mises yield criterion,

$$df = \frac{\partial f}{\partial \sigma_Y} \Delta\sigma_Y + \frac{\partial f}{\partial \sigma_x} \Delta\sigma_x + \frac{\partial f}{\partial \sigma_y} \Delta\sigma_y + \frac{\partial f}{\partial \tau_{xy}} \Delta\tau_{xy} = 0 \tag{6.9}$$

The incremental stress-strain relation gives:

$$\Delta\sigma = E\left[\Delta\varepsilon - \Delta\varepsilon^p\right] \tag{6.10}$$

and $$\Delta \varepsilon = \lambda \left[\frac{\partial f}{\partial \sigma}\right] \qquad \text{(Prandtl-Reuss flow rule)} \qquad (6.11)$$

Combining equations 6.8, 6.10 and 6.11 the plastic strain rate multiplier is obtained:

$$\lambda = \frac{\left[\frac{\partial f}{\partial \sigma}\right]^T E \Delta \varepsilon + \left[\frac{\partial f}{\partial \sigma_Y}\right] \Delta \sigma_Y}{\left[\frac{\partial f}{\partial \sigma}\right]^T E \left[\frac{\partial f}{\partial \sigma}\right]} \qquad (6.12)$$

The modified incremental stress-strain relation therefore becomes:

$$\Delta \sigma = E^* \Delta \varepsilon + \Delta \sigma_c \qquad (6.13)$$

where $$\Delta \sigma_c = -E \left[\frac{\partial f}{\partial \sigma_Y}\right] \Delta \sigma_Y \frac{\left[\frac{\partial f}{\partial \sigma}\right]}{\left[\frac{\partial f}{\partial \sigma}\right]^T E \left[\frac{\partial f}{\partial \sigma}\right]} \qquad (6.14)$$

On the von Mises yield surface,

$$\left[\frac{\partial f}{\partial \sigma_Y}\right] \Delta \sigma_Y = -\frac{2 \Delta \sigma_y}{\sigma_Y^3} \left(\sigma_x^2 + \sigma_y^2 + 3\tau_{xy}^2 - \sigma_x \sigma_y \right) =$$

$$= -\frac{2 \Delta \sigma_Y}{\sigma_Y} \qquad (6.15)$$

Substituting from 6.15 in 6.11,

$$\Delta \sigma_c = \frac{2\Delta\sigma_Y}{\sigma_Y} \frac{E\left[\frac{\partial f}{\partial \sigma}\right]}{\left[\frac{\partial f}{\partial \sigma}\right]^T E\left[\frac{\partial f}{\partial \sigma}\right]} \tag{6.16}$$

The stress increments on the yield surface arising from the effect of strain rate therefore are:

$$\Delta\sigma_{xc} = \frac{2\Delta\sigma_Y}{\sigma_Y} \frac{E}{1-\nu^2} \frac{1}{r}\left[\frac{\partial f}{\partial \sigma_x} + \nu\frac{\partial f}{\partial \sigma_y}\right] \tag{6.17a}$$

$$\Delta\sigma_{y\,c} = \frac{2\Delta\sigma_Y}{\sigma_Y} \frac{E}{1-\nu^2} \frac{1}{r}\left[\frac{\partial f}{\partial \sigma_y} + \nu\frac{\partial f}{\partial \sigma_x}\right] \tag{6.17b}$$

$$\Delta\tau_{xy\,c} = \frac{2\Delta\sigma_Y}{\sigma_Y} \frac{E}{1-\nu^2} \frac{1}{r} \frac{1-\nu}{2} \frac{\partial f}{\partial \tau_{xy}} \tag{6.17c}$$

where $$r = \left[\frac{\partial f}{\partial \sigma}\right]^T E\left[\frac{\partial f}{\partial \sigma}\right] \tag{6.18}$$

The above treatment is based on (135) in which the von Mises yield criterion was used but shear stresses were not included (plate strip approach). The effect of strain rate was seen to be of importance in previous work and was introduced using a relationship originally proposed by Cowper and Symonds [139] and recommended by Jones [137]. In this the material is assumed elastic visco-perfectly plastic and the dynamic stress is related to the static yield stress as follows:

$$\frac{\sigma_{yd}}{\sigma_0} = 1 + \left[\frac{\dot{\varepsilon}_e}{D}\right]^{1/p} \tag{6.19}$$

where σ_0 is the static yield stress and D and p are material constants which take values of 40.4 s^{-1} and 5 for mild steel. The equivalent strain rate was obtained using a relationship given by Jones [137]:

$$\dot{\varepsilon}_e = \left(\frac{2}{3} \dot{\varepsilon}_{ij} \dot{\varepsilon}_{ij} \right)^{1/2} \tag{6.20}$$

where $\dot{\varepsilon}_{ij}$ is the strain rate tensor given by :

$$\dot{\varepsilon}_{ij} = \frac{\varepsilon_{ij}}{\Delta t} = \begin{bmatrix} \varepsilon_x & \varepsilon_{xy} & \varepsilon_{xz} \\ \varepsilon_{yx} & \varepsilon_y & \varepsilon_{yz} \\ \varepsilon_{zx} & \varepsilon_{zy} & \varepsilon_z \end{bmatrix} \frac{1}{\Delta t} \tag{6.21}$$

For plane stress problems, $\sigma_z = \tau_{yz} = \tau_{zx} = 0$. Therefore $\varepsilon_{zy} = \varepsilon_{yz} = \varepsilon_{xz} = \varepsilon_{zx} = 0$ and the expression (6.20) is evaluated using the Einstein summation convention to give:

$$\varepsilon_{ij}\,\varepsilon_{ij} = \varepsilon_x^2 + \varepsilon_{xy}\varepsilon_{yx} + \varepsilon_x\varepsilon_{xy} + \varepsilon_{xy}\varepsilon_y + \varepsilon_{yx}\varepsilon_x + \varepsilon_y\varepsilon_{yx} + \varepsilon_{yx}\varepsilon_{xy} + \varepsilon_y^2 + \varepsilon_z^2$$

Since $\varepsilon_{xy} = \frac{\gamma_{xy}}{2}$, $\varepsilon_{yx} = \frac{\gamma_{yx}}{2}$, this reduces to:

$$\varepsilon_{ij}\,\varepsilon_{ij} = \varepsilon_x^2 + \varepsilon_y^2 + \varepsilon_z^2 + \gamma_{xy}\,(\varepsilon_x + \varepsilon_y + \gamma_{xy}/2) \tag{6.22}$$

where $\varepsilon_z = -\frac{\nu}{E}(\sigma_x + \sigma_y)$ in the elastic and the elasto-plastic range since the flow rule shows that plastic strain increments are zero in the transverse direction.

At this stage it is necessary to consider how the DR cycle should be modified in order that the dynamic transient response can be analysed and the effect of strain rate included. The changes considered up to this point are:

i) the equations of equilibrium do not now contain damping terms and the time increment is calculated using equation 6.3.

ii) the elasto-plastic rigidities which were previously found at the end of each load increment now have to be calculated within each cycle. They are used in the subsequent cycle to find the multilayer incremental stresses.

iii) the yield stress which is a function of strain rate is now calculated within each cycle.

These changes are indicated in Fig. 6.1 which summarises the new sequence of calculations leading to the evaluation of multilayer stresses and the yield function. It is seen that the plastic strain rate multiplier, λ, is now calculated before the yield function f. The sign of λ is again used to check whether loading or unloading is taking place at the yield surface. In the dynamic analysis, if elasto-plastic loading is occurring it is necessary to also evaluate the stress increments $\Delta\sigma_c$ which are added to the static stress increments at each layer, as indicated by equation 6.13.

When dynamic unloading occurs, it is assumed that the yield surface contracts at the same rate such that the value of the yield function remains equal to unity. During unloading elastic rigidities are used as in the static analysis.

6.4 Impact Analysis of Flat Plates

During the period 1982-84 a series of small-scale collision tests was conducted and results were compared with a numerical procedure developed at Glasgow University [135].

In this section, the application of the Real-Time procedure to simulate the test results will be described. During the tests a flat plate was supported along its boundaries and was hit by a rigid striker of known mass and velocity. Conditions along the boundaries of the impacted plate were modelled in a simplified manner since no accurate account could be taken of energy losses to the adjoining structure. The boundaries were thus treated as rotationally clamped and restrained in the three orthogonal directions.

The impact was simulated by applying uniform velocities to the plate nodes along the line of contact, at time t = 0. The effect of the mass of the striker was allowed for by increasing the mass of the struck nodes accordingly.

At time t, the total kinetic energy absorbed by the plate is given by:

$$U(t) = \iiint (\sigma(t) \ \varepsilon(t)) \ dx \ dy \ dz \qquad (6.23)$$

where σ (t) = total stress at time t

ε (t) = total strain at time t

at any point in the plate. Since

$$U(t) = U_e(t) + W_p(t) \qquad (6.24)$$

where U_e = recoverable elastic strain energy stored in the plate at time t

W_p = plastic work dissipated in time t,

the recoverable elastic strain energy can be found from :

$$U_e(t) = U(t) - W_p(t) =$$

$$= U(t) - (W_p(t-\Delta t) + \int dW_p(t)) =$$

$$= U(t) - (W_p(t-\Delta t) + \iiint \sigma(t) \ \Delta\varepsilon^p(t) \ dx\, dy\, dz) \qquad (6.25)$$

where $\Delta\varepsilon^p$ is the incremental plastic strain at time t, evaluated using the flow rule.

It is assumed that following separation, the plate will continue to oscillate about what is its permanent deflection, since the motion is undamped. The point at which separation occurs is assumed to be that at which the recoverable (elastic) part of the total kinetic energy imparted to the plate by the striker reduces to zero. Detailed results for one impact test are given in Figs 6.2-6.7, as predicted by the numerical procedure. Input data are given in the following table.

Table 6.1 Impact Test Data

Plate dimensions	mm	243 x 243 x 0.79
Young's Modulus	kN/mm^2	207.0
Poisson's ratio		0.30
Yield stress	N/mm^2	220
Mass of striker	kg	55.4
Velocity of striker	m/s	2.0
Length of line of impact	mm	145.0

Figure 6.2 shows that the central deflection of the plate increases monotonically until

the peak deflection is reached. It then decreases regularly until separation occurs and the analysis is terminated. The variation of the out-of-plane velocity at the same position is shown in Fig. 6.3. During the initial part of the response the reduction is small but after 3 milliseconds the velocity gradient increases and reaches a constant value which is maintained until separation occurs (11 millisecs). The variation in elastic kinetic energy absorbed by the struck plate is shown in Fig. 6.4. The plastic work done is also illustr ated in this diagram and it is seen that at separation the plate behaves elastically ($dW_p = 0$).

The material behaviour is described in further detail in Figs 6.5 and 6.6. The number of nodes behaving elasto-plastically during the period of impact are shown in Fig. 6.5. A peak occurs before the maximum deflection is reached (8.5 millisecs), following which unloading occurs.

The effect of strain rate is shown in Fig. 6.6. The average dynamic yield stress increases rapidly following loading and levels off at nearly three times the static value. During unloading, a slight decrease is noted.

Results for other cases are summarised in Fig. 6.7 in which test data are compared with theory. In this diagram the maximum available energy to cause structural damage is plotted against final deflection. It is seen that the test data lie between the curves obtained using the present approach, a plate-strip approach and an analytical method [140] in which rigid-plastic behaviour was assumed. The results obtained using the present approach involving the complete plate are seen to lie closest to the test data and quite good correlation is achieved.

The numerical approaches are seen to predict a response which is not as stiff as that observed during the tests. Several factors contribute to this, probably the most important being that energy losses to the adjoining structure are not accounted for. One other difference between the theoretical and test results was observed in the final transverse profile of the plate. The test results indicated that a local indentation was

produced along the line of impact. This can be attributed to the knife edge of the striker and could not be reproduced theoretically because a rectangular mesh of constant dimensions is used in the finite difference representation. Energy dissipation along the line of impact was not therefore modelled in an exact manner and some differences in the distributions of elasto-plastic zones should be expected. Nonetheless, good agreement is obtained in the global response and the method gives results which overall are on the conservative side.

CHAPTER SEVEN

CONCLUSIONS AND PROPOSALS FOR FURTHER WORK

7.1 Conclusions

The work presented in this thesis represents an effort to come to terms with the problem of the flexural-torsional response of stiffened plates in the large-deflection elasto-plastic range. In the past this has been handled in an approximate manner and analytical solutions have been proposed for the elastic range. Inelastic effects have usually been allowed for by use of tangent-stiffness relations (Ostenfeld-Bleich, Johnson). However interaction effects complicate the behaviour and in certain cases can lead to premature failure of the cross-section. This has not yet been taken fully into account although the effect of plate failure on stiffener response has been included in analytical equations for stiffener tripping.

- An extensive survey of stiffener tripping has been conducted. Although it was found that the energy method has proved effective in solving design problems, it cannot rigorously handle the effects of interaction nor the geometrical and material nonlinearities needed to fully understand the failure mechanisms in stiffened plates, especially those related to flexural-torsional behaviour. One study specifically concluded that the absence of equations governing stiffener distortions was the most serious shortcoming of the method although an allowance for stiffener distortions was included by assuming that

the stiffener behaved as a cantilever beam. For axial compression good agreement was obtained with finite element solutions but for lateral pressure the agreement was not as satisfactory because of the more complicated failure modes and distortions.

- The primary objective of this work has been to develop a numerical model of the behaviour of flat plates and attached flatbar stiffeners which includes the effects of interaction between the two components. The Marguerre large-deflection thin plate equations were used to represent both the plate and the stiffener so enabling the lateral-torsional behaviour of the stiffener to be accurately modelled. Complete interaction was achieved by satisfying the full set of equilibrium and kinematic conditions acting at the stiffener-plate junction. Material nonlinearity has been modelled using the von Mises yield criterion in conjunction with the Prandtl-Reuss flow rule on a multilayer basis. Interframe buckling was accounted for by the introduction of a coupled beam-column equation.

The procedure was extended to include T-stiffeners via the plate equations to model local buckling of the flange, full interaction between the web and the flange and the use of a coupled beam-column equation for overall buckling of the flange.

Dynamic Relaxation was the numerical technique used to solve the governing equations when written in a finite difference form. Although used successfully in studies of isolated elements, interaction and the rapid growth of out-of-plane movement associated with buckling in the stiffened plates raised difficulties when checking convergence. It was found necessary to check convergence for each group of geometries to be analysed particularly at buckling stress levels. Frequent load increments were required to accurately monitor the spread of plasticity through the structure as the failure load was approached.

The discretisation of the finite difference model was found to be affected by the geometry of the structure.

Other than choosing appropriate damping factors, load intervals and mesh spacings, two other measures were taken to assist convergence. These were the factorisation of displacements at the beginning of each load increment and a parallel shift of each line of nodes at the intersection of the plate and the stiffener. The latter was introduced in order to avoid the propagation of a 'flexural' wave arising from the imposition of the out-of-plane boundary condition ('w' deflection) within each cycle.

It was found possible to analyse the dynamic behaviour of flat plates using the real-time version of Dynamic Relaxation. In this case convergence problems do not arise and stability is governed by the size of the time increment. This was determined using the same criterion as for the static solution but involving actual densities rather than the fictitious ones and unit time steps used in the static problem. The effect of strain rate on yield stress was modelled using an existing empirical relationship.

• Preliminary studies involving isolated stiffeners and stiffened plates were performed to validate the procedure at each stage of its development and to provide a basis for the direct comparison of the effects of different boundary conditions, interaction and material behaviour. In a study of isolated flatbar stiffeners in the elastic range it was found that:

- buckling stresses for simply supported stiffeners were found to closely model those given by classical theory.

- clamping of boundaries not surprisingly increased buckling stresses particularly for short stiffeners. Again these closely match classical results.

- for slender stiffeners a postbuckling reserve of strength was observed.

When including plasticity in the analyses of isolated flatbars it was found that:

- simply supported stiffeners showed no sudden drop-off after peak load.

- clamped stiffeners demonstrated a rapid fall-off after peak load.

Flatbar stiffened plates were examined under various loading configurations and good agreement was obtained with elementary beam and plate theory thus validating the interaction equations.

This was followed by a study of the effect of the presence of attached shell plating on the elastic behaviour of flatbar stiffeners behaving elastically. Plate buckling did not arise in the cases considered and it was found that the presence of the plating did not affect the buckling stress of the stiffener. However, in the postbuckling regime the isolated plate experienced a rapid drop in load whereas the attached stiffener did exhibit a reserve of strength.

- A simulation of small-scale stiffened plates tested at Glasgow University under axial compression and lateral pressure was undertaken. It was found that

- elastic buckling could not be predicted with great accuracy for individual test data

- elasto-plastic buckling could be predicted well primarily in relation to loads

With regard to the test programme in question,

- in some cases axiality of the load was not achieved and it was not easy to determine the extent of eccentricity accurately. Although combined axial load and moment were applied in the correlation studies it was only found to give similar stress distributions at particular load levels.

- it was not possible to have detailed knowledge of the magnitude and distribution of the load across the loaded edges of the cross-section because of the size of the specimens and the necessity to weld the specimens to the box sections.

In the case of the combined load test, careful monitoring of the axial load seemed difficult because the tests were conducted in a pressure chamber and were not accessible.

A comparison of the test results for stiffener buckling under axial compression with predicted values obtained using several analytical formulations showed that it is necessary to allow for the effect of rotational restraint, particularly for slender stiffeners.

The correlation of the dynamic analysis procedure with a series of tests on flat plates under lateral impact showed close agreement in the prediction of final deflections. These were in general slightly larger than those observed the main reason for this being that energy losses to the adjoining structure are not accounted for.

- In a series of studies on the local elasto-plastic behaviour of stiffened plates under axial compression the following parameters were considered:

- aspect ratio
- initial geometrical imperfections
- base plate and stiffener slendernesses
- stiffener/plate area ratio
- yield stress
- boundary conditions

With regard to aspect ratio it was found that the value at which minimum strength is observed in the base plate is 0.60. This is similar to the results obtained by other researchers for isolated plates.

For short stiffeners it was seen that the peak load decreases with increasing aspect ratio but reaches a constant value in the range $1 < a/b < 2$. For larger plate aspect ratios (3, 4), collapse was more sudden for both the plate and stiffener but no further decrease in the peak load was observed. These findings support Faulkner's recent criticism of the

prevailing belief that the tripping stress is dependent upon the length of the cross-section and that therefore the use of tripping brackets should be questioned.

Imperfections have an important influence in this respect and this needs further study, in conjunction with beam-column interaction. It was found that base plate and stiffener imperfections cause reductions in both the stiffness and maximum strength and that stiffener imperfections are less likely to affect plate behaviour than vice versa.

A comparison of stiffened plates designed to DnV and BS5400 rule tolerances showed that the DnV rules permit weaker plates and stiffeners to be used (20% and 30% respectively for the cases considered).

Subsequent studies were carried out for short panels (a/b = 0.60) for the practical range of plate and slendernesses. For the plate the range considered was $85 > b/t_p > 30$ and for the stiffener the range considered was $40 > d/t_w > 8$.

A study on the effect of increasing base plate and stiffener slenderness showed that both reduced the stiffener and plate stiffness. Increases in plate slenderness also cause reductions in stiffener peak load.

For short panels it was found that for the practical range of stiffener slendernesses failure is caused by yielding along the free edge of the stiffener at midlength which progressively spreads towards the plate until the peak load is reached. In general failure follows the onset of yielding fairly rapidly. The study of the effect of stiffener/plate area ratio showed that increases in this ratio increased the stiffener strength. This was in agreement with results obtained by other researchers.

The effect of plate and stiffener slenderness on stiffener behaviour is seen in the maximum strength - peak load curves presented. When flatbar stiffeners are attached to stocky plates (b/t_p = 30, 40) their strength reduces below the squash load when their slenderness is increased beyond $d/t_w = 30$. For a plate slenderness of 60 the strength

reduces for values of 20 and for $b/t_p = 85$ the value is 10. In the light of these findings design rules in use are judged to be conservative, particularly for stocky cross-sections.

When the yield stresses of both the plate and stiffener are increased their relative strengths decrease. The same is observed when only the yield stress of either the plate or the stiffener is increased.

The effect of clamping along the transverse loaded edges and the longitudinal plate edges gives rise to increases in stiffness for both the plate and stiffener. The maximum strength is correspondingly increased, the largest increases occurring in the case of slender plates. In general the stiffener strength is only marginally increased since for the simply supported condition it is close to the squash load.

7.2 Proposals for Further Work

The stiffened plate program in its present form can examine both the static and the dynamic response of stiffened plates as follows:

- local interactive buckling between flat plates and stiffeners of flatbar and teebar cross-section

- local interactive and interframe buckling of flatbar stiffened plating by analysing either short sections of stiffened plate subjected to combinations of axial load and moment or complete spans between transverses.

- combined local interactive and interframe buckling of teebar stiffened plating, and

- any form of initial distortions and/or thicknesses in the plating and the stiffener.

Comprehensive parametric studies can therefore be performed with a view to derive design guidance on such factors as:

- flatbar and teebar flange depth to thickness ratios to ensure stiffener instability does not affect stiffened plate strength

- the effect of plate and teebar web slenderness on this if any

- teebar web depth to thickness ratios to ensure stiffened plate strength is not affected.

- for teebar stiffeners, ratios of elastic torsional buckling stresses to yield stress to ensure stiffened panel strength is not compromised.

- strength curves for flatbar stiffeners

- closed form strength solutions for teebar stiffeners

The above would need to be conducted using appropriate levels of initial geometrical distortions. To be of most relevance, however, welding residual stresses would also have to be considered.

For the teebar stiffened plate, the effect of tripping brackets could be simulated by the introduction of stiff springs acting transversely to the flange. The load on these could then be evaluated so that tripping bracket design could be put on a rational basis.

The success of the isolated plate dynamic analysis indicates the stiffened plate program could be implemented along similar lines so that the effect of impacts of one form or another on stiffened plates could be considered.

REFERENCES

1. Smith C.S. 'Compression Strength of Welded Steel Ship Grillages', Trans. R.I.N.A., 1975.

2. Faulkner D. 'Towards a Better Understanding of Compression Induced Stiffener Tripping', in 'Advances, Design and Construction', Intl Conference on Steel Structures, Cardiff Univ, July 1987.

3. Hooke R. **De Potentia Restitutiva**, London, 1678.

4. Bernoulli D. in P.H. Fuss **Correspondance Mathematique et Physique de quelques celebres geometres du XVIII siecle ...**, letter 26, Vol. 2, St. Petersburg, 1843.

5. Bernoulli J. **Opera**, Vol. 2, Geneva, 1744.

6. Euler L. **Mechanica Sive Motus Scientia Analytice Exposita**, Vols 1, 2, St. Petersburg, 1736.

7. Navier L. Bulletin Soc. Phil. Math., Paris, 1823.

8. Kirchhoff G.R. **Vorlesungen uber Mathematische Physik, Mechanik**, 2nd edition, 1877.

9. Foppl A. **Technische Mechanik**, Vol. 5, 1907.

10. von Karman T. 'Beitrage zur Technischen Physik und Technischen Mechanik', Festschrift August Foppl, Springer, Berlin, 1923.

11. Marguerre K. 'Zur Theorie der Gekrummter Platte Grosser Formanderung', Proc. Fifth Intl Congress Applied Mechanics,

Cambridge, 1938.

12. Bryan G.H. 'On the Stability of a Plane Plate under Thrusts in its own Plane, with Application to the Buckling of the Sides of Ships', Proc. London Math Soc, Vol. 22, 1891.

13. Timoshenko S.P. Bulletin Polytech. Inst. Kiev (in Russian), 1907. Published later as 'Einige Stabilitatsprobleme der Elasticitatstheorie', Zeitsch. fur Math. und Physik, 1910.

14. Hencky H. Z. angew. Math. Mech., Vol. I, 1921.

15. Way S. 'Uniformly Loaded Clamped Rectangular Plates With Large Deflections', Proc. Fifth Intl Congress on Applied Mechanics, Cambridge, 1938.

16. Levy S. 'Bending of Rectangular Plates with Large Deflections', NACA Report No. 737, 1942.

17. Coan J.M. 'Large Deflection Theory for Plates with Small Initial Curvature Loaded in Edge Compression', Jrnl App Mech, Vol. 18, June 1951.

18. Yamaki N. 'Postbuckling Behaviour of Rectangular Plates with Small Initial Curvature Loaded in Edge Compression', Jrnl App Mech, Vol. 26, September 1959.

19. Walker A.C. 'The Post-buckling Behaviour of Simply Supported Square Plates', Aeronautical Quarterly, Vol. 20, 1969.

20. von Mises R. Gottinger Nachrichten, math.-phys. Klasse, 1913.

21. Ilyushin A.A. **Plasticite**, Editions Eyrolles, Paris, 1965.

22. Ivanov G.V. 'Inzheneryi Zhurnal Mekhanika Tverdogo, TELA, No. 6, Vol. 74, 1967.

23. Crisfield M.A. 'On an Approximate Yield Criterion for Thin Steel Shells', TRRL Laboratory Report No. 658, Dept of the Environment, 1974.

24. Reuss A. Zeits. ang. Math. Mech., Vol. 10, 1930.

25. Huber M.T. 'Die Grundlagen einer Rationeller Berechnung der Kreuzweise Bewehrten Eisenbetonplatten', Zeits. Osterreichischen Ing. und Arch Verein ,Vol. 66, 1914.

26. Smith C.S. 'Bending, Buckling and Vibration of Orthotropic Plate-Beam Structures', Jrnl Ship Research, December 1968.

27. Horne M.R., Narayanan R. 'Design of Axially Loaded Stiffened Plates', A.S.C.E., Jrnl Struct Div, November 1977.

28. Dwight J.B., Moxham K.E. 'Welded Steel Plates in Compression', The Structural Engineer, No. 2, Vol. 47, February 1969.

29. Crisfield M.A. 'Full Range Analysis of Steel Plates and Stiffened Plating under Uniaxial Compression', Proc. Instn Civil Engrs, Vol. 59, 1975.

30. Crisfield M.A. 'A Combined Rayleigh-Ritz/Finite Element Method for the Non-linear Analysis of Stiffened Plated Structures', Computers and Structures, Vol. 8, 1978.

31. Szilard R. **Theory and Analysis of Plates - Classical and Numerical Methods**, Prentice Hall, Englewood Cliffs, New Jersey, 1974.

32. Shade H.A. 'The Effective Breadth Concept of Stiffened Plating Under Bending Loads', Trans S.N.A.M.E., Vol. 60, 1952.

33. Reissner E. 'Uber der Berucksichtigung der Gurtsteifigkeit bei der Berechnung der Mittragenden Breite', Schweizerische Bauzeitung, Vol. 108, 1936.

34. Odqvist F. 'On the Effective Width of Reinforced Plane Plates', Royal Swedish Air Board, Tran.slation No. 5, 1948.

35. 'Dowling P.J. 'Some Approaches to the Non-linear Analysis of Plated Structures' in Structural Analysis - Behaviour and Techniques, TRRL Symposium, Supplementary Report No. 164UC, 1975.

36. Dwight J.B., Little G.H. 'Stiffened Steel Compression Flanges - A Simpler Approach', The Structural Engineer, Vol. 54, (12), 1976.

37. Harris H.G., Pifko A.B. 'Elastic-Plastic Buckling of Stiffened Rectangular Plates', A.S.C.E. Symposium on Application of Finite Element Methods in Civil Engineering, Nashville, U.S.A., November 1963.

38. Komatsu S., Nara S., Kitada T. 'Elasto-plastic Analysis of Orthogonally Stiffened Plates with Initial Imperfections under Uniaxial Compression', Computers and Structures, Vol .11, 1980.

39. Szabo B.A., Chen K.C., Tsai C.-T. 'Conforming Finite Elements Based on Complete Polynomials', Computers and Structures, Vol. 4, 1974.

40. Rossow M.P., Ibrahimkhail A.K. 'Constraint Method of Analysis of Stiffened Plates',Computers and Structures, Vol. 8, 1978.

41. Frieze P.A. 'Ultimate Load Behaviour of Steel Box Girders and Their Components', Ph.D. Thesis, Imperial College, London, October 1975.

42. Moolani F.M., Dowling P.J. 'Ultimate Load Behaviour of Stiffened Plates in Compression', in Steel Plated Structures Symposium, ed.

Dowling P.J., Harding J.E., Frieze P.A., London, 1978.

43. Murray N.M. 'Analysis and Design of Stiffened Plates for Collapse Load', The Structural Engineer, Vol. 53, No. 3, March 1976.

44. Djahani P. 'Large Deflection Elasto-plastic Analysis of Discretely Stiffened Plates', Ph.D. Thesis, Imperial College, London, 1977.

45. Webb S.E., Dowling P.J. 'Large Deflexion Elasto-Plastic Behaviour of Discretely Stiffened Plates', Proc. Inst. Civ. Engrs, Part 2, Vol. 69, June 1980.

46. van der Neut A. 'Mode Interaction with Stiffened Panels', in 'Buckling of Structures', IUTAM Symposium, Cambridge U.S.A., June 1974, Springer Verlag 1976.

47. Koiter W.T., Pignataro M. 'An Alternative Approach to the Interaction between Local and Overall Buckling in Stiffened Panels', in 'Buckling of Structures', IUTAM Symposium, Cambridge U.S.A., June 1974, Springer Verlag 1976.

48. Thomson J.M.T., Tulk J.D., Walker A.C. 'An Experimental Study of Imperfection Sensitivity in the Interactive Buckling of Stiffened Plates', in 'Buckling of Structures', IUTAM Symposium, Cambridge U.S.A., June 1974, Springer Verlag 1976.

49. Tulk J.D., Walker A.C. 'Model Studies of the Elastic Buckling of a Stiffened Plate', Jrnl Strain Analysis, Vol. 11, No. 3, 1976.

50. Fok W.C., Rhodes J., Walker A.C. 'Local Buckling of Outstands in Stiffened Plates', Aeronautical Quarterly, Vol. 27, Part 4, November 1976.

51. Fok W.C., Walker A.C., Rhodes J. 'Buckling of Locally Imperfect

Stiffeners in Plates', Proc A.S.C.E., Eng Mech Div, EM5, Vol. 103, No.5, October 1977.

52. Croll J.G.A. 'Model of Interactive Buckling of Stiffened Plates', Proc A.S.C.E., Jrnl Eng. Mech. Div.,Vol. 101, October 1975.

53. Tvergaard V. 'Influence of Post-buckling Behaviour on Optimum Design of Stiffened Panels',.Intl Jrnl of Solids and Structures, Vol. 9, 1973.

54. Svensson S.E., Croll J.G.A. 'Interaction between Local and Overall Buckling', Intl Jrnl of Mechanical Sciences, Vol. 17, 1975.

55. Maquoi R., Massonet Ch. 'Intercation between Local Plate Buckling and Overall Buckling in Thin-walled Compression Members - Theories and Experiments' in 'Buckling of Structures', IUTAM Symposium, Cambridge U.S.A., June 1974, Springer Verlag 1976.

56. Graves Smith T.R. 'The Ultimate Strength of Locally Buckled Columns of Arbitrary Length', Symposium on Thin Walled Steel Structures, ed. Rockey K.C., Hill H.V., Crosby Lockwood, 1969.

57. Frieze P.A., Dowling P.J. 'Interactive Buckling Analysis of Box Sections using Dynamic Relaxation', Computers and Structures, Vol. 9, 1978.

58. Frieze P.A. 'Elasto-plastic Buckling in Short Thin-Walled Beams and Columns', Proc Instn Civil Engrs, Part 2, December 1978.

59. Timoshenko S.P. 'Sur la Stabilite des Systemes Elastiques', Ann. des Ponts et Chaussees, Paris, 1913.

60. Barbre R. 'Beulspannungen von Rechteckplatten mit Langssteifen bei Gleichmassiger Druckbeanspruchung', Vol. 17, No. 25/26, June 1936.

61. Seide P. 'The Effect of Longitudinal Stiffeners Located on one Side of a

Plate on the Compressive Buckling Stress of the Plate-Stiffener Combination', NACA Tech. Note 2873, January 1953.

62. Wagner H. 'Verdrehung und Knikung von Offenen Profilen', Technische Hochschule, Danzig, 25th anniversary number, 1929 (also in English 'Torsion and Buckling of Open Sections', NACA Tech Memorandum No. 807, 1936).

63. Bleich F., Bleich H. 'Bending Torsion and Buckling of Bars Composed of Thin Walls', Prelim Pub 2nd Cong Intl Assoc Bridge and Structural Eng, English edition, Berlin 1936.

64. Bleich F. **Buckling Strength of Metal Structures**, McGraw Hill Book Co, 1952.

65. Kappus R. 'Drillknicken zentrisch Gedrukter stabe mit Offenem Profil im Elastischen Bereich', Luftfahrtforschung, Vol. 14, No. 9, September 1937 (in English as 'Twisting Failure of Centrally Loaded Open-Section Columns in the Elastic Range', NACA Tech. Memorandum No. 851, 1938).

66. Lundquist E.E., Fligg C.M. 'A Theory for Primary Failure of Straight Centrally Loaded Columns', NACA Tech. Report No. 582, 1937.

67. Timoshenko S.P. 'Theory of Bending Torsion and Buckling of Thin Walled Structures of Open Cross-Section', Jrnl of the Franklin Institute, Vol. 239, April and May 1945.

68. Goodier J.N. 'The Buckling of Compressed Bars by Torsion and Flexure', Cornell Univ Expt Sta Bulletin No. 37, December 1941.

69. Lloyds' Register of Shipping, **Rules and Regulations for the Classification of Ships, Part 4, Ship Structures**, London, January 1984.

70. Det norske Veritas, **Rules for the Design, Construction and Inspection of Offshore Structures, Appendix C - Steel Structures**, Oslo, 1979.

71. Windenburg D.F. 'The Elastic Stability of Tee-Stiffeners', USEMB Report No. 457, November 1938.

72. Harvey Evans J. (ed.) **Ship Structural Design Concepts**, Cornell Maritime Press, 1975.

73. Adamchak J.C. 'Design Equations for Tripping of Stiffeners under Inplane and Lateral Loads', DTNSRDC - 79/064, October 1979.

74. Argyris J.H., Dunne P.E. **Handbook of Aeronautics, Part 2 Structural Analysis - Structural Principles and Data**, No.1, Fourth Edition, New Era Publishing Co, London 1952.

75. Faulkner D., Adamchak J.C., Snyder G.J., Vetter M.F. 'Synthesis of Welded Grillages to Withstand Compression and Normal Loads', Computers and Structures, Vol. 3, 1973.

76. Faulkner D. 'Compression Strength of Welded Ship Panels', Archiwum Budowy Maszyn, Tom XXIV, 1977.

77. Bijlaard F.S.K. 'The Design of Transverse and Longitudinal Stiffeners for Stiffened Plate Panels', Heron, Vol. 27, No. 4, 1982.

78. Carlsen C.A. 'Torsional Buckling of Flatbar Stiffeners - Part 1', DnV Report No. 80 - 0562, Oslo, 1980.

79. Carlsen C.A. 'Experimental and Theoretical Analysis of Post-buckling Strength of Flatbar Stiffeners Subjected to Tripping', DnV Report No. 80 - 149, Oslo, 1980.

80. Skaloud M., Kristek V. 'Folded Plate Theory Analysis of the Effect of the

Stiffener Configuration upon the Buckling of Longitudinally Stiffened Compression Members', Acta Tech CSAV, No. 5, 1977.

81. Guedes Soares C., Soreide T.H. 'Behaviour and Design of Stiffened Plates under Predominantly Compressive Loads', Intl Shipbuilding Progress, Vol. 30, 1982.

82. Ellinas C.P., Croll J.G.A. 'Post-critical Analysis of Torsionally Buckled Stiffened Plates', Intl Jrnl of Solids and Structures, Vol. 17, 1981.

83. Rogers N.A., Dwight J.B. 'Outstand Strength', in Steel Plated Structures Symposium, ed. Dowling P.J., Harding J.E., Frieze P.A., London, 1978.

84. Dowling P.J., Frieze P.A. 'Residual Stresses in Welded Steel Box Girder Flanges', W.I. Conference on Residual Stresses in Welded Construction and their Effects, London, November 1977.

85. Smith C.S., Kirkwood W.C. 'Elastic Bending and Buckling of Panels with Unsymmetrical Stiffeners', Tech. Memorandum AMTE(S) TM 83469, Dunfermline, March 1983.

86. Bradfield C.D. 'Collapse of Rectangular Outstands Loaded in Compression', Proc Intl Colloquium on Stability of Steel Structures (Prelim Report), Liege, April 1977.

87. Wagner H., Pretschner W. 'Verdrehung und Knickung von Offenen Profilen', Luftfahrtforschung, Vol. 11, No. 6,December 1934.

88. Ramberg W., McPherson A.E., Levy S. NACA Tech. Note No. 684, 1939.

89. Rogers N.A. 'Compression Tests on Plain Flat Outstands', Cambridge Univ Report No. CUED/TR 52, 1976.

90. Horne M.R., Montague P., Narayanan R.'Ultimate Capacity of Axially Loaded Stiffened Plates Collapsing by Outstand Failure', Manchester Univ Report, Simon Engineering Laboratories, January 1976.

91. Horne M.R., Narayanan R. 'Ultimate Capacity of Longitudinally Stiffened Plates used in Box Girders', Proc Instn Civil Engrs, Part 2, Vol. 61, June 1976.

92. Scheer J., Nolke H. 'The Background to the German Plate Buckling Design Rules', in Steel Plated Structures, ed. Dowling P.J., Harding J.E., Frieze P.A., London, 1978.

93. Faulkner D. 'A Review of Effective Plating for Use in the Analysis of Stiffened Plating in Bending and Compression', Jrnl of Ship Research, Vol. 19, No. 1, March 1975.

94. British Standards Institution **Steel , Concrete and Composite Bridges, BS5400 Part 3 - Code of Practice for Design of Steel Bridges**, 1982.

95. Drymakis E.C. 'An Examination of Several Methods on Tripping of Stiffeners', Final Year Project, Dept of Naval Architecture and Ocean Engineering, Glasgow Univ, 1979.

96. Hill R. **The Mathematical Theory of Plasticity**, Clarendon Press, Oxford, 1950.

97. Harding J.E., Hobbs R.E., Neal B.G. 'The Elasto-Plastic Analysis of Imperfect Square Plates Under In-plane Loading', Proc Instn Civil Engrs Part 2, Vol. 63, March 1977.

98. Brush D.O., Almroth B.O. **Buckling of Bars, Plates, and Shells**, McGraw Hill Book Co, New York, 1975.

99. Timoshenko S.P., Woinowsky-Kreiger S. **Theory of Plates and Shells**, McGraw Hill Kogakusha, Second Edition, 1959.

100. Donnell L.H. **Beams, Plates and Shells**, McGraw Hill Book Co, 1976.

101. Washizu K. **Variational Methods in Elasticity and Plasticity**, Second Edition, Pergamon Press, 1975.

102. Basu A.K., Djahani P., Dowling P.J. 'Elastic Post-buckling Behaviour of Discretely Stiffened Plates', Symposium on Stability of Steel Structures, (Prelim Report), Liege, April 1977.

103. Lamas A.R.G. 'Influence of Shear Lag on the Collapse of Wide-Flange Girders', Ph.D. Thesis, Imperial College, London, 1979.

104. Sachinis A. 'Ultimate Strength of Stiffened Cylinders in Compression', Ph.D. Thesis, Glasgow Univ, 1981.

105. Ames W.F. **Nonlinear Partial Differential Equations in Engineering**, Academic Press, New York, 1965.

106. Richardson L.F. 'The Approximate Arithmetical Solution by Finite Differences of Physical Problems involving Differential Equations, with an Application to the Stresses in a Masonry Dam', Phil. Trans. Roy. Soc. (London), Vol. A210, 1910.

107. Otter J.R.H., Day A.S. 'Tidal Computations', The Engineer, January 1965.

108. Otter J.R.H. 'Computations for Pre-stressed Concrete Reactor Pressure Vessels using Dynamic Relaxation', Nucl Struct Engng, Vol. 1, 1965.

109. Day A.S. 'Analysis of Plates by Dynamic Relaxation with Special Reference to Boundary Conditions', Intl Symp Use of Elect. Digital

Computers in Struct Engng, University of Newcastle-upon-Tyne, 1936.

110. Underwood P. 'Dynamic Relaxation - A Review', Appl Mech Lab Report, Lockheed Palo Alto Research Lab, California, U.S.A., April 1981.

111. Rushton K.R. 'Dynamic Relaxation Solution for the Large Deflection of Plates with Specified Boundary Stresses', Jrnl Strain Analysis, Vol. 3, No. 1, 1968.

112. Rushton K.R. 'Dynamic Relaxation of Elastic Plate Problems', Jrnl Strain Analysis, Vol. 3, No. 1, 1968.

113. Rushton K.R. 'Postbuckling of Rectangular Plates with Various Boundary Conditions', Aeronautical Quarterly, May 1970.

114. Rushton K.R. 'Large Deflection of Plates with Unsupported Edges', Jrnl Strain Analysis, Vol. 7, 1972.

115. Frieze P.A., Hobbs R.E., Dowling P.J. 'Application of Dynamic Relaxation to the Large Deflection Elasto-Plastic Analysis of Plates', Computers and Structures, Vol. 8, 1978.

116. Drymakis E. 'A Numerical Elasto-Plastic Buckling Analysis for Stiffened Plates', M.Sc. Thesis, Glasgow Univ, 1981.

117. Cassell A.C., Kinsey P.J., Sefton D.J. 'Cylindrical Shell Analysis by Dynamic Relaxation', Proc Instn Civil Engrs, Vol. 39, 1968.

118. Cassell A.C. 'Shells of Revolution under Arbitrary Loading and the Use of Fictitious Densities in Dynamic Relaxation', Proc Instn Civil Engrs, Vol. 45, 1970.

119. Cassell A.C., Hobbs R.E. 'Numerical Stability of Dynamic Relaxation

Analysis of Non-linear Structures', Intl Jrnl Numerical Methods, 1976.

120. Engeli M., Ginsburg Th., Rutishauser H., Stiefel E. 'Refined Iterative Methods for Computation of the Solution and the Eigenvalues of Self-Adjoint Boundary Value Problems', Birkhauser Verlag, Basel/Stuttgart, 1959.

121. Wood W.L. 'On an Explicit Numerical Method for Solving the Biharmonic Equation', Numerische Mathematik, Vol. 11, 1968.

122. Papadrakakis M. 'A Method for the Automatic Evaluation of the Dynamic Relaxation Parameters', Computer Methods in Applied Mechanics and Engineering, Vol. 25, 1981.

123. Brew J.S., Brotton D.M. 'Nonlinear Structural Analysis by Dynamic Relaxation', Intl Jrnl Numerical Methods, Vol. 3, 1971.

124. Gilles D.C. 'The Use of Interlacing Nets for the Application of Relaxation Methods to Problems Involving Two Dependent Variables', Proc Roy Soc (London), Vol. A193, 1948.

125. Crisfield. M.A. 'Large Deflection Elasto-Plastic Buckling Analysis of Plates Using Finite Differences', TRRL Report LR593, 1973.

126. Moffat K.R., Dowling P.J. 'Parametric Study on the Shear Lag Phenomenon in Steel Box Girder Bridges', CESLIC Report BG 17, Imperial College, London, 1972.

127. Sands J.G., Frieze P.A. 'Torsional Buckling Tests on Flat-Bar Stiffened Flat Panels - Part 1: Experimental Procedure and Test Results', Report No. NAOE-84-66, Glasgow Univ, December 1984.

128. Clarkson J. 'A New Approach to the Design of Plates to Withstand Lateral Pressure', Trans R.I.N.A., Vol. 98, 1956.

129. Young A.G. 'Ship Plating Loaded Beyond the Elastic Limit', Trans R.I.N.A., Vol. 101, 1959.

130. Jones N., Walters R.M. 'Large Deflections of Rectangular Plates', Jrnl Ship Research, June 1971.

131. Ueda Y., Tall L. 'Inelastic Buckling of Plates with Residual Stresses', Publ Inst Assoc Bridge Structural Engineering, 1967.

132. Moxham K.E. 'Buckling Tests on Individual Welded Steel Plates in Compression', Report No CUED/C - Struct/TR3, Engineering Dept, Cambridge Univ, 1971.

133. Carlsen C.A. 'A Parametric Study of Collapse of Stiffened Plates in Compression', The Structural Engineer, Vol. 58B, No. 2, June 1980.

134. Frieze P.A., Drymakis E. 'An Examination of Shakeout in Stiffened Plates', in Behaviour of Thin-Walled Structures, ed. Rhodes J., Spence J., Elsevier Applied Science Publishers, London, 1984.

135. Samuelides E. 'Structural Dynamic and Rigid Body Response Coupling in Ship Collisions', Ph.D. Thesis, Glasgow Univ, 1984.

136. Johnson W. **Impact Strength of Materials**, Edward Arnold, London, 1972.

137. Jones N. 'A Literature Review on the Dynamic Plastic Response of Structures', The Shock and Vibration Digest, Vol. 7, No. 8, August 1975.

138. Jones N. 'A Theoretical Study of the Dynamic Plastic Behaviour of Beams and Plates with Finite-Deflections', Intl Jrnl of Solids and Structures, Vol. 7, 1971.

139. Cowper G.R., Symonds P.S. 'Strain-hardening and Strain-Rate Effects in the Impact Loading of Cantilever Beams', Tech Rep No. 28, Brown Univ, Rhode Island, 1957.

140. de Oliveira J.G. 'Design of Steel Structures against Impact Loads due to Dropped Objects', Proc 3rd Intl Symp on Offshore Engineering Structures, ed. Carneiro et al., Coppe, Rio de Janeiro, 1981.

141. Sadden J.A. 'Primary Strength Design for Destroyers and Frigates', Steel Plated Structures Symposium, ed. Dowling P.J. Harding J.E. Frieze P.A., London, 1978.

142. Department of the Navy, **Design Data Sheets DDS100-4 - Strength of Structural Members**, Naval Ship Engineering Centre, August 1969.

143. Mathewson J.I., Viner A.C. 'Buckling as a Mode of Failure in Ship Structures', Lloyds Register of Shipping, London, 1970.

144. Timoshenko S.P., Gere J.M. **Theory of Elastic Stability,** McGraw Hill Kogakusha, Second Edition, Tokyo, 1961.

145. Carlsen C.A., Shao W.J., Fredheim S. 'Experimental and Theoretical Analysis of Post-buckling Strength of Flat-bar Stiffeners Subjected to Tripping', Det norske Veritas Report No. 80 - 0149, February 1980.

APPENDIX A : TRIPPING STRESS FORMULAE PRESENTED FOR DESIGN PURPOSES

A.1 British Bridge Design Code (BS5400 Part 3) [94]

For flatbar stiffeners, the proportions should be such that

$$\frac{h_s}{t_s}\sqrt{\frac{\sigma_{ys}}{355}} \leq 10$$

where h_s, t_s are the depth and thickness of the stiffener.

For tee-bar stiffeners,

$$\frac{b_{so}}{t_{so}}\sqrt{\frac{\sigma_{ys}}{355}} \leq 10 \qquad \frac{d_s}{t_s}\sqrt{\frac{\sigma_{ys}+\sigma_a}{355}} \leq 41 \qquad \frac{d_s}{t_s}\sqrt{\frac{\sigma_{ys}}{355}} \leq 7$$

where t_{so} is the average thickness of the flange outstand of width b_{so}

d_s is the effective stiffener depth, measured from the underside of the flange plate

σ_a is the longitudinal stress for the ultimate state at the centroid of the effective section of the stiffener.

A.2 Det norske Veritas Rules for Offshore Structures [70]

Flatbar stiffeners should be proportioned such that

$$\frac{h}{t_w} \leq 0.4\sqrt{\frac{E}{f_y}}$$

For flanged profiles, $\sigma_{TE} \geq 2.5\, f_y$, where the torsional buckling stress is given by

$$\sigma_{TE} = \frac{GI_t}{I_{po}} + \frac{\pi^2 E h_s^2 I_z}{I_{po}^{\ 2}}$$

where I_t is the Saint Venant torsional stiffness of the stiffener

I_{po} is the polar moment of inertia of the stiffener about the toe

I_z is the momemt of inertia of the stiffener about the neutral axis normal to the plate

a is the length between transverse girders

h_s is the distance from the stiffener toe to the shear centre

f_y is the yield stress

A.3 Royal Navy [141]

The maximum average stress across the edges of a stiffened plate is given by:

$$\sigma_{tr} = \frac{(\sigma_T A_s + \sigma_p bt)}{(A_s + bt)}$$

where $$\sigma_T = \frac{GJ}{I_0} + E\,(I_z d^2 + \Gamma)\frac{\pi^2}{I_0 a^2}$$ (longitudinal tripping stress)

$$\sigma_p = \frac{\pi^2 E}{12\,(1 - \nu^2)} \left(\frac{t}{b}\right)^2 \left[\frac{a}{b} + \frac{b}{a}\right]^2$$ (plate buckling stress)

and

A_S	=	Stiffener cross-sectional area
a, b, t	=	Plate length, breadth, thickness
G	=	Shear modulus
J	=	Saint Venant torsion constant for stiffener
I_0	=	Polar second moment of area about axis of enforced rotation
I_z	=	Second moment of area about stiffener toe
d	=	Distance from shear centre to stiffener toe
Γ	=	Torsional warping constant

A.4 Lloyd's Register of Shipping Rules [69]

For general cargo ships, the strength/weather deck longitudinals located outside lines of

openings are to have a section modulus given by

$$Z = 0.0106\, s\, k\, l_e^2\, K$$

where s is the spacing of secondary stiffeners

k is a higher tensile steel factor

l_e is the effective length of the stiffening member (not to be taken less than 1.5 m)

K is a factor dependent on freeboard

The thickness of flatbar longitudinals located outside lines of openings are to be not less than

$$t = \frac{d_w}{18\sqrt{k}}$$

where the longitudinal is continuous through the bulkhead.

A.5 U.S. Navy [142]

The maximum ratio of stiffener span to flange width (a/f_w) for which support is only required at the ends is given by:

$$\left(\frac{a}{f_w}\right) = \frac{\left(\frac{\pi}{\sqrt{\sigma}}\right)\sqrt{\frac{E}{\sigma_0}}}{\left[1 + \frac{1}{3}\left(\frac{d}{f_w}\right)\left(\frac{t_w}{t_f}\right) - \left(\frac{E}{7.8\sigma_0}\right)\left(\frac{t_f}{t_w}\right)^2\left(\frac{f_w}{d}\right)^2\right]}$$

where E = Young's Modulus

σ_0 = Yield stress

d, t_w, t_f = Web depth, thickness, flange thickness

A.6 Adamchak [73]

i) Axial compressive loading

For flanged stiffeners $$\sigma_{tr} = \left(\frac{1}{I_p}\right)\left[GJ + E\left(I_z \bar{z}^2 + \Gamma\right)\left(\frac{m\pi}{a}\right)^2 + C\left(\frac{a}{m\pi}\right)^2\right]$$

For flatbars $$\sigma_{tr} = \frac{1}{3}\frac{D_w d}{I_p}\left[\left(\frac{m\pi}{a}\right)^2 d^2 + 6(1-\nu)\right] + \frac{C}{I_p}\left(\frac{a}{m\pi}\right)^2$$

ii) Constant moment loading

For flanged stiffeners $$M_{cr} = \left(\frac{I}{S}\right)\left[E(I_z\bar{z}^2 + \Gamma)\left(\frac{m\pi}{a}\right)^2 + GJ + \left(\frac{a}{m\pi}\right)^2 C\right]$$

For flatbars $$M_{cr} = \left(\frac{I}{S}\right)\left[\frac{D_w d}{3}\left\{\left(\frac{m\pi}{a}\right)^2 d^2 + 6(1-\nu)\right\} + \left(\frac{a}{m\pi}\right)^2 C\right]$$

iii) Lateral loading

For flanged stiffeners $$q_{cr} = -\frac{12IGJ}{Sa^2}\frac{H_m(k)}{F_m(k)}$$

For flatbars $$q_{cr} = -\frac{4IdD_w}{Sa^2}\frac{\bar{H}(k)}{F_m(k)}$$

where $H_m(k)$, $\bar{H}_m(k)$ and $F_m(k)$ are quadratic functions of the scalar k.

iv) Combined axial compression and lateral loading

$$\sigma_{cr} = \frac{GJH_m(k) + \frac{1}{12}\left(\frac{qa^2}{I}\right) S F_m(k)}{Ip\left(m^2k^2 + (m+2)^2(k-1)^2\right)}$$

Interaction formula: $$\frac{\sigma}{\sigma_{cr}} + \frac{M}{M_{cr}} + \frac{q}{q_{cr}} = 1$$

Inelastic effects are considered by using the structural proportional limit, p_r.

A.7 Bleich [63]

The elastic tripping stress is given by:

$$\sigma_{tr} = \frac{\pi^2 E}{l^2}\left[\frac{a^2 I_y + \Gamma}{I_{pc}} + \frac{G}{\pi^2 E}\frac{l^2 k}{I_{pc}}\right]$$

A.8 Faulkner et al. [74]

$$\sigma_{TE} = \frac{G}{I_0}\left[J_t + \frac{Cs^2}{G\pi^2}\right]$$

where s = length of each half-sine wave

$C = Et^3/3b$

J = stiffener twisting rigidity

I_0 = stiffener polar moment of inertia about its toe

A.9 Faulkner [72]

$$\sigma_{TEI} = (GJ_t + Et^3 l^2 / 3\pi^2 b) / I_o (1 + Et^3 l^2 / 3\pi^2 b \sigma_{PE} I_o)$$

where $J_t = J + \pi^2 E (I_z \bar{z}^2 + \Gamma) / Gl^2$

$$\sigma_{PE} = 0.905 E (t/b)^2 (\alpha + 1/\alpha)^2$$

A.10 Mathewson and Viner [143]

$$\sigma_{cr} = \frac{\pi^2 Et}{I_p l^2}\left[\eta I_f a^2 + 0.0390 J_e l^2\right]$$

where $I_p = A_f a^2 + \frac{t_w a^3}{3} + I_f$

$$I_f = \frac{b^3 t_f}{12}$$

η = 1 for a symmetric flange

Inelastic effects are considered by use of the Ostenfeld-Bleich quadratic parabola for $\sigma > \sigma_0/2$.

A.11 Timoshenko and Gere [144].

The critical elastic buckling stress for an isolated plate (stiffener) with one edge free is given by:

$$\sigma_{cr} = k \frac{\pi^2 D}{b^2 h}$$

where k depends on the stiffener and plate geometry. For long plates, the coefficient k takes the following values:

S-S-S-F edges $k = 0.456 + (b/a)^2$

S-C-S-F edges $k = 1.328$

A.12 Argyris and Dunne [74]

Flexural failure $\sigma_1 = (\frac{1}{A_e})\left[(\frac{\pi}{\lambda})^2 E_t I_e + (\frac{\lambda}{\pi})^2 k\right]$ where $k = 4E(\frac{t}{b})^2$

Torsional failure $\sigma_2 = (\frac{1}{I_p})\left[GJ + (\frac{\pi}{\lambda})^2 E_t \Gamma + (\frac{\lambda}{\pi})^2 k\right]$

Combined torsional and flexural failure:

$$\sigma_{cr} = \frac{1}{2}\left[\sigma_1 + \sigma_2 + \sqrt{(\sigma_1 - \sigma_2)^2 + 4(S/i_{pR})^2 \sigma_{xy}^2}\right]$$

where $\sigma_{xy} = \dfrac{\pi^2 E_t I_{xy}}{\lambda^2 (A_s + A_p/S)}$

i_{pR} = polar radius of gyration

S = distance of shear centre

A.13 Rogers and Dwight [83]

σ_{cr} is the lower root of $(\sigma_o - \sigma_{cr}) (\sigma_E - \sigma_{cr}) = \eta \sigma_E \sigma_{cr}$

$D = \sqrt{\dfrac{I_o}{J}}$ where D is the 'slenderness' of the flatbar stiffener

$D_1 = 0.62 \sqrt{\dfrac{E}{\sigma_0}}$

$D_o = 0.4 \sqrt{\dfrac{E}{\sigma_0}} - 0.0012 \dfrac{E}{\sigma_0}$ = extent of plateau along flatbar stiffener strength curve

where $D < D_1$ $\quad \sigma_E = \dfrac{G}{D^2}$

$D > D_1$ $\quad \sigma_E = \{ (\dfrac{D_1}{D}) - (\dfrac{D_1}{D})^4 + (\dfrac{D_1}{D})^5 \} \sigma_0$

$D < D_o$ $\quad \eta = 0$

$D_o < D < D_1$ $\quad \eta = \alpha_0 (D - D_0)$

$D_1 < D$ $\quad \eta = \alpha_0 (D_1 - D_0)$

$\alpha_0 = 0.01$

A.14 Carlsen, Shao and Fredheim [145]

The plastic collapse bending moment is given by:

$$M_p = \frac{\sigma_0 h A_w}{2}\left[1 - \frac{\sigma_m}{\sigma_0} - \frac{bz^2}{t_w h^2} + \left(1 + \frac{\sigma_m}{\sigma_0} \right) \frac{t_p^2 b}{t_w^2 h} \right]$$

where $$z = \left(\frac{1}{2b}\right)\left(A_t \frac{\sigma_m}{\sigma_0} + \left(A_p - A_w \right) \right)$$

APPENDIX B : STABILITY BOUNDS FOR THE VON KARMAN AND BEAM - COLUMN EQUATIONS OF EQUILIBRIUM

Gershgorin's theorem states that the largest eigenvalue, b_G, is bounded by the numerical sum of the absolute values of the coefficients of each row of the stiffness matrix (Section 3.2). For the equation of equilibrium of a flat plate in the out-of-plane direction at each node (i,j), the Gershgorin bound is given by:

$$b_{Gw} = \overline{\frac{\partial^2 M_x}{\partial x^2}} + 2\,\overline{\frac{\partial^2 M_{xy}}{\partial x \partial y}} + \overline{\frac{\partial^2 M_y}{\partial y^2}} + \overline{N_x}\left(\left|\frac{\partial^2 w}{\partial x^2}\right| + \left|\frac{\partial^2 w_o}{\partial x^2}\right|\right) +$$

$$2\,N_{xy}\left(\left|\frac{\partial^2 w}{\partial x \partial y}\right| + \left|\frac{\partial^2 w_0}{\partial x \partial y}\right|\right) + \overline{N_y}\left(\left|\frac{\partial^2 w}{\partial y^2}\right| + \left|\frac{\partial^2 w_0}{\partial y^2}\right|\right) +$$

$$\overline{N_y}\left(\left|\frac{\partial^2 w}{\partial y^2}\right| + \left|\frac{\partial^2 w_0}{\partial y^2}\right|\right)$$

where the horizontal bar denotes the Gershgorin bound of the individual term. In the in-plane directions, stability is ensured if

$$b_{Gu} = \overline{\frac{\partial N_x}{\partial x}} + \overline{\frac{\partial N_{xy}}{\partial y}} \qquad \text{(A2.2)}$$

$$b_{Gv} = \overline{\frac{\partial N_y}{\partial y}} + \overline{\frac{\partial N_{xy}}{\partial x}} \qquad \text{(A2.3)}$$

Each Gershgorin term is obtained from the absolute values of the coefficients of the corresponding finite difference term. For example,

$$\overline{\frac{\partial^2 M_x}{\partial x^2}} = \frac{|\overline{M_x}(i+1,j)|\,|-2|\,|\overline{M_x}(i,j)|\,|+1|\,|\overline{M_x}(i-1,j)|}{\Delta x^2} \qquad \text{(A2.4)}$$

where

$$\overline{M_x} = |-D|\left(\overline{\frac{\partial^2 w}{\partial y^2}} + \nu\,\overline{\frac{\partial^2 w}{\partial x^2}}\right) = 4D\left(\frac{1}{\Delta x^2} + \frac{\nu}{\Delta y^2}\right) \qquad \text{(A2.5)}$$

$$\therefore \quad \overline{\frac{\partial^2 M_x}{\partial x^2}} = \frac{16D}{\Delta x^2}\left(\frac{1}{\Delta x^2} + \frac{\nu}{\Delta y^2}\right) \qquad \text{(A2.6)}$$

Formal requirements stipulate that in the elasto-plastic range it is necessary to consider the full set of elasto-plastic coefficients. It has been found however that coefficients valid in the elastic range ensure stability in the plastic range as well and for this reason only the elastic terms have been used throughout the loading path.

The stability bound b_G^s for equation 2.48a which represents beam-column action, is found at each node i from:

$$b_G^s(i) = \frac{1}{\Delta x^2}\left[\overline{M}(i+1) + 2\overline{M}(i) + \overline{M}(i-1)\right] + |P_i|\frac{4}{\Delta x^2} +$$

$$\overline{P_i}\left(\left|\frac{\partial^2 s}{\partial x^2}\right| + \left|\frac{\partial^2 s_o}{\partial x^2}\right|\right) + |z|\left(\frac{4}{\Delta x^2}\right) \qquad \text{(A2.7)}$$

where

$$\overline{P_i} = \sum_{j=2}^{jmax} \overline{N_x^G}(i,j) \;.\; (\text{rule multiplier}) \qquad \text{(A2.8)}$$

$$\overline{M_i} = \sum_{j=2}^{jmax} \overline{N_x^G}(i,j) \;.\; z \;.\; (\text{rule multiplier}) \qquad \text{(A2.8)}$$

and $\overline{N_x^G}(i,j)$ is the Gershgorin bound of the global longitudinal stress resultant. As in the analysis of local behaviour, elastic expressions are used.

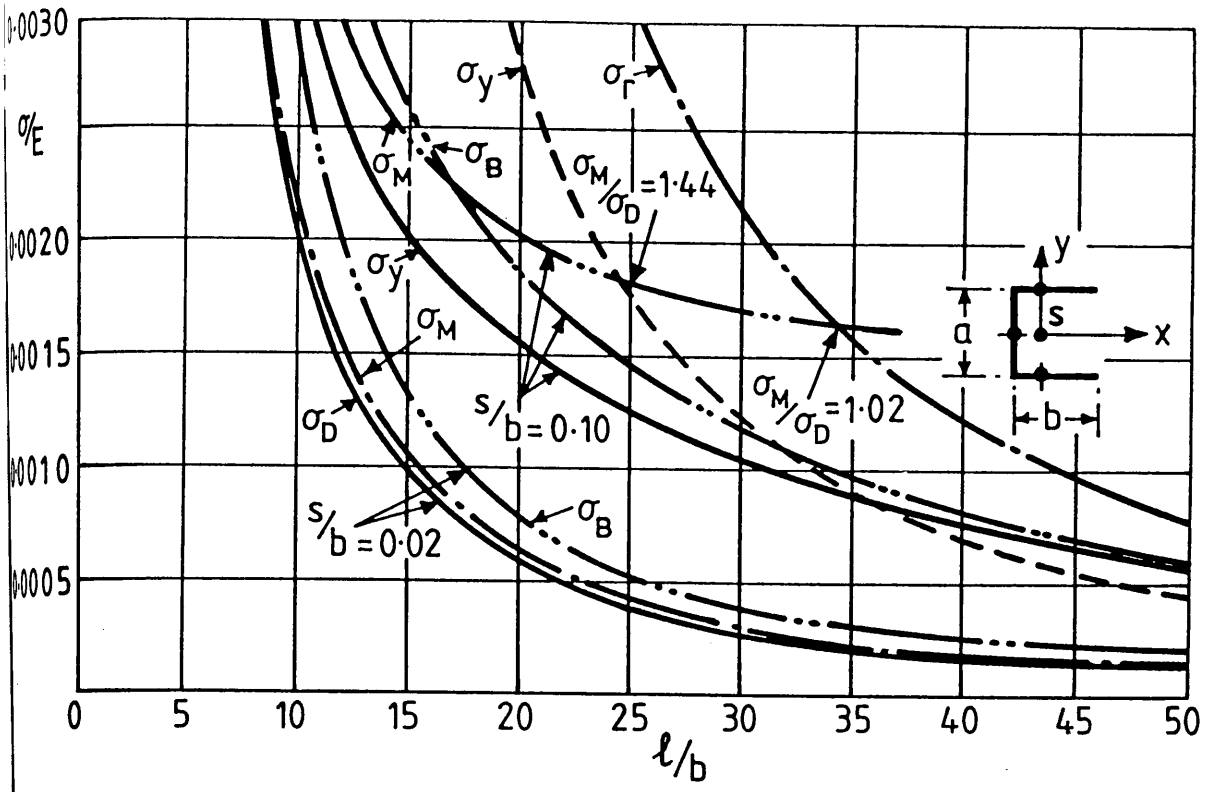

EULER EQUATIONS:

$$\sigma_x = 0 \cdot 1944 \frac{\pi^2 E}{(\ell/b)^2}$$

$$\sigma_y = 0 \cdot 1111 \frac{\pi^2 E}{(\ell/b)^2}$$

KAPPUS (64):

$$\sigma_D = \frac{\sigma_s + \sigma_x}{2} \; (\mp) \; \sqrt{\frac{(\sigma_s - \sigma_x)^2}{2} + \rho_x^2} \quad ; \quad \rho_x = -0 \cdot 2680 \frac{\pi^2 E}{(\ell/b)^2}$$

WAGNER:

$$\sigma_M = \left[0 \cdot 002239 + 0 \cdot 001466 \left(\frac{s}{b}\right)^2 \left(\frac{\ell}{b}\right)^2 \right] \frac{\pi^2 E}{(\ell/b)^2}$$

BLEICH:

$$\sigma_B = 0 \cdot 1994 \left[1 - \frac{0 \cdot 3593}{0 \cdot 4345 + 0 \cdot 04251 \left(\frac{s}{b}\right)^2 \left(\frac{\ell}{b}\right)^2} \right] \frac{\pi^2 E}{(\ell/b)^2}$$

1.1 CLASSICAL METHODS – VARIATION OF TWISTING FAILURE STRESS WITH LENGTH FOR CHANNEL SECTIONS WITH a/b = 1 (64)

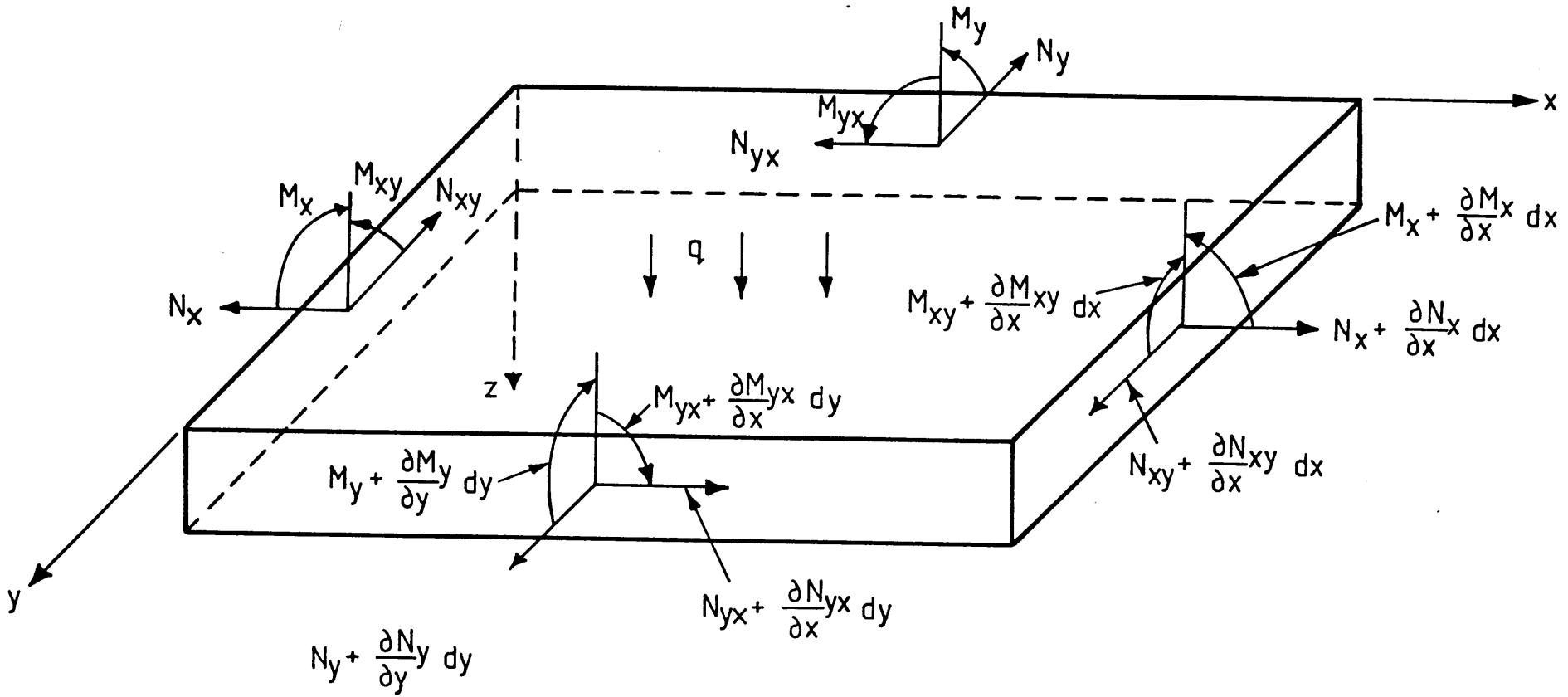

Fig. 2·1. FORCES AND MOMENTS ACTING ON A PLATE SECTION.

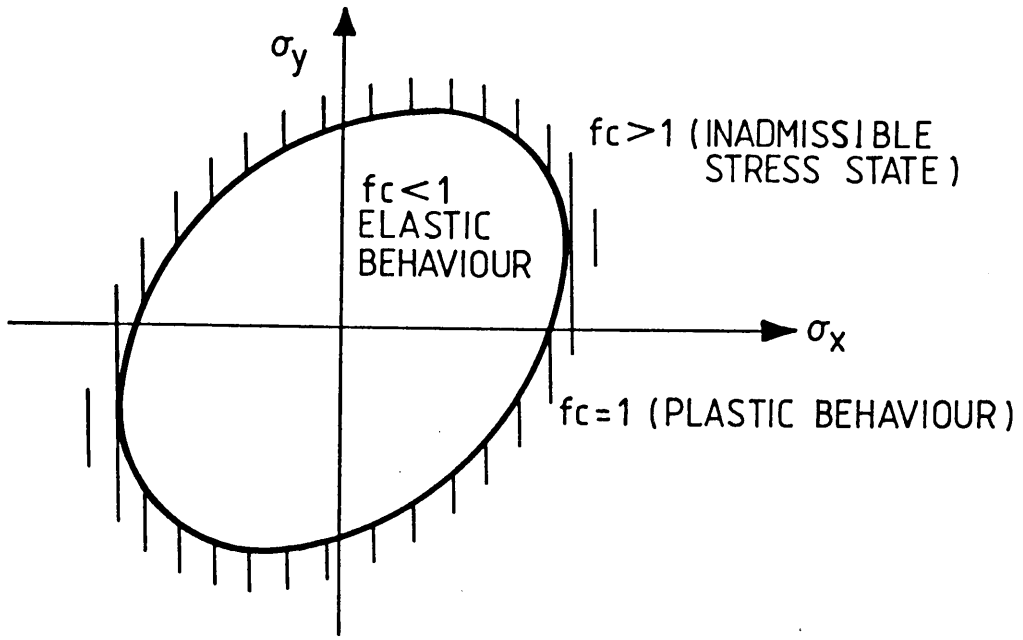

$$fc = (\sigma_x^2 + \sigma_y^2 - \sigma_x \sigma_y + 3\tau_{xy}^2) / \sigma_Y^2 \leq 1{\cdot}0$$

(a) THE VON MISES YIELD CRITERION IN 2-D SPACE

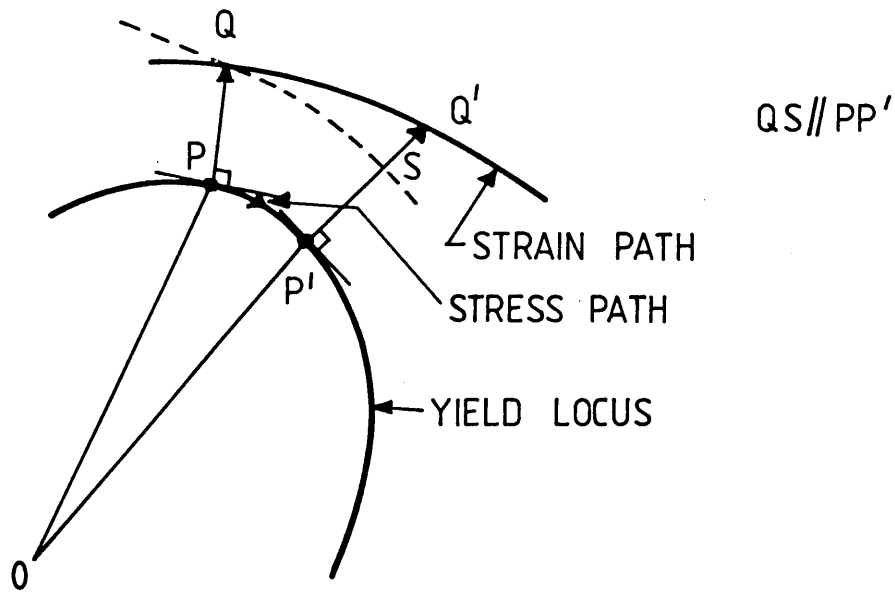

(b) PERMISSIBLE STRESS AND STRAIN PATHS IN STRESS SPACE

Fig. 2·2 STRESS-STRAIN BEHAVIOUR FOR A NON-WORKHARDENING MATERIAL

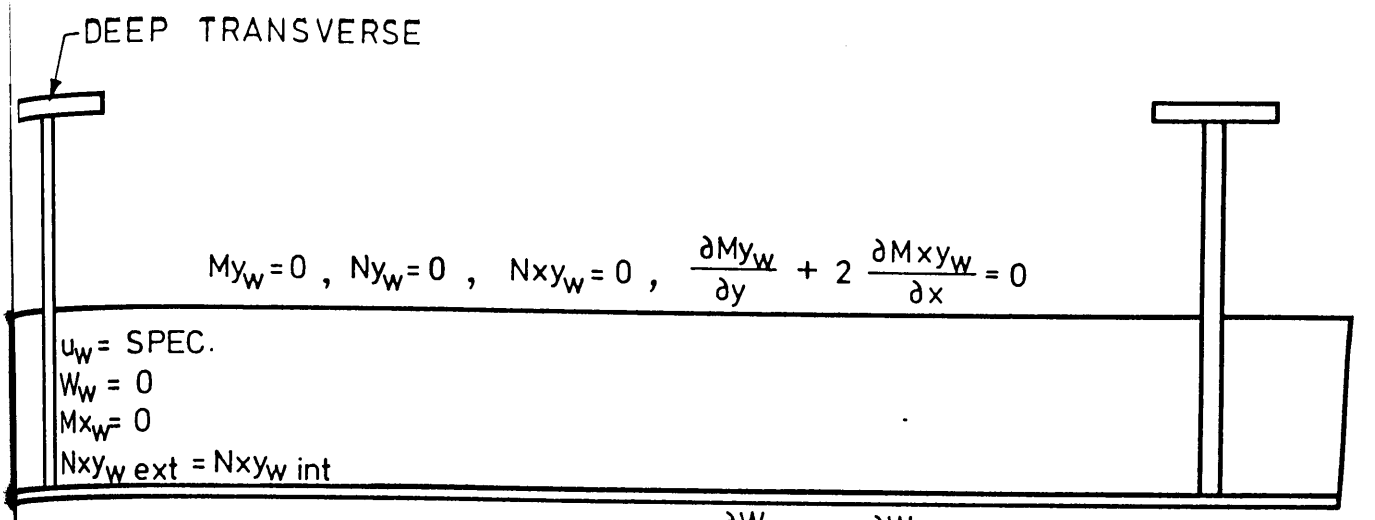

$$W_w = V_p \quad , \quad Ny_w = Q_p \quad , \quad \frac{\partial W_w}{\partial y} = \frac{\partial W_p}{\partial y}$$

$$\left(\frac{\partial Nx_p}{\partial x} + \frac{\partial Nxy_p}{\partial y}\right)\left(\frac{\Delta y_p}{\Delta y_p + \Delta y_w/2}\right) + \left(\frac{\partial Nx_w}{\partial x} + \frac{\partial Nxy_w}{\partial y}\right)\left(\frac{\Delta y_w/2}{\Delta y_p + \Delta y_w/2}\right) = 0$$

a) STIFFENER

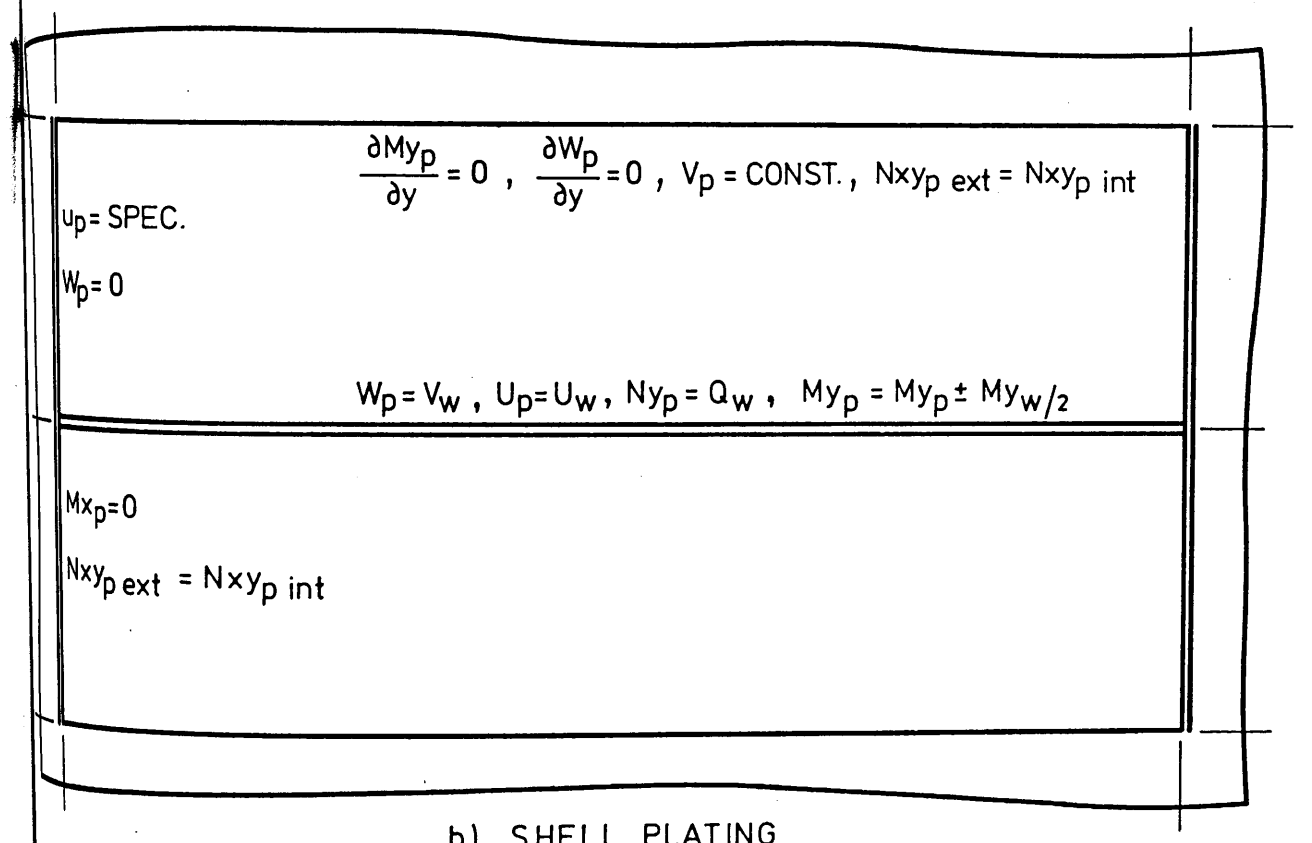

b) SHELL PLATING

10.2.3 BOUNDARY CONDITIONS FOR STIFFENED PLATING FORMING PART OF A UNIAXIALLY COMPRESSED GRILLAGE

DISPLACEMENT BOUNDARY CONDITIONS

(1.) $W_p = -V_w$

(2.) $W_w = V_p$

(3.) $U_p = U_w$

(4.) $\frac{\partial w_w}{\partial y} = \frac{\partial w_p}{\partial y}$

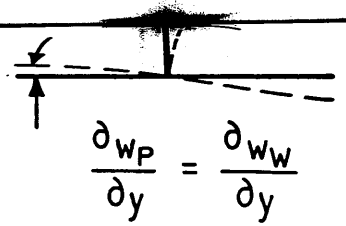

$$\frac{\partial w_p}{\partial y} = \frac{\partial w_w}{\partial y}$$

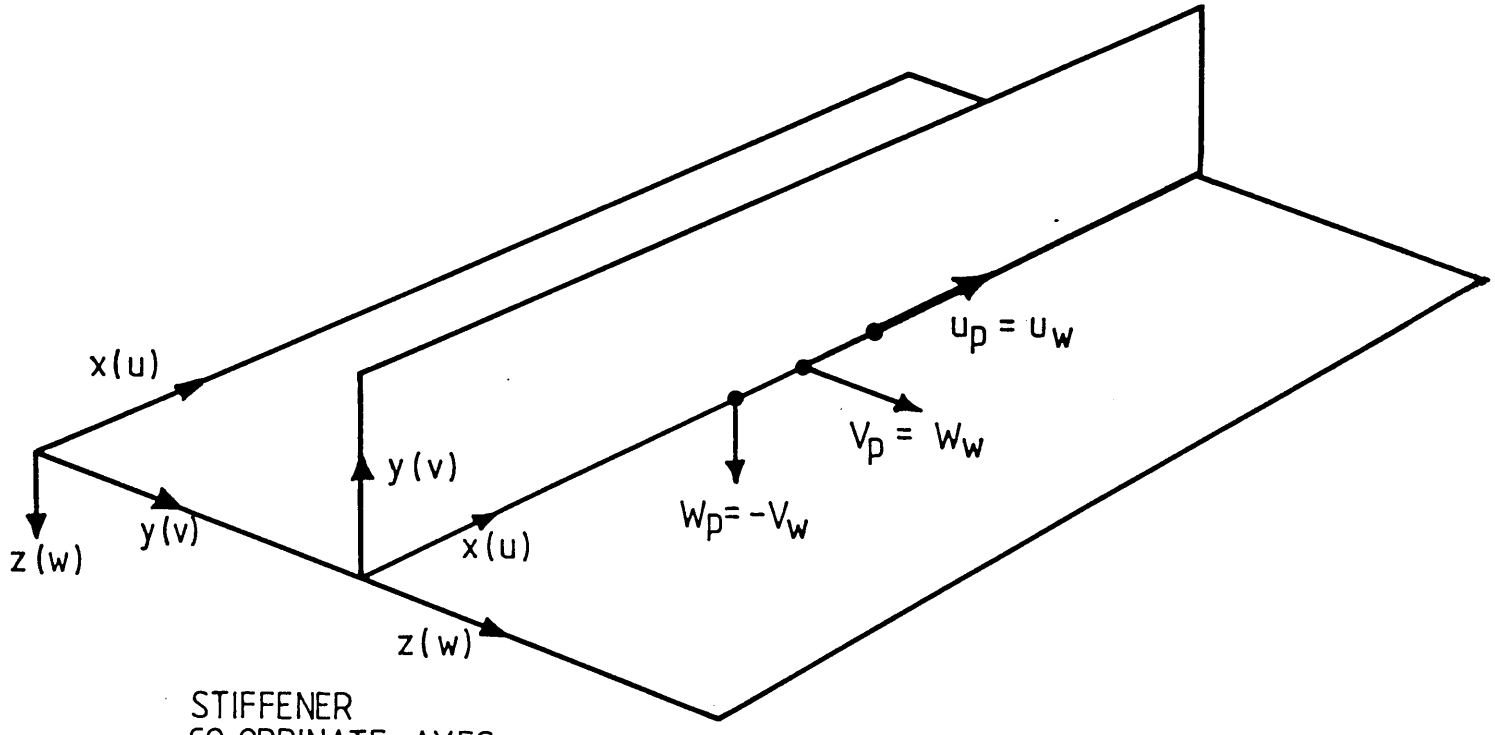

PLATE CO-ORDINATE AXES

SUBSCRIPTS p, w REFER TO PLATE, STIFFENER RESPECTIVELY

STIFFENER CO-ORDINATE AXES

Fig.2·4(a) FLAT STIFFENED PLATE — COMPATIBILITY of DISPLACEMENTS and ROTATIONS

EQUILIBRIUM BOUNDARY CONDITIONS

(1) $N_{yw} = -\left(\frac{\partial M_{yp}}{\partial y} + 2\frac{\partial M_{xy}}{\partial x}p\right)$

(2.) $N_{yp} = \left(\frac{\partial M_{yw}}{\partial y} + 2\frac{\partial M_{xyw}}{\partial x}\right)$

(3.) $N_{xyw} = N_{xyr} - N_{xy\ell}$

(4.) $M_{yp_{\ell,r}} = M_{yp} \mp M_{yw}/2$

SUBSCRIPTS p,w REFER TO PLATE, STIFFENER RESPECTIVELY

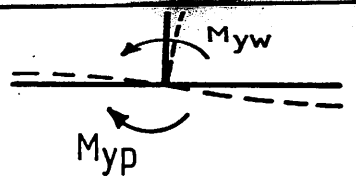

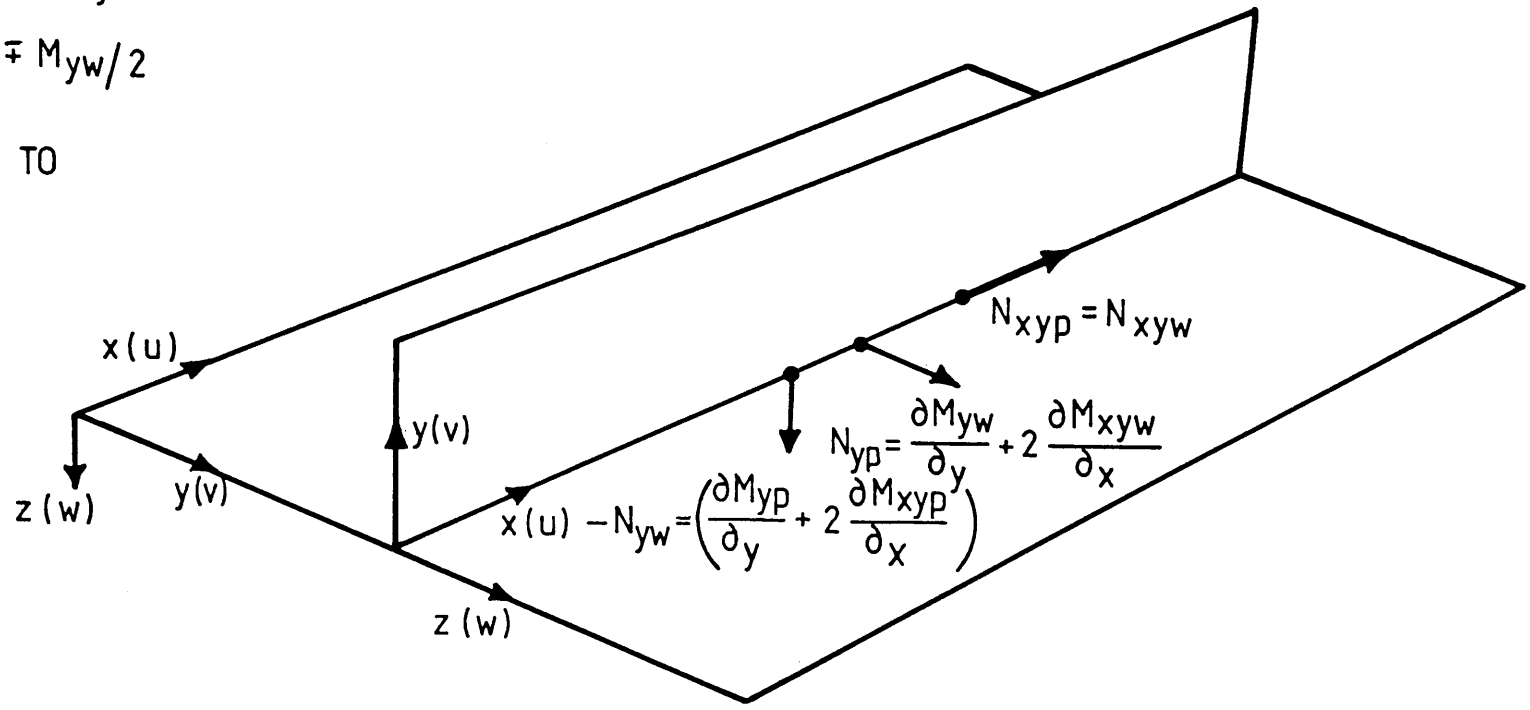

Fig. 2·4(b) FLAT STIFFENED PLATE — COMPATIBILITY of FORCES and MOMENTS

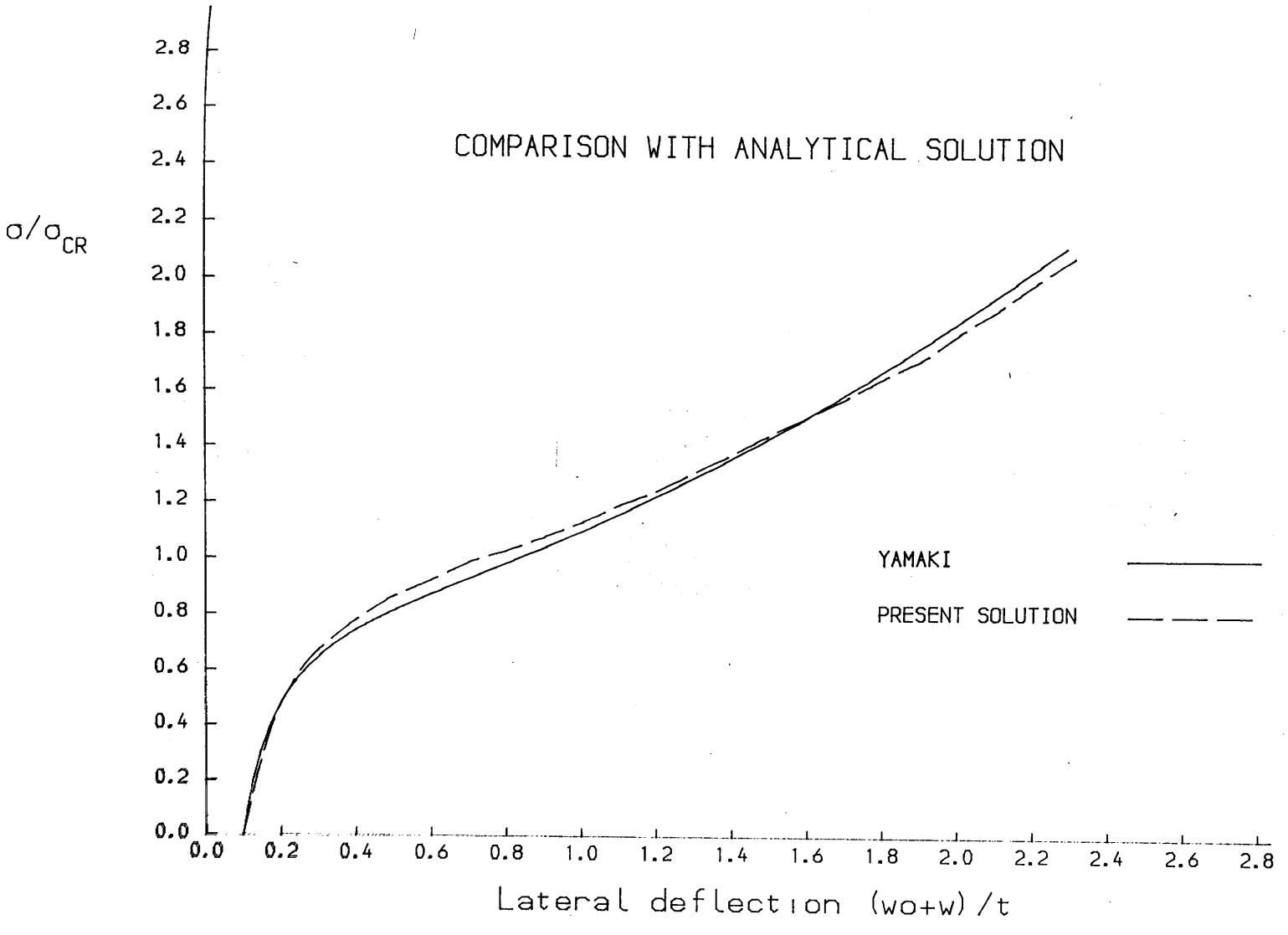

FIG. 3.1 ELASTIC RESPONSE OF A SIMPLY-SUPPORTED SQUARE PLATE

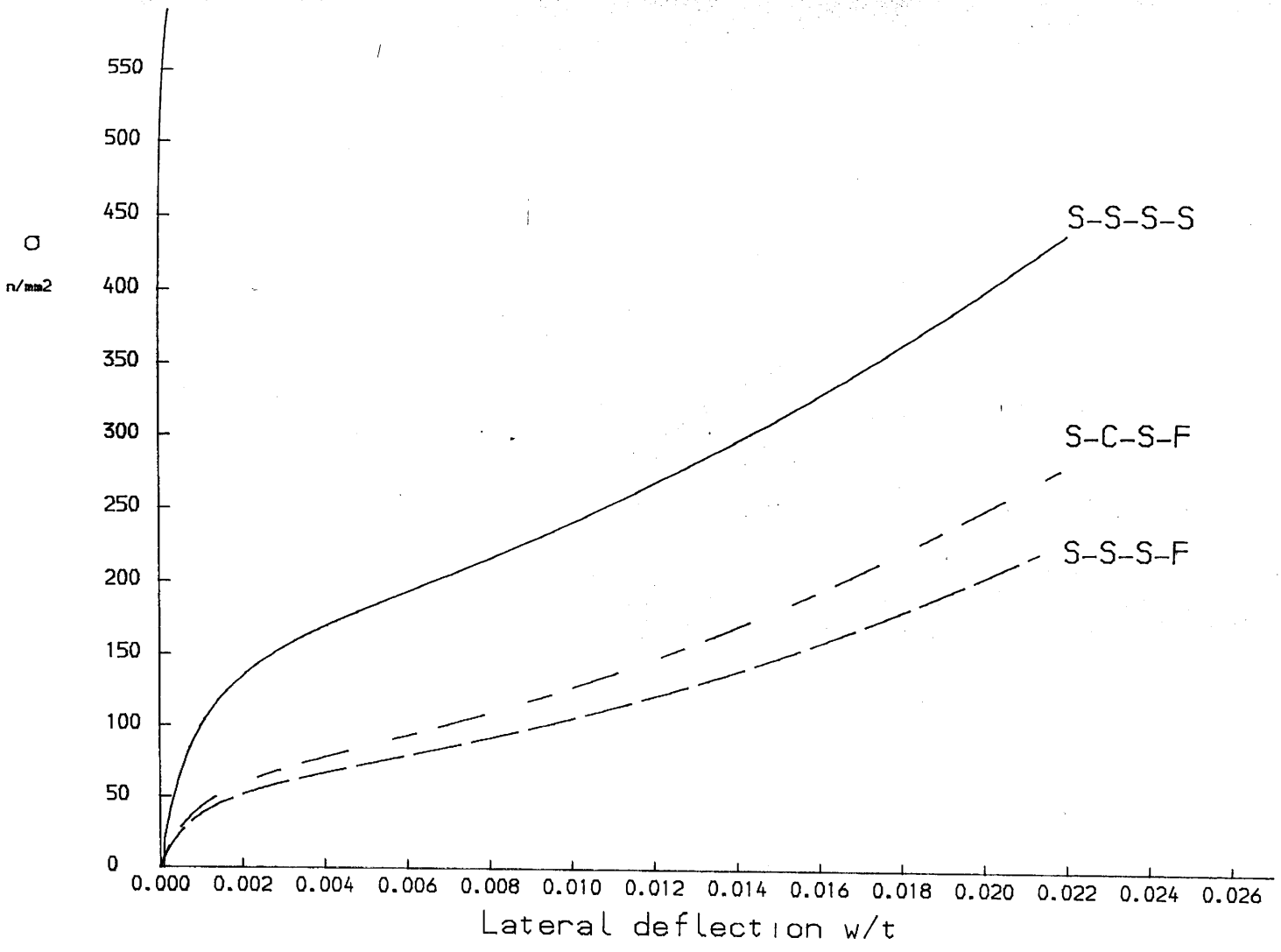

FIG. 3.2 ELASTIC RESPONSE OF A SIMPLY-SUPPORTED SQUARE PLATE

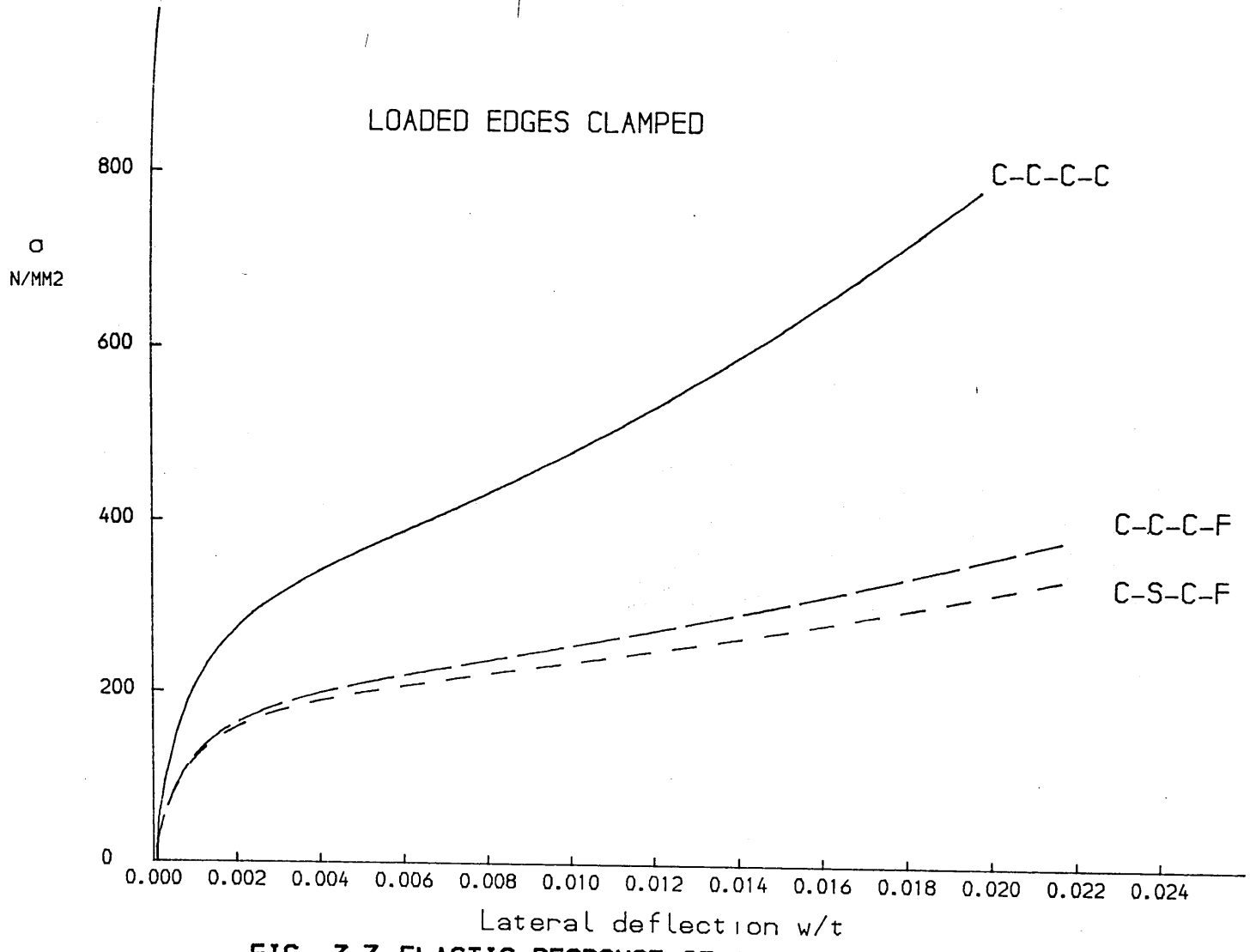

FIG. 3.3 ELASTIC RESPONSE OF A SIMPLY-SUPPORTED SQUARE PLATE

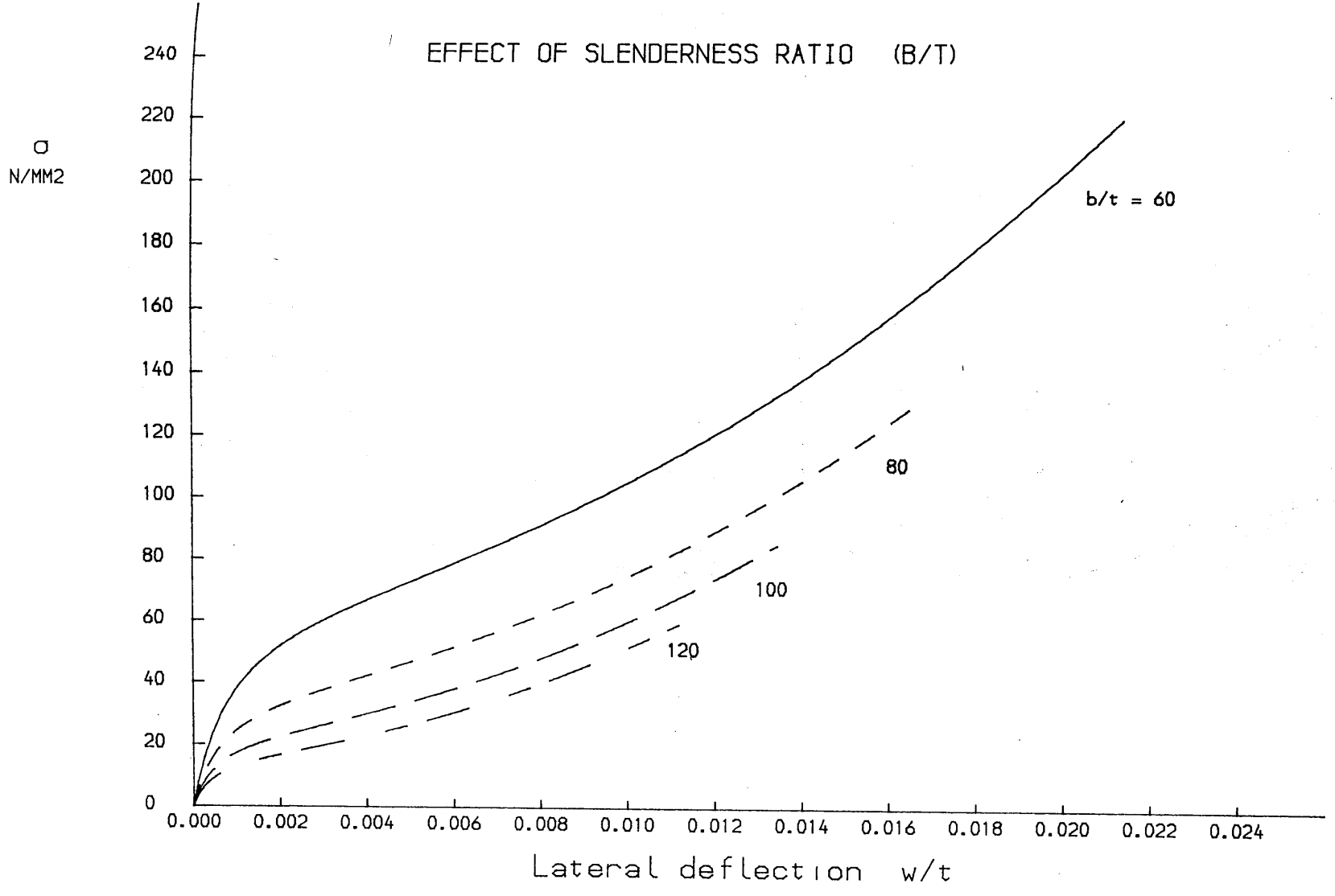

FIG. 3.4 ELASTIC RESPONSE OF A SQUARE PLATE WITH ONE EDGE FREE

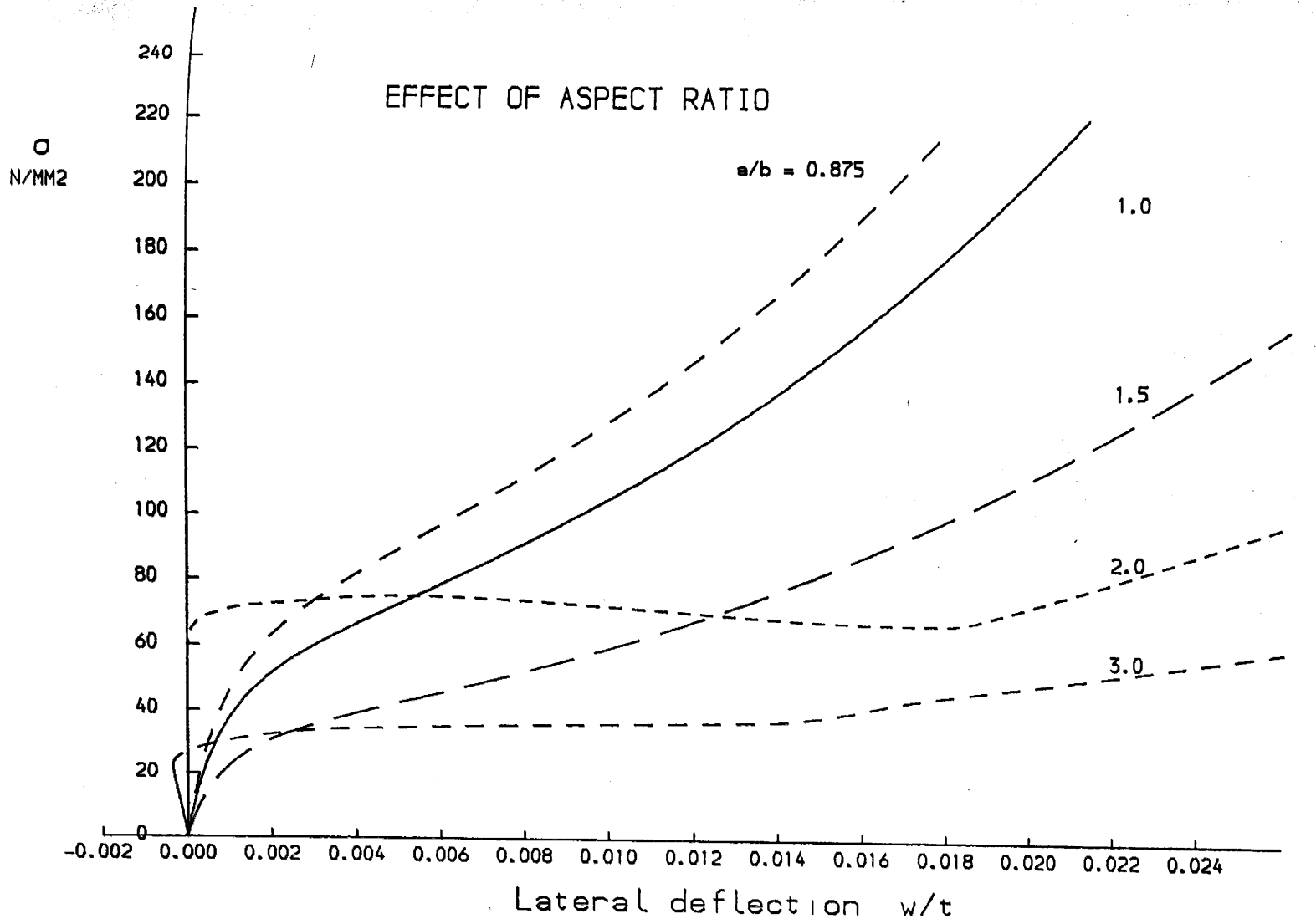

FIG. 3.5 ELASTIC RESPONSE OF A SQUARE PLATE WITH ONE EDGE FREE

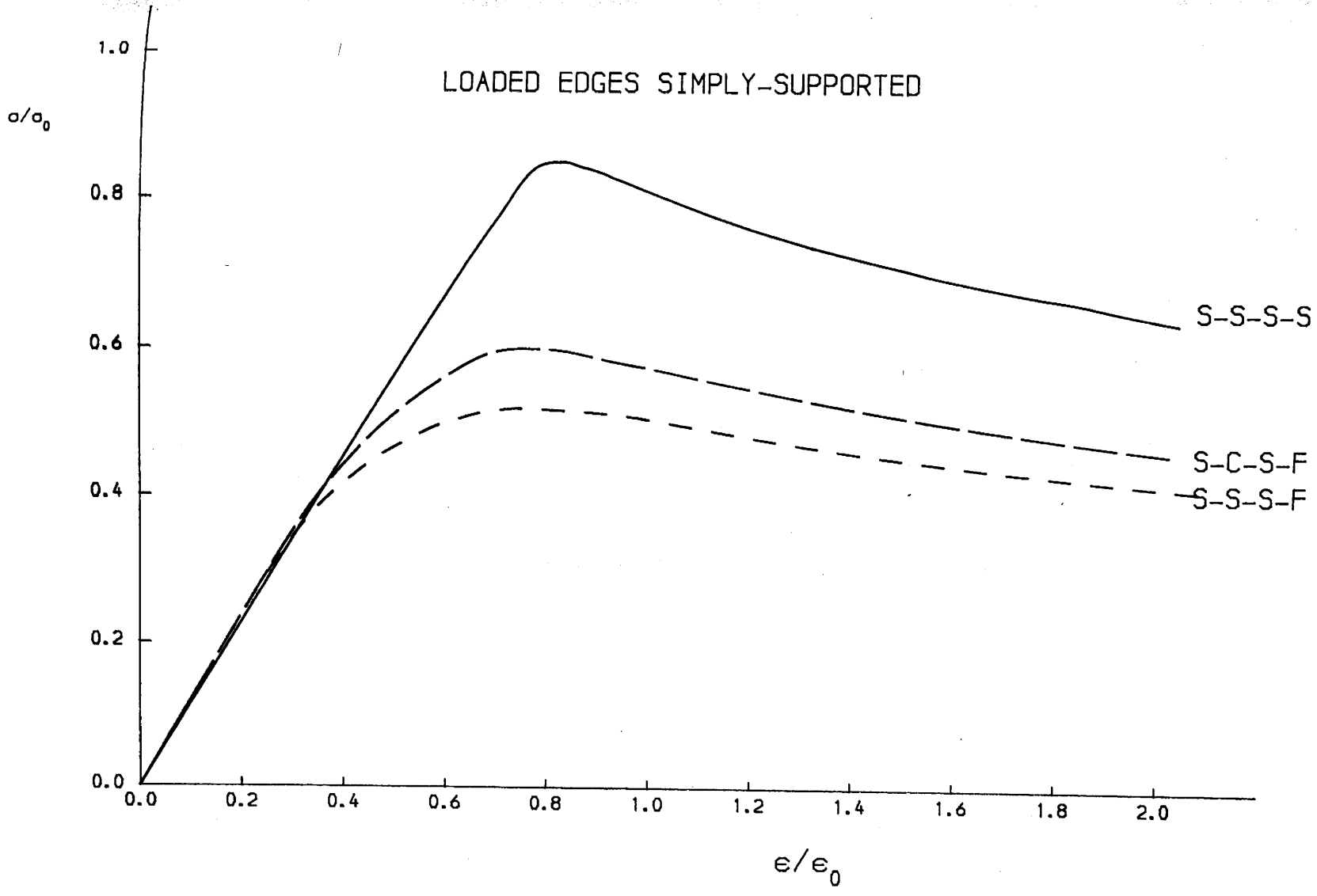

FIG. 3.6(A) ELASTO-PLASTIC RESPONSE OF A SQUARE PLATE

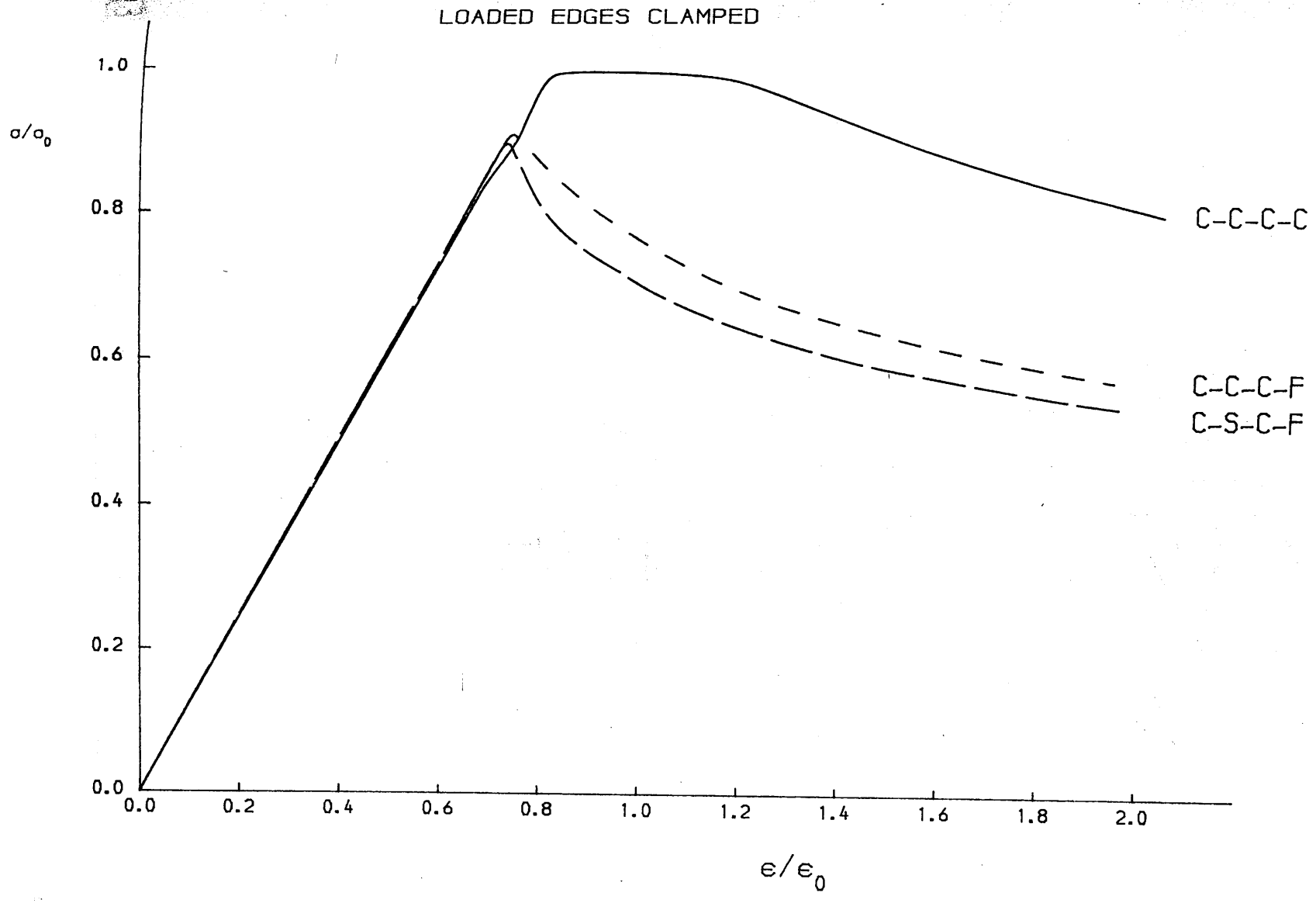

FIG. 3.6(B) ELASTO-PLASTIC RESPONSE OF A SQUARE PLATE

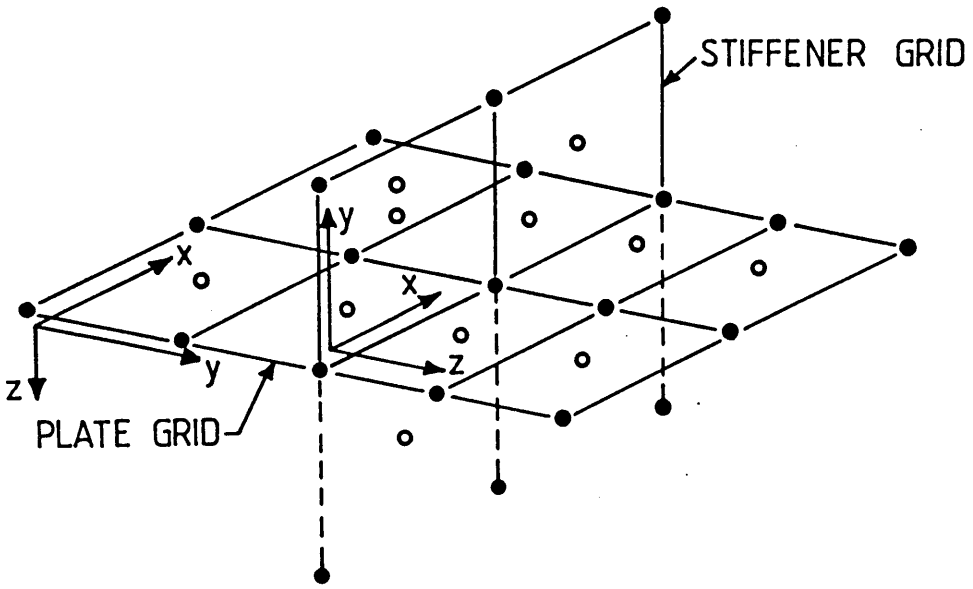

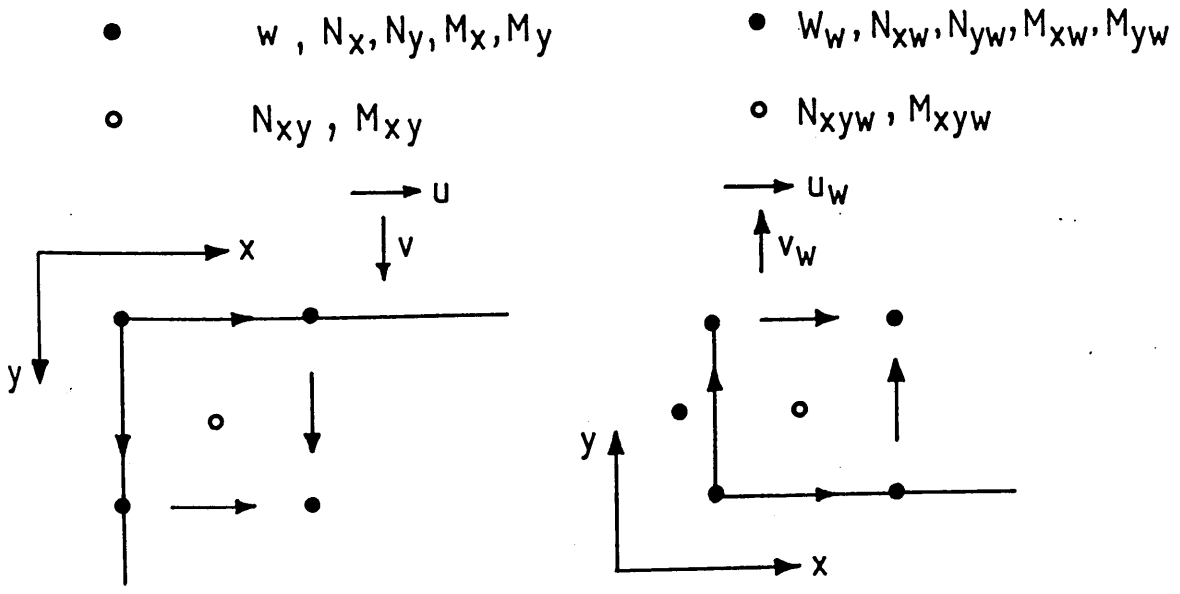

PLATE GRID – PLAN VIEW

STIFFENER GRID – PLAN VIEW

Fig. 3·7 MESH ARRANGEMENT FOR FINITE DIFFERENCES

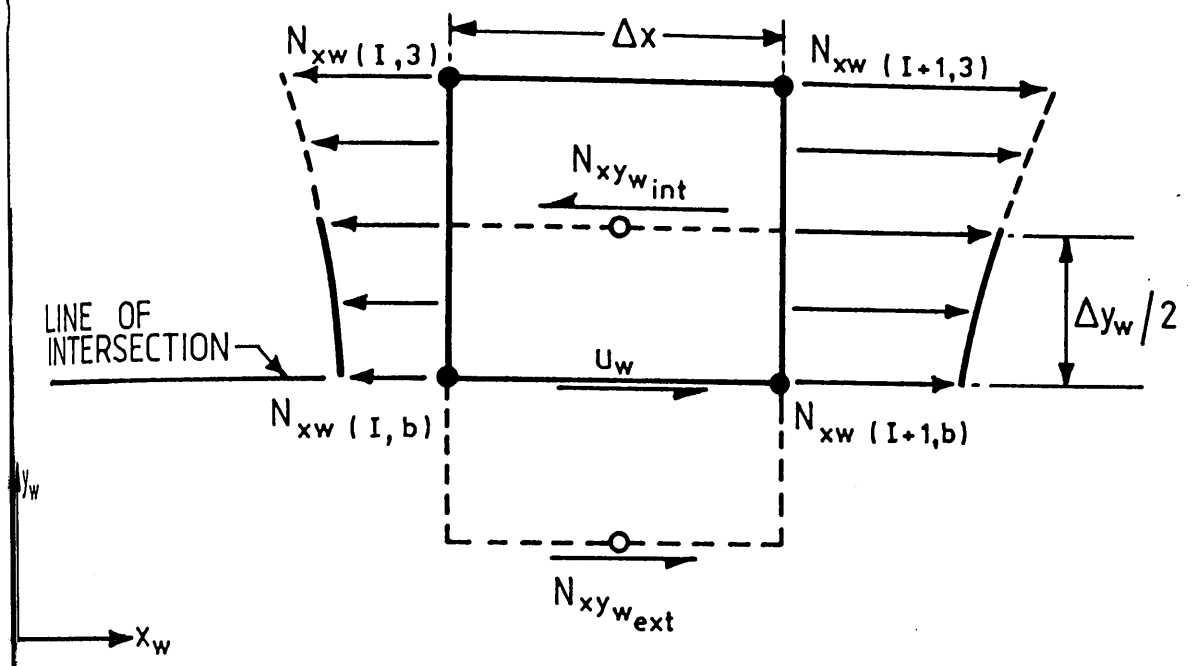

(a) STIFFENER FORCES

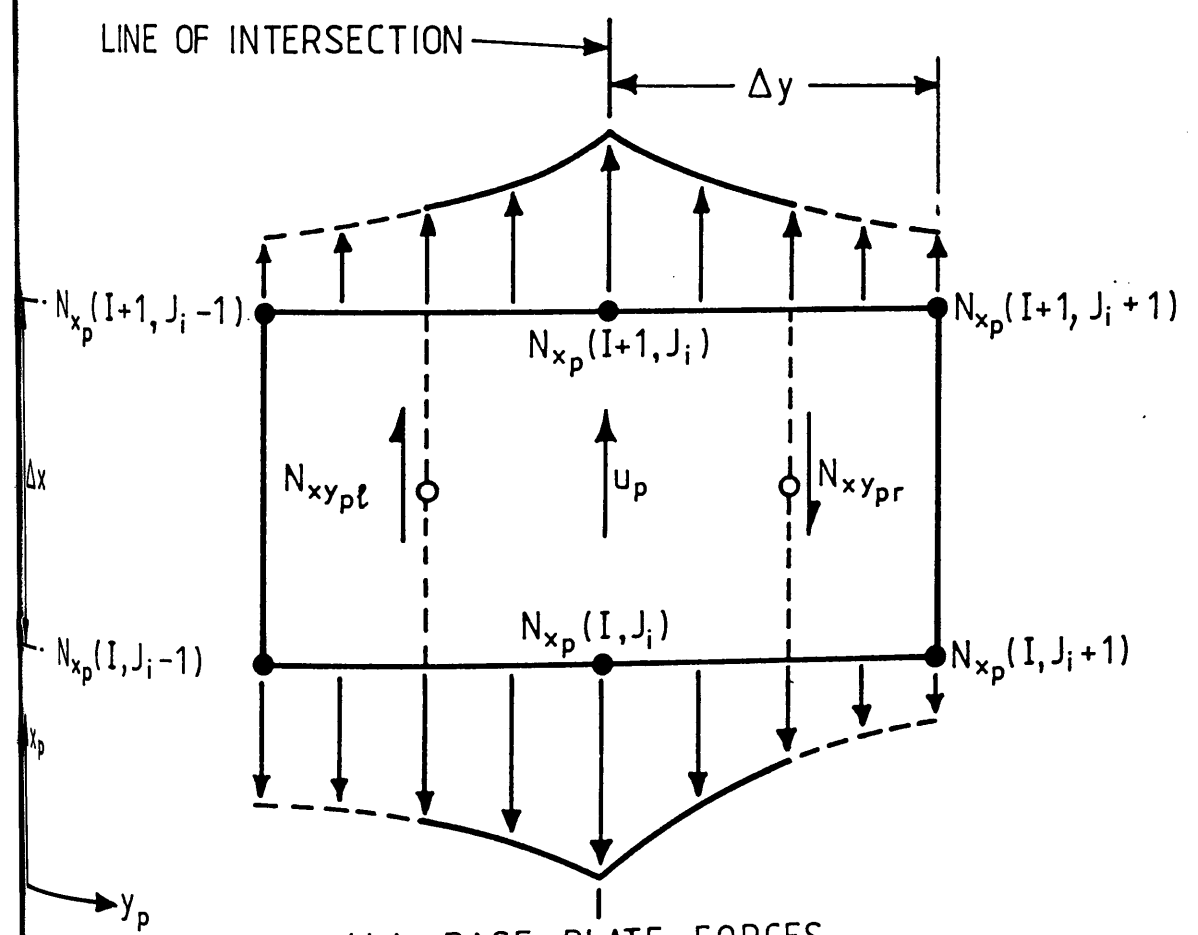

(b) BASE PLATE FORCES

Fig. 3·8 LONGITUDINAL EQUILIBRIUM AT STIFFENER - PLATE INTERSECTION

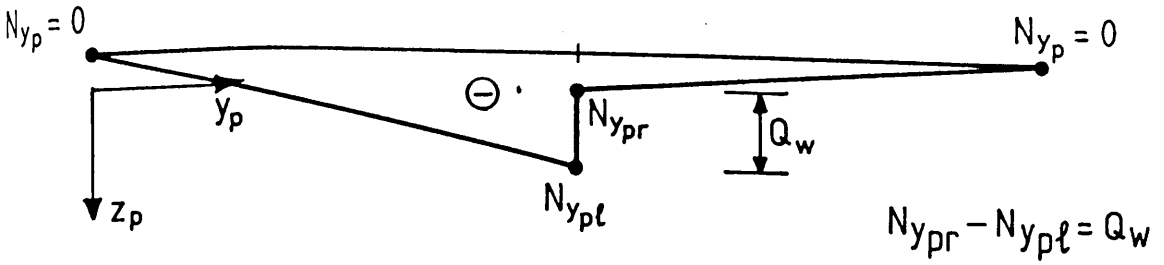

a) TRANSVERSE IN-PLANE FORCES IN BASE PLATE

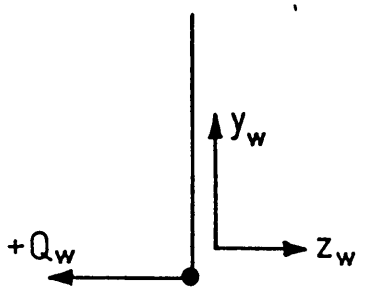

b) POSITIVE DIRECTION OF KIRCHHOFF FORCE ACTING ON LOWER FACE OF STIFFENER

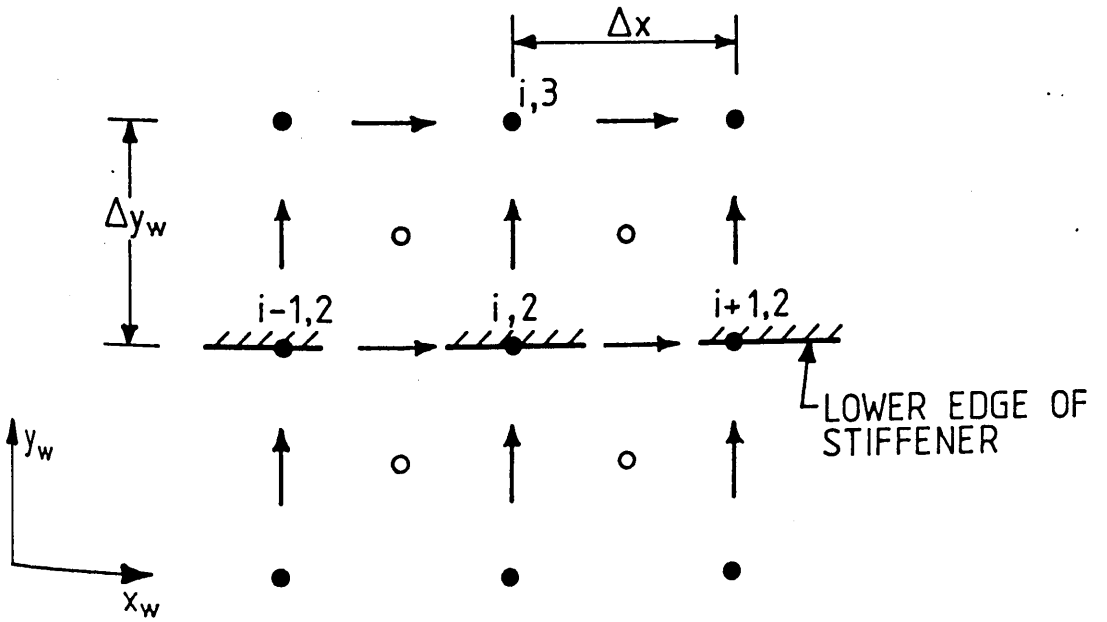

$$Q_{w(i)} = \frac{M_{yw(i,3)} - M_{yw(i,2)}}{\Delta_{yw}} + 2\,\frac{M_{xyw(i+1,2)} - M_{xy(i-1,2)}}{2\Delta_x}$$

c) DETERMINATION OF KIRCHHOFF FORCE Q_w USING FINITE DIFFERENCE GRID

Fig.3·9 TRANSVERSE EQUILIBRIUM AT STIFFENER-PLATE INTERSECTION

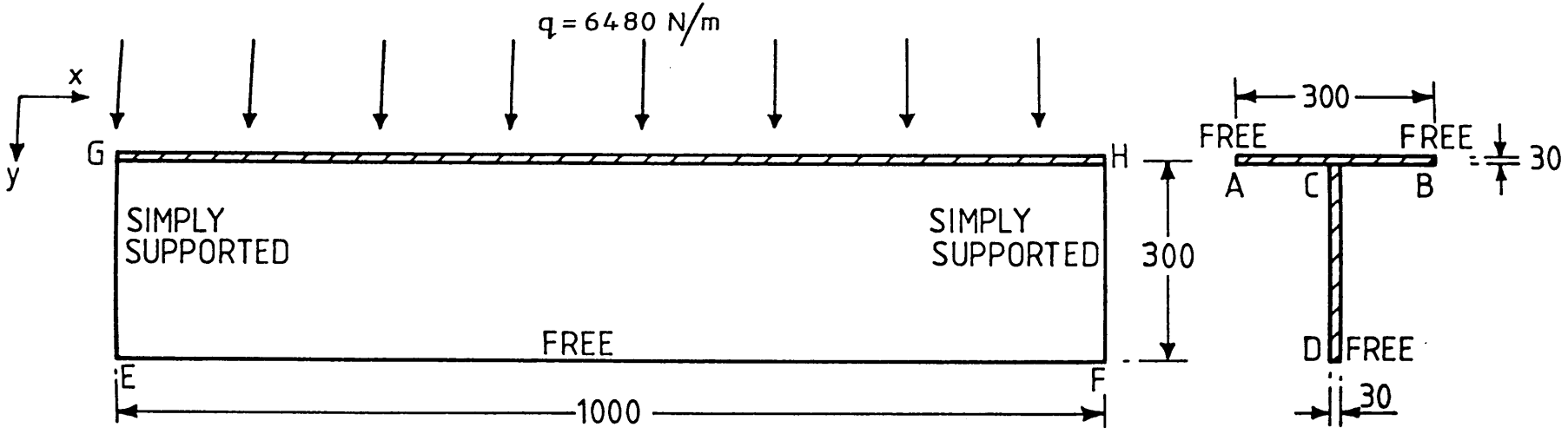

BOUNDARY CONDITIONS

AB, CD; $W=0$ $M_x=0$ $N_x=0$ $\frac{\partial N_{xy}}{\partial x}=0$ (SIMPLY SUPPORTED)

EF, GH; $M_y=0$ $N_y=0$ $N_{xy}=0$ $\frac{\partial M_y}{\partial y}+2\frac{\partial M_{xy}}{\partial x}=0$ (FREE)

ALL DIMENSIONS IN mm

Fig. 3·10 GEOMETRY of SIMPLY-SUPPORTED LATERALLY LOADED BEAM

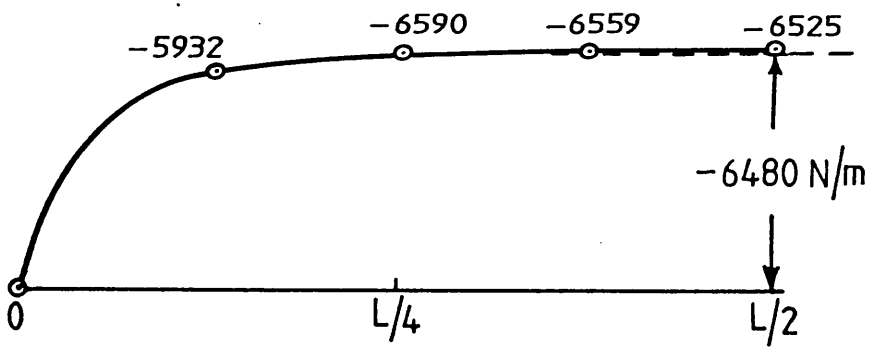

a) KIRCHHOFF FORCE ON STIFFENER ALONG INTERSECTION

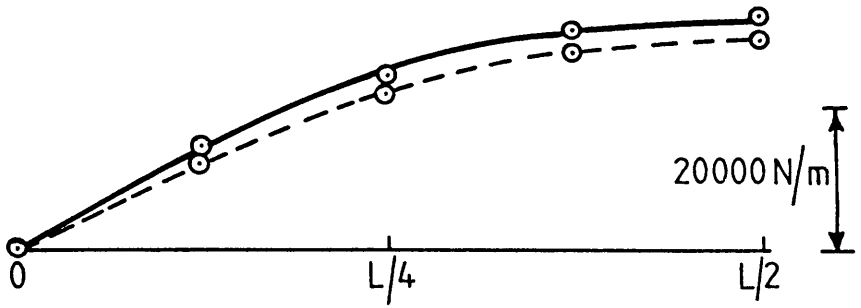

b) LONGITUDINAL FORCE ALONG STIFFENER TIP (Nxw)

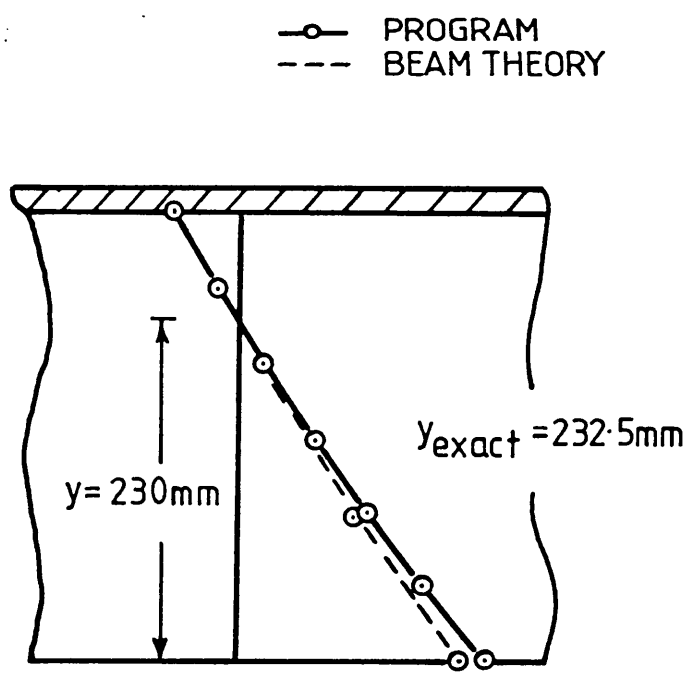

c) LONGITUDINAL FORCE IN STIFFENER (Nxw) AT x=L/2 (Nm/m)

Fig. 3·11 LATERALLY LOADED REAM– ANALYTICAL AND NUMERICAL RESULTS

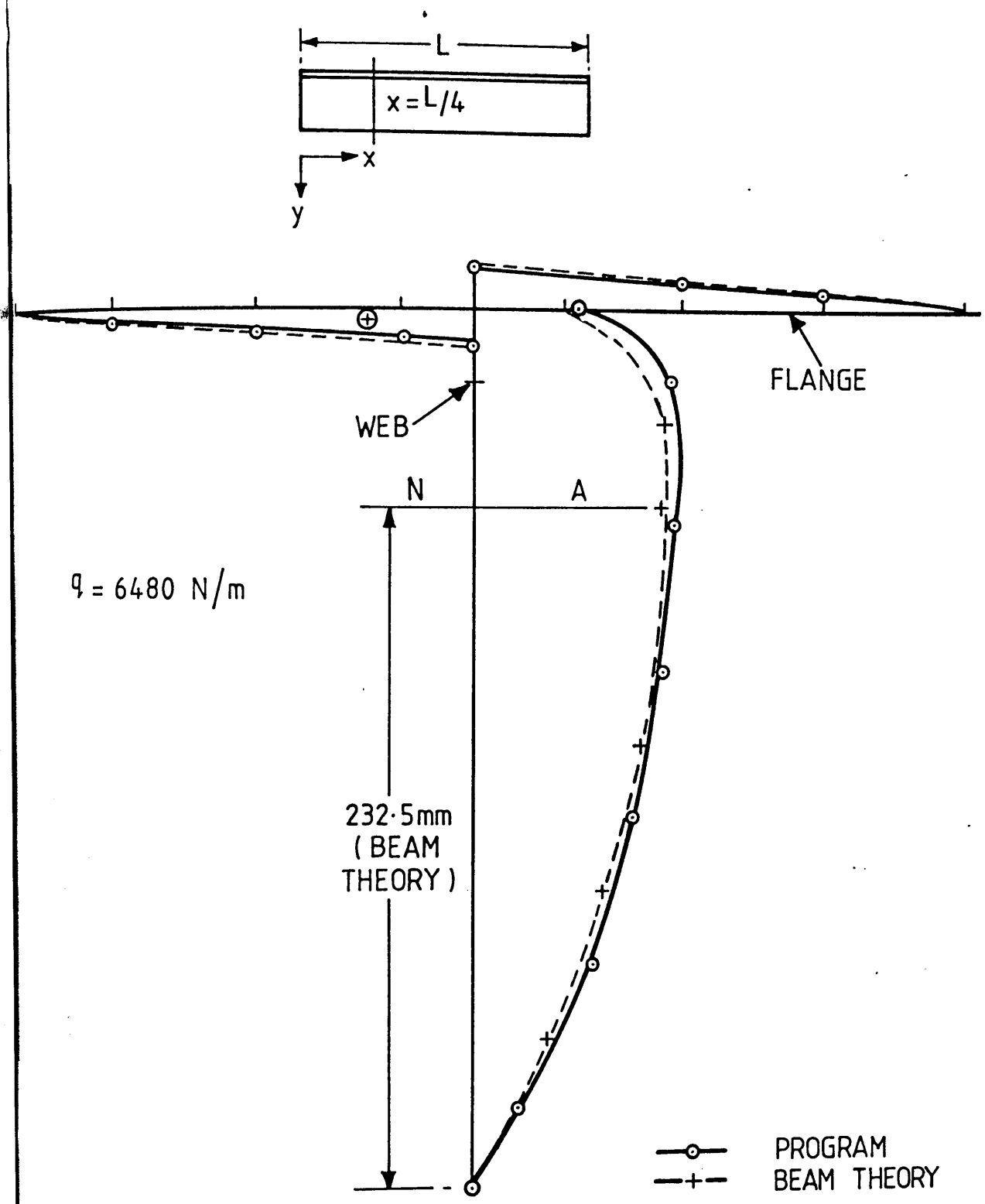

3·12 DISTRIBUTION of SHEAR FLOW in LATERALLY LOADED BEAM AT L/4

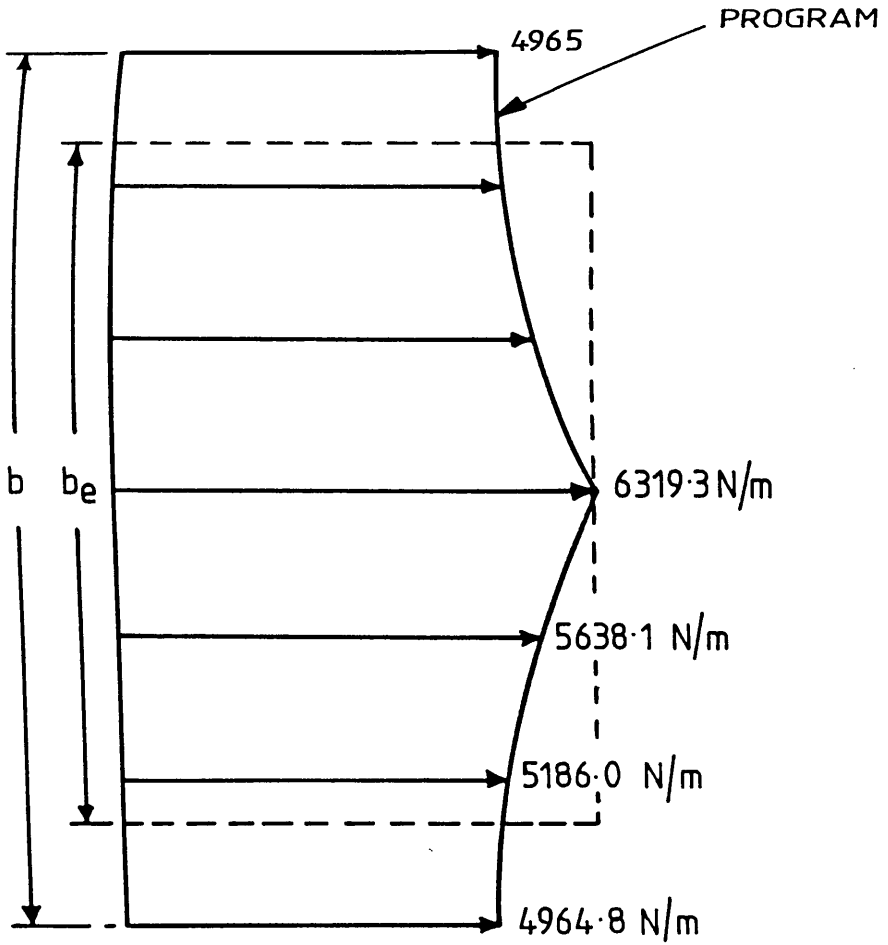

TOTAL LOAD = 1646·6N

$\therefore b_e = \frac{1646 \cdot 6}{6319 \cdot 3} = 0 \cdot 260\,m$

MOFFAT AND DOWLING

EFFECTIVE BREADTH FACTOR: $\psi_u = 0 \cdot 78$

$\therefore b_e = 0 \cdot 78 \times 0 \cdot 300 = 0 \cdot 234\,m$

Fig. 3·13 DISTRIBUTION of LONGITUDINAL FORCES in FLANGE at x = L/2
EFFECTIVE BREADTH of FLANGE.

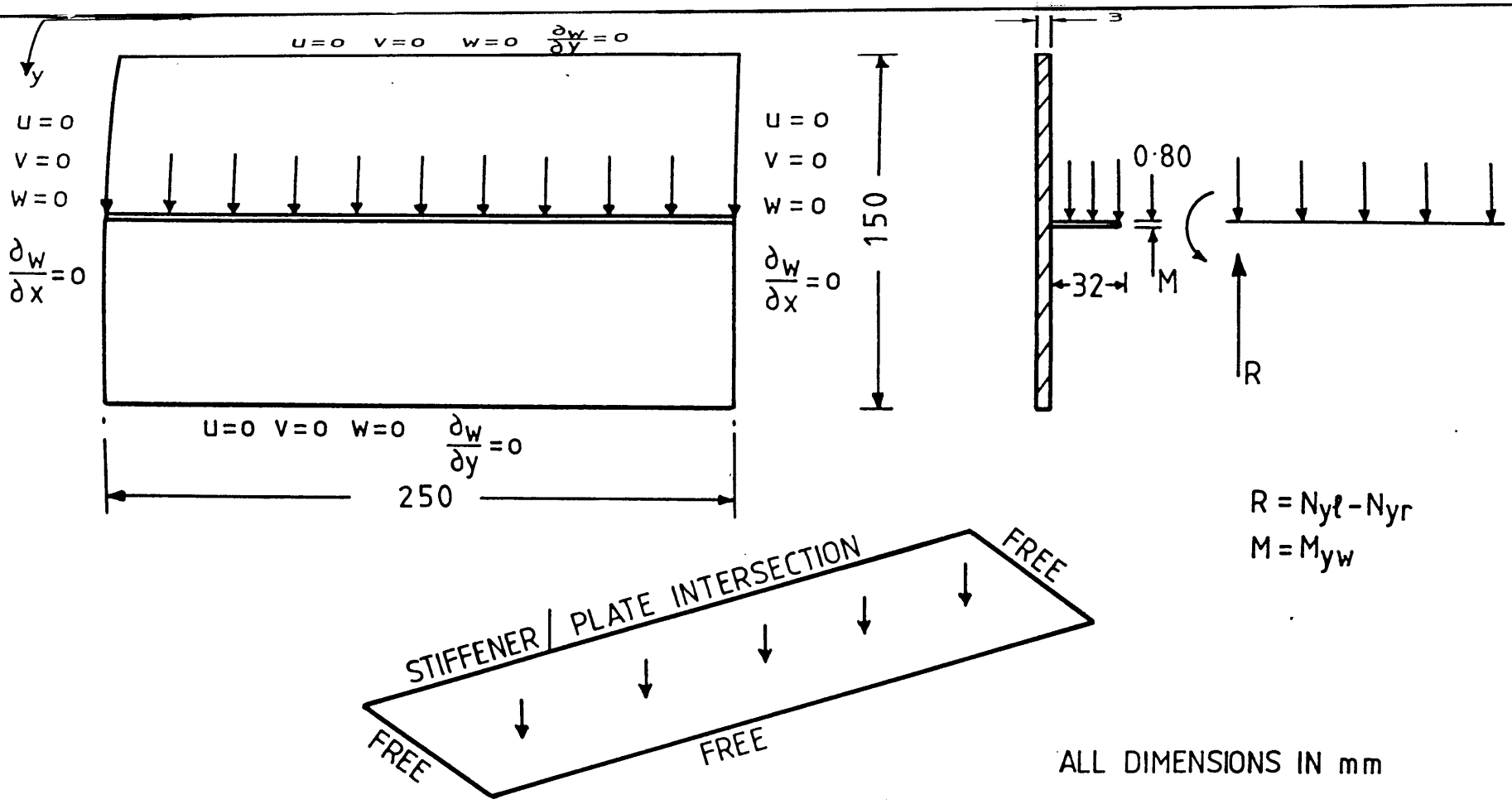

Fig.3·14 CANTILEVER DIMENSIONS AND BOUNDARY CONDITIONS.

$$W = \frac{qL^4}{8EI} = 0.148\,mm$$

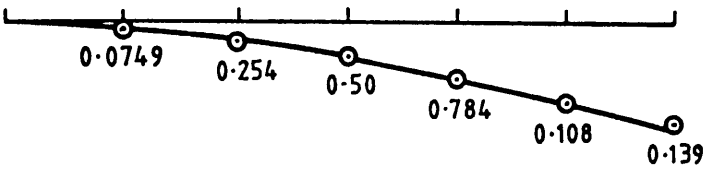

(a) VERTICAL DEFLECTION OF CANTILEVER AT $X = L/2$

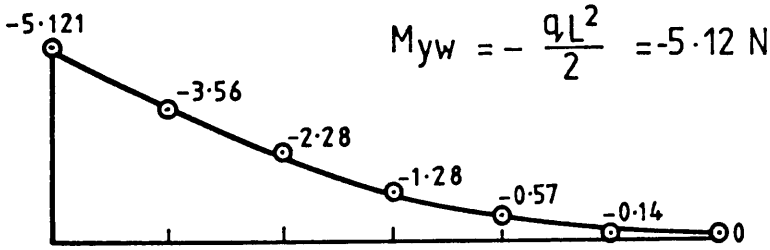

$$M_{yw} = -\frac{qL^2}{2} = -5{\cdot}12\ Nm/m$$

(b) BENDING MOMENT IN CANTILEVER (M_{yw}) AT $X = L/2$

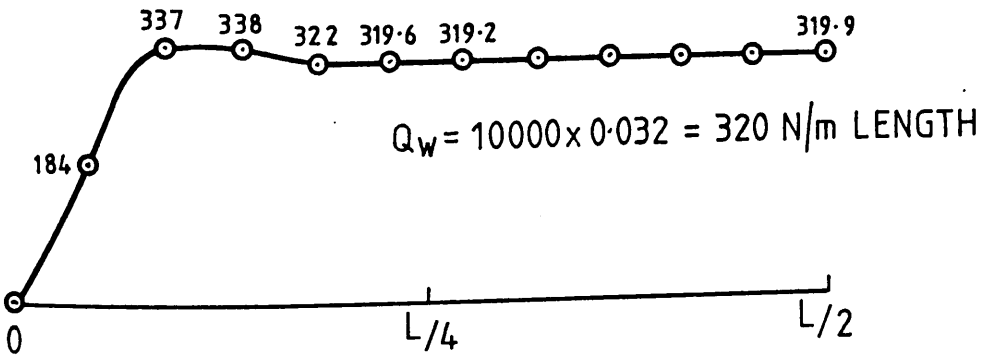

$$Q_w = 10000 \times 0{\cdot}032 = 320\ N/m\ LENGTH$$

(c) KIRCHHOFF FORCE IN BASE PLATE ALONG INTERSECTION ($Q_w = Ny\ell - Nyr$)

Fig 3·15 CANTILEVER – ANALYTICAL and NUMERICAL RESULTS.

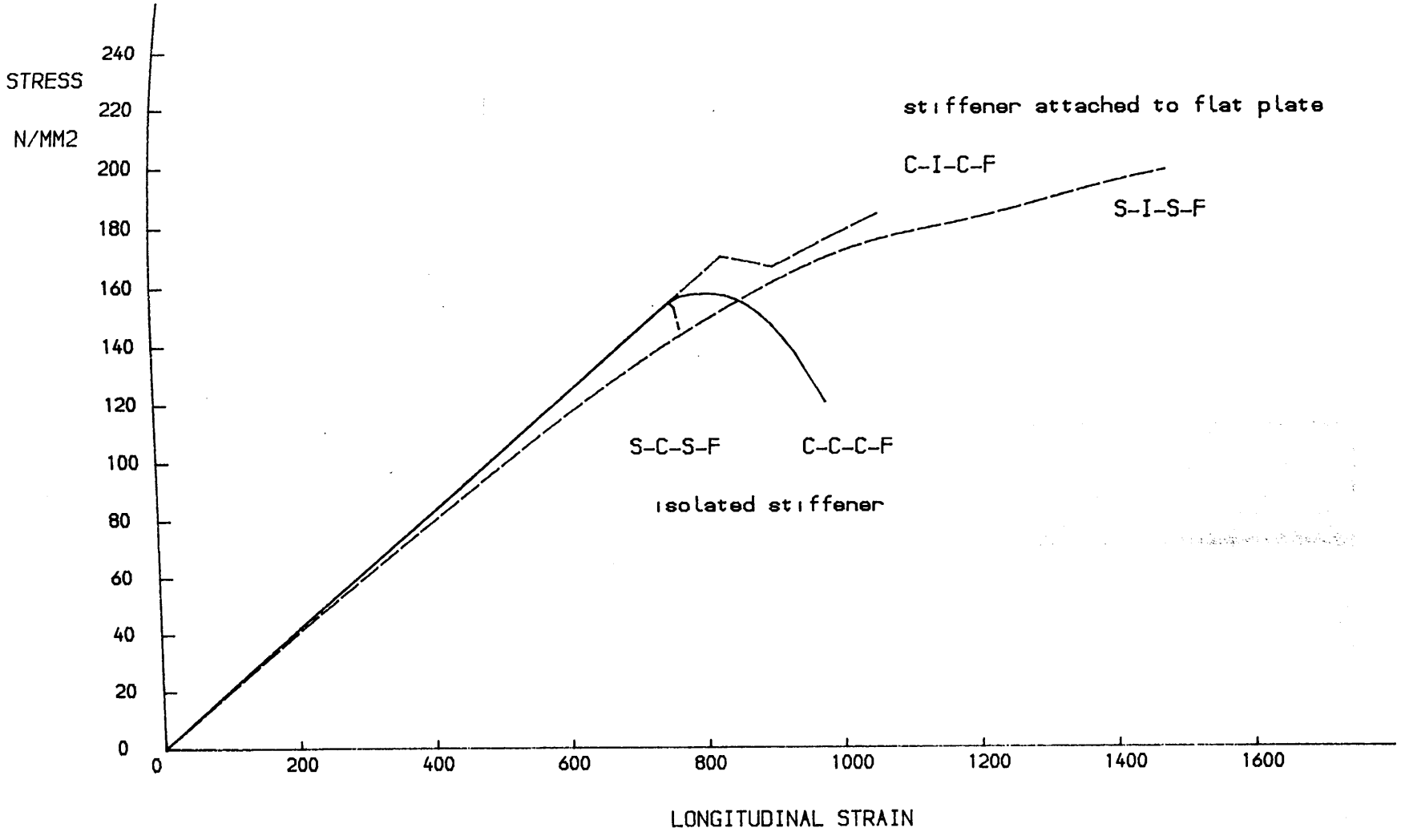

FIG. 3.16 AVERAGE STRESS-STRAIN CURVES FOR STIFFENERS

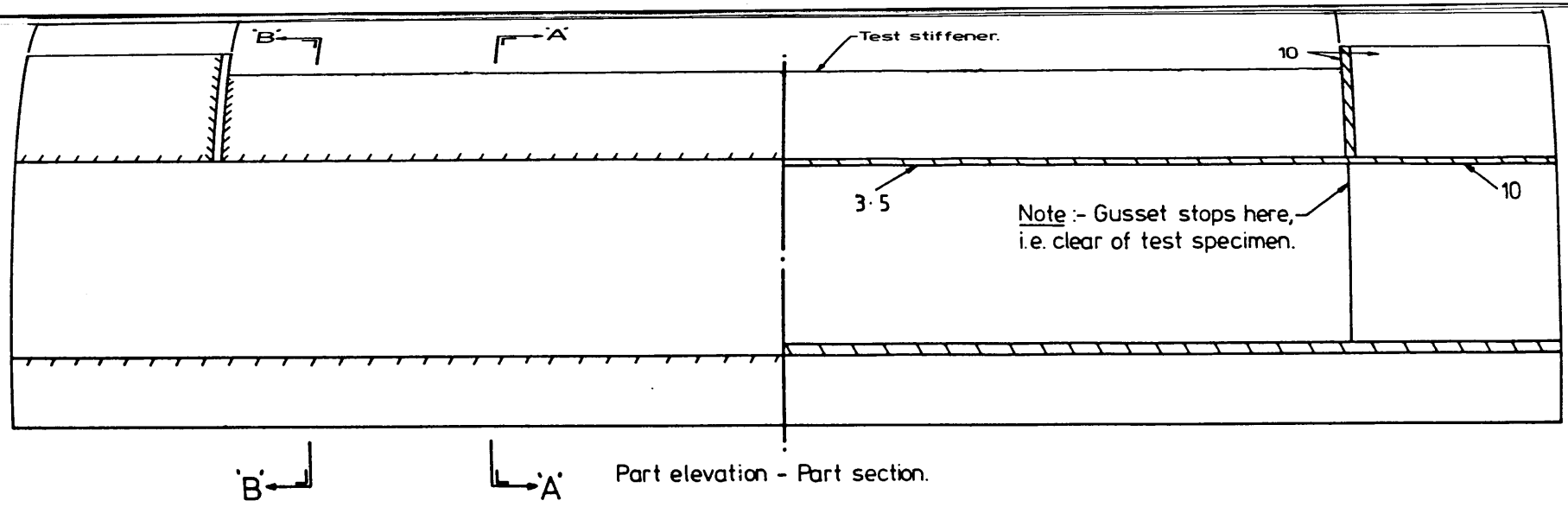

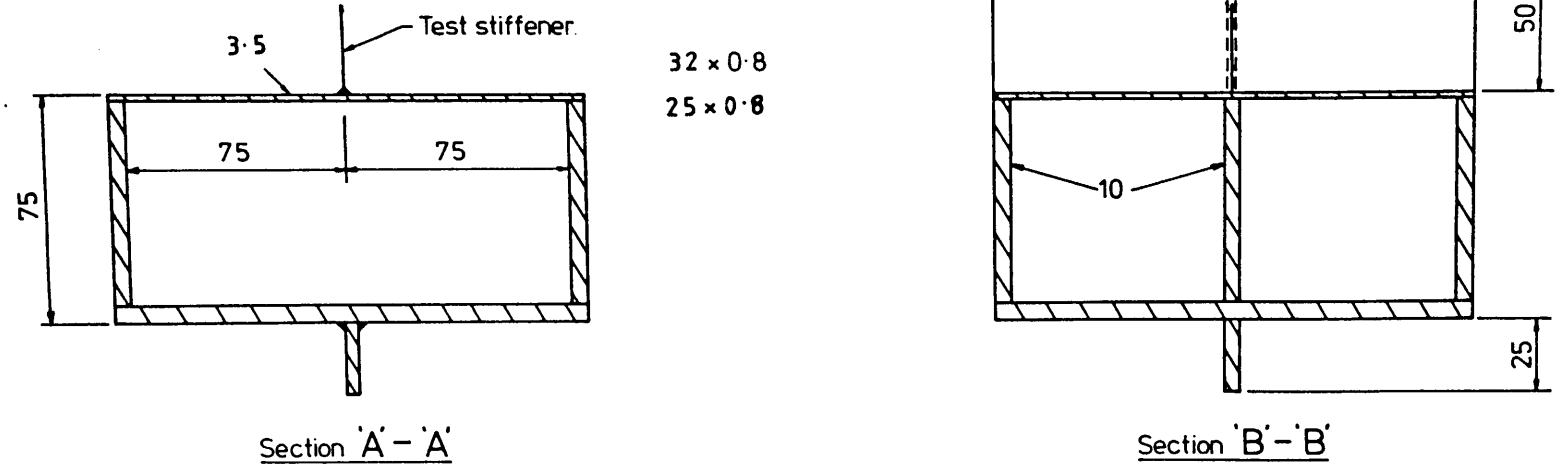

Fig 4·1 ELEVATION / LONGITUDINAL AND TRANSVERSE SECTIONS OF TEST MODELS

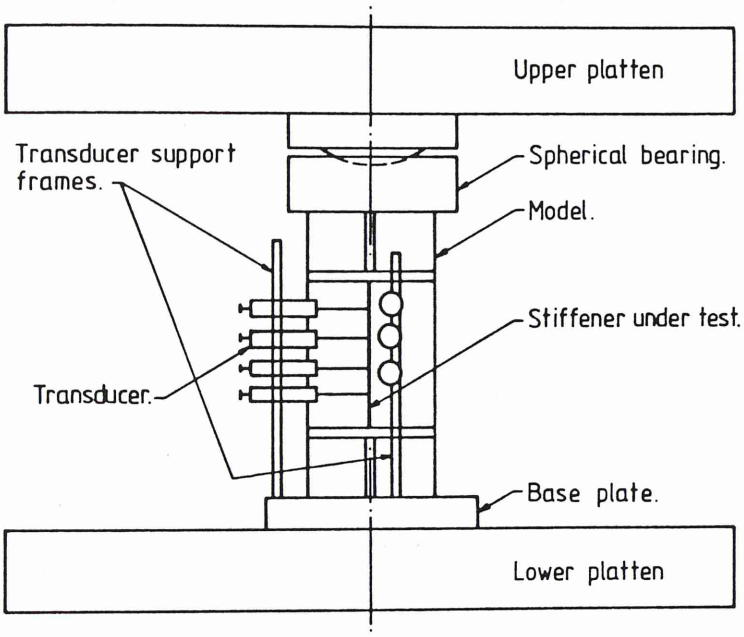

Fig. 4·2(a) SCHEMATIC DIAGRAM OF AXIAL LOAD TEST RIG.

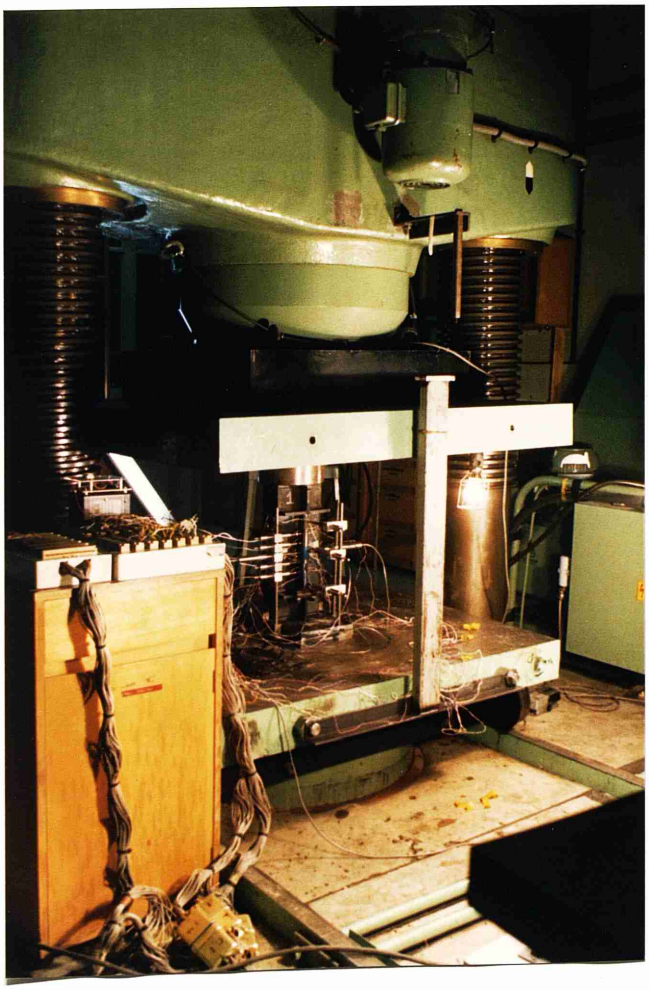

Fig 4·2(b) AXIAL LOAD TEST RIG.

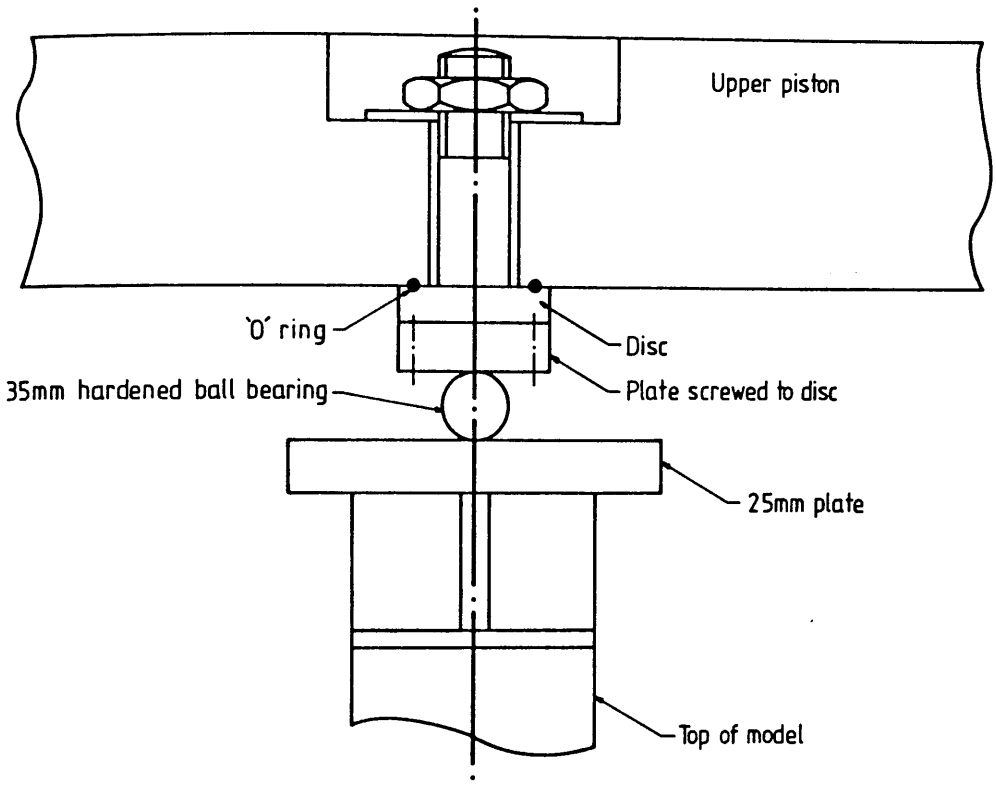

Fig 4·3(a). COMBINED LOAD SET UP FOR MODEL 7

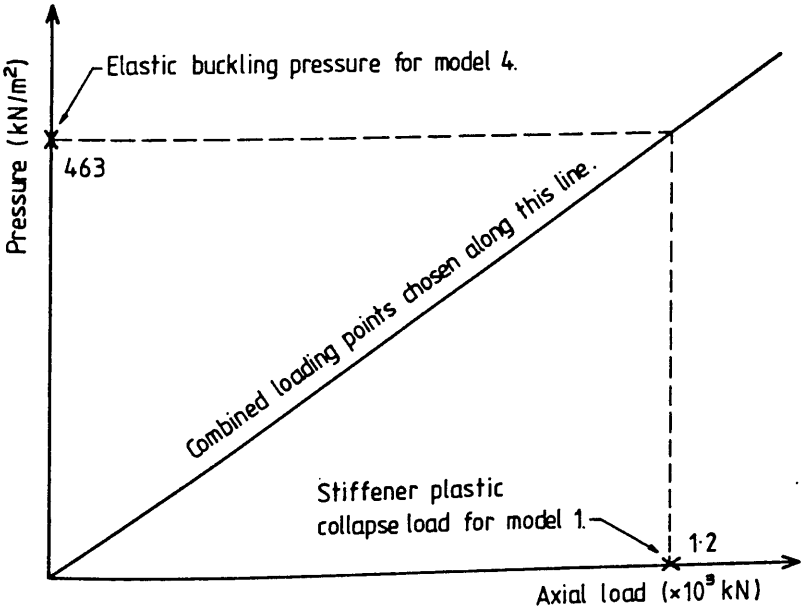

Fig. 4·3(b) DETERMINATION OF LOAD COMBINATIONS.

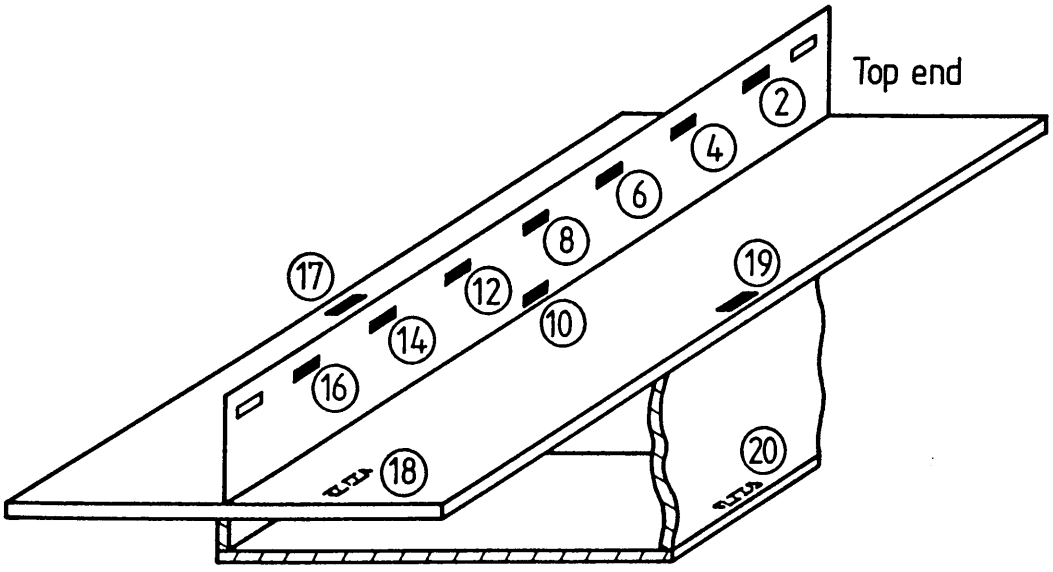

Identifies strain gauge numbers for models 1-5 & 8.

Identifies additional gauges for models 6 & 7.

Gauges 1, 3, 5, ..., 15 are opposite gauges 2, 4, 6, ..., 16 respectively.

Fig. 4·4 FLAT BAR STIFFENERS :-
STRAIN GAUGE IDENTIFICATION

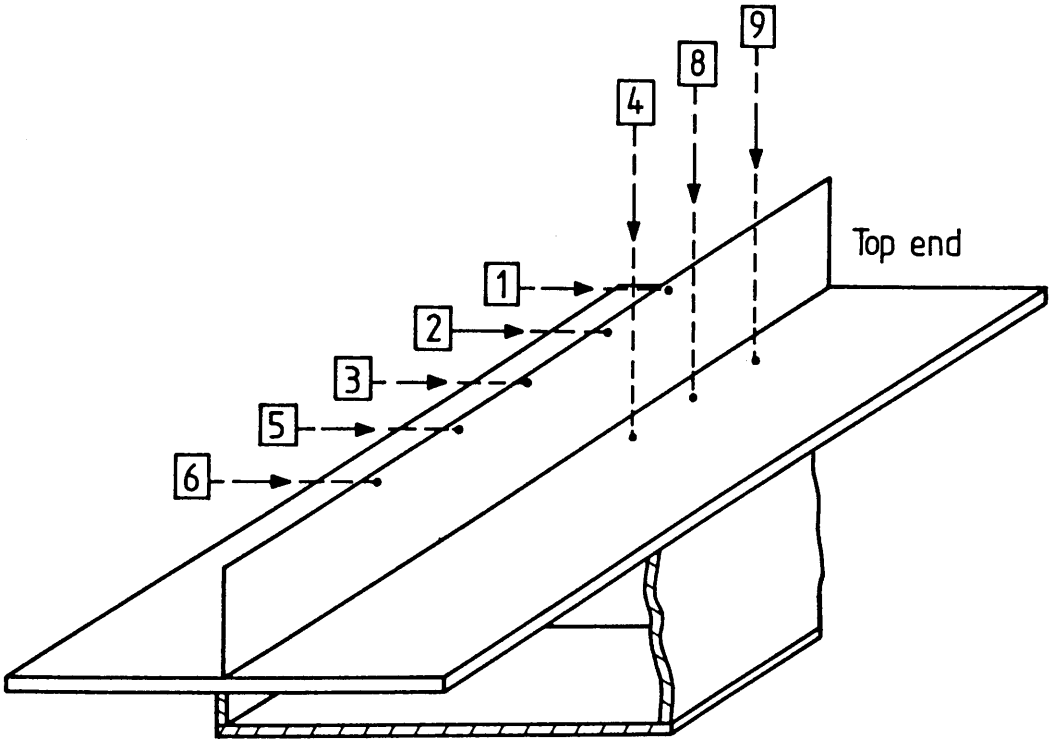

□—→- - - • Identifies transducer number.

Transducer N°. 7 is fitted along the line of the stiffener and is clamped to the bottom end plate.

Fig.4·5. FLAT BAR STIFFENERS :-
TRANSDUCER IDENTIFICATION

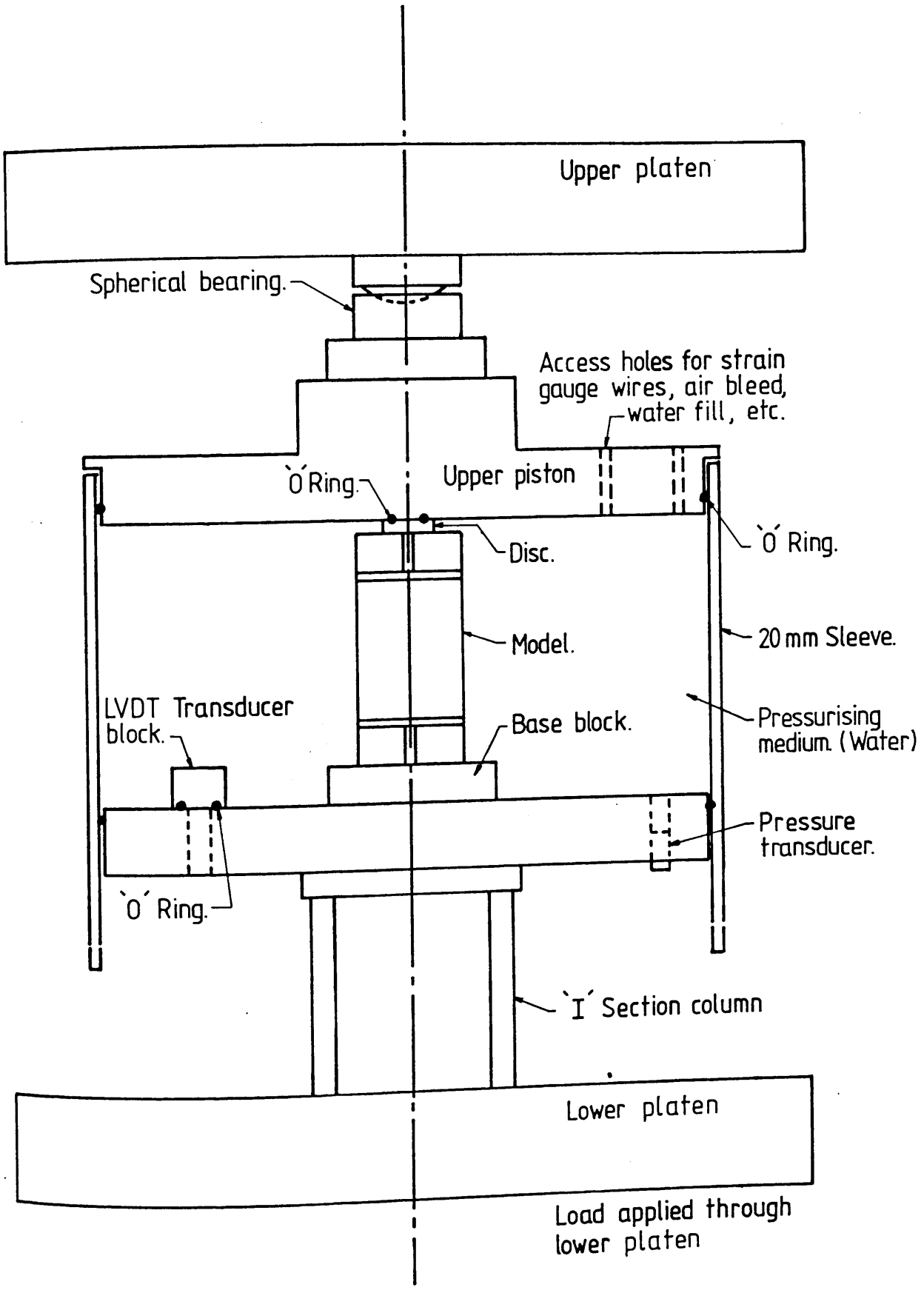

Fig.4·6. TEST RIG FOR PRESSURE LOADING AND COMBINED LOADING TESTS

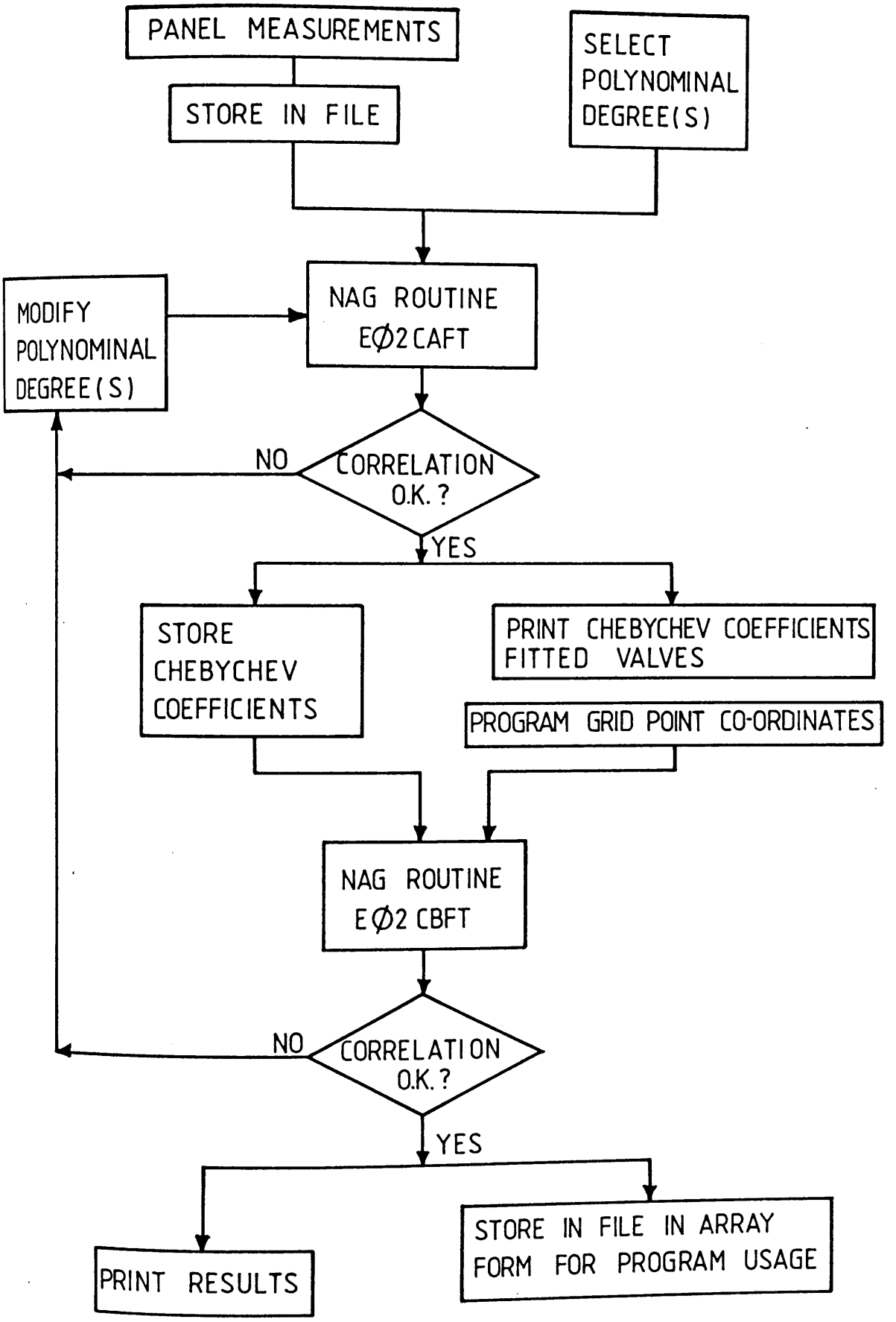

Fig.4.7 FLOW CHART FOR GENERATION OF PANEL COMPONENT SURFACES USING NAG ROUTINES

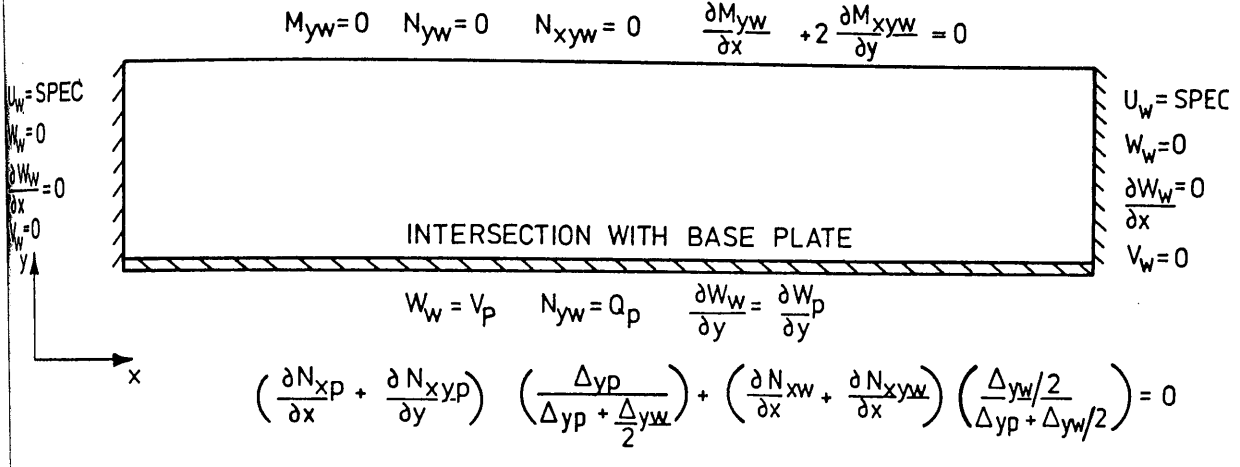

a) STIFFENER

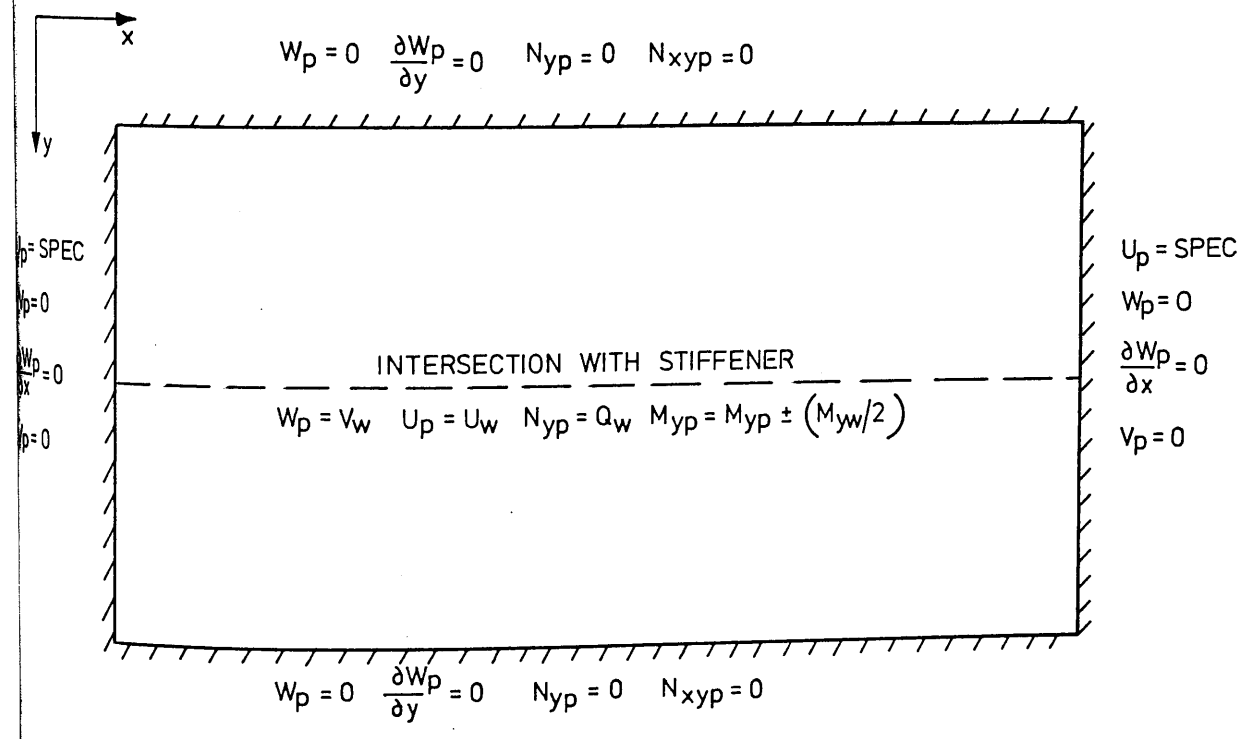

b) BASE PLATE

Fig.4·8 BOUNDARY CONDITIONS FOR STIFFENED PLATE COMPONENTS (CORRELATION STUDIES)

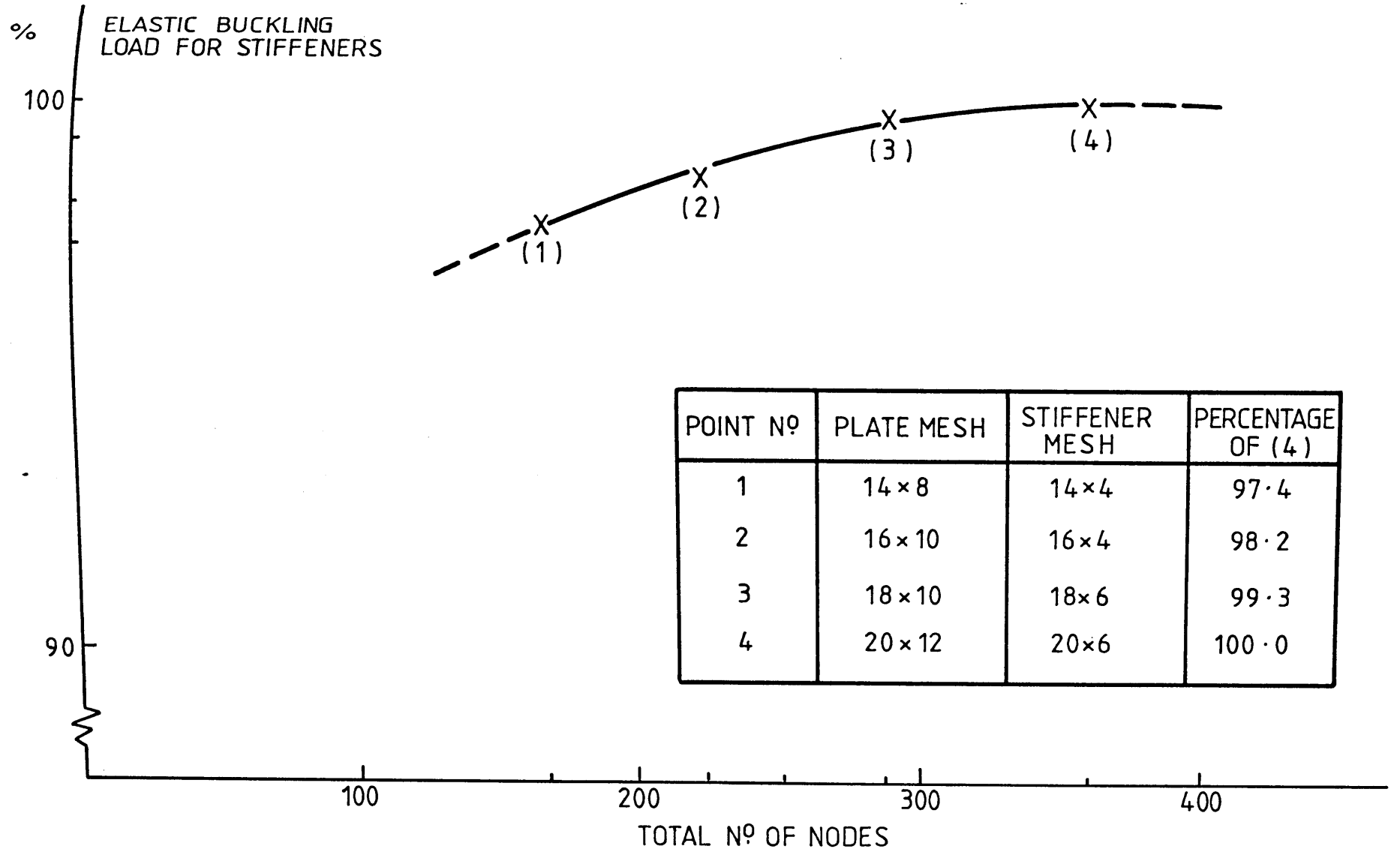

POINT Nº	PLATE MESH	STIFFENER MESH	PERCENTAGE OF (4)
1	14×8	14×4	97·4
2	16×10	16×4	98·2
3	18×10	18×6	99·3
4	20×12	20×6	100·0

Fig. 4·9a. CONVERGENCE STUDY—AXIAL EDGE COMPRESSION

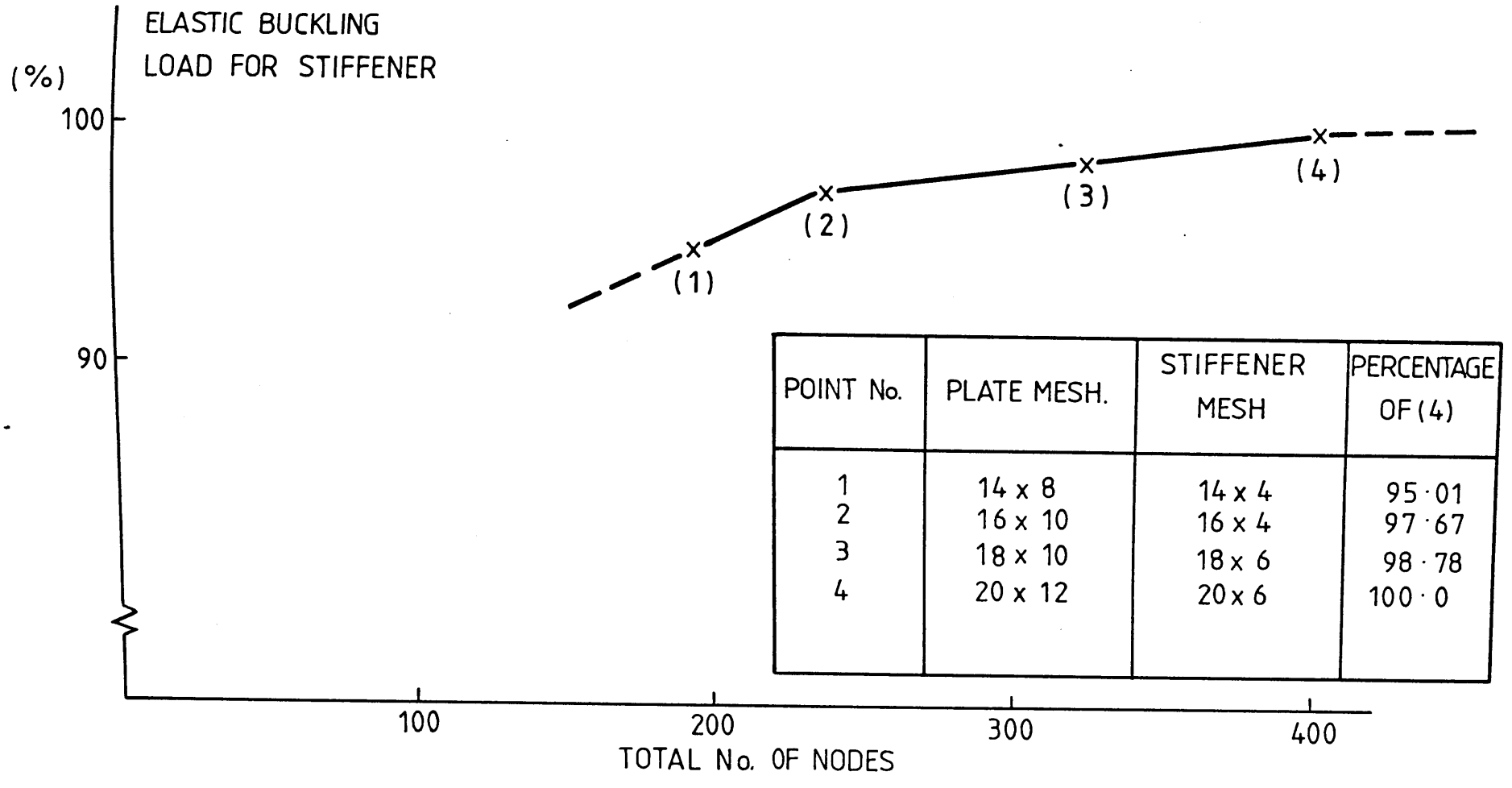

POINT No.	PLATE MESH.	STIFFENER MESH	PERCENTAGE OF (4)
1	14 x 8	14 x 4	95·01
2	16 x 10	16 x 4	97·67
3	18 x 10	18 x 6	98·78
4	20 x 12	20 x 6	100·0

Fig. 4·9b. CONVERGENCE STUDY – LATERAL PRESSURE ON BASE PLATE.

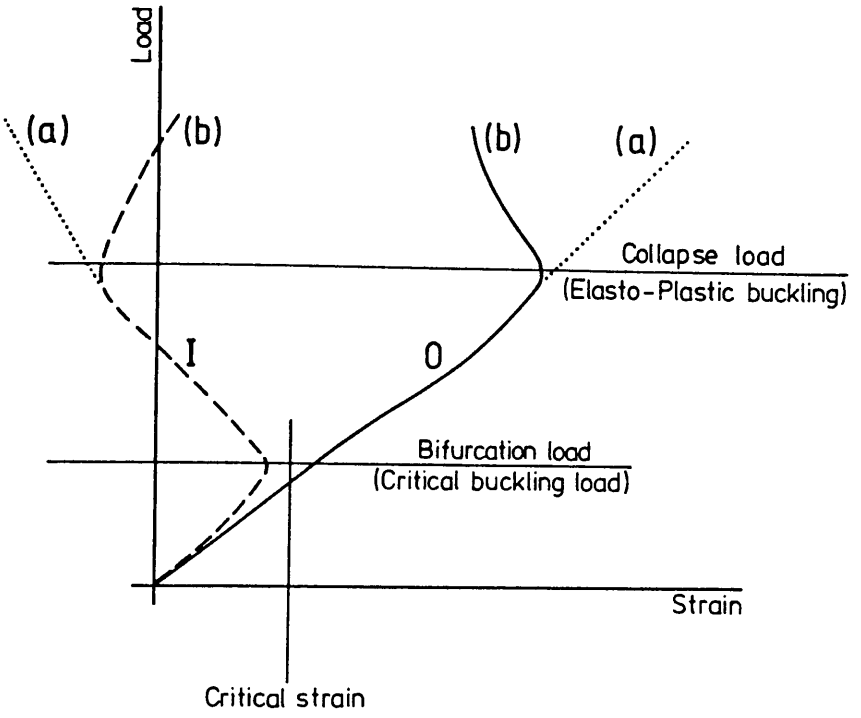

Fig 4·10(a) FLAT BAR STIFFENERS
GENERAL STRAIN - LOAD RESPONSE.

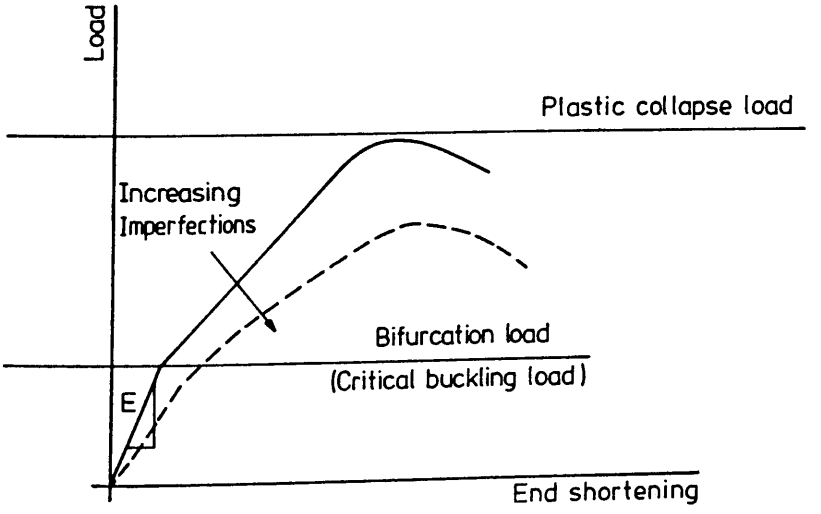

4·10 (b) GENERAL LOAD-END SHORTENING RESPONSE.

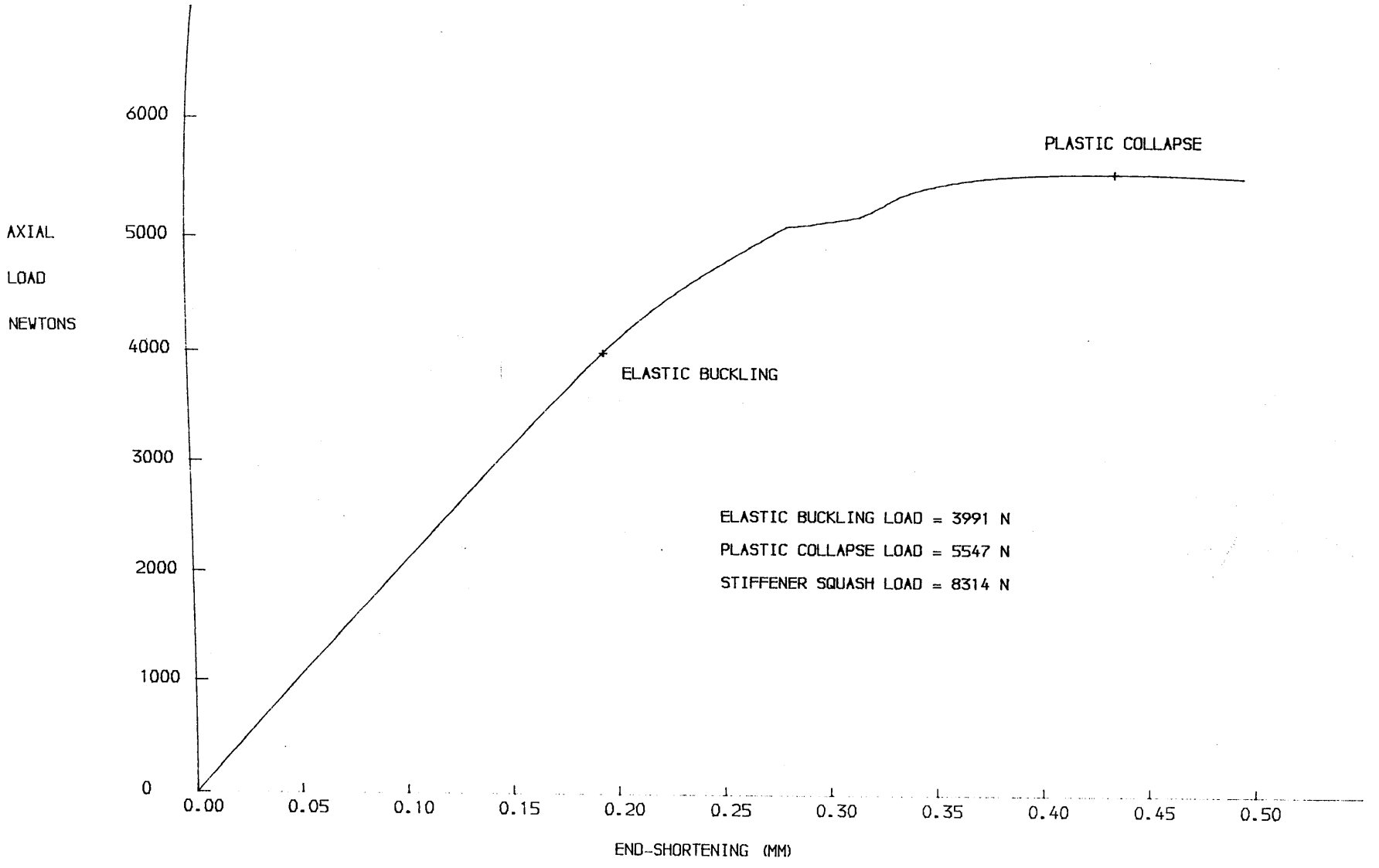

FIG. 4.11 MODEL NO. 1 - STIFFENER LOAD END-SHORTENING CURVE

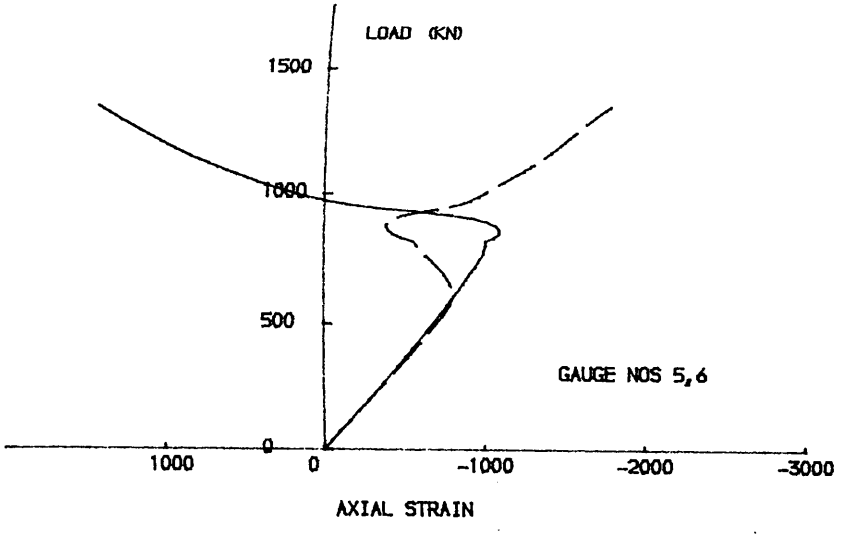

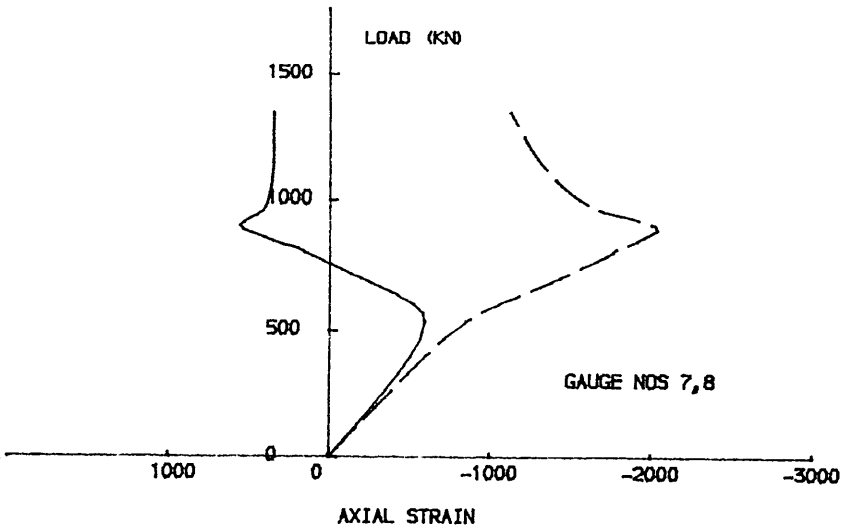

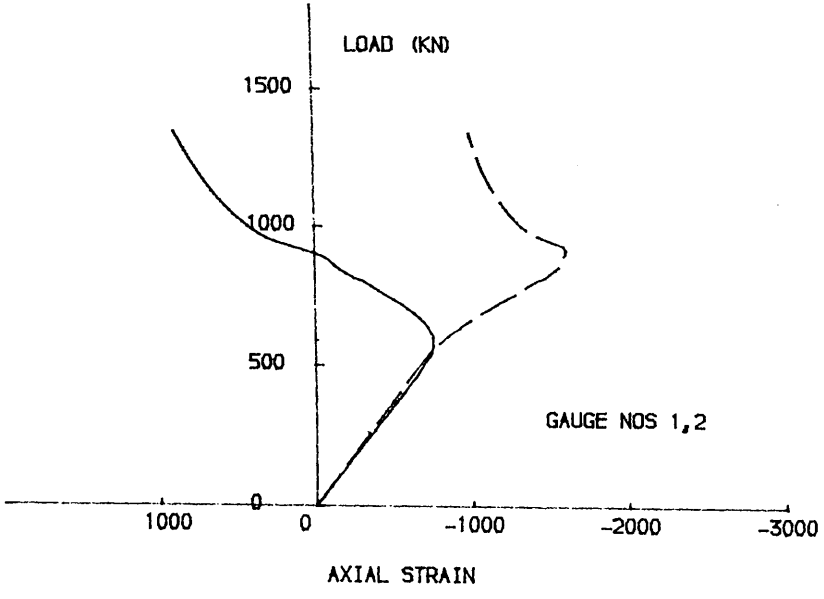

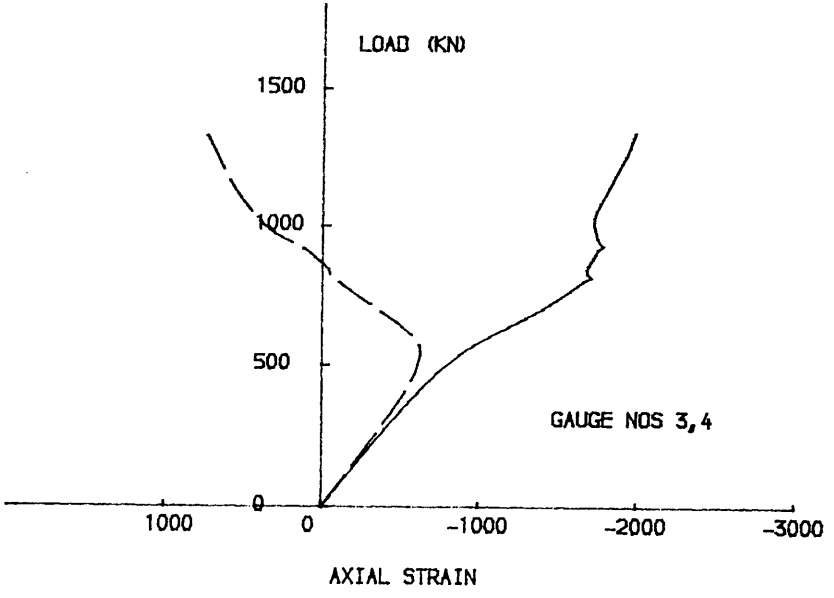

FIG.4.12a MODEL NO. 1 - LOCAL STIFFENER TIP STRAINS

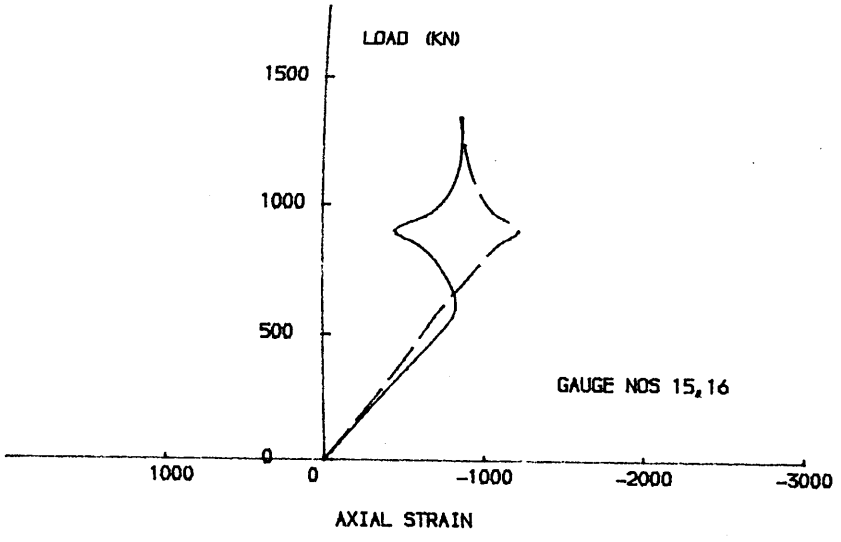

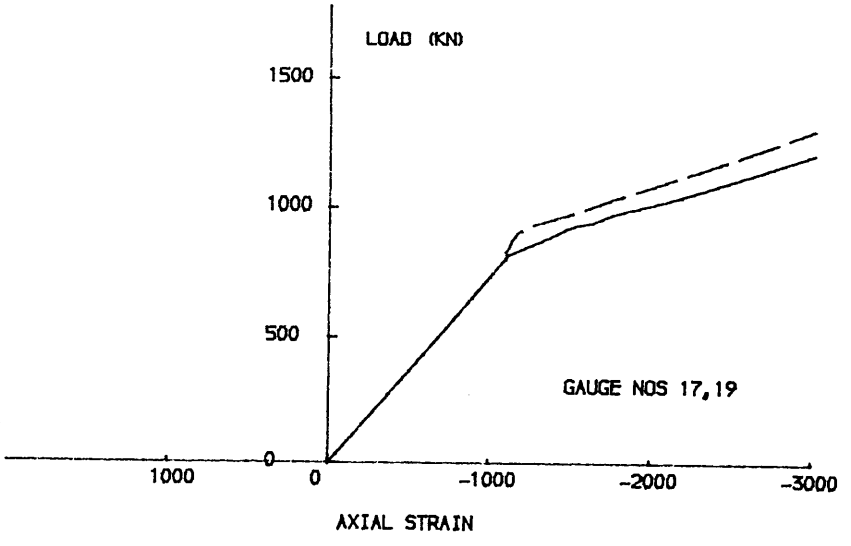

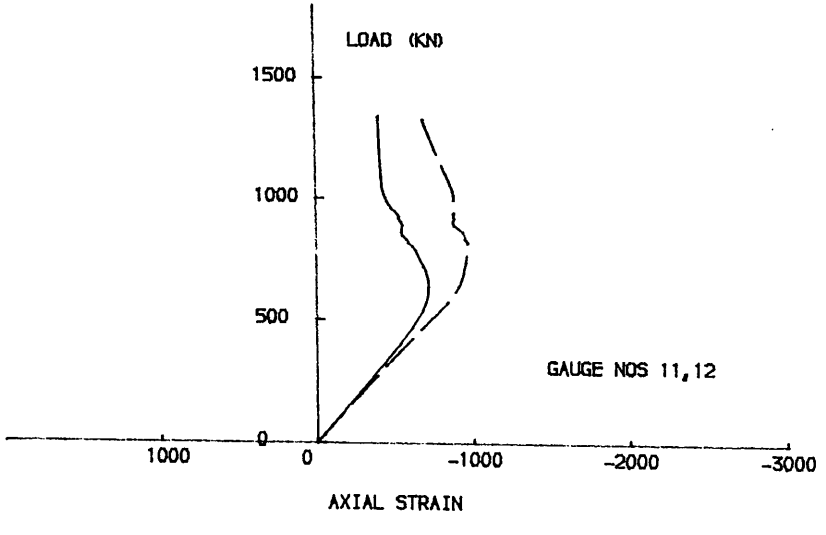

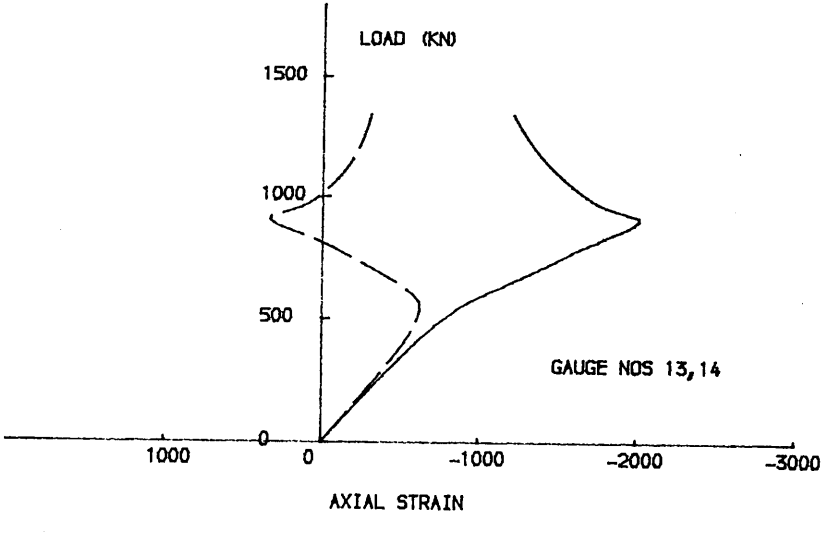

FIG.4.12bMODEL NO. 1 - LOCAL STIFFENER TIP STRAINS

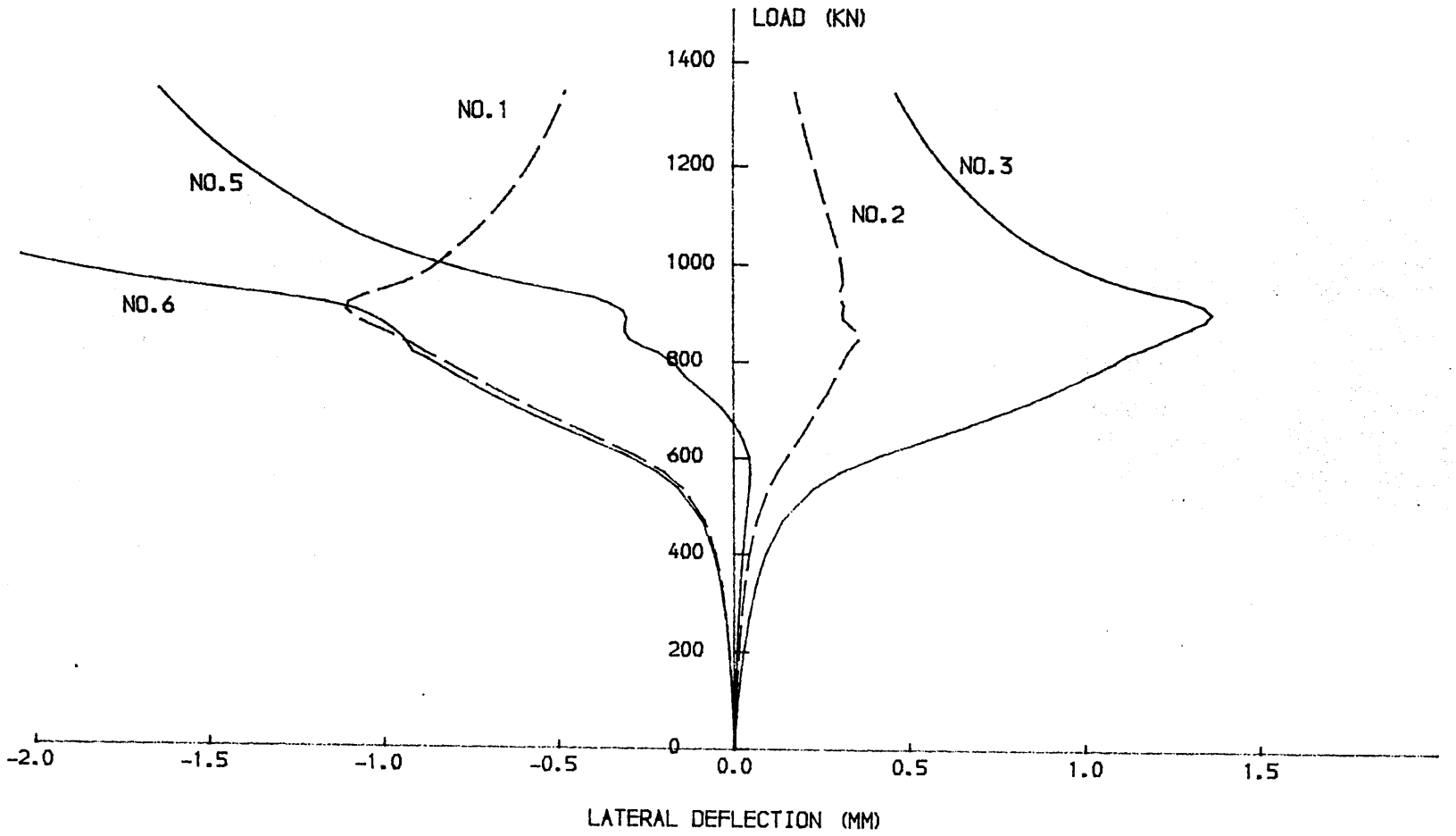

FIG. 4.13 MODEL NO. 1 STIFFENER TIP LATERAL DEFLECTIONS

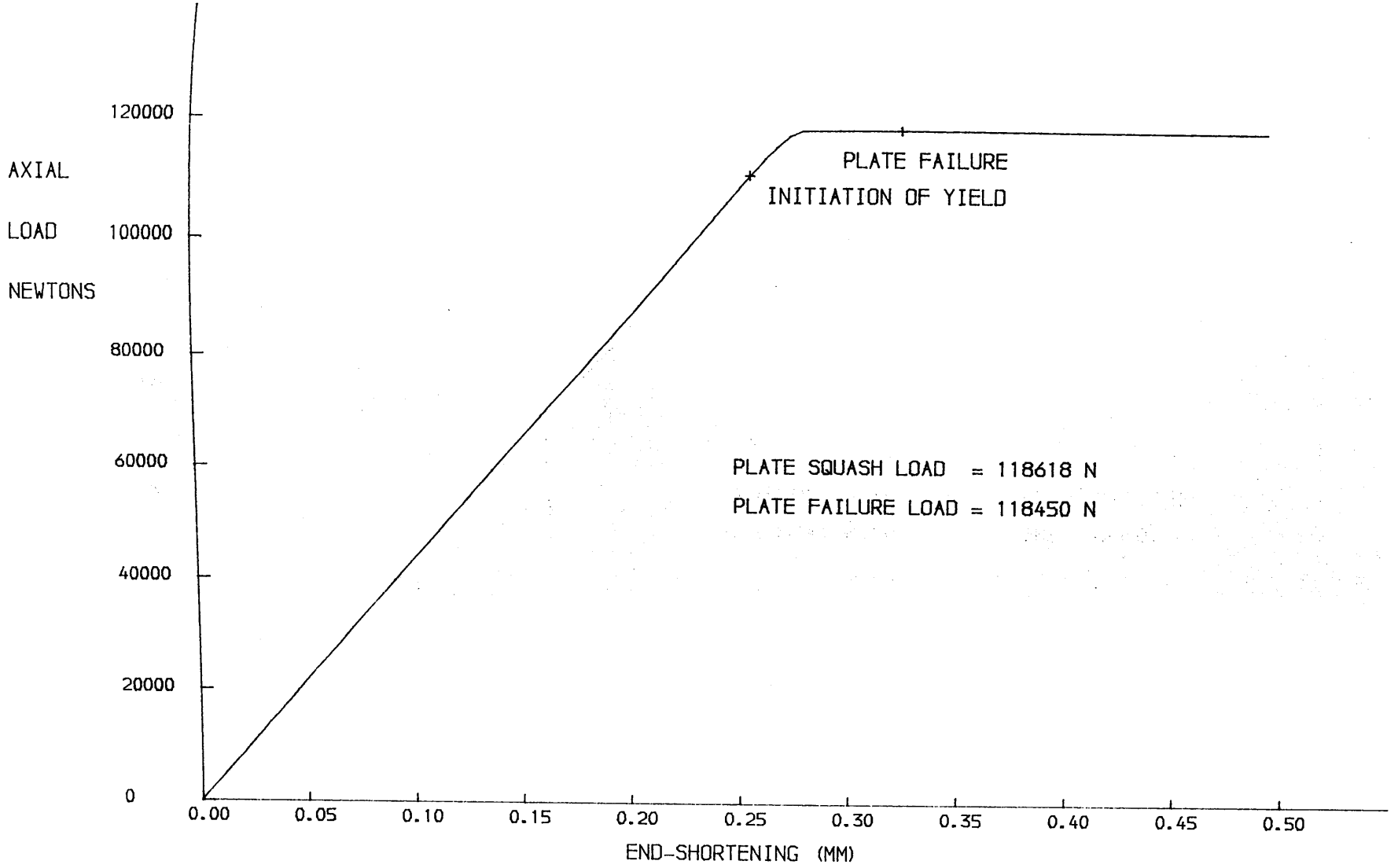

FIG.4.14 MODEL NO.1 - BASE PLATE LOAD END-SHORTENING CURVE

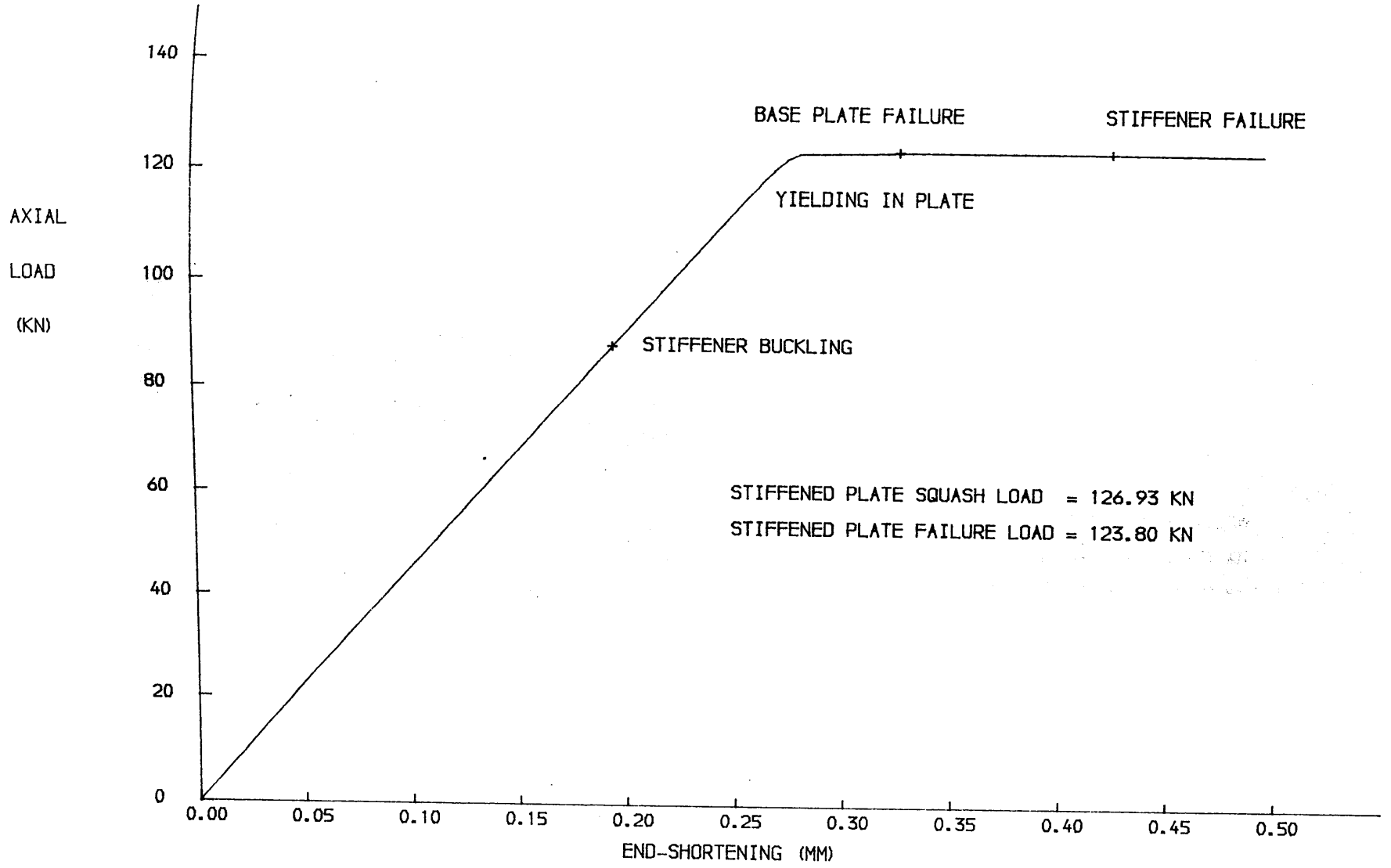

FIG. 4.15 MODEL NO. 1 - STIFFENED PLATE LOAD END-SHORTENING CURVE

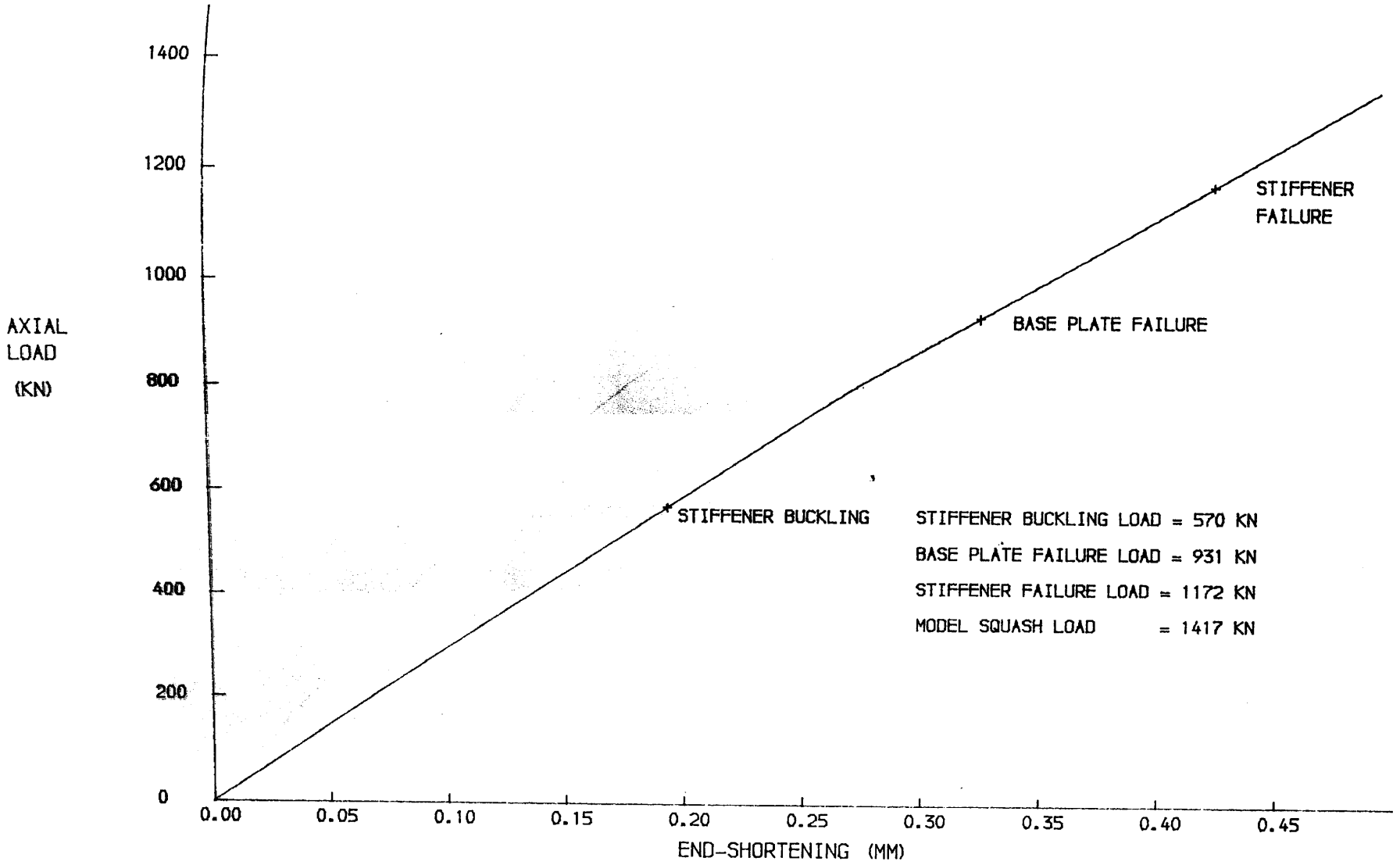

FIG.4.16 MODEL NO.1 - MODEL LOAD END-SHORTENING CURVE

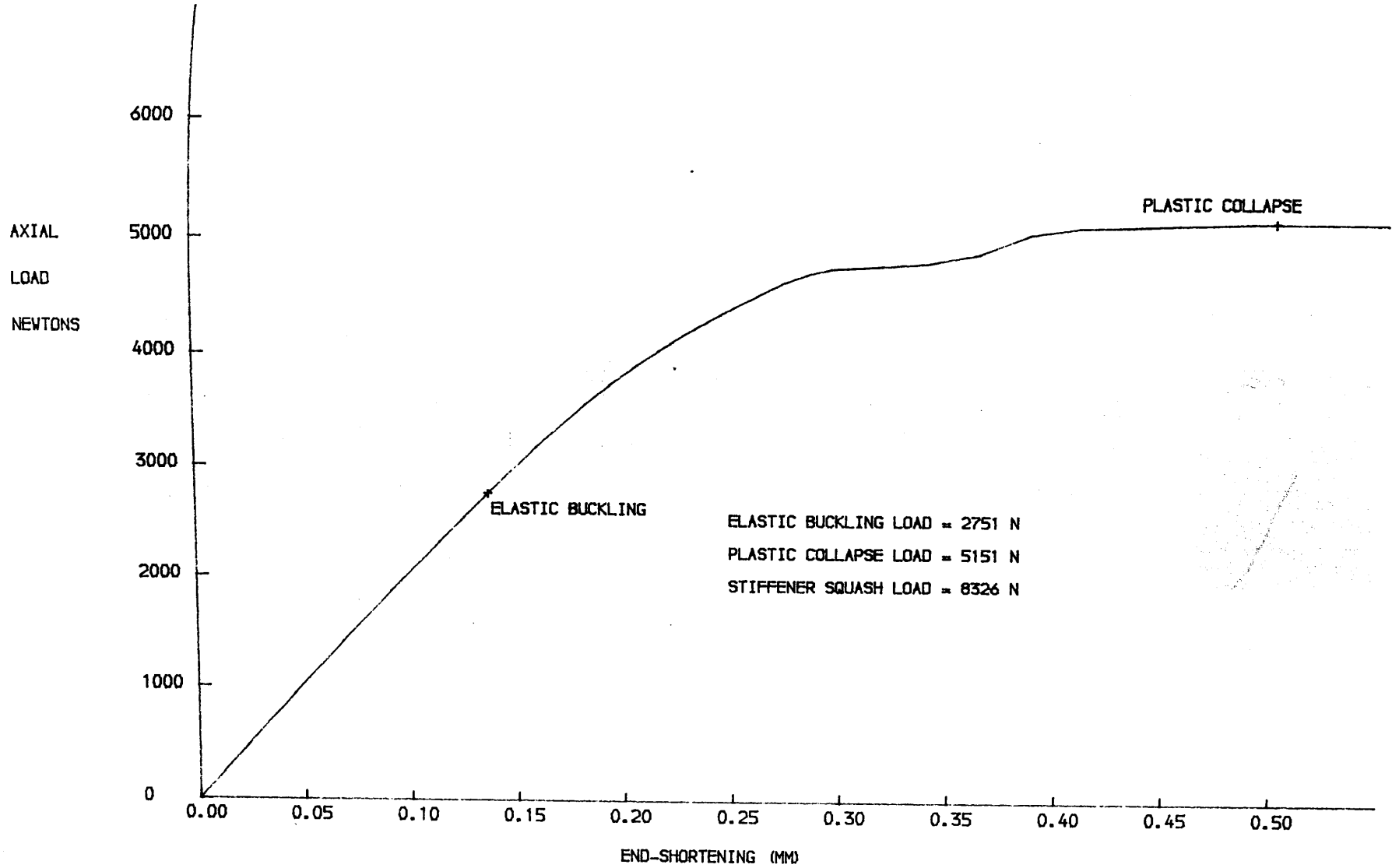

FIG. 4.17 MODEL NO.2 - STIFFENER LOAD END-SHORTENING CURVE

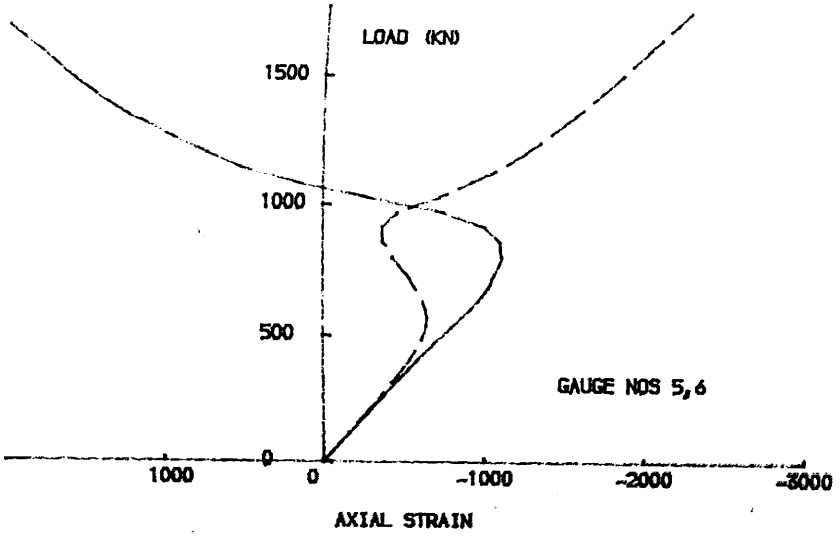

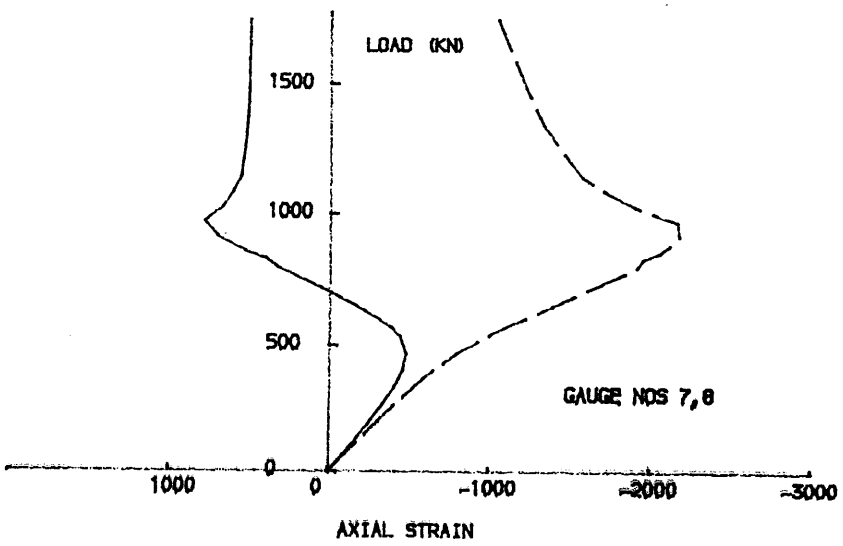

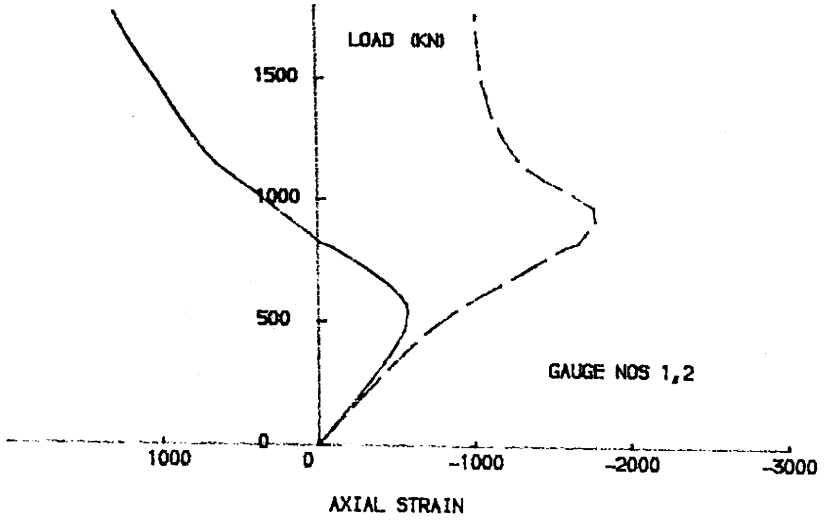

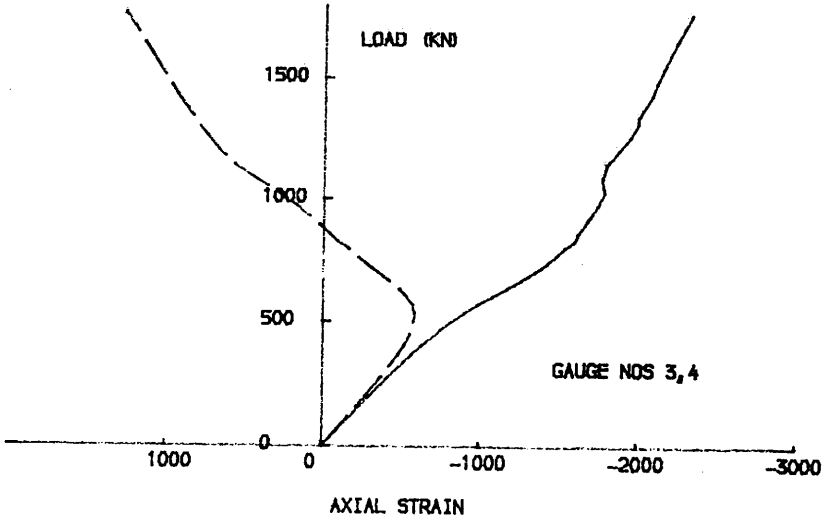

FIG.4.18a MODEL NO. 2 - LOCAL STIFFENER TIP STRAINS

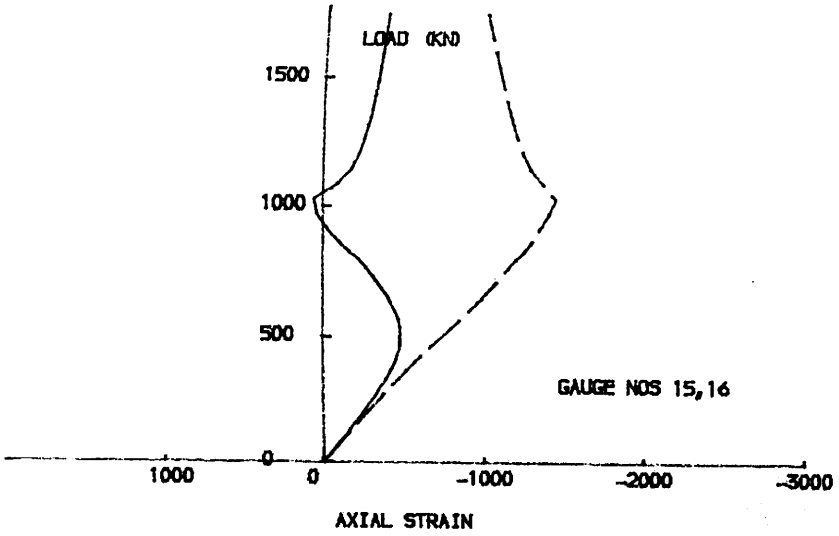

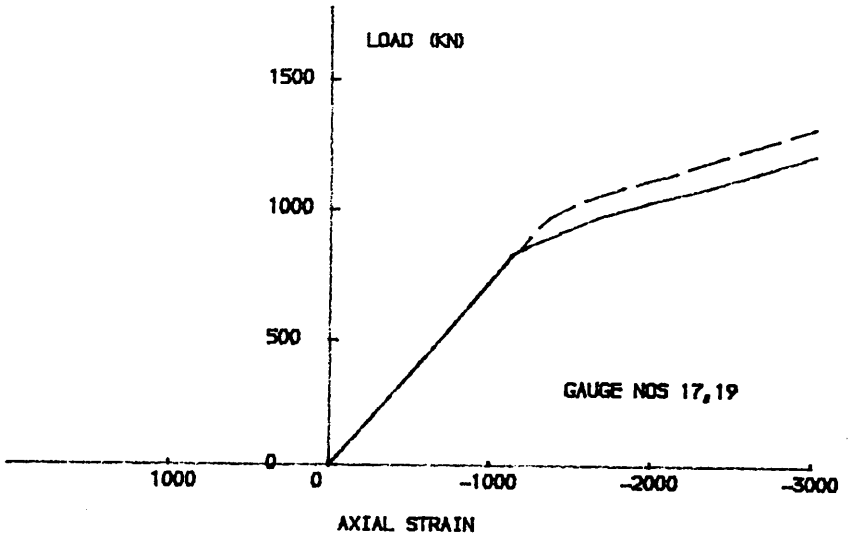

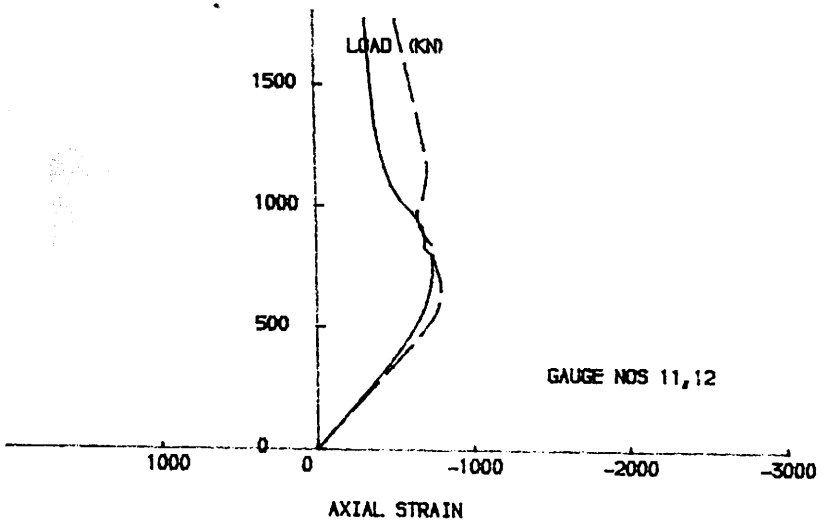

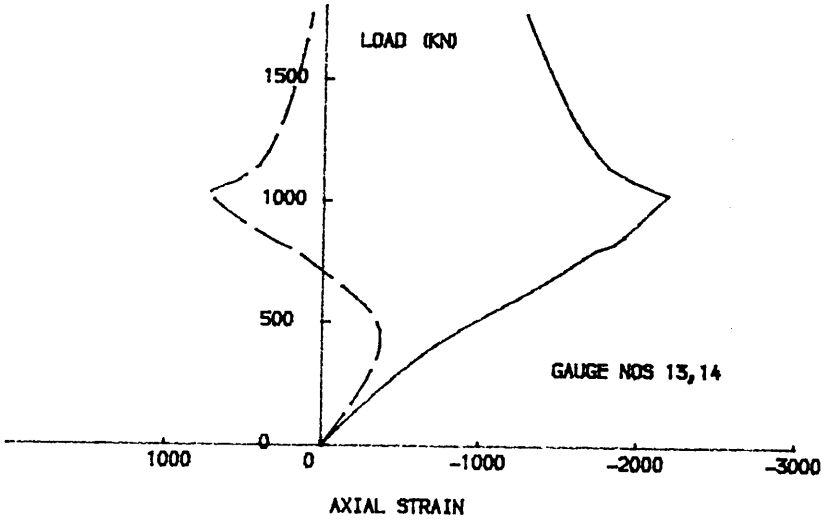

FIG.4.18b MODEL NO. 2 - LOCAL STIFFENER TIP STRAINS

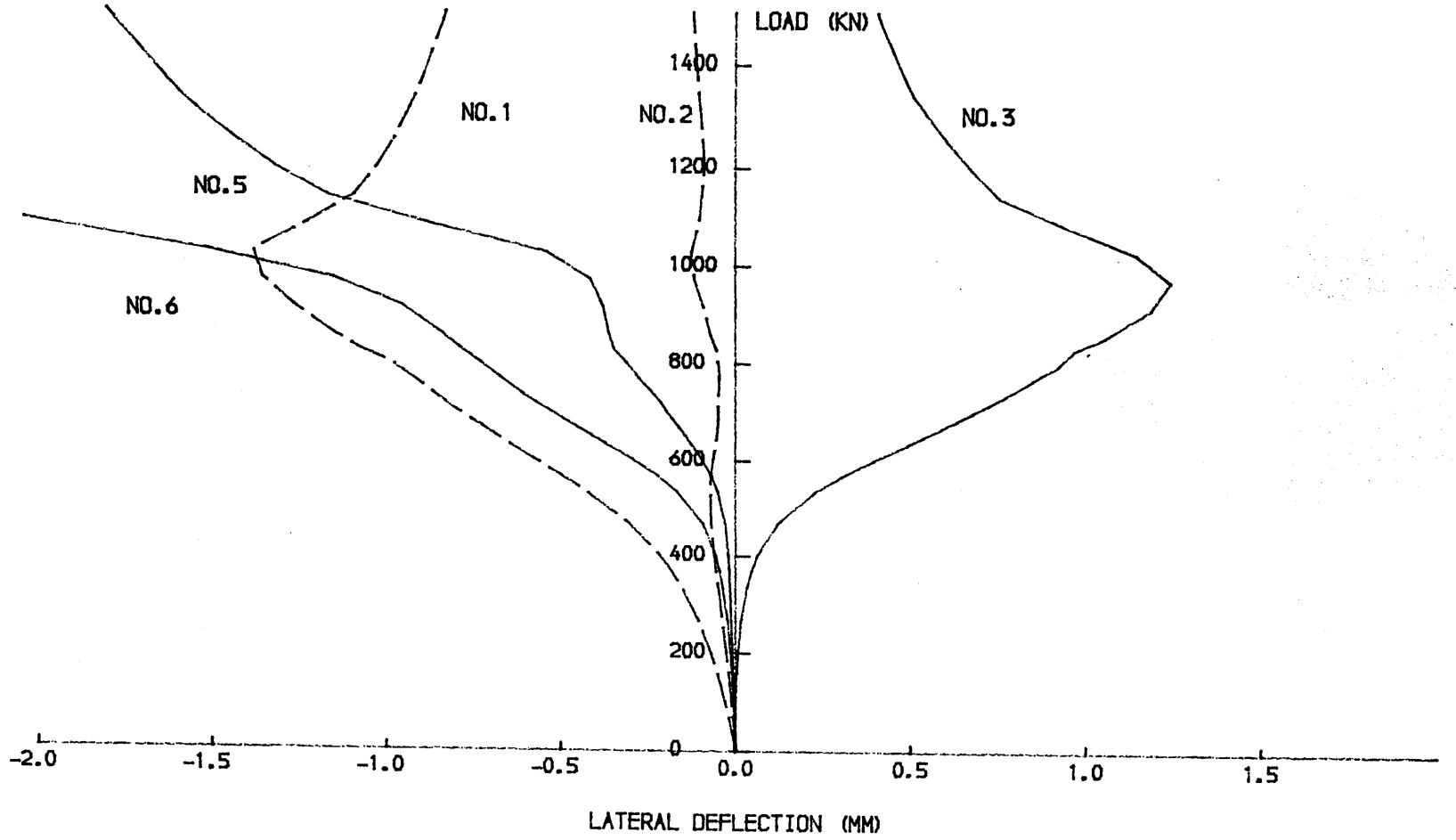

FIG.4.19 MODEL NO.2 STIFFENER TIP LATERAL DEFLECTIONS

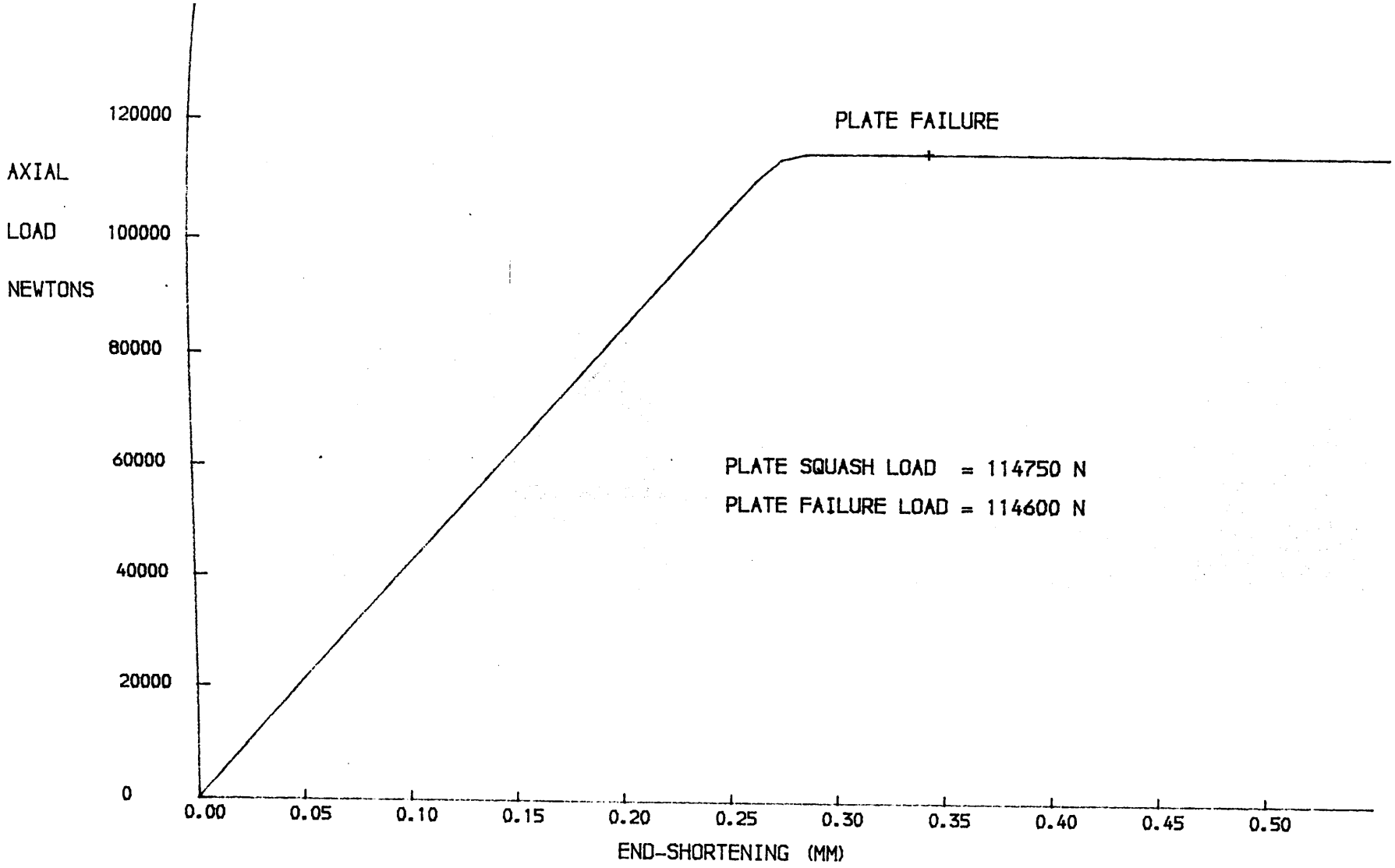

FIG.4.20 MODEL NO.2 - BASE PLATE LOAD END-SHORTENING CURVE

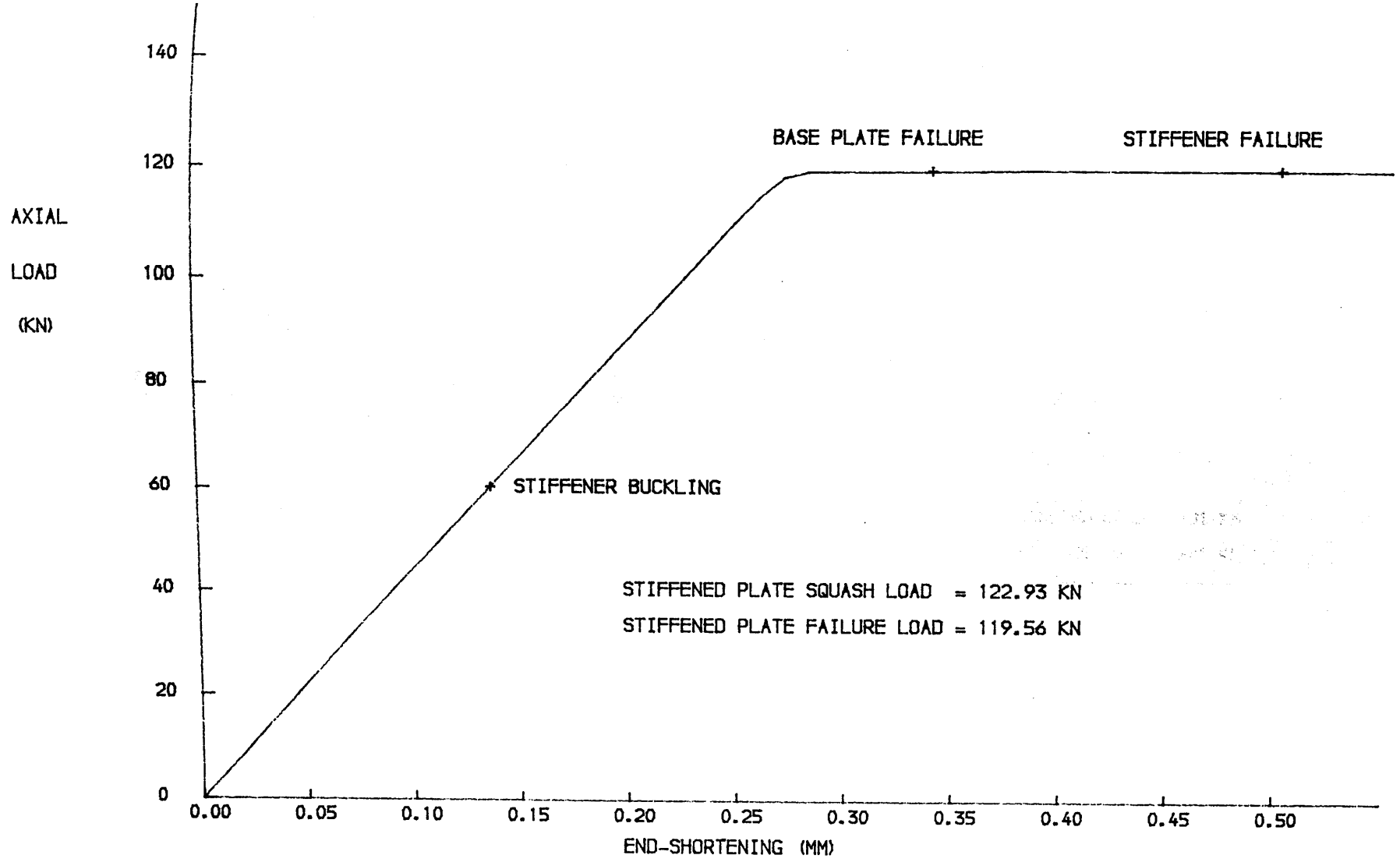

FIG. 4.21 MODEL NO.2 - STIFFENED PLATE LOAD END-SHORTENING CURVE

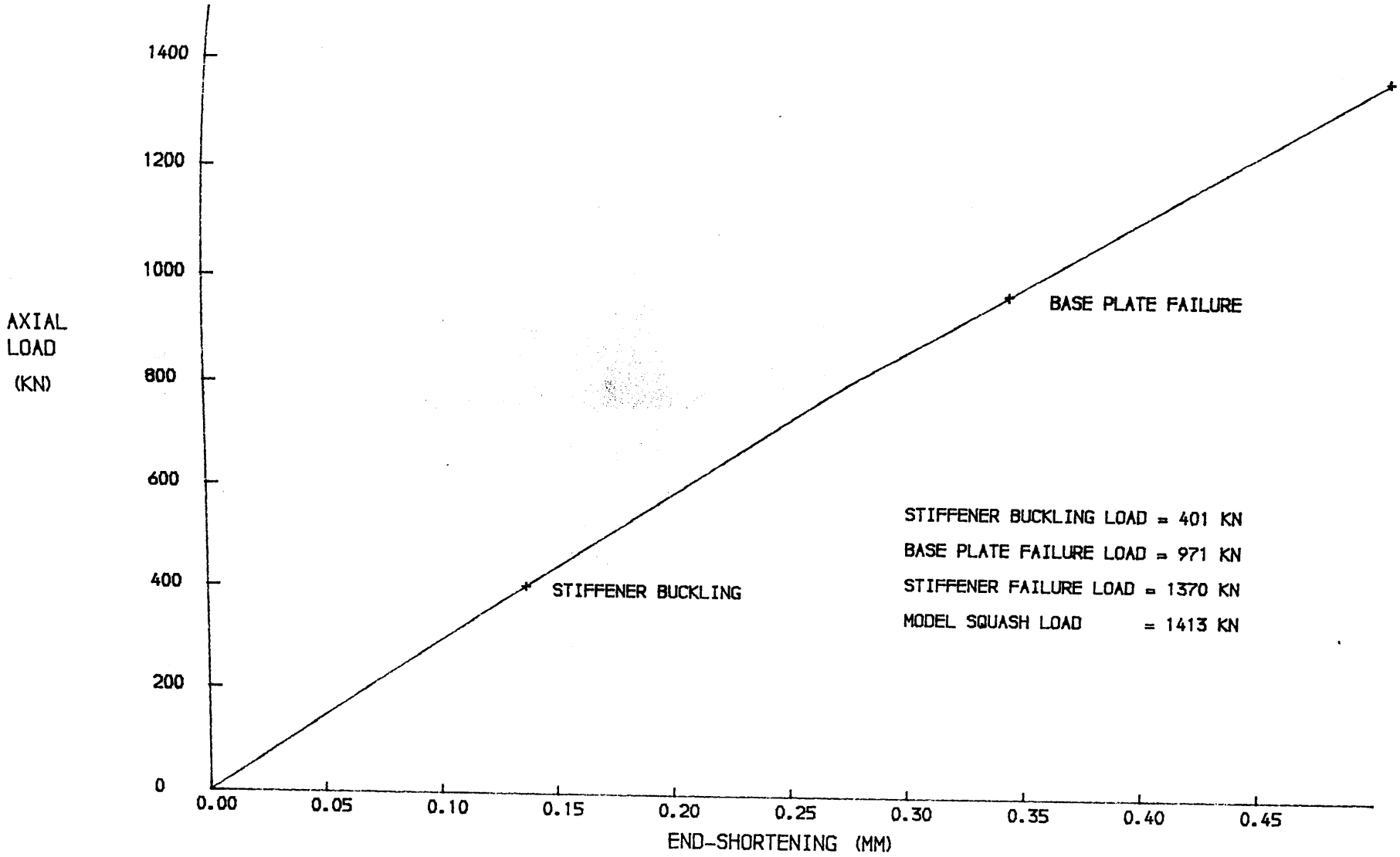

FIG.4.22 MODEL NO.2 - MODEL LOAD END-SHORTENING CURVE

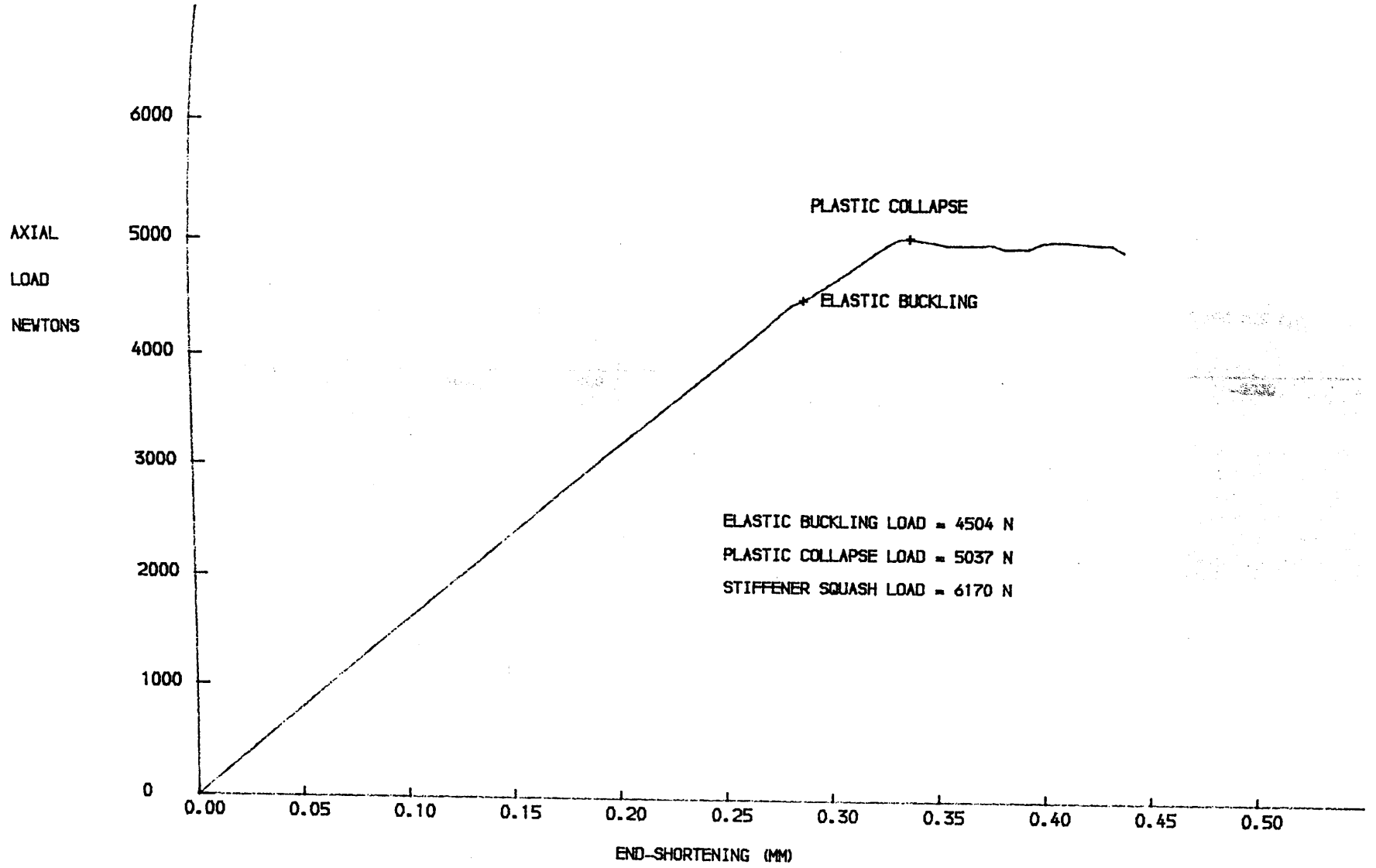

FIG.4.23 MODEL NO.5 - STIFFENER LOAD END-SHORTENING CURVE

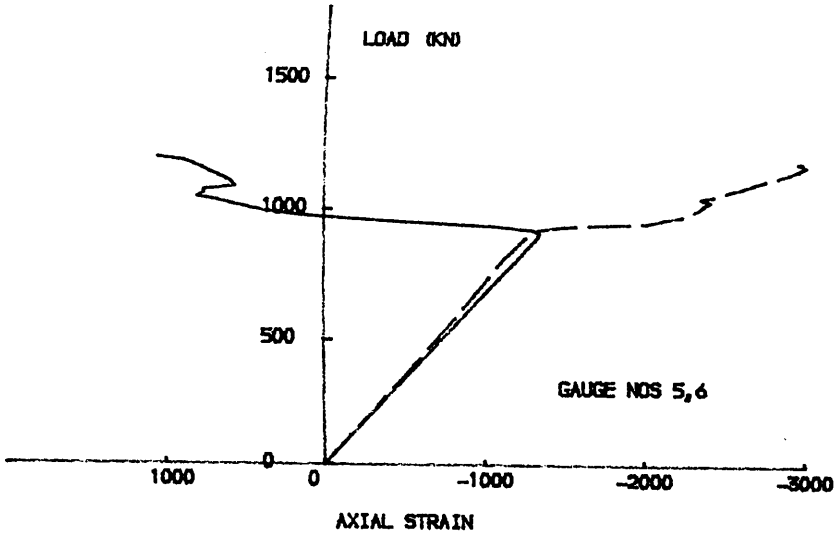

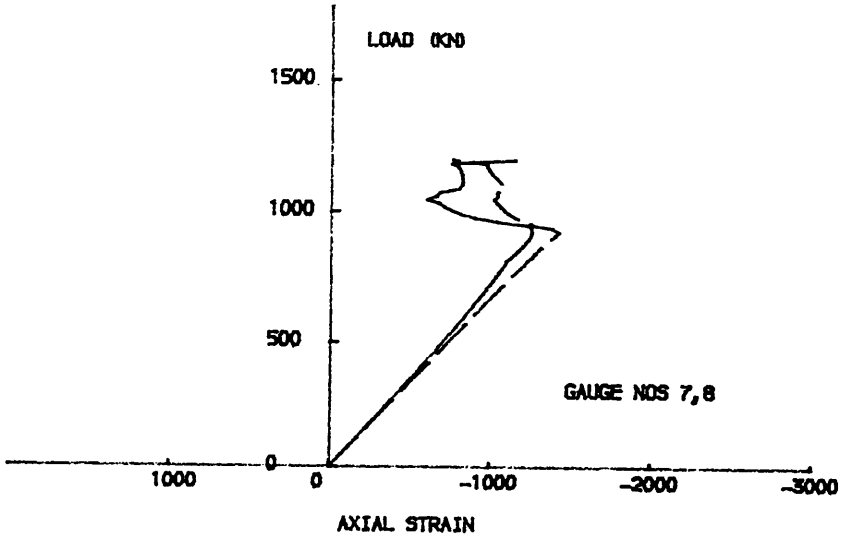

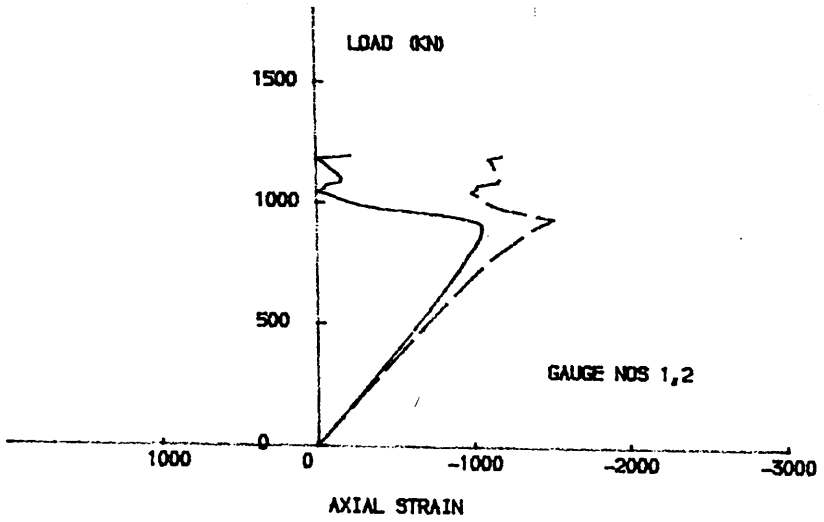

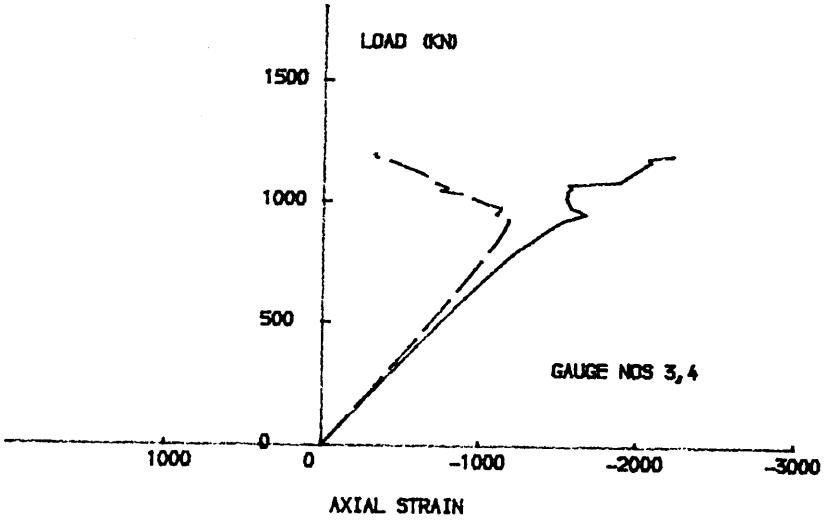

FIG.4.24aMODEL NO. 5 - LOCAL STIFFENER TIP STRAINS

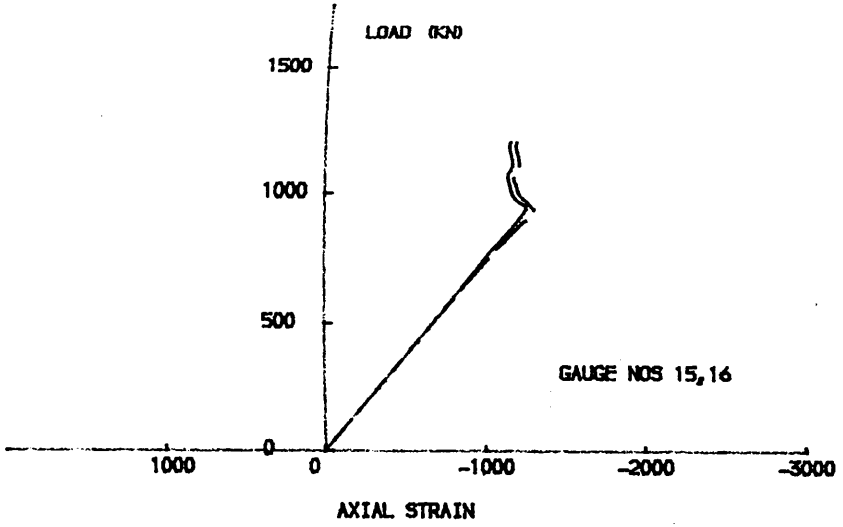

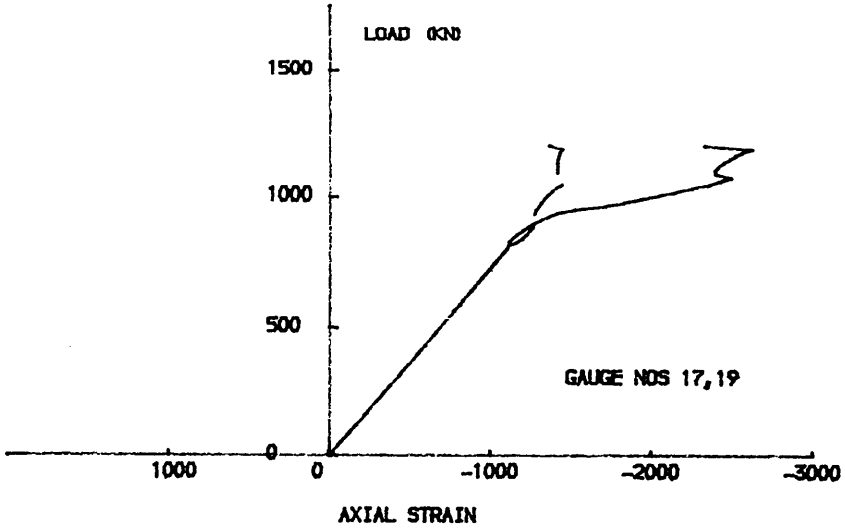

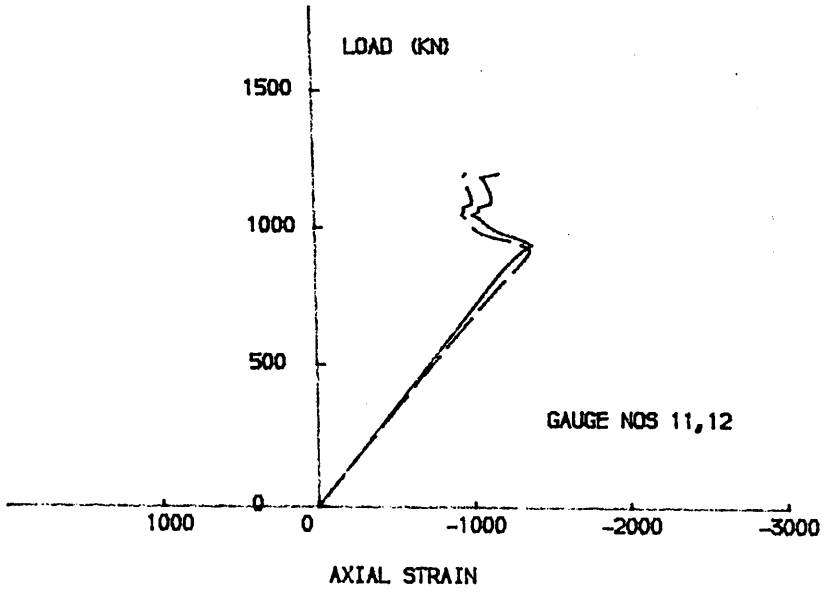

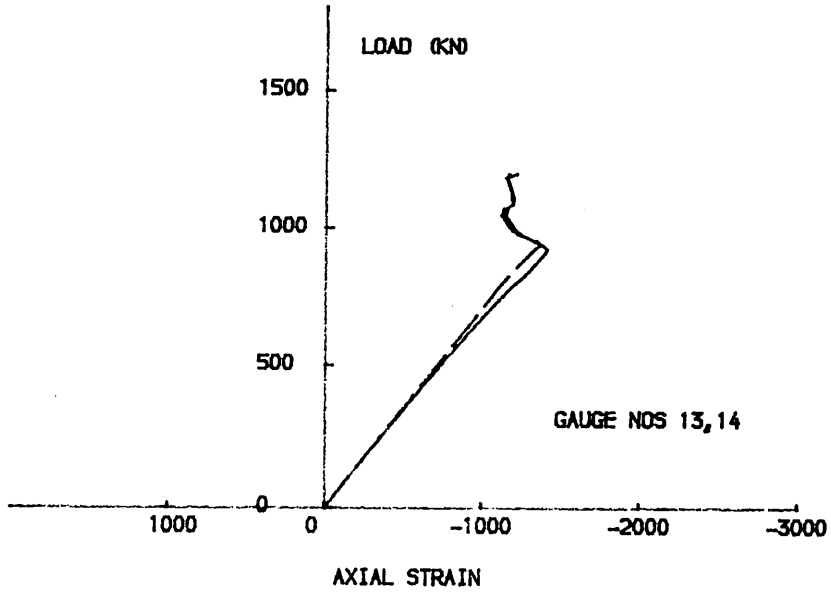

FIG.4.24b MODEL NO. 5 - LOCAL STIFFENER TIP STRAINS

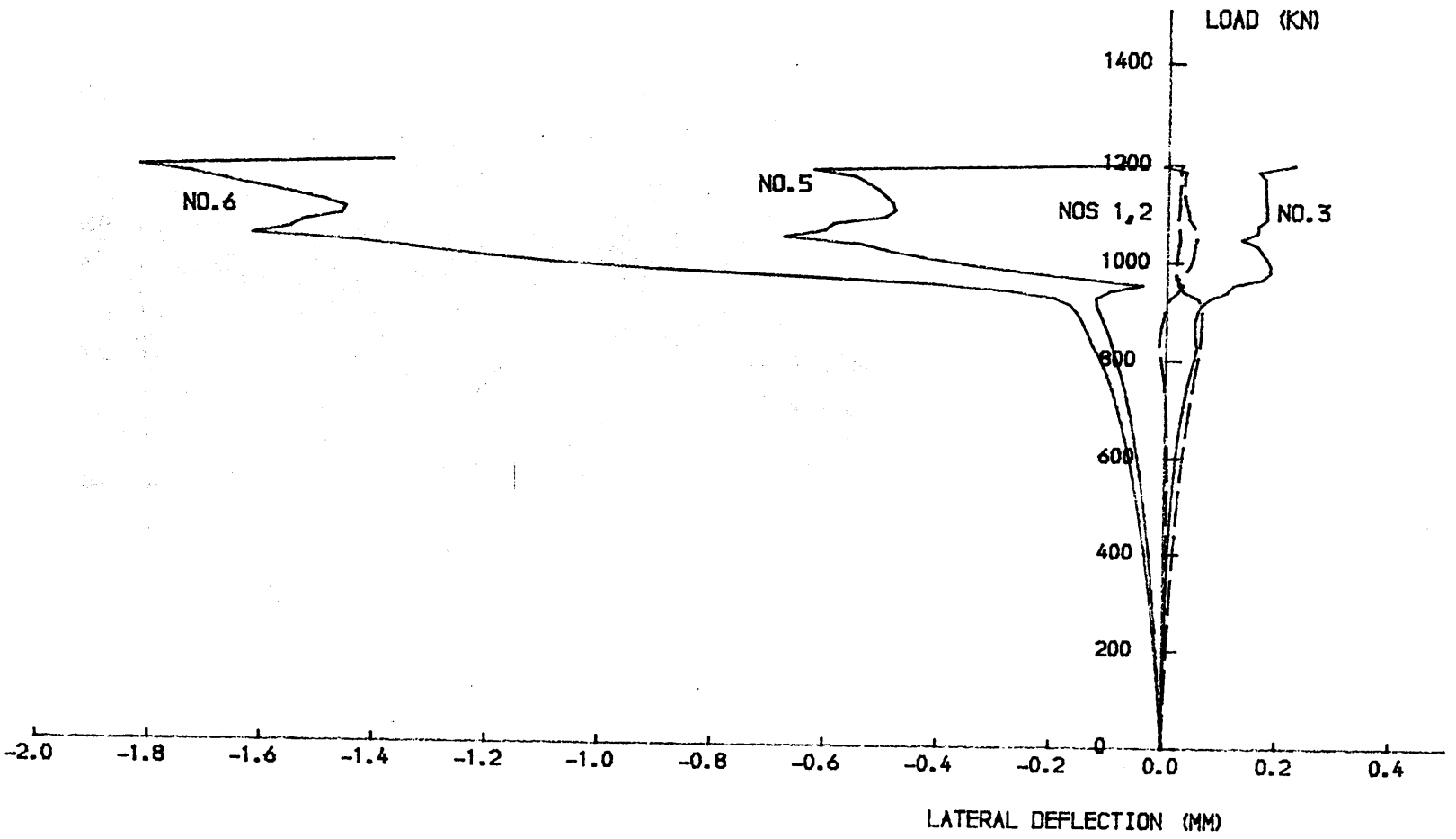

FIG.4.25 MODEL NO.5 STIFFENER TIP LATERAL DEFLECTIONS

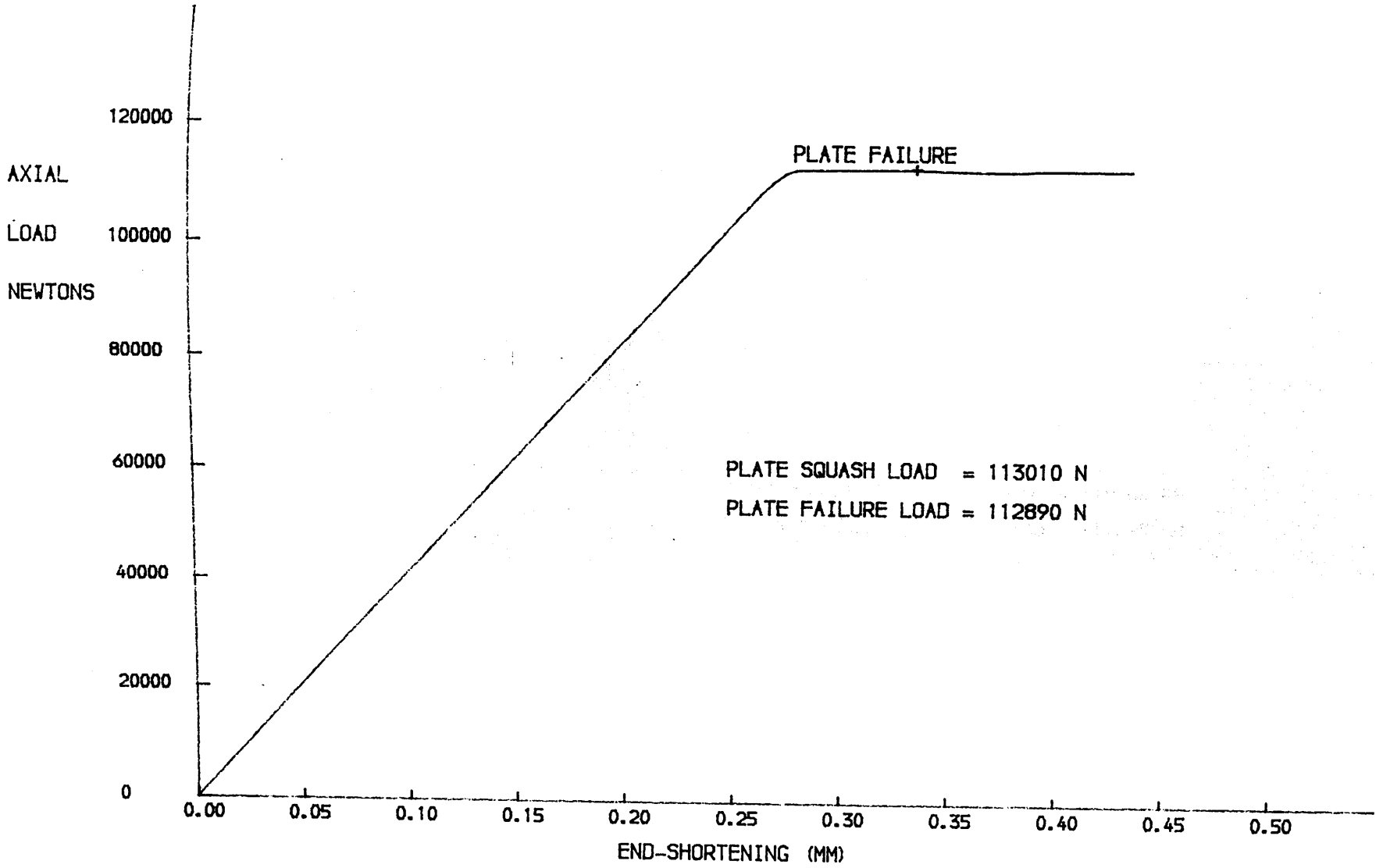

FIG. 4.26 MODEL NO.5 - BASE PLATE LOAD END-SHORTENING CURVE

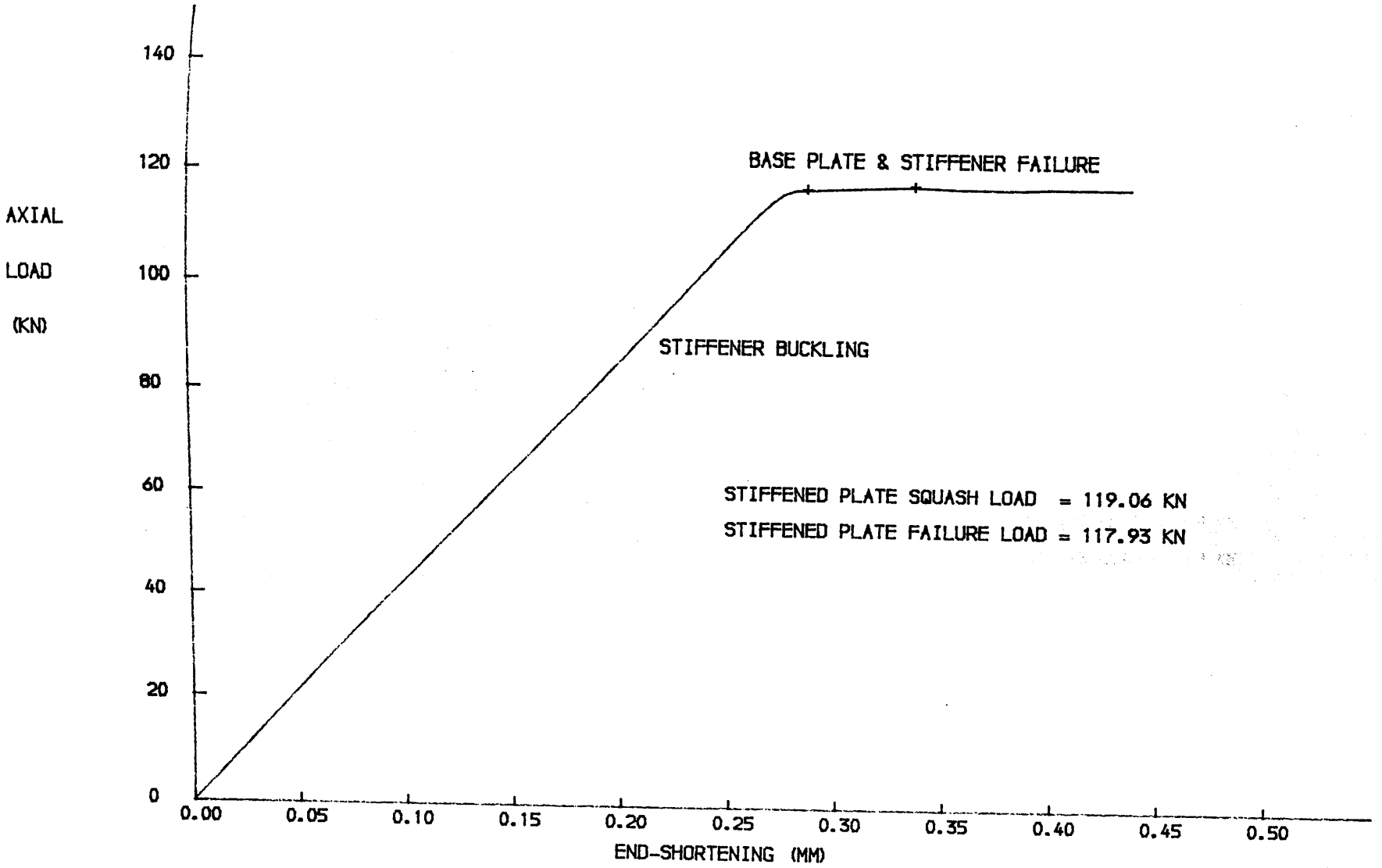

FIG. 4.27 MODEL NO.5 - STIFFENED PLATE LOAD END-SHORTENING CURVE

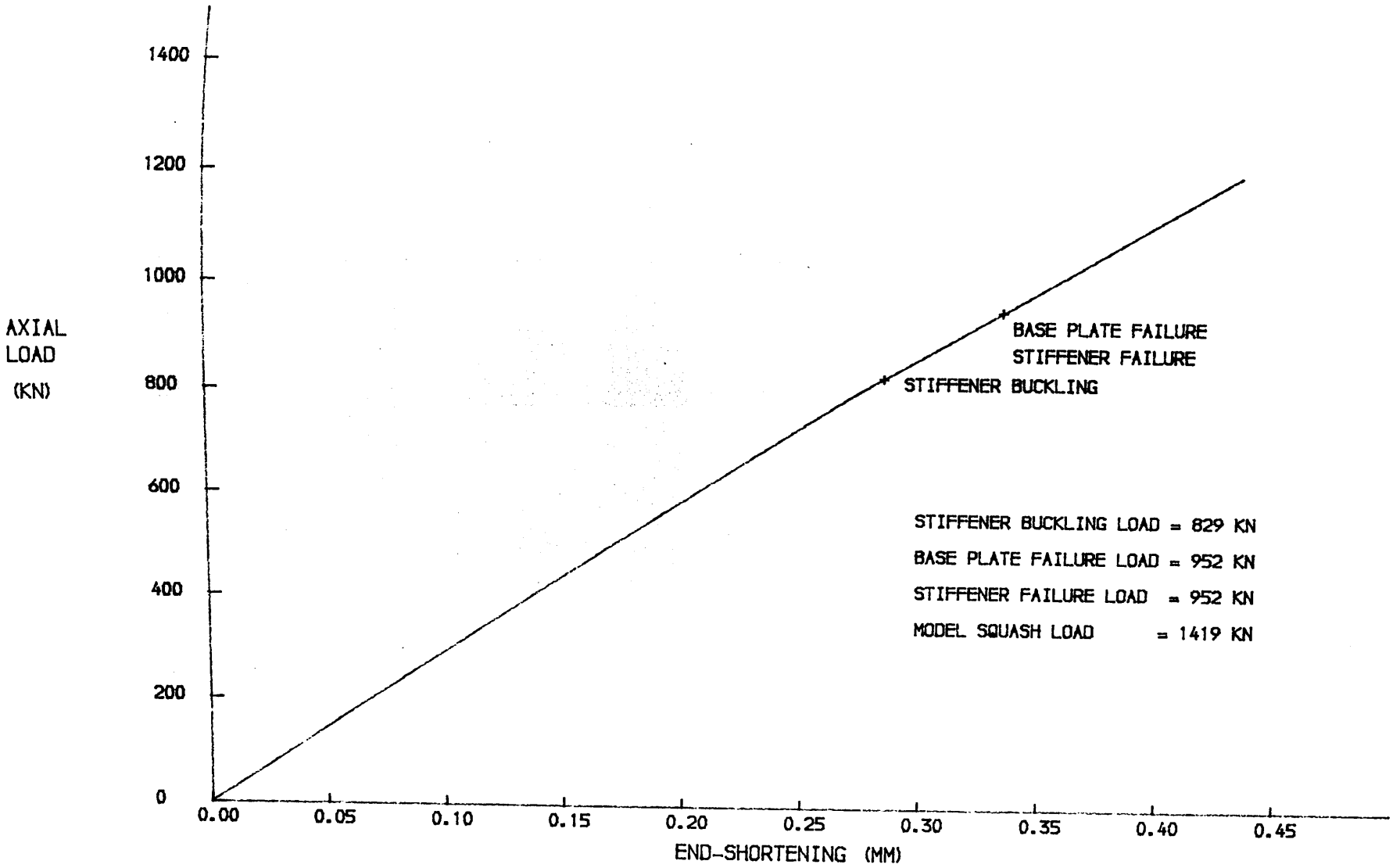

FIG.4.28 MODEL NO.5 - MODEL LOAD END-SHORTENING CURVE

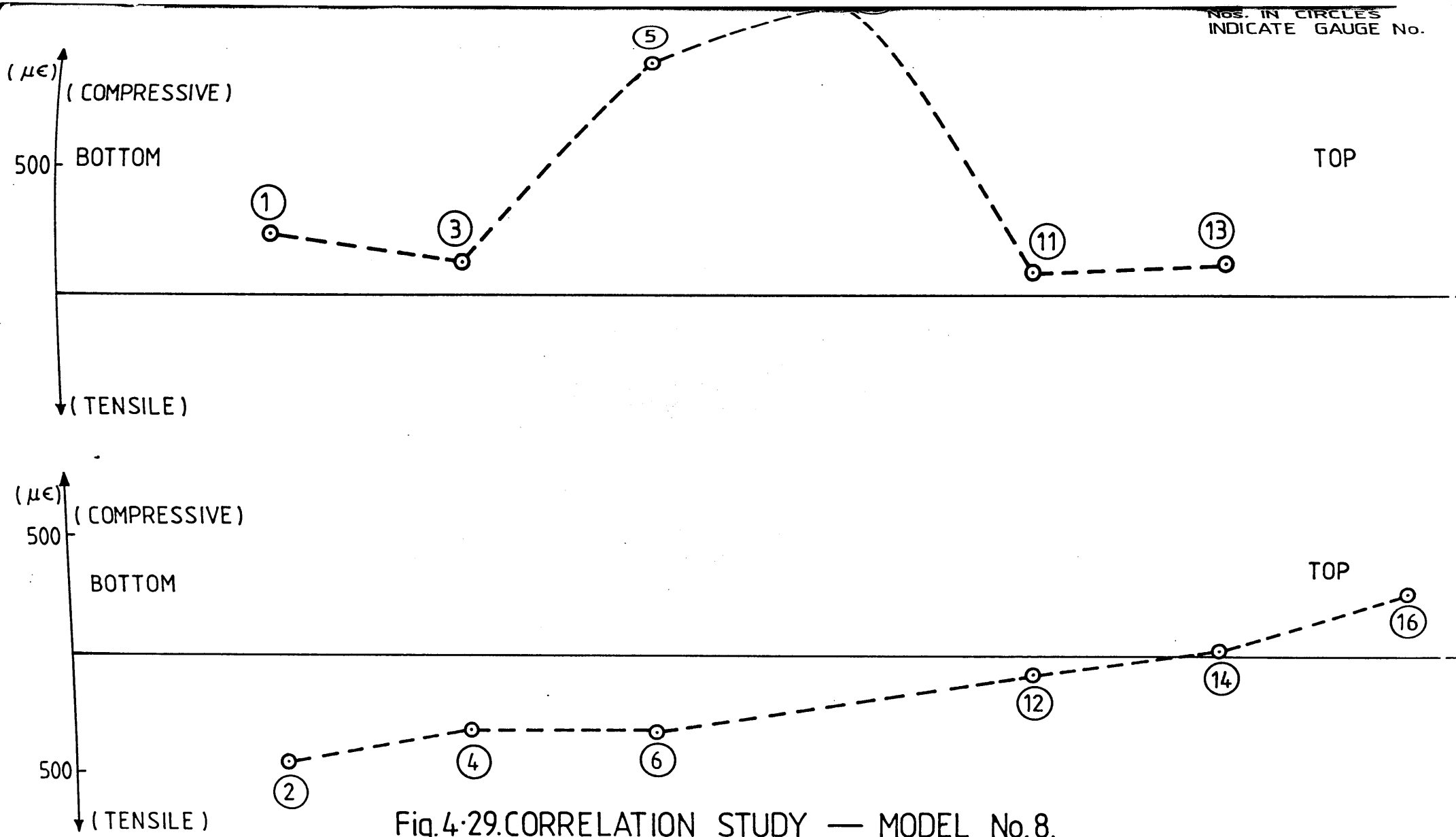

Fig.4·29.CORRELATION STUDY — MODEL No.8.
DISTRIBUTION OF RESIDUAL STRAINS ALONG STIFFENER TIP (TEST RESULTS)

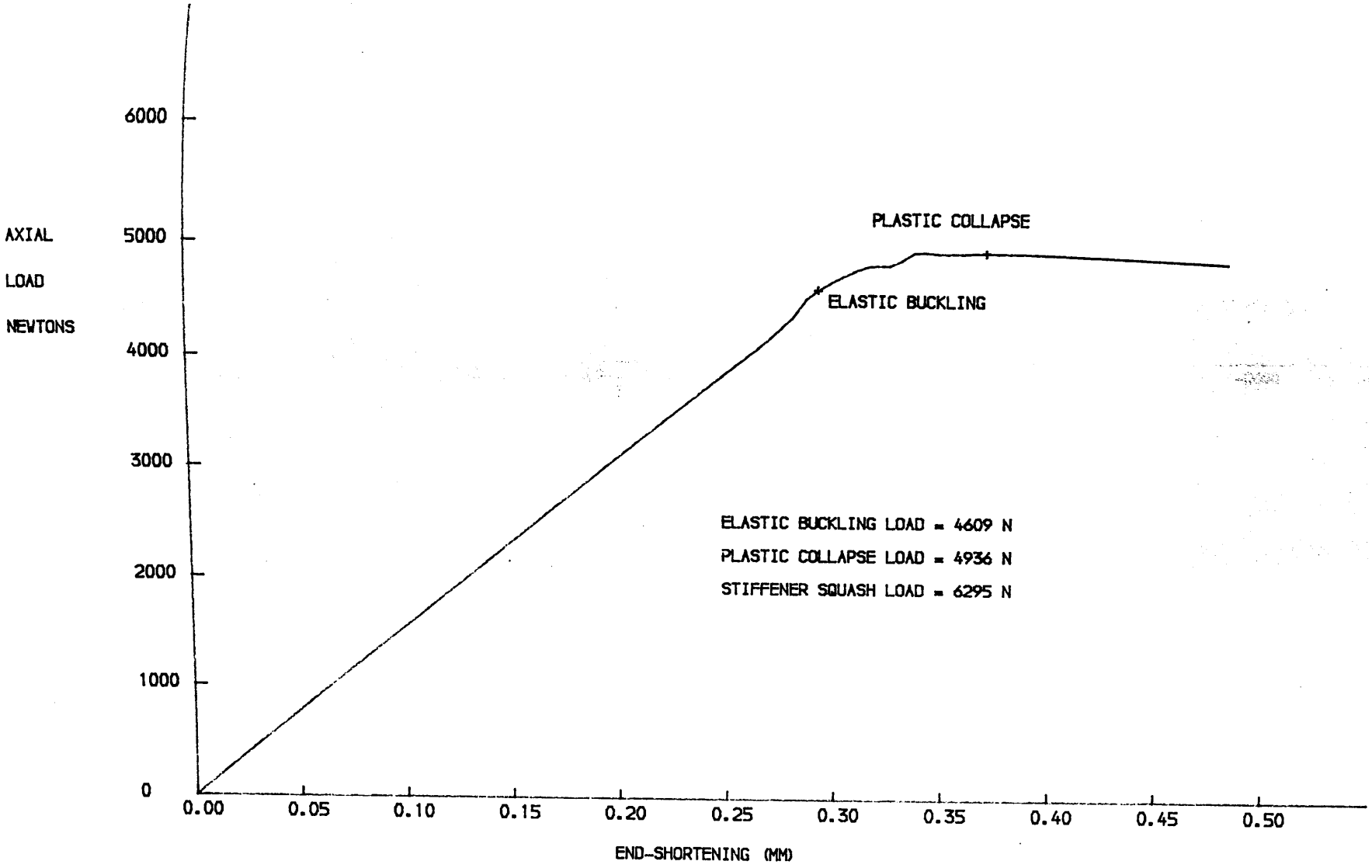

FIG. 4.30 MODEL NO.8 - STIFFENER LOAD END-SHORTENING CURVE

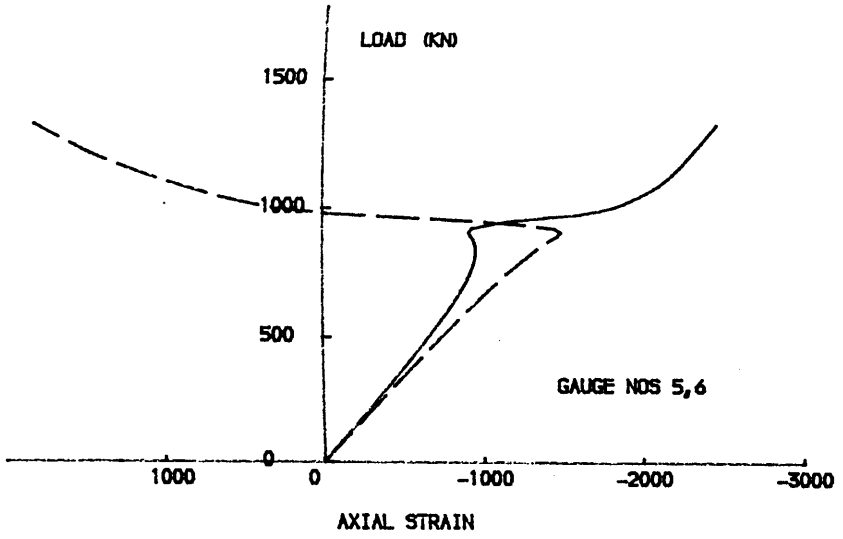

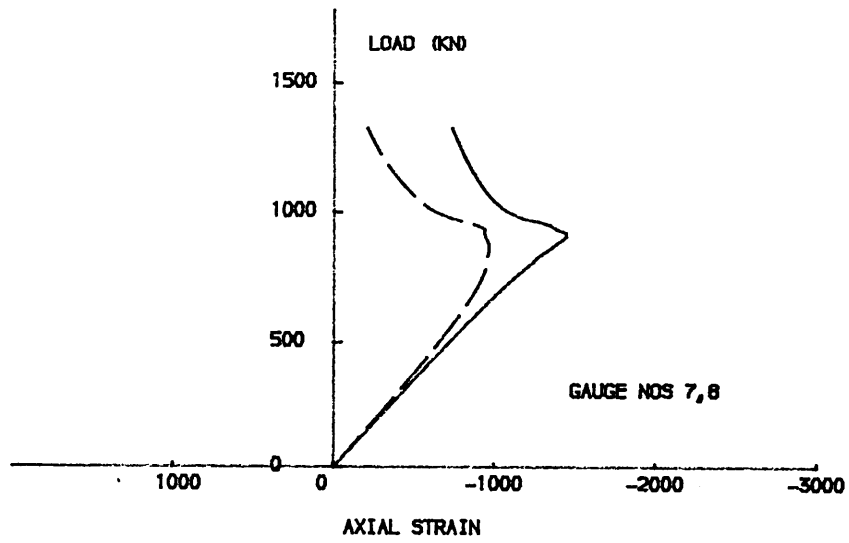

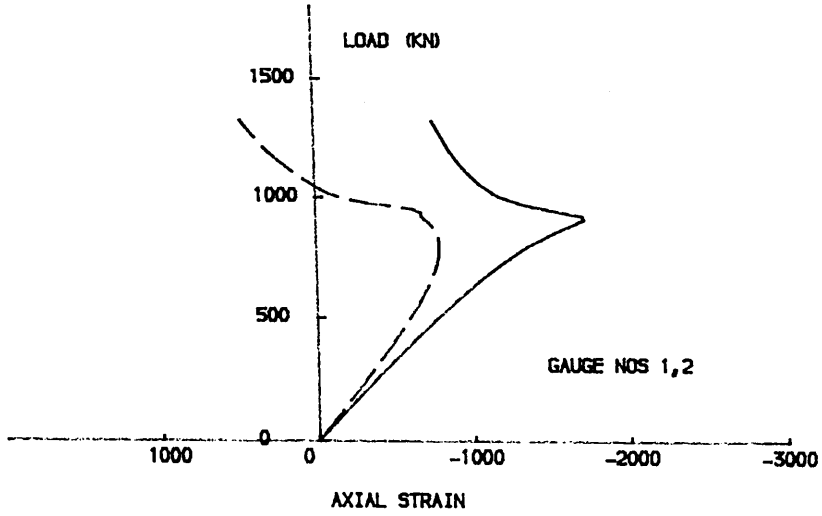

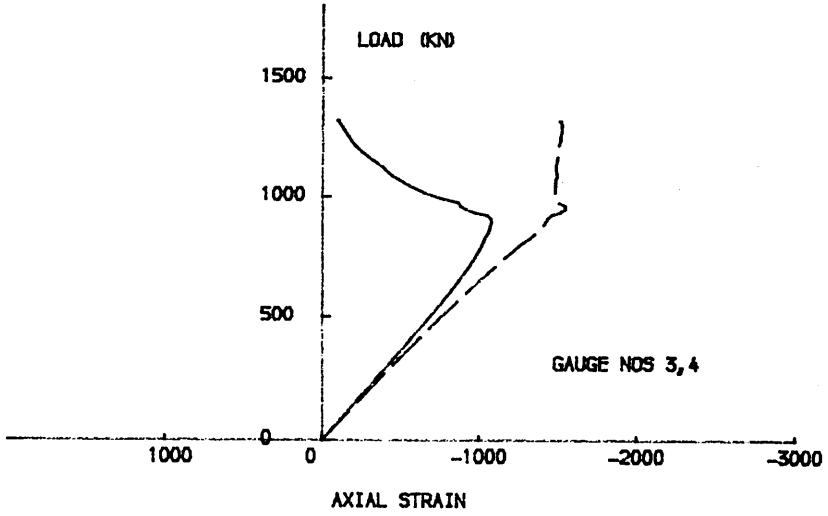

FIG. 4.31 (A) MODEL NO. 8 - LOCAL STIFFENER TIP STRAINS

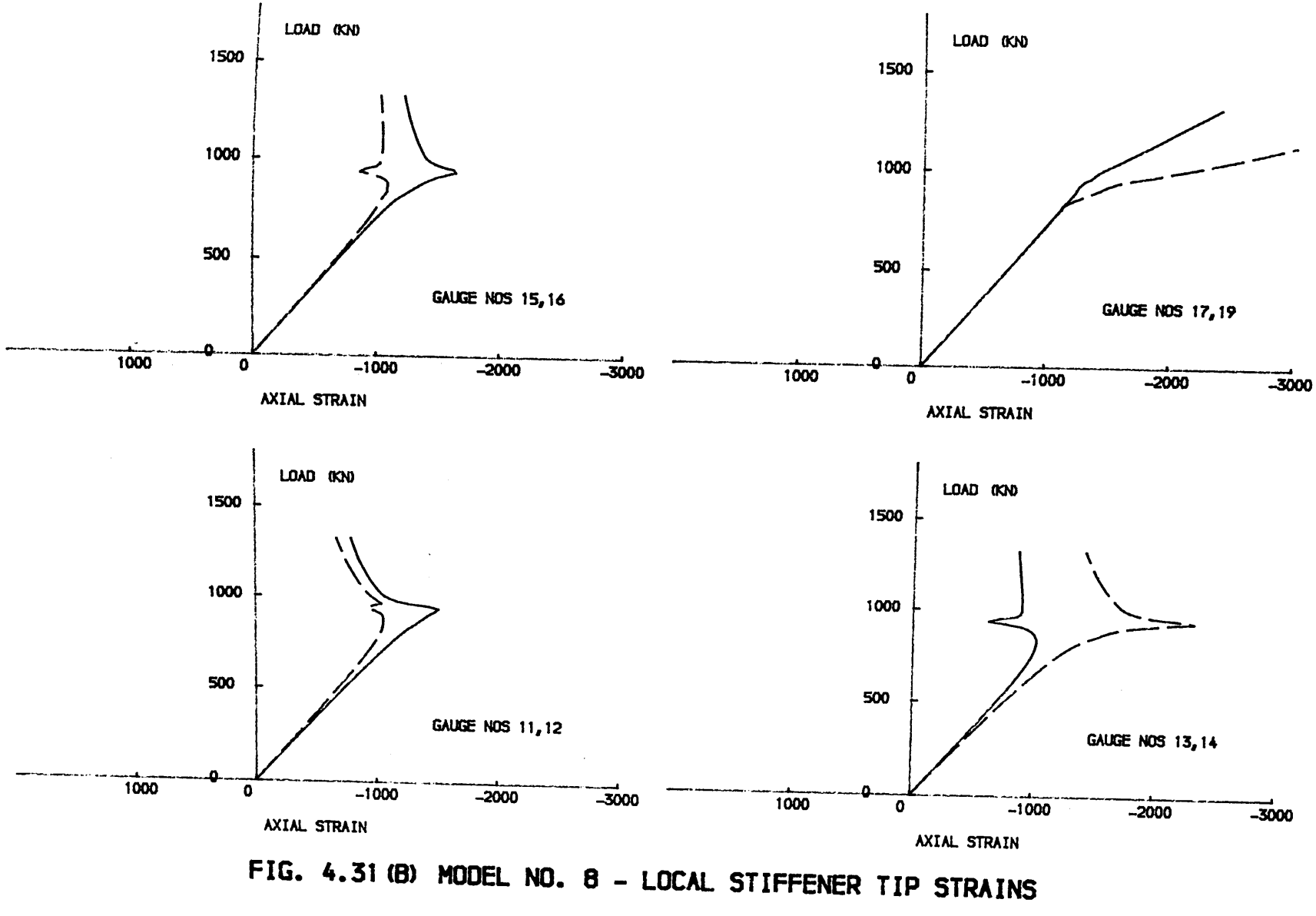

FIG. 4.31 (B) MODEL NO. 8 - LOCAL STIFFENER TIP STRAINS

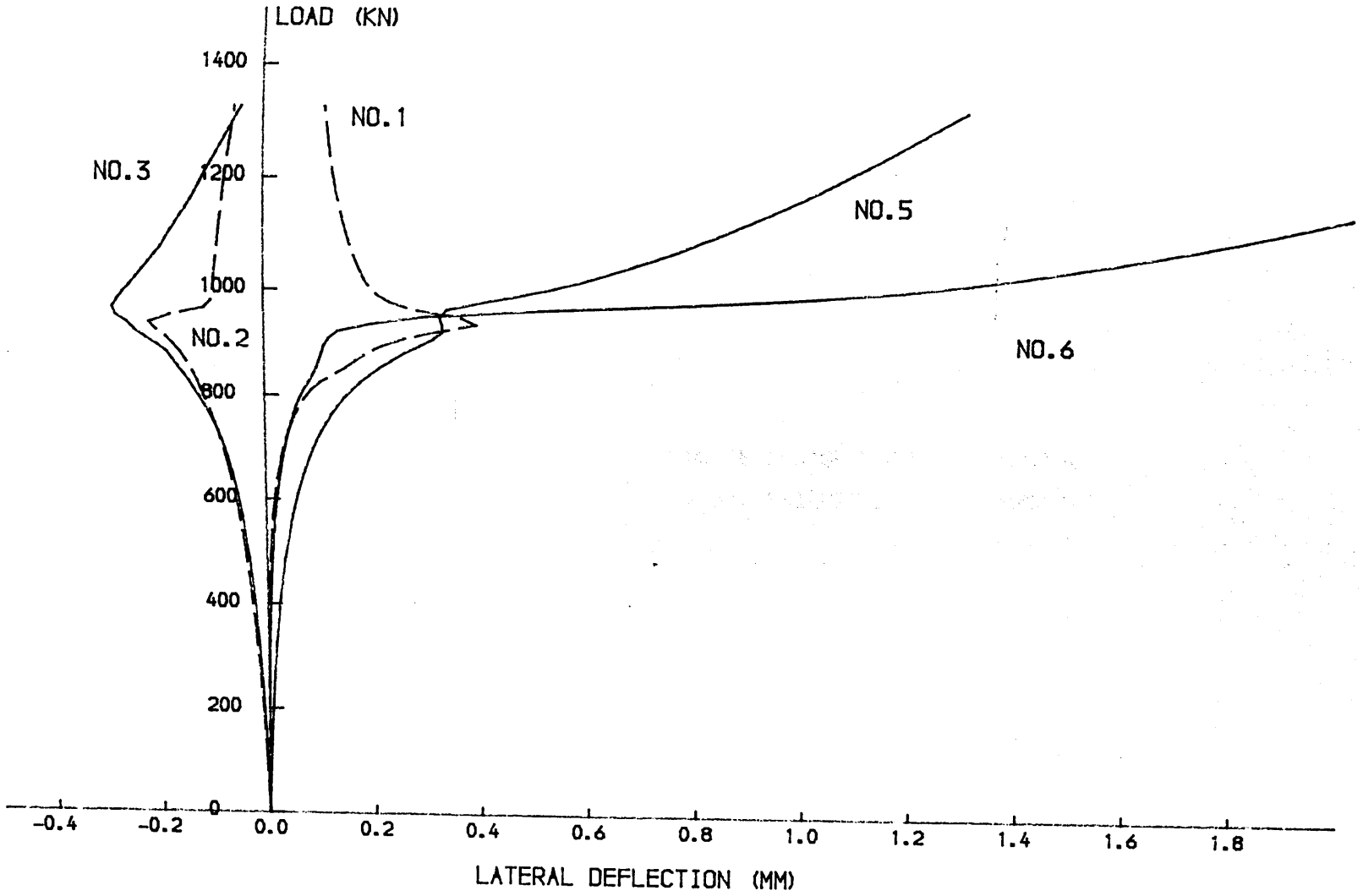

FIG. 4.32 MODEL NO.8 STIFFENER TIP LATERAL DEFLECTIONS

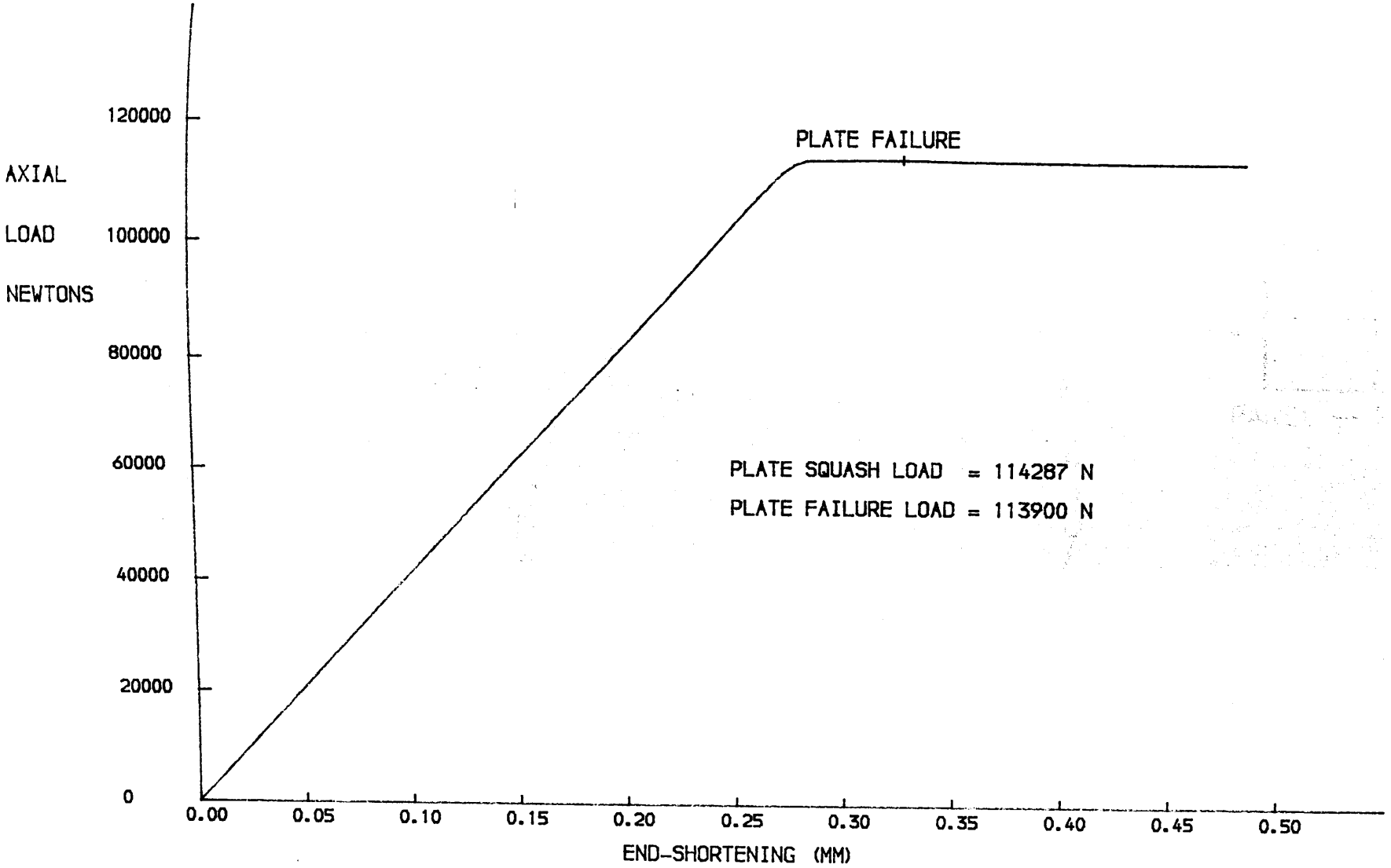

FIG. 4.33 MODEL NO.8 - BASE PLATE LOAD END-SHORTENING CURVE

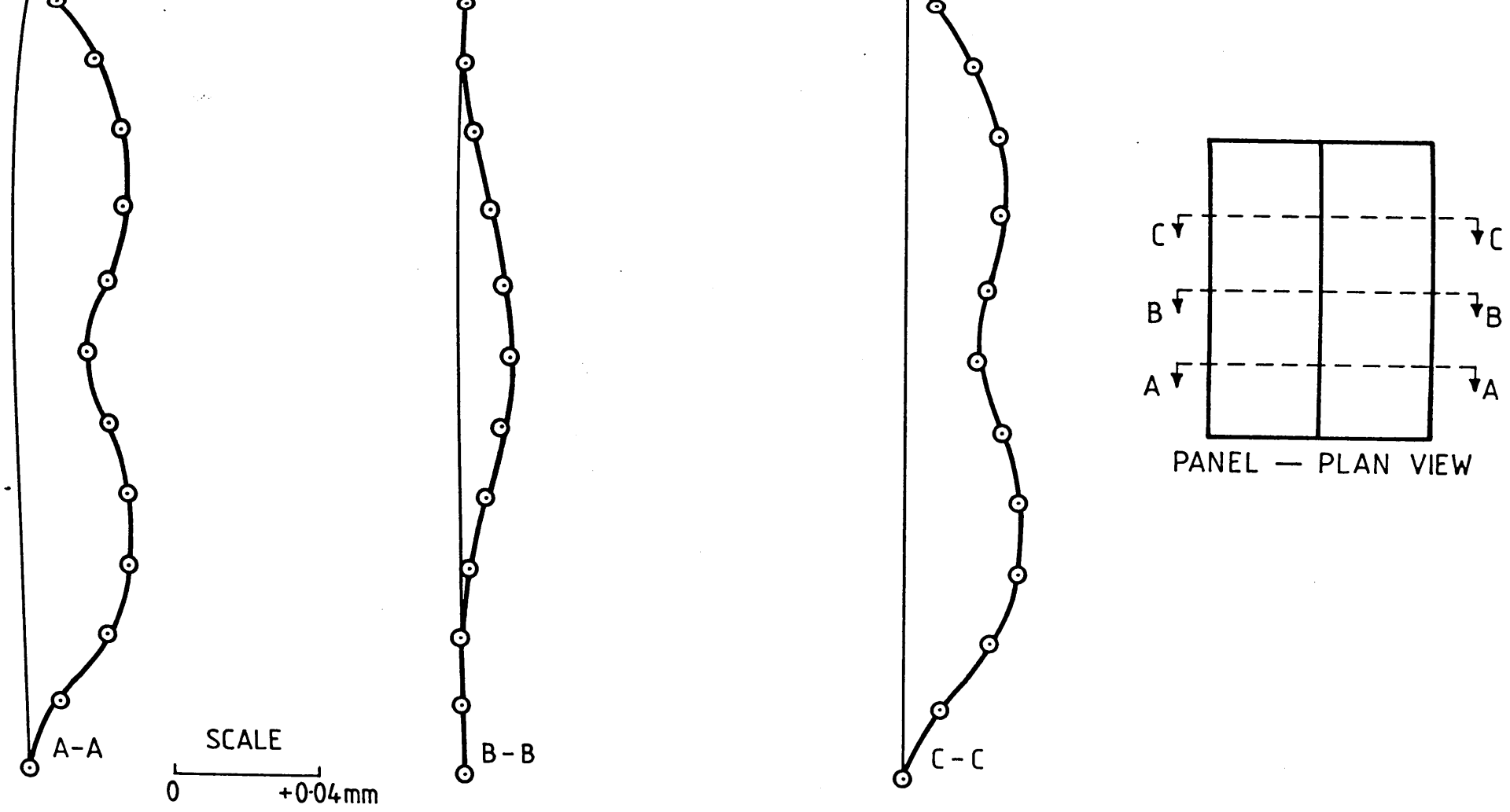

Fig.4·34. CORRELATION STUDY — MODEL No.8
BASE PLATE PROFILES OF DEFLECTED SHAPE IN TRANSVERSE DIRECTION (PRE-BUCKLING RANGE)

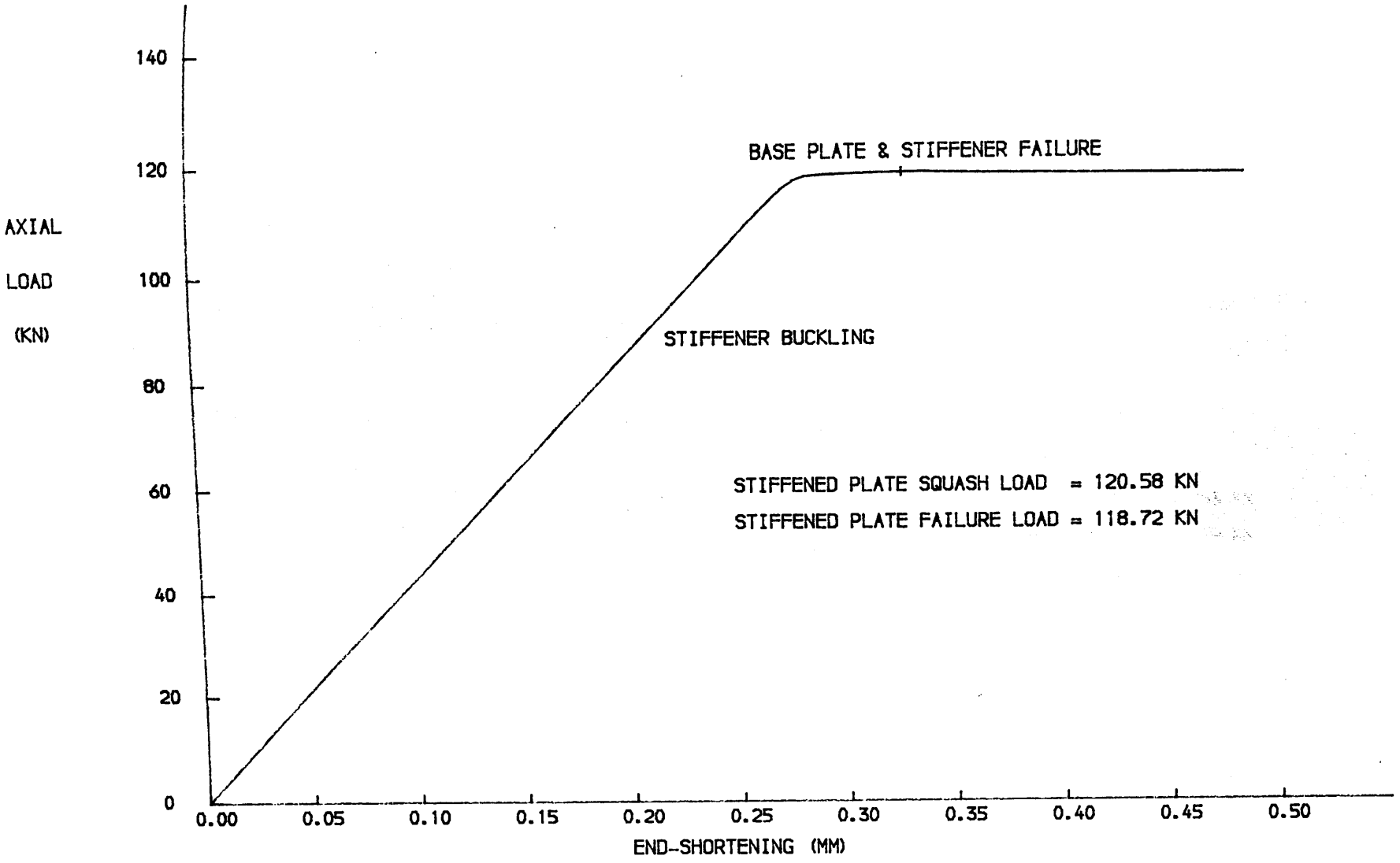

FIG. 4.35 MODEL NO.8 - STIFFENED PLATE LOAD END-SHORTENING CURVE

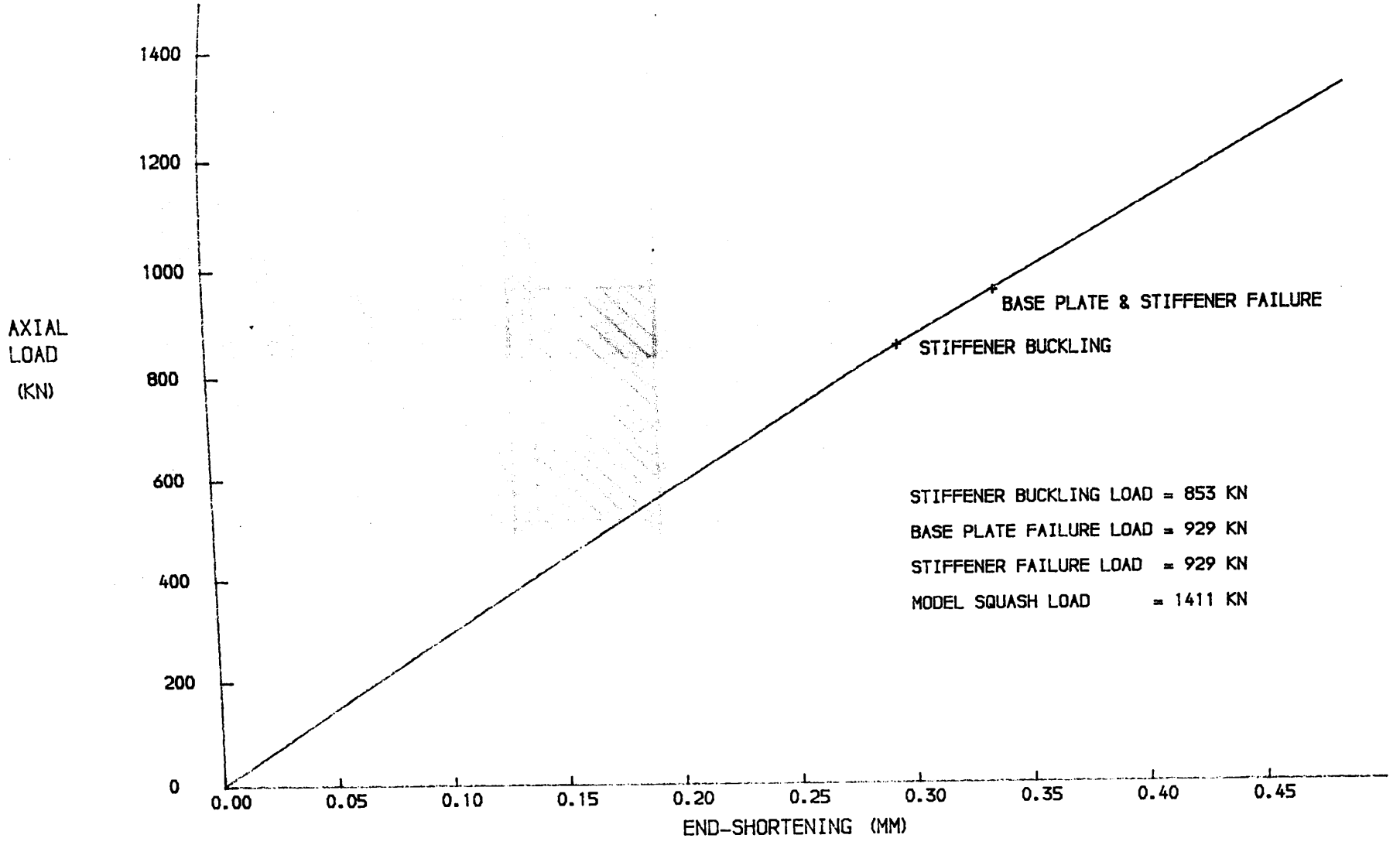

FIG. 4.36 MODEL NO.8 - MODEL LOAD END-SHORTENING CURVEH

EDGES AB, CD ARE WELDED TO BOX
EDGE BC IS WELDED TO THE BASE PLATE
EDGE AD IS FREE

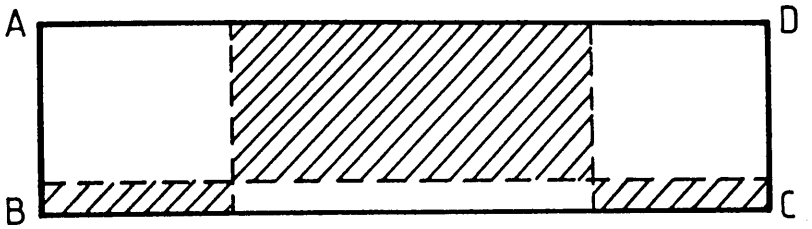

(a) PREBUCKLING RANGE (250kN/m^2)

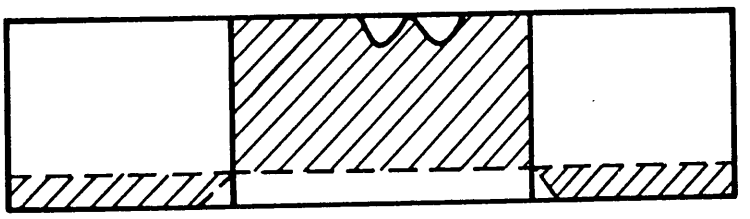

(b) STIFFENER POSTBUCKLING RANGE (725 kN/m^2)

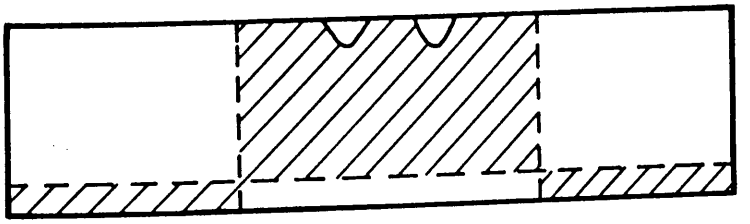

(c) POST FAILURE (850 kN/m^2)

///// INDICATES REGIONS OF COMPRESSIVE STRAIN

Fig. 4·37. CORRELATION STUDY — MODEL No. 4
DISTRIBUTION OF LONGITUDINAL MEMBRANE STRAINS
IN STIFFENER AT VARIOUS STAGES OF LOADING

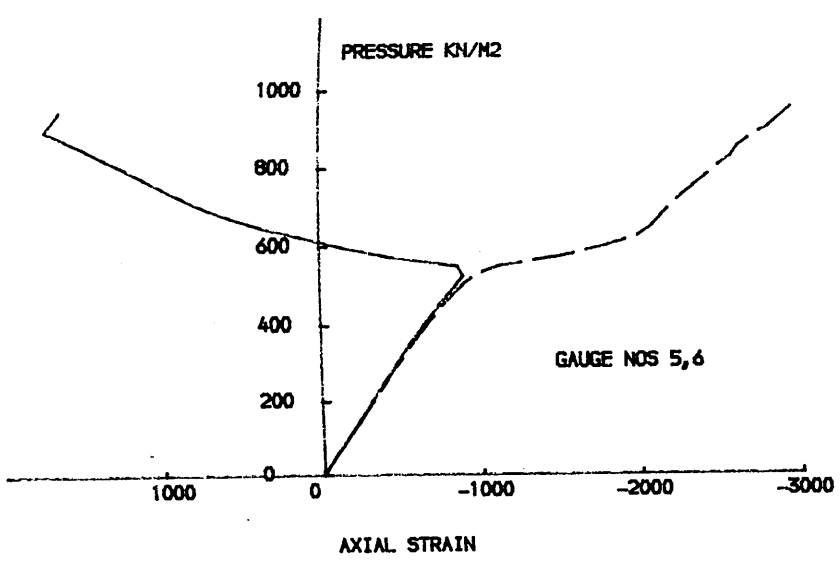

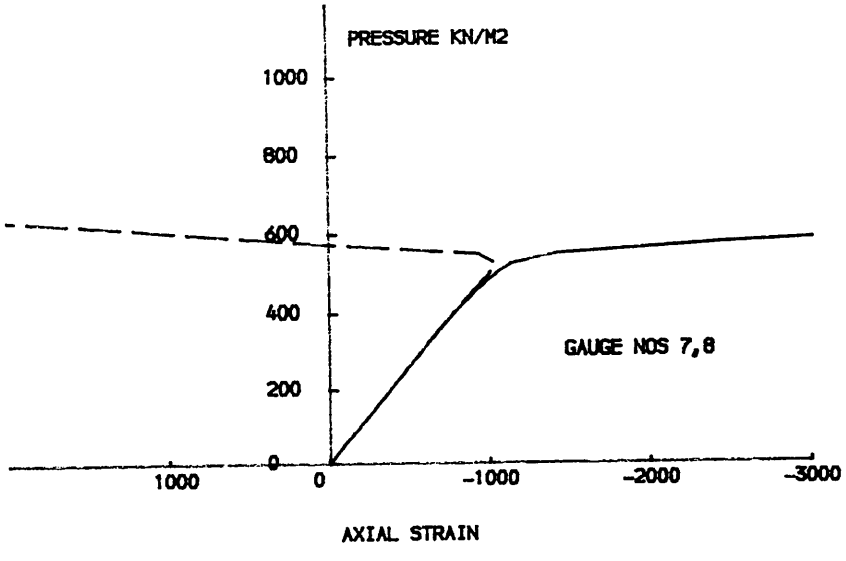

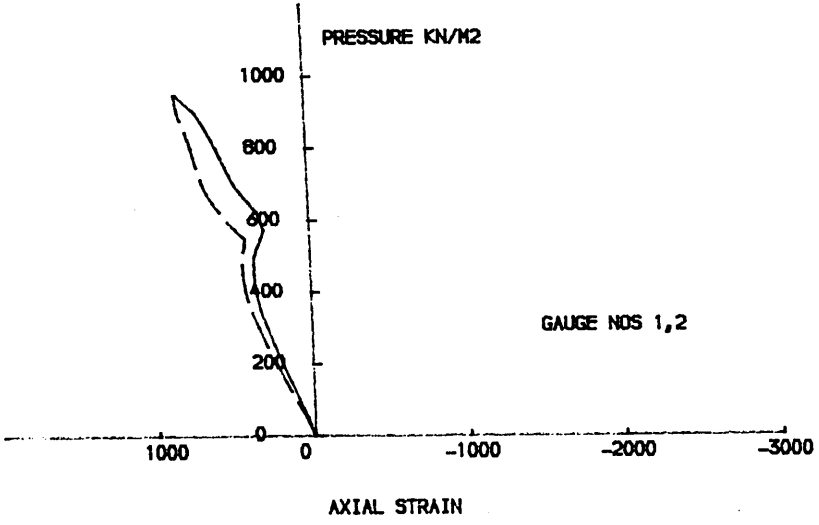

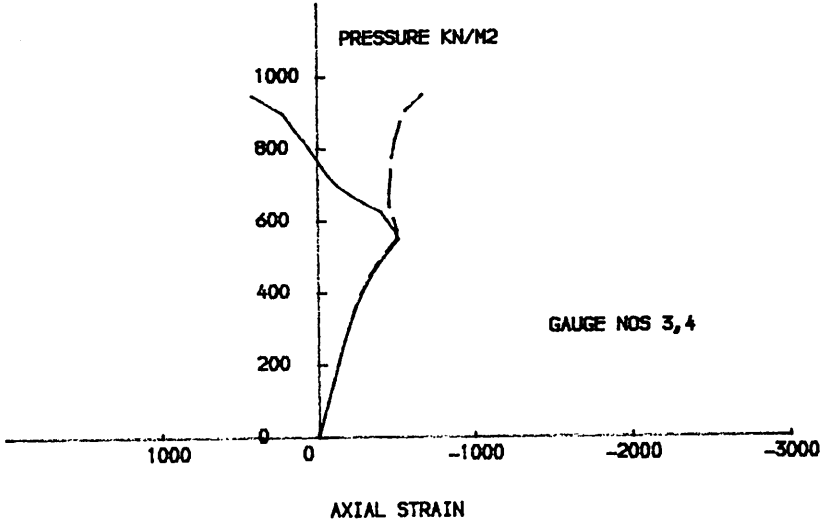

FIG. 4.38(A) MODEL NO. 4 - LOCAL STIFFENER TIP STRAINS

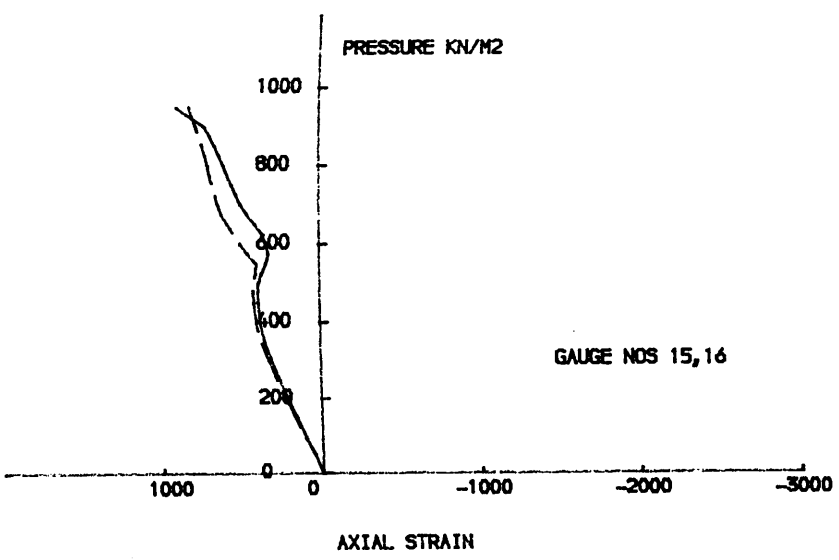

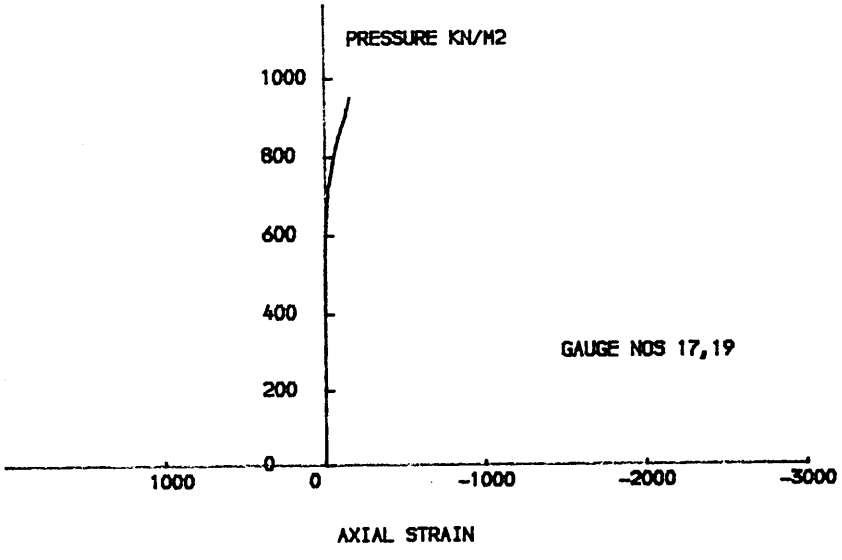

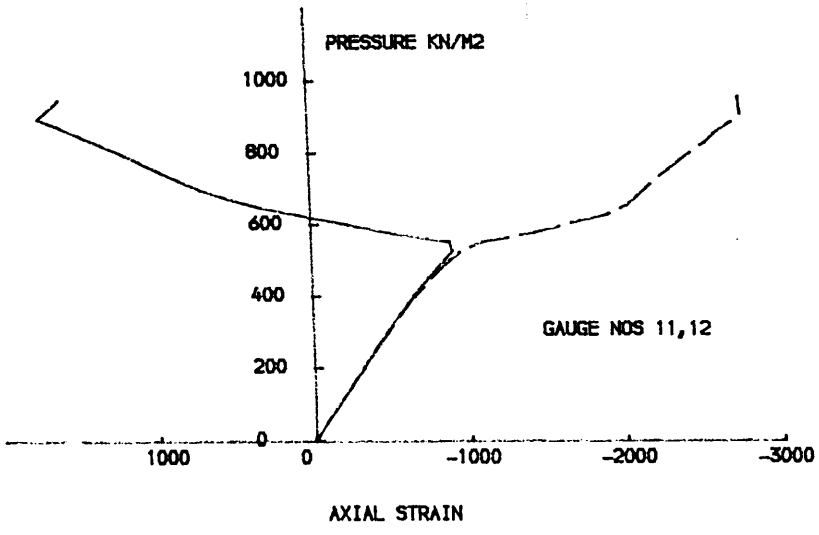

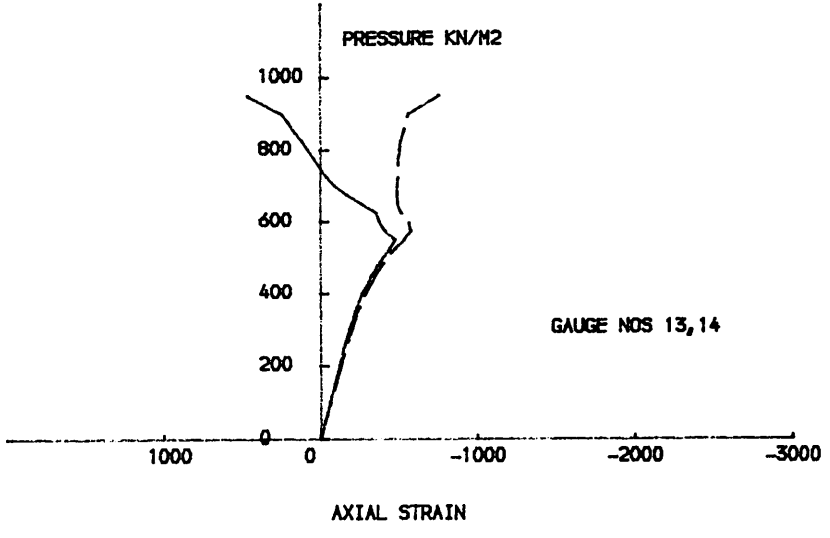

FIG. 4.38(B) MODEL NO. 4 - LOCAL STIFFENER TIP STRAINS

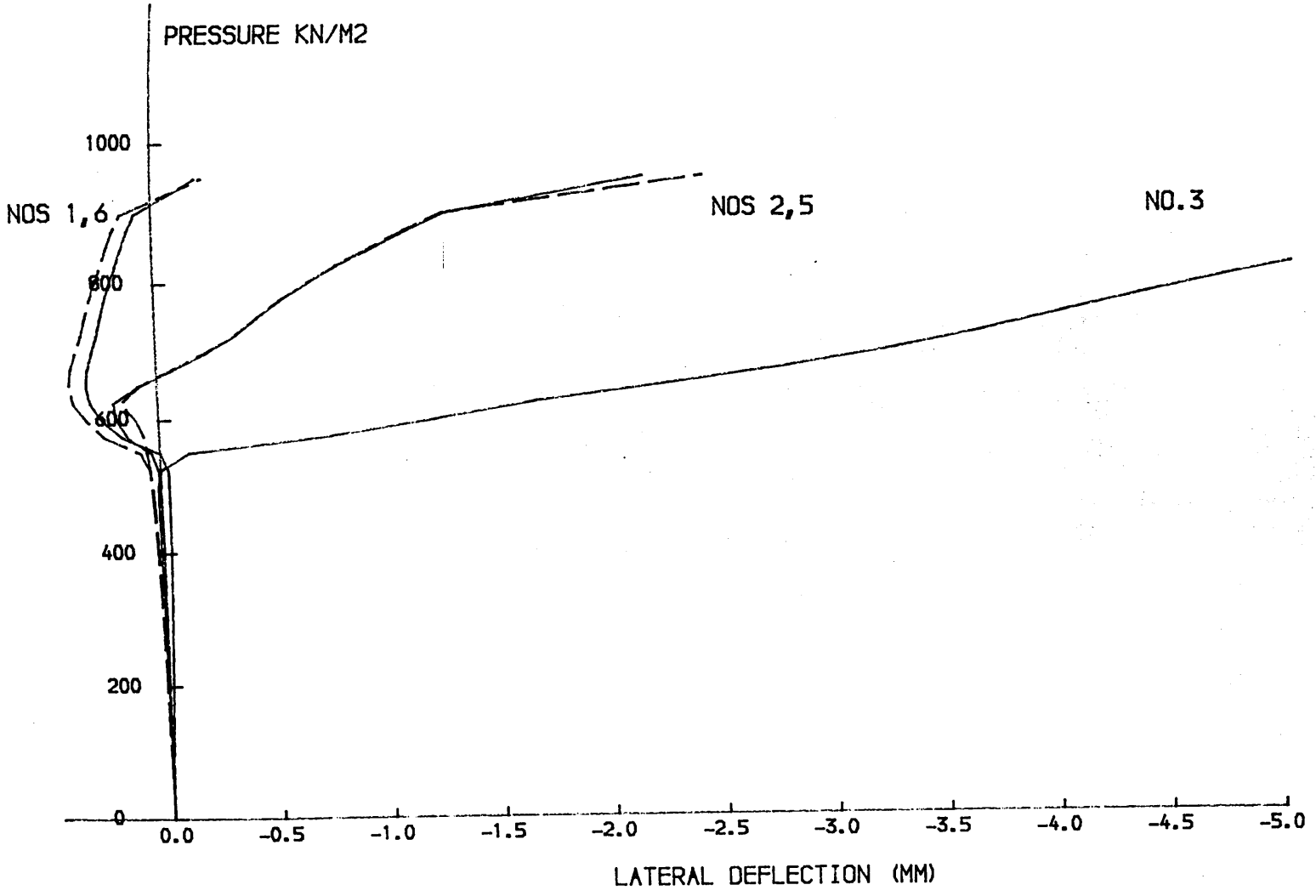

FIG. 4.39 MODEL NO.4 STIFFENER TIP LATERAL DEFLECTIONS

EDGES AB, CD ARE WELDED TO THE BOX
EDGE BC IS WELDED TO THE BASE PLATE
EDGE AD IS FREE

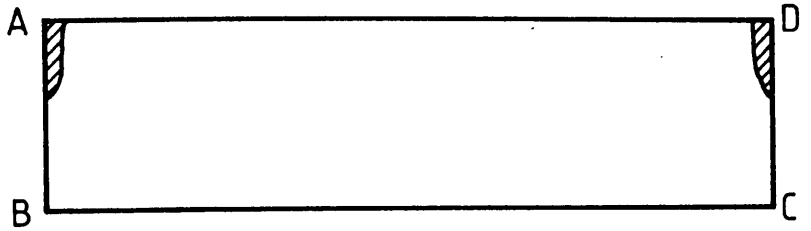

(a) PREBUCKLING RANGE (250 kN/m^2)

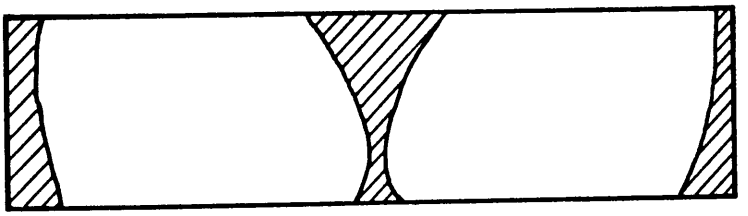

(b) STIFFENER POSTBUCKLING RANGE (600 kN/m^2)

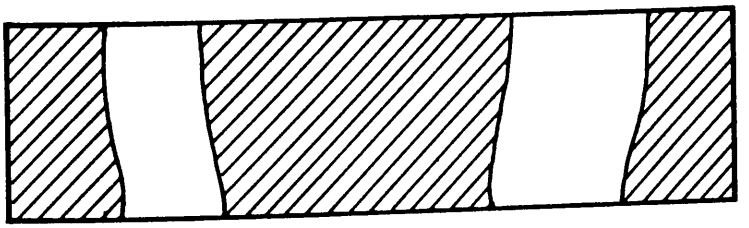

(c) POST PLATE FAILURE (850 kN/m^2)

Fig. 4·40 CORRELATION STUDY MODEL No. 4 GROWTH OF PLASTICITY IN STIFFENER AT VARIOUS STAGES OF LOADING

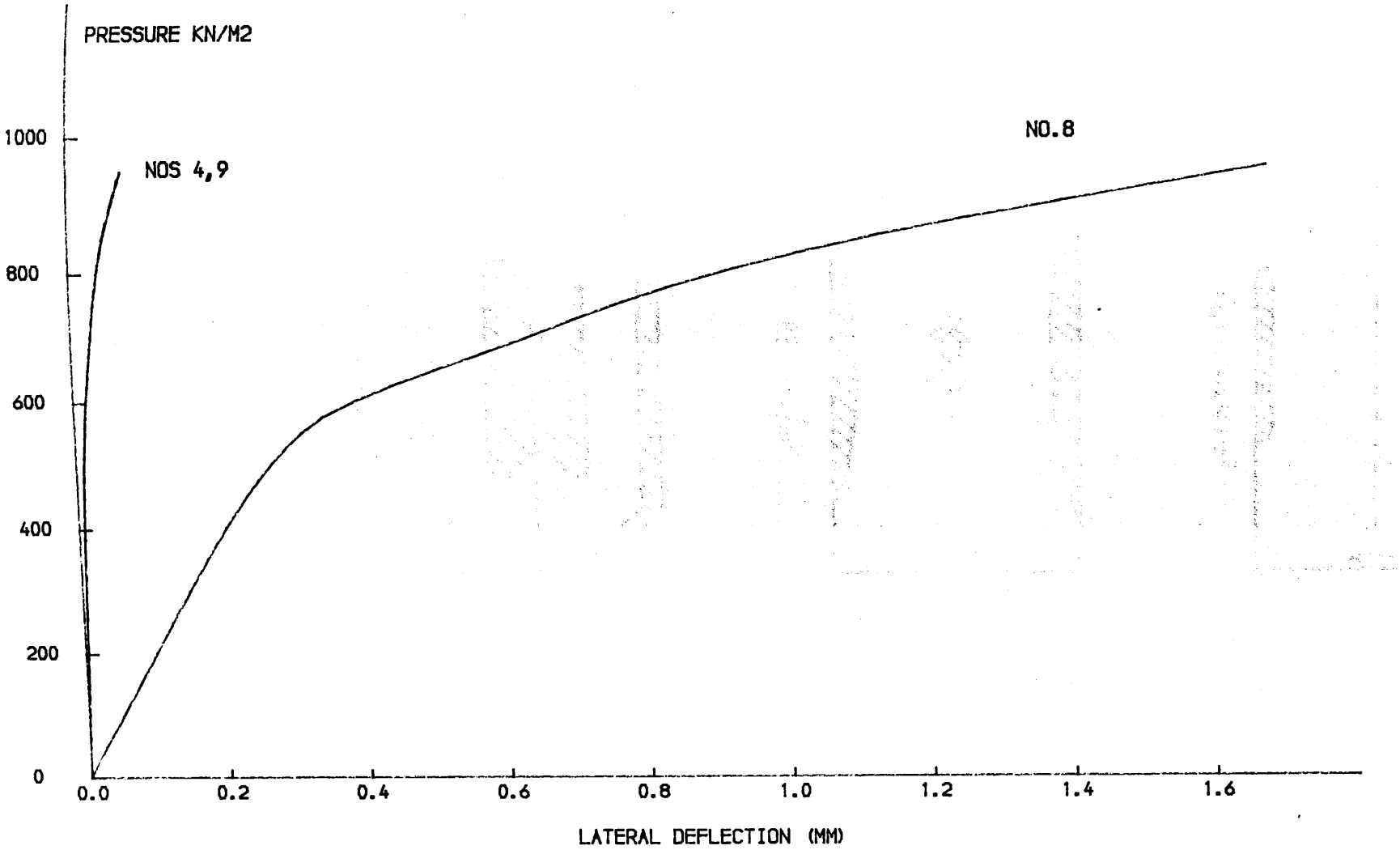

FIG. 4.41 MODEL NO.4 BASE PLATE OUT-OF-PLANE DEFLECTIONS

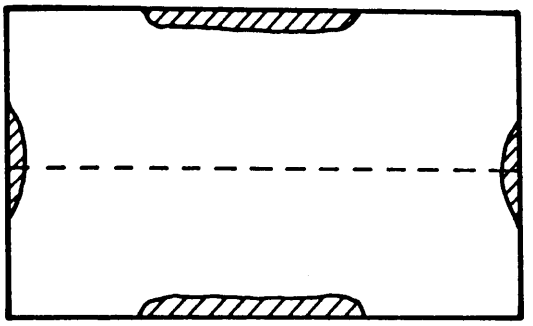

(a) 600kN/m^2

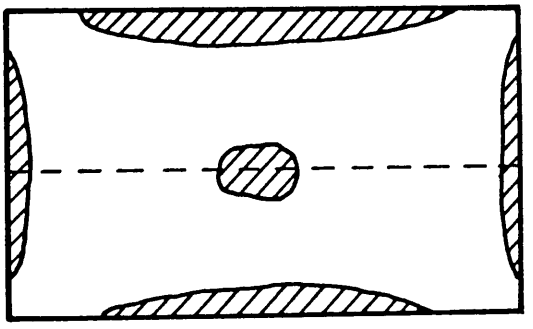

(b) 850 kN/m^2

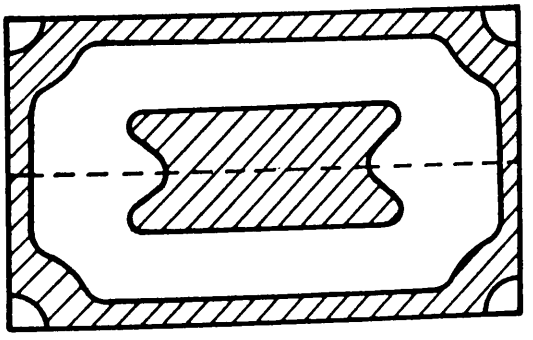

(c) 1000 kN/m^2

Fig.4·42 CORRELATION STUDY — MODEL No. 4
GROWTH OF PLASTICITY IN BASE PLATE AT
VARIOUS STAGES OF LOADING

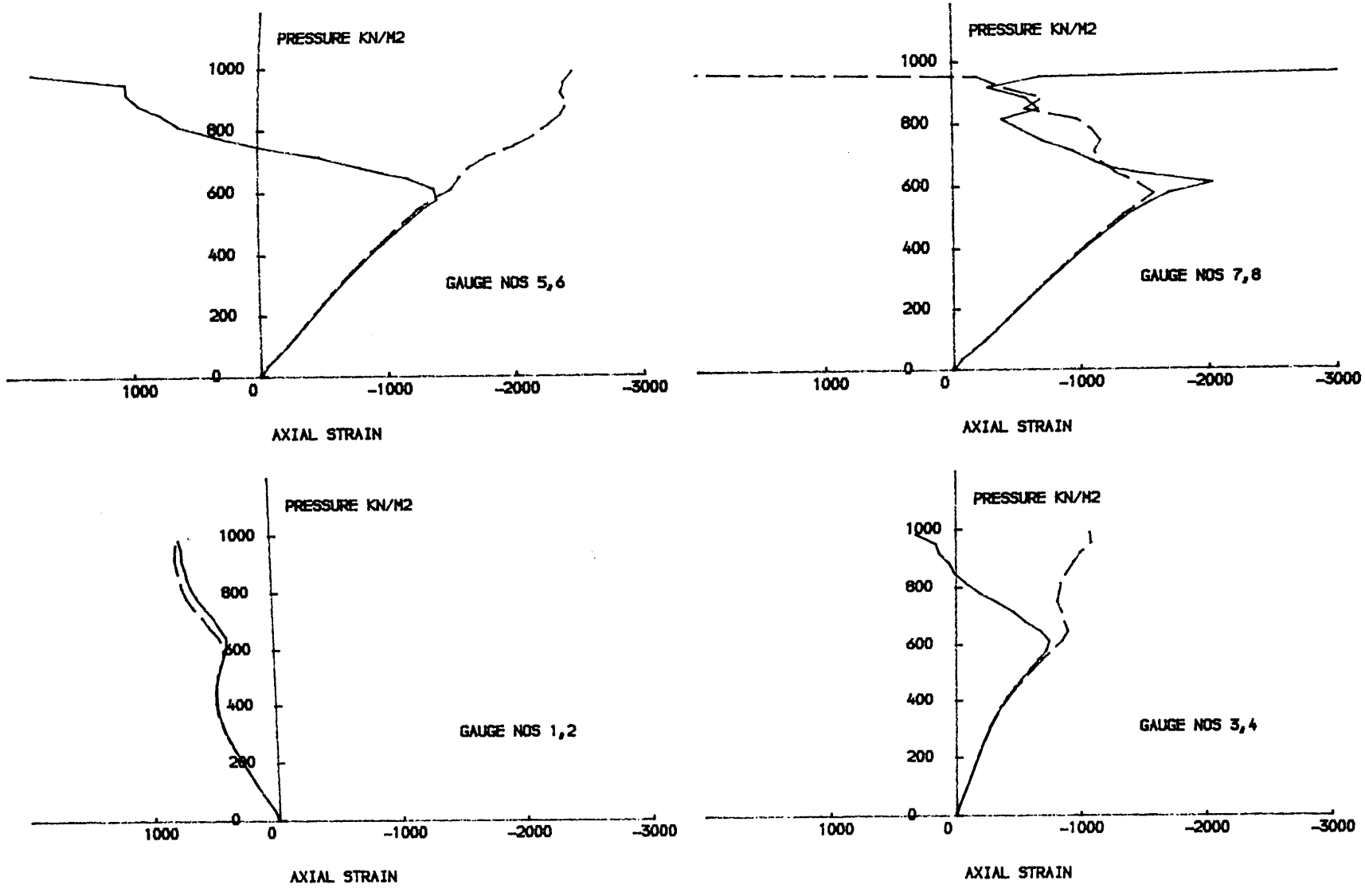

FIG. 4.43(A) MODEL NO. 6 - LOCAL STIFFENER TIP STRAINS

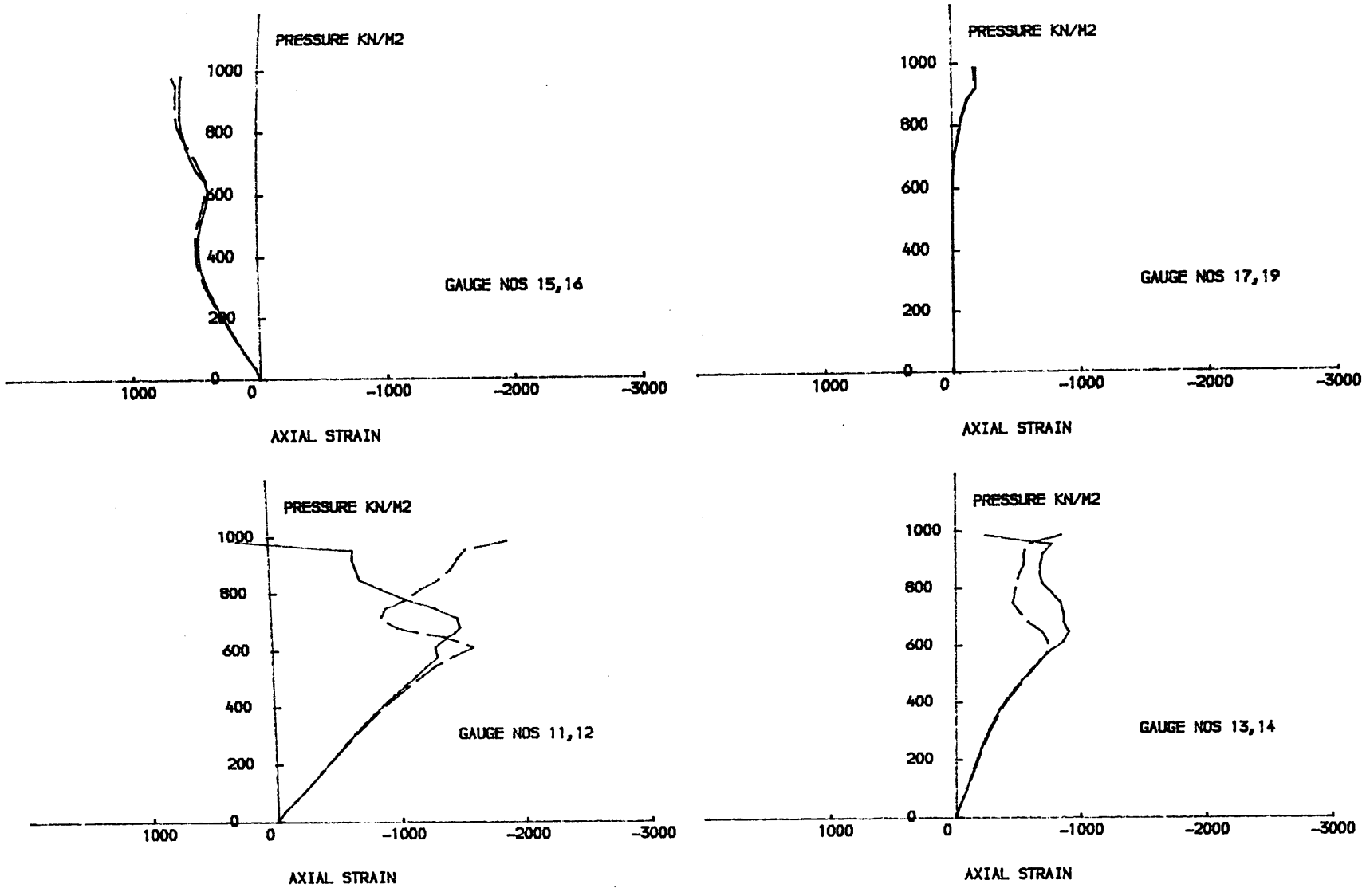

FIG. 4.43(B) MODEL NO. 6 - LOCAL STIFFENER TIP STRAINS

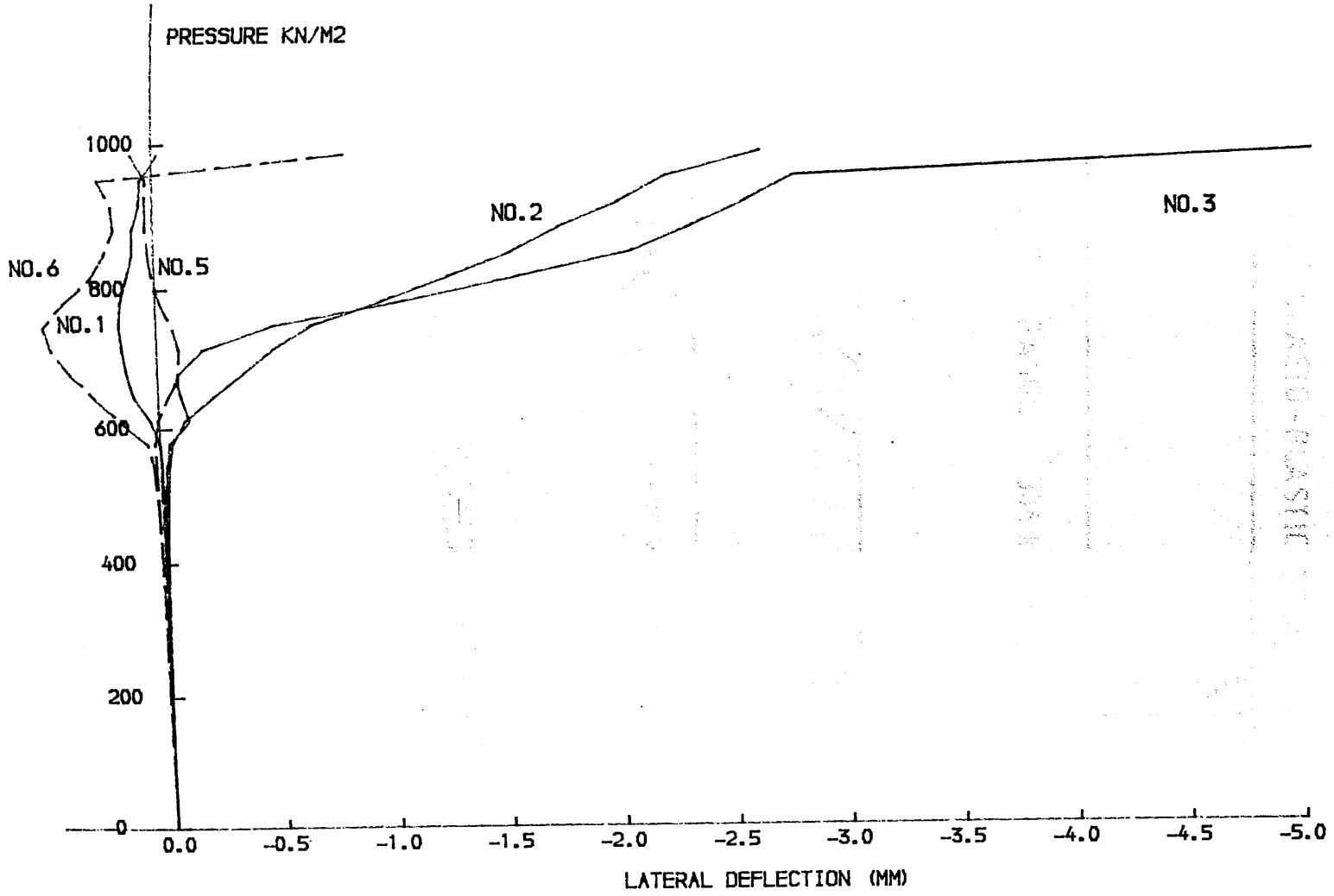

FIG. 4.44 MODEL NO.6 STIFFENER TIP LATERAL DEFLECTIONS

EDGES AB, CD WELDED TO THE BOX

EDGE BC IS WELDED TO THE BASE PLATE

EDGE AD IS FREE

/// INDICATES ELASTO-PLASTIC REGIONS

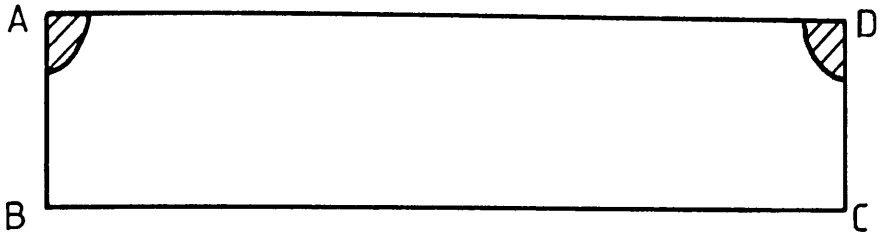

(a) PREBUCKLING RANGE (306 kN/m^2)

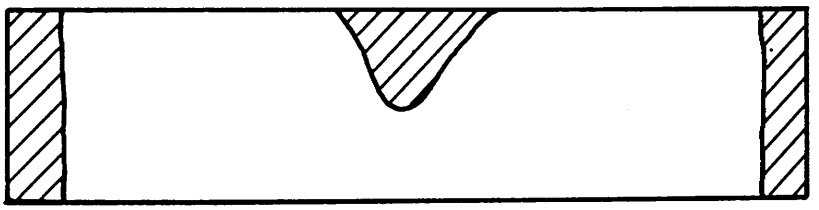

(b) BUCKLING (620 kN/m^2)

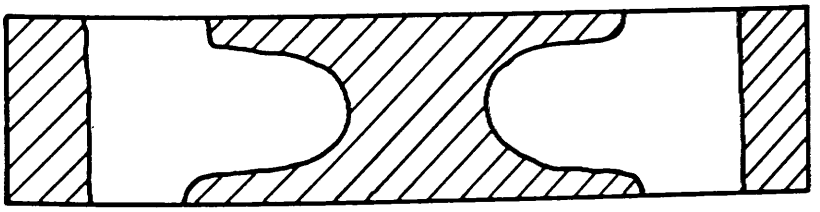

(c) POSTBUCKLING RANGE (750 kN/m^2)

Fig. 4·45 CORRELATION STUDY — MODEL Nº 6 GROWTH OF PLASTICITY IN STIFFENER AT VARIOUS STAGES OF LOADING

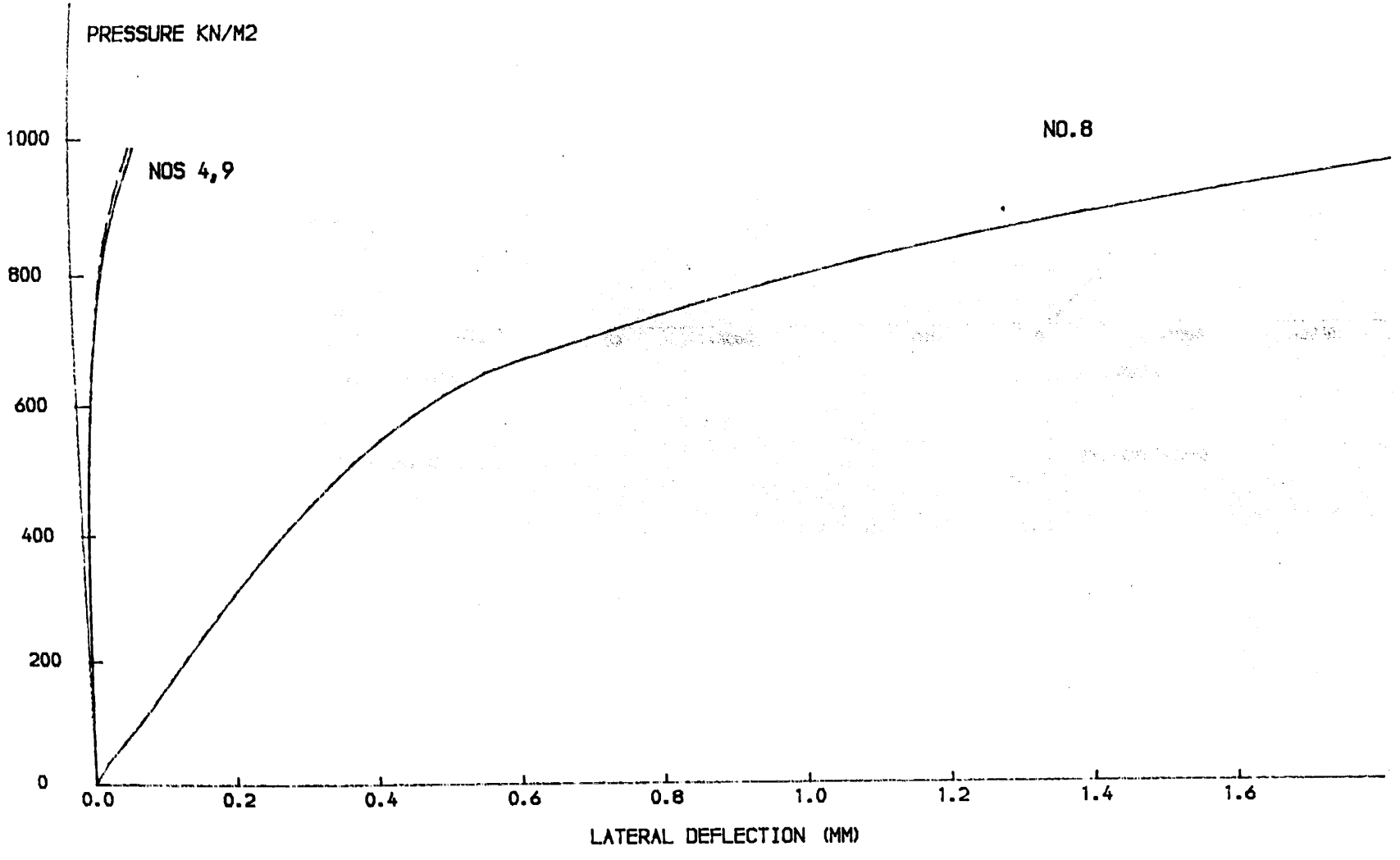

FIG. 4.46 MODEL NO.6 BASE PLATE OUT-OF-PLANE DEFLECTIONS

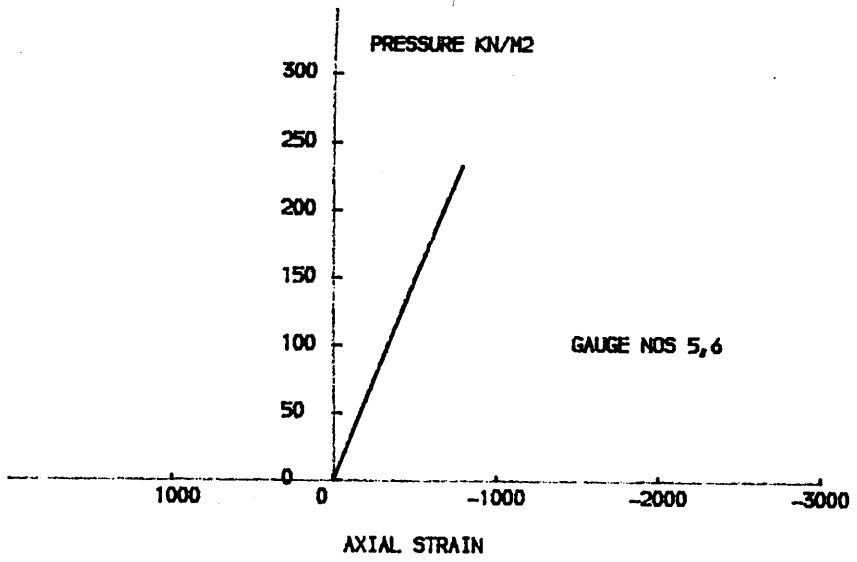

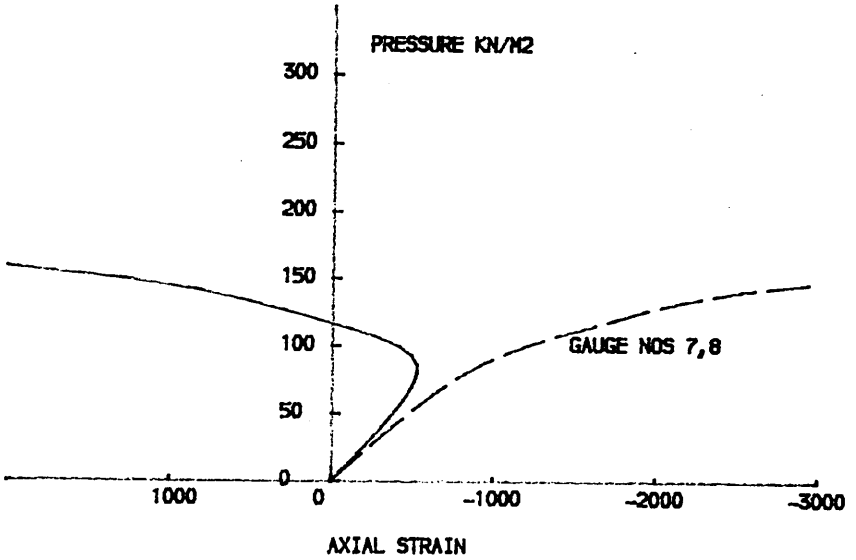

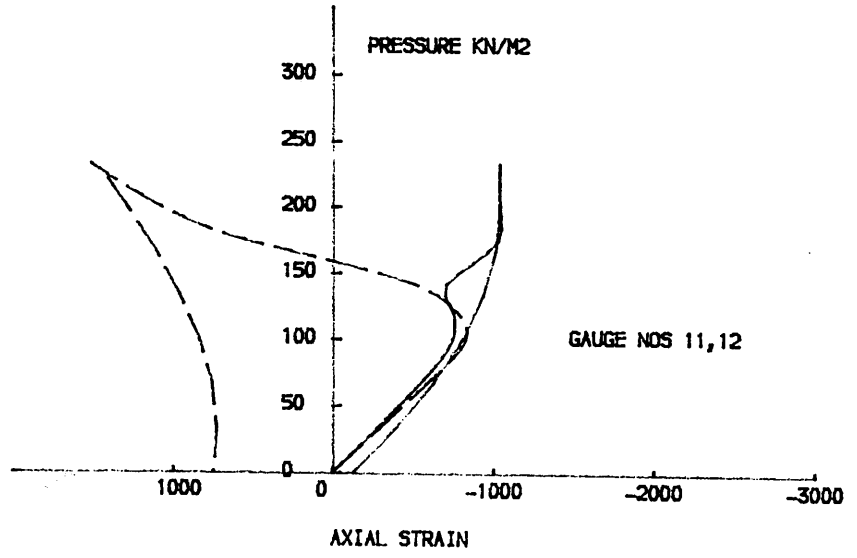

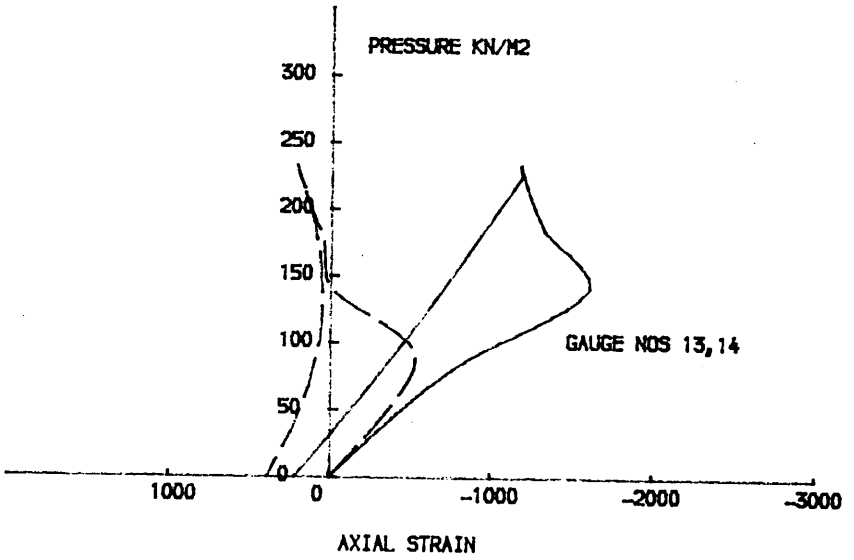

FIG. 4.47 MODEL NO. 3 - LOCAL STIFFENER TIP STRAINS

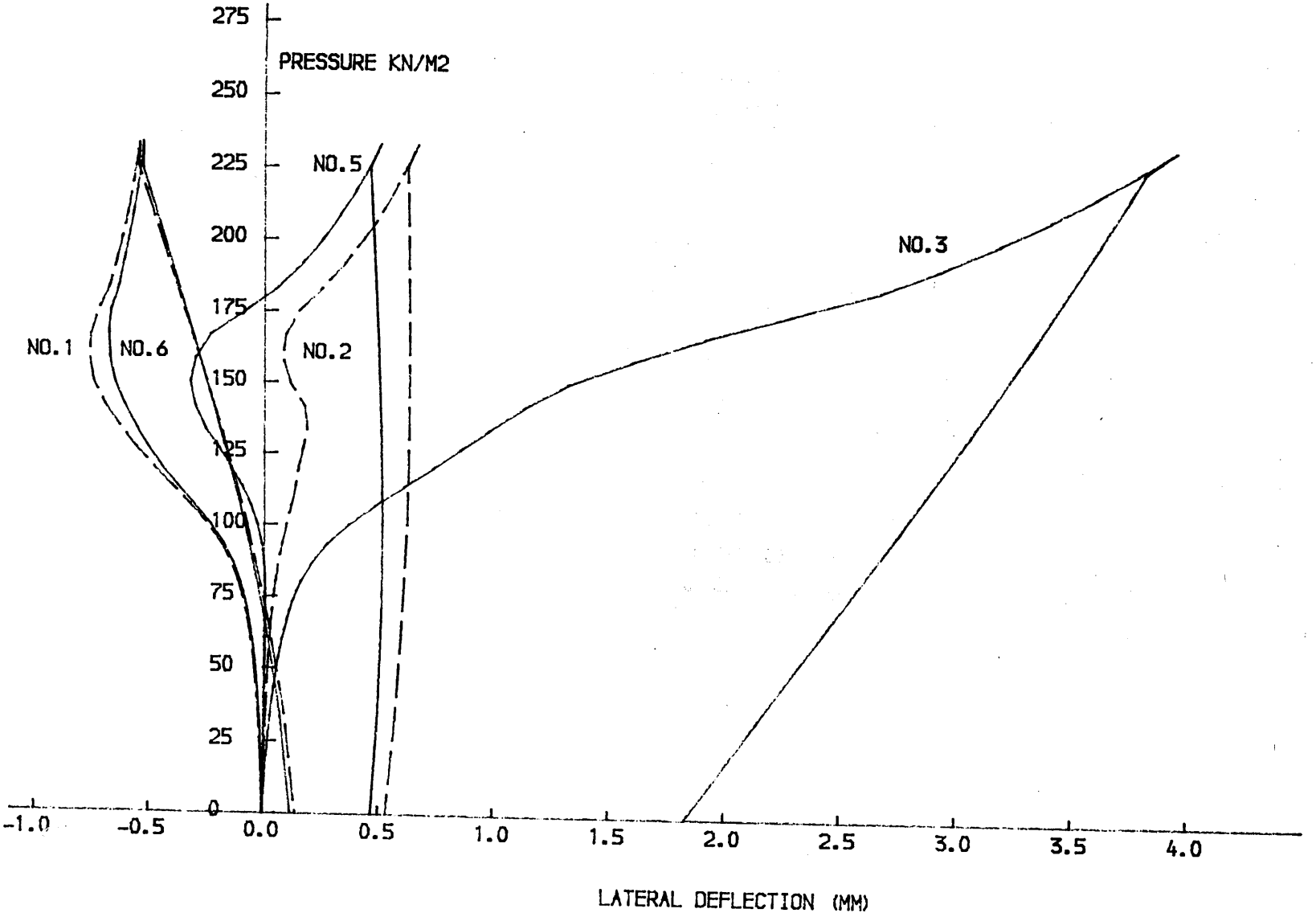

FIG. 4.48 MODEL NO.3 STIFFENER TIP LATERAL DEFLECTIONS

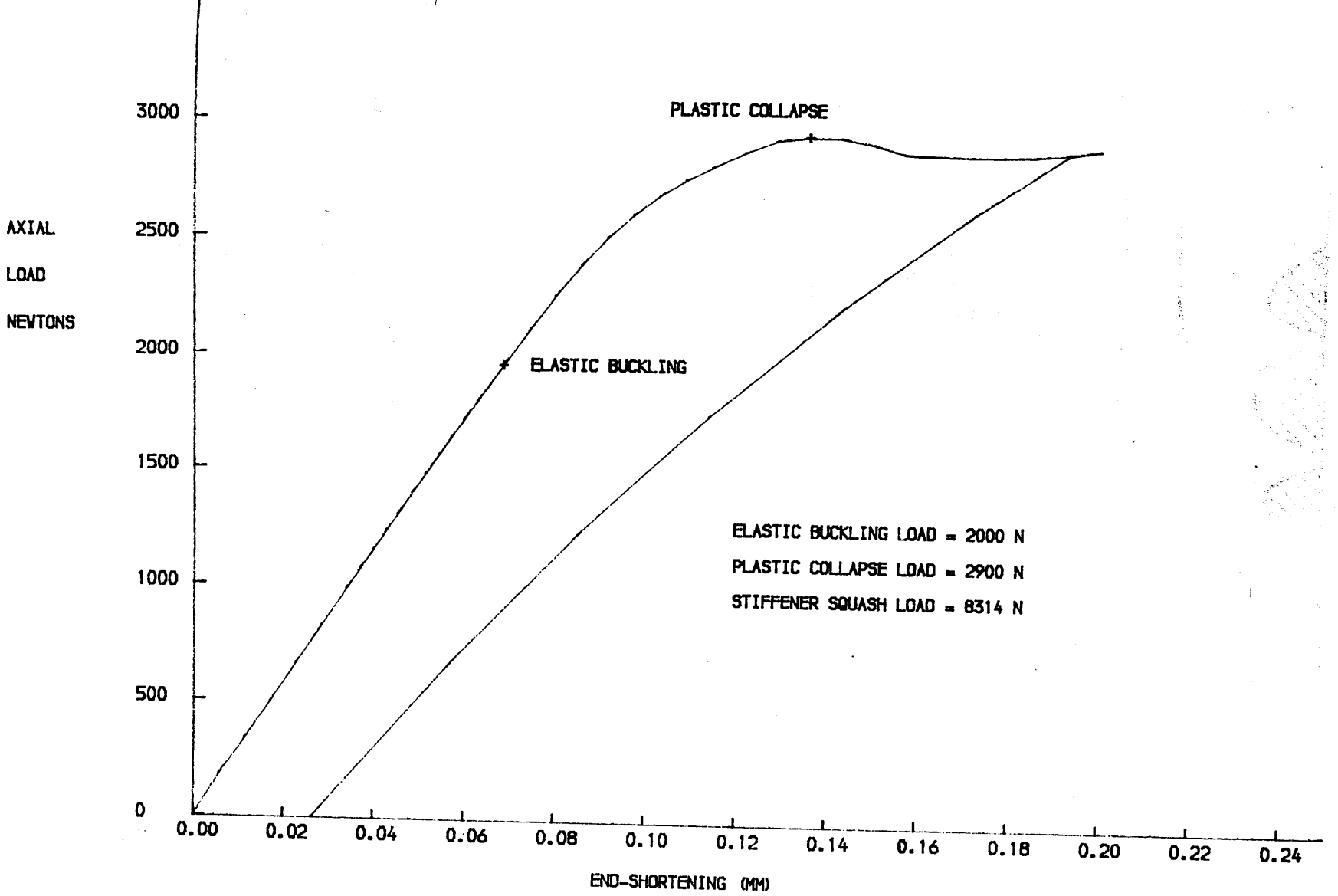

FIG. 4.49 MODEL NO.3 - STIFFENER LOAD END-SHORTENING CURVE

EDGES AB, CD ARE WELDED TO THE BOX
EDGE BC IS WELDED TO BASE PLATE
EDGE AD IS FREE

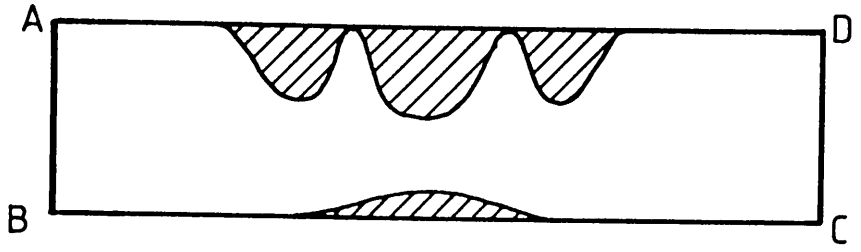

(a) INITIATION OF PLASTICITY ($126\,kN/m^2$ - $317\,kN$)

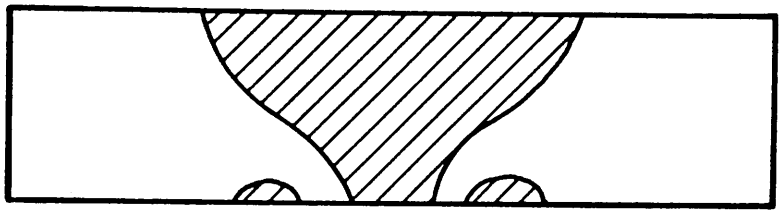

(b) PEAK LOAD ($233\,kN/m^2$ - $581\,kN$)

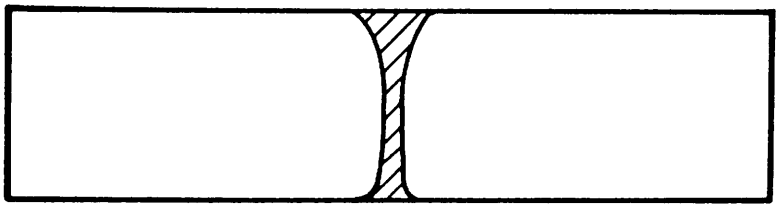

(c) RESIDUAL DISTRIBUTION FOLLOWING UNLOADING

Fig. 4·50 CORRELATION STUDY – MODEL No. 3
GROWTH OF PLASTICITY IN STIFFENER AT
VARIOUS STAGES OF LOADING

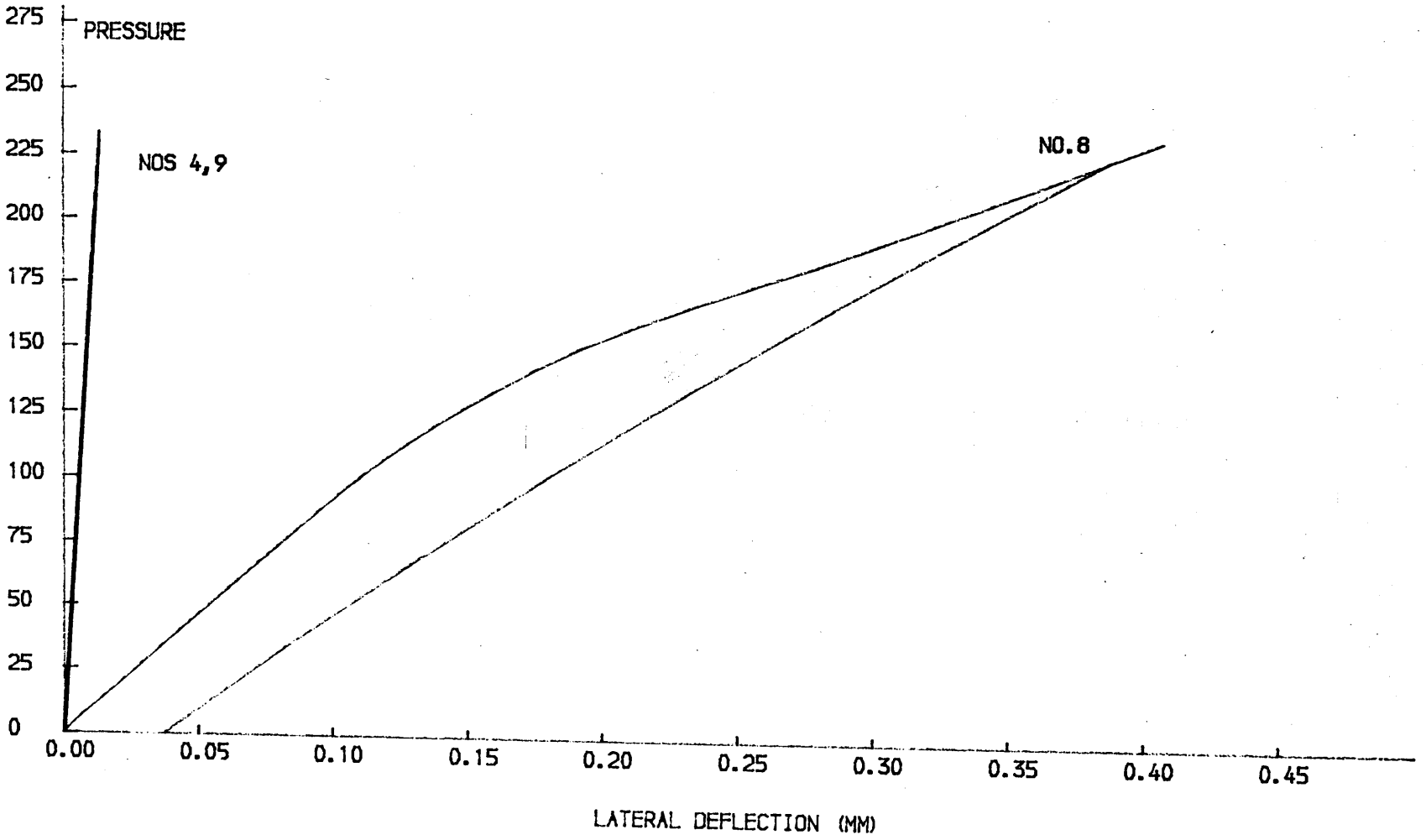

FIG. 4.51 MODEL NO.3 BASE PLATE OUT-OF-PLANE DEFLECTIONS

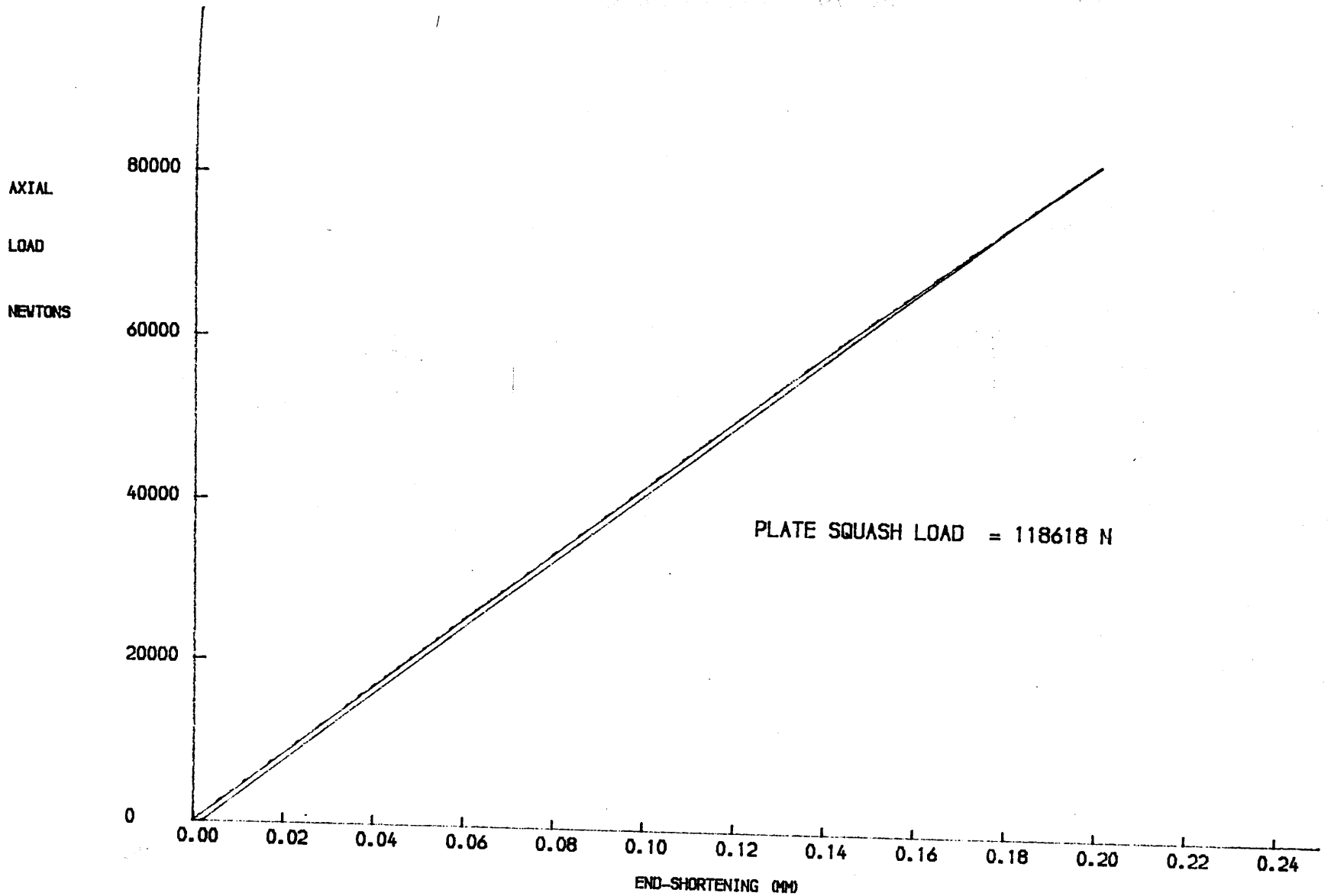

FIG. 4.52 MODEL NO.3 - BASE PLATE LOAD END-SHORTENING CURVE

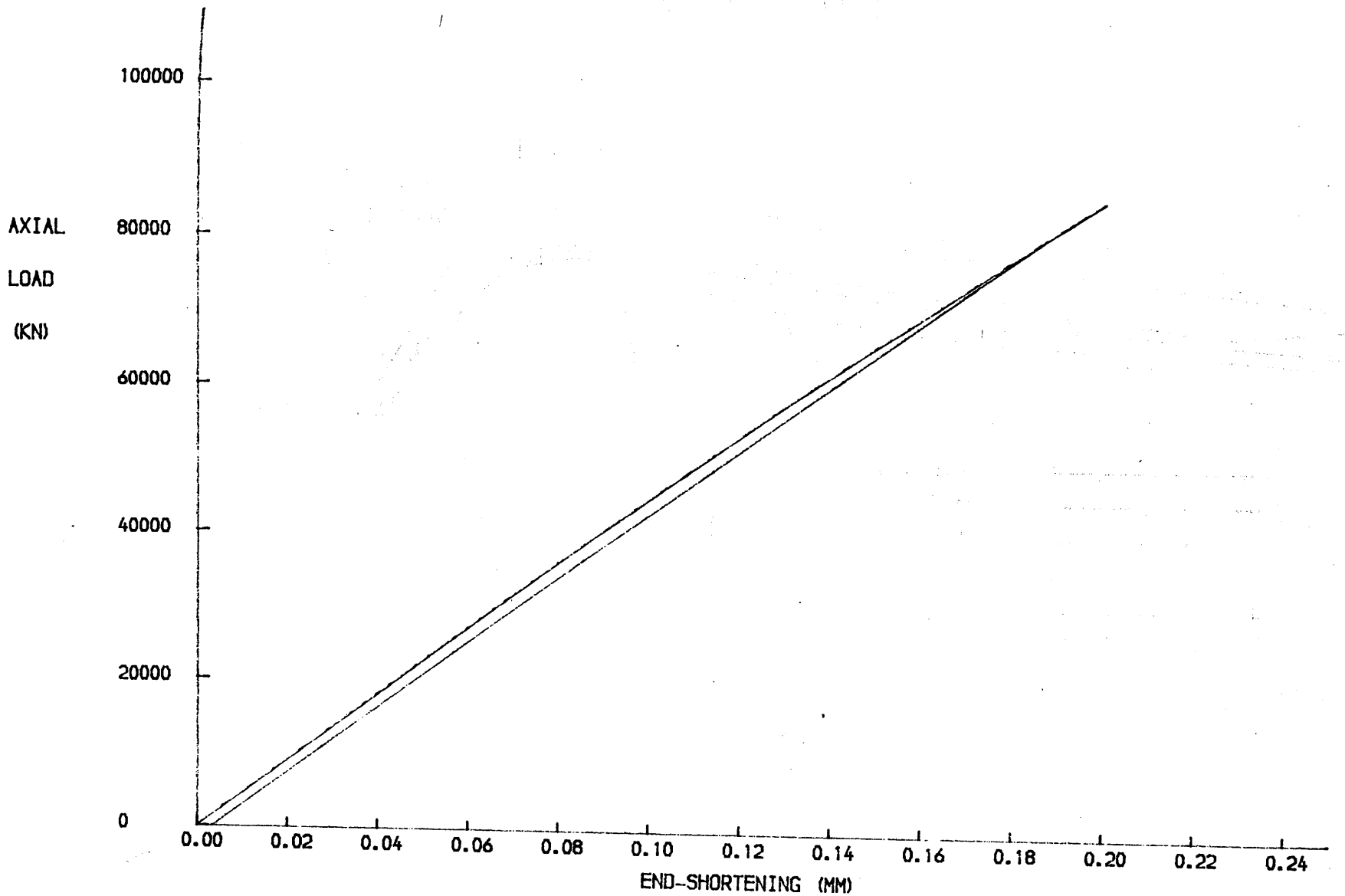

FIG. 4.53 MODEL NO.3 - STIFFENED PLATE LOAD END-SHORTENING CURVE

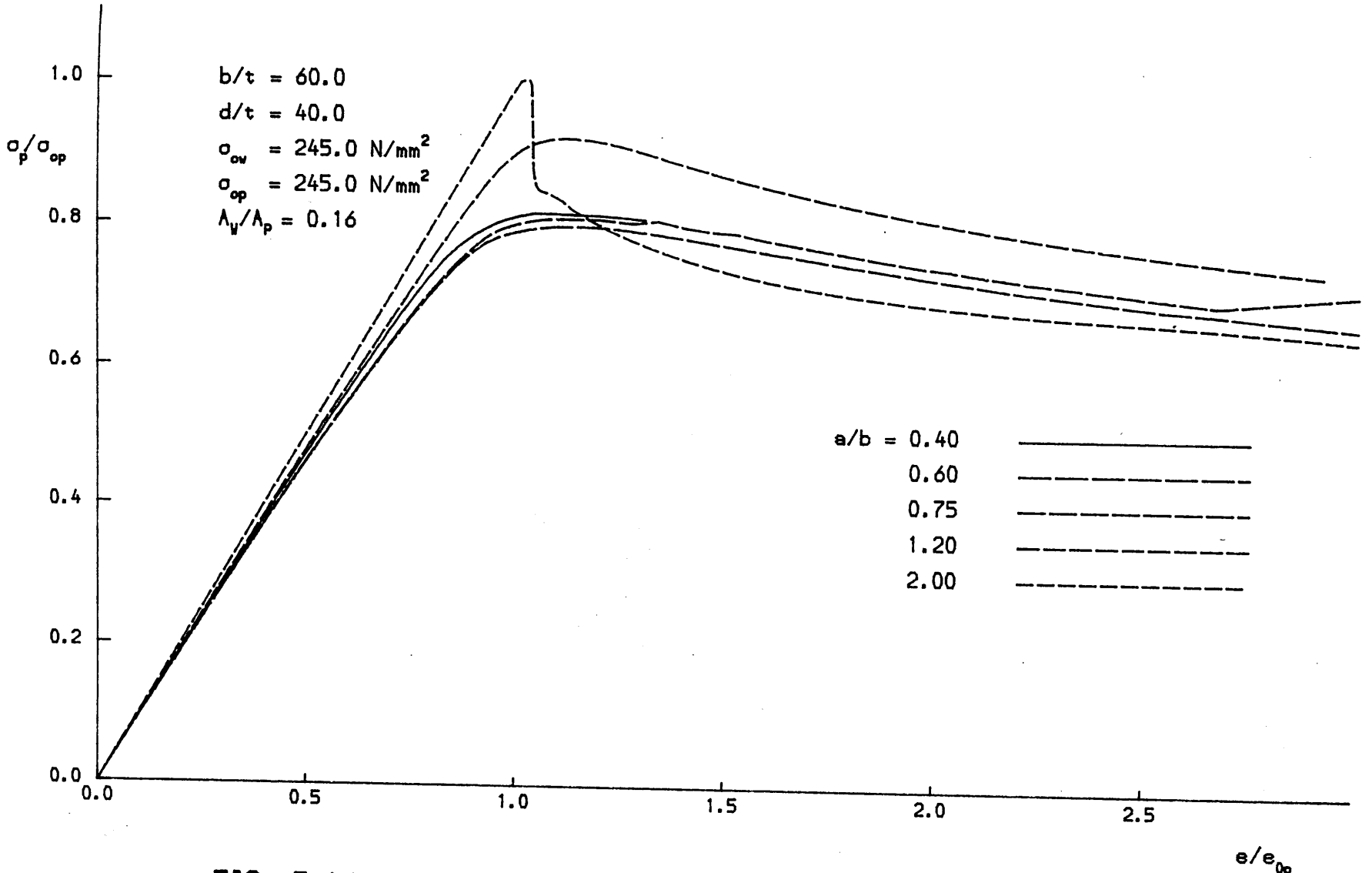

FIG. 5.1 (A) EFFECT OF ASPECT RATIO ON BASE PLATE RESPONSE

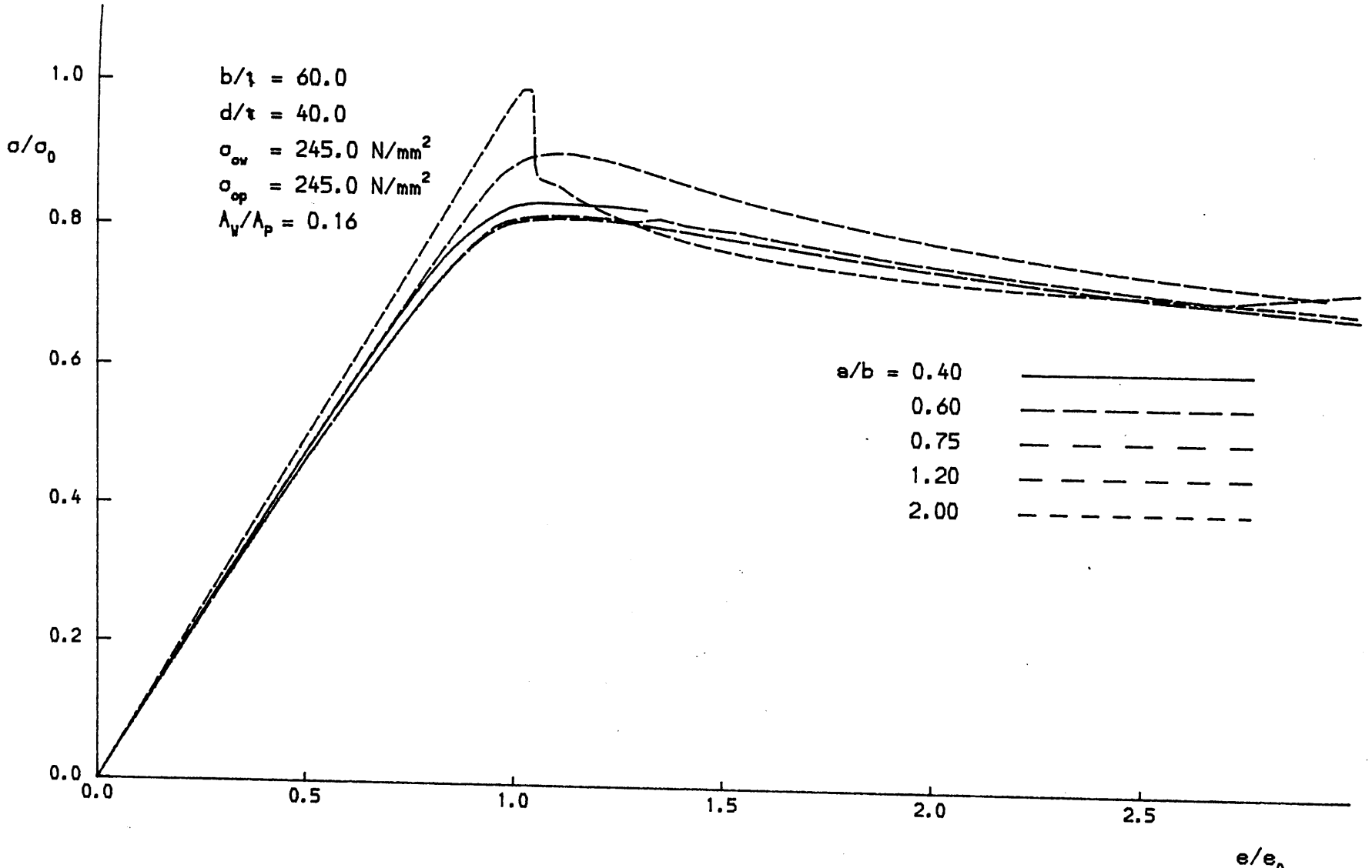

FIG. 5.1 (B) EFFECT OF ASPECT RATIO ON STIFFENED PLATE RESPONSE

$b/t_p = 6.0$ $\quad W_{op} = 0.145 \beta_p \, t_p \left(\frac{a}{b}\right)$

$d/t_w = 40$ $\quad W_{ow} = 0$

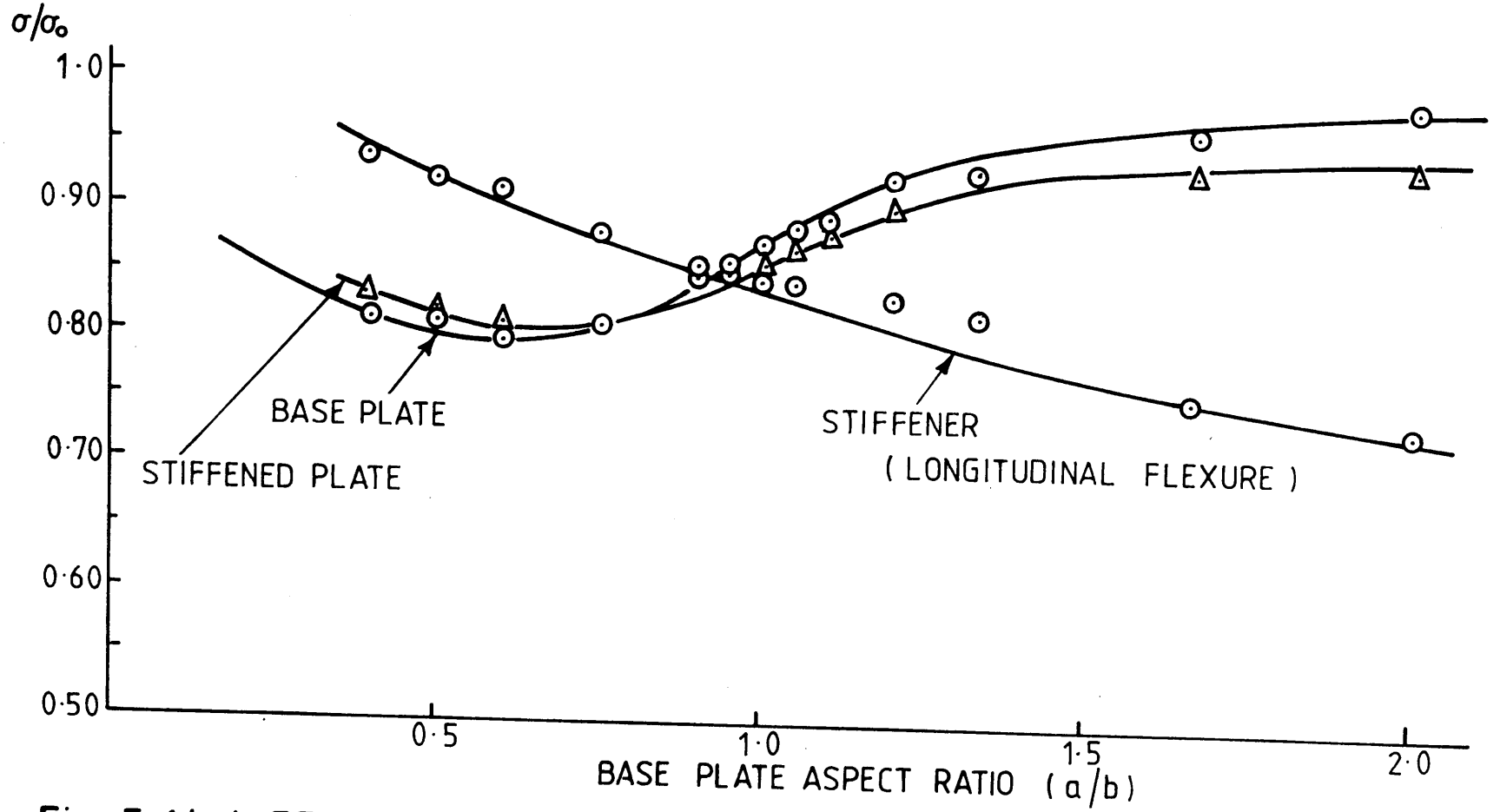

Fig. 5·1(c) EFFECT of ASPECT RATIO on ULTIMATE STRENGTH of BASE PLATE

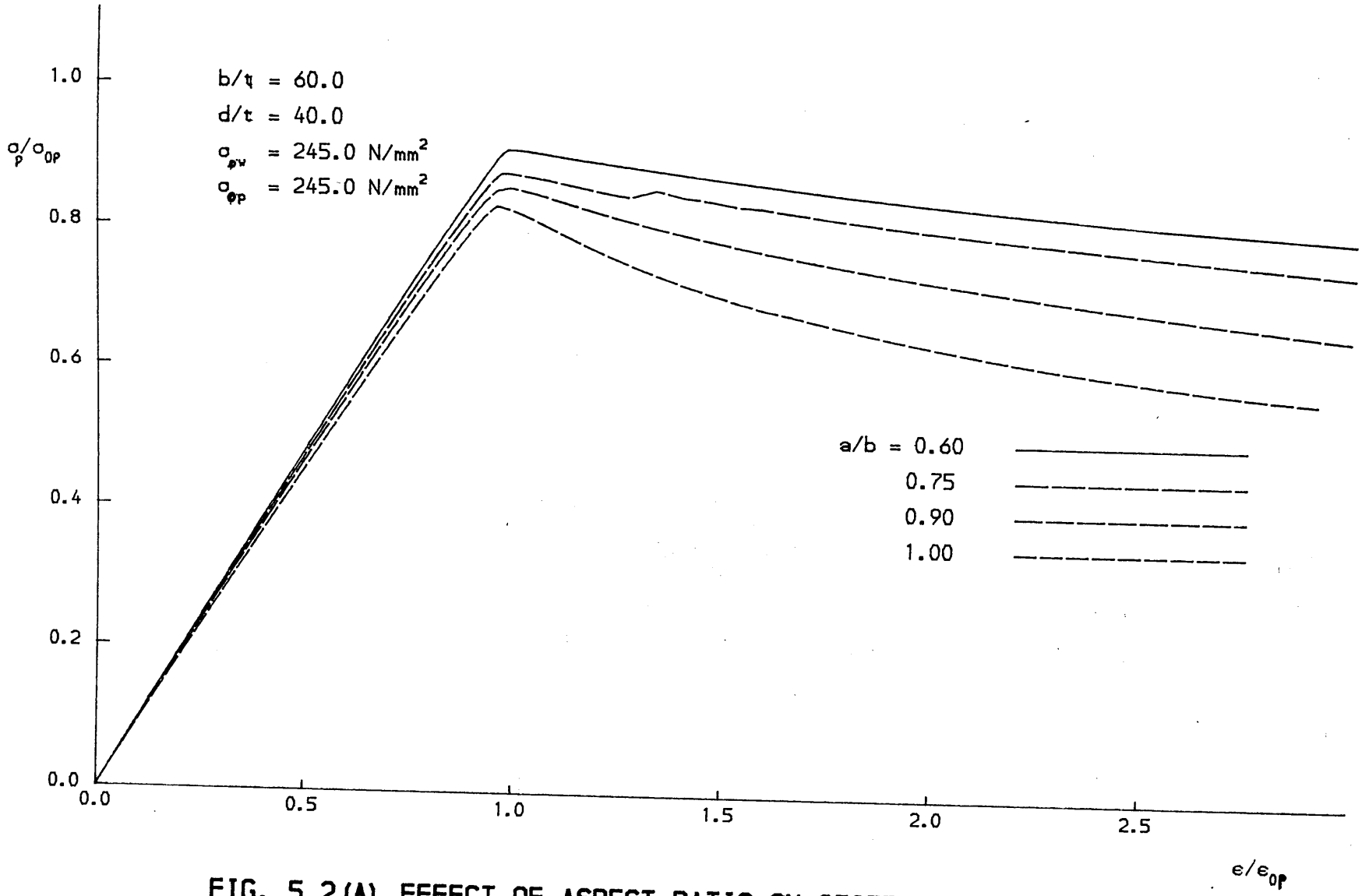

FIG. 5.2(A) EFFECT OF ASPECT RATIO ON STIFFENER RESPONSE (SHORT PLATES)

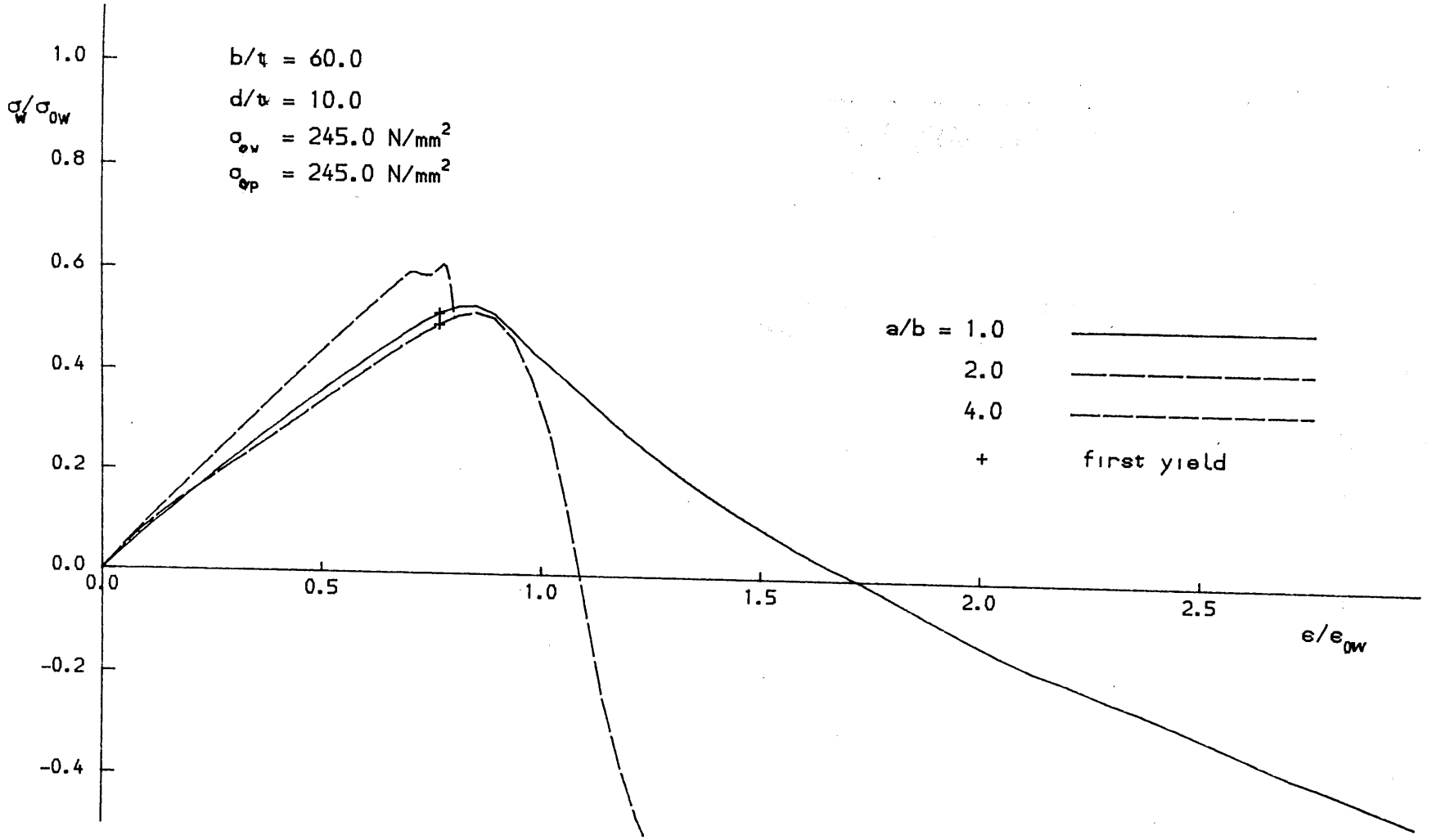

FIG. 5.2(B) EFFECT OF ASPECT RATIO ON STIFFENER RESPONSE (LONG PLATES)

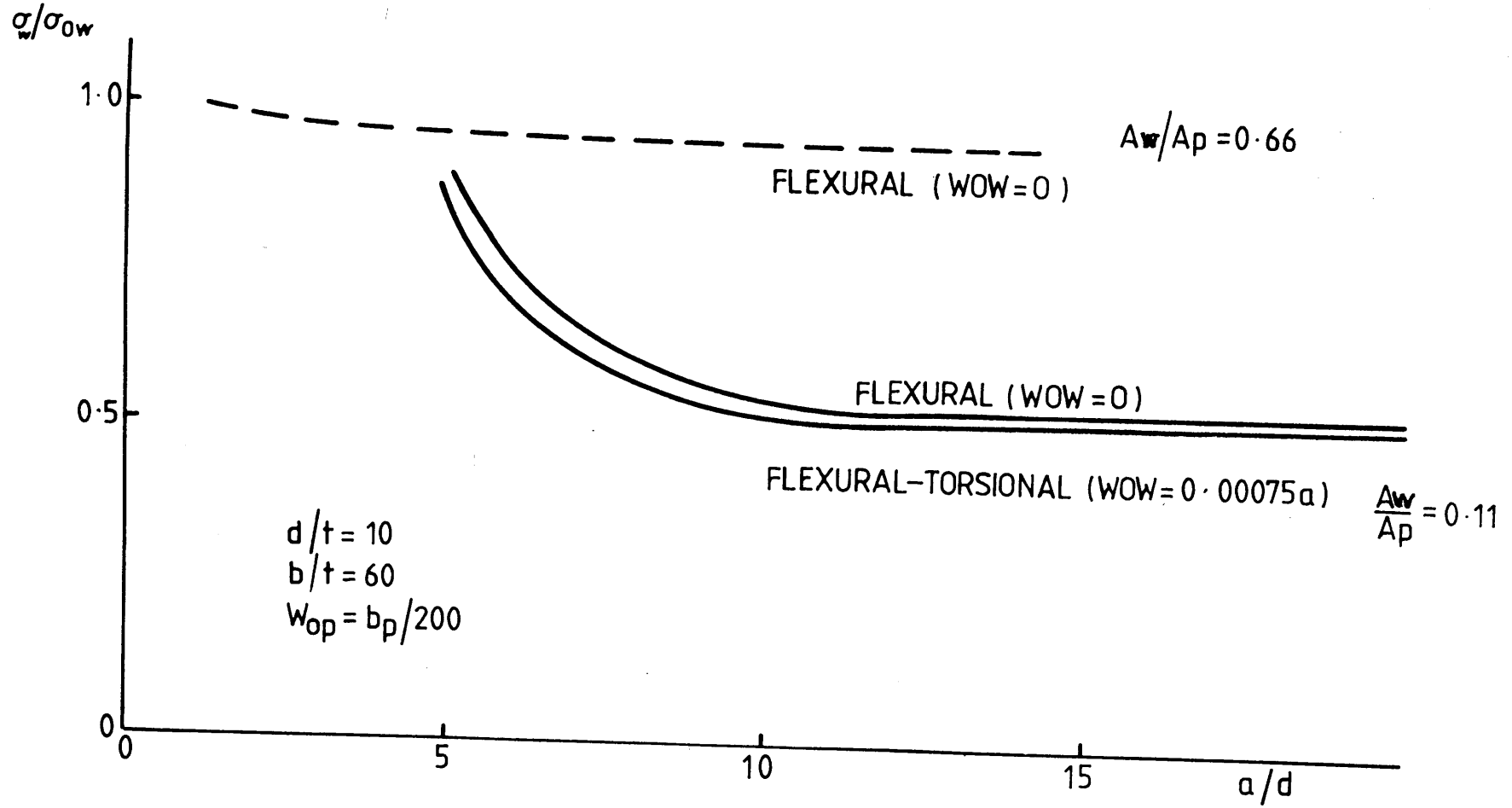

Fig. 5·2(c) EFFECT of ASPECT RATIO on ULTIMATE STRENGTH of FLATBAR STIFFENER.

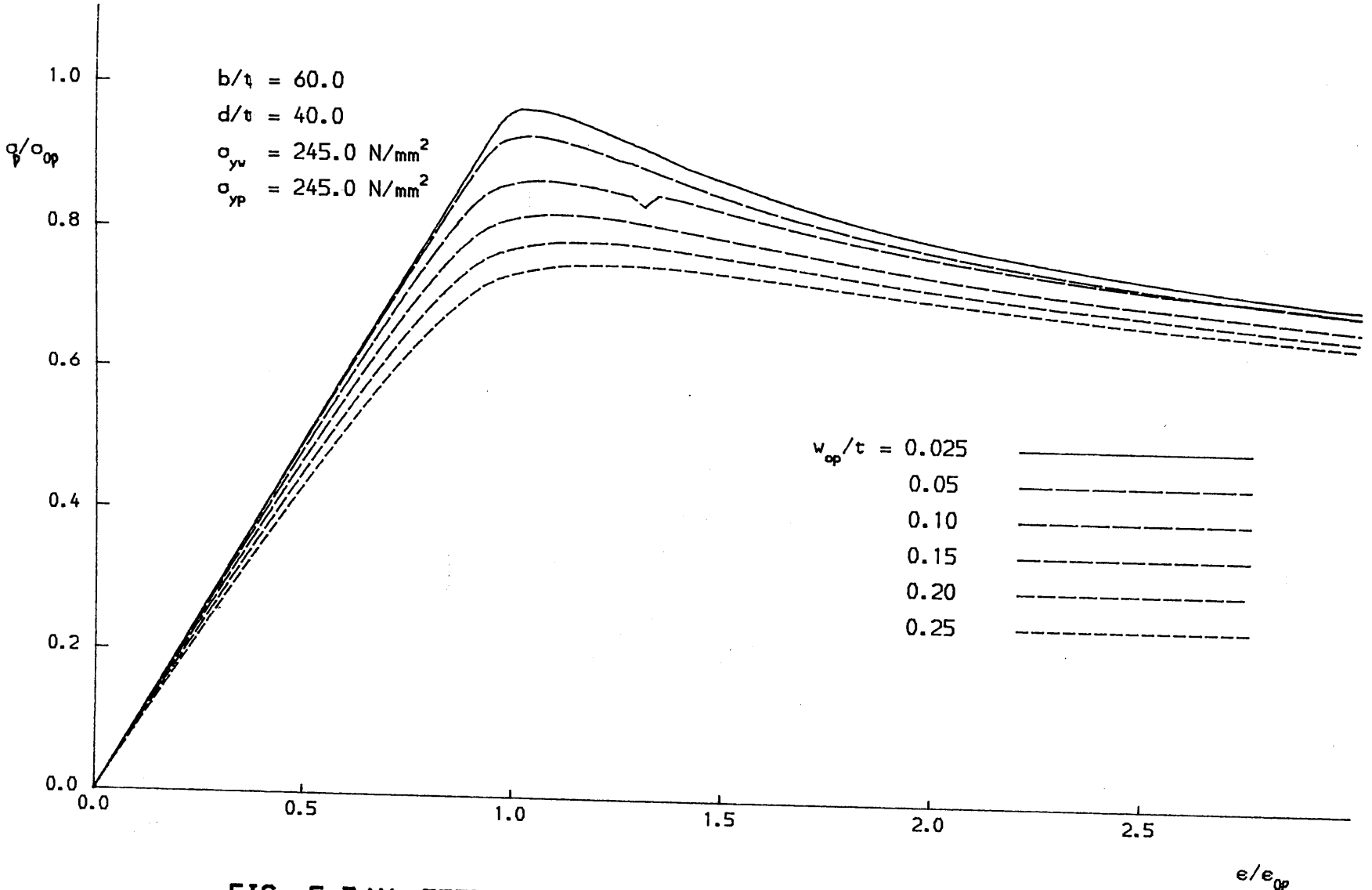

FIG. 5.3(A) EFFECT OF BASE PLATE IMPERFECTIONS ON BASE PLATE RESPONSE

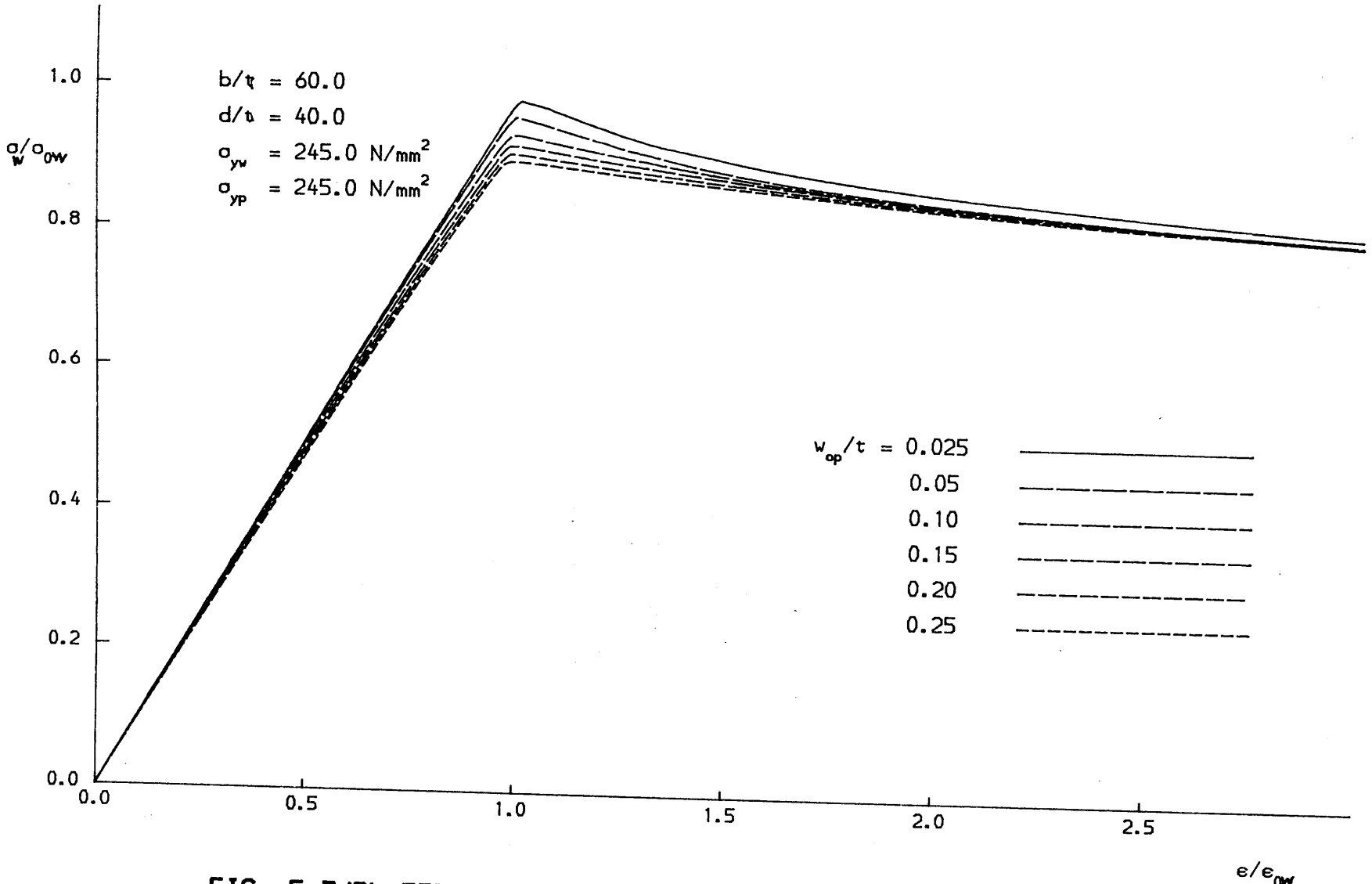

FIG. 5.3(B) EFFECT OF BASE PLATE IMPERFECTIONS ON STIFFENER RESPONSE

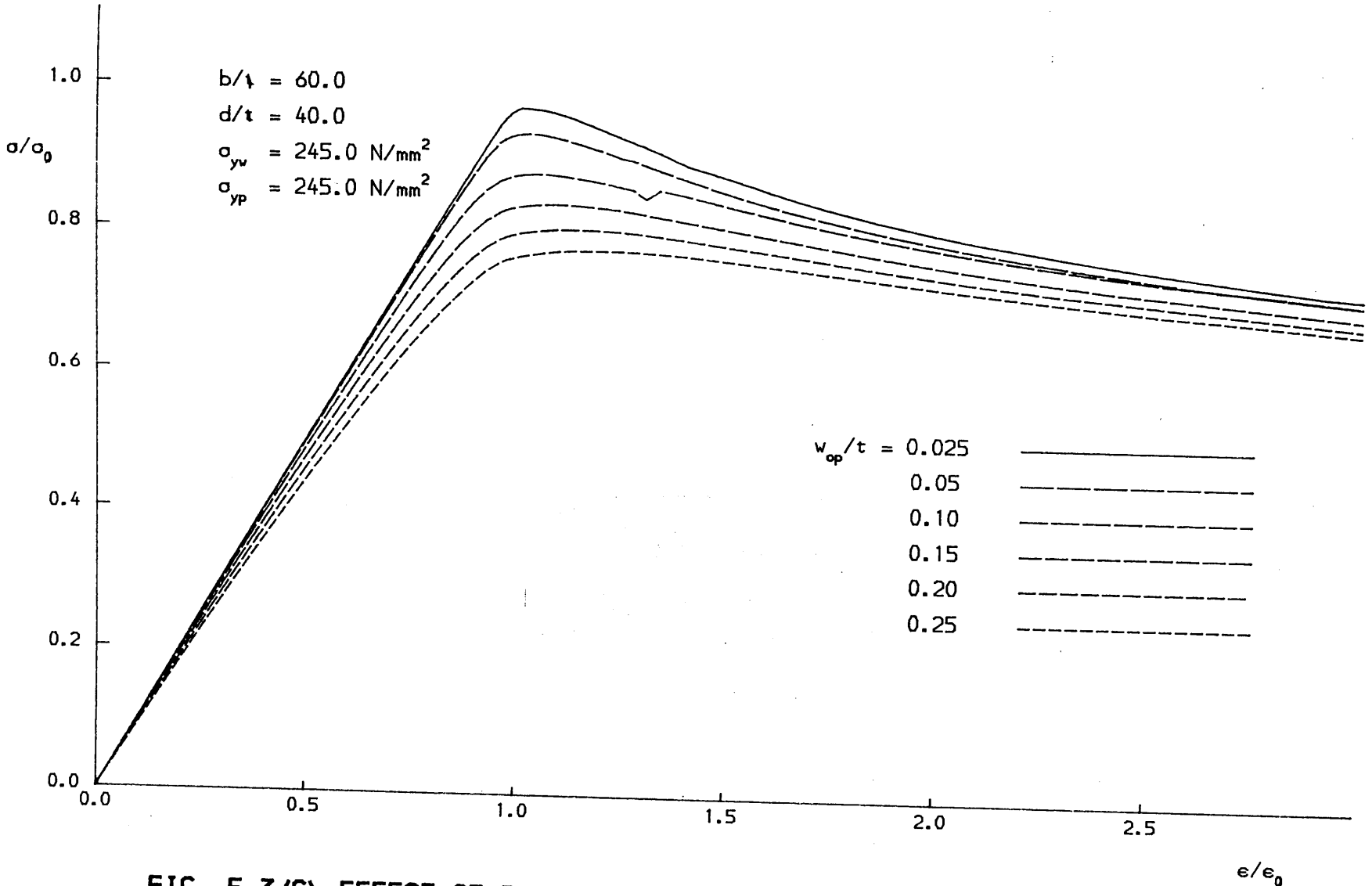

FIG. 5.3(C) EFFECT OF BASE PLATE IMPERFECTIONS ON STIFFENED PLATE RESPONSE

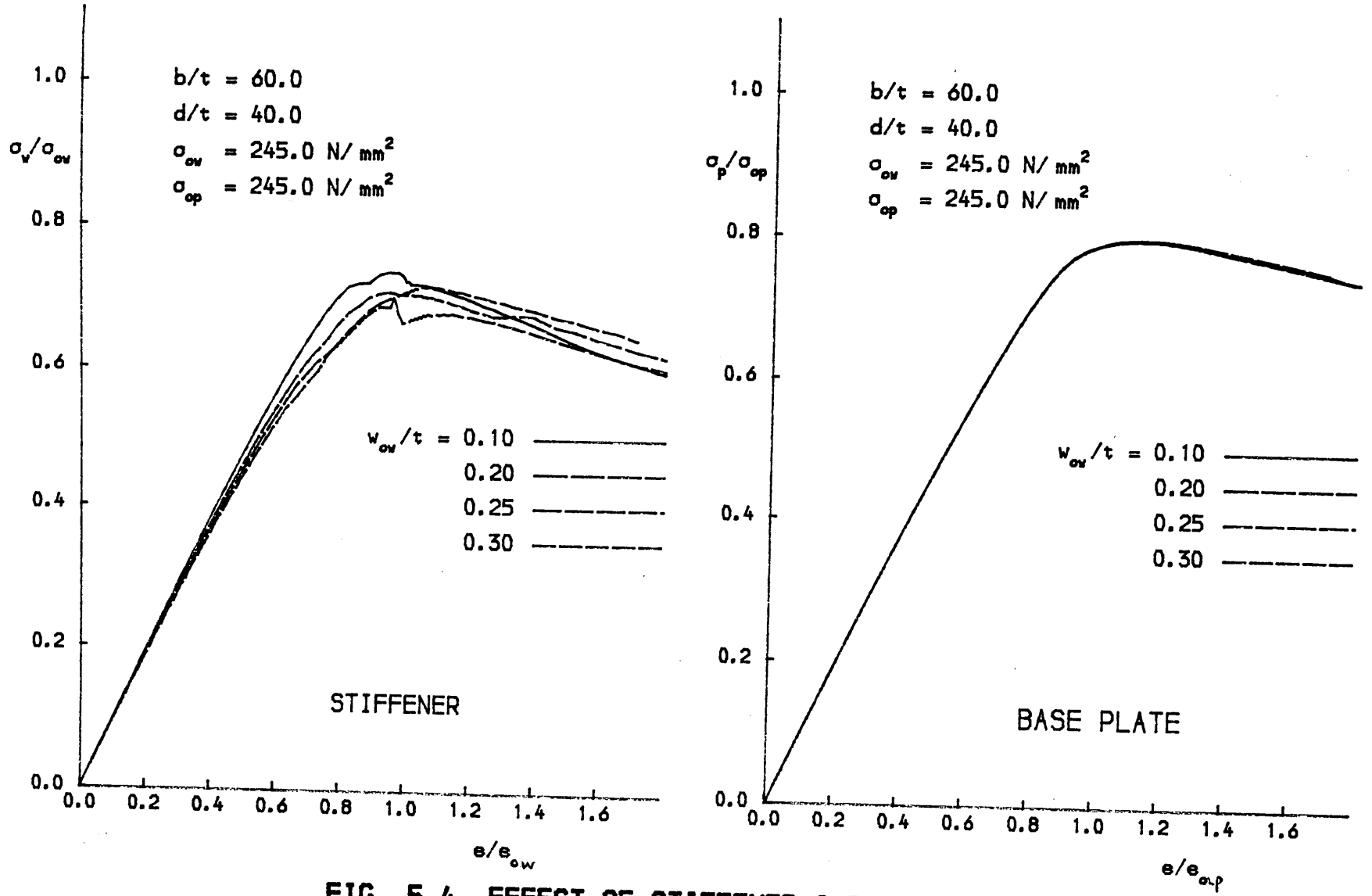

FIG. 5.4 EFFECT OF STIFFENER IMPERFECTIONS

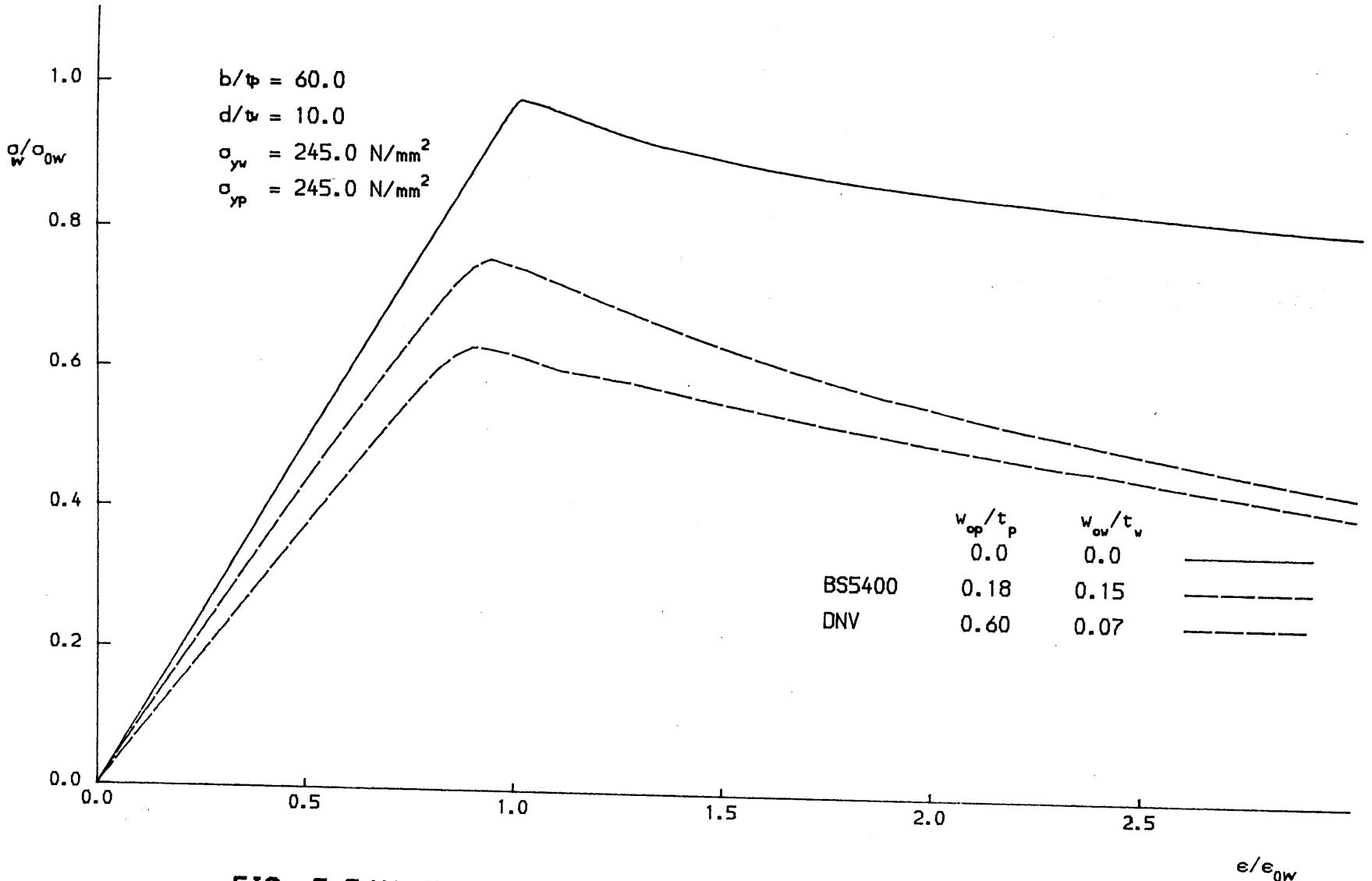

FIG. 5.5(A) EFFECT OF RULE IMPERFECTIONS ON STIFFENER RESPONSE

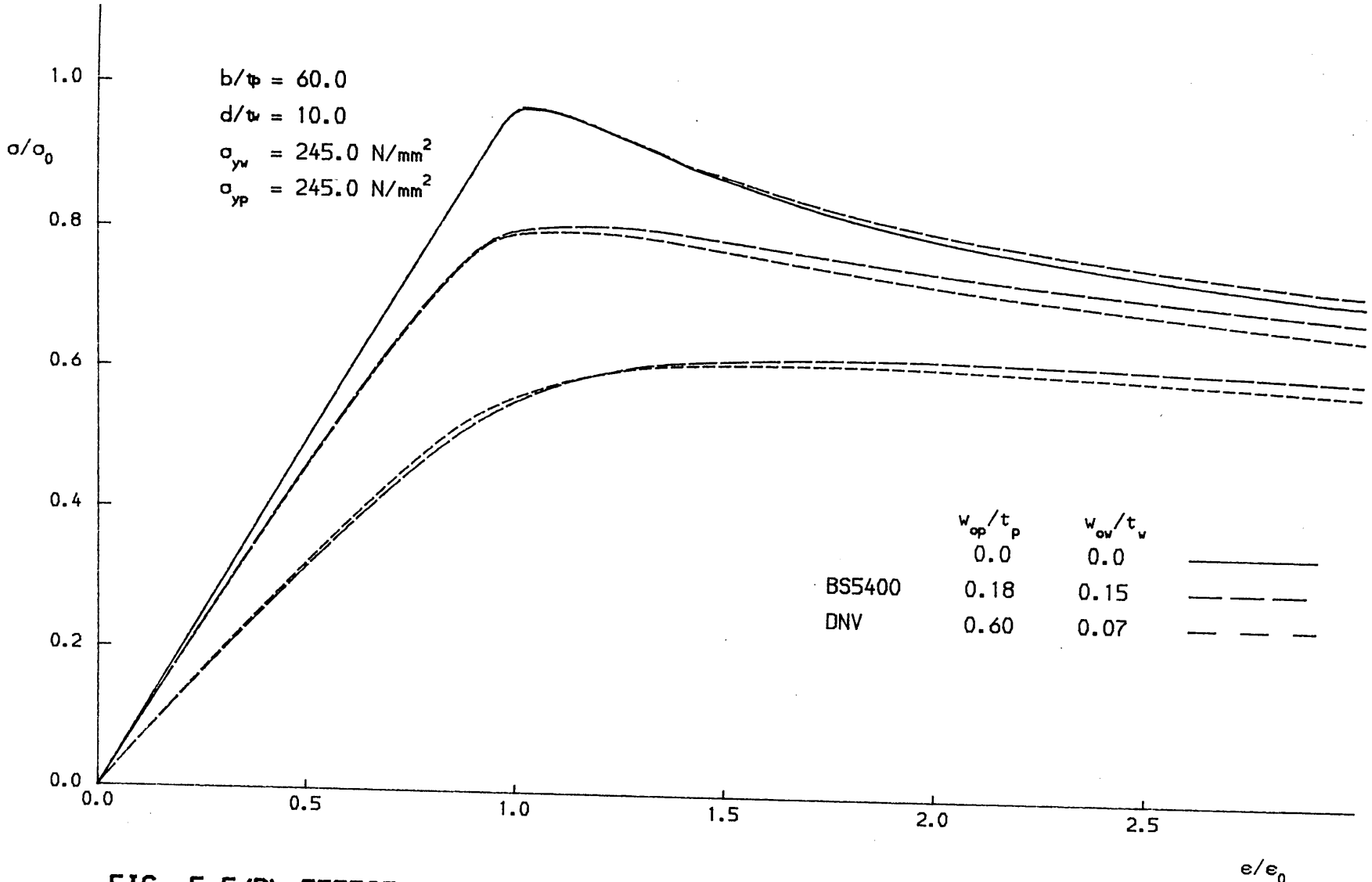

FIG. 5.5(B) EFFECT OF RULE IMPERFECTIONS ON PLATE AND STIFFENED PLATE RESPONSE

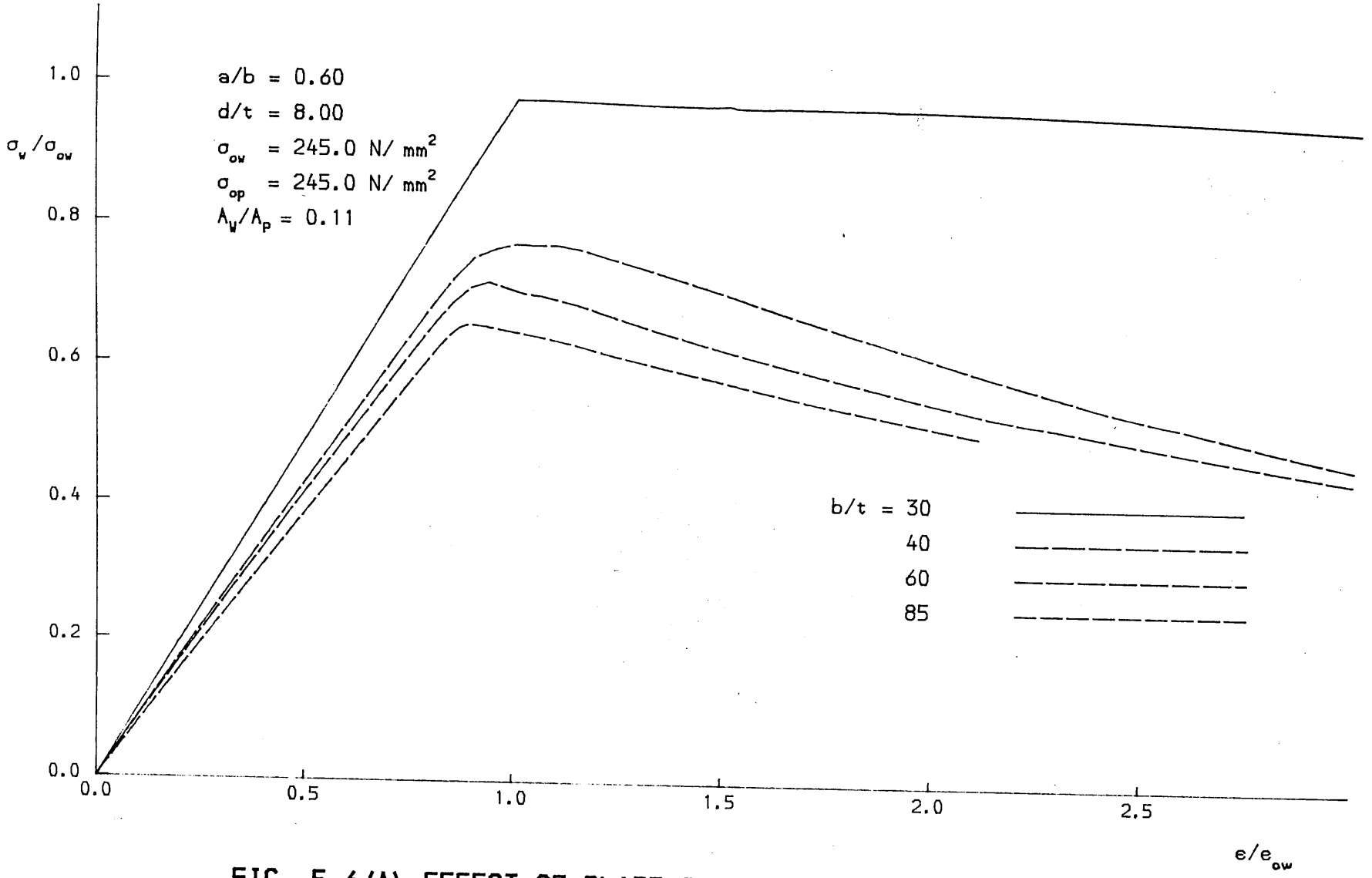

FIG. 5.6(A) EFFECT OF PLATE SLENDERNESS ON STIFFENER RESPONSE

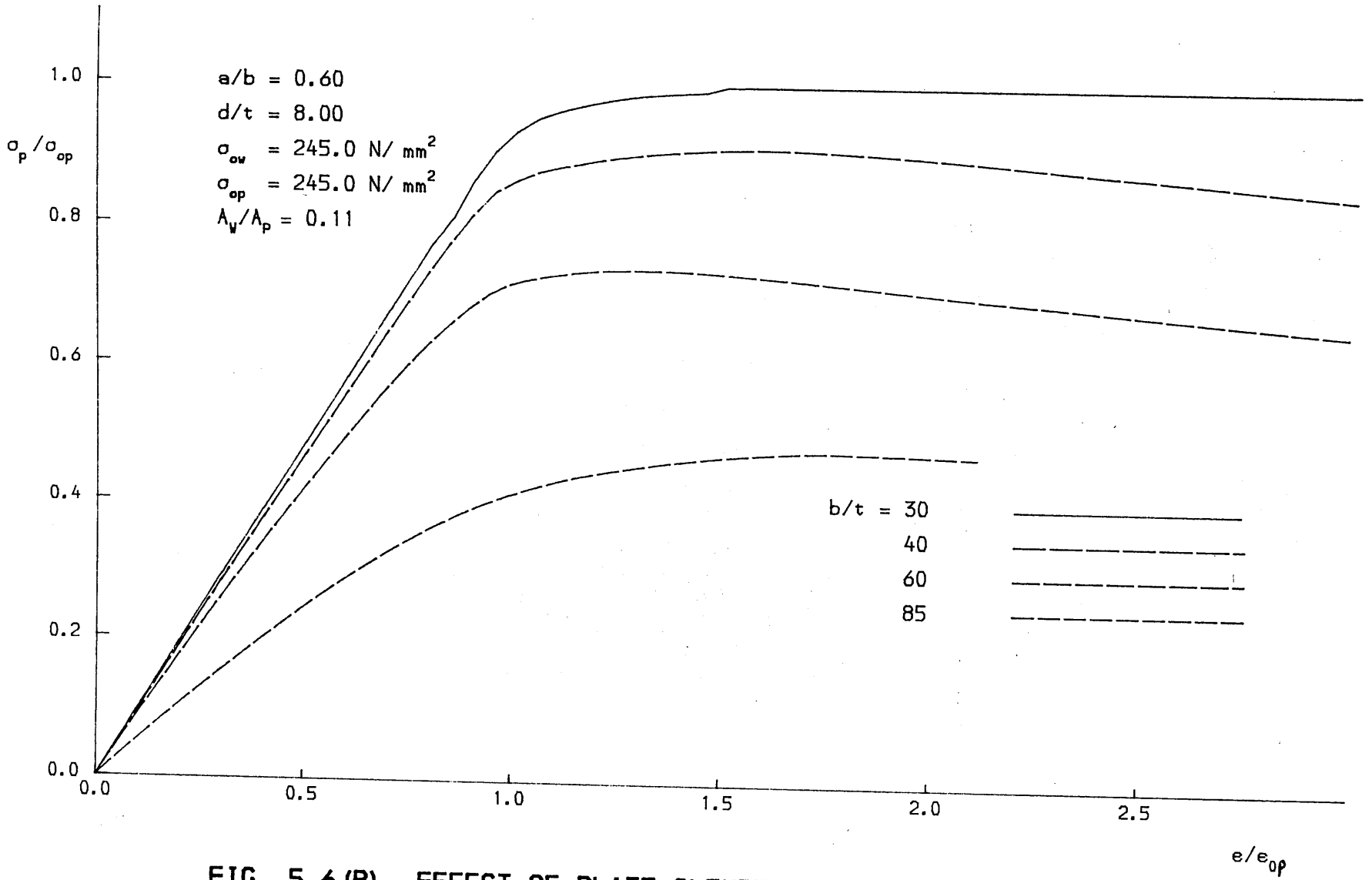

FIG. 5.6 (B) EFFECT OF PLATE SLENDERNESS ON BASE PLATE RESPONSE

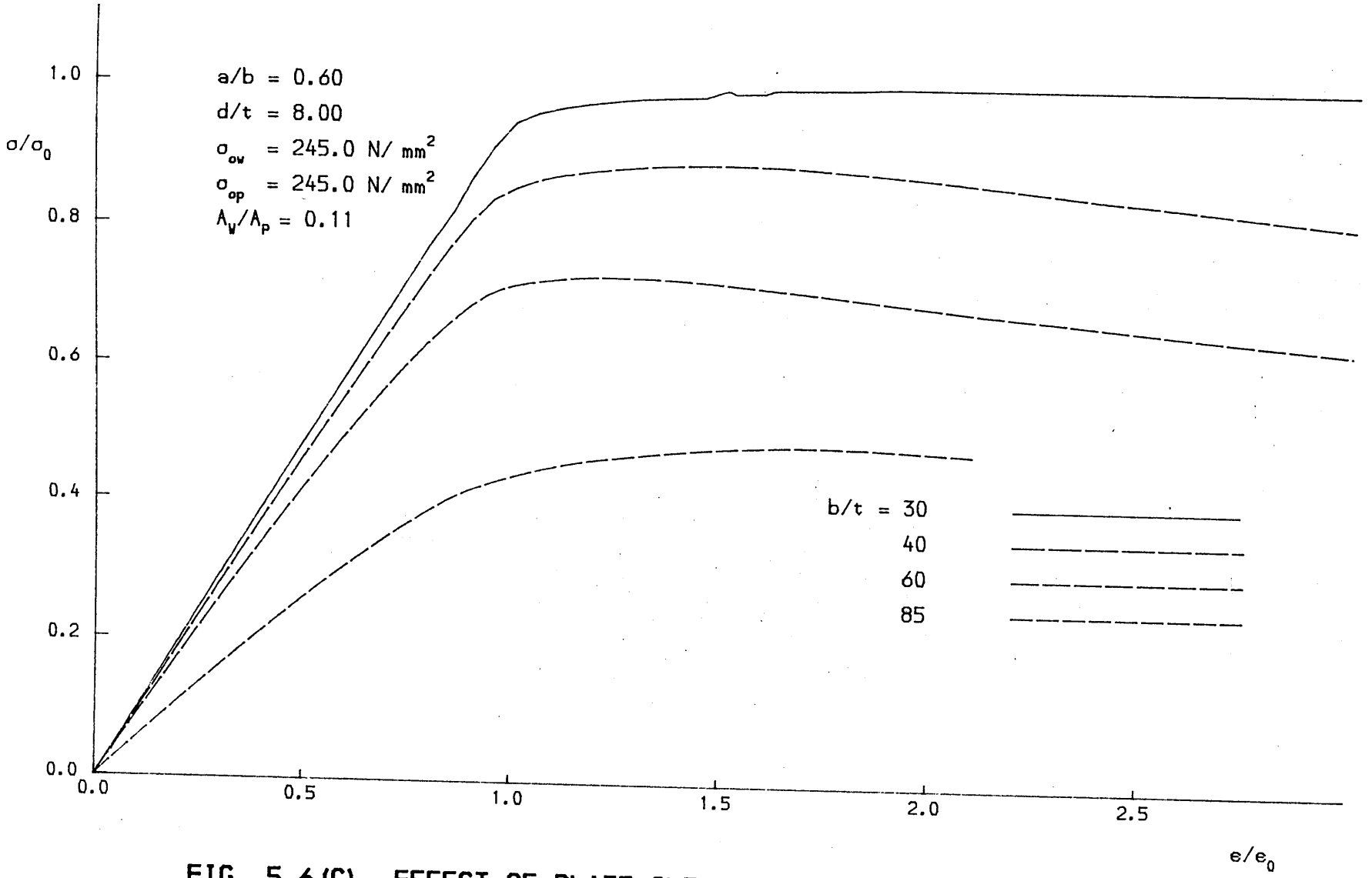

FIG. 5.6 (C) EFFECT OF PLATE SLENDERNESS ON STIFFENED PLATE RESPONSE

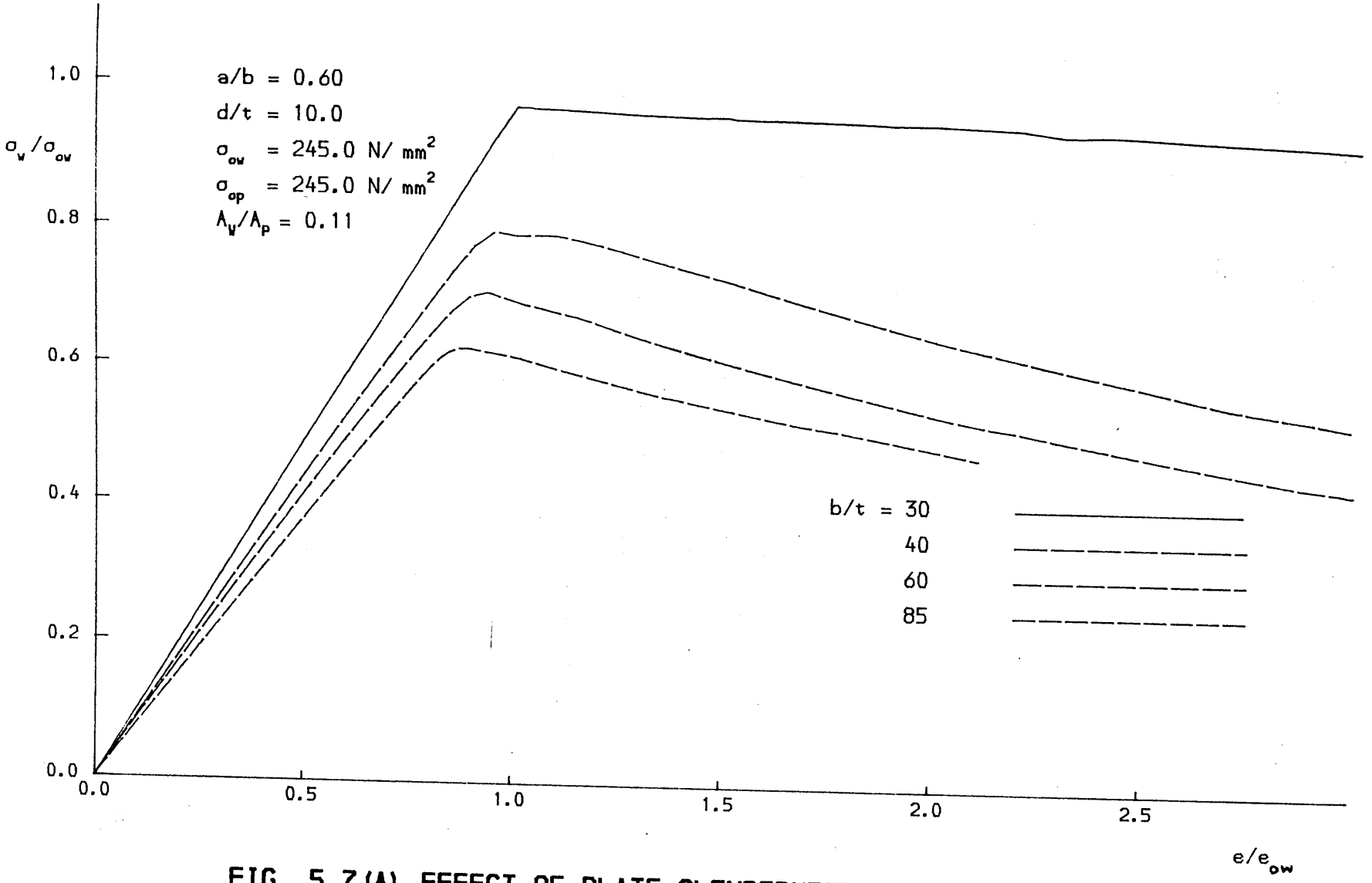

FIG. 5.7(A) EFFECT OF PLATE SLENDERNESS ON STIFFENER RESPONSE

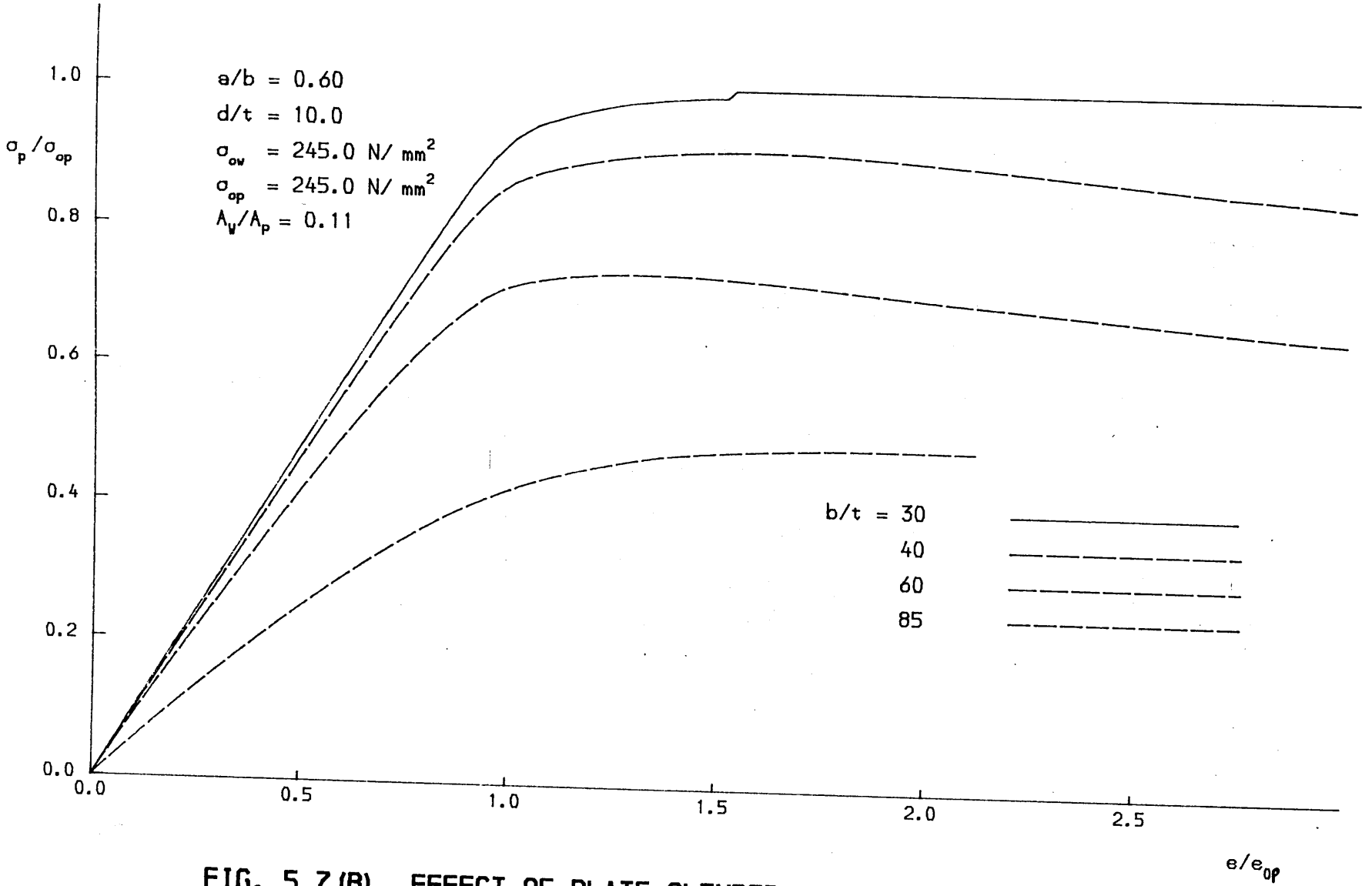

FIG. 5.7 (B) EFFECT OF PLATE SLENDERNESS ON BASE PLATE RESPONSE

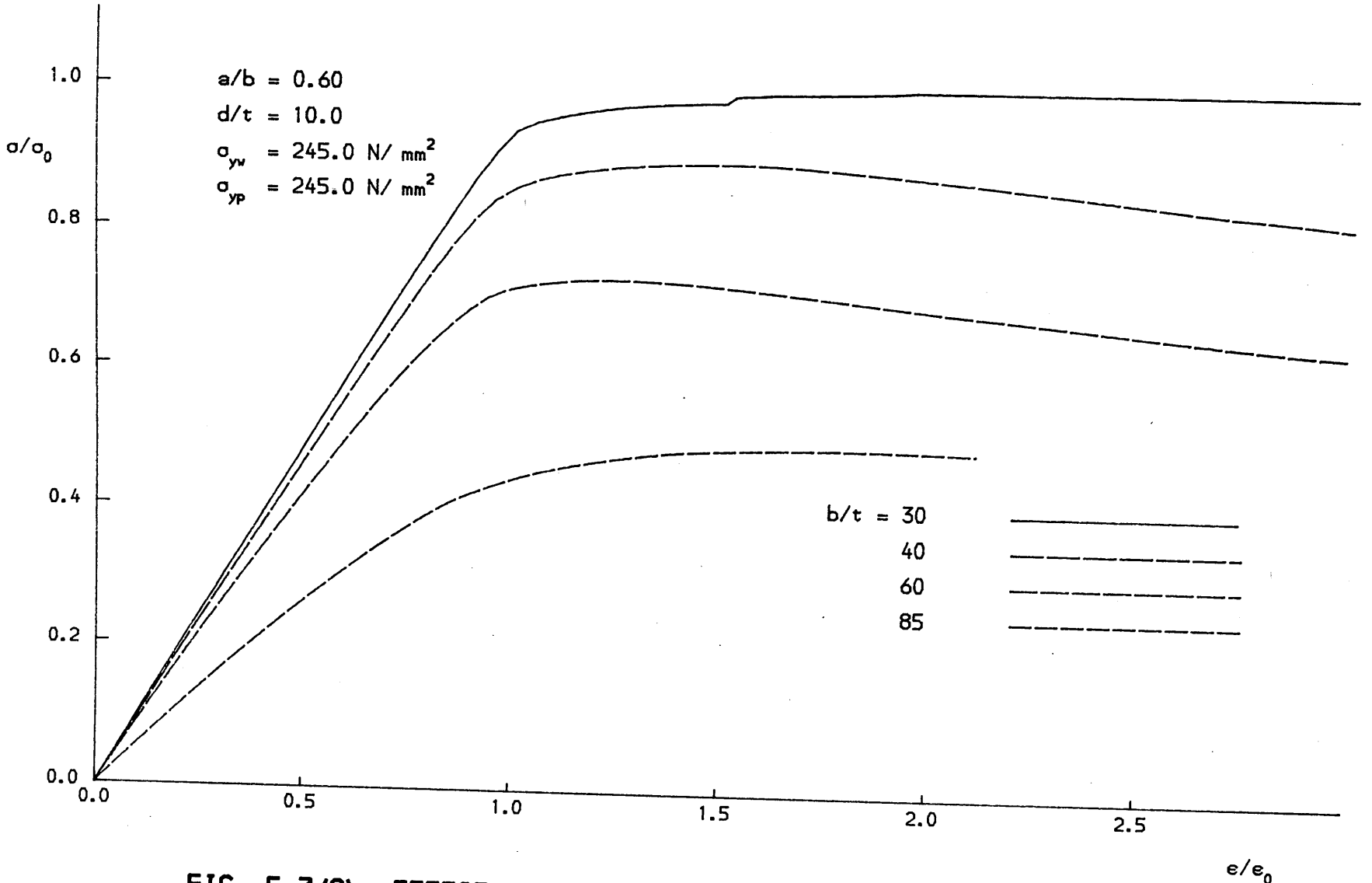

FIG. 5.7 (C) EFFECT OF PLATE SLENDERNESS ON STIFFENED PLATE RESPONSE

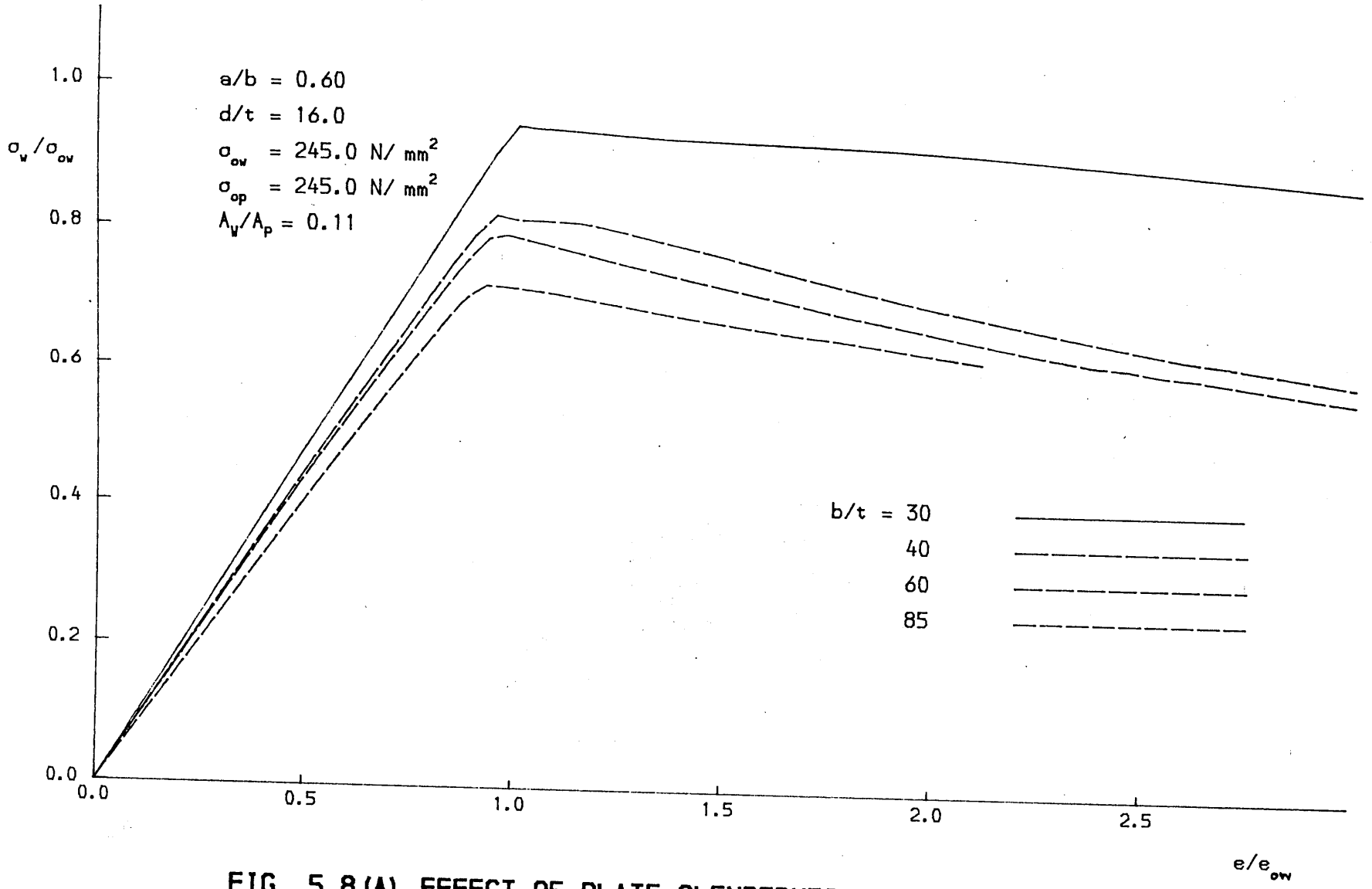

FIG. 5.8(A) EFFECT OF PLATE SLENDERNESS ON STIFFENER RESPONSE

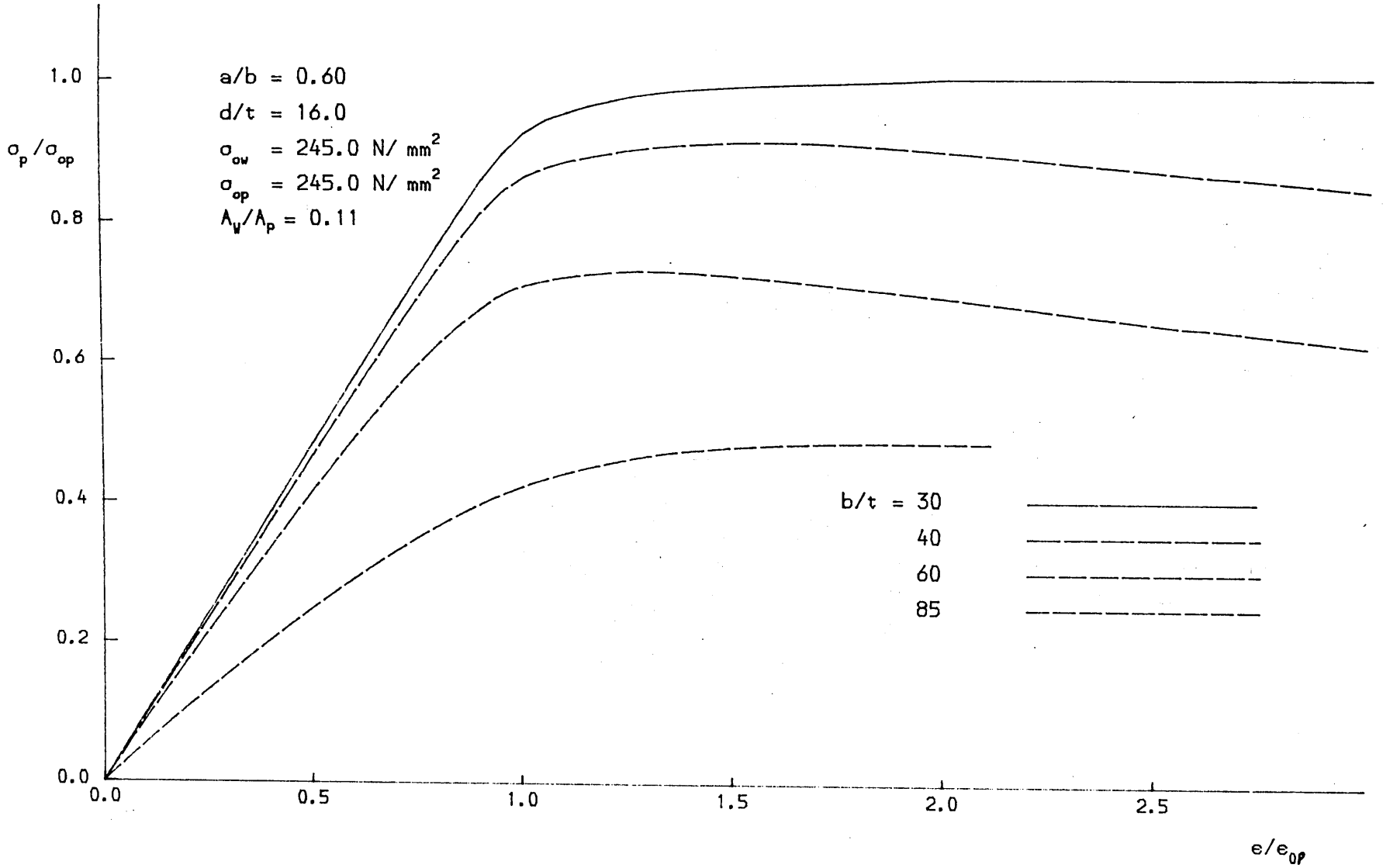

FIG. 5.8(B) EFFECT OF PLATE SLENDERNESS ON BASE PLATE RESPONSE

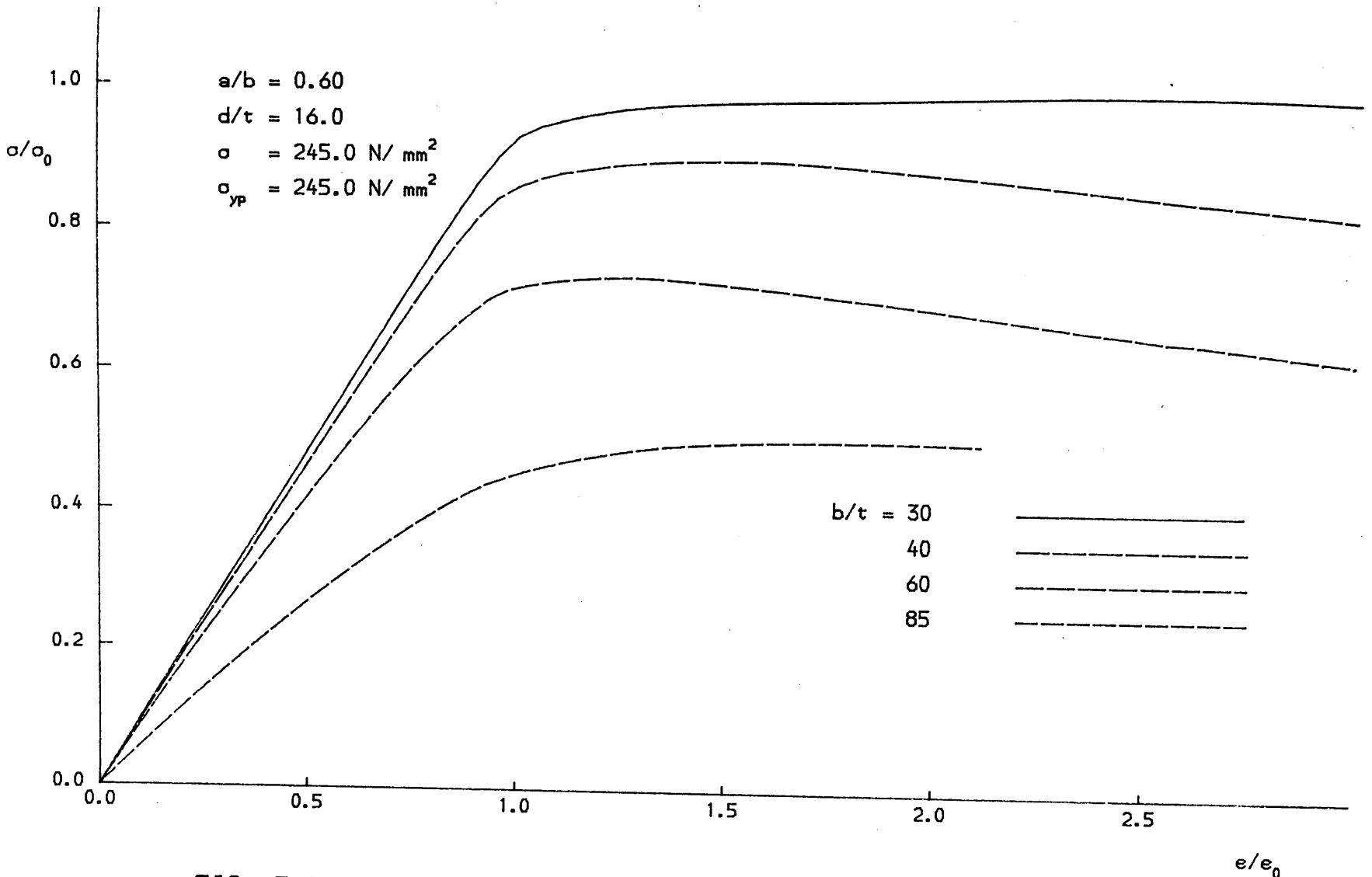

FIG. 5.8(C) EFFECT OF PLATE SLENDERNESS ON STIFFENED PLATE RESPONSE

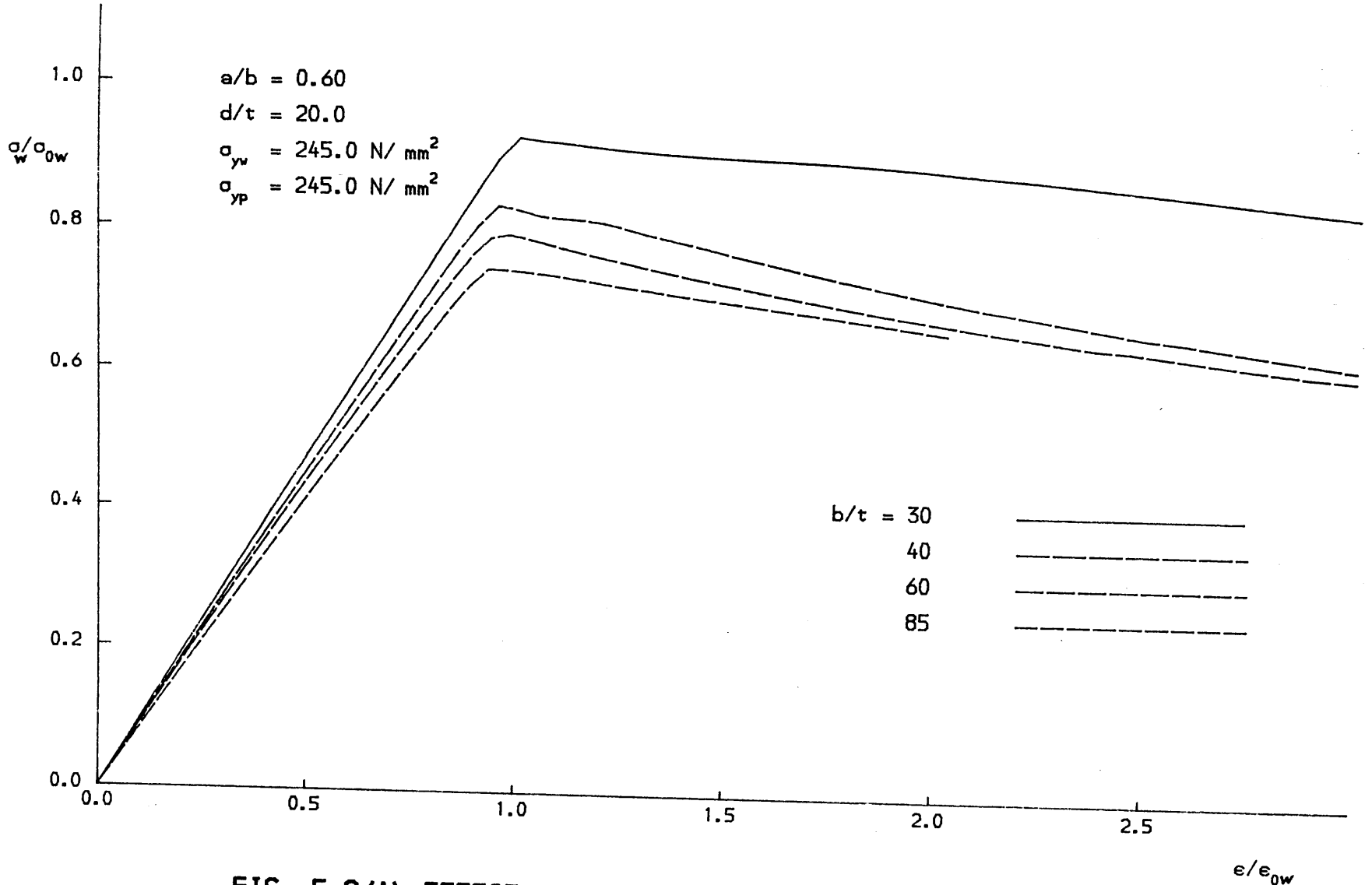

FIG. 5.9(A) EFFECT OF PLATE SLENDERNESS ON STIFFENER RESPONSE

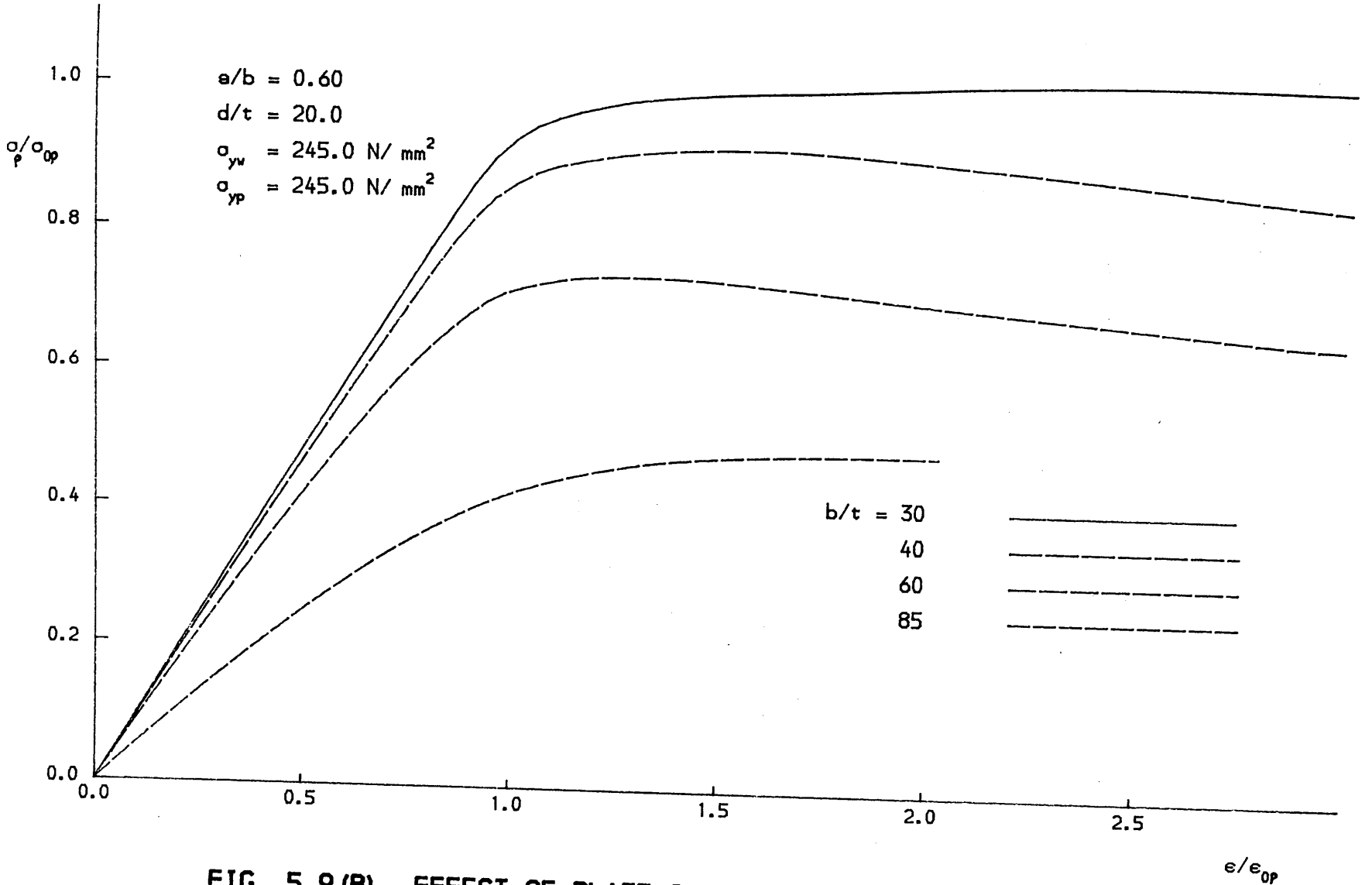

FIG. 5.9 (B) EFFECT OF PLATE SLENDERNESS ON BASE PLATE RESPONSE

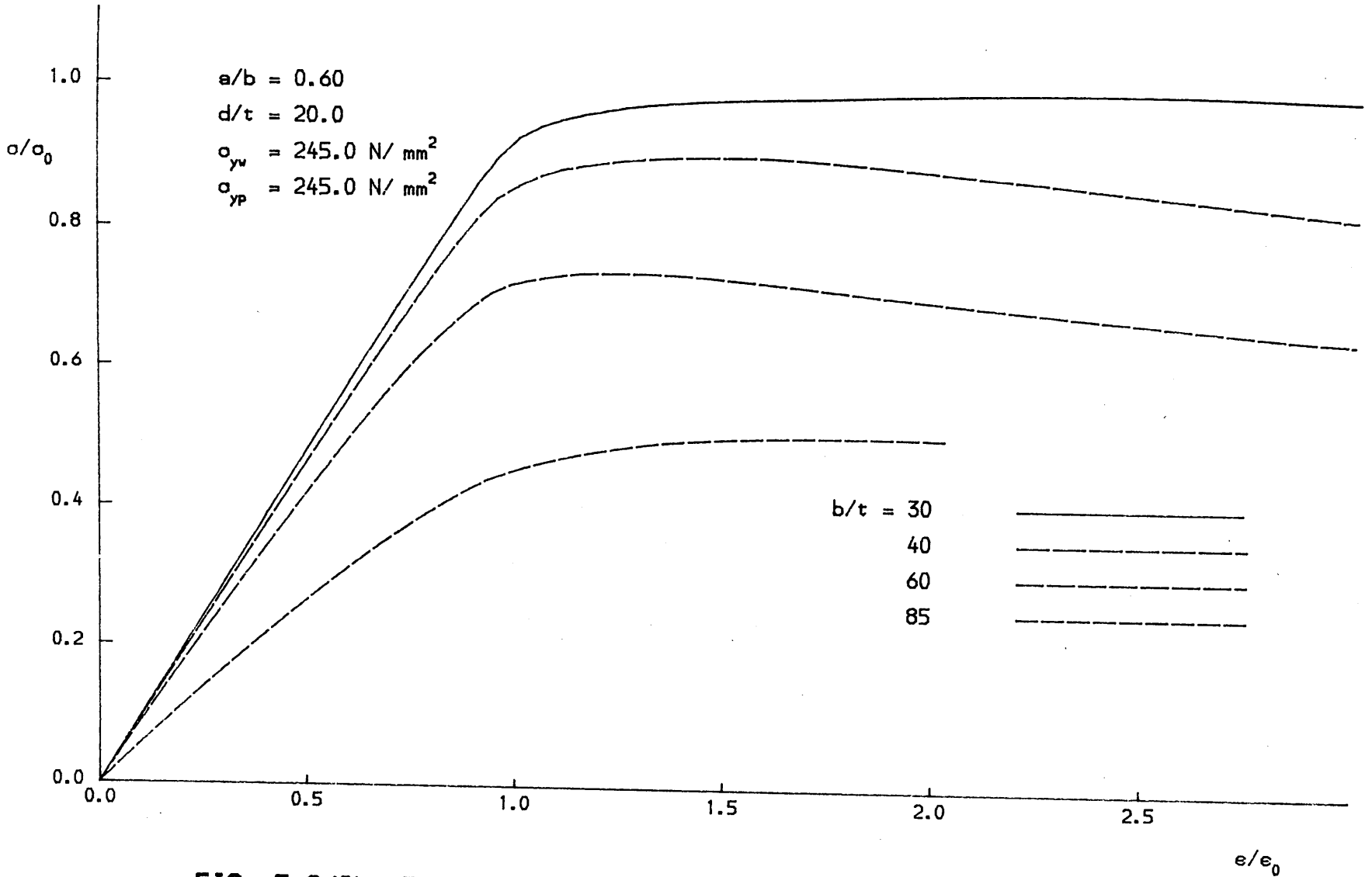

FIG. 5.9(C) EFFECT OF PLATE SLENDERNESS ON STIFFENED PLATE RESPONSE

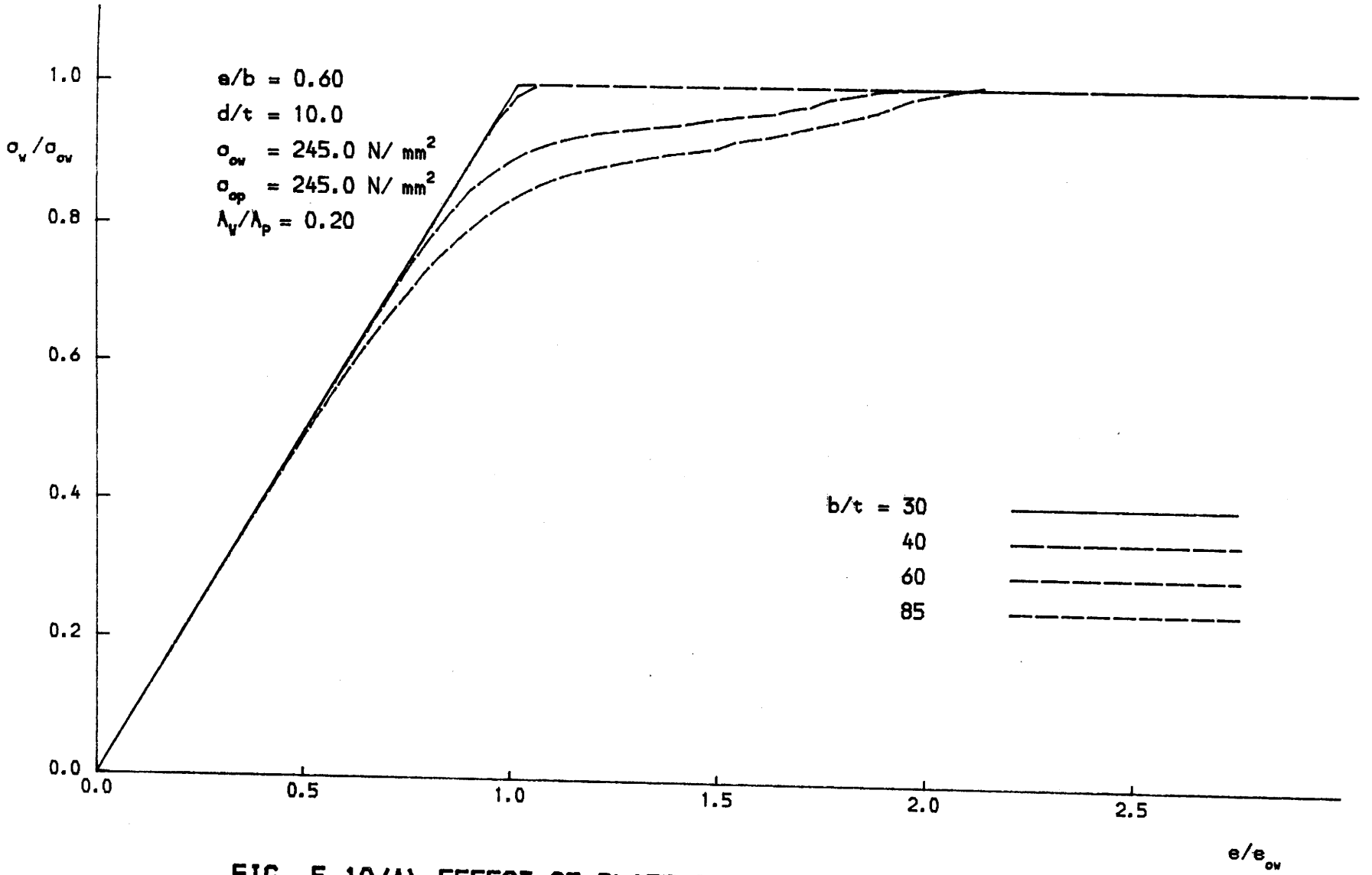

FIG. 5.10(A) EFFECT OF PLATE SLENDERNESS ON STIFFENER RESPONSE

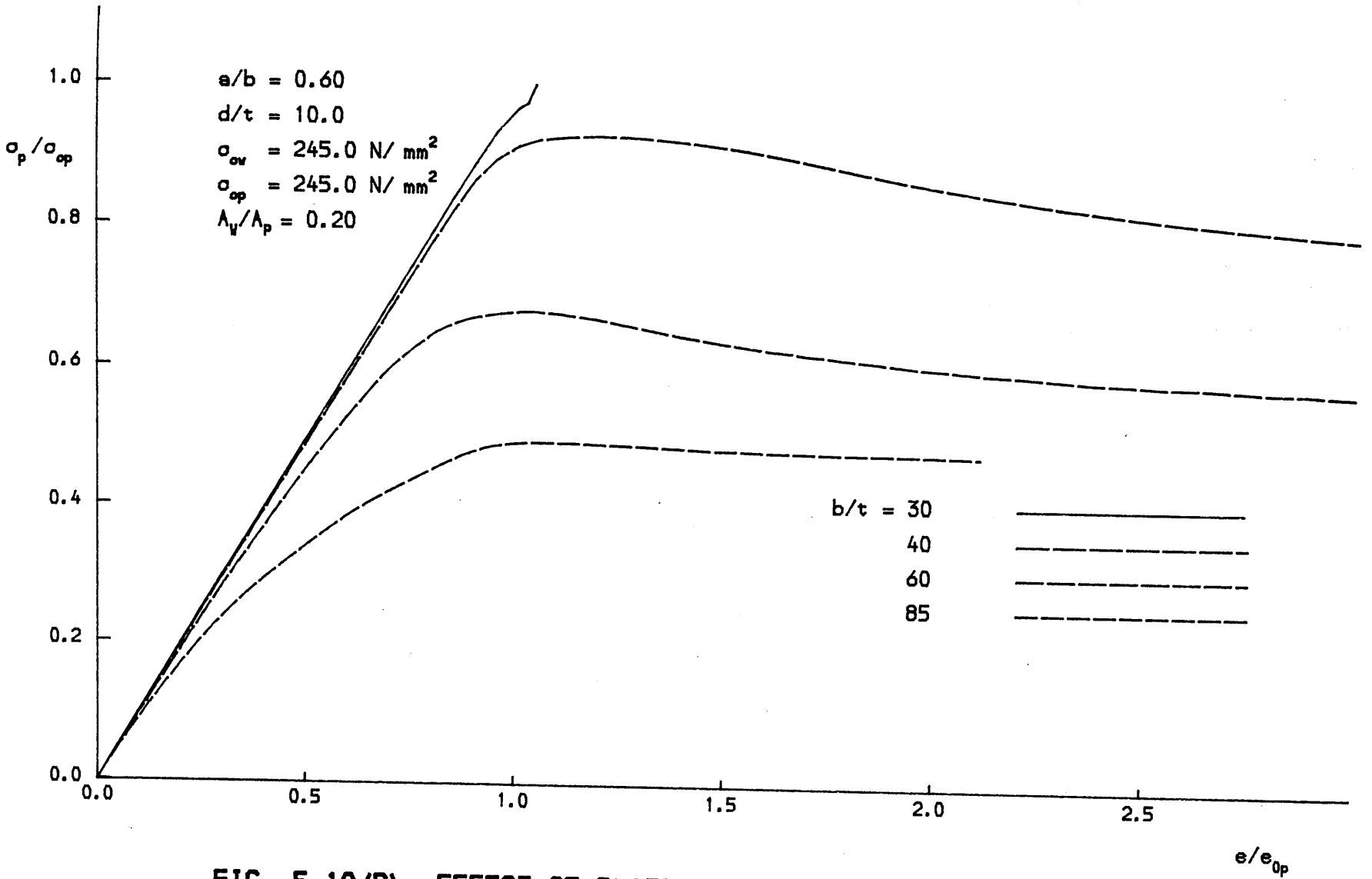

FIG. 5.10 (B) EFFECT OF PLATE SLENDERNESS ON BASE PLATE RESPONSE

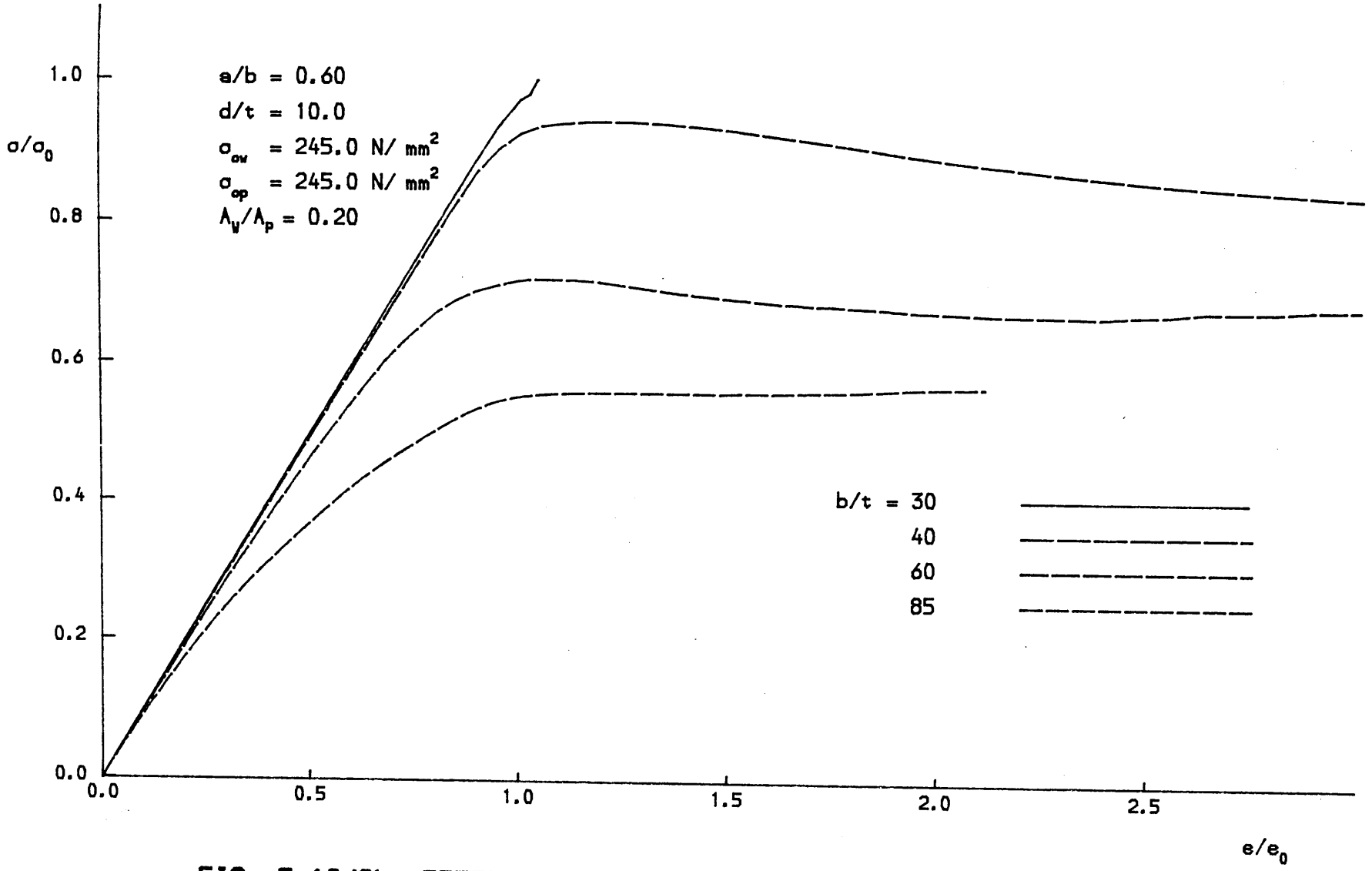

FIG. 5.10(C) EFFECT OF PLATE SLENDERNESS ON STIFFENED PLATE RESPONSE

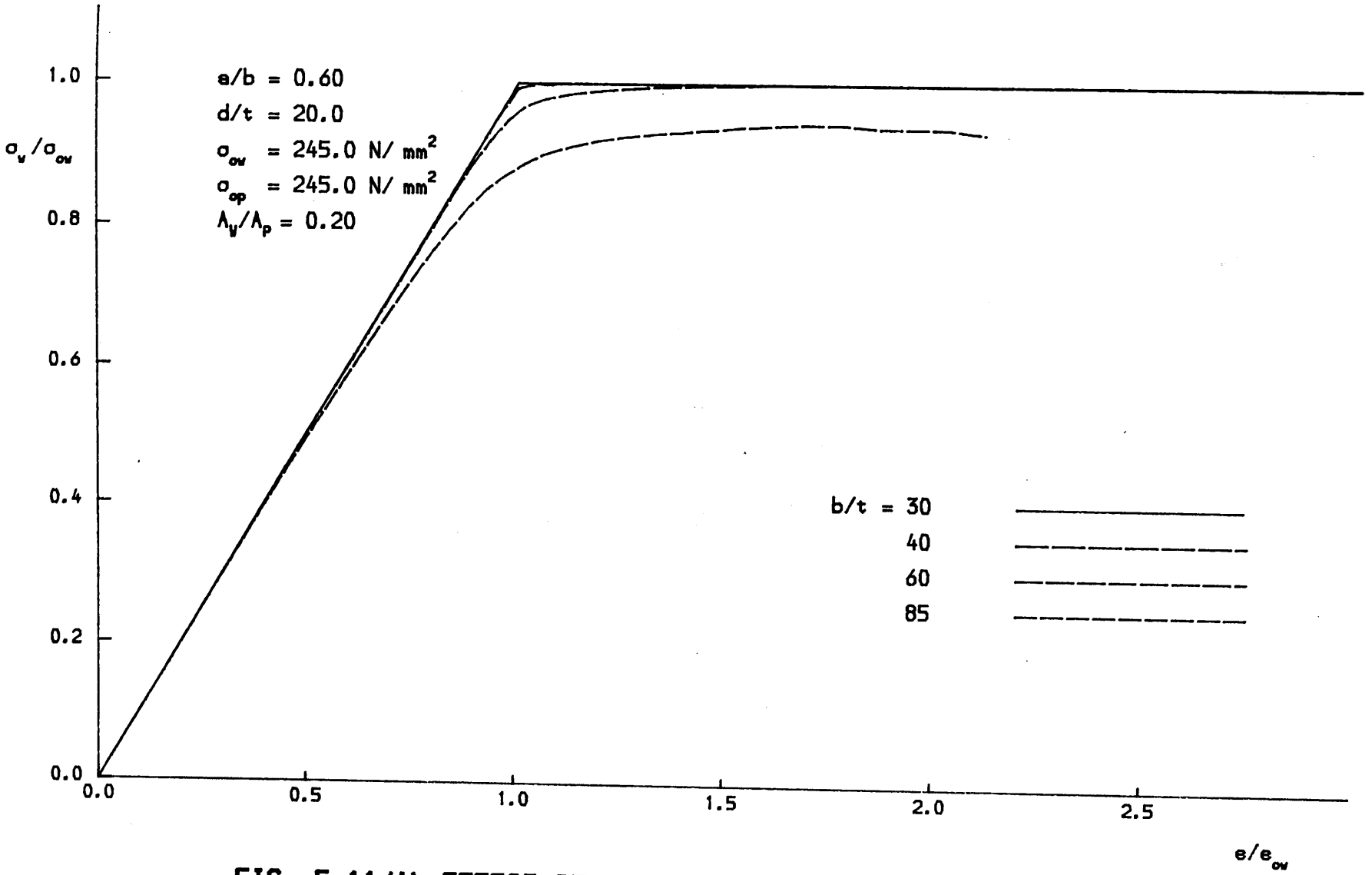

FIG. 5.11(A) EFFECT OF PLATE SLENDERNESS ON STIFFENER RESPONSE

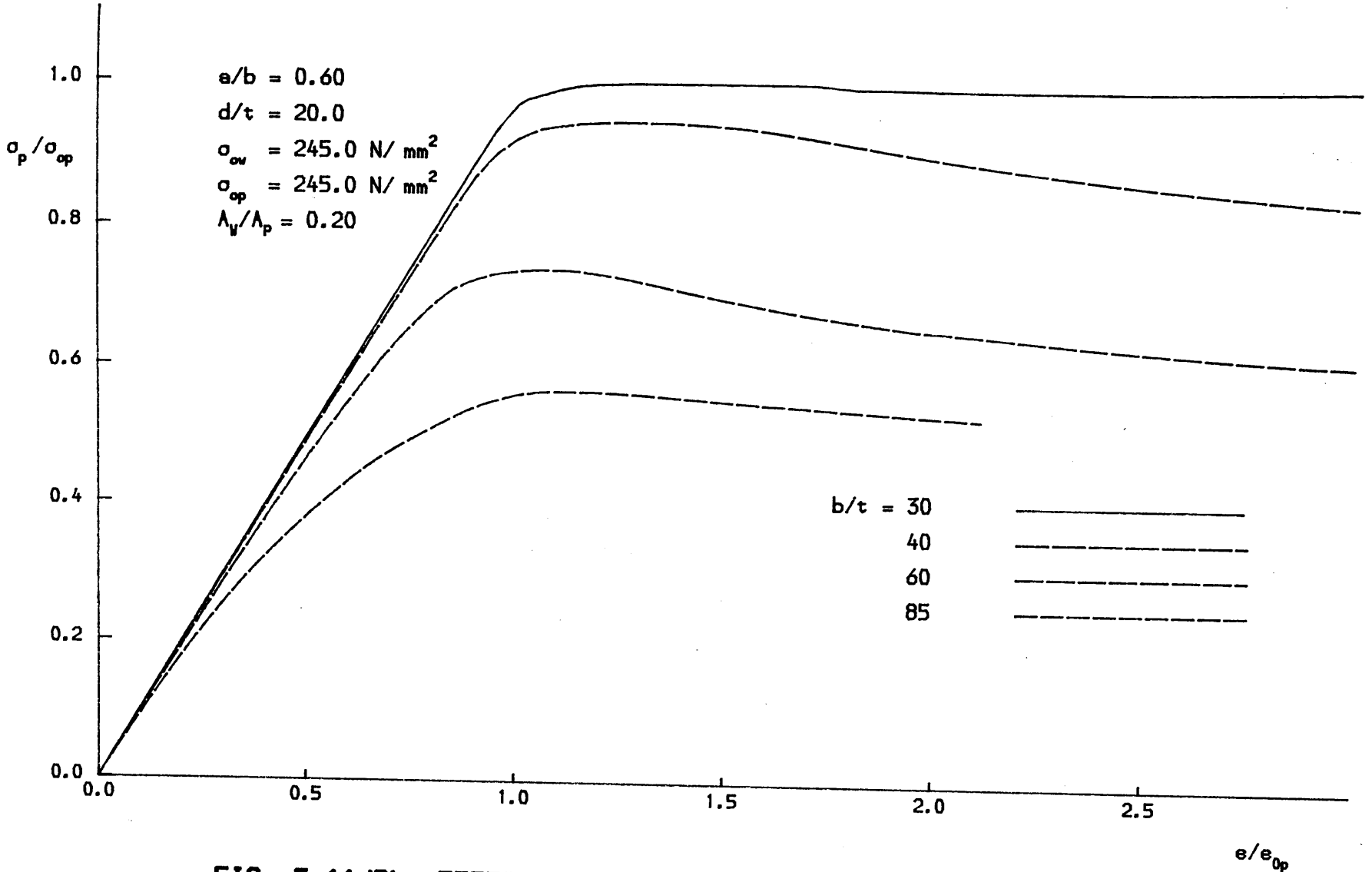

FIG. 5.11 (B) EFFECT OF PLATE SLENDERNESS ON BASE PLATE RESPONSE

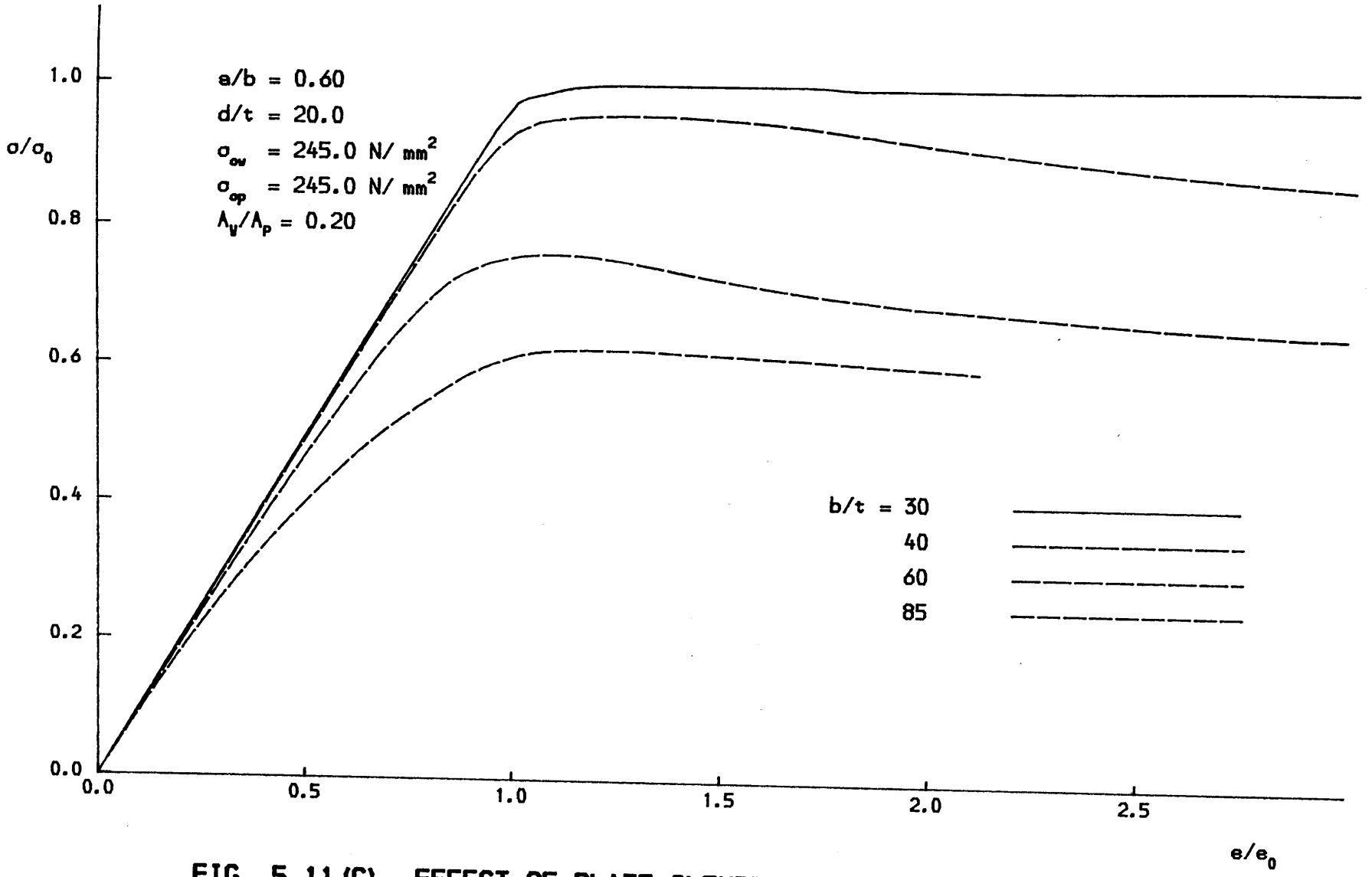

FIG. 5.11 (C) EFFECT OF PLATE SLENDERNESS ON STIFFENED PLATE RESPONSE

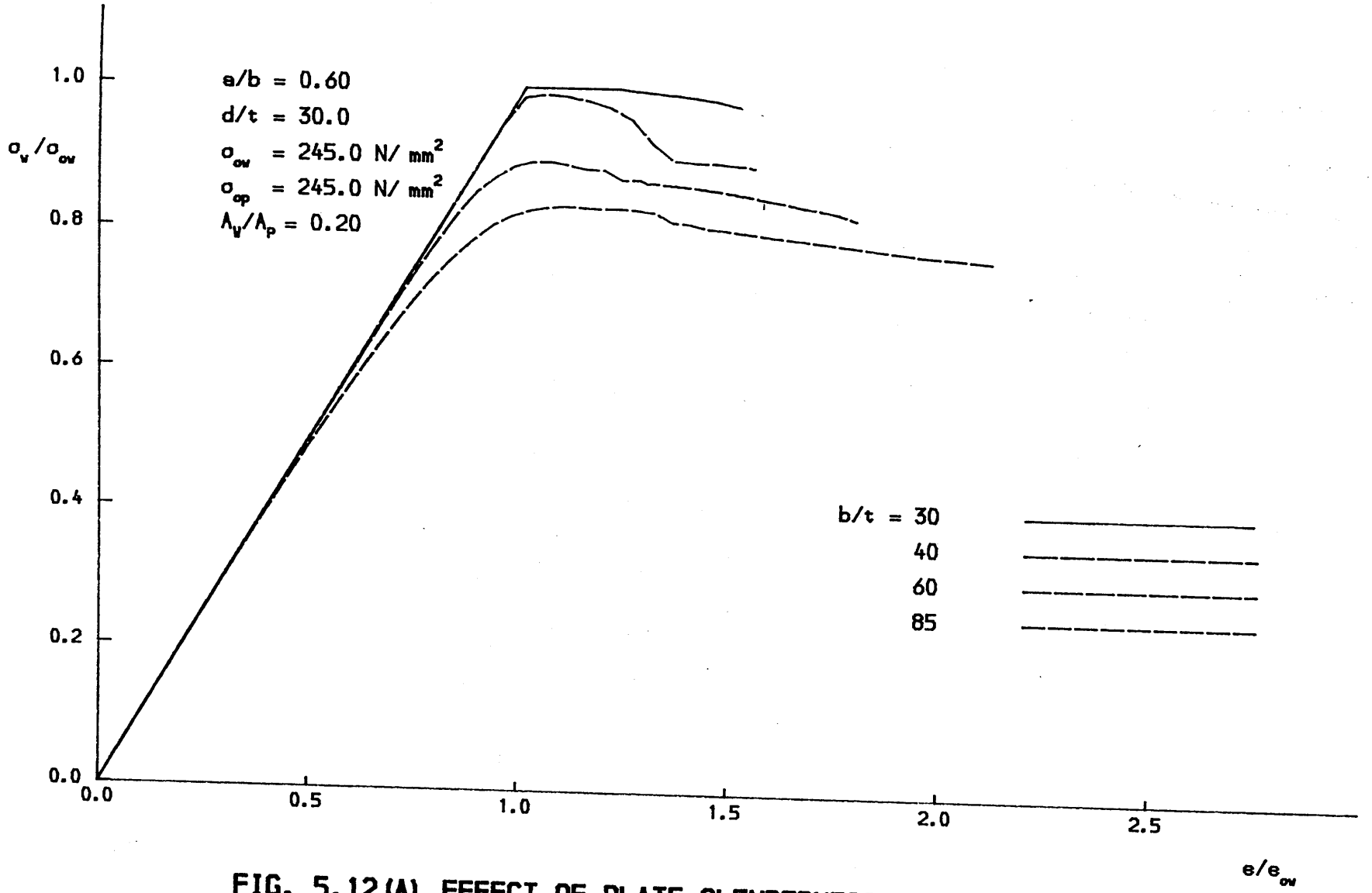

FIG. 5.12(A) EFFECT OF PLATE SLENDERNESS ON STIFFENER RESPONSE

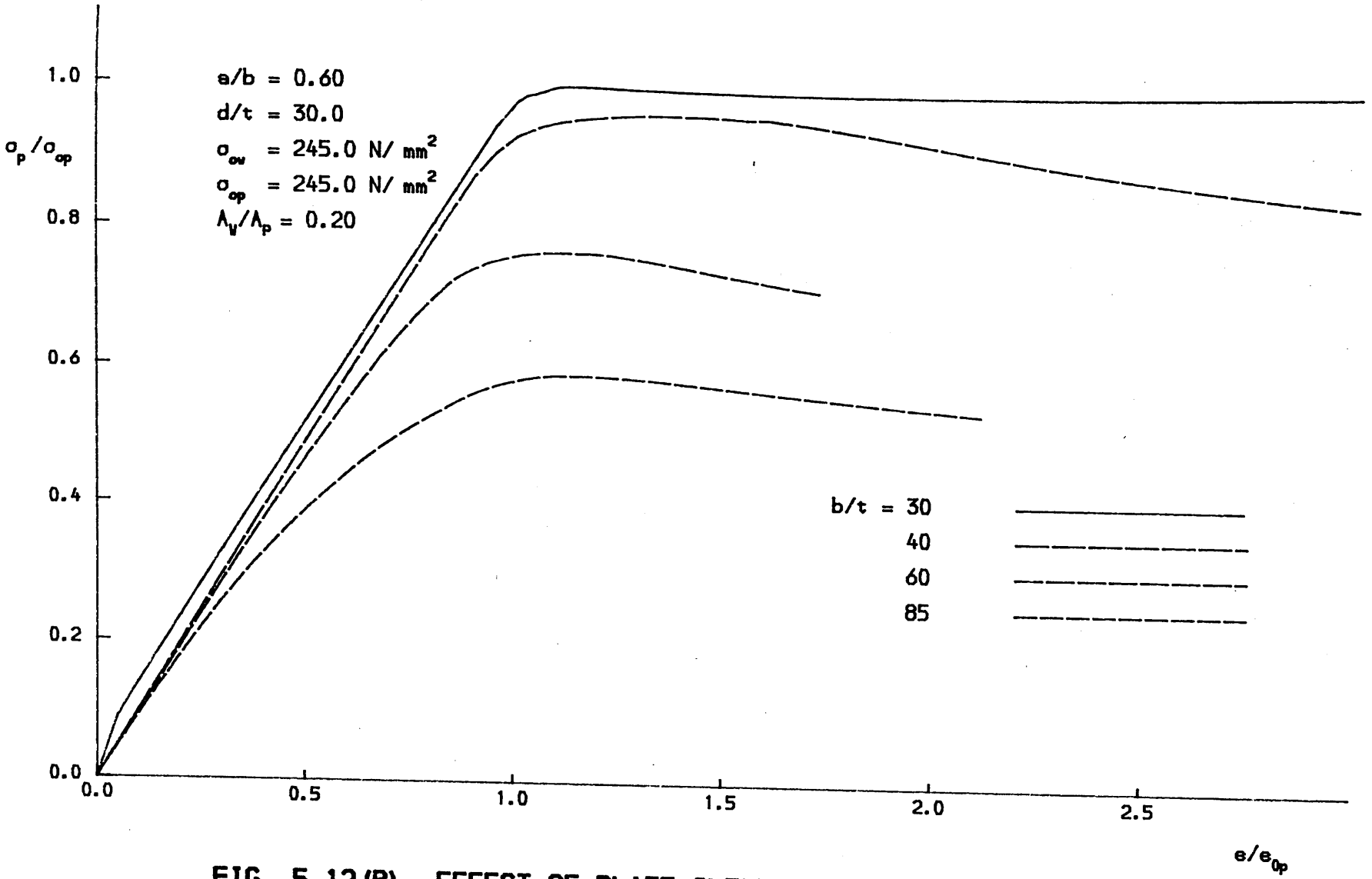

FIG. 5.12(B) EFFECT OF PLATE SLENDERNESS ON BASE PLATE RESPONSE

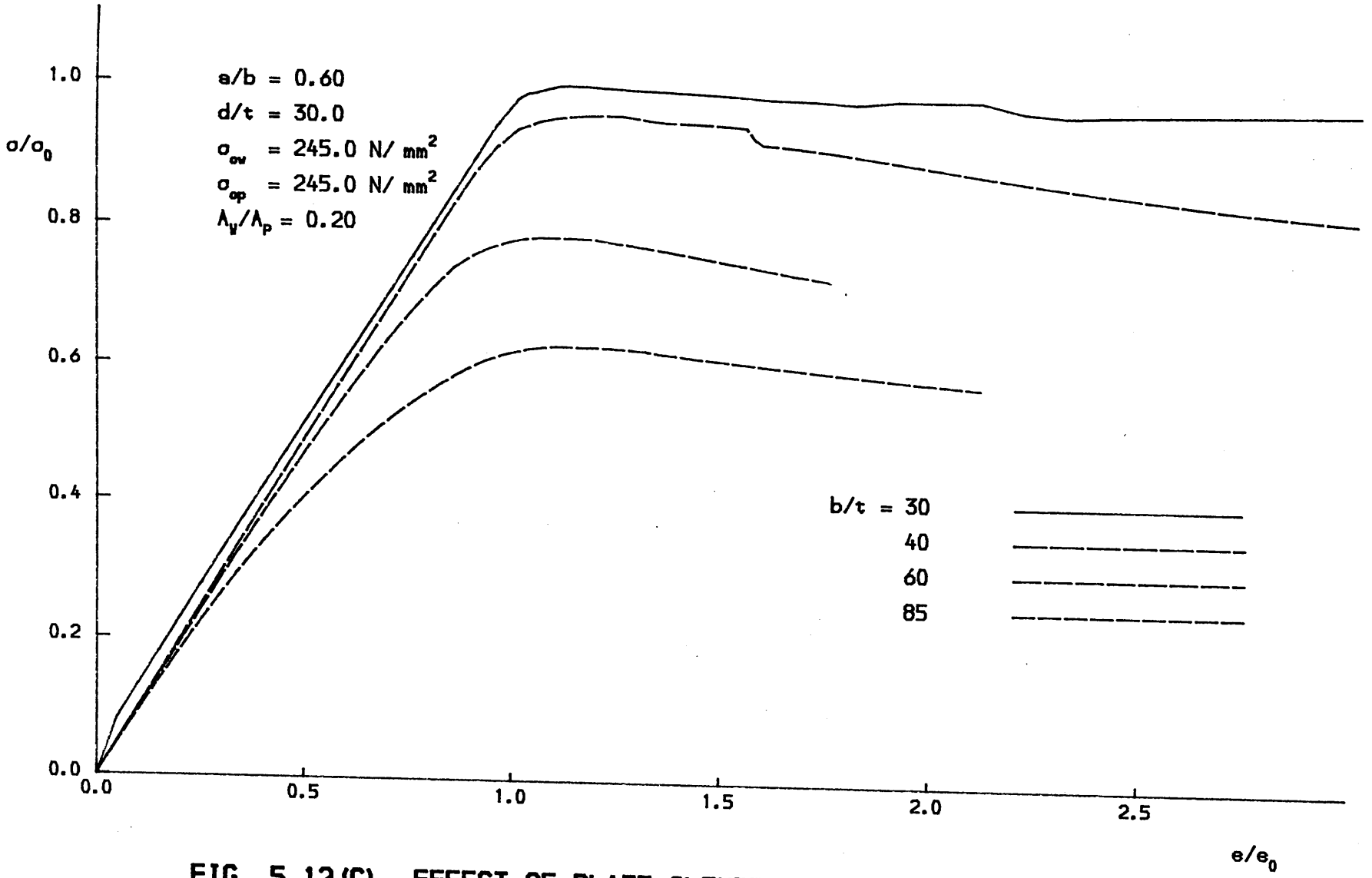

FIG. 5.12(C) EFFECT OF PLATE SLENDERNESS ON STIFFENED PLATE RESPONSE

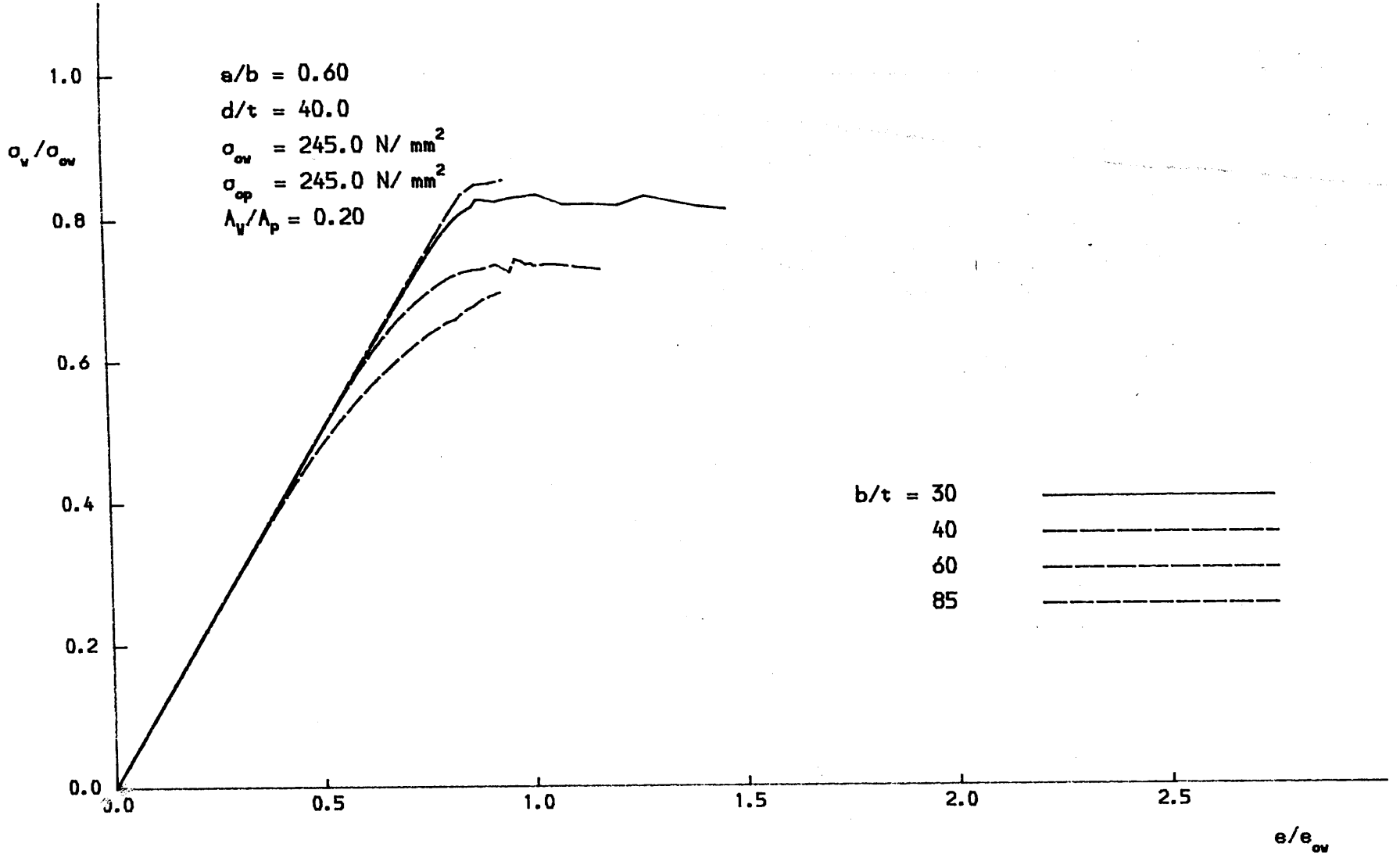

FIG. 5.13(A) EFFECT OF PLATE SLENDERNESS ON STIFFENER RESPONSE

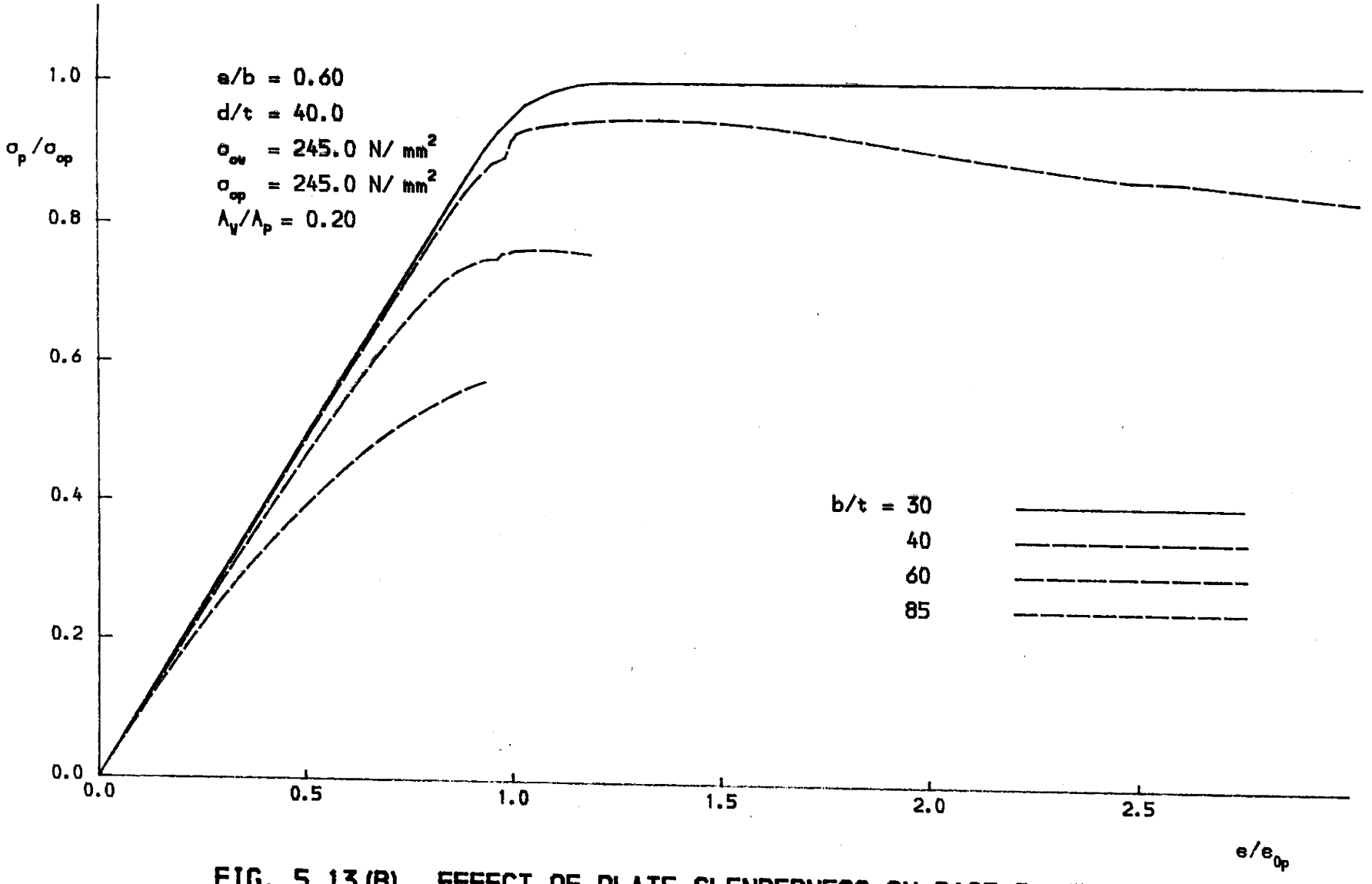

FIG. 5.13(B) EFFECT OF PLATE SLENDERNESS ON BASE PLATE RESPONSE

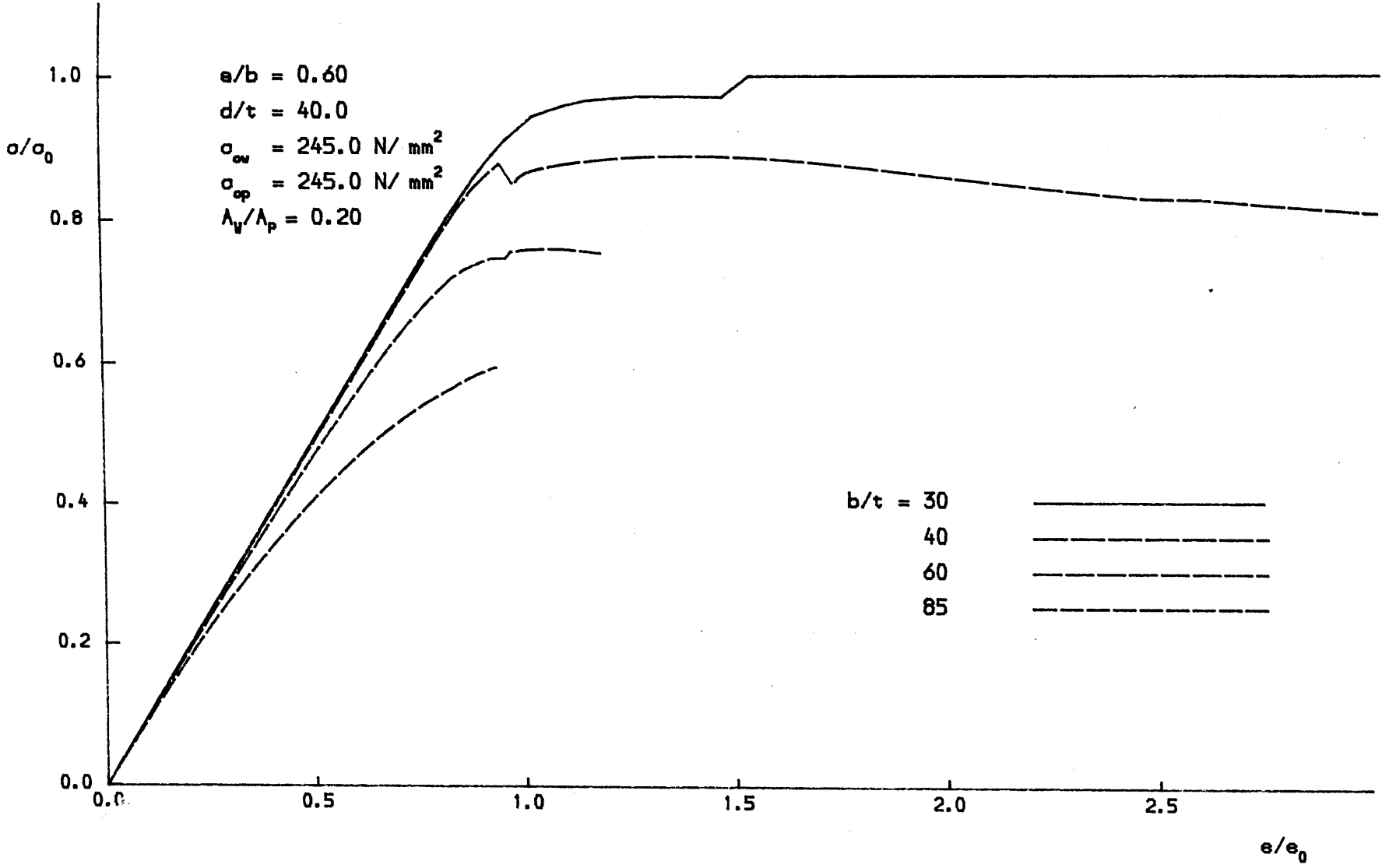

FIG. 5.13(C) EFFECT OF PLATE SLENDERNESS ON STIFFENED PLATE RESPONSE

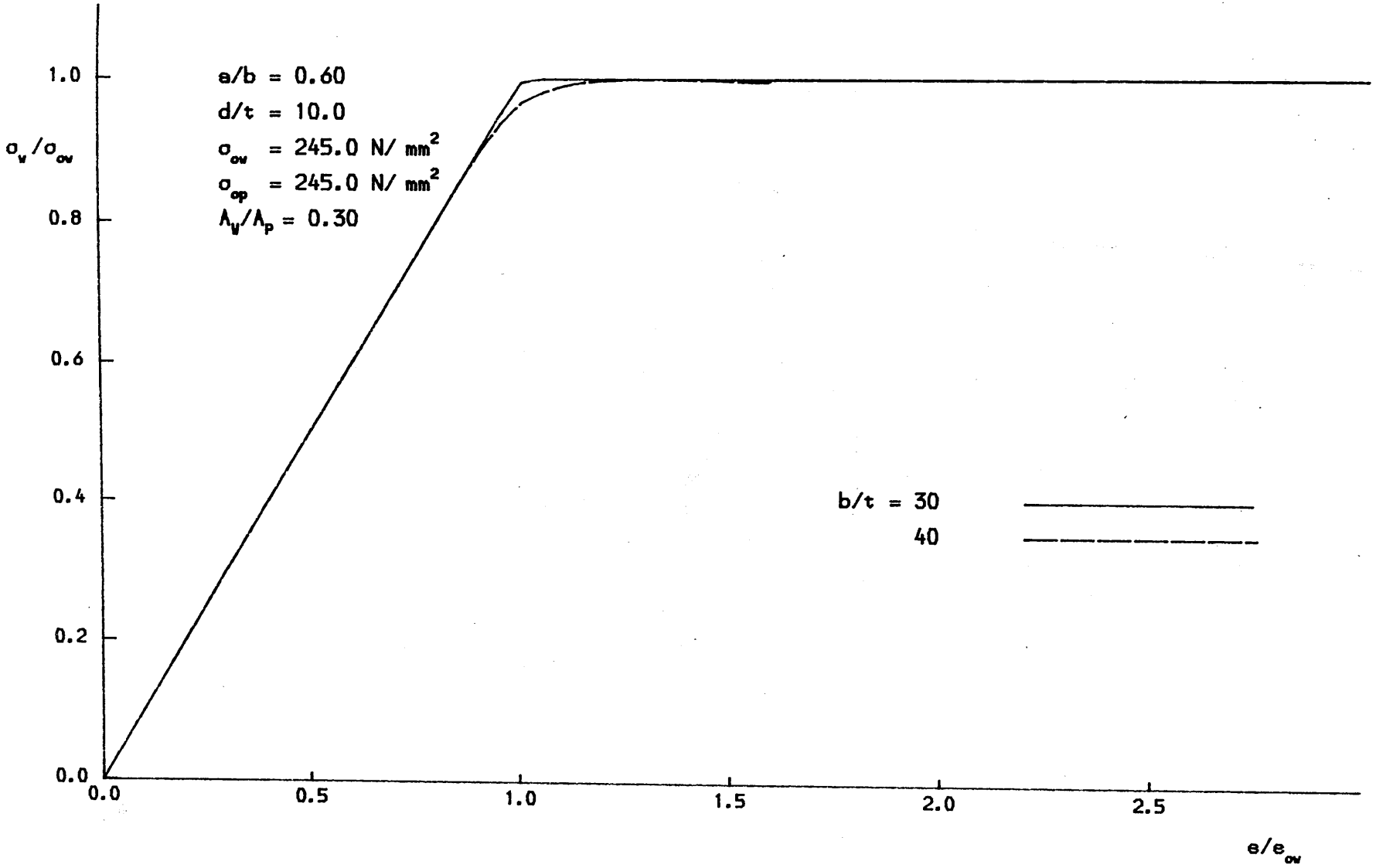

FIG. 5.14 (A) EFFECT OF PLATE SLENDERNESS ON STIFFENER RESPONSE

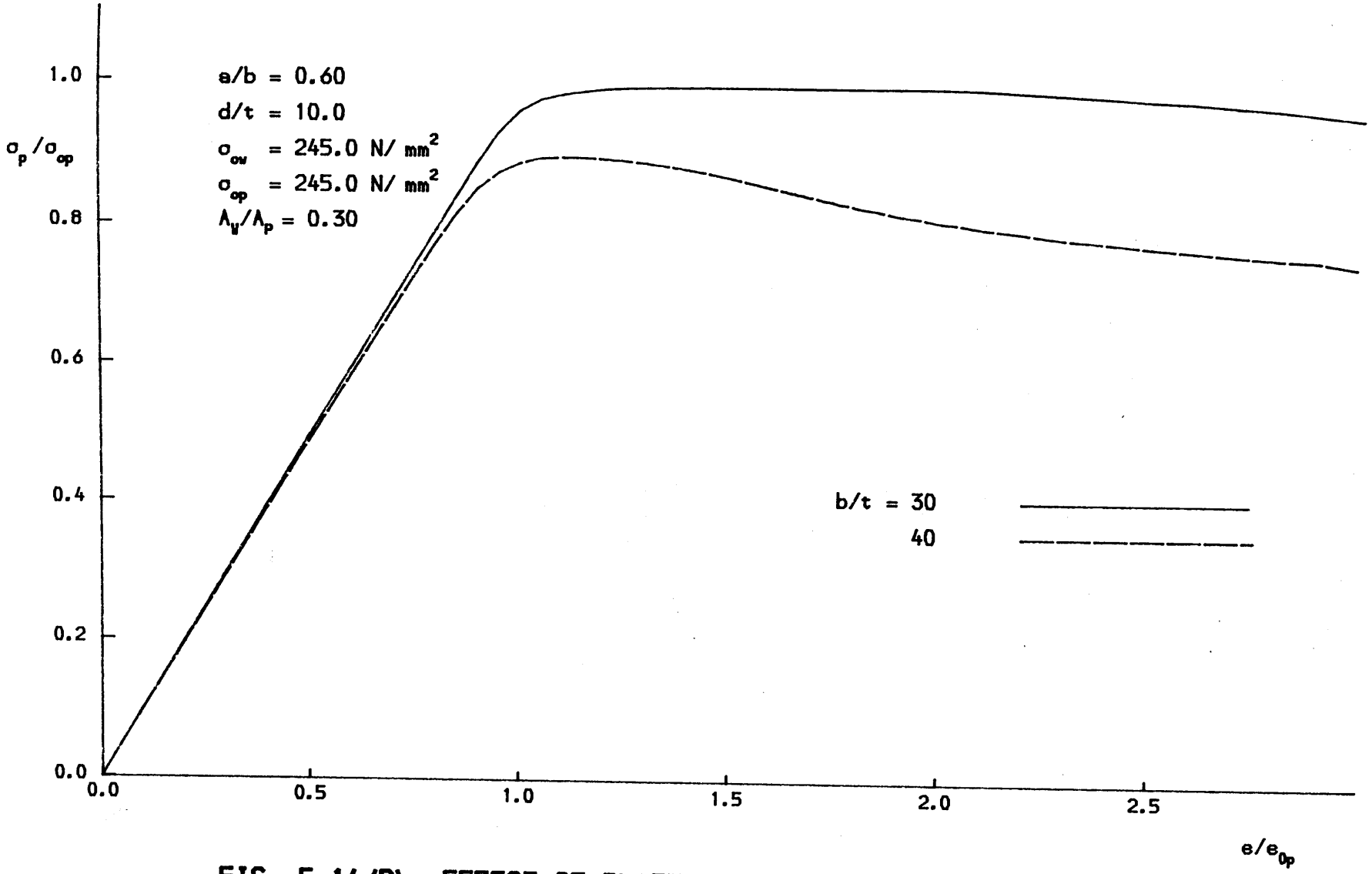

FIG. 5.14 (B) EFFECT OF PLATE SLENDERNESS ON BASE PLATE RESPONSE

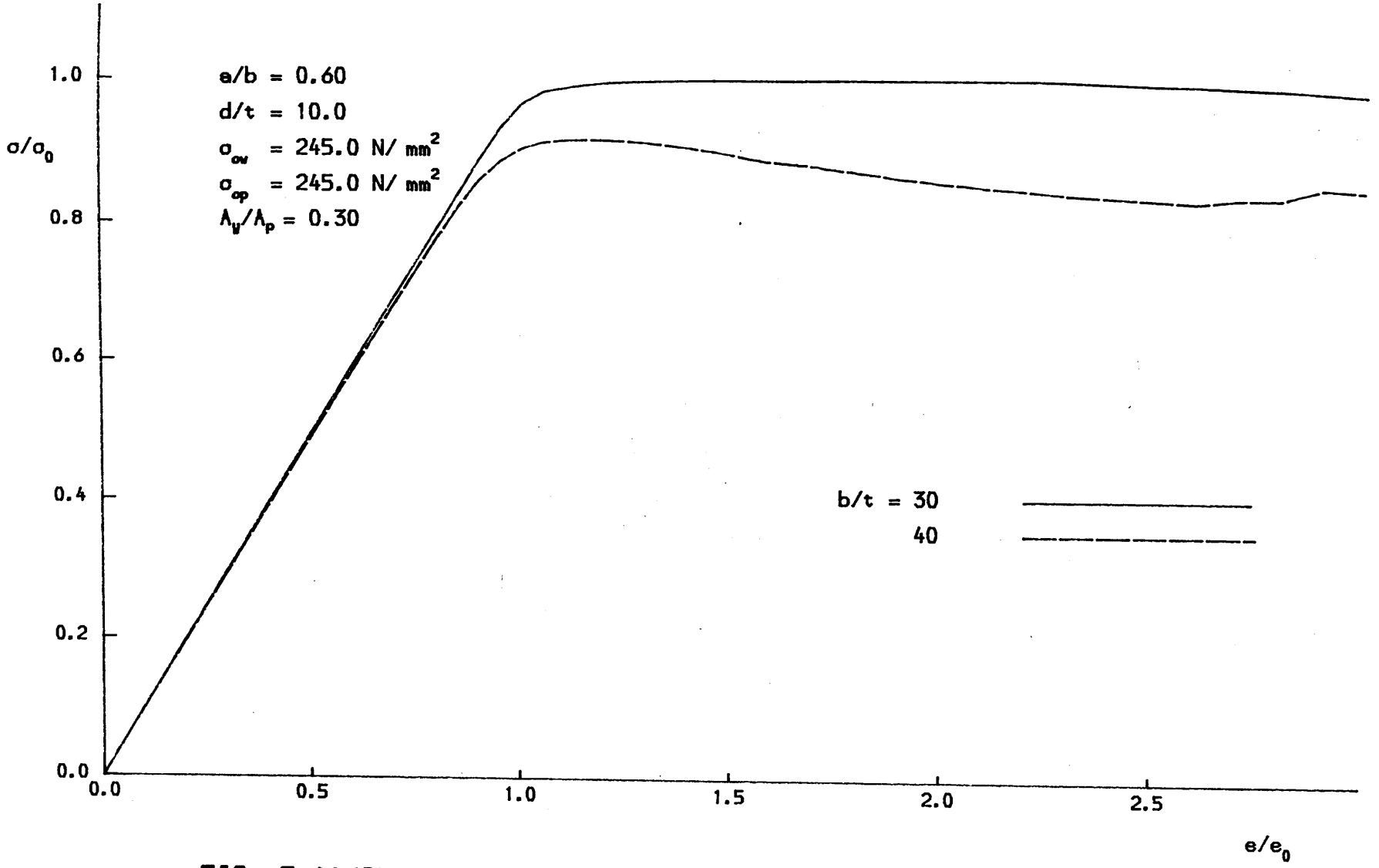

FIG. 5.14 (C) EFFECT OF PLATE SLENDERNESS ON STIFFENED PLATE RESPONSE

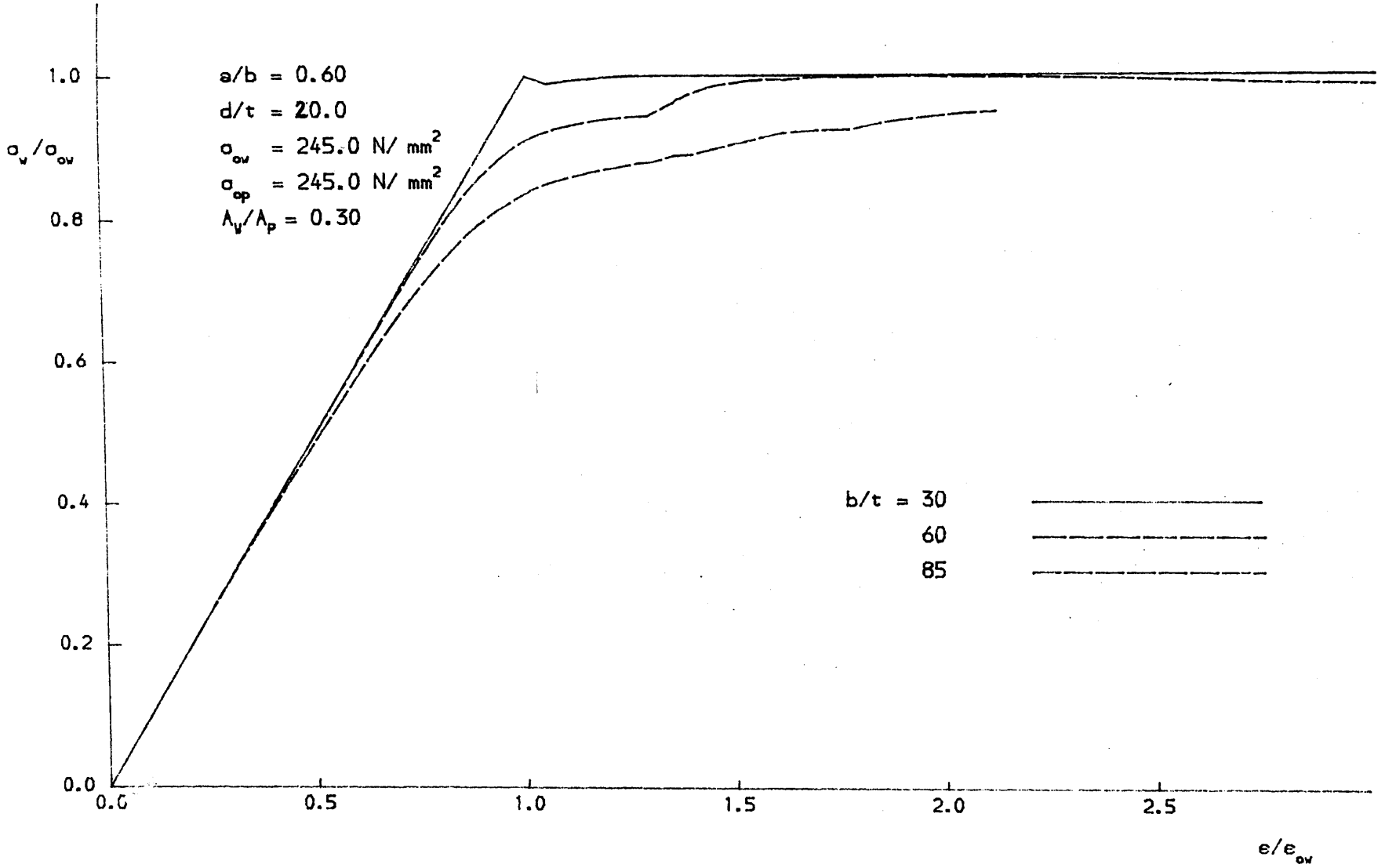

FIG. 5.15(A) EFFECT OF PLATE SLENDERNESS ON STIFFENER RESPONSE

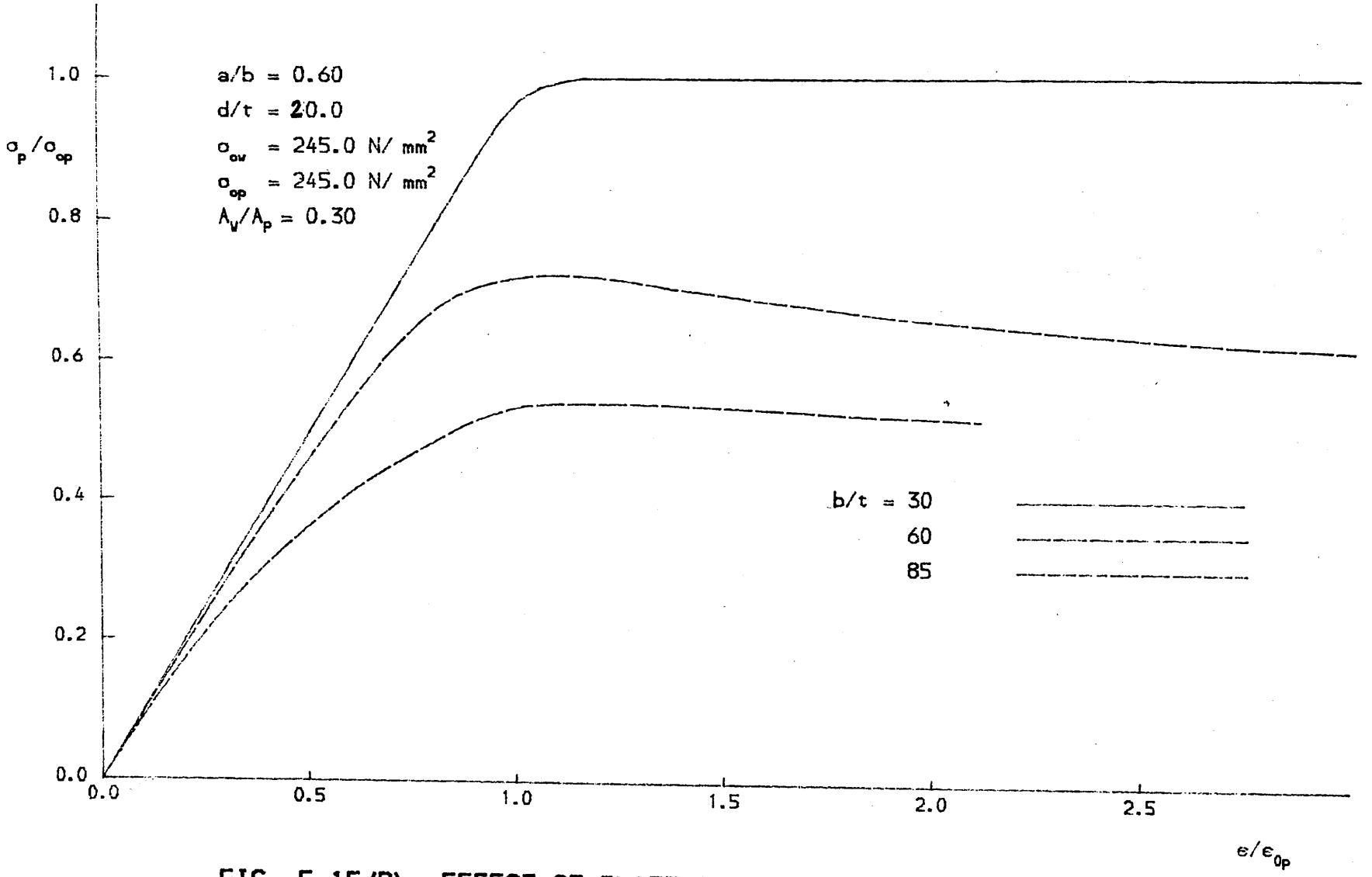

FIG. 5.15 (B) EFFECT OF PLATE SLENDERNESS ON BASE PLATE RESPONSE

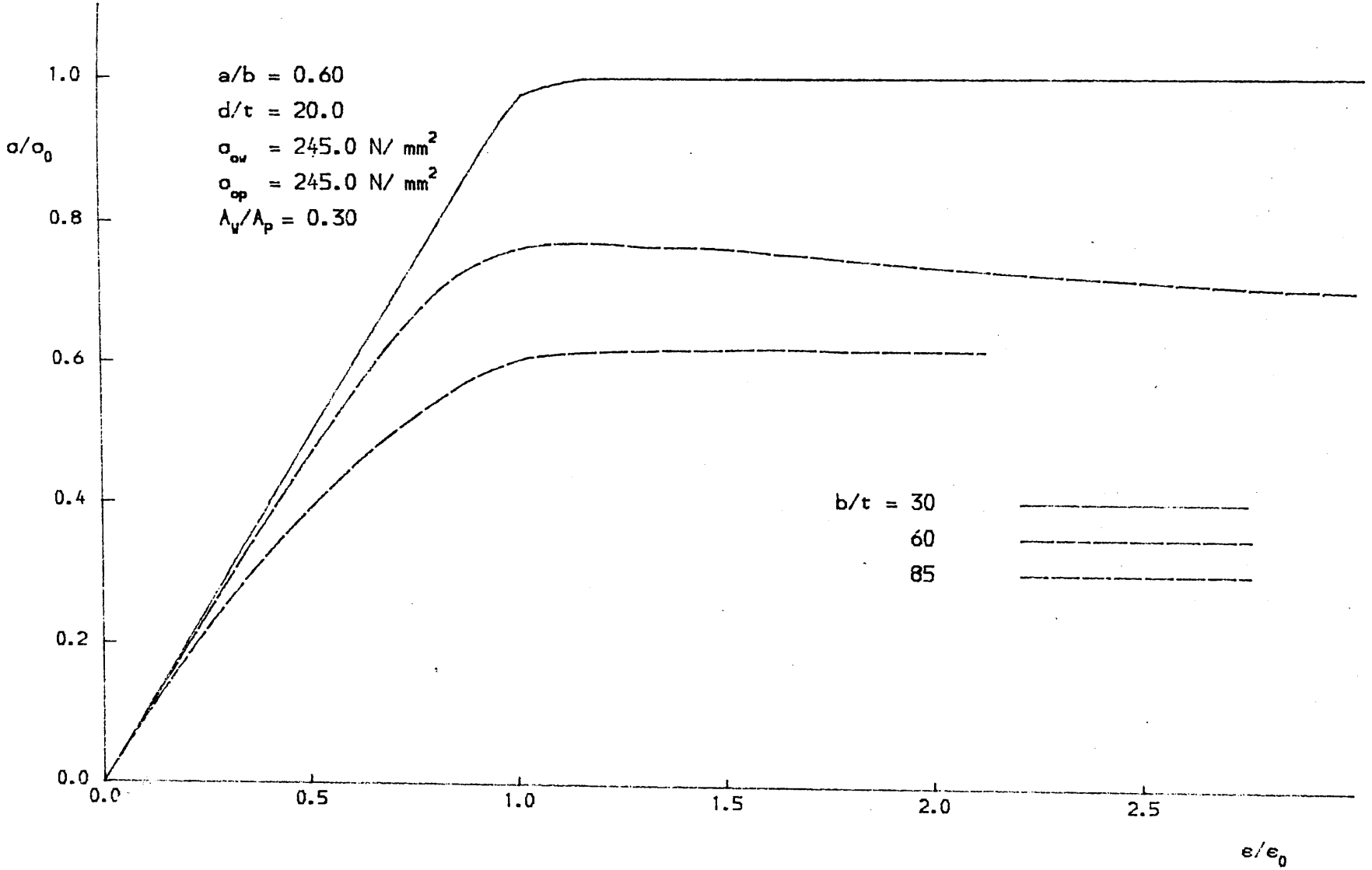

FIG. 5.15(C) EFFECT OF PLATE SLENDERNESS ON STIFFENED PLATE RESPONSE

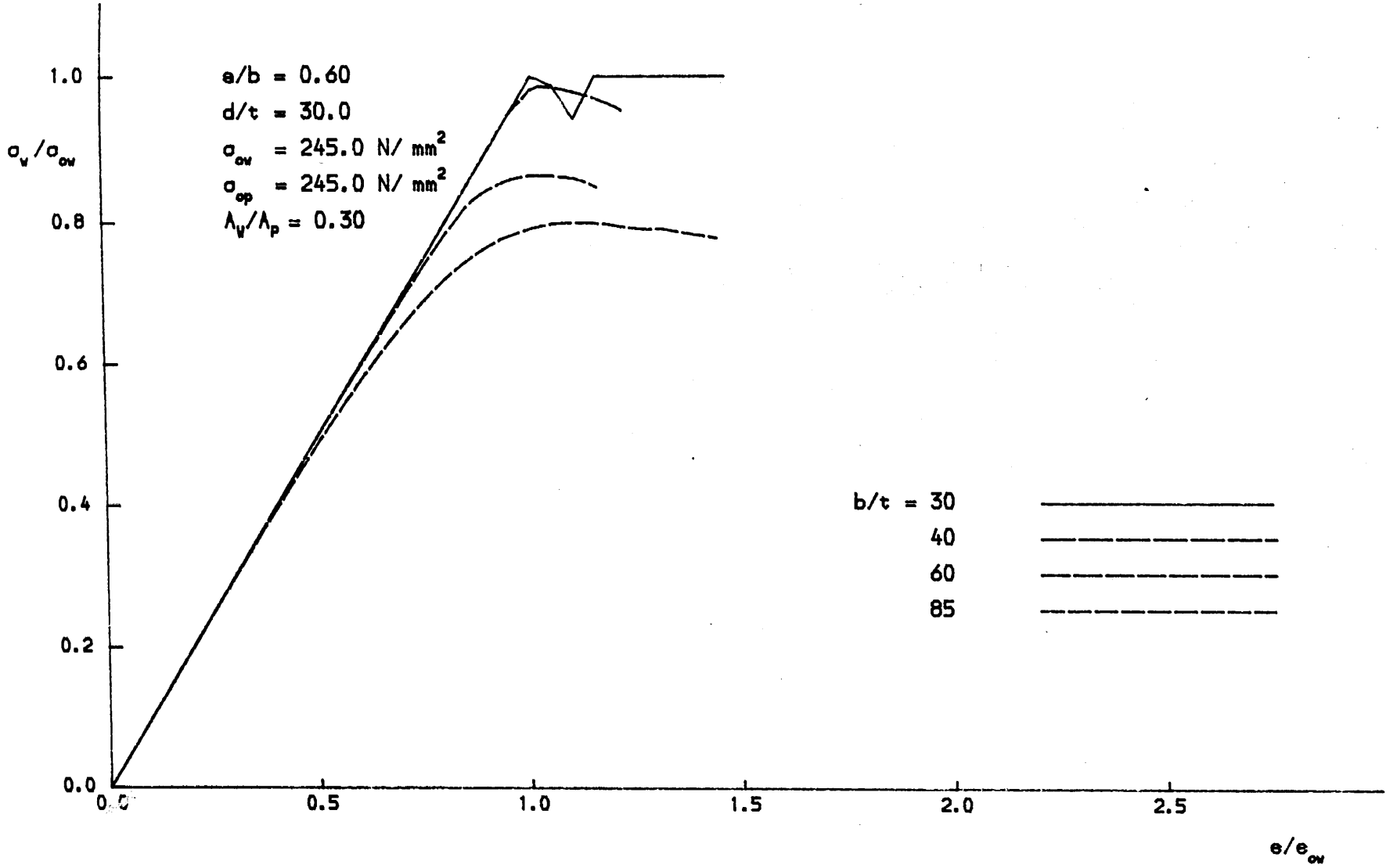

FIG. 5.16(A) EFFECT OF PLATE SLENDERNESS ON STIFFENER RESPONSE

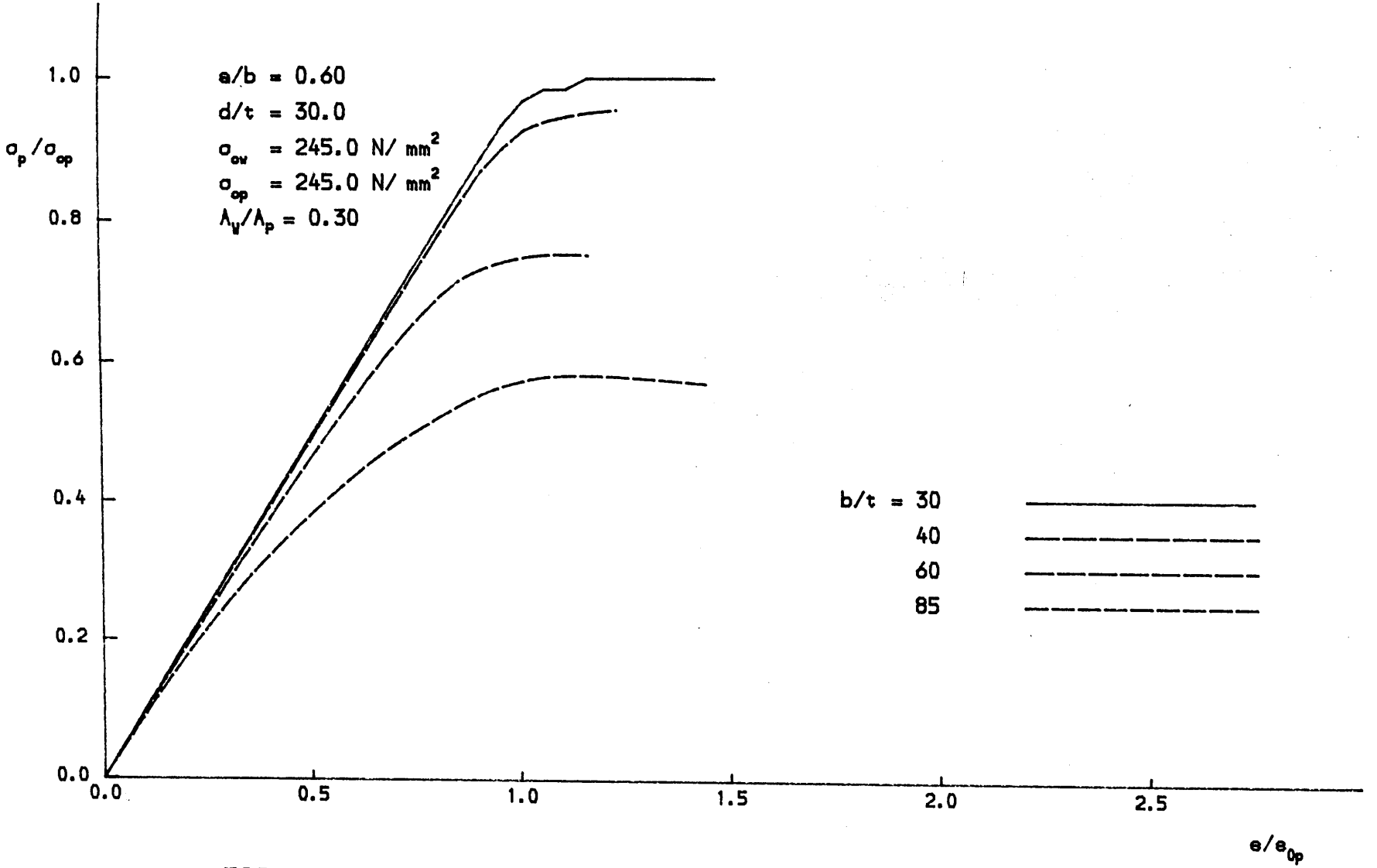

FIG. 5.16 (B) EFFECT OF PLATE SLENDERNESS ON BASE PLATE RESPONSE

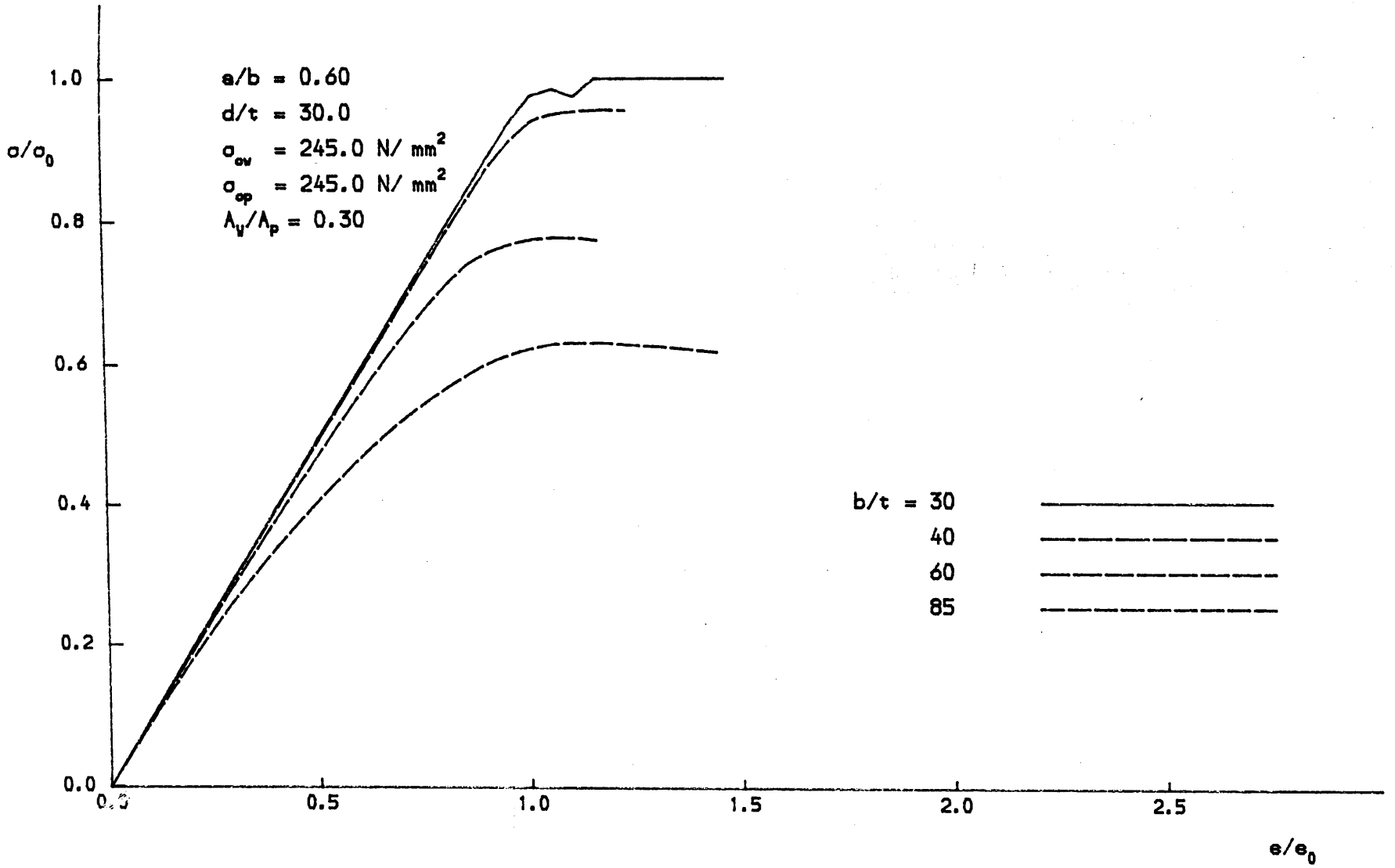

FIG. 5.16(C) EFFECT OF PLATE SLENDERNESS ON STIFFENED PLATE RESPONSE

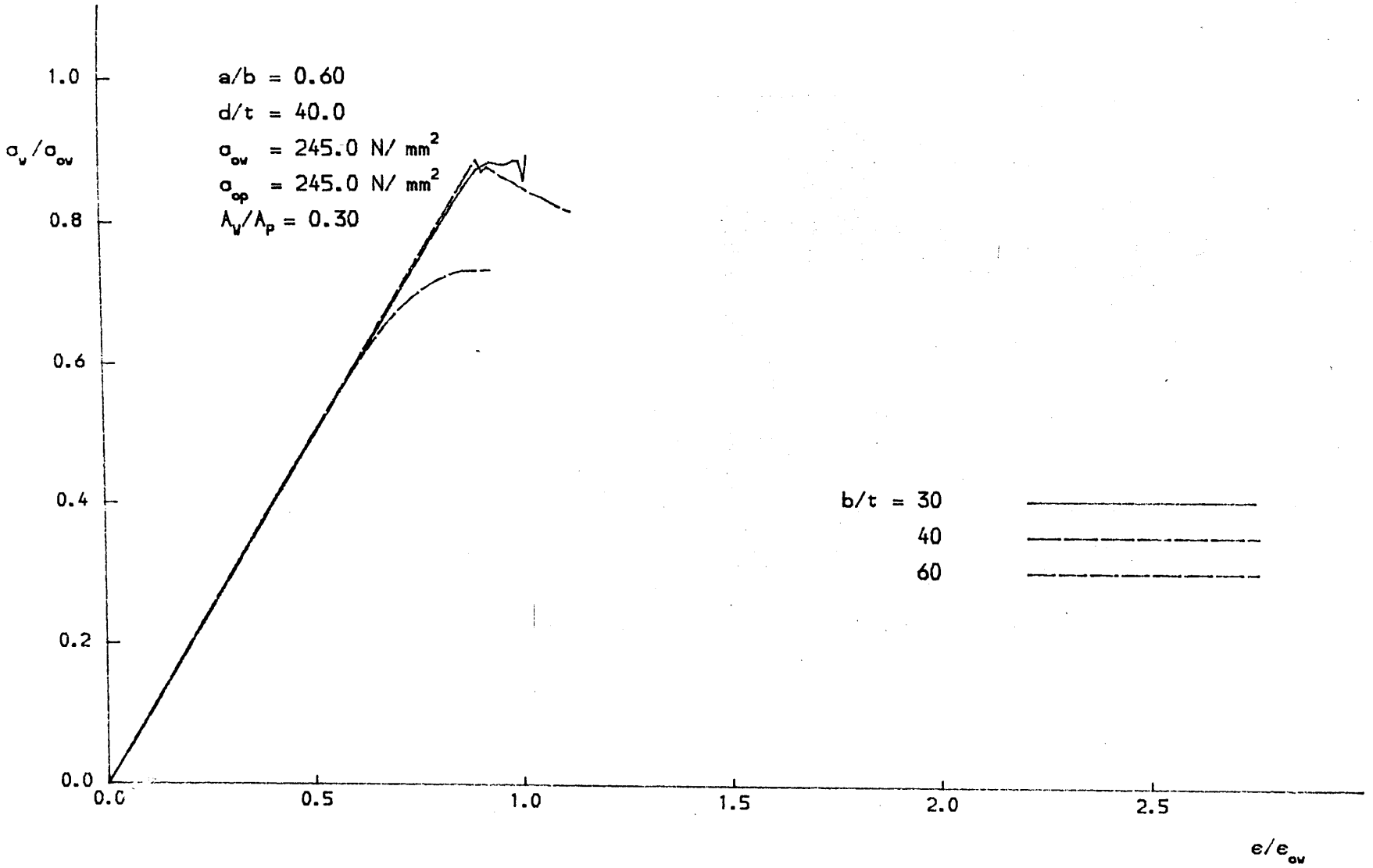

FIG. 5.17(A) EFFECT OF PLATE SLENDERNESS ON STIFFENER RESPONSE

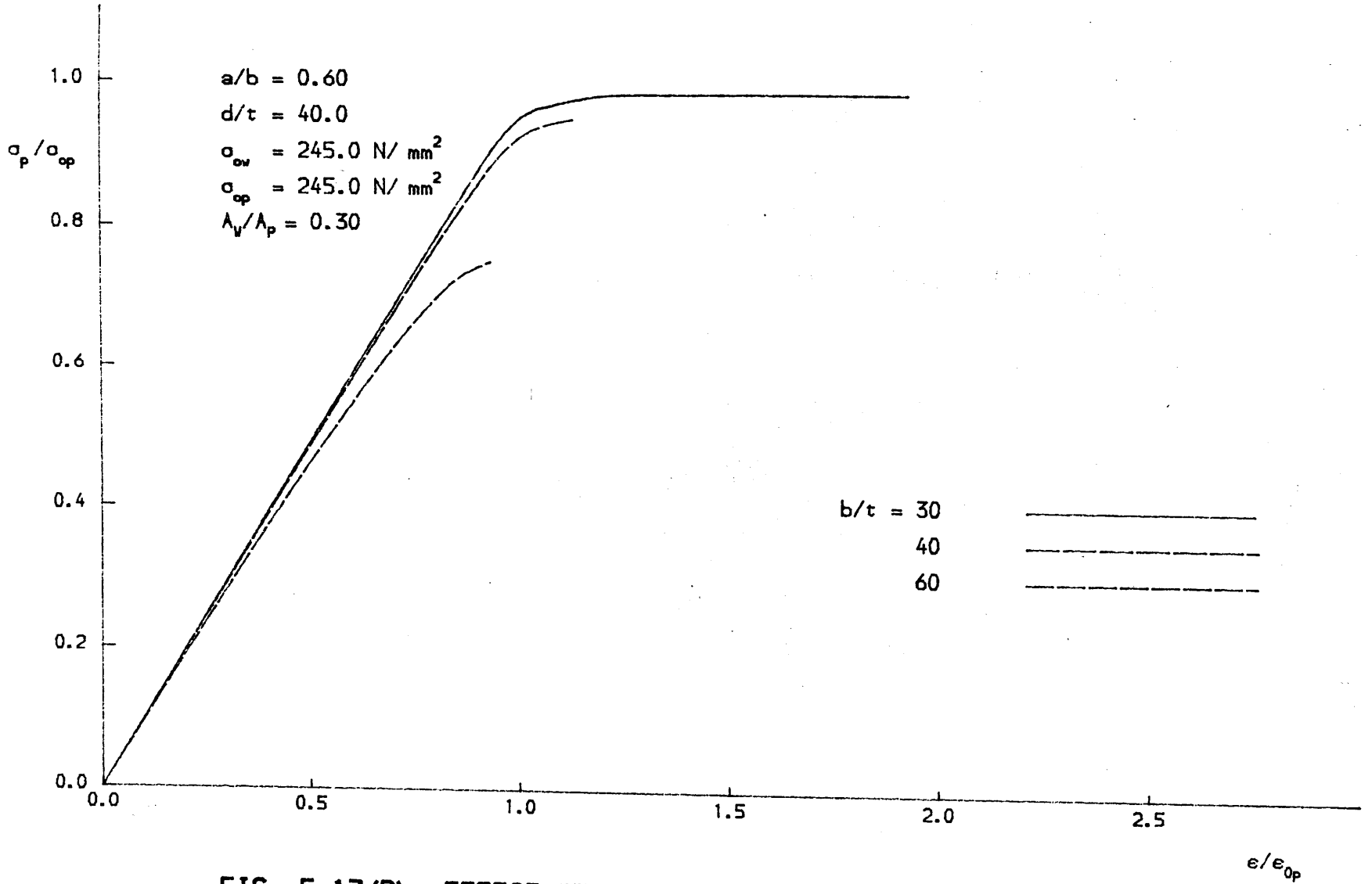

FIG. 5.17 (B) EFFECT OF PLATE SLENDERNESS ON BASE PLATE RESPONSE

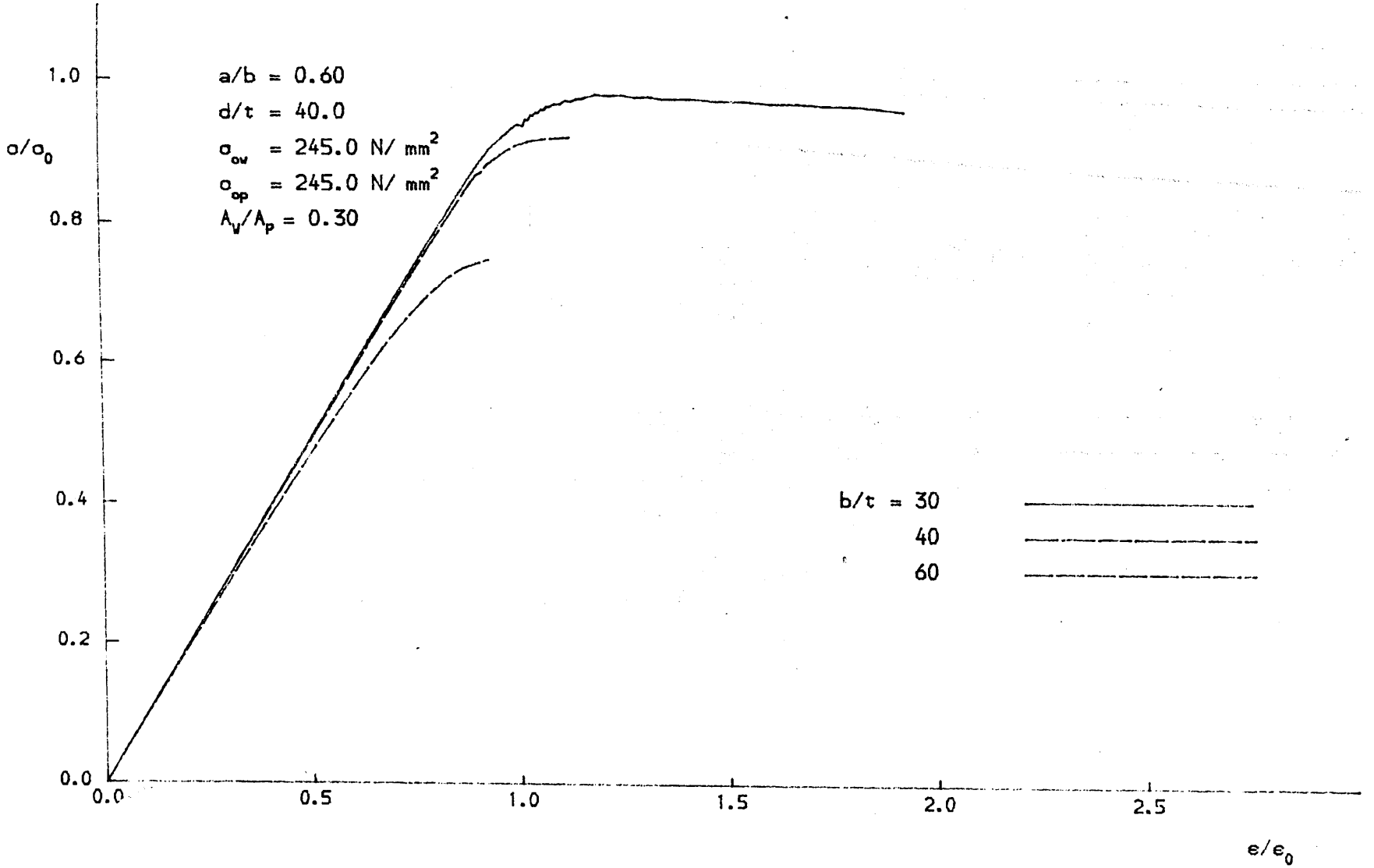

FIG. 5.17(C) EFFECT OF PLATE SLENDERNESS ON STIFFENED PLATE RESPONSE

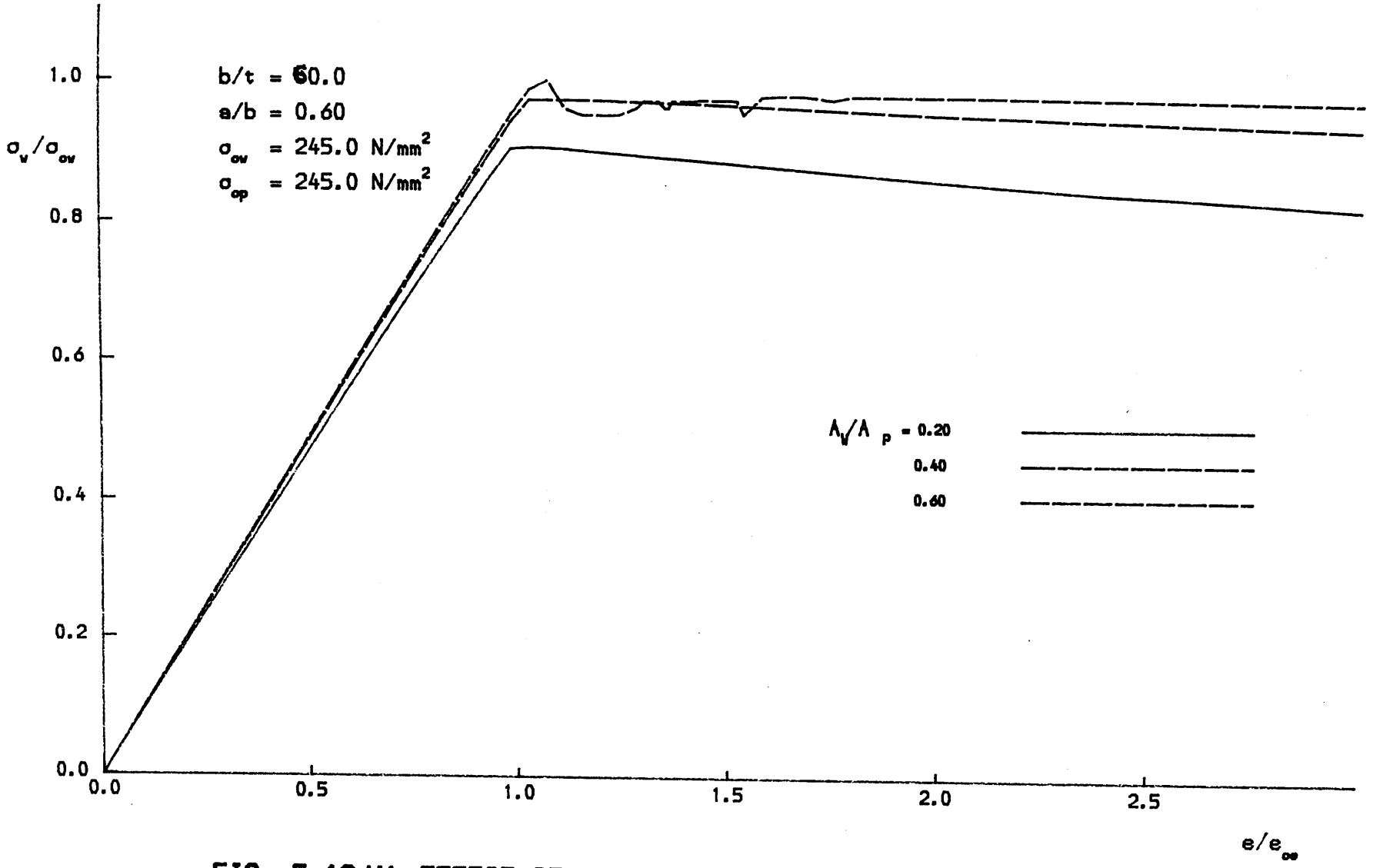

FIG. 5.18(A) EFFECT OF STIFFENER/PLATE AREA RATIO ON STIFFENER RESPONSE

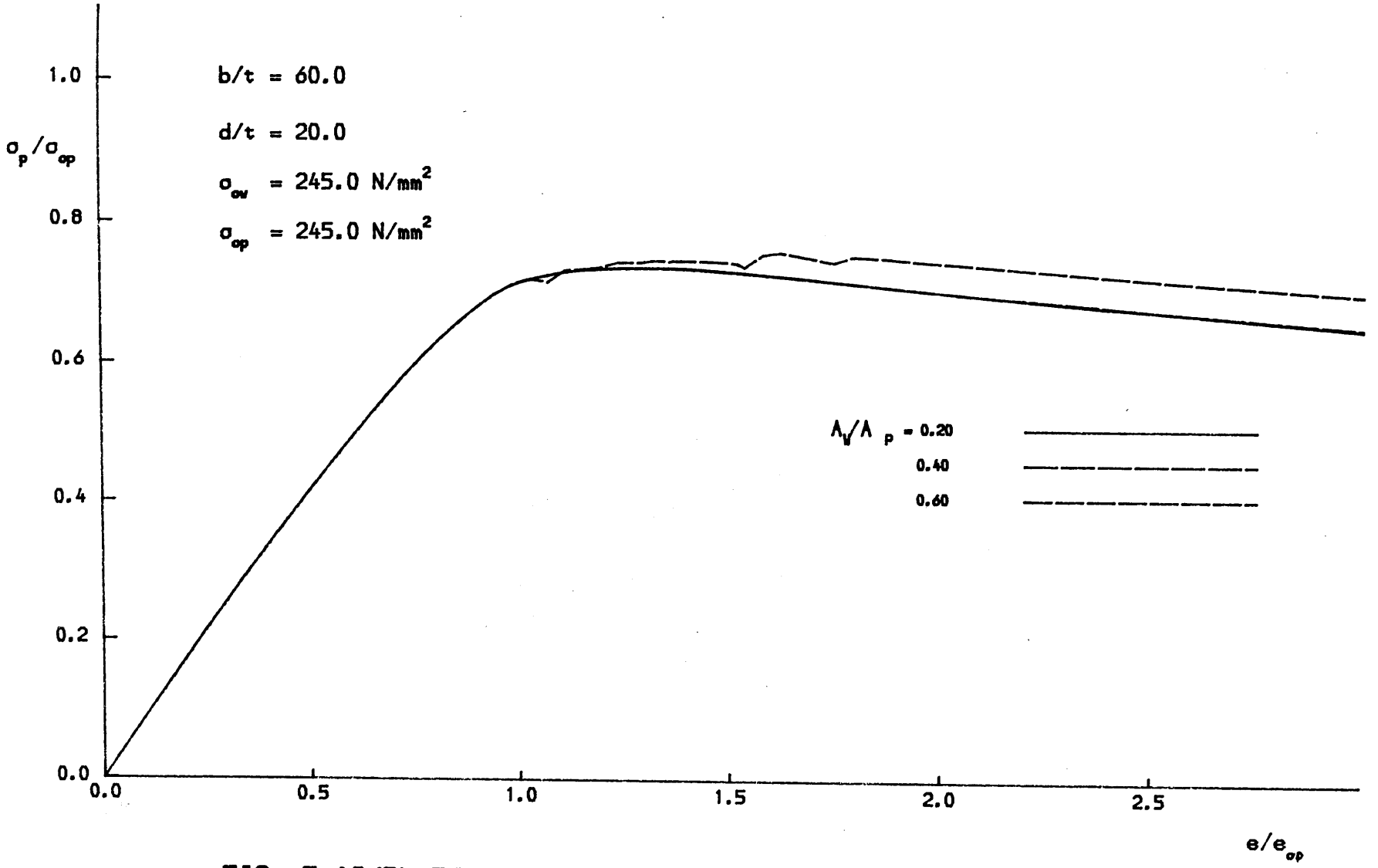

FIG. 5.18(B) EFFECT OF STIFFENER/PLATE AREA RATIO ON BASE PLATE RESPONSE

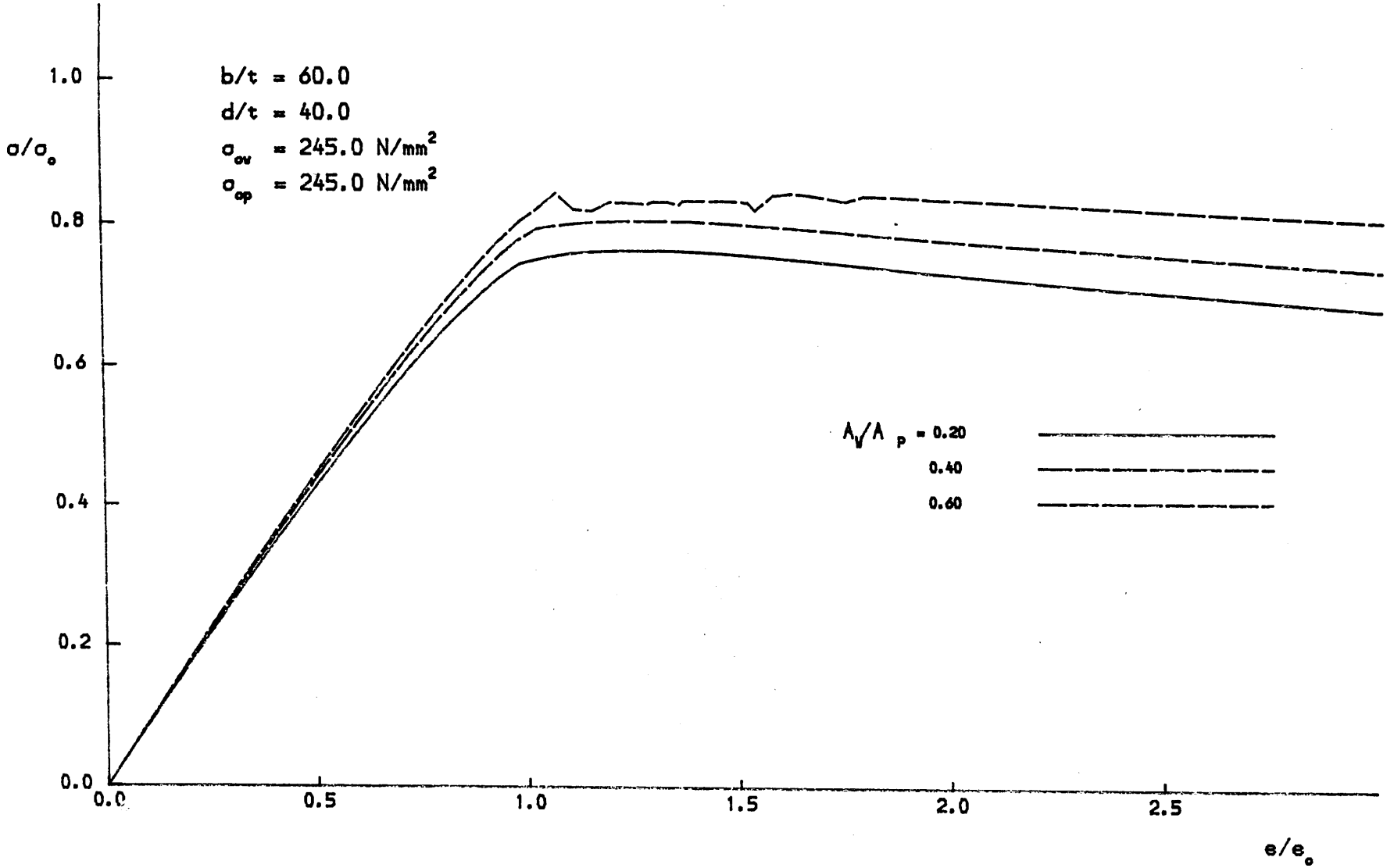

FIG. 5.18(C) EFFECT OF STIFFENER/PLATE AREA RATIO ON STIFFENED PLATE RESPONSE

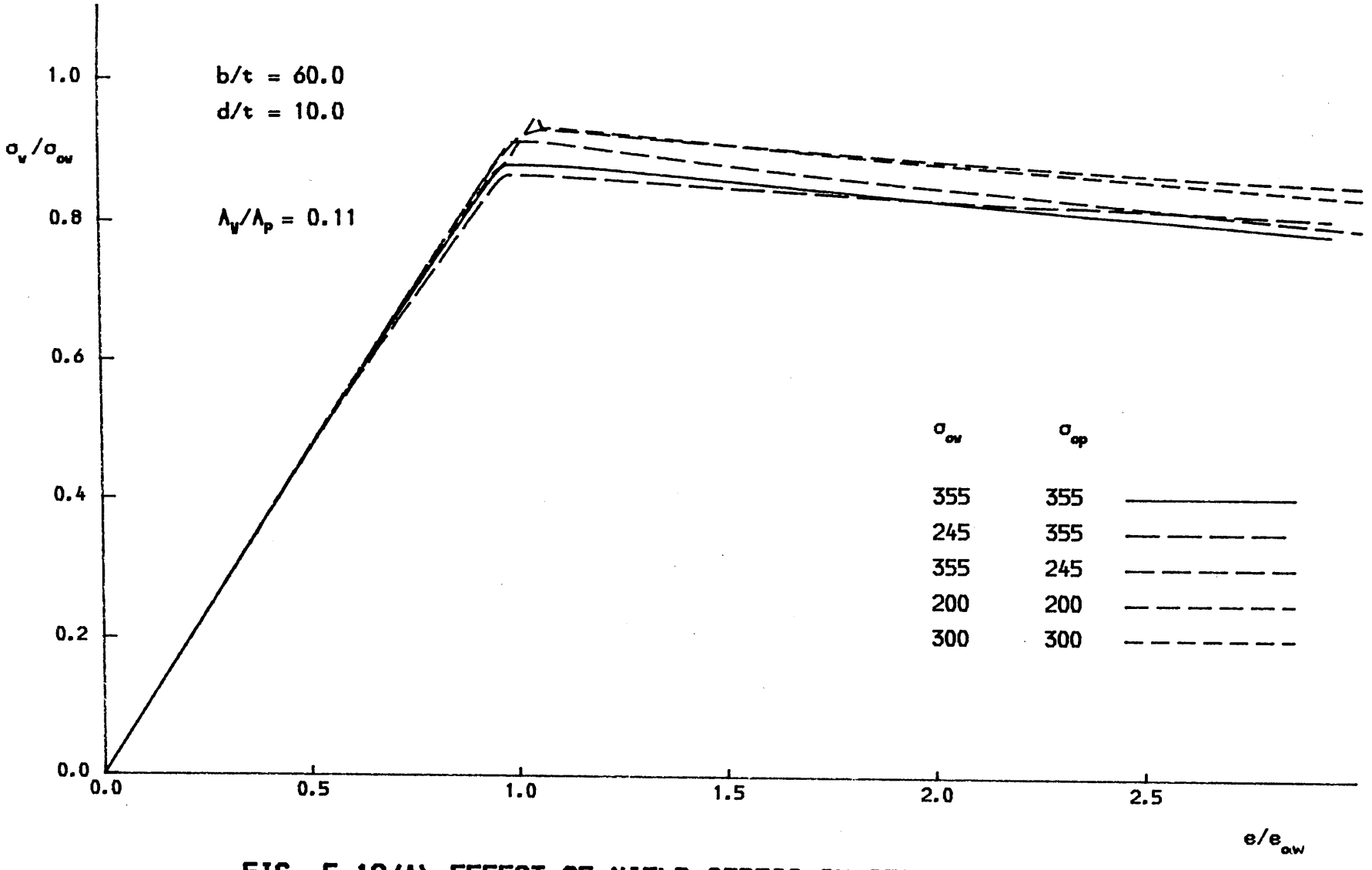

FIG. 5.19(A) EFFECT OF YIELD STRESS ON STIFFENER RESPONSE

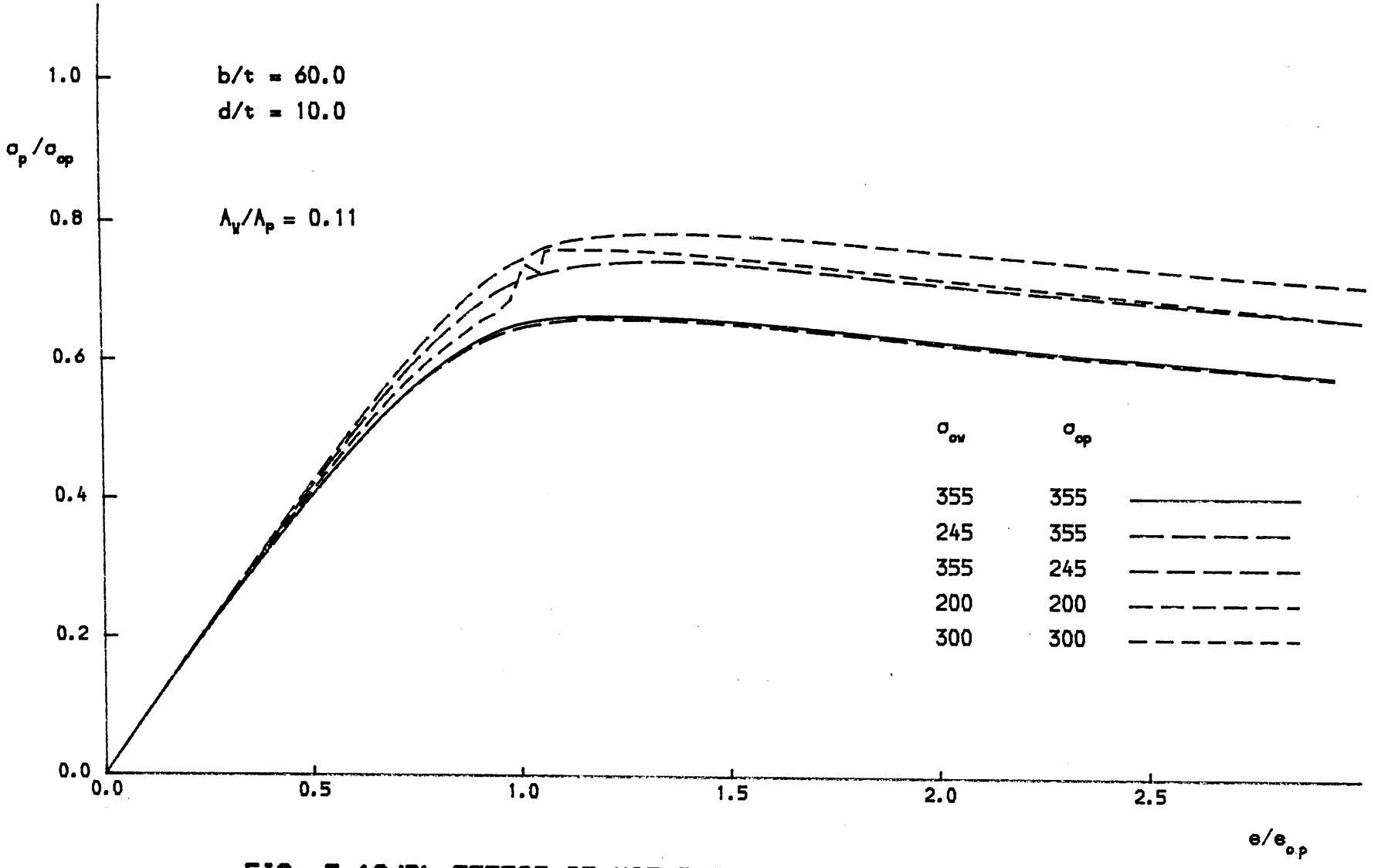

FIG. 5.19(B) EFFECT OF YIELD STRESS ON BASE PLATE RESPONSE

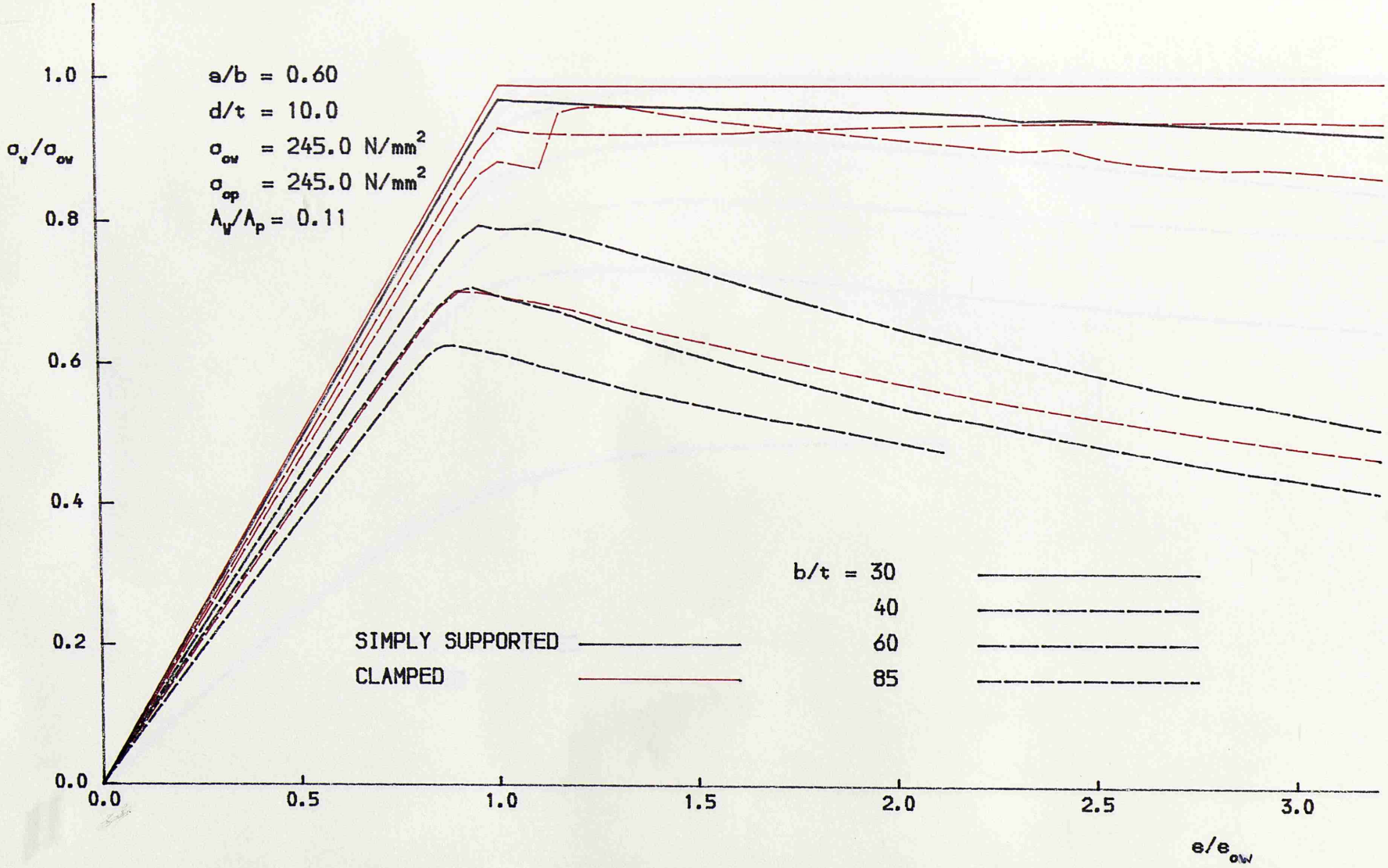

FIG. 5.20(A) EFFECT OF BOUNDARY CONDITIONS ON STIFFENER RESPONSE

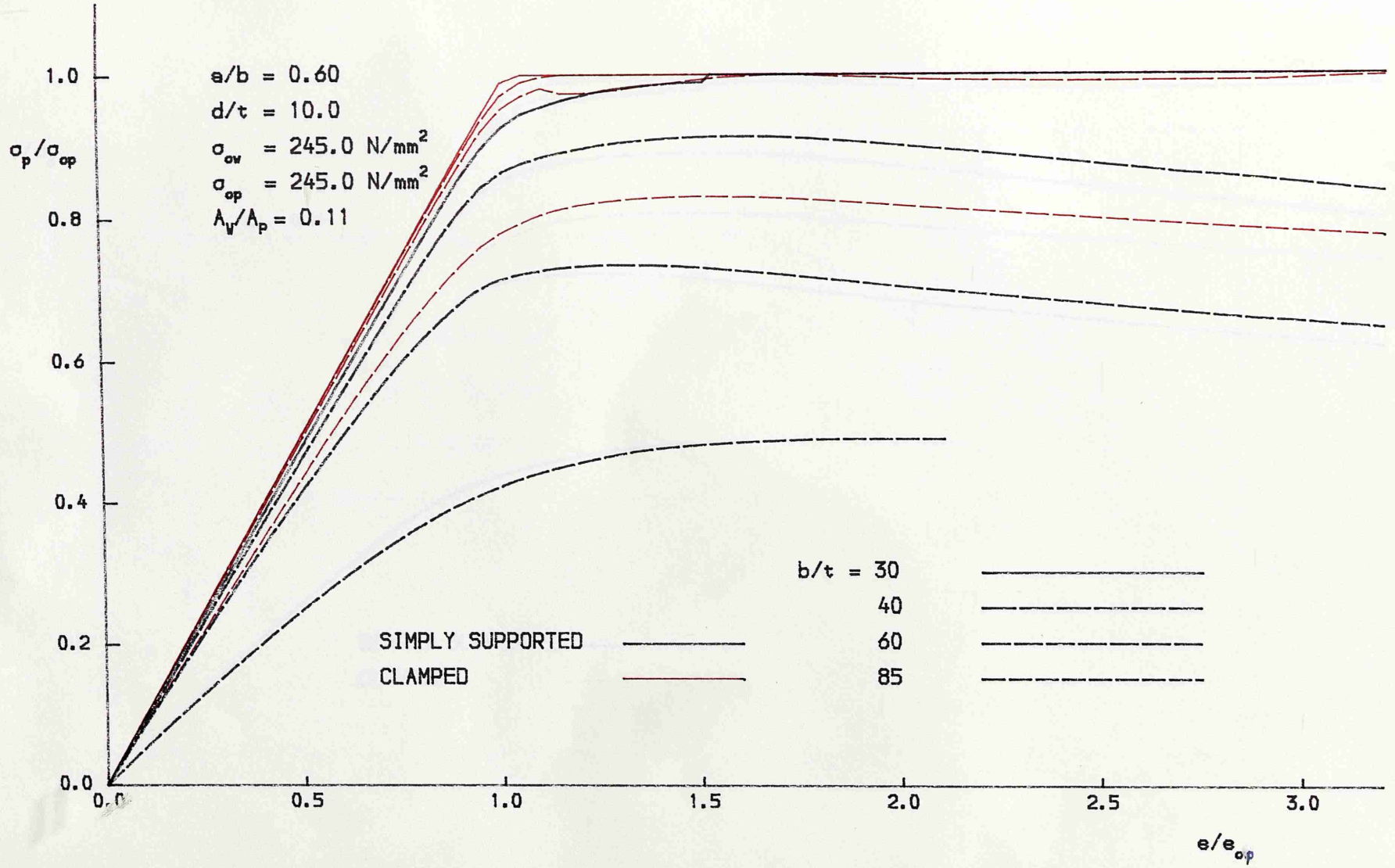

FIG. 5.20 (B) EFFECT OF BOUNDARY CONDITIONS ON BASE PLATE RESPONSE

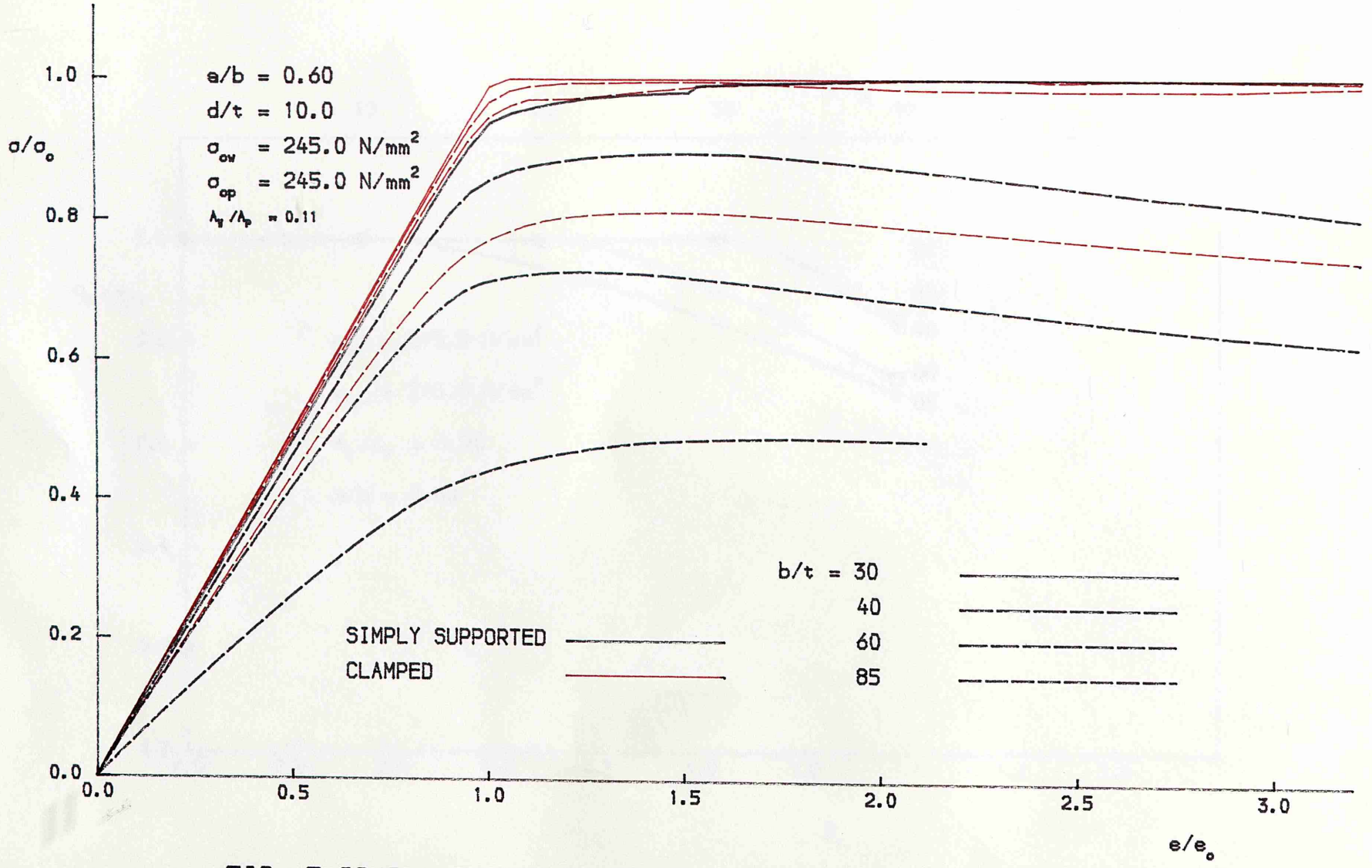

FIG. 5.20 (C) EFFECT OF BOUNDARY CONDITIONS ON STIFFENED PLATE RESPONSE

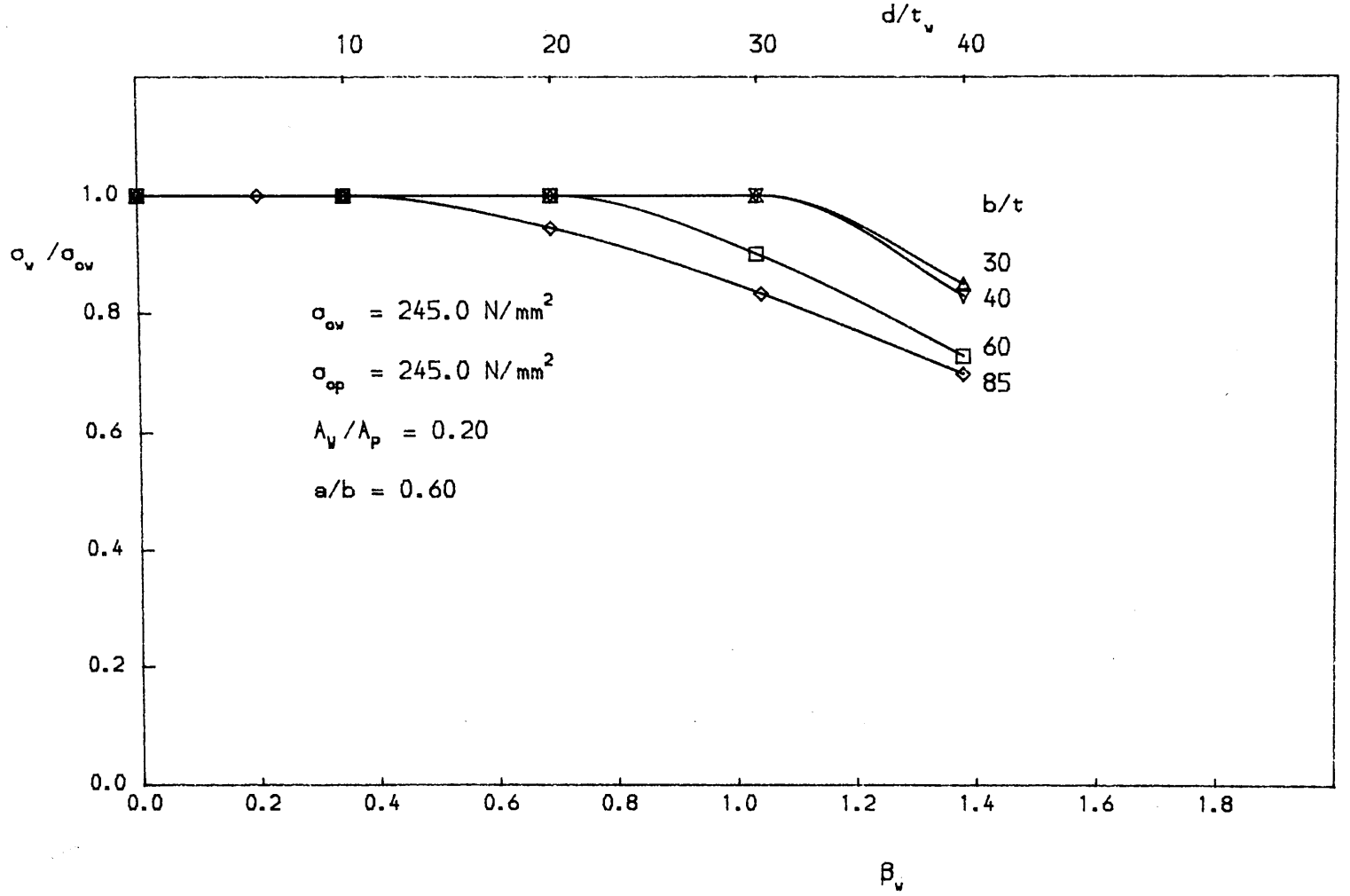

FIG 5.21 (A) MAXIMUM STRENGTH CURVES FOR FLATBAR STIFFENERS

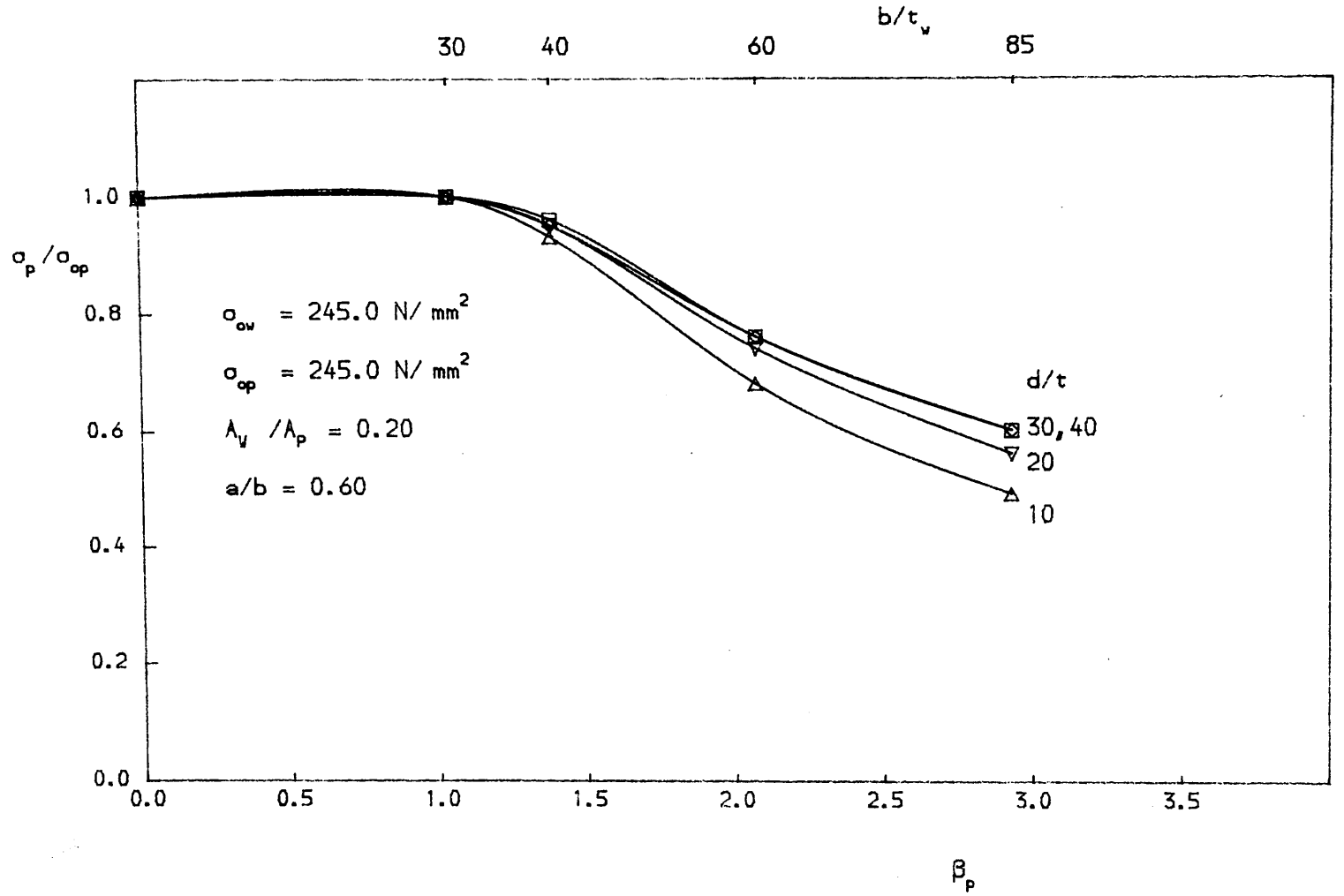

FIG 5.21 (B) MAXIMUM STRENGTH CURVES FOR BASE PLATE

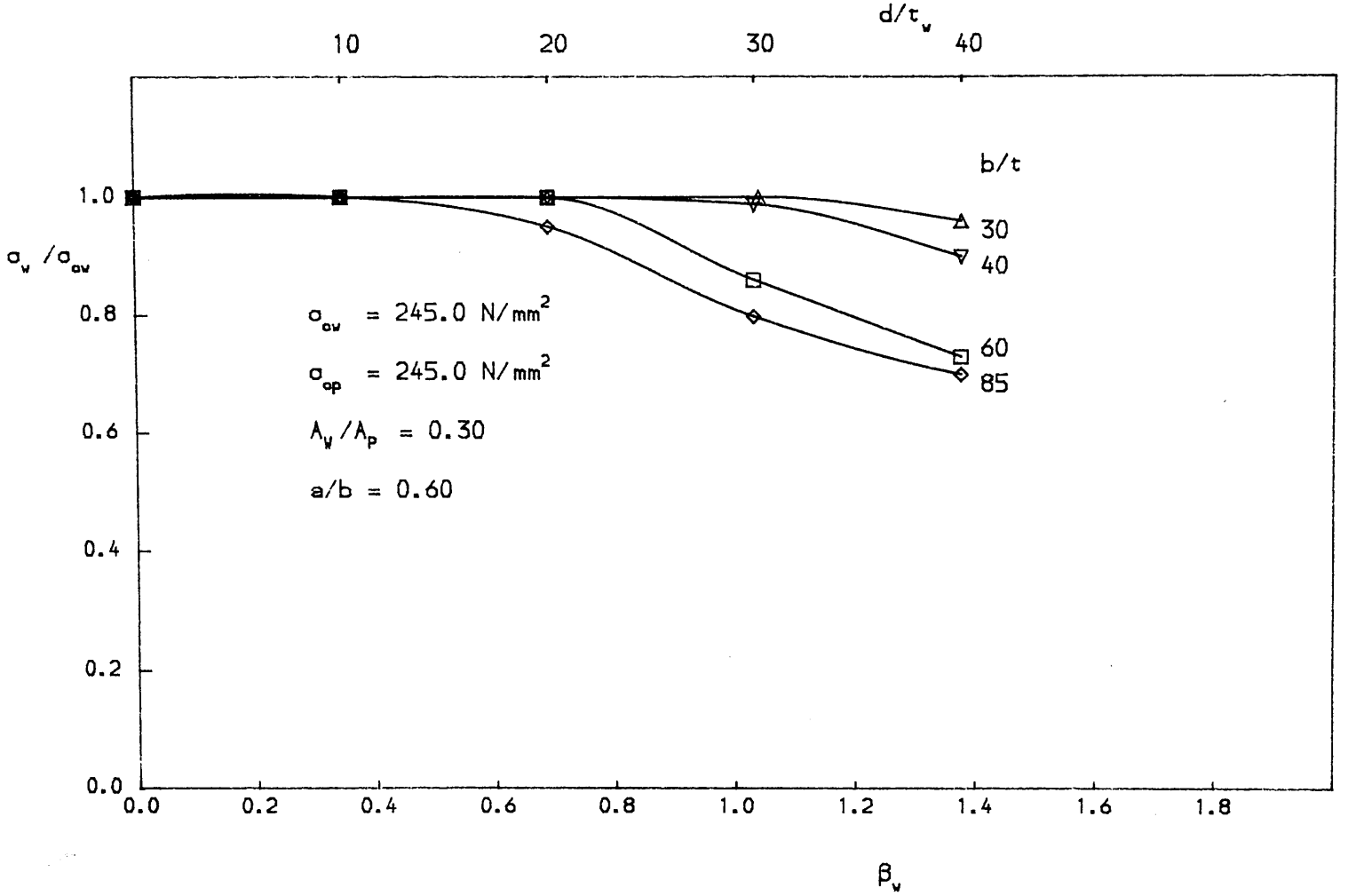

FIG 5.22(A) MAXIMUM STRENGTH CURVES FOR FLATBAR STIFFENERS

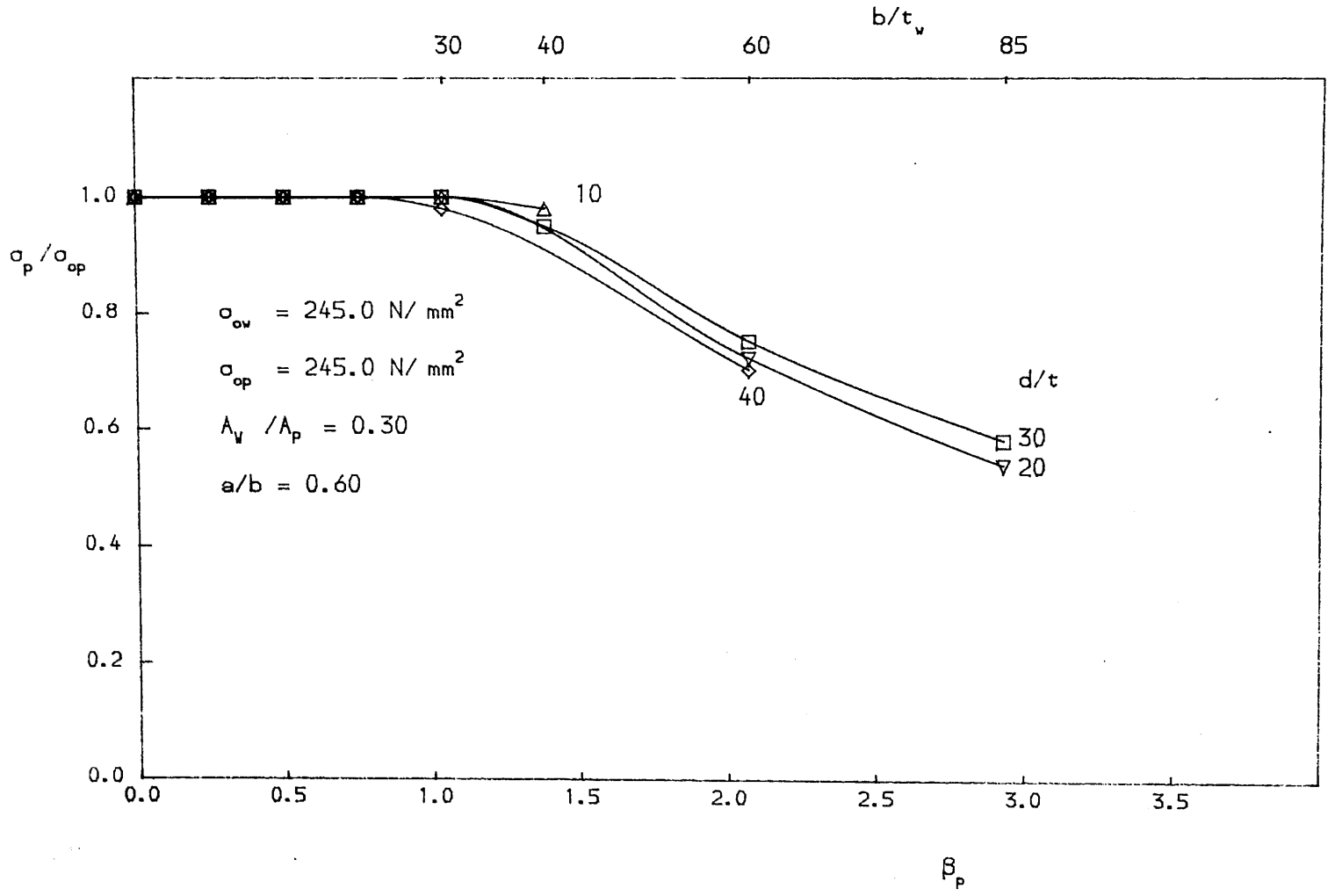

FIG 5.22 (B) MAXIMUM STRENGTH CURVES FOR BASE PLATE

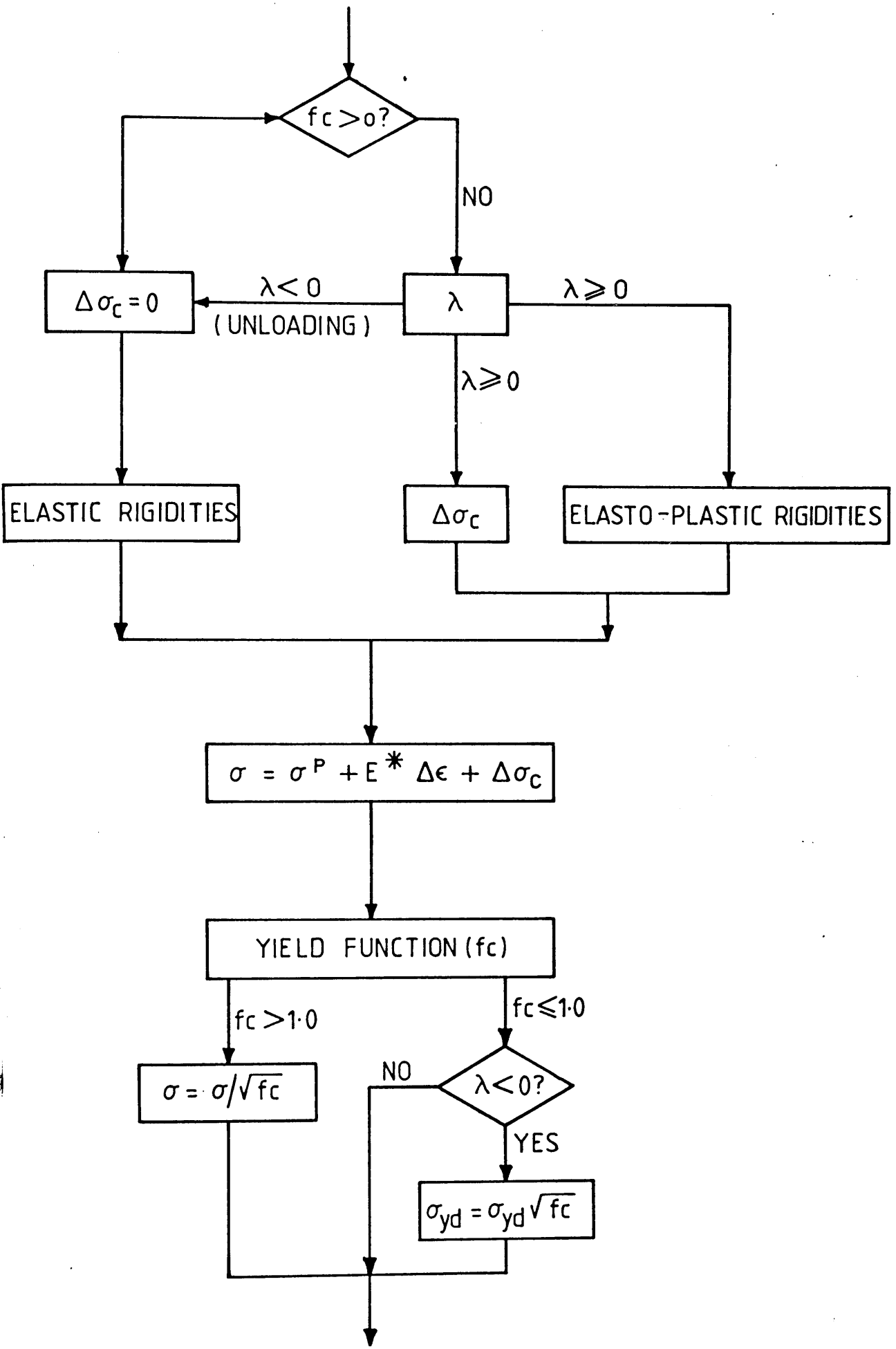

Fig. 6·1. DYNAMIC ANALYSIS CYCLE — YIELD FUNCTION and ELASTO-PLASTIC RIGIDITIES

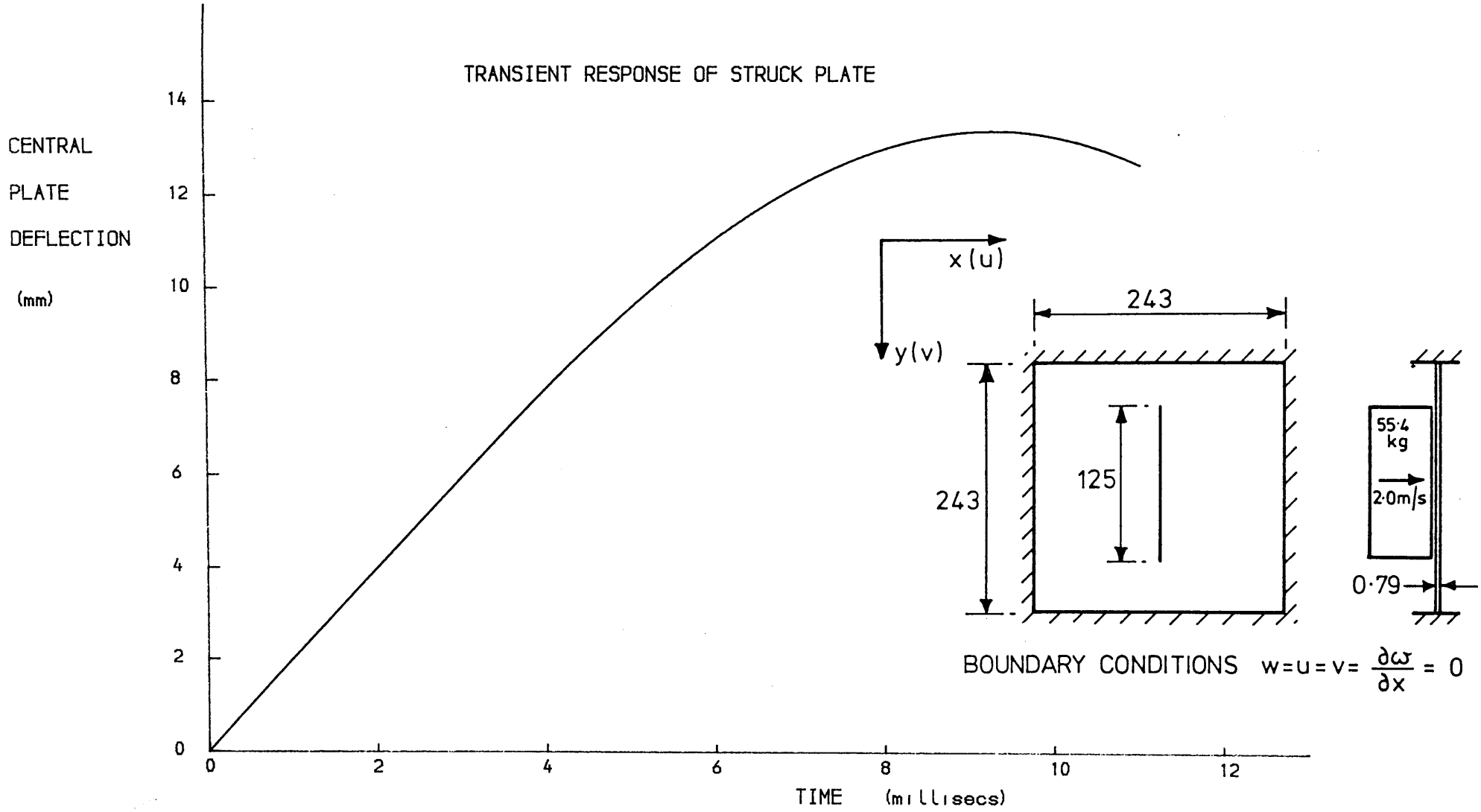

FIG. 6.2 FLAT PLATE UNDER LINE LOAD IMPACT

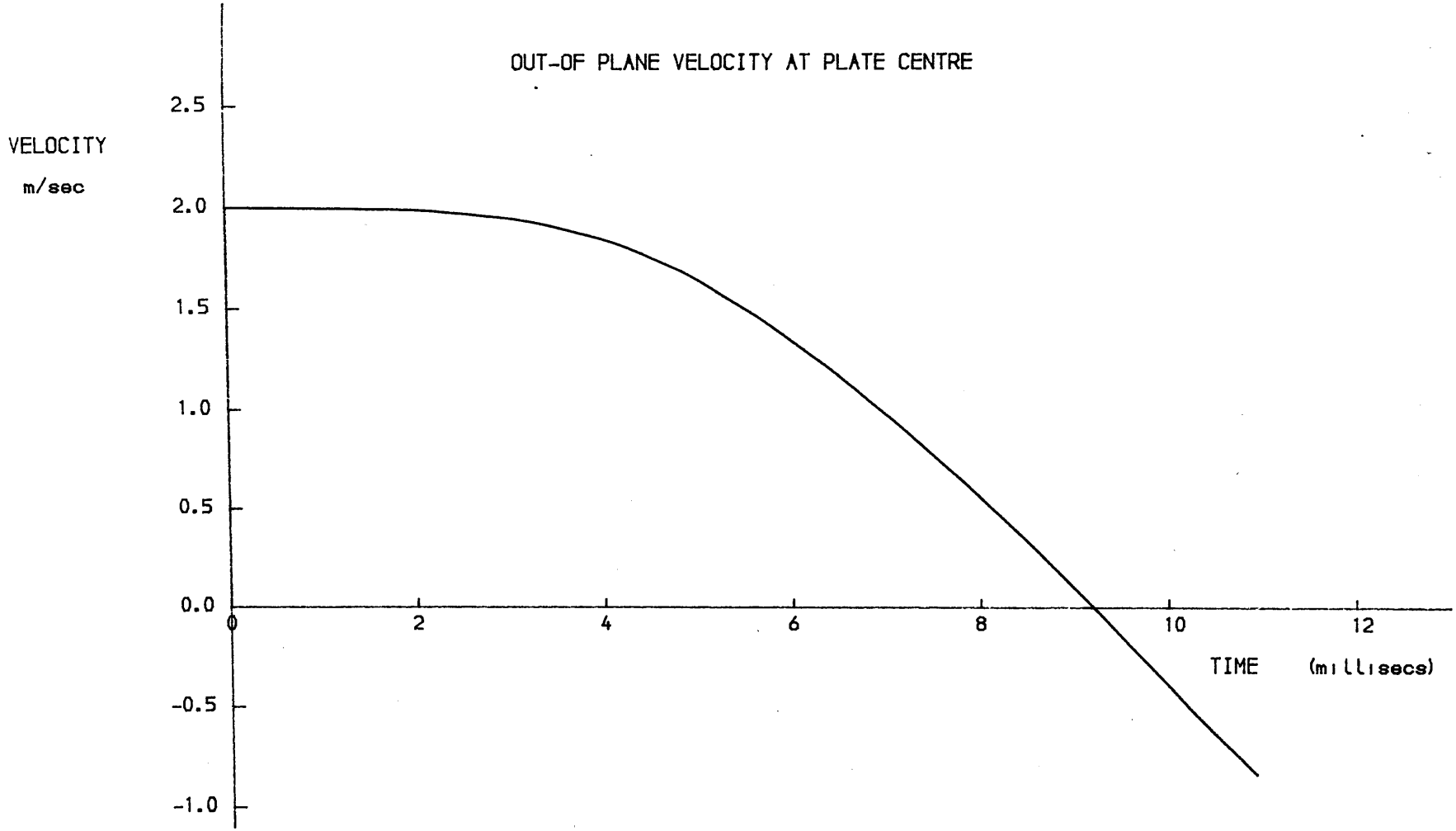

FIG. 6.3 FLAT PLATE UNDER LINE LOAD IMPACT

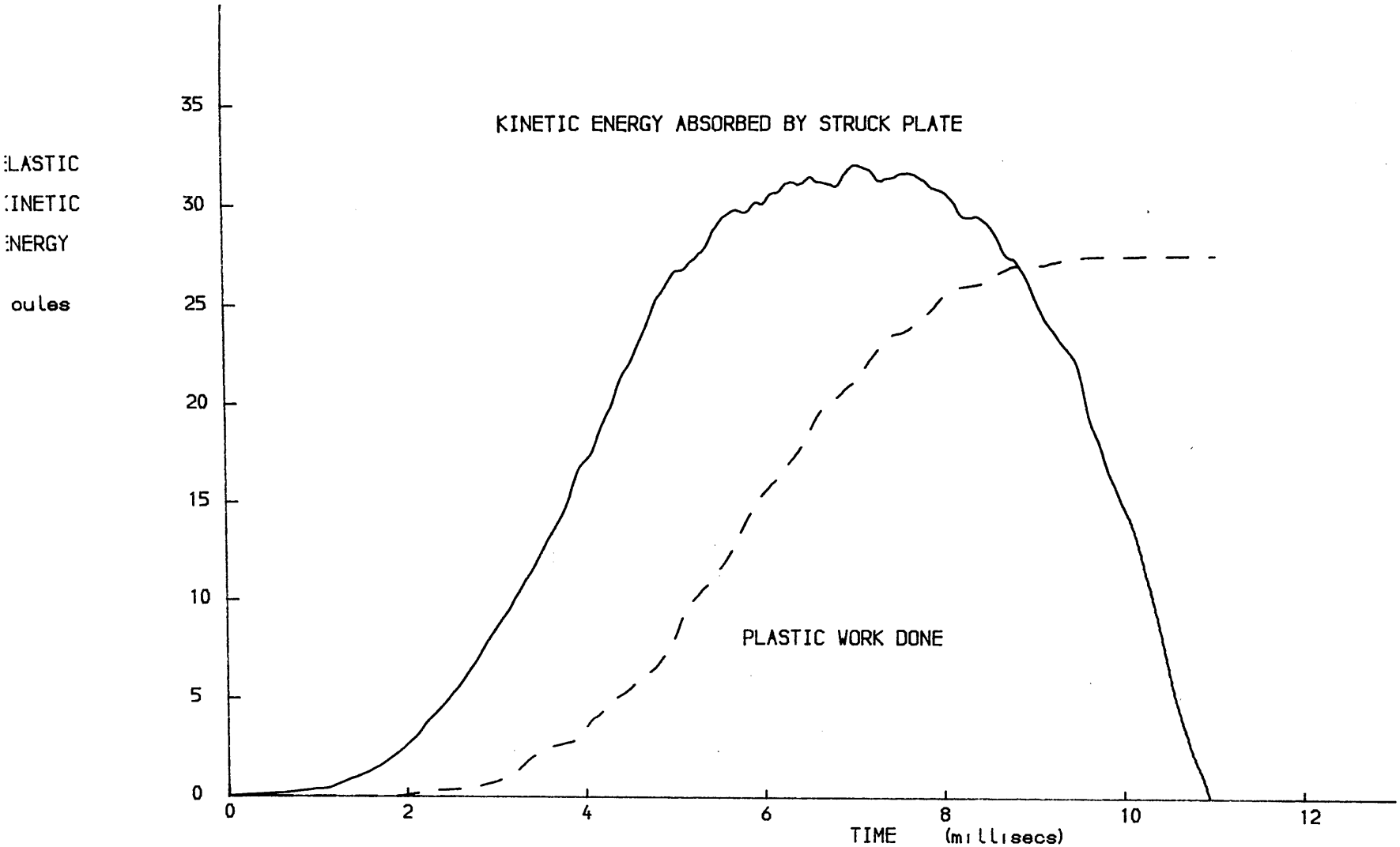

FIG. 6.4 FLAT PLATE UNDER LINE LOAD IMPACT

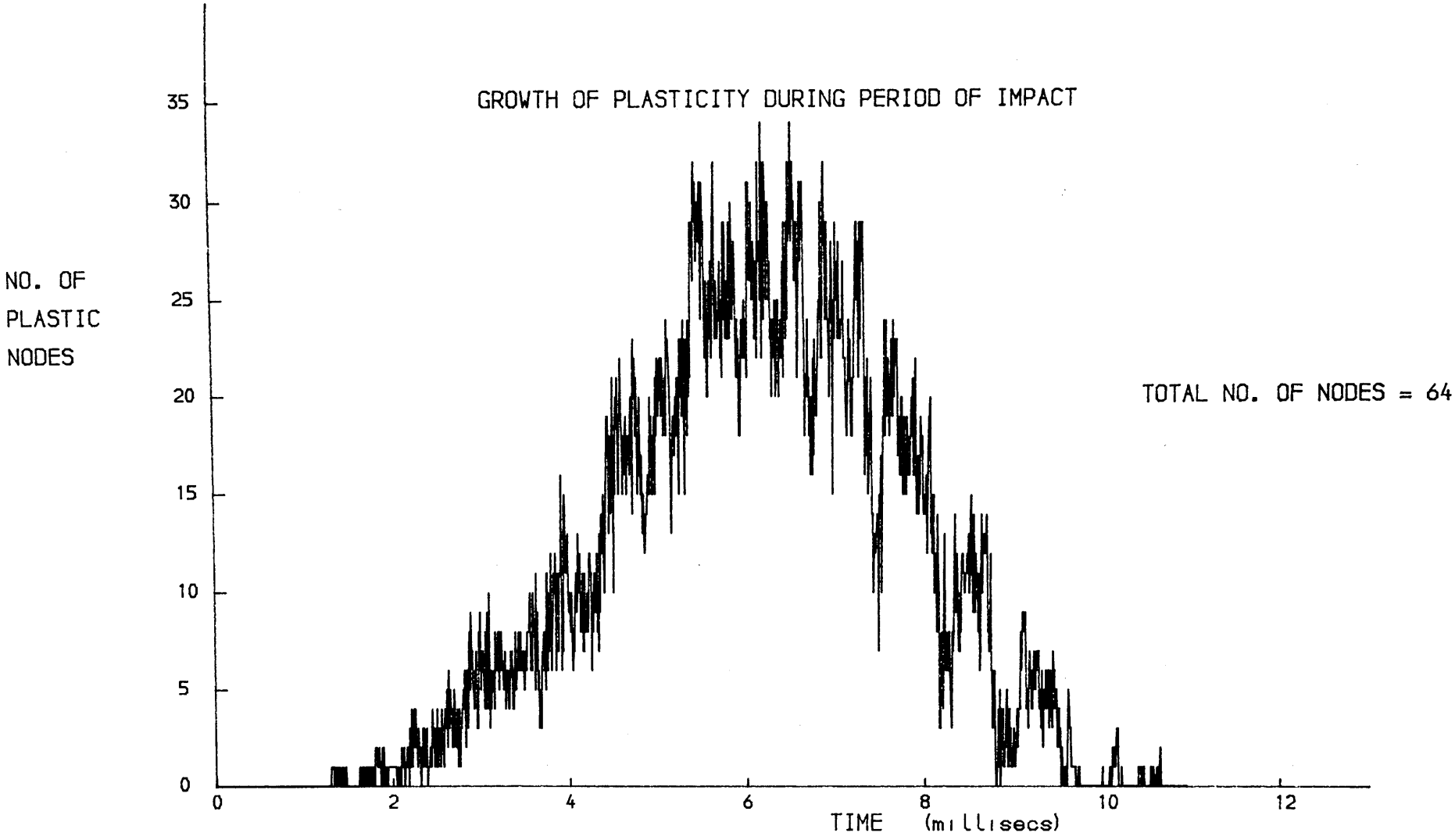

FIG. 6.5 FLAT PLATE UNDER LINE LOAD IMPACT

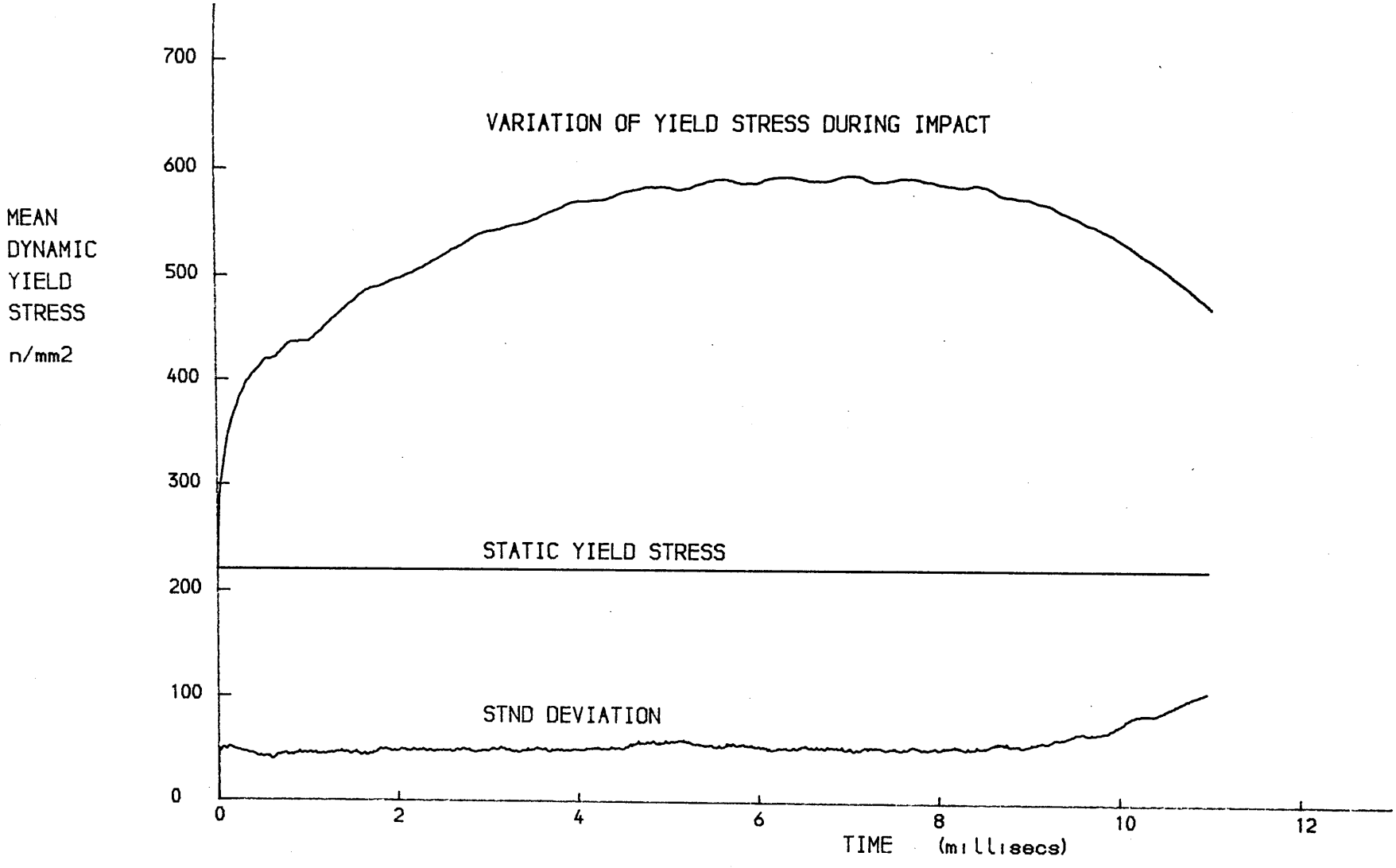

FIG. 6.6 FLAT PLATE UNDER LINE LOAD IMPACT

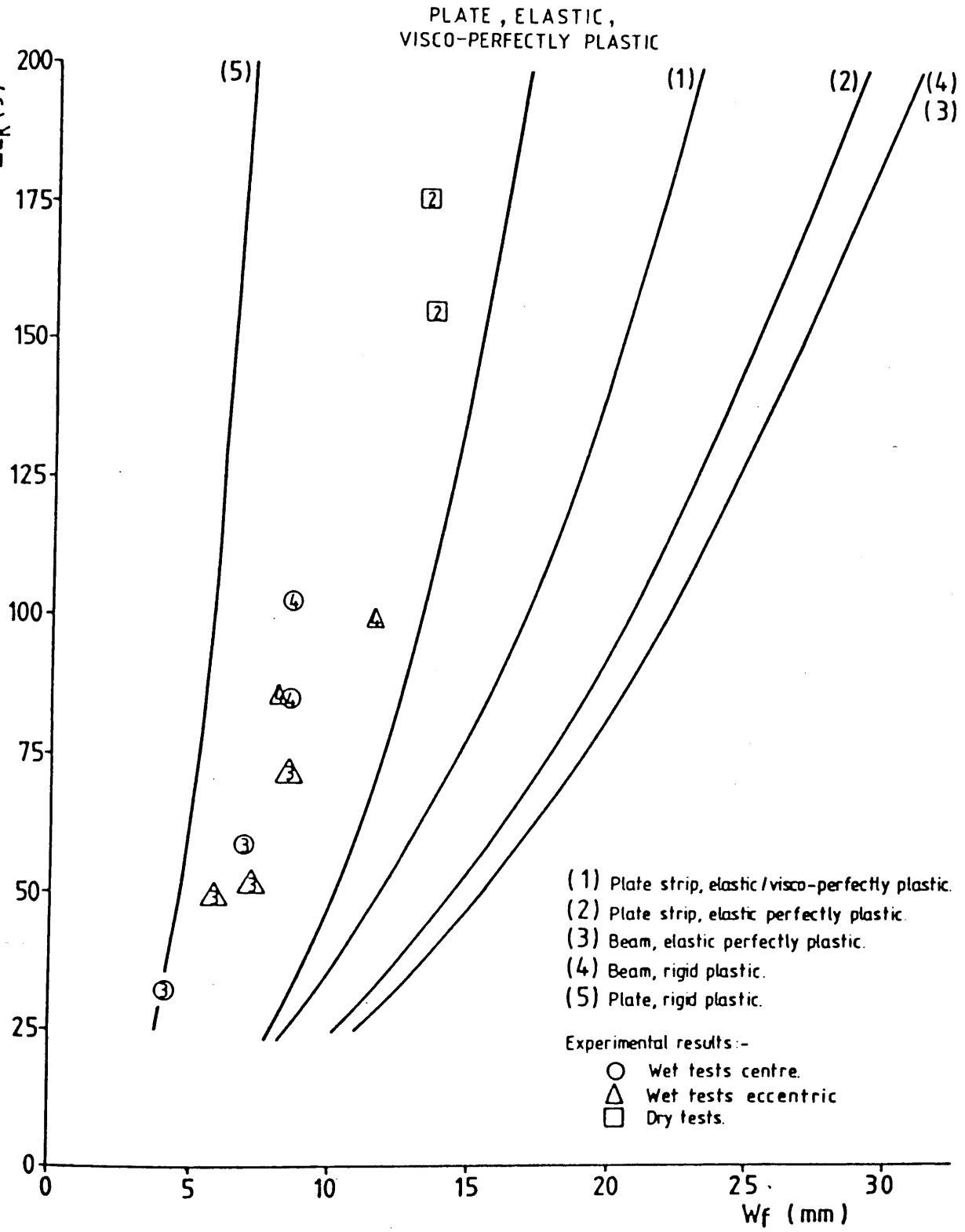

Fig. 6·7 Comparison of experimental and theoretical results.